EFFECTS OF STRUCTURAL PARAMETERS ON THE STATIC INDENTATION AND BENDING BEHAVIOR OF GRAPHITE/EPOXY LAMINATES

by

Stephen Andrew Thomas

B.S. Aerospace Engineering, University of Maryland (1989)

Submitted to the Department of Aeronautics and Astronautics
in partial fulfillment of the requirement for the degree of

Master of Science
in Aeronautics and Astronautics

at the

Massachusetts Institute of Technology

September 1993

Signature of Author______________________________
Department of Aeronautics and Astronautics
September 17, 1993

Certified by______________________________
Professor Paul A. Lagace
Thesis Supervisor

Accepted by______________________________
Professor Harold Y. Wachman
Chairman, Departmental Graduate Committee

EFFECTS OF STRUCTURAL PARAMETERS ON THE STATIC INDENTATION AND BENDING BEHAVIOR OF GRAPHITE/EPOXY LAMINATES

by

Stephen Andrew Thomas

Submitted to the Department of Aeronautics and Astronautics on September 17, 1993 in partial fulfillment of the requirements for the Degree of Master of Science

ABSTRACT

The effect of different structural parameters on the indentation and bending behavior of laminated plates was investigated through a nonlinear analysis and static indentation experiments using rigid backface support and clamped-clamped boundary conditions, and specimens with six different spans between 32 and 508 mm in the clamped-clamped condition. The specimens were graphite/epoxy laminates in a $[\pm45_2/0_2]_s$ layup made from Hercules AS4/3501-6 tape prepreg. The laminates were loaded at their geometrical center with a 12.7 mm hemispherical indentor, while recording force, deflection, indentation and strain data. The damage in the specimens was evaluated using X-ray photography and cross-sectioning. A nonlinear analysis of the bending of the plates was developed using nonlinear strain-displacement relations, laminated plate theory, and the Rayleigh-Ritz method to produce a set of nonlinear equations to be solved using the Newton-Raphson method. The indentation behavior of the plates was influenced by structural parameters as indentations were seen to be different at a given force level depending on the boundary condition and possibly, the span. A comparison between previous impact results and the static tests, for the same structural parameters, showed that static force-deflection behavior for the two boundary conditions tested bounds the behavior in the impact tests and that membrane effects are important in both impact and static events. The membrane behavior was observed to become more dominant for larger spans and at increased force levels. The analytical force-deflection and force-extensional strain curves fit the experimental data well using a fitting parameter which accounts for the flexibility of the in-plane boundary conditions. The initial damage in the specimens consists of matrix cracks near the backface of the specimens. These are accompanied by delaminations at higher force levels, which increase in extent toward the lower face of the laminate. The specimens tested with a rigid support show no damage (to loads of 1479 N) while the specimens tested with a clamped-clamped support show a progression of damage for the same forces tested, initiating between 507 N and 549 N, but with no variation with total span. Using force as the parameter for comparison, the type and through-thickness location of the damage are similar for both impact and static tests, but the overall extent of the damage is smaller for statically loaded specimens.

Thesis Supervisor:	Paul A. Lagace
Title:	Associate Professor, Department of Aeronautics and Astronautics, Massachusetts Institute of Technology

ACKNOWLEDGEMENTS

I must first express my love and gratitude to my wife, Mary. Her rationality when I was irrational, strength when I was weak, and unconditional love when I needed a friend allowed me to even think of completing this degree. I must also express my love and gratitude to my family and, especially, to my mother. Without her advice, support, and encouragement, I could not have made it through my college career.

Before I came to MIT, I expected an intense educational experience with highly intelligent and well qualified colleagues. When I arrived here, I found this to be the case, but I also found interesting friends who were eager to share a joke and have a good time. Mary and I were relieved to find other young couples, Mark and Elaine, Jeff and Becky, and Aaron and Ann, with whom we could always share a beer and get into a "guys vs. gals" game of Pictionary. I was relieved to find more "experienced" students, Wilson, Narendra, Mary Mahler, Ed, Laura, Mak, Hiroto, and Hari, who would patiently answer even the most ridiculously obvious questions I could ask (no one in the lab, during the time I was here, could ever repay the favors done for them by Wilson and Narendra). I was pleased to have a friend like Stacy, who was always willing to discuss a problem set, or get into a conversation on just about any topic. I have also been happy to get to know Brian, Lauren, Rich, Cecilia, Robin, and Tracy and pass on what I was taught by the more "experienced" students (of course, I probably learned more from them in the process). I also found friendship and help from the many undergraduates who worked in the lab, particularly Caleb White and Randy Stevens. The work those two gentlemen performed for me was invaluable.

Fortunately, students are not the only people at MIT I count as my friends. Debbie and Ping always did more than their job required, from cheering me up with a smile and a kind word to taking care of my problems by cutting through all the red tape. Al always seemed to have the answer to a desperate problem and a wise word of advice to think about while applying strain gages. Hugh and Michael enriched my education with their experiences. Professor Dugundji showed infinite patience in explaining some of the more subtle points in the nonlinear analysis and great wisdom by pointing out some of the directions that the research took. Paul was my advisor, teacher, benefactor, and friend. He made all of this possible and, for that, he will always have my deepest appreciation.

Finally, I just can't resist...

Most likely to take the bhat pole to the bhat cave: Narendra Bhat
Least likely to have a driver's license: Wilson Tsang
Most likely to take the qualifiers: Mary Mahler
Most likely to get a parking ticket: Ed Wolf
Most likely to date a "real man": Laura Kozel
Most likely to use the word dude: Mak
Most likely to visit Martha's Vineyard with a hangover: Hiroto Matsuhashi
Most likely to vacation where there is a natural disaster: Stacy Priest
Most likely to empty a building: Jeff Farmer
Most likely to say "But I don't get it": Mark Ciero
Most likely to write a book titled "1001 Bad Jokes About Canada": Aaron Bent
Most likely to be devastated when the batteries in his walkman die: Hari Budiman
Most likely to say "that's cool, huh, huh": Brian Wardle
Most likely to do the "Achy Breaky" while wearing an Orioles cap: Lauren Kucner
Most likely to be imitated by Hari: Rich Kroes
Least likely to have a pet mouse: Cecilia Park
Most likely to have Macintosh questions: Robin Olsson
Most likely to be mistaken for John Malkovich: Tracy Vogler
Most likely to wish they never heard of Steve Thomas: Randy Stevens and Caleb White
Most likely to succeed (in antagonizing anyone within earshot): Steve Thomas

FOREWORD

This investigation was conducted in the Technology Laboratory for Advanced Composites (TELAC) of the Department of Aeronautics and Astronautics at the Massachusetts Institute of Technology. This work was sponsored by the FAA under Navy Contract N00019-89-C-0058.

TABLE OF CONTENTS

TABLE OF CONTENTS (continued)

LIST OF FIGURES

LIST OF FIGURES (continued)

LIST OF FIGURES (continued)

LIST OF FIGURES (continued)

LIST OF FIGURES (continued)

LIST OF FIGURES (continued)

LIST OF FIGURES (continued)

LIST OF FIGURES (continued)

LIST OF FIGURES (continued)

LIST OF FIGURES (continued)

LIST OF FIGURES (continued)

LIST OF TABLES

NOMENCLATURE

a	plate dimension in x-direction
A_i	modal amplitude associated with u-displacement
A_{ij}	in-plane stiffness component of the plate ($i, j = 1, 2, 6$)
b	plate dimension in y-direction
B_i	modal amplitude associated with v displacement
B_{ij}	bending-stretching stiffness component of the plate ($i, j = 1, 2, 6$)
c_1	first constant of integration
c_2	second constant of integration
C_i	modal amplitude associated with ψ_x-displacement
C_{ij}	two-dimensional reduced plane stress material constants
D_i	modal amplitude associated with ψ_y-displacement
D_{ij}	bending stiffness component of the plate ($i, j = 1, 2, 6$)
E_i	modal amplitude associated with w-displacement
F	force
$f_i(x)$	mode shape in x-direction associated with u-displacement
$g_i(y)$	mode shape in y-direction associated with u-displacement
G_{ij}	transverse shear stiffness component of the plate ($i, j = 4, 5$)
$g^k(X)$	system of homogeneous nonlinear equations to be solved with Newton-Raphson method
h	thickness of plate
$h_i(x)$	mode shape in x-direction associated with v-displacement
i	modal amplitude index number
J^k	Jacobian matrix of equations $g^k(X)$, where k is the step in Newton-Raphson method

NOMENCLATURE (continued)

k	local contact stiffness
$\underline{K}_{I}$	stiffness matrix for linear term of complete system of equations
$\underline{K}_{I}^{*}$	stiffness matrix for linear term of reduced system of equations
$K_{I_{ij}}$	subcomponent of stiffness matrix for linear term of complete system of equations (i, j = a, b, c, d, e)
$\underline{K}_{II}$	stiffness matrix for nonlinear squared term of complete system of equations
$K_{II_{ij}}$	subcomponent of stiffness matrix for nonlinear squared term of complete system of equations (i, j = a, b, c, d, e)
$\underline{K}_{III}$	stiffness matrix for nonlinear cubic term of complete system of equations
$\underline{K}_{III}^{*}$	stiffness matrix for nonlinear cubic term of reduced system of equations
$\underline{K}_{III_{ee}}$	stiffness matrix for nonlinear cubic term of system of equations reduced with β
K_iK_j	shear correction factor
L	beam length
l_d	deformed length of plate
$l_i(y)$	mode shape in y-direction associated with v-displacement
l_o	original length of plate
M	total number of modes in the y-direction
$m_i(x)$	mode shape in x-direction associated with ψ_x-displacement
M_{ij}	bending moment resultants ($i, j = 1, 2$)
N	total number of modes in the x-direction
n	local contact nonlinearity exponent
$n_i(y)$	mode shape in y-direction associated with ψ_x-displacement

NOMENCLATURE (continued)

N_{ij}	in-plane stress resultants (i, j = 1, 2)
$o_i(x)$	mode shape in x-direction associated with ψ_y-displacement
p_i	transverse force per unit area
$p_i(y)$	mode shape in y-direction associated with ψ_y-displacement
Q_i	bending moment resultants (i = 1, 2)
$q_i(x)$	mode shape in x-direction associated with w-displacement
q_j	generalized coordinates for linear terms (j = 1, 2, ..., M)
$\underline{R}$	generalized force vector
R	radius of indentor
R^2	correlation factor
$r_i(y)$	mode shape in y-direction associated with w-displacement
R_{j_i}	generalized force vector associated with a modal amplitude (j = a, b, c, d, e)
S	surface area of the plate
U	internal strain energy
u	displacement component along the x-coordinate direction
v	displacement component along the y-coordinate direction
W	work done by the external forces
w	displacement component along the z-coordinate direction
x_1	direction equivalent to x-direction
x_2	direction equivalent to y-direction
x_3	direction equivalent to z-direction
X^k	generalized representation of the modal amplitudes, where k is the step in Newton-Raphson method

NOMENCLATURE (continued)

z_l	z-coordinate of lower face of laminate
z_u	z-coordinate of upper face of laminate
α	indentation at the contact point
β	geometrical nonlinearity factor
Δl	change of length of plate on through-thickness centerline
Δu	displacement of end of plate
ε_{ij}	strain tensor components ($i, j = 1, 2, 3$)
ε_l	strain on the lower face of the laminate
$\underline{\varepsilon}^o$	midplane extensional strains
$\varepsilon^o{}_{ij}$	strain tensor components at midplane ($i, j = 1, 2$)
ε_u	strain on the upper face of the laminate
$\underline{\gamma}$	transverse shear strains
$\underline{\kappa}$	plate curvatures
κ_{ij}	curvature tensor components ($i, j = 1, 2$)
μ	index number for y-direction mode shapes
Π_p	total potential energy
ψ_x	rotations of a plane section about the x-axis
ψ_y	rotations of a plane section about the y-axis
ζ	index number for x-direction mode shapes

Chapter 1

INTRODUCTION

Composites are becoming the material of the present in aircraft structures. Composite materials have found their way into an increasing percentage of the total structure of military and, more recently, commercial aircraft. Commercial aircraft companies have turned to composites in an attempt to give their designs an edge in an increasingly competitive market. Because of their high strength and stiffness to weight ratios, composites offer an attractive way to increase the profitability, performance, and safety of aircraft. Yet, composites have a largely underutilized potential due, in part, to the high safety factors and knockdowns required in designing with them while they gain acceptance as replacements for metallic structures. In order to take full advantage of the benefits of composite materials, the understanding of the issues which affect their structural performance must be matured to the point where they can be used in design with the confidence now associated with metals.

The performance of a structure that has been impacted by a foreign object is an issue of particular concern in composite materials. Low speed impact events such as a tool dropped on a skin panel, a composite part banged against a storage rack during manufacture, or debris kicked up during a takeoff roll can pose a serious threat to a composite aircraft. This threat comes from two basic characteristics of composite materials. First, low through-the-thickness strength, due to a lack of fiber reinforcement in that direction, makes composite materials susceptible to damage during lateral loading such as impact. Second, the existence of internal ply interfaces may result in an impact event causing significant damage to the structure internally while the surface of the laminate appears undamaged. While much work has been conducted in an attempt to understand these phenomena, the understanding of the impact behavior of composites lags behind that for metals.

As work has progressed to better understand how impact affects composite materials, the subject has been divided into two areas: damage resistance and damage tolerance. Damage resistance pertains to the amount of damage sustained by a material or structure when loaded. Damage tolerance pertains to the capability of a structure to perform with damage present [1]. Correct evaluation of damage tolerance requires an accurate definition of the damage state in the material. In order to do this properly for the case of impact, the damage resistance of the material must be well understood. Therefore, understanding damage tolerance with regard to impact relies on understanding damage resistance.

In understanding impact damage resistance of composites, there is not a distinct division between structure and material. In composites, material design is an integral part of structural design in that the material is built up in conjunction with the structure. This indicates that the response of a composite to impact is not a material property alone. It is therefore necessary to understand the effects of impact on both material and structural behavior to properly assess damage resistance.

The fact that both material and structural behavior are important to properly assessing a structural system is recognized in the building block approach to understanding failure phenomena [2]. The first step in this approach is to test small samples which allow the understanding of basic material behavior. The second step is to test samples more representative of actual structural size, shape, and boundary conditions to gain further understanding of material and structural behavior. Because of the connection between material and structural behavior in composites, the philosophy of these steps is the basis for the work presented here.

The structural effects on impact resistance of composite laminated plates are considered in the present research. This is done by examining the effects of varying the size and boundary conditions of a plate on its contact, bending, and damage behavior in a static indentation test. An analysis was also developed to model the bending of the plate for the same conditions. This work also contributes to understanding the ability and the validity of using static indentation tests for evaluating impact resistance. This is accomplished by comparing the contact and bending behavior, as well as the damage, from these static tests with existing experimental data from impact tests. This approach has been suggested and verified for certain configurations [1,2].

This investigation of the issues described above is presented in the following six chapters. In Chapter 2, the research needs identified by previous work on impact and static indentation are presented. The manufacturing techniques, the test matrix, the test methods, and the damage evaluation techniques used in this research are described in Chapter 3. The plate bending analysis is outlined in Chapter 4 through the derivation of the governing equations and the solution technique concluding in a description of the computer implementation of the analysis. Experimental and analytical results are presented in Chapter 5 followed by a discussion of those results in Chapter 6. This work concludes with a presentation of conclusions which are drawn from this investigation and recommendations for future work in Chapter 7.

Chapter 2

PREVIOUS WORK

Because impact is a major concern in the design and use of composite structure, there have been many investigations into impact behavior in the past two decades. Abrate [3] has conducted an extensive review of the work that has been done on impact of laminates. It has been shown that the topic of impact of composites can be divided into two issues which may be treated separately: damage resistance and damage tolerance. The issues may be separated because the details of how damage is created (damage resistance) does not affect the way the structure responds to that damage (damage tolerance) [4]. The present work addresses only aspects of the issue of impact damage resistance.

The impact damage resistance works examined herein can roughly be divided into four categories: correlation between static indentation and impact testing, contact behavior, bending behavior, and damage characteristics of an indented specimen. These categories, which may define the damage resistance of a structure under impact, yield a logical way to separate a large amount of work into comprehensible bits. However, the relationship between these categories of behavior may be different for static and dynamic events, leading to the question of when static indentation results are applicable to impact events. The lack of work in one or another of these categories may point to a deficiency in the understanding of the impact event in regards to that area.

2.1 Correlation of Static Indentation and Impact Testing

There is great motivation to use static tests to evaluate the damage resistance of a structure to impact. Static tests can be better controlled and more simply instrumented using "standard" testing equipment since such tests require fewer factors to be controlled during an experiment. Also, effects such as ringing in impact force measurements, which may mask behavior, are not present in static tests. Overall, static tests are less complicated than impact tests, thereby allowing better fidelity in the data gathered statically. The desire to use static tests to investigate the structural and material characteristics involved in impact resistance requires the establishment of a relationship between static tests and impact events.

To relate static and impact tests, the contact force between the indentor and plate has been shown to be the best parameter for comparison. The maximum force measured in an impact (which is related to the physical characteristics of the impact event) test may be used as the maximum force for a static test, allowing direct comparison between the two kinds of tests [1]. Also, the damage incipience (the onset of damage) has been observed to occur at a consistent contact force level in the two types of tests [5]. Because of this, the force history of the impact event is considered by many to be the most useful parameter in understanding impact damage mechanisms and correlating static and impact results [1, 2, 6].

A number of studies have shown that static indentation tests may yield useful information about contact behavior, failure mechanisms, and failure loads for composite plates under impact. In attempts to investigate the applicability of static tests to model impact events, similar results for both kinds of tests have been seen in experimental force-displacement and damage behavior for monolithic plates [5-8] and sandwich panels [9]. The displacement of the point of contact between a plate and an indentor has been found to be virtually the same for both static indentation and impact tests [5-9]. During both impact and static tests, the force at which a given level of damage occurs, generally incipience or penetration, was also seen to be essentially the same [5, 7, 9]. Once the damage occurred, evaluation techniques such as C-scan and X-ray photography showed that the size, type, and progression of damage with applied force result from both static and impact events [5-8]. These results indicate that static tests can be used to evaluate impact phenomena for composite laminated plates.

In response to the experimental results, there have been effective attempts to analytically clarify the reasons for the apparent similarity between static indentation and impact tests results and better define the limits of that similarity [2, 7, 8]. Among these, Jackson and Poe [2] cite cases when static indentation results may be applicable to impact events. They indicate that for large mass, low velocity[†] impact events, the contact duration is much longer than the time required for flexural waves to be reflected from the boundaries. This means that during a long contact period, the flexural waves have time to move to the boundaries and reflect repeatedly, resulting in a deformation mode approaching the static solution. However, it is also indicated that the size of the plate is important. For example, in larger plates (25.4 x 25.4 cm is cited) where flexural waves take longer to reflect from the boundaries, the static deformation mode may not develop during impact except for very large impactor masses. The

---

[†] No distinct definition of what bounds were set on "large" mass or "low" velocity were given.

conclusion is that quasi-static response is only applicable during impact if the target is relatively small (described in this specific case as less than 12.7 x 12.7 cm) and the impactor mass is relatively large.

There exists a good basis for comparing the two kinds of tests, but the range of applicability of static tests to impact tests is still unclear. In light of the investigation by Jackson and Poe, it must be noted that the previous studies considered plates under 15.3 cm in span [5-8] or sandwich panels [9]. The applicability of results from static indentation tests of larger panels to impact events is still in question. No investigations have been found that examine larger plates under static indentation or impact loading, except for the impact experiments of Jackson and Poe [2] and Wolf [10], whose results will be used in this work.

2.2 Contact Behavior

Contact behavior can be defined as the response of a structure to an object (the indentor) being pressed into its surface. A result of this interaction, if the indentor is rigid, is a reduction in the thickness of the structure, defined as indentation. Among the parameters of interest involved in this behavior are the size, shape, mass, and velocity (if the contact is dynamic) of the indentor, the local contact rigidity of the plate, and the force between the two objects in contact. Understanding contact behavior is a key to understanding damage because the extent of damage is dependent on the contact force, which can be related to the indentation [11].

Hertz developed the "classical" contact theory [12]†. Starting with the assumption of contact between an elastic sphere and a homogeneous

---

† A detailed discussion of Hertzian contact theory can be found in the book "Impact" by Goldsmith [13].

isotropic elastic half-space, a simple formula for the relationship between the force and indentation was determined:

$$F=k\alpha^{n} \tag{2.1}$$

where k is the local contact rigidity and the exponent n is equal to 3/2. Hertzian contact law has been shown to work well as a prediction tool for loading and reloading in certain cases. Some of the earliest work on static indentation of composite laminates conducted by Sun and colleagues [11, 14, 15] showed that Hertzian contact law was followed for loading and reloading of plates under indentation,. Unloading followed a similar power law with an exponent of n equal to 5/2. There are obvious limitations of this theory in regard to the impact of composite plates since plates may not be a good approximation of a half-space and composites are inhomogeneous and orthotropic. In order to overcome the limitations of Hertzian theory, there have been a number analyses [16-22] developed which have achieved some success in predicting force-indentation behavior for composite laminates.

Along with the limitations of Hertzian contact theory already noted, there is evidence that contact behavior may be affected by increasing deflection, increasing indentation, and the geometry of the plate being indented. Increasing the deflection of a beam specimen creates a larger contact area with the indentor, reducing the contact stresses and causing smaller indentations [15]. When indentations increase, and the region of contact increases, contact stresses redistribute away from Hertzian. The contact stresses may also change because the plate wraps around the indentor in the contact region when the contact area grows and the plate thickness decreases [17]. This behavior, called plate wrapping, is defined as a local bending of the plate to conform to the indentor [16]. This behavior is very different from that allowed by Hertz' elastic half-space. Also different from Hertzian assumptions is the behavior of a finite, simply-supported isotropic square plate. The geometry of the plate causes a reduction in the contact area corner-to-corner as indentation is increased, causing the contact stresses to be higher along the longitudinal and transverse axes. The result is a contact area in the shape of a four-lobed hypotrocoid (a square with rounded corners). In this case the hypotrocoid is oriented so that its "corners" point to the edges of the plate and its flat sides towards the plate corners. The hypotrocoid-shaped contact area was also seen to occur concurrently with wrapping as the indentation grows, causing a divergence from Hertzian contact behavior [23].

The works that are presented here clearly show that the contact behavior between a plate and an indentor may differ from Hertzian behavior. However, because Hertzian contact law is relatively simple and well-established as a first order model for indentation, it may be valid to use it as a basis of comparison for what effects boundary conditions and plate geometry have on contact behavior. Still, there is a lack of experimental work which attempts to define what structural parameters (boundary conditions, plate geometry, etc.) may affect the contact relationship.

2.3 Bending Behavior

Contact behavior is one form of deformation of a plate under indentation or impact load; the overall (global) bending of the plate is the other. Plate bending behavior is influenced by the geometry and boundary conditions of the plate: the larger the span of the plate between supports, the larger the bending deflection at the geometrical center for a given force.

The potential for large deflection bending under transverse loading increases with plate span.

Finite deflections of plates have been considered in many analyses throughout this century, based on equations developed by von Kármán [24]†. These equations represent a nonlinear theory that has been used to accurately predict the large deflection bending of both homogeneous [26] and composite laminated plates [27-30] under uniformly distributed loading. The references cited are not intended to represent the large quantity of work done but rather provide a source for the basics behind this theory. The volume of the work done on finite bending of plates precludes a general discussion of the work here. As previously stated, the current discussion is limited to the topic of impact resistance of composite laminated plates. Nonlinear dynamic analyses of composite plates have shown that nonlinear theory predicts smaller deflections in comparison to linear theory, attributed to membrane stiffening of the plate [31, 32]. Comparison of nonlinear dynamic analysis with experimental data shows that geometrical nonlinearity caused by finite deflections must be included and that boundary conditions must be correctly modeled to accurately predict the impact event [32].

Experimental investigations have shown that bending behavior can influence the contact behavior and the development of damage during an impact event. Increasing the deflection of a plate can result in a larger contact area with the indentor, reduce the contact stresses and cause smaller indentations which can be related to the damage size [15]. Longer plates, which bend more easily, experience damage which initiates as

---

† An explanation of von Kármán's equations for large deflections is presented by Timoshenko and Woinowsky-Kreiger in "Theory of Plates and Shells" [25].

splitting between lower surface fibers; while shorter plates, which do not bend as easily, show damage limited to the area immediately beneath the indentor [33].

However, the reported effects of bending seem to be somewhat in conflict. Comparison between support conditions which allowed bending (two sides clamped) and prohibit bending (rigid foundation) have shown similar effects in loading and damage [1]. Other tests have shown that varying the span of a specimen, which obviously changes how it bends, does not alter the damage that results in the plate [2].

Clearly there is a need for clarification of the effects of bending behavior. This behavior is greatly influenced by plate geometry and boundary conditions. No experimental work could be found that deals with the bending effects on the impact response of a wide range of plate sizes. There is also a lack of analytical work on impact resistance as it relates to large deflection bending. Only two analytical investigations could be found [31, 32] that deal with large bending effects of plates under impact and only one of these [32] compared the analysis with experimental data.

2.4 Damage Characteristics

The most important aspect of an impact or indentation event in regard to structural integrity may be the damage that occurs during the event. Damage is important in determining the ability of a structure to perform during and after an impact event. The force at which damage first occurs (incipience), the types of damage, and the extent of the damage in-plane and through-the-thickness are factors which are deemed important in understanding how a material and structure resist an impact or indentation event. One factor which appears common to impact and indentation events is that a particular contact force can be associated with a particular level of damage in the laminate [1, 2, 8, 11] (as cited in section 2.1). However, the force at which the damage occurs should be accompanied by descriptions of the type, extent, and through-the-thickness location of the damage as these factors are equally important in evaluating the damage resistance of the structure [1].

A number of studies [5, 6, 8, 10, 33, 34] have shown very similar modes of damage and sequences of damage growth for laminates. From observations made with a variety of techniques including X-ray photography, C-scan, deplying, sectioning and microscopic photography, and visual inspection after both static and impact tests, a general scheme of damage can be seen for tape laminates. As contact force is applied, damage initiates at a particular force level as matrix cracking. Increasing the force causes the damage to progress: the matrix cracks grow, link up and encounter ply interfaces, forming delaminations. The delaminations begin in an area between two matrix cracks, but as the contact force is increased further, the delaminations grow in size, become elliptical in shape, but remain bounded by the cracks. Final failure occurs when the force increases to the point where fibers begin to crack. After this the indentor may penetrate the plate.

Other types of plate geometries and boundary conditions will produce different modes of damage. Short thick beams (described as having length less than 75 mm and thickness less than 2 mm) and long thin beams (described as having length greater than 75 mm, and thickness greater than 2 mm) display different damage modes under the same impact conditions [33]. These "long and thin" targets experience flexural damage consisting of splitting between lower surface fibers since the structural bending stiffness for these types of specimens is low and the bending stresses, which are tensile on the lower surface of the laminate, cause damage to initiate there. The "short and thick" targets show contact failure consisting of matrix cracks originating from the edge of the contact zone and delaminations in the top plies. This type of damage results from high local contact stresses between the target and the impactor.

It is apparent that damage can occur in many different ways depending on a number of parameters which are not well understood. While there has been some work that addresses the affects of structural geometry on damage, there exists a need to better define how structural configuration influences the occurrence of damage and the relationship between damage occurring in static and impact tests.

From this discussion it can be seen that structural geometry and boundary conditions can affect the impact damage resistance of a composite laminated plate. However, the effects of structural geometry and boundary condition on the impact damage resistance and the applicability of using static tests to evaluate impact damage resistance of composite laminated plates need better definition.

Chapter 3

EXPERIMENTAL PROCEDURES

3.1 General Approach

The discussion in Chapter 2 indicates that there is a lack of understanding of how the geometry of a plate affects the contact relationship, the damage progression, and the relationship between static indentation and impact events in composite plates. In addition, the large deflections of these plates under impact conditions has not been widely investigated, so it is not fully understood how large deflections might affect the contact relationship and the damage that occurs. The objective of the current work is to understand how plate geometry affects the impact resistance of a laminate and to better understand the relationship between static indentation tests and impact tests for these laminates.

The behavior of the laminates was investigated by conducting static indentation tests which have been shown to yield useful information about the impact behavior [1, 5-9]. The tests were carried out using plates ranging in span from 32 mm to 508 mm and two boundary conditions, clamped-clamped (with respect to bending deflection) and rigid backface support. The contact relation that resulted from these tests was compared to the Hertzian contact law in an attempt to determine the effects of the combinations of plate size and boundary condition. The global bending characteristics of the plate under static indentation were also examined and compared with results from impact test data. A static nonlinear analysis of a plate under concentrated loading was developed with the intent of comparing results with the experimental data. Finally, the damage state of the laminates was examined after the tests were run and the extent of damage was compared with damage results from available impact test data using the force as the parameter for comparison.

3.2 Test Matrix and Description of Specimens

All tests were conducted on $[\pm45_2/0_2]_s$ laminates made from Hercules AS4/3501-6 graphite/epoxy. The layup and material system were chosen to allow direct comparison with previous experimental impact data [10]. Six different spans from 32 mm to 508 mm were considered. This range of spans was selected because it includes "short" span sizes (127 mm and smaller) similar to those tested in other investigations [5-8], 254 mm span specimens as used in previous work for direct comparison [10], and longer spans which have not been tested previously. The different spans were also chosen to provide a wide distribution in bending and membrane behavior during the indentation tests. In all cases, the width of the specimens was kept at 89 mm, which was the plate width previously used by Wolf [10]. The specimens were cut approximately 102 mm longer than the desired span length to allow 51 mm on each end of the specimen for gripping in the test fixture. The overall specimen dimensions are shown in Figure 3.1.

Two kinds of boundary conditions were used for the tests: clamped-clamped and rigid backface support. The clamped-clamped support fixed the out-of-plane deflection and rotation of the longitudinal ends of the specimen to zero, while the transverse sides were free. The distance between the two clamps was defined as the span of the specimen. This boundary condition was used because it may provide an approximation of a skin structure used in aircraft and was used previously by Wolf [10]. The rigid backface support consists of a thick (19 mm) steel plate on which the specimen rests, fixing out-of-plane deflection of the entire backface of the

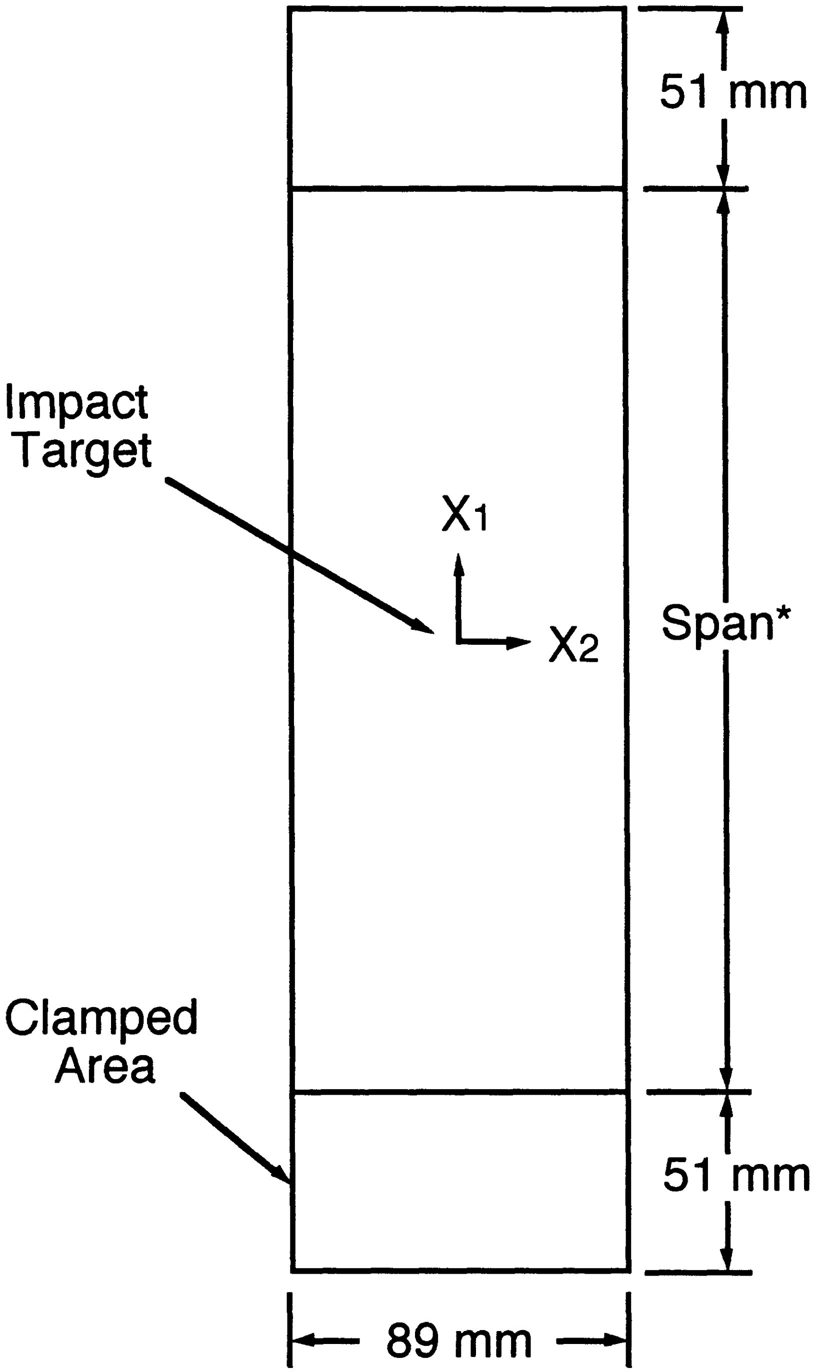

*See Table 3.1
Drawing Not to Scale

Figure 3.1 Static indentation specimen geometry.

plate to zero. Since bending is not allowed in this case, span has no meaning. The rigid backface support was used to eliminate all bending effects in the laminate in an attempt to provide conditions more closely approximating the Hertzian assumptions. This boundary condition may also provide a bounding case for indentation behavior in a laminate under impact loading. The two boundary condition cases were selected to parallel the previous work [1, 9].

The overall test matrix is shown in Table 3.1. All the tests were conducted with a 12.7 mm hemispherical indentor as has been used in a number of investigations [2, 5, 9-11, 14, 15, 33, 35]. The indentation took place at the center of the top face of each specimen.

The first specimens tested were the plates with a 254 mm span. For these tests, the long ends were clamped in a fixture originally designed to restrain motion both in-plane and out-of-plane, maintaining a clamped-clamped boundary condition. However, through a comparison of experiments using this fixture [10] with an analysis modeling these experiments [36], this fixture was found to exhibit in-plane flexibility. This type of boundary condition was chosen because it was the same as in previous experimental impact tests by Wolf [1, 10]. In order to observe the progression of damage, static tests were performed at various forces. Each of the forces chosen were based on the maximum contact force seen in an impact test conducted at a particular velocity by Wolf [10]. This enabled the comparison of the damage states resulting from static and impact tests. The range of forces represent impact test velocities which were selected to capture the entire range of damage from none to large amounts of matrix cracking and delamination [10]. In addition to measuring the force and damage of the plate, the indentation was measured to compare with the

Table 3.1 Test matrix[a].

Maximum Force, N	Span Length, mm					
	31.75	63.5	127	254	381	508
444				C[b] R		
507				C		
549				C R		
739				C		
930	C1	C1	C1	C R C1	C1	C1
1183				C		
1479	C2	C2	C2	C R C2	C2	C2

[a] One specimen for each configuration

[b] Indicates boundary condition and test scheme:
C - Clamped - Clamped Support, No Strain Gages
R - Rigid Backface Support, No Strain Gages
C1 - Strain Gage Scheme A, Clamped - Clamped Support
C2 - Strain Gage Scheme B, Clamped - Clamped Support

analytical contact law and the deflection was measured to compare with previous experimental impact results [10] and the static analysis presented later in this work.

The next set of specimens were tested with the rigid support behind the entire backface of the laminate. The rigid support was provided by a 19 mm thick steel plate. The bending of the plate was also measured to ensure that the boundary condition was truly rigid. The steel plate deflected less than 0.35 mm under the maximum force of 1479 N tested in this investigation (a detailed description of this evaluation is presented in section 3.4). This provides an essentially rigid support. Since the entire backface of the laminate is supported, span length is irrelevant in a test of this kind. Specimens with a length of 254 mm were used because they were the easiest to manufacture. Force, indentation, and damage were measured for these specimens. The force is measured as the correlation factor for the other quantities, the indentation was measured to compare with Hertzian contact law, and the damage was measured to compare with the previous impact tests and the other static tests.

The specimens with a range of spans were tested last, using the clamped-clamped boundary condition. The specimens were tested at two force levels used in the first set of tests: 930 N which was seen to be the approximate level of damage incipience from the first set of tests, and 1479 N which was a high enough force to allow delamination damage to occur. Both forces were high enough so that large deflection bending effects could fully develop. In addition to collecting force, indentation, and damage data for these tests to compare with the previously collected data, strain data was collected at different points on the top and bottom of the specimen along the longitudinal centerline of the plates. Two different gage schemes were used for the two force levels. The first scheme, illustrated in Figure 3.2, was used with the tests to 930 N in order to get a distribution of longitudinal strains along the plate for comparison with the bending analysis. The second scheme, illustrated in Figure 3.3, was used with the tests to 1479 N in an attempt to determine the effects of the boundary condition on the distribution of strain near the end of the plate and to determine if the plate-wrapping effect, noted in previous analyses [16, 23], could be observed.

The strain gages were placed on the plate to capture the bending and membrane behavior in the plates. The strain gages were placed on the top and bottom of the plate so that bending and extensional strain could be separated during data reduction. The gages in "scheme A" (Figure 3.2) were placed at one-eighth span intervals across half the span of a specimen in order to determine the bending and extensional strain distributions on the longitudinal centerline of a plate. In "scheme B" (Figure 3.3), the centerline of the gages at the end of the plate were placed 7 mm from the clamps to put them as close as possible to the clamps while leaving approximately 2 mm between the gage and the clamp so that the specimen could be aligned without damaging the gage with the clamp. These gages were placed at the end of the plate to determine if the plate was slipping in-plane in the grips during the test. If slippage was occurring, extensional strain was expected to be nonexistent or smaller than would be expected if the clamps were perfect. The centerline of gages 4 and 5 were placed 9 mm from the transverse centerline of the plate. This is the minimum distance possible to the point of contact without having the indentor touch the gage (and damage it) during the test. Gages 6 and 7 were butted up against gages 4 and 5, placing their centerline 14 mm from the transverse centerline of the plate. The centerline of gage 3 was placed directly on the

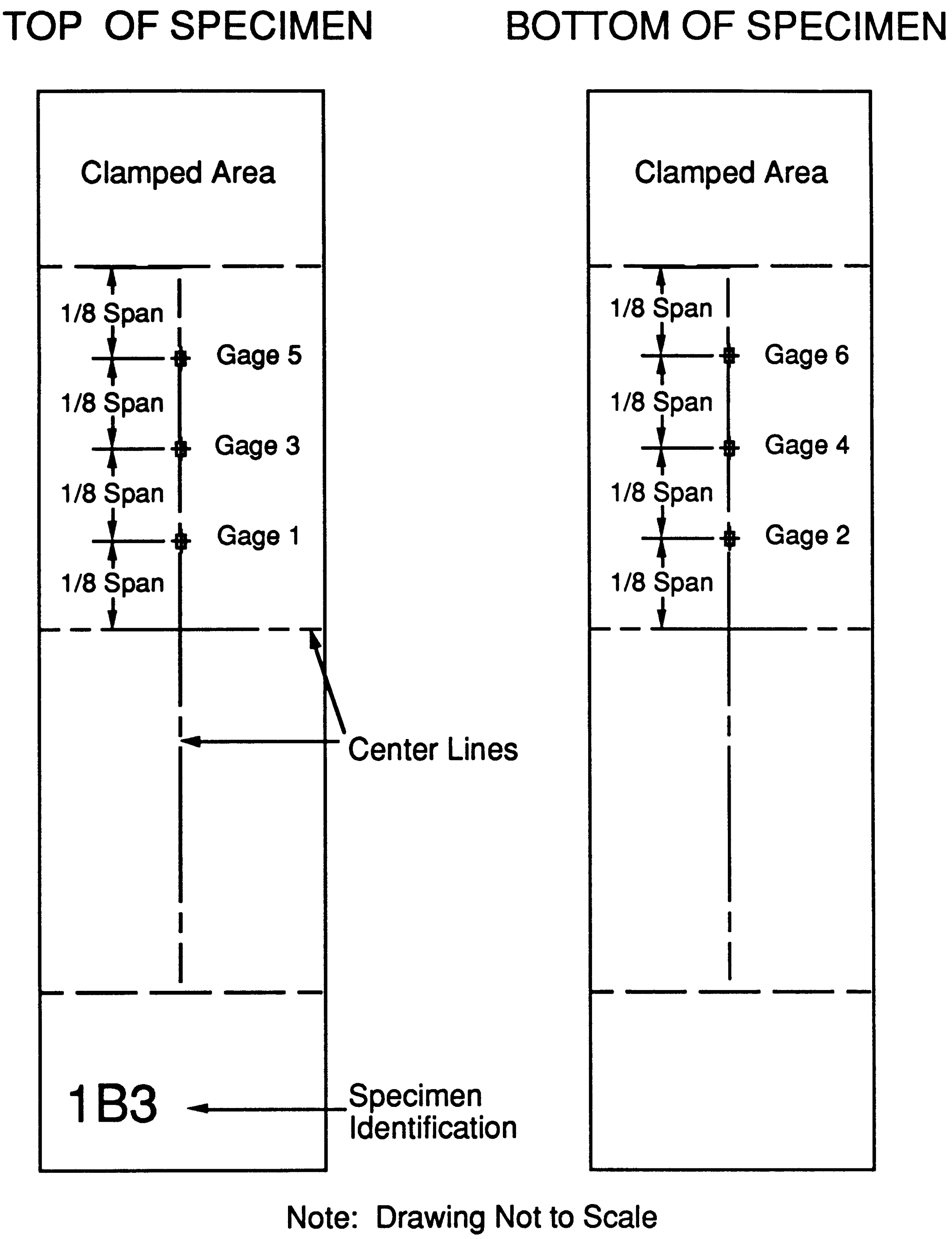

Figure 3.2 Illustration of strain gage scheme A.

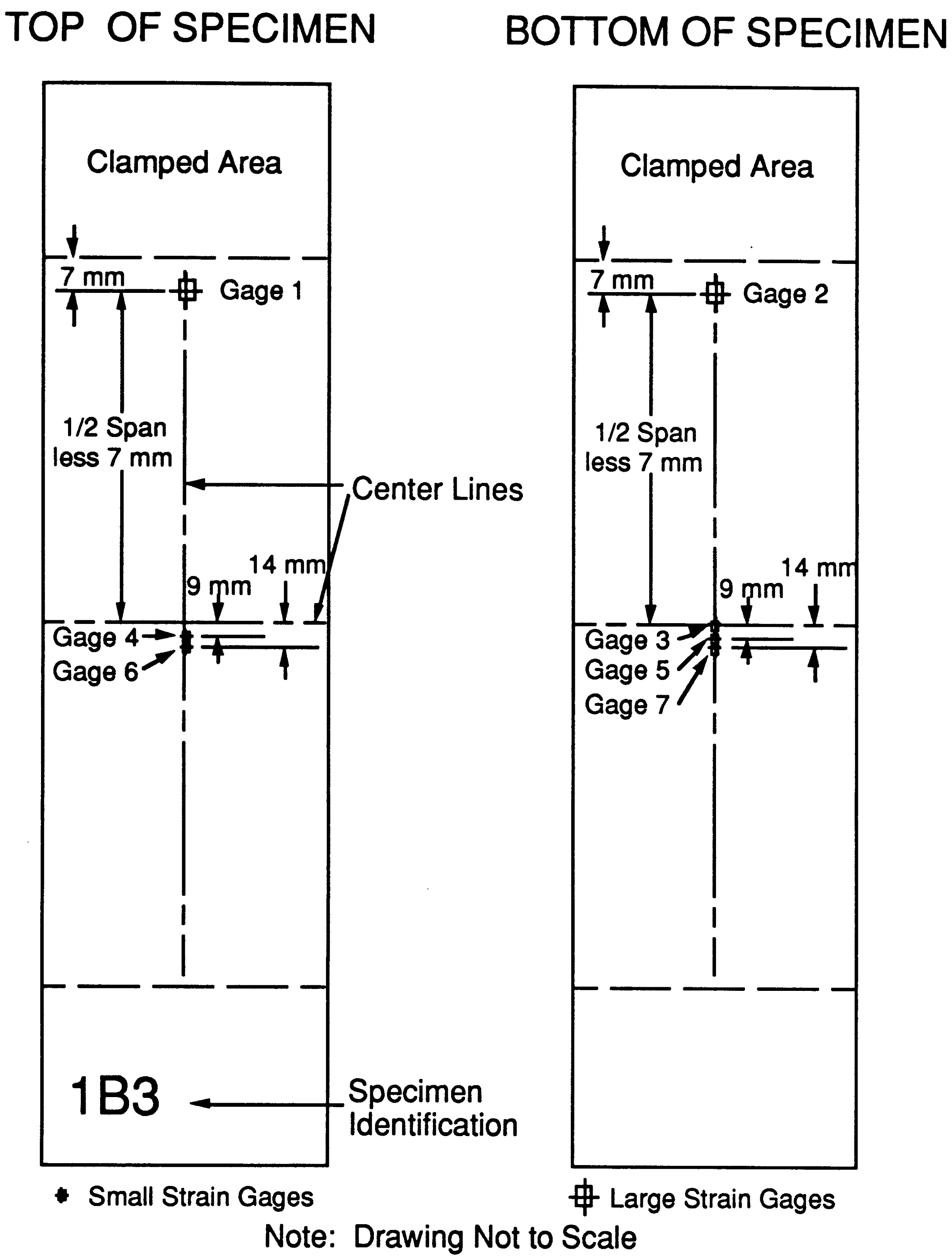

Figure 3.3 Illustration of strain gage scheme B.

transverse centerline of the plate, putting it on the backface of the plate directly opposite the point of contact with the indentor. These gages were placed near the contact point in an attempt to catch plate wrapping around the indentor. If the plate was wrapping around the indentor, a change in the bending behavior in the region where the gages were placed was expected to be observed. Because of a lack of space, gages 1 and 2 were omitted from the 32 mm span plates in both schemes.

3.3 Manufacturing Procedures

The specimens mentioned were manufactured according to TELAC standard procedures [37] except where noted. The Hercules AS4/3501-6 prepreg material, supplied in 305 mm rolls, consists of AS4 graphite fibers impregnated with 3501-6 matrix system with a resin content of 41%. Until needed, the prepreg is stored in a sealed bag in a freezer at a temperature below -18°C. Before layup, the prepreg is removed from the freezer and allowed to warm up inside its bag for approximately 30 minutes, or until it is no longer cold to the touch. The material is kept in the bag while it warms up to prevent moisture, which may affect the quality of the specimens, from condensing on it.

The plies for the specimens are carefully cut so that proper angles can be maintained. The prepreg was unrolled and the necessary plies were cut using teflon-coated aluminum patterns, a teflon-coated straight edge, and a sharp utility knife. Two sizes of plies cut, 365 mm by 305 mm for "normal" panels and 685 mm by 305 mm for "large" panels. The zero degree plies were easily made by cutting the tape at the correct length for the desired plate. The angle plies for the normal panels were cut from the tape with two templates, one in the shape of a parallelogram to make an initial cut from the tape, the other a quadrilateral to cut the parallelogram-shaped piece of tape into two parts (see Figure 3.4). The resulting two pieces were then reassembled into a rectangular shape of the desired dimensions with the seam running parallel to the fiber direction of the tape. A matrix joint such as this, as opposed to a fiber joint, is necessary to ensure the desired high quality of the laminate. The large angle plies were cut similarly except that three pieces were used (see Figure 3.5). The pieces which make up the ends of the ply were cut by the same procedure as for the normal plies. The length of the ply was then increased by cutting a center piece using the parallelogram-shaped template. This piece was then measured to the correct length with a ruler and cut to that length against the teflon-coated straight edge. The three pieces were placed together, now with two matrix joints, to make a ply. Angle plies of any length could be made using this procedure simply by placing different numbers and lengths of center pieces between the original two end pieces. Once all the plies are cut, the roll of prepreg is returned to its bag and the freezer.

With the proper number of plies cut, the laminates were assembled. The individual plies are stacked in proper sequence using an L-shaped aluminum jig to provide alignment of the angles in the laminate. The corner of the laminate which was placed in the corner of the aluminum jig is assumed to have the most accurate ply stacking and is marked as the "good corner" for future reference. The laminate is trimmed with a sharp utility knife and aluminum pattern to the nominal dimensions. Peel ply one-half inch larger than the plate on three edges and two inches larger on the short edge adjacent to the good corner, is placed on both top and bottom surfaces to provide a subtly textured surface for good gripping in the test fixture and for ease of applying strain gages. The laminates were sealed in

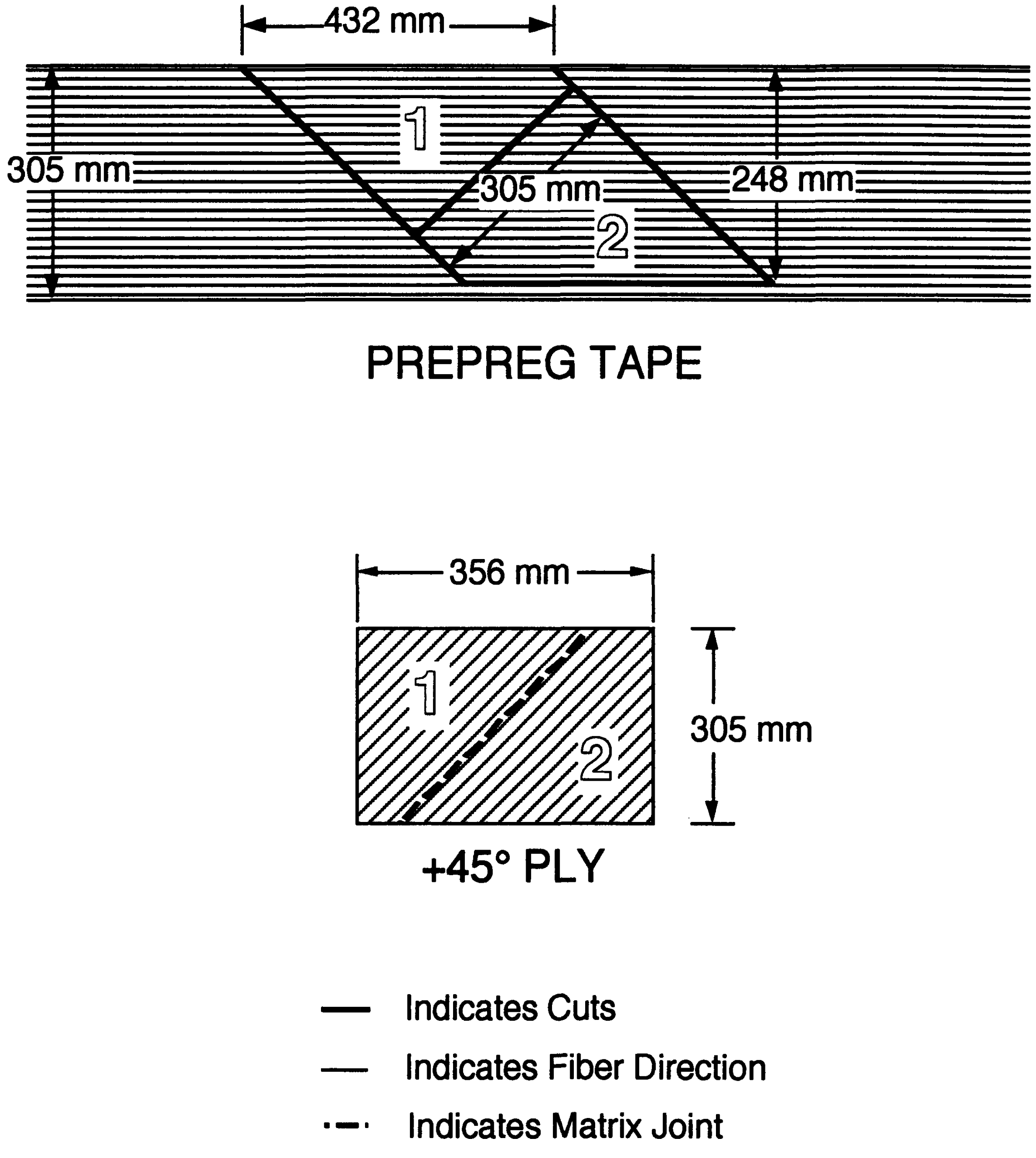

Figure 3.4 Illustration of ply assembly for "normal" specimens.

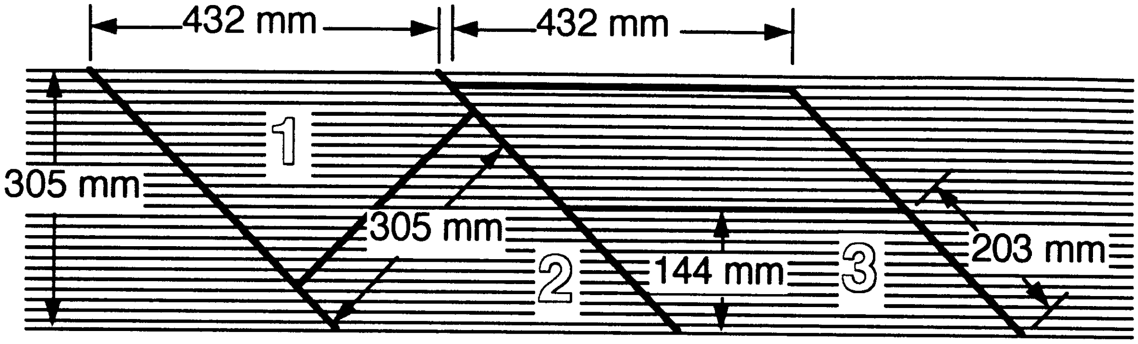

PREPREG TAPE

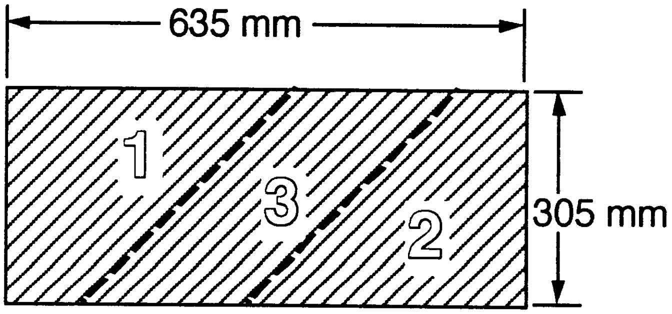

+45° PLY

━ Indicates Cuts

— Indicates Fiber Direction

·–· Indicates Matrix Joint

Figure 3.5 Illustration of ply assembly for "long" specimens.

a vacuum bag and left out for no longer than twenty-four hours before curing.

The laminates were cured according to the manufacturer's recommended procedure for AS4/3501-6. The arrangement of packaging material placed on the aluminum cure plate is shown in Figure 3.6. The aluminum parts are sprayed with a release agent and covered with guaranteed nonporous teflon (GNPT) to prevent resin from adhering to them. The laminate with peel ply is placed on top of the sheets of nonporous teflon and is constrained by cork and aluminum dams. The "good corner" of each laminate (marked during layup) is placed into the corner of an aluminum T-dam to maintain the correct alignment of plies. The T-dams are sized so that a normal-sized laminate will have two sides bordered by an aluminum dam and two sides bordered with cork dams. Since the T-dams did not extend all the way to the end of the large laminates, cork was used to complete the dam around their perimeter. One sheet of porous teflon is placed on top of the laminate followed by one sheet of bleeder paper for every two plies in the laminate, and an aluminum top plate. The bleeder paper soaks up excess resin that is released from the laminate during the cure. The entire cure plate is covered by a sheet of porous teflon and a layer of fiberglass airbreather. The airbreather provides an airway so that vacuum can be applied evenly over the entire cure plate. Finally, a vacuum bag is placed over the entire assembly and attached to the cure plate by vacuum tape to create an airtight seal between the bag and the plate.

A vacuum check is performed on the cure plate before it is rolled into the autoclave. This is done by applying a vacuum of 760 mm Hg to the plate, sealing it, and then shutting off the vacuum pump. The vacuum seal is considered satisfactory if less than 130 mm Hg is lost after five minutes had

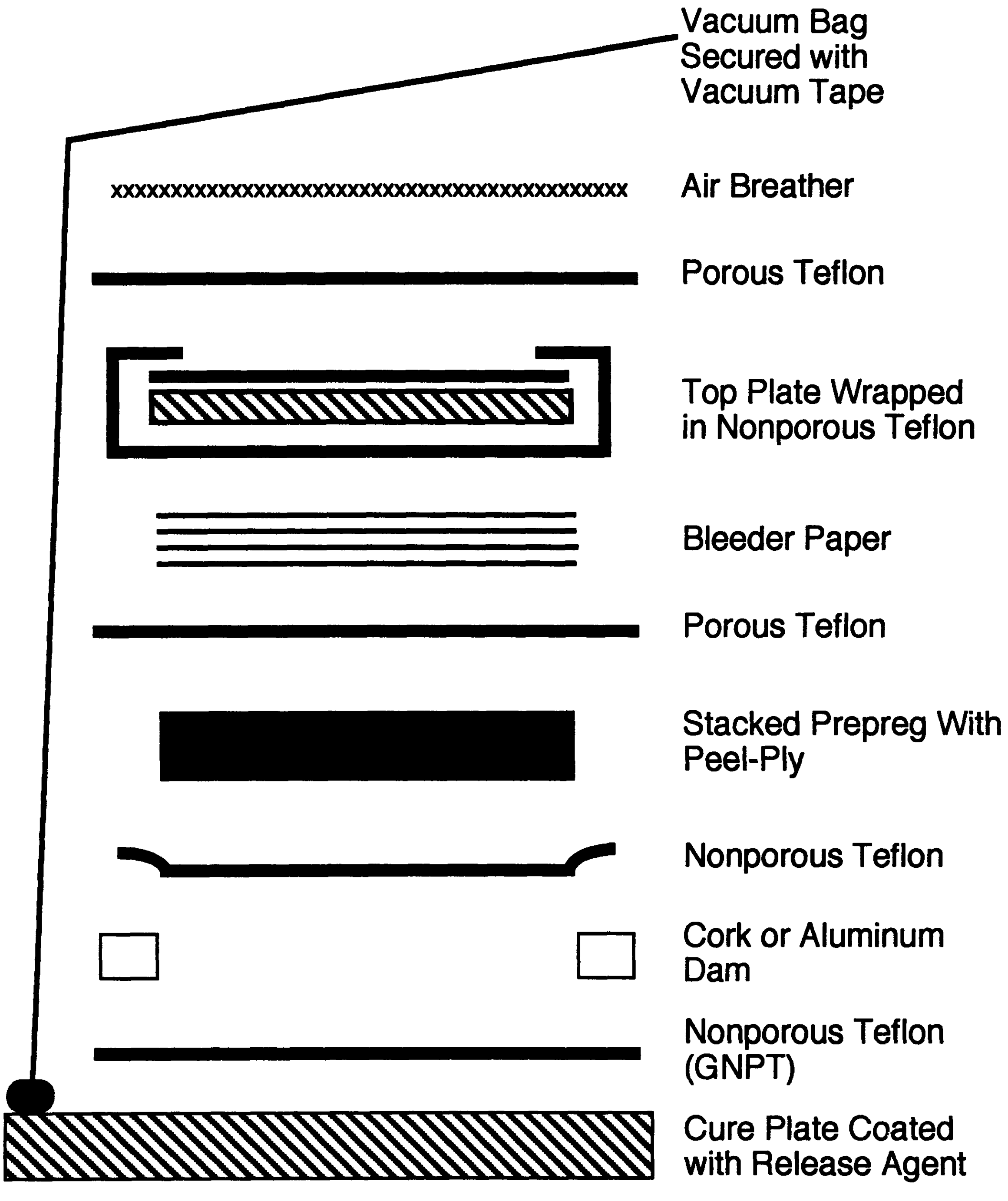

Figure 3.6 Schematic of materials used in cure.

elapsed. If the seal is not good, attempts are made to find and repair any leaks in the vacuum bag or tape or, in the extreme, the entire bag is replaced. When the seal is found to be satisfactory, the cure plate is rolled into the autoclave on a cart and the vacuum check repeated.

Once the autoclave is sealed with the plate inside, a vacuum of 760 mm Hg is maintained on the plate. The autoclave pressure is raised to 0.59 MPa and held. After this pressure is reached, the autoclave temperature is raised at a rate of 1-3°C per minute to 116°C. After an hour at 116°C, the temperature is raised at the same rate to 177°C and held for two hours. The cure is completed by decreasing the temperature at 3-5°C per minute to 80°C, at which time the pressure is slowly released. The pertinent cycles for the cure are illustrated in Figure 3.7. Finally, the laminates are postcured at 177°C for eight hours in an oven without applying vacuum or pressure.

The final specimens were milled from the cured panels with a 220-grit diamond cutting wheel. The milling is done with a 254 mm diameter, water-cooled cutting wheel rotating at 1100 rpm. The laminate is fed past on a table at 279 mm per minute. The specimens are aligned for cutting by placing a trimmed edge against a reference bar bolted to the milling table that has been predetermined as parallel to the cutting blade. To provide extra spacing for different width cuts, square steel and aluminum scraps are placed between the reference bar and the specimen to be cut. With this setup, the rough edges of each panel were trimmed off (approximately 5 mm on each side). Next, the 89 mm width dimensions were cut by aligning the good corner of the laminate to the reference bar. The desired length specimen was then cut from the panels by measuring the length dimension

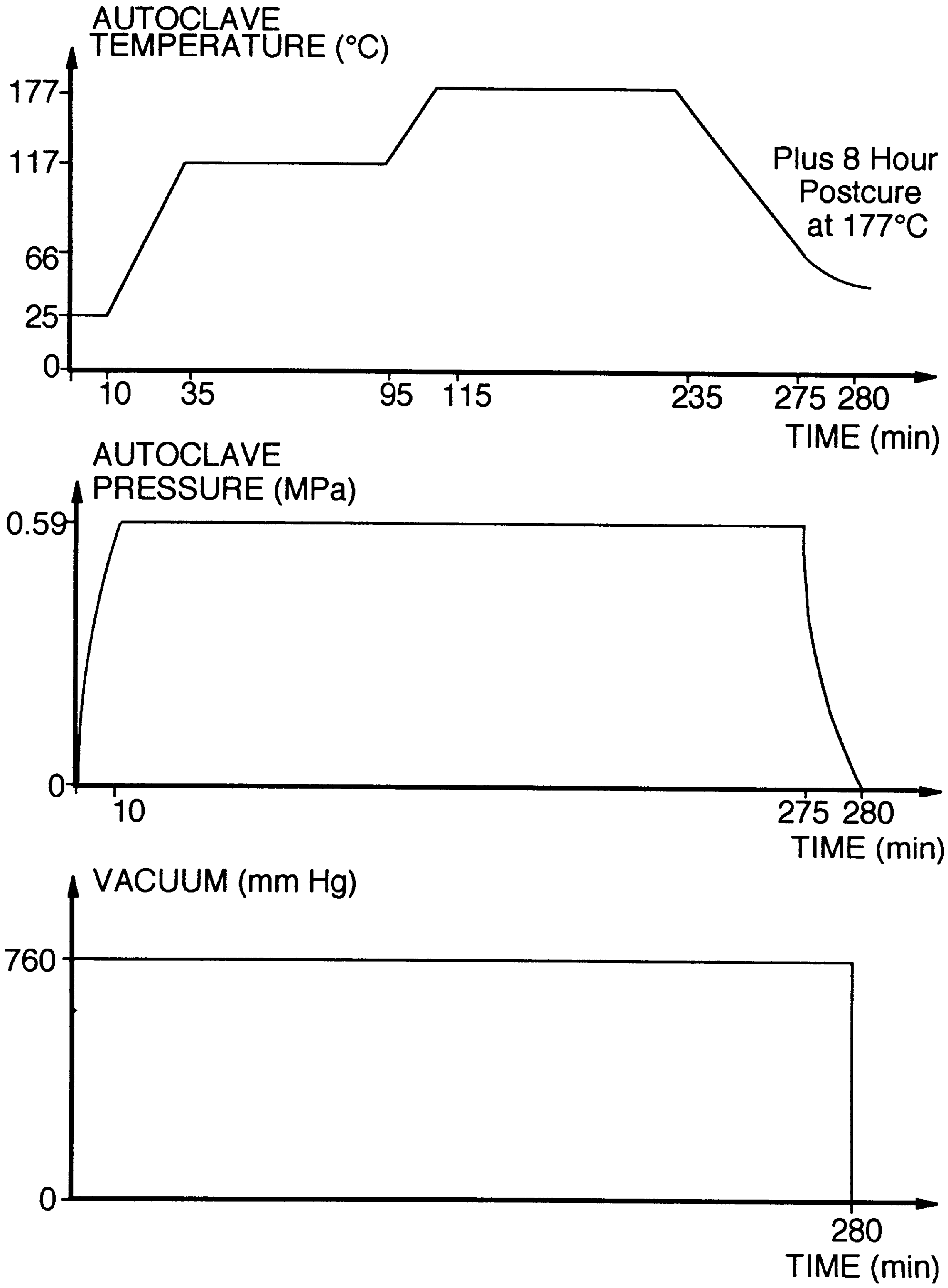

Figure 3.7 AS4/3501-6 cure cycle.

from the good corner and milling across the width at that point, again aligning the good corner for a specimen with the reference bar.

After the specimens were milled, marks were applied to the laminate with a white paint marker so that measurements could be taken at consistent points and so that the laminate could be aligned properly in the test fixture. The dimensions of each laminate were measured to check the results of the manufacturing procedure at a number of locations (see Figure 3.8): nine points for thickness, three points for width, and one point for length. The average ply thickness of all the specimens was 0.136 mm compared to the nominal ply thickness of 0.134 mm.

The last procedure in the preparation of the specimens was to apply strain gages to the appropriate specimens. The strain gages used were Micro-Measurements EA-06-125AD-120 (large gages) and EA-06-031DE-120 (small gages). The large gages have an element size of 3.18 mm by 3.02 mm and the small gages have an element size of 0.79 mm by 0.79 mm. All the strain gages were applied by the standard TELAC procedure [37] using a cyanoacrylate adhesive. The gages were applied at the locations shown in Figures 3.2 and 3.3. Once attached, copper lead wires were soldered to the terminals of the gage and a terminal strip. If the gage read the nominal value 120 Ω (±1 Ω) when checked with an ohmmeter, it was considered acceptable. If not, the lead wires and gage were checked and replaced or repaired if necessary.

3.4 Static Indentation Test Procedures

All the static indentation tests were conducted using an MTS-810 uniaxial testing machine and the setup illustrated in Figure 3.9. The test fixture used to hold a specimen during a test was mounted in the lower grip

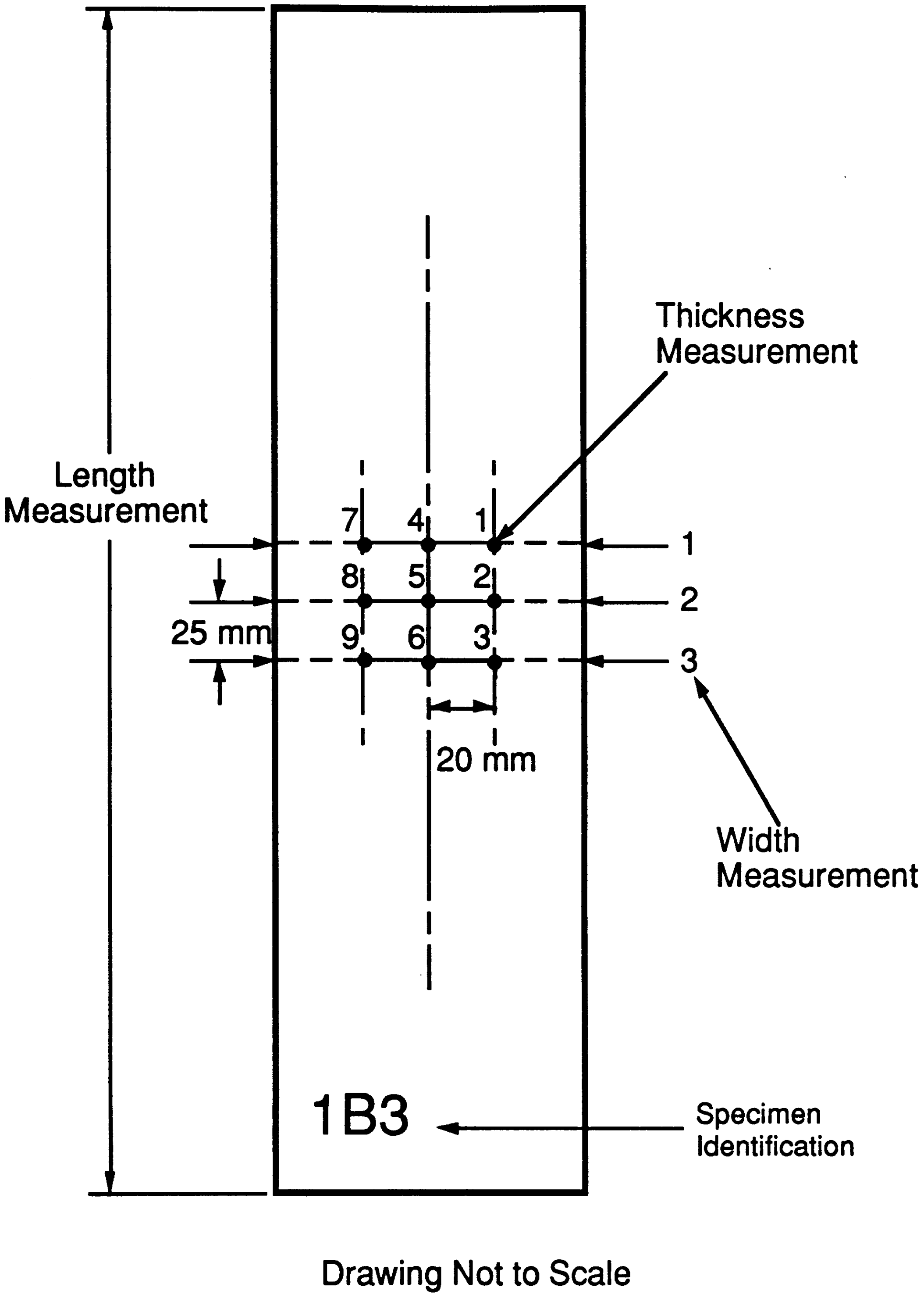

Figure 3.8 Specimen measurement locations.

of the machine. The same basic setup is used for both the clamped-clamped boundary condition, shown in Figure 3.9, and the rigid backface support boundary condition, shown in Figure 3.10 (the details of how these boundary conditions are achieved is discussed below). A stainless steel, 12.7 mm diameter hemispherical indentor and an MTS 8896 N (2000 lb) load cell were mounted in the upper grip of the machine. A Trans-Tek 0350-0000 Linear Variable Displacement Transducer (LVDT) was clamped to a stationary frame which allowed it to be positioned beneath the indentor. By raising the lower crosshead, the fixture moves up which raises the clamped ends of the laminate. The LVDT and tup are fixed in space, so the indentation of the specimen is measured directly by the movement of the LVDT as the laminate thickness reduces under load. The deflection of the specimen is also measured directly by the testing machine stroke as the motion of the fixture. The setup shown in Figure 3.9 allows the measurement of both the indentation and deflection of the specimen using a clamped-clamped boundary condition. The setup shown in Figure 3.10 allows the measurement of both the indentation and deflection of the specimen using a rigid backface support boundary condition. However, bending deflection is effectively prevented by the 19 mm-thick steel plate used to achieve this boundary condition.

The setups illustrated in Figures 3.9 and 3.10 are the same basic test fixture, the details of which are shown in Figures 3.11 through 3.15. The holding jig shown in Figure 3.11 was used to provide the clamped boundary condition. This is the same as the jig used in the impact tests by Wolf [10]. This was to ensure that the clamped-clamped boundary condition were the same as in that previous work. The specimen was held between two aluminum blocks with 80-grit sandpaper applied with double-sided tape to

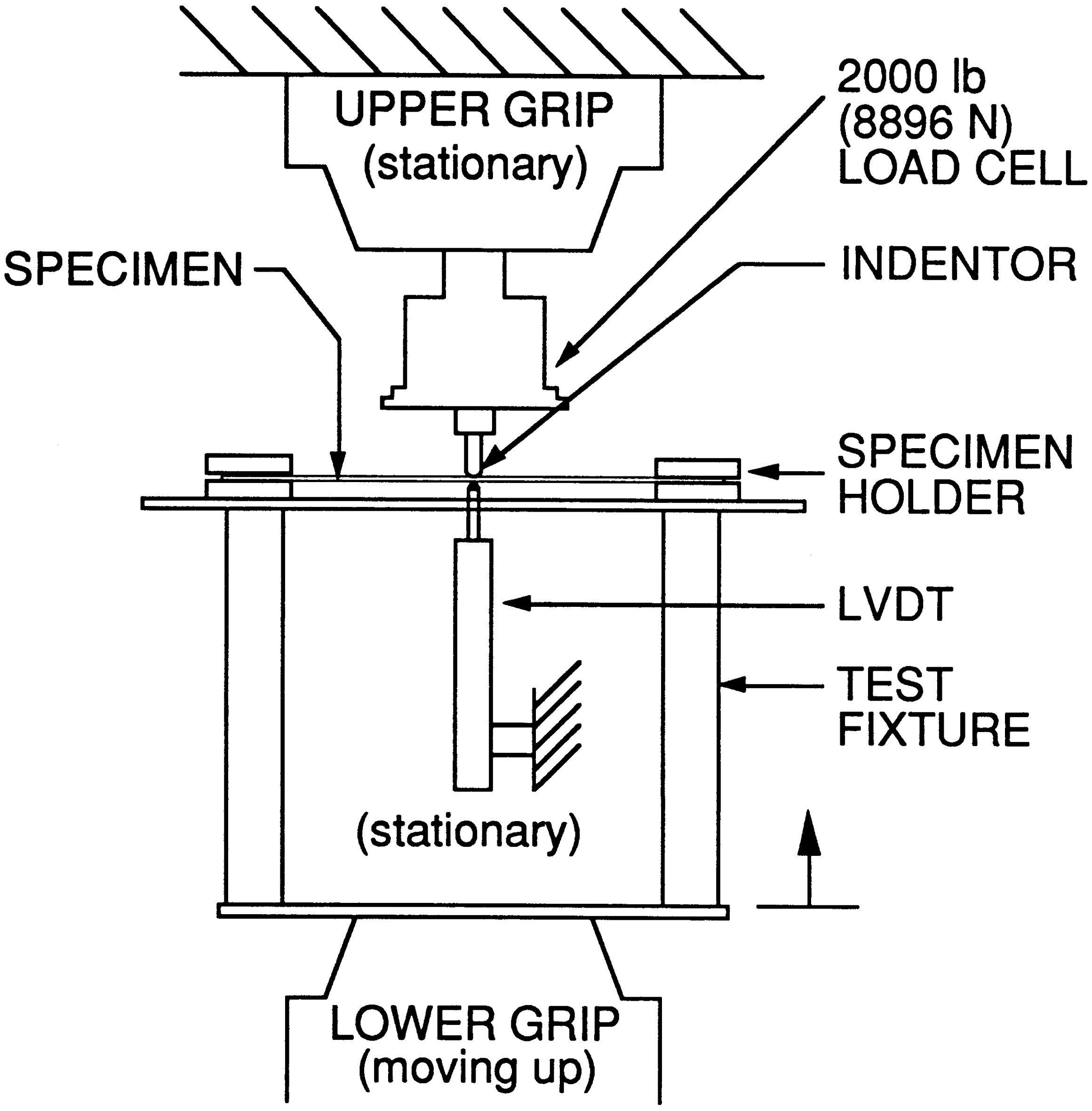

Figure 3.9 Illustration of test setup for clamped-clamped boundary condition.

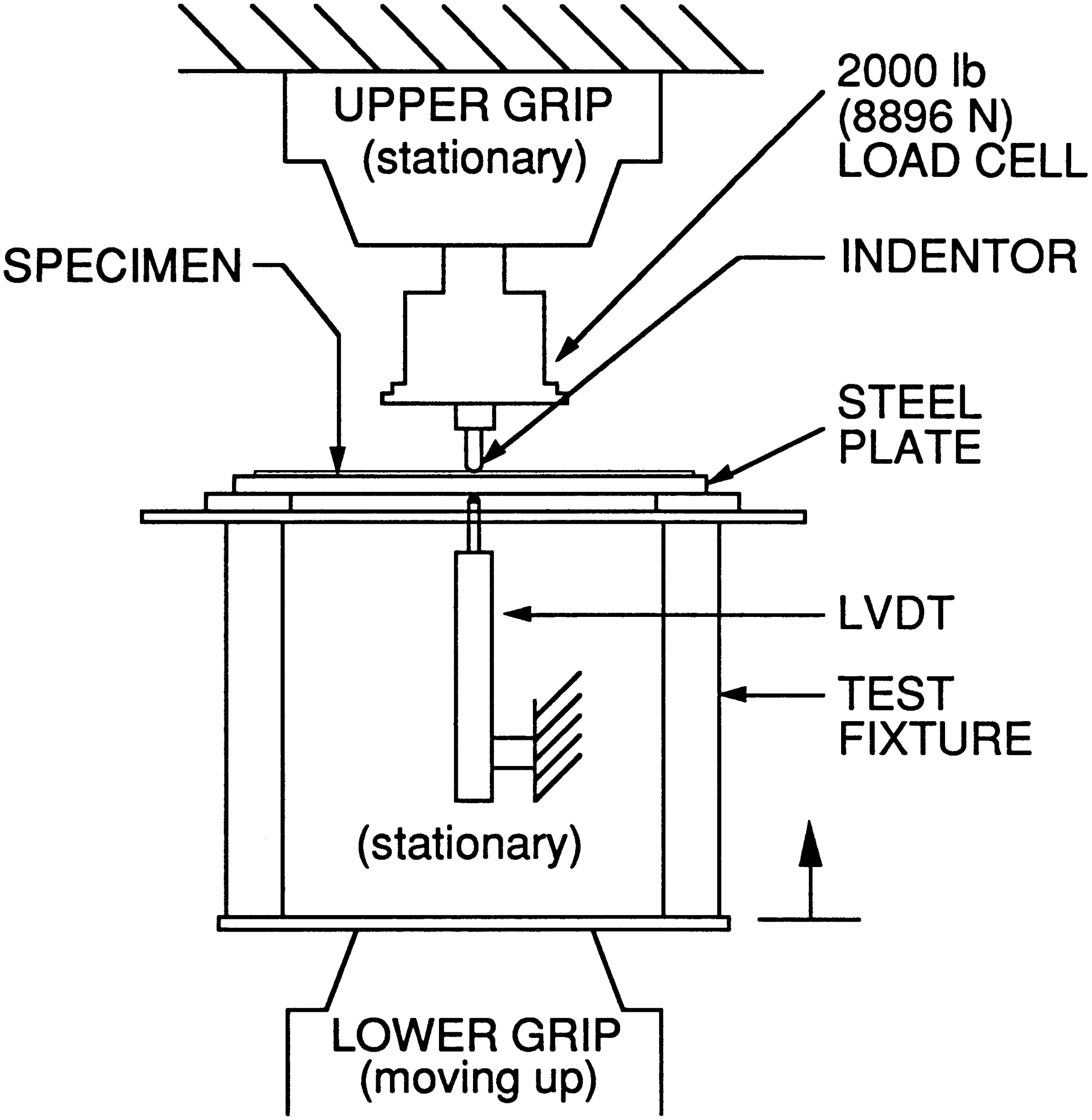

Figure 3.10 Illustration of test setup for rigid backface support boundary condition.

the clamping faces. The blocks were secured to the test fixture and each other by eight bolts, lubricated with SAE 20 weight oil and torqued to 10 Newton-meters. The sandpaper was changed after every two tests to ensure uniformity of the boundary condition and prevent slippage during the test. The gripping blocks were bolted to a fixture, illustrated in Figure 3.12, that could be adjusted to the correct span length by moving the grip mounting plates in or out.

The testing fixture illustrated in Figure 3.12 consists of three major parts: the channel/fixture support assembly, the channel mounting plates, and the grip mounting plates. The details of these parts are illustrated in Figures 3.13-3.15 All the components are constructed of aluminum except the channel, which is steel. The grip mounting plates, illustrated in Figure 3.15, were secured to the rest of the jig by bolting them in holes that were pre-drilled at locations in the channel mounting plates, illustrated in Figure 3.14, to provide the correct spans for the tests. The channel mounting plates were bolted to the channel to fix the whole grip assembly to the fixture support, illustrated in Figure 3.13.

The rigid backface support condition was provided by placing a 19 mm thick flat steel plate on the grip mounting plates. The laminate was placed backface down on the steel plate as shown in Figure 3.10. The steel plate had been tested beforehand to confirm that its indentation and deflection were negligible in comparison to that in the laminate. The deflection and indentation of the steel plate at the maximum contact force tested, 1479 N, were 0.35 mm and 0.004 mm respectively. The deflection and indentation of a laminate tested to the same contact force of 1479 N were 23.0 mm and 0.18 mm, respectively. The deflection and indentation of the steel plate represent 1.5% and 2.2%, respectively, of the deflection and

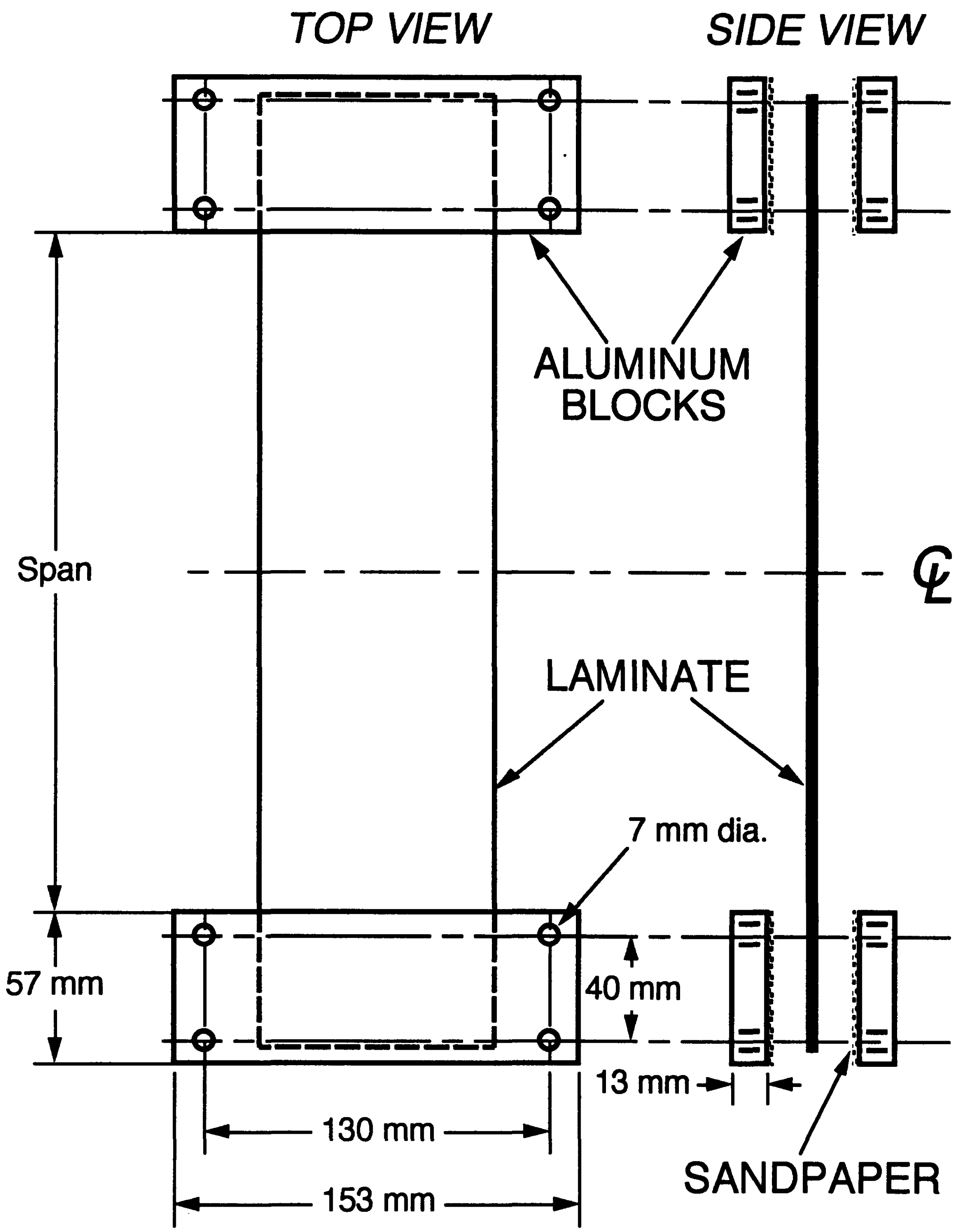

Note: Drawing Not to Scale

Figure 3.11 Illustration of specimen holding jig (grips).

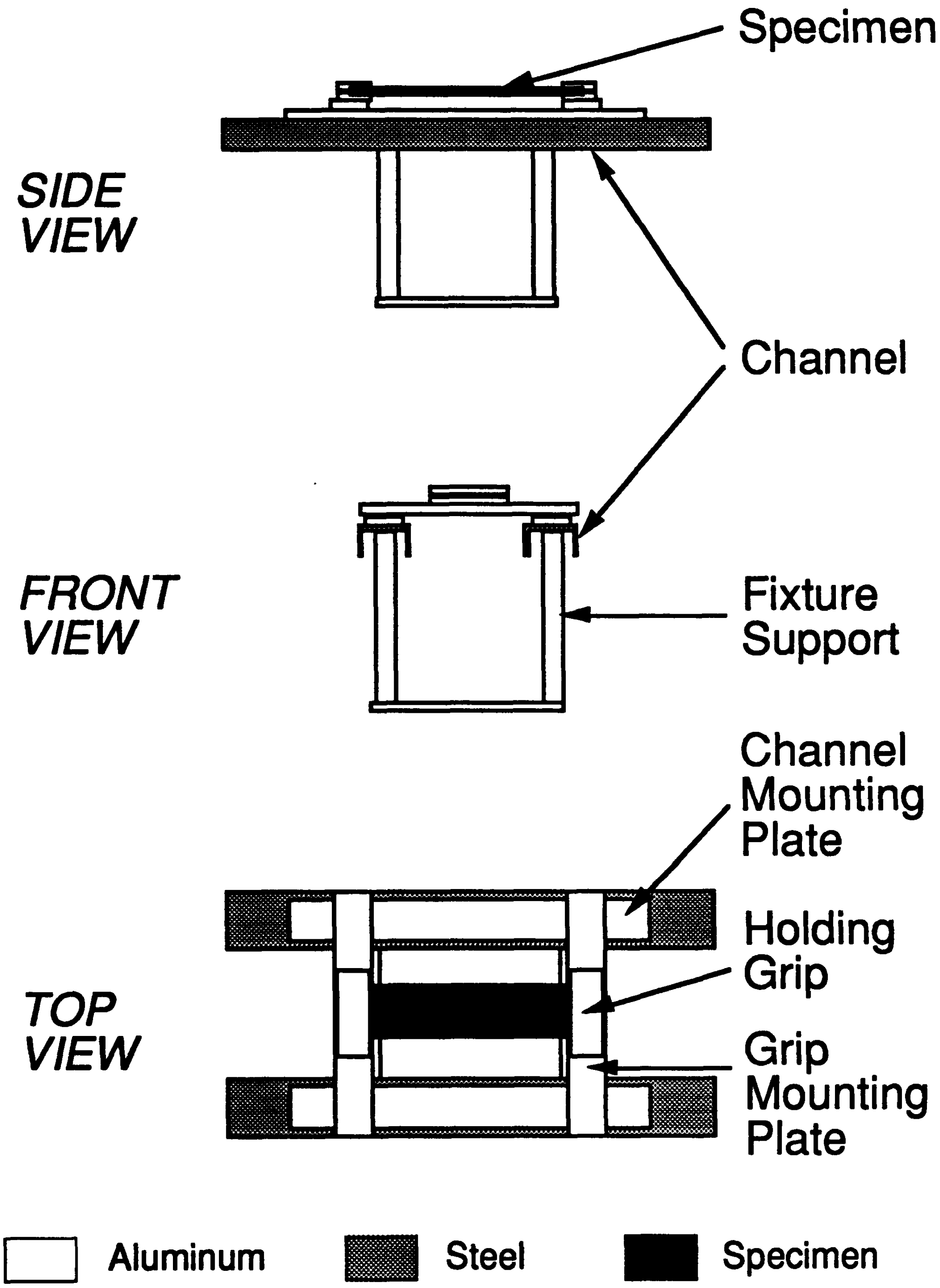

Figure 3.12 Illustration of testing fixture.

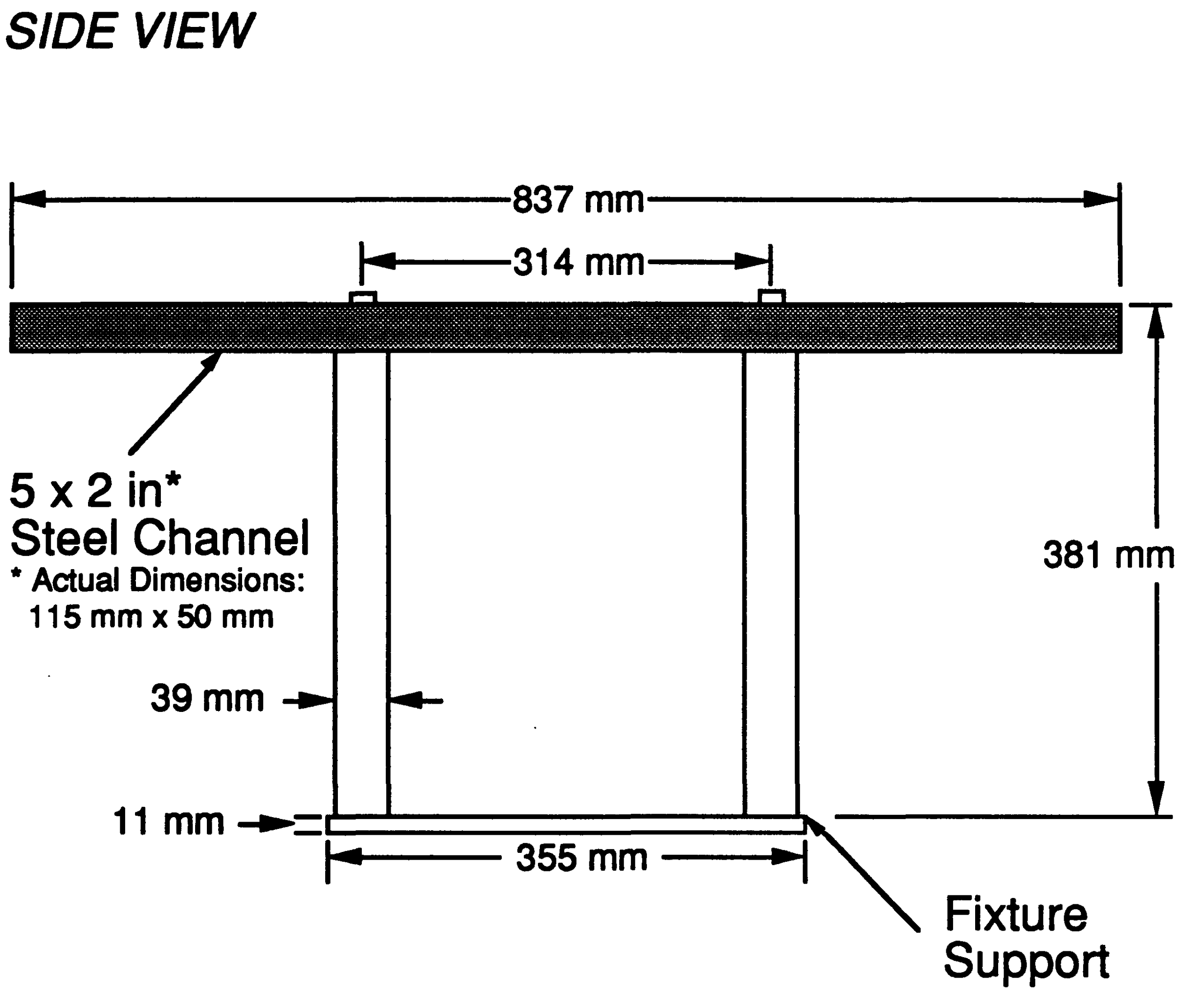

Figure 3.13 Illustration of fixture support and steel channel.

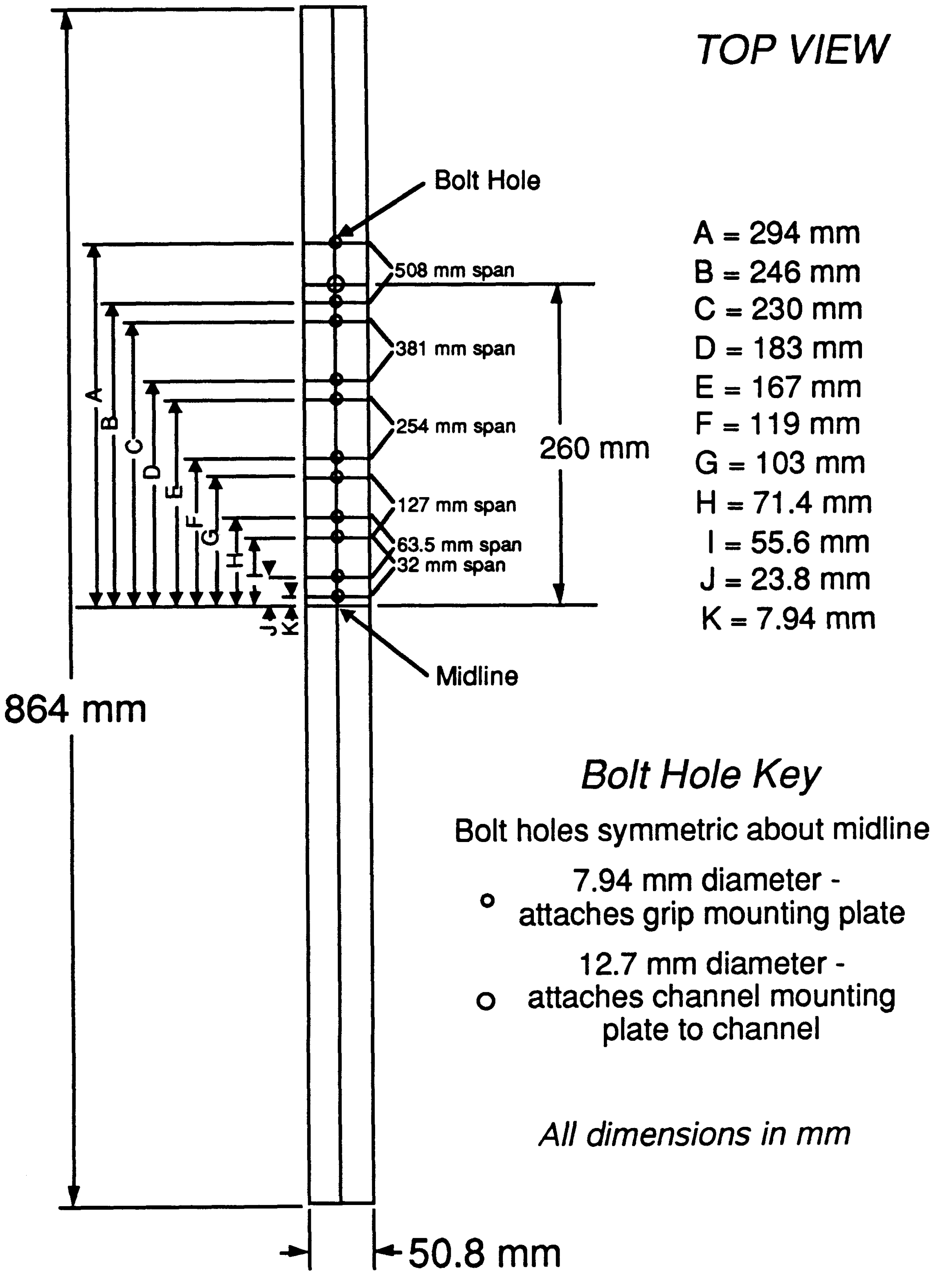

Figure 3.14 Illustration of channel mounting plate.

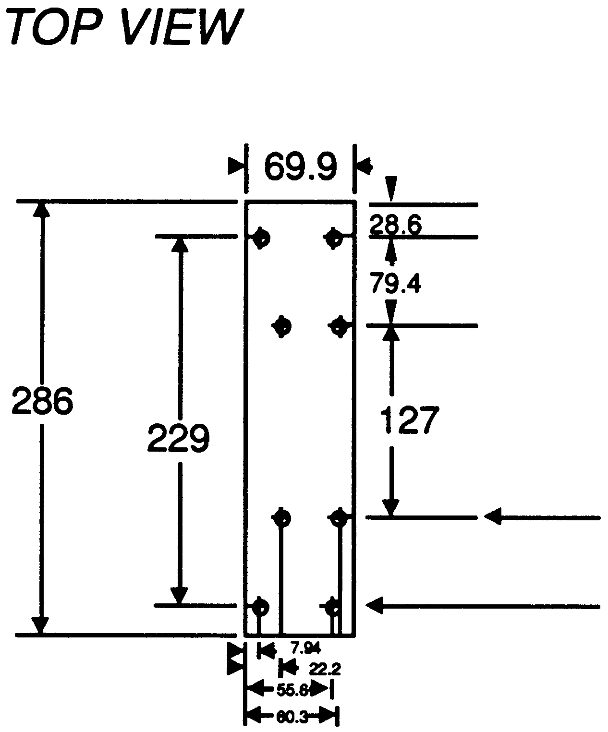

Bolt holes used to attach this plate to channel mounting plate.

Bolt holes used to attach gripping blocks to this plate.

○ 7.94 mm Diameter Bolt Holes

All dimensions in mm

Figure 3.15 Illustration of grip mounting plate.

indentation of the composite specimen at the maximum force tested, making the steel plate essentially rigid.

A computer data acquisition system was used to record load and stroke from the MTS machine, indentation from the LVDT, and strain from the strain gages. This system consists of a GW Instruments MacADIOS II analog/digital converter connected to a Macintosh IIx computer. Since the data acquisition system was limited to eight channels, the specimens with strain gages required the sacrifice of certain measurements. When strain gage scheme A was used, involving six gages, stroke was measured by a voltmeter and only the maximum value was recorded. When strain gage scheme B was used, involving seven gages, both stroke and indentation were measured by voltmeters, again recording only the maximum values.

The static indentation tests were carried out as follows. The fixture was adjusted to the necessary span by moving the grip mounting plates so they were aligned with the correct holes shown in Figure 3.14. The grip mounting plate was secured in position by bolts torqued to 10 Newton-meters into the aligned holes. The plate was then placed loosely into the grips. If the plate had strain gages, they were balanced and zeroed before the grips were tightened. This was to prevent zeroing out strain in the plate caused by any preload created by clamping the plate in the fixture. The specimen was aligned by eye and a small square by matching up paint markings on the specimen and alignment marks scribed on the fixture. Using these marks for alignment ensured that the plate was square with the clamps and that the indentor contacted the center of the plate. The grips were then tightened as previously mentioned. Once the specimen was secured in the desired boundary condition and at the proper span, the upper crosshead was lowered until the indentor was approximately 2 mm from the test specimen. The lower crosshead was then moved up using the zeroing knob until a preload of not more than 5 N was seen. At this point, the LVDT was brought into contact with the backside of the laminate directly opposite the indentation point and its offset was recorded in the data acquisition system. The crosshead movement rate was set to 0.0127 mm/sec for rigid support tests, 0.0730 mm/sec for clamped-clamped tests of spans 254 mm and greater, and 0.0726 mm/sec for clamped-clamped tests of spans less than 254 mm. These rates were selected because they provided a loading rate that was considered quasi-static and because they provided a rate which allowed data to be taken slowly enough to determine the loading curves completely. The stroke range was set to the 10% range (±12.7 mm) for rigid support tests, the 50% (±63.5 mm) range for clamped-clamped tests of spans 254 mm and greater, and the 20% (±25.4 mm) range for clamped-clamped tests of spans less than 254 mm. These ranges were chosen to accommodate the maximum deflection that was expected for each specimen given the load to be applied. The load range for the 8896 N (2000 lb) load cell was changed between 50% (±44.5 kN), 20% (±17.8 kN), and 10% (±8.9 kN) depending on the maximum contact force desired in the test.

The MTS machine was run in compression mode and stroke control. Data was recorded during the test by the acquisition system at a rate of 2 Hz. The fixture was moved upward, with the lower crosshead, into the fixed indentor. The specimen could bend (in the clamped-clamped tests) while the LVDT base and indentor remained in a fixed position. With the LVDT in contact with the back surface, the movement of the laminate relative to the indentor (the indentation) was measured. The movement of the center point of the laminate relative to the test fixture (the deflection) was measured by the stroke of the testing machine. Once the maximum contact force for the test was reached, the crosshead was reversed. The test was completed when the crosshead returned to its original position.

3.5 Damage Evaluation Procedures

Three methods were used for damage evaluation: visual inspection, X-ray photography, and sectioning. After an indentation test, observations made from a visual inspection of all specimens were recorded in a notebook. The specimens were then x-rayed to determine the interior damage in the laminate. To accomplish this, a 0.74 mm diameter hole was drilled through the specimen at the indentation point with a Dremel Moto-Tool® equipped with a 220-grit diamond grit drill bit. A piece of flash tape was placed over the exit hole on the back face (opposite the point of indentation) of the laminate. The specimen was then placed on a flat surface and 1,4-Diiobutane (DiB) dye was injected into the hole. Enough dye is injected so that a small bubble forms over the hole. This is to ensure that sufficient dye seeps into the cracks and delaminations in the laminate. Because the cracks and delaminations are transparent to X rays, the X ray opaque dye is necessary to show the damage as dark spots on an X-ray photograph. The specimen was left for forty-five minutes so that the dye would have sufficient opportunity to flow into the damage features. At the end of that time, the remaining dye was absorbed with a paper towel and the flash tape was removed from the backface.

The specimen was then x-rayed with a Scanray Torrex 150D X ray Inspection System. Using the TIMERAD control, the specimen was exposed to 240 mR at 3 milli-amps and 50 V potential. An image was obtained by placing a piece of Polaroid Type 52 PolaPan film behind the laminate during the exposure and then developing it. A typical X-ray photograph is shown in Figure 3.16. The orientation of the specimen was set so that the x_1 (longitudinal) direction of the specimen (defined in Figure 3.1) is aligned vertically with the page.

Once the X-ray photographs were taken, one cross-section was made through the center of the area of damage indicated in the photographs. This location was aligned with the hole drilled to insert dye into the specimen for X-ray photography. The specimens were again cut with a 220 grit diamond cutting wheel. As before, the cutting was done with a 254 mm diameter water-cooled cutting wheel rotating at 1100 rpm, while the laminate fed past on a table at 279 mm per minute. The sectioned edges were then buffed by a felt cylinder rotating in a drill press while a slurry mixture of polishing powder and water was applied to create a smooth surface. A smooth surface was necessary to identify the location of the damage through the thickness of the laminate through a microscope.

An Olympus SZ-Tr Zoom Stereo Microscope was used to examine all specimen cross-sections. The damaged region was magnified 5X to 20X to identify delaminations, matrix cracks, and fiber damage. Matrix cracks could be observed as light lines through the matrix between the fibers. Delaminations could be observed as lightened areas between plies which had separated. In one case, fiber damage was observed as an area where fibers were seen to be loose or missing from a ply. The damage showed up light because the white powder used to polish the cross-sectioned surface accumulated in the cracks and delaminations. Transcriptions of the damage were made, when damage was apparent, by examining the specimens under the microscope at the magnifications described above.

The specimen was then photographed under 5X magnification as this allowed the full extent of the damage to be seen in all cases. The photographs were made using a Polaroid camera with a 55 mm aperture and a lens magnifying the subject five times. The specimen was held between two blocks of 25.4 mm thick plastic joined together by two bolts. This simple fixture secured the specimen and assured that it was held perpendicular to the flat surface beneath the camera. A scale divided into 0.5 mm increments was attached to the specimen at the damaged area. The camera was focused on the cross-sectioned edge of the specimen and the specimen was then adjusted until the damaged area was centered in the camera's viewfinder. Lighting was concentrated on the specimen at the damaged area and adjusted while looking through the camera's viewfinder until the damage was highlighted. The camera was loaded with Polaroid Type 52 PolaPan film which was then exposed. The picture was developed using the standard procedures accompanying the film. The quick processing of the Polaroid film was of great benefit as poor photographs frequently resulted from vibrations or poor lighting. As a result, adjustments to the setup and lighting could be made immediately and better photographs could be made. In order to provide a comparison, a typical photograph and transcription are shown in Figure 3.17. Because the transcription provides a clearer and equally accurate representation of the damage that occurs through-the-thickness, the cross-sections will be represented by transcriptions throughout this work.

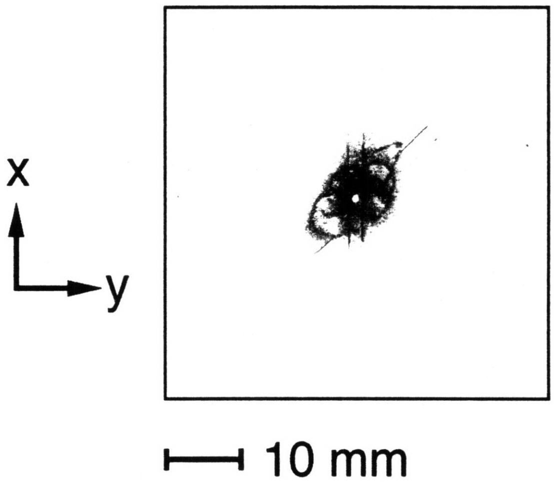

Figure 3.16 Typical X-ray photograph of the damage in a 127 mm specimen in a clamped-clamped support tested to a maximum contact force of 1479 N.

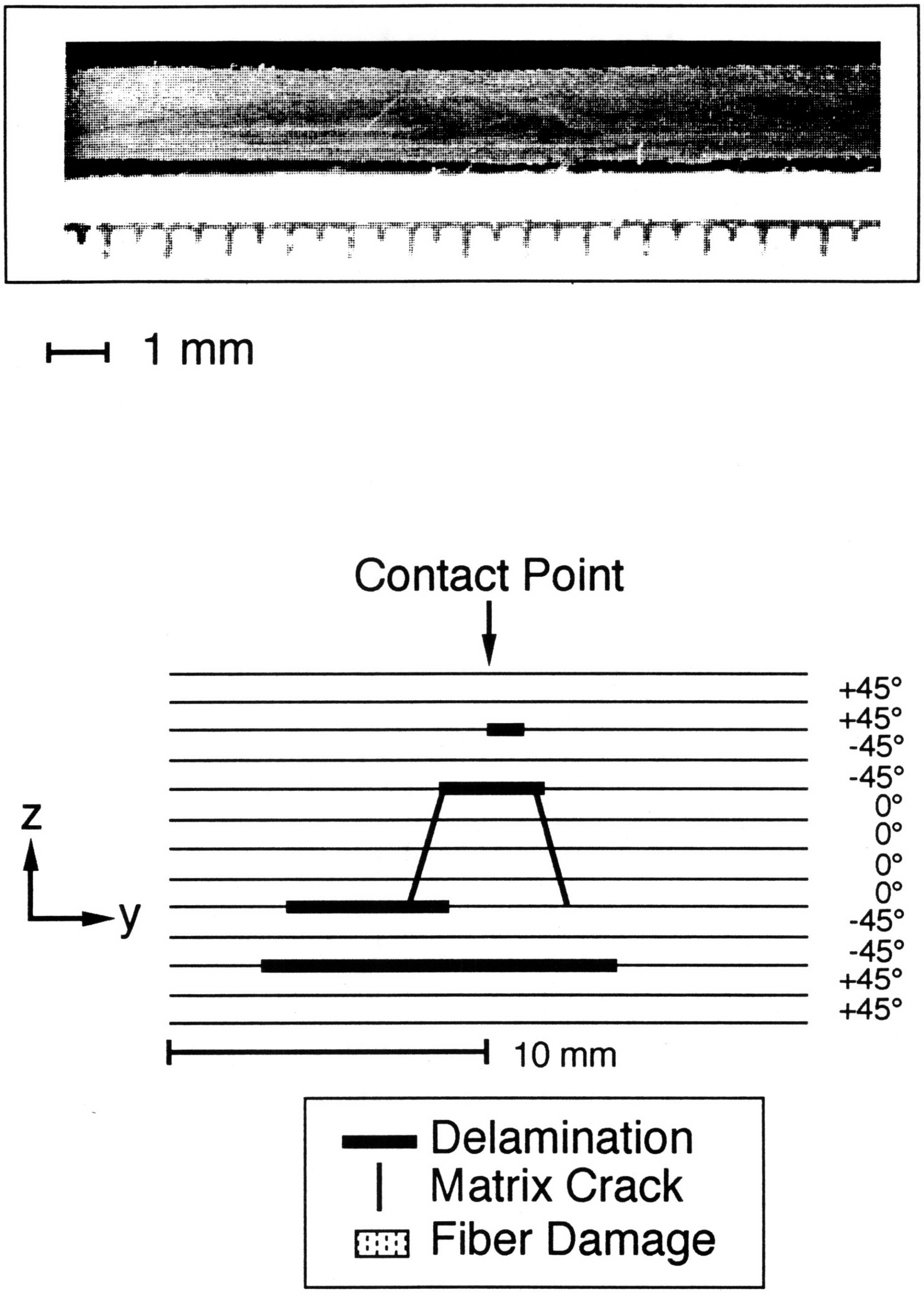

Figure 3.17 Typical cross-section of damage in a 127 mm specimen in a clamped-clamped support tested to a maximum contact force of 1479 N via *(top)* magnified photograph and *(bottom)* transcription.

Chapter 4

ANALYTICAL MODEL

The need for better understanding of large deflection bending behavior of laminated plates under impact loading is clear from the discussion in Chapter 2. In response to this need, a model for the response of composite laminated plates under indentation loading was developed to aid in identifying how the global bending of the plate affects the impact damage resistance of the plate. Shear deformable nonlinear plate theory is used following the analysis developed by Matsuhashi [32, 36] for the impact case. Nonlinear strain-displacement relations are used with constitutive equations based on linear stress-strain relations and laminated plate theory to develop energy equations for the plate. Using the principle of minimum potential energy and the Rayleigh-Ritz method, a system of nonlinear equations for the bending of the plate is determined. The system of equations are solved using the Newton-Raphson method to find the roots of the equation for a particular contact force. The results are force-deflection and force-strain behavior for the plate under static indentation loading.

4.1 Linear Wide Beam Analysis

Before the nonlinear plate analysis was developed, a simple linear beam analysis was developed as a basis for comparison with the nonlinear analysis. It is important to compare the nonlinear analysis with an accepted analysis, such as the linear wide beam analysis, to ascertain whether they are in agreement for simple cases before comparison with experimental data is attempted. This is accomplished by comparing the nonlinear analysis with the linear analysis for small deflections. The nonlinear analysis should provide results which match the linear analysis for small deflections.

The linear analysis is referred to as a wide beam analysis since the loading that is assumed is a moment acting about the transverse direction causing bending along the longitudinal axis only. This is also known as cylindrical bending [25]. This type of loading makes the plate essentially a beam, hence wide beam analysis. An illustration of this configuration is provided in Figure 4.1. The coordinate system used in the development of this analysis is illustrated in Figure 4.2. The axes are centered at the left end of the plate. The x-axis is aligned with the longitudinal centerline of the plate and the y-axis is oriented in the transverse direction of the plate on the through-the-thickness centerline of the plate. The z-axis begins at the through-the-thickness centerline and is perpendicular to the back surface of the plate (away from the point of application of force).

A linear strain-displacement relationship between the longitudinal strain and the second derivative of the bending deflection, w, is assumed:

$$\varepsilon_{11}(x) = z\kappa_{11}(x) = -z\frac{\partial^2 w(x)}{\partial x^2} \tag{4.1}$$

where $\varepsilon_{11}(x)$ is the longitudinal strain and $\kappa_{11}(x)$ is the curvature. The constitutive equations used are those for a laminated plate under bending only (with no twisting):

$$\begin{Bmatrix} M_{11} \\ M_{22} \end{Bmatrix} = \begin{bmatrix} D_{11} & D_{12} \\ D_{12} & D_{22} \end{bmatrix} \begin{Bmatrix} \kappa_{11} \\ \kappa_{22} \end{Bmatrix} \tag{4.2}$$

In this case, the transverse moment M_{22} is equal to zero. Solving equation (4.2) for κ_{11} yields,

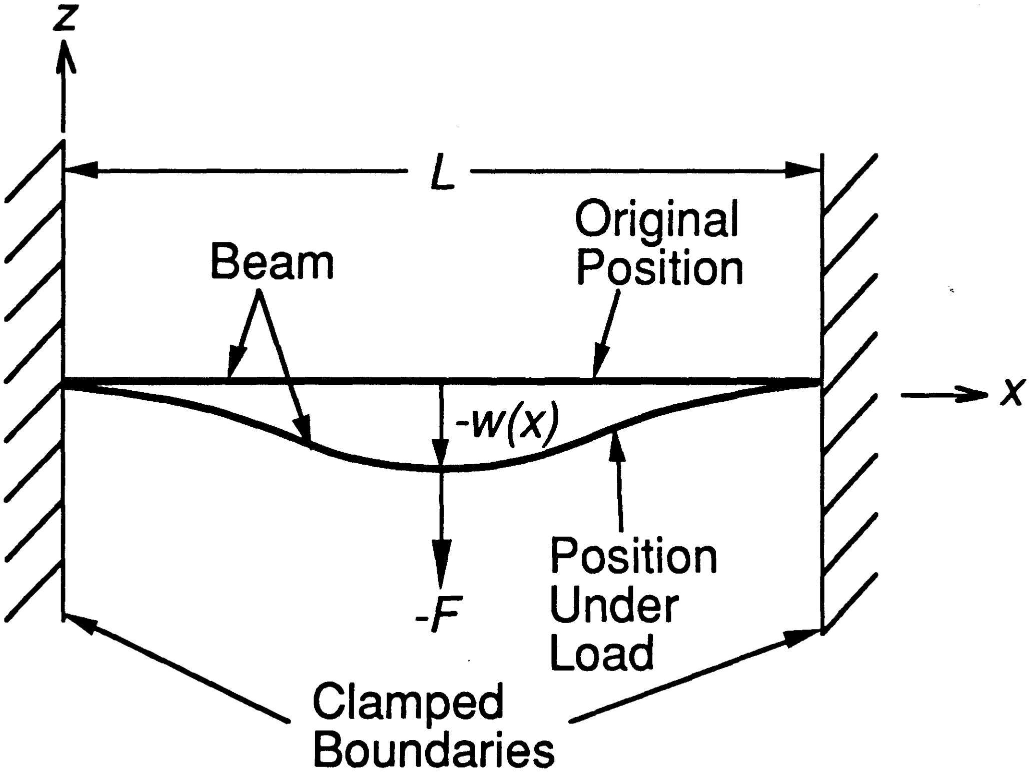

Figure 4.1 Illustration of the bending of a clamped-clamped beam under point load.

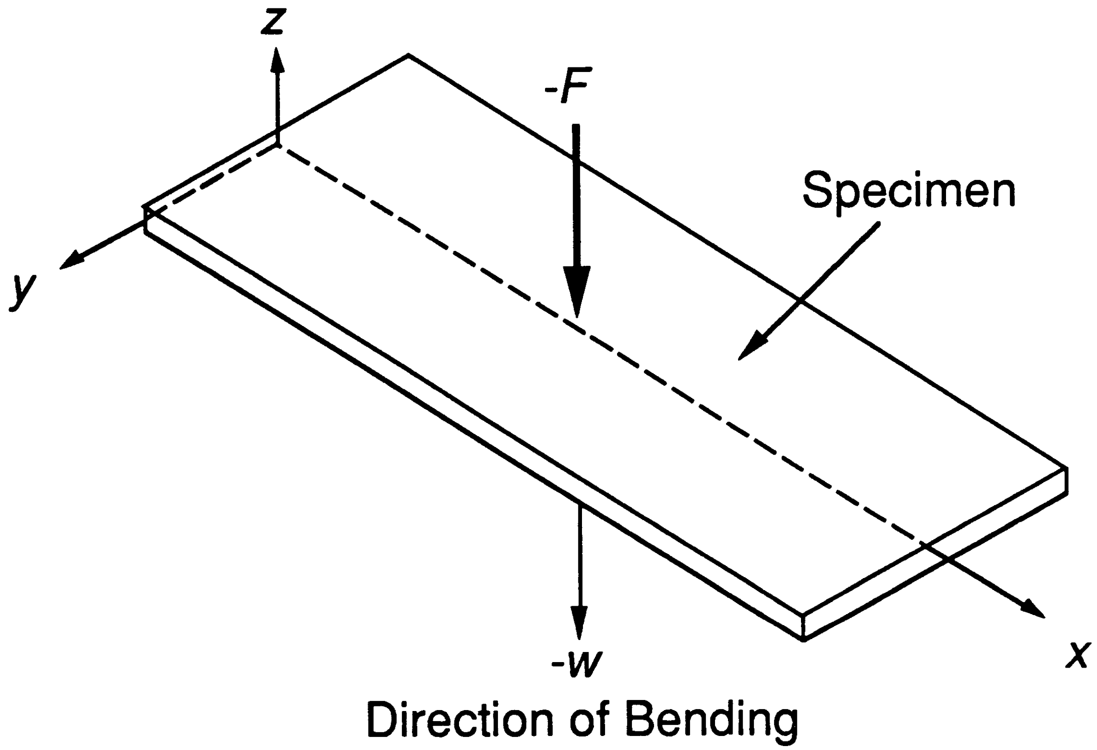

Figure 4.2 Definition of coordinate system.

$$\kappa_{11} = M_{11}\left(\frac{D_{22}}{D_{22}D_{11} - D_{12}^{2}}\right) \tag{4.3}$$

By assuming a clamped-clamped boundary condition at the ends and a point load acting at the center point on a beam, an expression for M_{11} can be found in terms of the load F and the length L of the wide beam [38]:

$$M_{11} = -\frac{F}{2}\left(x - \frac{L}{4}\right) \tag{4.4}$$

Combining equations (4.3) and (4.4) and applying the strain-displacement relationship (4.1) yields a differential equation for the deflection in terms of the geometry of the wide beam, the material constants, and the loading.

$$\kappa_{11} = -\frac{\partial^{2} w(x)}{\partial x^{2}} = -\frac{F}{2}\left(x - \frac{L}{4}\right)\left(\frac{D_{22}}{D_{22}D_{11} - D_{12}^{2}}\right) \tag{4.5}$$

Equation (4.5) may be twice integrated with respect to x, after canceling the minus signs, to give an equation for the deflection,

$$\frac{\partial w(x)}{\partial x} = \frac{F}{2}\left(\frac{x^{2}}{2} - \frac{Lx}{4} + c_{1}\right)\left(\frac{D_{22}}{D_{22}D_{11} - D_{12}^{2}}\right) \tag{4.6}$$

$$w(x) = \frac{F}{2}\left(\frac{x^{3}}{6} - \frac{Lx^{2}}{8} + c_{1}x + c_{2}\right)\left(\frac{D_{22}}{D_{22}D_{11} - D_{12}^{2}}\right) \tag{4.7}$$

where c_1 and c_2 are constants of integration. For the case of clamped-clamped boundary conditions, these are set to zero because the deflection and slope at the ends of the plate are zero. The bending strain in the beam is given from equation (4.1) as:

$$\varepsilon_{11} = z\kappa_{11} = -z\frac{F}{2}\left(x - \frac{L}{4}\right)\left(\frac{D_{22}}{D_{22}D_{11} - D_{12}^{2}}\right) \tag{4.8}$$

This analysis provides a way of checking the nonlinear plate analysis with a simple, linear analysis. If the nonlinear analysis is done properly, it should match the linear analysis over a range for "small" deflections.

4.2 Governing Equations for Nonlinear Analysis

The deflection in a static indentation problem is comprised of two parts: the indentation and the global bending. The difference between these two kinds of deformation under a contact load F is illustrated in Figure 4.3. The indentation α is equivalent to the reduction in the thickness of the plate under the point of contact. The global bending w is the deflection of the plate midplane relative to the undeformed state. Only the global bending is considered in the current analysis. This is because the bending is two orders of magnitude larger than the indentation (as will be seen in Chapter 5), making the contribution of the indentation to the total deformation negligible.

The development of the following analysis from the strain-displacement relations through the Rayleigh-Ritz method is taken from the nonlinear transient analysis developed by Matsuhashi [36]. The only divergence from Matsuhashi's analysis is the assumption that the event is considered quasi-static as the current analysis models a static indentation event, whereas Matsuhashi modeled an impact event. Therefore, the equations for the analysis developed here exclude the time-varying terms in Matsuhashi's analysis.

The coordinate system used in the development of this analysis is illustrated in Figure 4.2. The axes are centered at the left end of the plate. The x-axis is aligned with the longitudinal centerline of the plate. The y-axis is oriented in the transverse direction of the plate on the through-the-

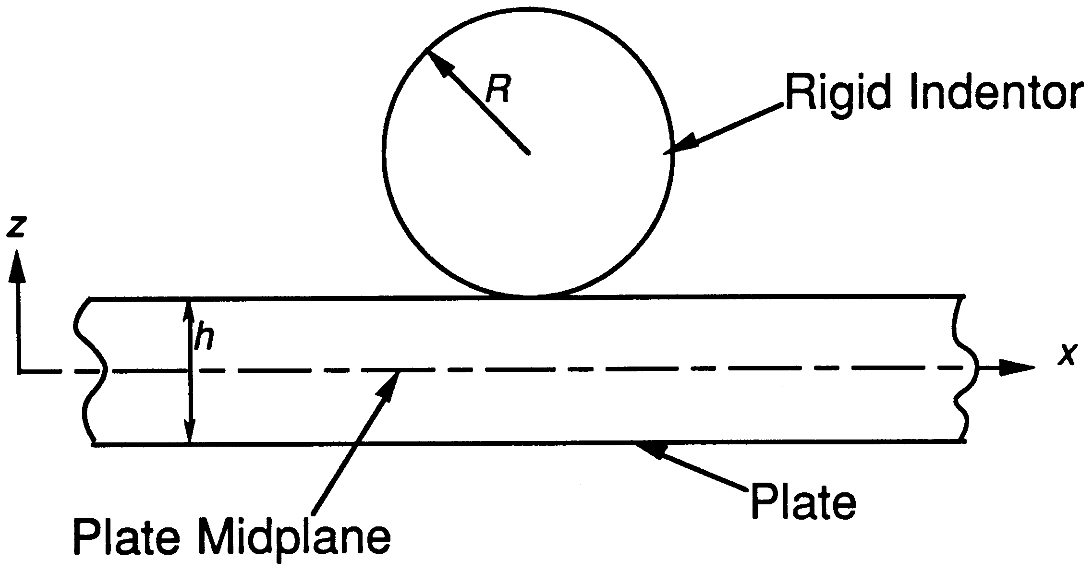

Before Application of Force

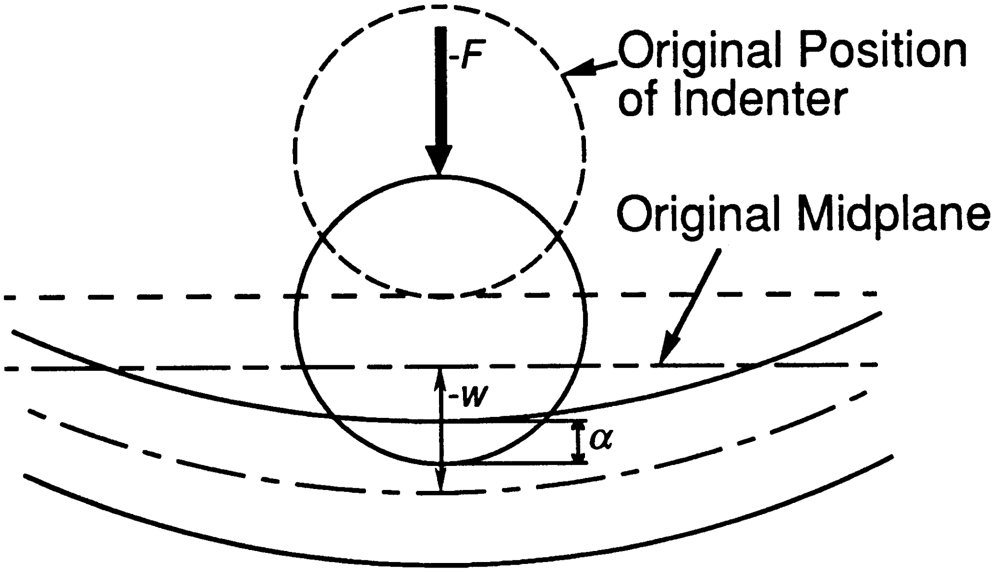

After Application of Force

Figure 4.3 Illustration of global bending and indentation.

thickness centerline of the plate. The z-axis begins at the through-the-thickness centerline and is perpendicular to the upper surface of the plate (the surface on which the force is applied). The model assumes that the contact force acts at the geometrical center of the upper surface of the plate.

4.2.1 Strain-Displacement Relations

In order to model the geometric nonlinearity in the plate due to the large deflections seen in tests (on the order of ten times the thickness), the strain-displacement relations include second order nonlinear terms in the mid-plane strains. The Green-Lagrange strain relations [39] are used:

$$\varepsilon_{ij} = \frac{1}{2}\left(\frac{\partial u_i}{\partial x_j} + \frac{\partial u_j}{\partial x_i} + \frac{\partial u_k}{\partial x_i}\frac{\partial u_k}{\partial x_j}\right) \tag{4.9}$$

with the independent variables x_1, x_2, x_3 representing the coordinates x, y, z.

The effects of shear are included in the analysis by using shear deformable plate theory [40]. It is assumed that plane sections remain plane but not necessarily perpendicular to the midplane. An illustration of the deformation of an element with end sections originally perpendicular to the midplane is shown in Figure 4.4. The independent quantity, ψ, represents the rotation of the plane section from a plane perpendicular to the midplane before deformation. The deformations ψ_x and ψ_y represent rotations in the $x-z$ and $y-z$ planes, respectively. The displacements in the x, y, and z directions are u_1, u_2, and u_3, respectively, and u, v, and w are the associated midplane displacements. Because the indentations are considered negligible in this analysis (the thickness of the plate never changes), the out-of-plane displacements are a function only of the in-plane

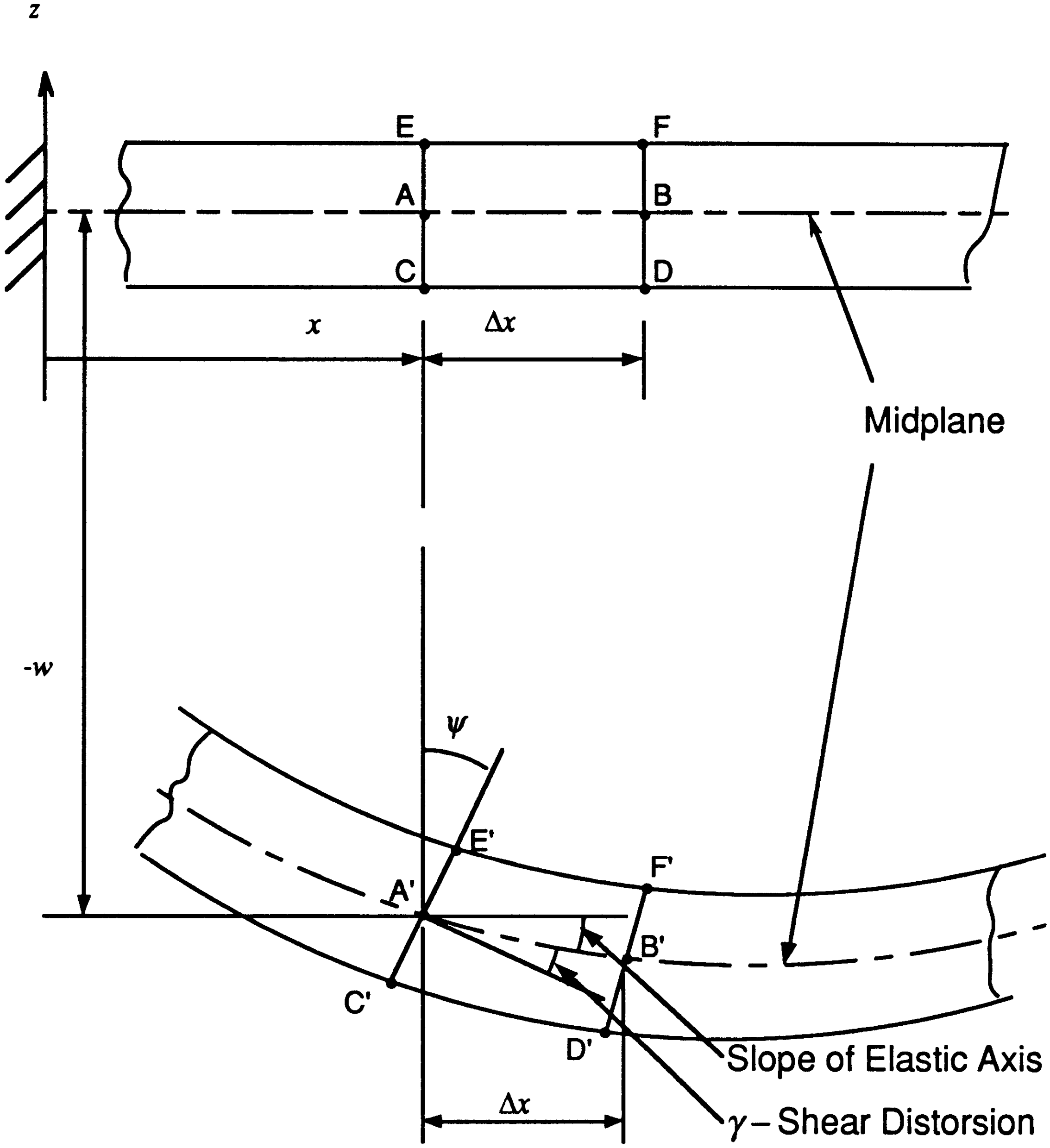

Figure 4.4 Geometry of shear deformation.

coordinates, x and y. The displacement of a point on the plate can therefore be represented by:

$$\begin{aligned} u_1(x,y,z) &= u(x,y) + z\psi_x(x,y) \\ u_2(x,y,z) &= v(x,y) + z\psi_y(x,y) \\ u_3(x,y,z) &= w(x,y) \end{aligned} \qquad (4.10)$$

The strain can be expressed simply with vector notation.

$$\begin{aligned} \underline{\varepsilon}(x,y,z) &= \underline{\varepsilon}^{\circ}(x,y) + z\,\underline{\kappa}(x,y) \\ \underline{\gamma}(x,y,z) &= \underline{\gamma}(x,y) \end{aligned} \qquad (4.11a)$$

where,

$$\underline{\varepsilon} = \begin{Bmatrix} \varepsilon_{11} \\ \varepsilon_{22} \\ 2\varepsilon_{12} \end{Bmatrix}, \qquad \underline{\gamma} = \begin{Bmatrix} 2\varepsilon_{23} \\ 2\varepsilon_{13} \end{Bmatrix} = \begin{Bmatrix} \psi_x - \dfrac{\partial w}{\partial x} \\ \psi_y - \dfrac{\partial w}{\partial y} \end{Bmatrix}$$

$$\underline{\varepsilon}^{\circ} = \begin{Bmatrix} \varepsilon^{\circ}_{11} \\ \varepsilon^{\circ}_{22} \\ \varepsilon^{\circ}_{12} \end{Bmatrix} = \begin{Bmatrix} \dfrac{\partial u}{\partial x} + \dfrac{1}{2}\left(\dfrac{\partial w}{\partial x}\right)^2 \\ \dfrac{\partial v}{\partial y} + \dfrac{1}{2}\left(\dfrac{\partial w}{\partial y}\right)^2 \\ \dfrac{\partial u}{\partial y} + \dfrac{\partial v}{\partial x} + \dfrac{\partial w}{\partial x}\dfrac{\partial w}{\partial y} \end{Bmatrix}, \qquad \underline{\kappa} = \begin{Bmatrix} \kappa_{11} \\ \kappa_{22} \\ \kappa_{12} \end{Bmatrix} = \begin{Bmatrix} \dfrac{\partial \psi_x}{\partial x} \\ \dfrac{\partial \psi_y}{\partial y} \\ \dfrac{\partial \psi_x}{\partial y} + \dfrac{\partial \psi_y}{\partial x} \end{Bmatrix} \qquad (4.11b)$$

The $\underline{\varepsilon}^{\circ}$ represent the midplane extensional strains, the $\underline{\kappa}$ represent the curvatures of the plate, and the $\underline{\gamma}$ represent the transverse shear strains. The difference between the nonlinear strain-displacement relations in equations (4.11a) and (4.11b) and the linear relations are the second-order terms in the $\underline{\varepsilon}^{\circ}$ expressions.

4.2.2 Constitutive Equations

In the analysis it is assumed that the material properties do not change during the indentation event. The implications of this assumption are that the occurrence of damage is not taken into account in this analysis and that the material behaves in a linearly elastic manner. This assumption allows the constitutive equations for a general laminate to be used:

$$\begin{Bmatrix} \{N\} \\ \{M\} \end{Bmatrix} = \begin{bmatrix} [A] & [B] \\ [B]^T & [D] \end{bmatrix} \begin{Bmatrix} \underline{\varepsilon}^{o} \\ \underline{\kappa} \end{Bmatrix}$$
$$\begin{Bmatrix} Q_x \\ Q_y \end{Bmatrix} = \begin{bmatrix} G_{55} & G_{45} \\ G_{45} & G_{44} \end{bmatrix} \begin{Bmatrix} \varepsilon_5 \\ \varepsilon_4 \end{Bmatrix} \tag{4.12}$$

where $[A]$, $[B]$, and $[D]$ are the in-plane, bending-stretching, and bending stiffnesses of the plate, respectively. Each of the matrix components are given by:

$$\left(A_{ij},\ B_{ij},\ D_{ij}\right) = \sum_{n=1}^{N} \int_{z_n}^{z_{n+1}} C_{ij}{}^{(n)}\left(1,\ z,\ z^2\right) dz \qquad (i, j = 1, 2, 6) \tag{4.13}$$

where n is the nth ply out of a total of N plies. The C_{ij} are assumed to be the plane stress material constants. The components of the transverse shear stiffness matrix $[G]$ are defined as:

$$G_{ij} = \sum_{n=1}^{N} K_i K_j \int_{z_n}^{z_{n+1}} C_{ij}{}^{(n)}\, dz \qquad (i, j = 4, 5) \tag{4.15}$$

where the shearing correction term, $K_i K_j$, is assumed to be the isotropic correction factor of 5/6, which may be used for laminates made from thin plies [41]. The indices i, j become 1,2,4,5,6 because the strains are represented with the following notation:

$$\underline{\varepsilon}=\begin{Bmatrix}\varepsilon_{11}\\ \varepsilon_{22}\\ 2\varepsilon_{12}\end{Bmatrix}=\begin{Bmatrix}\varepsilon_{1}\\ \varepsilon_{2}\\ \varepsilon_{6}\end{Bmatrix}, \qquad \underline{\gamma}=\begin{Bmatrix}2\varepsilon_{23}\\ 2\varepsilon_{13}\end{Bmatrix}=\begin{Bmatrix}\varepsilon_{4}\\ \varepsilon_{5}\end{Bmatrix} \tag{4.14}$$

4.2.3 Energy Expressions

The potential energy of the plate under static loading comes from two sources, the strain energy stored in the plate and the work done on the plate. The strain energy for linear stress-strain behavior can be written,

$$U=\frac{1}{2}\iiint_V C_{ij}\varepsilon_i\varepsilon_j\,dV \tag{4.16}$$

where the integral is taken over the volume, V, of the plate. The work that transverse external forces do on the plate can be represented as,

$$W=\iint_S p_i w_i\,dS \qquad i=1,2,3 \tag{4.17}$$

where the integral is taken over the surface, S, of the plate. Additionally, p_i is the transverse force per unit area and w_i is the transverse displacement of the plate.

By inserting the strain equations, (4.11a) and (4.11b), into equation (4.16) and integrating through the thickness, a strain energy expression which is a function only of the displacements is produced.

$$U=\frac{1}{2}\iint_S\left(\underline{\varepsilon}^{oT}[A]\,\underline{\varepsilon}^{o}+2\underline{\varepsilon}^{oT}[B]\,\underline{\kappa}+\underline{\kappa}^{T}[D]\,\underline{\kappa}+\underline{\gamma}^{T}[G]\,\underline{\gamma}\right)dS \tag{4.18}$$

The strain energy in equation (4.18) can be written as the sum of four parts:

$$U=U_{\mathrm{I}}+U_{\mathrm{II}}+U_{\mathrm{III}}+U_{\mathrm{IV}} \tag{4.19}$$

where each of the four terms represents a physical relationship between the strains and material constants in the plate. The term U_{I} represents the in-plane stretching, the geometric coupling between in-plane and out-of-plane deformations, and the terms accounting for large deformation. The term U_{II} contains linear terms representing the material coupling between in-plane and out-of-plane deformations that may occur in unsymmetric laminates (B-matrix) and the nonlinear terms representing in-plane strains. The term U_{III} represents the bending energy of the plate. And the term U_{IV} represents transverse shear deformation in the plate.

Finally, the total potential energy of the system can be written:

$$\Pi_p = \mathrm{U} + \mathrm{W} \tag{4.20}$$

which is the sum of the potential energy of the plate and the work done by external forces.

4.3 Raleigh-Ritz Method

Assumed mode shapes for the displacements are used in conjunction with the principle of minimum potential energy to create a system of equations. Each of the displacements are approximated by a series whose terms are comprised of a modal amplitude and mode shapes in both the x and y directions.

$$\psi_x(x,y) = \sum_{\varsigma}\sum_{\mu} A_{\varsigma\mu}\, f_{\varsigma}(x) g_{\mu}(y) \tag{4.21a}$$

$$\psi_y(x,y) = \sum_{\varsigma}\sum_{\mu} B_{\varsigma\mu}\, h_{\varsigma}(x) l_{\mu}(y) \tag{4.21b}$$

$$u(x,y) = \sum_{\varsigma}\sum_{\mu} C_{\varsigma\mu}\, m_{\varsigma}(x) n_{\mu}(y) \tag{4.21c}$$

$$v(x,y) \ = \sum_{\varsigma}\sum_{\mu} D_{\varsigma\mu}\, o_{\varsigma}(x) p_{\mu}(y) \tag{4.21d}$$

$$w(x,y) \ = \sum_{\varsigma}\sum_{\mu} E_{\varsigma\mu}\, q_{\varsigma}(x) r_{\mu}(y) \tag{4.21e}$$

or, combining the double summation into a single summation,

$$\psi_x(x,y) = \sum_{i} A_i\, f_{\varsigma}(x) g_{\mu}(y) \tag{4.22a}$$

$$\psi_y(x,y) = \sum_{i} B_i\, h_{\varsigma}(x) l_{\mu}(y) \tag{4.22b}$$

$$u(x,y) \ = \sum_{i} C_i\, m_{\varsigma}(x) n_{\mu}(y) \tag{4.22c}$$

$$v(x,y) \ = \sum_{i} D_i\, o_{\varsigma}(x) p_{\mu}(y) \tag{4.22d}$$

$$w(x,y) \ = \sum_{i} E_i\, q_{\varsigma}(x) r_{\mu}(y) \tag{4.22e}$$

The modal amplitudes to be determined from the analysis are $A_i, B_i, C_i, D_i,$ and E_i. The single summation makes the equations simpler to manipulate, but the index numbers, $i, \varsigma,$ and μ, must be related through the relationship:

$$i = M \times [\zeta - 1] + \mu \tag{4.23}$$

where M is the total number of modes (the maximum value of μ) in the y-direction. Also, N is defined as the total number of modes in the x-direction. The mode shapes, $f, g, h, l, m, n, o, p, q,$ and r are beam functions defined by Dugundji [42] and outlined in Appendix A. Because the Raleigh-Ritz method requires that only geometric, or displacement, boundary conditions be met, selecting the correct beam functions to represent the physical constraints to be modeled is all that is necessary to define the boundary conditions.

The second step in using the Raleigh-Ritz technique is to apply the principle of minimum potential energy to equation (4.20). Since the degrees of freedom in the energy expressions have been transformed into the modal amplitudes by the assumption of mode shapes, the principle of minimum potential energy becomes,

$$\frac{\partial \Pi_p}{\partial q_j} = 0 \qquad j = 1, 2, \ldots, M \tag{4.24}$$

where q_j are the modal amplitudes, A_i, B_i, C_i, D_i, and E_i. The total number of degrees of freedom, M, is simply the number of generalized coordinates (the modal amplitudes) multiplied by the number of modes in each direction: $M = 5 \times i = 5 \times \varsigma \times \mu$. By substituting the series expressions for the displacements (4.22) into the expressions for potential energy (4.18) and work (4.17), which are then substituted into equation (4.24), a system of equations is derived,

$$[\underline{K}_{\mathrm{I}}]\begin{Bmatrix} \underline{A}_i \\ \underline{B}_i \\ \underline{C}_i \\ \underline{D}_i \\ \underline{E}_i \end{Bmatrix} + [\underline{K}_{\mathrm{II}}]\begin{Bmatrix} \underline{A_k E_l} \\ \underline{B_k E_l} \\ \underline{C_k E_l} \\ \underline{D_k E_l} \\ \underline{E_k E_l} \end{Bmatrix} + [\underline{K}_{\mathrm{III}}]\begin{Bmatrix} \underline{A_k E_l E_m} \\ \underline{B_k E_l E_m} \\ \underline{C_k E_l E_m} \\ \underline{D_k E_l E_m} \\ \underline{E_k E_l E_m} \end{Bmatrix} = -F\{\underline{R}\} \tag{4.25}$$

where F is an externally applied force and where,

$$[\underline{K}_{\mathrm{I}}] = \begin{bmatrix} \underline{K}_{\mathrm{I}aa} & \underline{K}_{\mathrm{I}ab} & \underline{K}_{\mathrm{I}ac} & \underline{K}_{\mathrm{I}ad} & \underline{K}_{\mathrm{I}ae} \\ \underline{K}_{\mathrm{I}ab}^{\mathrm{T}} & \underline{K}_{\mathrm{I}bb} & \underline{K}_{\mathrm{I}bc} & \underline{K}_{\mathrm{I}bd} & \underline{K}_{\mathrm{I}be} \\ \underline{K}_{\mathrm{I}ac}^{\mathrm{T}} & \underline{K}_{\mathrm{I}bc}^{\mathrm{T}} & \underline{K}_{\mathrm{I}cc} & \underline{K}_{\mathrm{I}cd} & \underline{0} \\ \underline{K}_{\mathrm{I}ad}^{\mathrm{T}} & \underline{K}_{\mathrm{I}bd}^{\mathrm{T}} & \underline{K}_{\mathrm{I}cd}^{\mathrm{T}} & \underline{K}_{\mathrm{I}dd} & \underline{0} \\ \underline{K}_{\mathrm{I}ae}^{\mathrm{T}} & \underline{K}_{\mathrm{I}be}^{\mathrm{T}} & \underline{0} & \underline{0} & \underline{K}_{\mathrm{I}ee} \end{bmatrix} \tag{4.26a}$$

$$[\underline{K}_{\mathrm{II}}]=\begin{bmatrix} \underline{0} & \underline{0} & \underline{0} & \underline{0} & \underline{K}_{\mathrm{II}_{ae}} \\ \underline{0} & \underline{0} & \underline{0} & \underline{0} & \underline{K}_{\mathrm{II}_{be}} \\ \underline{0} & \underline{0} & \underline{0} & \underline{0} & \underline{K}_{\mathrm{II}_{ce}} \\ \underline{0} & \underline{0} & \underline{0} & \underline{0} & \underline{K}_{\mathrm{II}_{de}} \\ \underline{K}_{\mathrm{II}_{ea}} & \underline{K}_{\mathrm{II}_{eb}} & \underline{K}_{\mathrm{II}_{ec}} & \underline{K}_{\mathrm{II}_{ed}} & \underline{0} \end{bmatrix} \tag{4.26b}$$

$$[\underline{K}_{\mathrm{III}}]=\begin{bmatrix} \underline{0} & \underline{0} & \underline{0} & \underline{0} & \underline{0} \\ \underline{0} & \underline{0} & \underline{0} & \underline{0} & \underline{0} \\ \underline{0} & \underline{0} & \underline{0} & \underline{0} & \underline{0} \\ \underline{0} & \underline{0} & \underline{0} & \underline{0} & \underline{0} \\ \underline{0} & \underline{0} & \underline{0} & \underline{0} & \underline{K}_{\mathrm{III}_{ee}} \end{bmatrix} \tag{4.26c}$$

and

$$\{\underline{R}\}=\begin{Bmatrix} \underline{R}_{ai} \\ \underline{R}_{bi} \\ \underline{R}_{ci} \\ \underline{R}_{di} \\ \underline{R}_{ei} \end{Bmatrix} \tag{4.26d}$$

Each element of the stiffness matrices for the linear term $[\underline{K}_I]$ and nonlinear terms $[\underline{K}_{II}]$ and $[\underline{K}_{III}]$, and the generalized force vector $\{\underline{R}\}$ is itself a matrix or a vector. The individual terms in these matrices are defined in reference [36].

4.4 Reduction Of Equations

The size of the matrices in equation (4.25) are determined by the number of modes assumed. The stiffness matrices $[\underline{K}_{\mathrm{I}}]$, $[\underline{K}_{\mathrm{II}}]$, and $[\underline{K}_{\mathrm{III}}]$ have dimensions $(5\times N\times M)$ by $(5\times N\times M)$, $(5\times N\times M)$ by $(5\times(N\times M)^2)$, and $(5\times N\times M)$ by $(5\times(N\times M)^3)$ respectively. Elements in each of the stiffness matrices, such as $\underline{K}_{\mathrm{I}_{aa}}$, $\underline{K}_{\mathrm{II}_{ae}}$, and $\underline{K}_{\mathrm{III}_{ee}}$ have dimensions $(N\times M)$ by $(N\times M)$, $(N\times M)$ by $(N\times M)^2$, and $(N\times M)$ by $(N\times M)^3$ respectively. From these general expressions, it can be seen that the sizes of the matrices increase geometrically with the number of modes. Therefore, reducing this set of equations is important for the calculations to be carried out in a reasonable amount of time.

The assumption that the laminates considered are symmetric ($B_{ij} = 0$) leads to a reduction in the system of equations. Some of the components of the stiffness matrices from equation (4.26) include only the B_{ij} laminate constants. Their elements become zero in the reduced set of matrices:

$$[\underline{K}_{\mathrm{I}}] = \begin{bmatrix} \underline{K}_{\mathrm{I}aa} & \underline{K}_{\mathrm{I}ab} & \underline{0} & \underline{0} & \underline{K}_{\mathrm{I}ae} \\ \underline{K}_{\mathrm{I}ab}^{\mathrm{T}} & \underline{K}_{\mathrm{I}bb} & \underline{0} & \underline{0} & \underline{K}_{\mathrm{I}be} \\ \underline{0} & \underline{0} & \underline{K}_{\mathrm{I}cc} & \underline{K}_{\mathrm{I}cd} & \underline{0} \\ \underline{0} & \underline{0} & \underline{K}_{\mathrm{I}cd}^{\mathrm{T}} & \underline{K}_{\mathrm{I}dd} & \underline{0} \\ \underline{K}_{\mathrm{I}ae}^{\mathrm{T}} & \underline{K}_{\mathrm{I}be}^{\mathrm{T}} & \underline{0} & \underline{0} & \underline{K}_{\mathrm{I}ee} \end{bmatrix} \tag{4.27a}$$

$$[\underline{K}_{\mathrm{II}}] = \begin{bmatrix} \underline{0} & \underline{0} & \underline{0} & \underline{0} & \underline{0} \\ \underline{0} & \underline{0} & \underline{0} & \underline{0} & \underline{0} \\ \underline{0} & \underline{0} & \underline{0} & \underline{0} & \underline{K}_{\mathrm{II}ce} \\ \underline{0} & \underline{0} & \underline{0} & \underline{0} & \underline{K}_{\mathrm{II}de} \\ \underline{0} & \underline{0} & \underline{K}_{\mathrm{II}ec} & \underline{K}_{\mathrm{II}ed} & \underline{0} \end{bmatrix} \tag{4.27b}$$

$$[\underline{K}_{\mathrm{III}}] = \begin{bmatrix} \underline{0} & \underline{0} & \underline{0} & \underline{0} & \underline{0} \\ \underline{0} & \underline{0} & \underline{0} & \underline{0} & \underline{0} \\ \underline{0} & \underline{0} & \underline{0} & \underline{0} & \underline{0} \\ \underline{0} & \underline{0} & \underline{0} & \underline{0} & \underline{0} \\ \underline{0} & \underline{0} & \underline{0} & \underline{0} & \underline{K}_{\mathrm{III}ee} \end{bmatrix} \tag{4.27c}$$

Since this analysis is not concerned with the details of the local indentation, the indentor is modeled as a point load. This was found to yield satisfactory results in the impact analysis by Matsuhashi [36]. However this type of modeling may cause inaccuracies in the region near the contact point. The point load acting in the z-direction allows the force vector to be written:

$$\{\underline{R}\} = \begin{Bmatrix} \underline{0} \\ \underline{0} \\ \underline{0} \\ \underline{0} \\ \underline{R}_{ei} \end{Bmatrix} \tag{4.27d}$$

With the new stiffness matrices in equations (4.27a-c), expanding equation (4.25) yields a set of equations which may be solved simultaneously for the modal amplitudes, A_i, B_i, C_i, D_i, and E_i.

$$\underline{K}_{\mathrm{I}aa}\underline{A}_i + \underline{K}_{\mathrm{I}ab}\underline{B}_i + \underline{K}_{\mathrm{I}ae}\underline{E}_i = \underline{0} \tag{4.28a}$$

$$\underline{K}_{\mathrm{I}ab}{}^{\mathrm{T}}\underline{A}_i + \underline{K}_{\mathrm{I}bb}\underline{B}_i + \underline{K}_{\mathrm{I}be}\underline{E}_i = \underline{0} \tag{4.28b}$$

$$\underline{K}_{\mathrm{I}cc}\underline{C}_i + \underline{K}_{\mathrm{I}cd}\underline{D}_i + \underline{K}_{\mathrm{II}ce}\underline{E_k E_l} = \underline{0} \tag{4.28c}$$

$$\underline{K}_{\mathrm{I}cd}{}^{\mathrm{T}}\underline{C}_i + \underline{K}_{\mathrm{I}dd}\underline{D}_i + \underline{K}_{\mathrm{II}de}\underline{E_k E_l} = \underline{0} \tag{4.28d}$$

$$\begin{aligned} &\underline{K}_{\mathrm{I}ae}{}^{\mathrm{T}}\underline{A}_i + \underline{K}_{\mathrm{I}be}{}^{\mathrm{T}}\underline{B}_i + \underline{K}_{\mathrm{I}ee}\underline{E}_i \\ &\qquad + \underline{K}_{\mathrm{II}ec}\underline{C_k E_l} + \underline{K}_{\mathrm{II}ed}\underline{D_k E_l} + \underline{K}_{\mathrm{III}ee}\underline{E_k E_l E_m} = -F\underline{R}_{ei} \end{aligned} \tag{4.28e}$$

However, it should be noted that four of the modal amplitudes may be written in terms of the fifth. The most convenient amplitude to write the equations in is $\underline{E}_i$. Solving for $\underline{A}_i$ and $\underline{B}_i$ in terms of $\underline{E}_i$ in equations (4.28a) and (4.28b) yields,

$$\begin{Bmatrix} \underline{A}_i \\ \underline{B}_i \end{Bmatrix} = -\begin{bmatrix} \underline{K}_{\mathrm{I}aa} & \underline{K}_{\mathrm{I}ab} \\ \underline{K}_{\mathrm{I}ab}{}^{\mathrm{T}} & \underline{K}_{\mathrm{I}bb} \end{bmatrix}^{-1} \begin{bmatrix} \underline{K}_{\mathrm{I}ae} \\ \underline{K}_{\mathrm{I}be} \end{bmatrix} \{\underline{E}_i\} \tag{4.29}$$

which may be inserted into equation (4.28e) with the result,

$$\underline{K}_{\mathrm{I}}{}^{*}\underline{E}_i + \underline{K}_{\mathrm{II}ec}\underline{C_k E_l} + \underline{K}_{\mathrm{II}ed}\underline{D_k E_l} + \underline{K}_{\mathrm{III}ee}\underline{E_k E_l E_m} = -F\underline{R}_{ei} \tag{4.30}$$

where,

$$\underline{K}_{\mathrm{I}}{}^{*} = \underline{K}_{\mathrm{I}ee} - \begin{bmatrix} \underline{K}_{\mathrm{I}ae}{}^{\mathrm{T}} & \underline{K}_{\mathrm{I}be}{}^{\mathrm{T}} \end{bmatrix} \begin{bmatrix} \underline{K}_{\mathrm{I}aa} & \underline{K}_{\mathrm{I}ab} \\ \underline{K}_{\mathrm{I}ab}{}^{\mathrm{T}} & \underline{K}_{\mathrm{I}bb} \end{bmatrix}^{-1} \begin{bmatrix} \underline{K}_{\mathrm{I}ae} \\ \underline{K}_{\mathrm{I}be} \end{bmatrix} \tag{4.31}$$

Equations (4.28c) and (4.28d) can also be reduced by solving for $\underline{C}_i$ and $\underline{D}_i$ in terms of $\underline{E_iE_j}$, producing,

$$\begin{Bmatrix} \underline{C}_i \\ \underline{D}_i \end{Bmatrix} = -\begin{bmatrix} \underline{K}_{\mathrm{I}cc} & \underline{K}_{\mathrm{I}cd} \\ \underline{K}_{\mathrm{I}cd}{}^{\mathrm{T}} & \underline{K}_{\mathrm{I}dd} \end{bmatrix}^{-1} \begin{bmatrix} \underline{K}_{\mathrm{II}ce} \\ \underline{K}_{\mathrm{II}de} \end{bmatrix} \left\{ E_iE_j \right\} \tag{4.32}$$

which, when inserted into equation (4.30), gives the result:

$$\begin{aligned} &\underline{K}_{\mathrm{II}ec}\underline{C_kE_l} + \underline{K}_{\mathrm{II}ed}\underline{D_kE_l} = \\ &\qquad -\left[\underline{K}_{\mathrm{II}ec} \quad \underline{K}_{\mathrm{II}ed} \right] \left\{ \left(\begin{bmatrix} \underline{K}_{\mathrm{I}cc} & \underline{K}_{\mathrm{I}cd} \\ \underline{K}_{\mathrm{I}cd}{}^{\mathrm{T}} & \underline{K}_{\mathrm{I}dd} \end{bmatrix}^{-1} \begin{bmatrix} \underline{K}_{\mathrm{II}ce} \\ \underline{K}_{\mathrm{II}de} \end{bmatrix} \left\{ \underline{E_iE_j} \right\} \right)_k \underline{E}_l \right\} \end{aligned} \tag{4.33}$$

Through manipulation of the indices, equation (4.33) can be used to produce,

$$\left[\underline{K}_{\mathrm{I}}{}^{*} \right] \left\{ \underline{E}_i \right\} + \left[\underline{K}_{\mathrm{III}}{}^{*} \right] \left\{ \underline{E_kE_lE_m} \right\} = -F\left\{ \underline{R}_{ei} \right\} \tag{4.34}$$

where,

$$\begin{aligned} &\left[\underline{K}_{\mathrm{III}}{}^{*} \right] \left\{ \underline{E_kE_lE_m} \right\} = \left[\underline{K}_{\mathrm{III}ee} \right] \left\{ \underline{E_kE_lE_m} \right\} \\ &\qquad -\left[\underline{K}_{\mathrm{II}ec} \quad \underline{K}_{\mathrm{II}ed} \right] \left\{ \left(\begin{bmatrix} \underline{K}_{\mathrm{I}cc} & \underline{K}_{\mathrm{I}cd} \\ \underline{K}_{\mathrm{I}cd}{}^{\mathrm{T}} & \underline{K}_{\mathrm{I}dd} \end{bmatrix}^{-1} \begin{bmatrix} \underline{K}_{\mathrm{II}ce} \\ \underline{K}_{\mathrm{II}de} \end{bmatrix} \left\{ \underline{E_iE_j} \right\} \right)_k \underline{E}_l \right\} \end{aligned} \tag{4.35}$$

The system of equations can be solved for the modal amplitudes, $\underline{E}_i$. Once $\underline{E}_i$ has been determined, it can be substituted into equations (4.29) and (4.32) to evaluate the other four modal amplitudes.

4.5 Flexible Boundary Conditions

In this work, the analysis was used to model the bending of a plate which is clamped on the two sides perpendicular to the longitudinal direction of the plate and free on the two sides perpendicular to the transverse direction of the plate. When the clamped boundary condition is used, as in this work, the analysis assumes that the boundary condition is perfectly rigid: there is no displacement or rotation of the ends of the plate in any direction, x, y, or z. It is important to recognize the distinction between in-plane boundary conditions and the out-of-plane boundary condition. The out-of-plane clamped boundary condition requires that the out-of-plane displacement, w, be equal to zero at the ends of the plate. The in-plane clamped boundary condition, as used here, requires the in-plane displacements, u and v, to be zero at the ends of the plate. However, in realistic cases, the in-plane clamped boundary condition might not be perfectly rigid: small, but nonzero, in-plane displacements (u and v) at the ends of the plate may occur during the indentation event. These small displacements due to the slightly flexible in-plane boundary condition can significantly affect the membrane force which must be taken into account. The in-plane flexibility enters the analysis through the stiffness terms in equations (4.28c) and (4.28d). The stiffnesses from these equations affect the nonlinear stiffness term $[\underline{K}_{\mathrm{III}}{}^{*}]$ in equation (4.34). This effect can be accounted for by applying a geometrical nonlinearity factor, β [32]. Since only the subtracted term in equation (4.35) involves the effects of the flexibility, it is useful to combine the effects of that term and the flexibility as:

$$\beta\left[\underline{K}_{\mathrm{III}_{ee}}\right] = \left[\underline{K}_{\mathrm{III}}{}^{*}\right] \tag{4.36}$$

Equation (4.36) results in a modification of equation (4.34):

$$\left[\underline{K}_{\mathrm{I}}{}^{*}\right]\left\{\underline{E}_i\right\} + \beta\left[\underline{K}_{\mathrm{III}_{ee}}\right]\left\{\underline{E_k E_l E_m}\right\} = -F\left\{\underline{R}_{ei}\right\} \tag{4.37}$$

Note the use of β imposes a relationship between the linear and nonlinear terms in the midplane strains. Physically, β represents a range of flexibility of the boundary conditions from clamped-perfectly-sliding, ($\beta = 0$), to clamped-perfectly-rigid, ($\beta = 1$). Referring to Figure 4.5, β can be seen as the degree to which in-plane sliding is allowed. The factor is quantified as the ratio of the change in length of the plate to the difference between this change in length and the displacement of the ends of the plate, where the length of the plate is measured on the through-the-thickness centerline, following the curve of the plate:

$$\beta = \frac{\text{Change in Length of the Plate}}{\text{Change in Length of Plate } - \text{ Displacement of Plate Ends}}$$

or,

$$\beta = \frac{\Delta l}{\Delta l - \Delta u} \tag{4.38}$$

The change in length of the plate on the through-the-thickness centerline, Δl, is simply how much the plate itself stretches (measured following the curve of the plate) during the application of load. This change in length of the plate can be found by integrating the midplane strain over the length of the plate:

$$\Delta l = \int_0^l \left[\frac{\partial u}{\partial x} + \frac{1}{2}\left(\frac{\partial w}{\partial x}\right)^2 \right] dx \tag{4.39}$$

The deflection of the end of the plate, Δu, is the sliding which is allowed by the flexible in-plane boundary condition. This movement of the end of the plate can be found by taking the average in-plane deflection of the plate over its length:

$$\Delta u = \int_0^l \frac{\partial u}{\partial x} dx \tag{4.40}$$

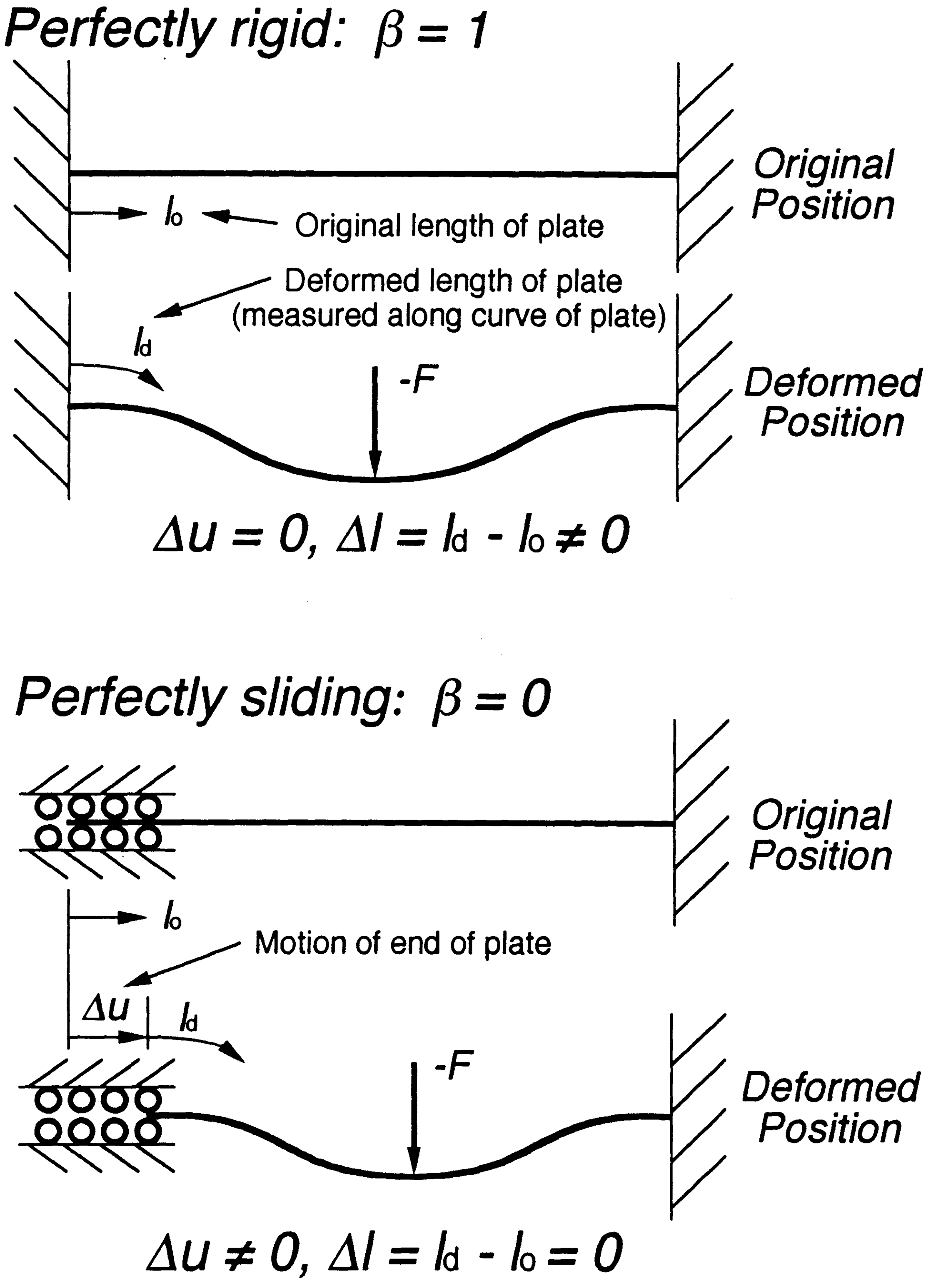

Figure 4.5 Illustration of *(upper)* perfectly rigid and *(lower)* perfectly sliding in-plane boundary conditions.

These expressions are substituted into equation (4.38) to yield:

$$\beta = \frac{\int_0^l \left[\frac{\partial u}{\partial x} + \frac{1}{2}\left(\frac{\partial w}{\partial x} \right)^2 \right] dx}{\int_0^l \left[\frac{\partial u}{\partial x} + \frac{1}{2}\left(\frac{\partial w}{\partial x} \right)^2 \right] dx - \int_0^l \frac{\partial u}{\partial x} dx} \tag{4.41}$$

Manipulation of equation (4.41) results in a relationship between the nonlinear and linear terms in the expression for midplane strain:

$$\frac{\partial u}{\partial x} = \frac{[\beta - 1]}{2}\left(\frac{\partial w}{\partial x} \right)^2 \tag{4.42}$$

By manipulating the definition of longitudinal extensional strain, ε_{11}°, from equation (4.11b) and inserting it into equation (4.42) (solve for the partial of u with respect to x and insert into (4.42), then solve the result for ε_{11}°), a modified expression for midplane strain results:

$$\varepsilon_{11}^{\circ} = \frac{\beta}{2}\left(\frac{\partial w}{\partial x} \right)^2 \tag{4.43}$$

Using equation (4.43) to determine the midplane, or extensional, strain in the plate eliminates the need to solve for $\underline{C}_i$ and $\underline{D}_i$ to determine the in-plane strains. It should be noted that this ignores the pointwise shell (i.e. large displacement) effect, but only characterizes the geometric nonlinearity on a global basis.

The β-factor also has the desirable effect of eliminating the need to employ equation (4.35), incorporating its effect on the nonlinear term in equation (4.34) into the nonlinearity factor. This significantly simplifies and shortens solving the equations for $\underline{E}_i$.

There are certain limitations to the β-factor which must be noted. It is an empirical parameter which must be fit with experimental data, so only the rigidly clamped or perfectly sliding case can be determined analytically. It does not account for variations in the "degree" to which the plate is clamped across the width in that different β-factors may be required at different locations along the width of the plate. This would arise, for example, if the edges of the plate were closer to an ideal clamped condition, while the center of the plate is closer to a sliding condition, due to the details of how the clamping is accomplished. Because the β-factor is derived by integrating over the length of the plate, the non-ideal boundary condition is averaged over the span of the plate. Also, since only one β-factor is used across the width in this analysis, the non-ideal boundary condition is effectively averaged over the width of the plate as well. All this means that the β-factor must be determined empirically for a unique degree of flexibility, remembering the limitation that it is an averaged effect over the span and width of the plate.

4.6 Solution Method

The key set of equations to be solved in the previous section are the set of equations given by (4.37). This nonlinear set of equations must be solved using a numerical method. The Newton-Raphson method was chosen because of its simplicity, ease in programming, and fast convergence when the initial guess is near the solution. A thorough discussion of this method is presented in reference [43]. The Newton-Raphson equation can be written,

$$\left[J^k\right]\left\{X^{k+1}-X^k\right\}=-\left\{g^k(X)\right\} \tag{4.44}$$

where $\left[J^k\right]$ is the Jacobian matrix of the equations $g^k(\mathrm{X})$, given as,

$$\left[J^k\right]=\begin{bmatrix} \partial g_1^k/\partial \mathrm{X}_1 & \partial g_1^k/\partial \mathrm{X}_2 & \cdots & \partial g_1^k/\partial \mathrm{X}_j \\ \partial g_2^k/\partial \mathrm{X}_1 & \partial g_2^k/\partial \mathrm{X}_2 & \cdots & \partial g_2^k/\partial \mathrm{X}_j \\ \cdot & \cdot & \cdot & \cdot \\ \cdot & \cdot & \cdot & \cdot \\ \cdot & \cdot & \cdot & \cdot \\ \partial g_i^k/\partial \mathrm{X}_1 & \partial g_i^k/\partial \mathrm{X}_2 & \cdots & \partial g_i^k/\partial \mathrm{X}_j \end{bmatrix} \tag{4.45}$$

and $g^k(\mathrm{X})$ are the system of homogeneous nonlinear equations to be solved. In this case:

$$g^k(\mathrm{X})=\left[\underline{K}_{\mathrm{I}}{}^*\right]\left\{\underline{E}_i\right\}^k+\beta\left[\underline{K}_{\mathrm{III}_{ee}}\right]\left\{\underline{E_k E_l E_m}\right\}^k+F\left\{\underline{R}_{ei}\right\}^k \tag{4.46}$$

The X^k are the modal amplitudes, $\underline{E}_i$, which the method is attempting to determine. The superscript, k, denotes the step of the iteration. The method is executed by assuming a trial solution†, X^0, for the modal amplitudes, which is used to calculate the value of the equations and the Jacobian. The next trial solution, X^1, is then found by solving the matrix equation (4.44). The steps are repeated until the change between the next trial solution and the current trial solution is less than a tolerance prescribed by the user (this will be discussed in the section on computer implementation).

---

† Reference [43] presents a full discussion on the "proper" choice of trial solutions and their implication on convergence of the Newton-Raphson method.

The modal amplitudes, $\underline{E}_i$, representing the out-of-plane displacement, w, are determined from the Newton-Raphson method and are used in equations (4.29) and (4.32) to determine the other modal amplitudes. Once these are determined, the modal amplitudes are used in equations (4.22a-e), to evaluate the shape functions at the points of interest to arrive at the displacements ψ_x, ψ_y, u, v, and w at those points. Equations (4.22a-e) can also be combined with equations (4.11) or equation (4.43) to determine the strains in the plate.

4.7 Computer Implementation

The analysis and solution technique described in sections 4.2 and 4.3 were implemented in a FORTRAN 77 program called "STATIC1". The program code is listed in Appendix C. STATIC1 is divided into two main parts: the calculation of the stiffness matrices and the solution of the system of equations, roughly dividing the topics as in sections 4.2 and 4.3†. Each of the parts is further subdivided into subprograms which carry out individual processes. An illustration of the program flow through the subroutines is shown in Figure 4.6.

The first set of subprograms calculates and stores the matrices $\underline{K}_{\mathrm{I}}^*$ and $\underline{K}_{\mathrm{III}_{ee}}$ to be used in solving equation (4.37) and the matrices necessary to determine A_i and B_i using equation (4.29). To begin calculating the stiffness matrices, an input file named "Stiff.dat" containing information such as plate dimensions, laminate constants, and solution parameters (a full listing is given in Table 4.1) is read by the subprogram INPUT. Based on this information, parameters for the mode shapes (see Appendix A) are

---

† Much of the first part of the program was taken directly from the nonlinear impact analysis program "GLOBAL2" written by Matsuhashi [36].

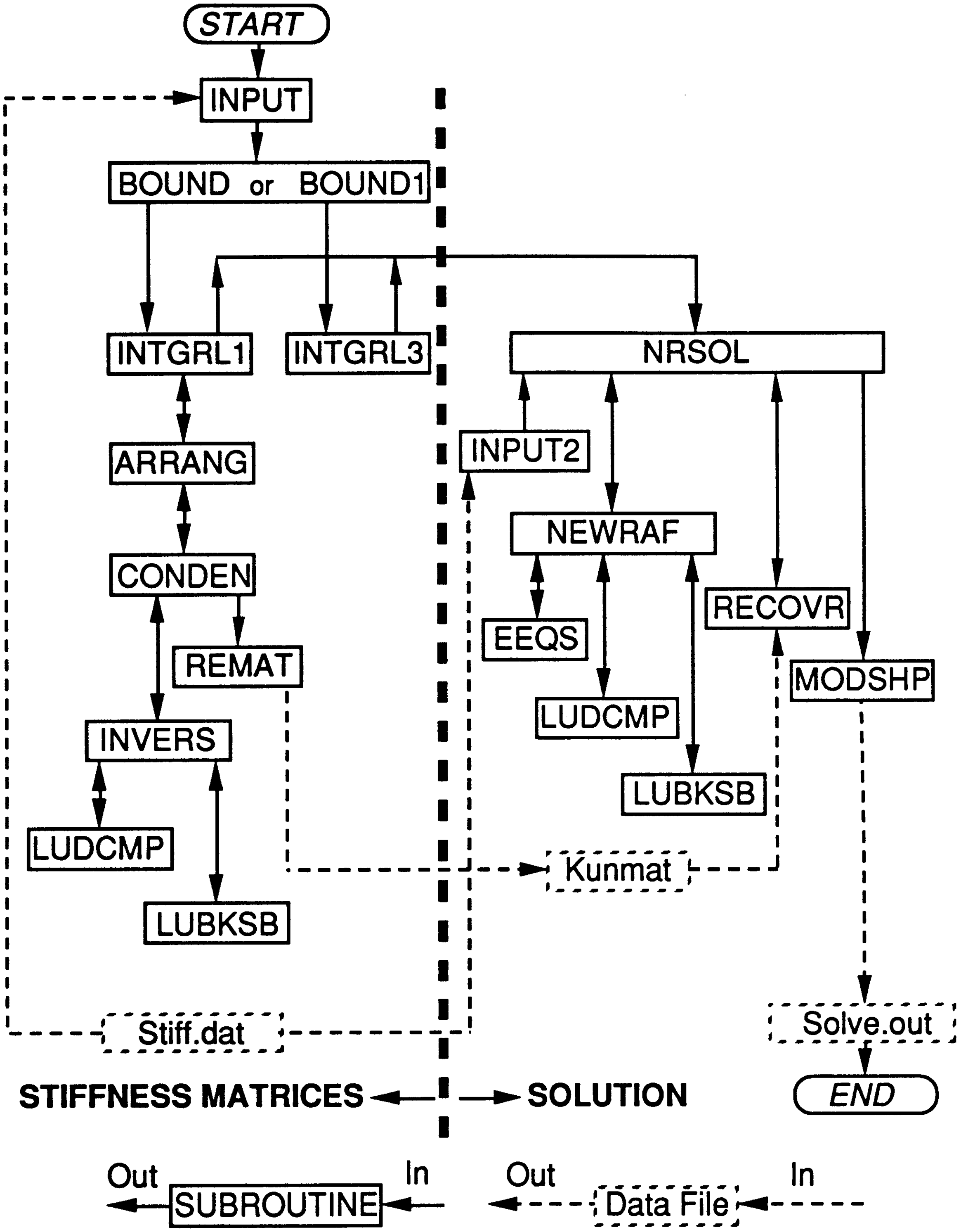

Figure 4.6 Structure of the program STATIC1.

assigned for either all modes, via subprogram BOUND, or for odd modes only, via subprogram BOUND1. Odd modes only may be used to reduce the computational time without loss in accuracy if the bending is expected to be symmetric, as would occur in symmetrically laminated plates with no bending-twisting coupling [36]. However, despite the fact that the laminate analyzed here has finite bending-twisting coupling, the difference between odd modes only and all modes was not investigated in this work. The assumption that odd modes only were sufficient was based on the comparison between odd modes only and all modes results presented by Matsuhashi [36] for the same laminate investigated here. Once the mode shape parameters are assigned, the subprogram INTGRL1 calculates components of the stiffness matrices $\underline{K}_{\mathrm{I}_{aa}}$, $\underline{K}_{\mathrm{I}_{ab}}$, $\underline{K}_{\mathrm{I}_{ae}}$, $\underline{K}_{\mathrm{I}_{bb}}$, $\underline{K}_{\mathrm{I}_{be}}$, and $\underline{K}_{\mathrm{I}_{ee}}$ by using the extended trapezoidal rule [44] to carry out the necessary integrations numerically. Because the shape functions for free-free boundary conditions are used in the y-direction, the inverted term in equation (4.31) becomes singular and cannot be inverted without some rearrangement. Normally, some of the rows and columns are all zeroes and may be eliminated, so the next subprogram, ARRANG, checks for zero rows and columns in the matrix, removes them, and compresses the matrix so that it can be inverted. The subprogram CONDENS carries out equation (4.31) by inverting and multiplying out the terms of the stiffness matrices to arrive at $\underline{K}_{\mathrm{I}}^{*}$, which is stored for use in the solution part of the program. The inversion is done in the subprogram INVERS by performing LU-decomposition[†] and back substitution using the subprograms LUDCMP and LUBKSB. The subprogram CONDENS also provides the inverted matrix to the subprogram REMAT, which multiplies terms in equation

---

[†] A standard method for solving linear matrix equations, described in reference [43].

(4.29) and outputs them to the data file "Kunmat" which is used in the solution part of the program to recover $\underline{A}_i$ and $\underline{B}_i$. The nonlinear stiffness matrices are computed in the subprogram INTGRL3, which uses the same techniques as INTGRL1 to calculate the components of the stiffness matrix $\underline{K}_{\mathrm{III}_{ee}}$. The stiffness matrices are calculated once for a case and then passed to the solution portion of the program for repeated use.

The second set of subprograms uses the information from the first set to build and solve equation (4.37) and calculate the final results of deflection, extensional strain, and bending strain. The parent subprogram, NRSOL, coordinates the input and output of data and increments the force levels for use in the solution subprograms. New data, including the nonlinearity factor, the maximum force level for the current case, and the initial trial solution for the Newton-Raphson method, are read from the file "Stiff.dat" by the subprogram INPUT2. The matrices $\underline{K}_{\mathrm{I}}^*$ and $\underline{K}_{\mathrm{III}_{ee}}$, the current trial solution for $\underline{E}_i^k$, the nonlinearity factor β, the generalized force vector $\underline{R}_{e_i}$, and the current indentation force F_z are all passed to NEWRAF, the subprogram which carries out the Newton-Raphson method, equation (4.44). The subprogram EEQS determines $g^k(X)$ and its Jacobian for use in NEWRAF. The derivatives in the Jacobian are found by determining what their form will be from the indices of the modal amplitudes and then inserting the current data into that form. The subprogram NEWRAF then solves equation (4.44) for the next trial solution using LU-decomposition and back substitution using the subprograms LUDCMP and LUBKSB. The value of the modal amplitudes is returned to NRSOL if the difference between the next and current trial solutions is less than the error given in the file "Stiff.dat"; otherwise, the procedure within NEWRAF executes until the error condition is met or a nonconvergence condition (exceeding a prescribed number of steps) is met. Since the number of iteration steps to completion is written to both the screen and the output file, it is immediately obvious when the method has not converged in the maximum number of steps prescribed (in all cases, increasing the maximum number of steps allowed solved any problems of this nature). The modal amplitudes $\underline{E}_i$ are then passed to the subprogram RECOVR which uses equation (4.29) and the data from the file "Kunmat" to determine the modal amplitudes $\underline{A}_i$ and $\underline{B}_i$. Finally, the modal amplitudes that have been determined are used in the subprogram MODSHP along with the mode shapes to determine the transverse deflection:

$$w(x,y)=\sum_i E_i q_\varsigma(x) r_\mu(y) \tag{4.47}$$

the longitudinal extensional strain:

$$\varepsilon_{11}{}^{\circ}(x,y)=\frac{\beta}{2}\left(\frac{\partial w(x,y)}{\partial x}\right)^2=\frac{\beta}{2}\left(\sum_i E_i \frac{\partial q_\varsigma(x)}{\partial x} r_\mu(y)\right)^2 \tag{4.48}$$

and the bending strain:

$$z\,\kappa_{11}{}^{\circ}(x,y)=z\frac{\partial \psi_x(x,y)}{\partial x}=z\sum_i A_i \frac{\partial f_\varsigma(x)}{\partial x} g_\mu(y) \tag{4.49}$$

at points on the plate requested in the file "Stiff.dat". Equation (4.47) is a reiteration of equation (4.22e); equations (4.48) and (4.49) are a combination of equations (4.11b) with equations (4.22a) and (4.22e), using the definition from equation (4.43). The entire procedure is repeated to create load-deflection and load-strain curves by incrementing the load from zero to the desired maximum load. The load-deflection and load-strain data are output to the file "Solve.out" for further data reduction.

Because STATIC1 encodes a quasi-static analysis similar in many respects to the transient analysis carried out in Matsuhashi's GLOBAL2 [36], it encounters similar problems due to computer hardware constraints. STATIC1 deals with a relatively large stiffness matrix for the nonlinear (cubic) term from equation (4.37). For example, using 13 by 13 odd modes only (or 7 by 7 actual modes, the largest number of modes attempted for this work) results in a 49 by 117,649 non-square $\underline{K}_{\mathrm{III}_{ee}}$ matrix. Because of the size of this matrix, STATIC1 requires much more memory (RAM) than would be necessary for a linear analysis. The case cited above used all of the 64 Megabytes on the DEC 5000/133 on which it was run. The size of the nonlinear stiffness matrix affects not only the memory required, but the computational time (CPU time). Running a 13 by 13 odd modes only case significantly taxed the DEC 5000/133, as the program ran continuously for ninety-one hours to calculate the deflection, extensional strain and bending strain data for the twenty forces necessary to calculate curves similar to those in Figures 4.7 through 4.9. The required CPU time is strongly dependent on the number of modes used as input. The 9 by 9 odd modes only case used as the example in the next section required approximately forty minutes to complete, whereas the next odd modes only case, 11 by 11 took approximately three hours to complete. Increasing the number of modes seems to increase the CPU time at a geometrical rate. The conclusion is that the computer must be fast to run the program in a reasonable amount of time, but it must have enough memory (RAM) to run large mode cases at all.

4.8 Numerical Example

A 254 mm by 89 mm AS4/3501-6 graphite/epoxy plate with a $[\pm45_2/0_2]_s$ stacking sequence under indentation to a maximum contact force of 930 N was used as the example case. The data used for this example is presented in Table 4.1. Force, deflection, extensional strain, and bending strain were the data output from the program. Reduction and presentation of the data output from STATIC1 was done on Apple Macintosh® computers using commercial software. The data are plotted as functions of force, as this has been determined to be the critical factor for comparison of impact phenomena [1]. A plot of force versus center point deflection is provided in Figure 4.7. Plots of force versus extensional strain and force versus bending strain for a point 63.5 mm from the transverse centerline and on the longitudinal centerline (strain gage locations 3 and 4 from strain gage scheme A, illustrated in Figure 3.2) are provided in Figures 4.8 and 4.9 respectively. These plots display the typical format and type of data used for comparison with experimental results to be presented and discussed in Chapters 5 and 6.

As previously mentioned, the β-factor must be determined empirically. This is done by using different values of β in the analysis program until a curve which matches the experimental data is found. Using this process, β equal to 0.03 was found to fit the experimental data best. This process also points out how the force-deflection curves vary with β. This is illustrated in Figure 4.10 where results for the extremes of β values, 0 and 1, and the best fit value, 0.03 are shown. When β equals zero, the plate is perfectly clamped-sliding and behaves linearly as the plate does not stiffen with increasing load. When β equals one, the plate is clamped-

Laminate Material System	AS4/3501-6 Graphite/Epoxy
Lay-up	$[\pm 45_2/0_2]_s$
x-direction Boundary Condition	Clamped-Clamped
y-direction Boundary Condition	Free-Free
Plate Length (x-direction)	254 mm
Plate Width (y-direction)	89 mm
Plate Thickness	1.608 mm
A_{1111}	125,542,700 N/m
A_{1122}	37,682,300 N/m
A_{1112}	0.00 N/m
A_{2222}	54,249,900 N/m
A_{2212}	0.00 N/m
A_{1212}	42,568,300 N/m
D_{1111}	17.072 N-m
D_{1122}	11.272 N-m
D_{1112}	5.121 N-m
D_{2222}	15.365 N-m
D_{2212}	5.121 N-m
D_{1212}	12.325 N-m
G_{44}	6.92 MN/m
G_{45}	0.00 MN/m
G_{55}	8.06 MN/m
Shear Correction Factor	0.833
Nonlinearity Factor β	0.030
Number of Modes in x-direction	9 (odd modes only)
Number of Modes in y-direction	9 (odd modes only)
Maximum Contact Force	930 N
Number of Force Increments	20

Table 4.1 Inputs for STATIC1 – Example Problem.

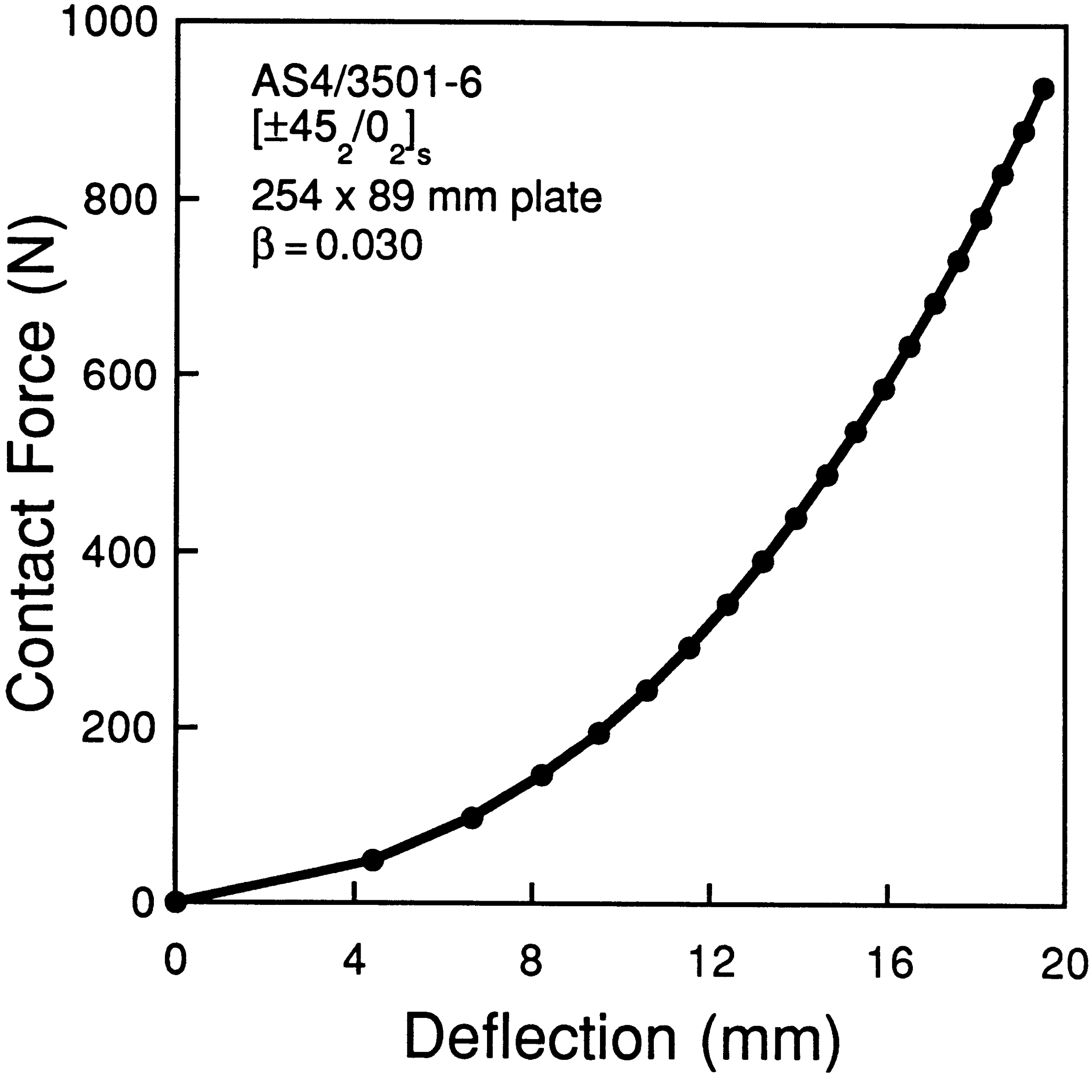

Figure 4.7 Analytical force-deflection curve for an AS4/3501-6 $[\pm 45_2/0_2]_s$ 254 mm span specimen indented to 930 N.

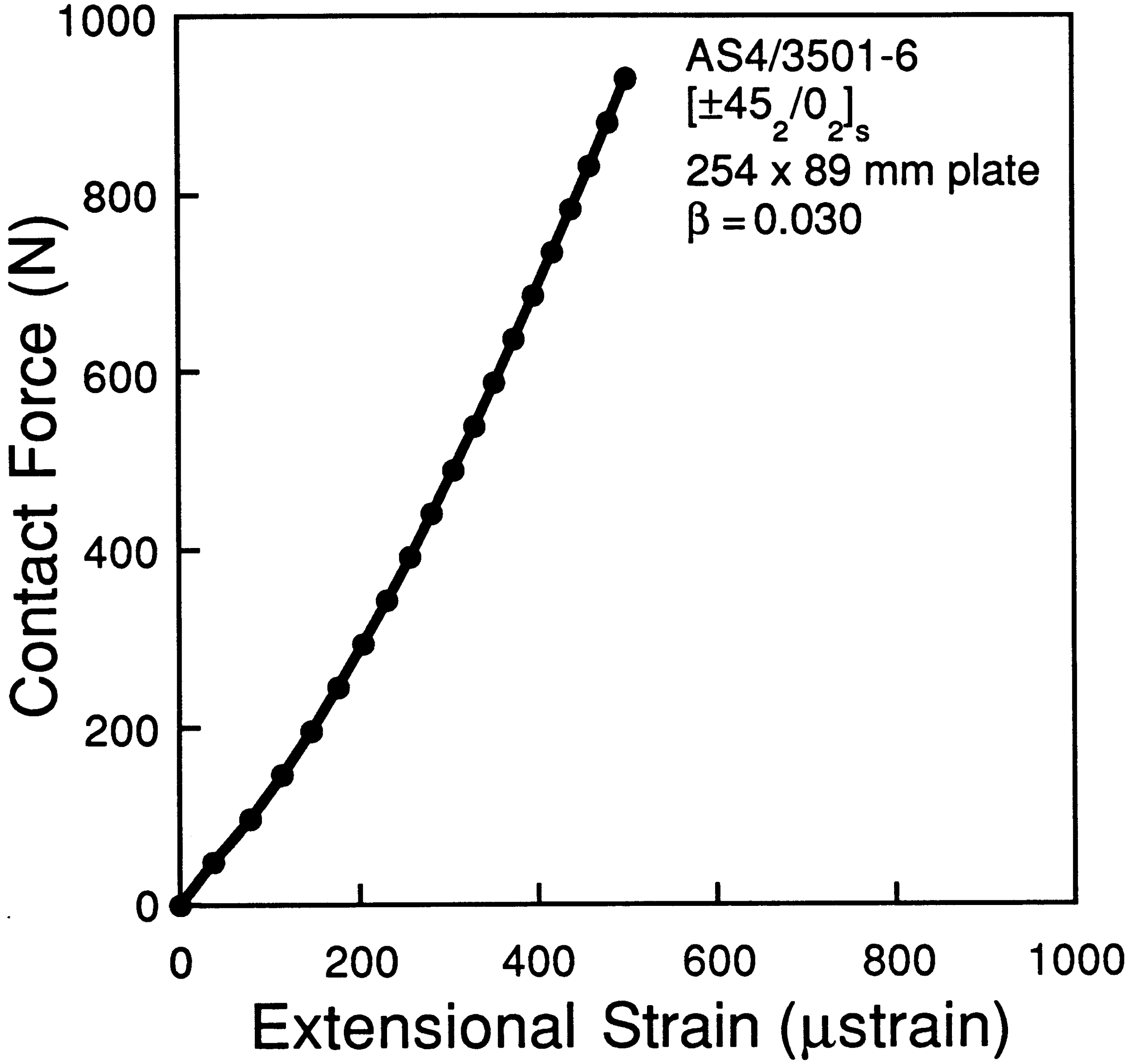

Figure 4.8 Analytical force-extensional strain curve at position 3-4 (strain gage scheme A) for an AS4/3501-6 [±45$_2$/0$_2$]$_s$ 254 mm span specimen indented to 930 N.

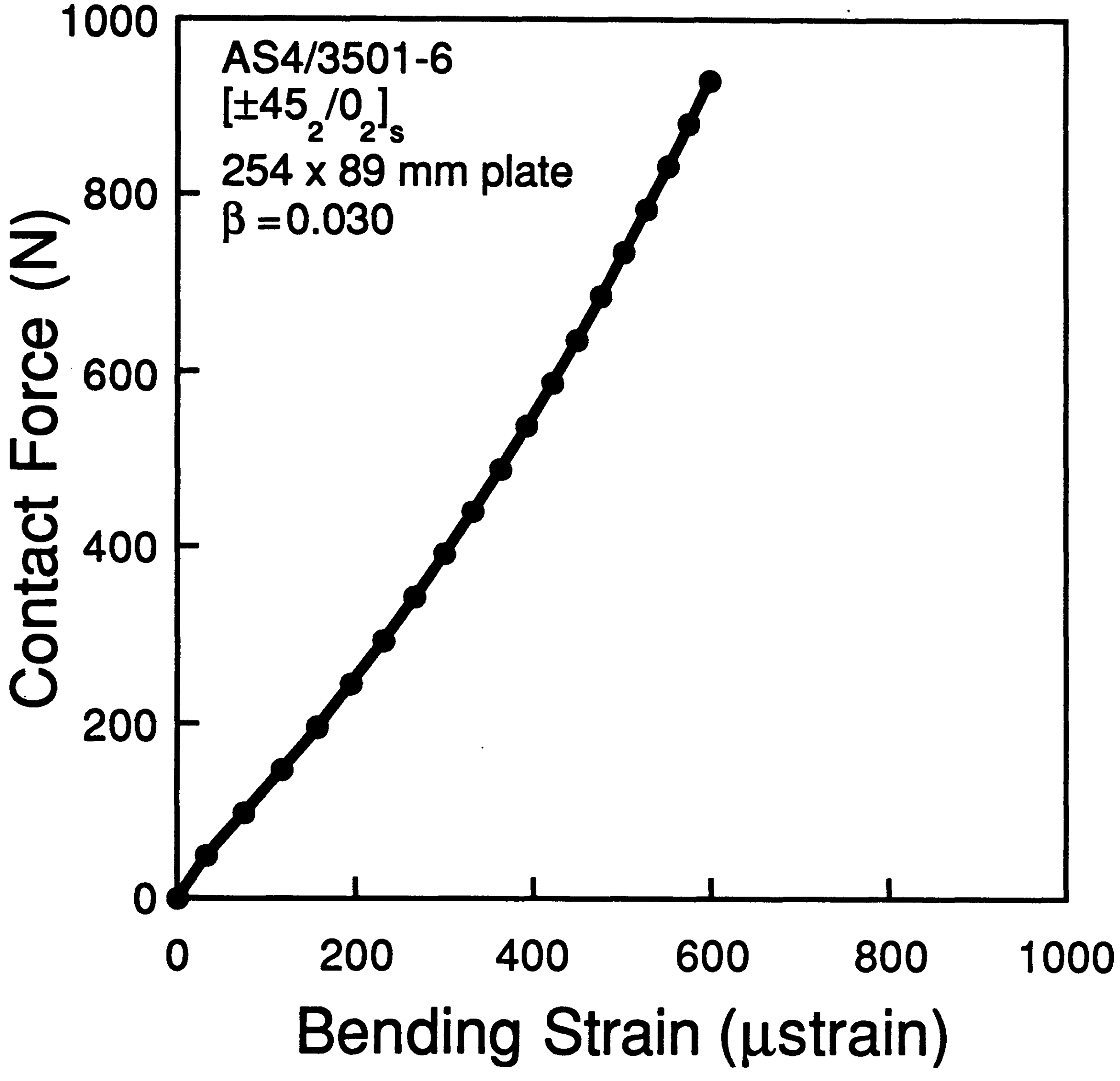

Figure 4.9 Analytical force-bending strain curve for gage 4 (strain gage scheme A) for an AS4/3501-6 [±45$_2$/0$_2$]$_s$ 254 mm span specimen indented to 930 N.

perfectly rigid as the plate stiffens to the maximum amount as load increases.

The analysis was run using from 5 by 5 odd modes to 13 by 13 odd modes. The analytical curves for deflection, extensional strain, and bending strain for each mode case are compared with each other to check for convergence of the analysis. The analytical curves are also compared with experimental curves to check if the method is converging to actual data. The convergence comparison for the force-deflection curves is shown in Figure 4.11. The analysis converges very quickly and matches the experimental data well when using $\beta = 0.03$ as even the 5 by 5 odd modes case appears to be well converged. On this basis, $\beta = 0.03$ is used for all further convergence comparisons.

Since the analysis is displacement-based, the convergence is obviously based on the displacement. Therefore, poor or non-convergence of the strains should not be surprising. Because the extensional strain is the first derivative of the displacement and the bending strain is based on the second derivative of the displacement, the error in basing their convergence on the displacement should result in poor convergence of the strains. A convergence comparison for a force-extensional strain curve is shown in Figure 4.12. The analysis does not converge as quickly as the force-deflection curves, but appears to be converged after 9 by 9 odd modes. A convergence comparison for a force-bending strain curve is shown in Figure 4.13. For this case, the analysis does not appear converged after 13 by 13 odd modes. Further mode cases were not tried because computer hardware limitations made it impossible.

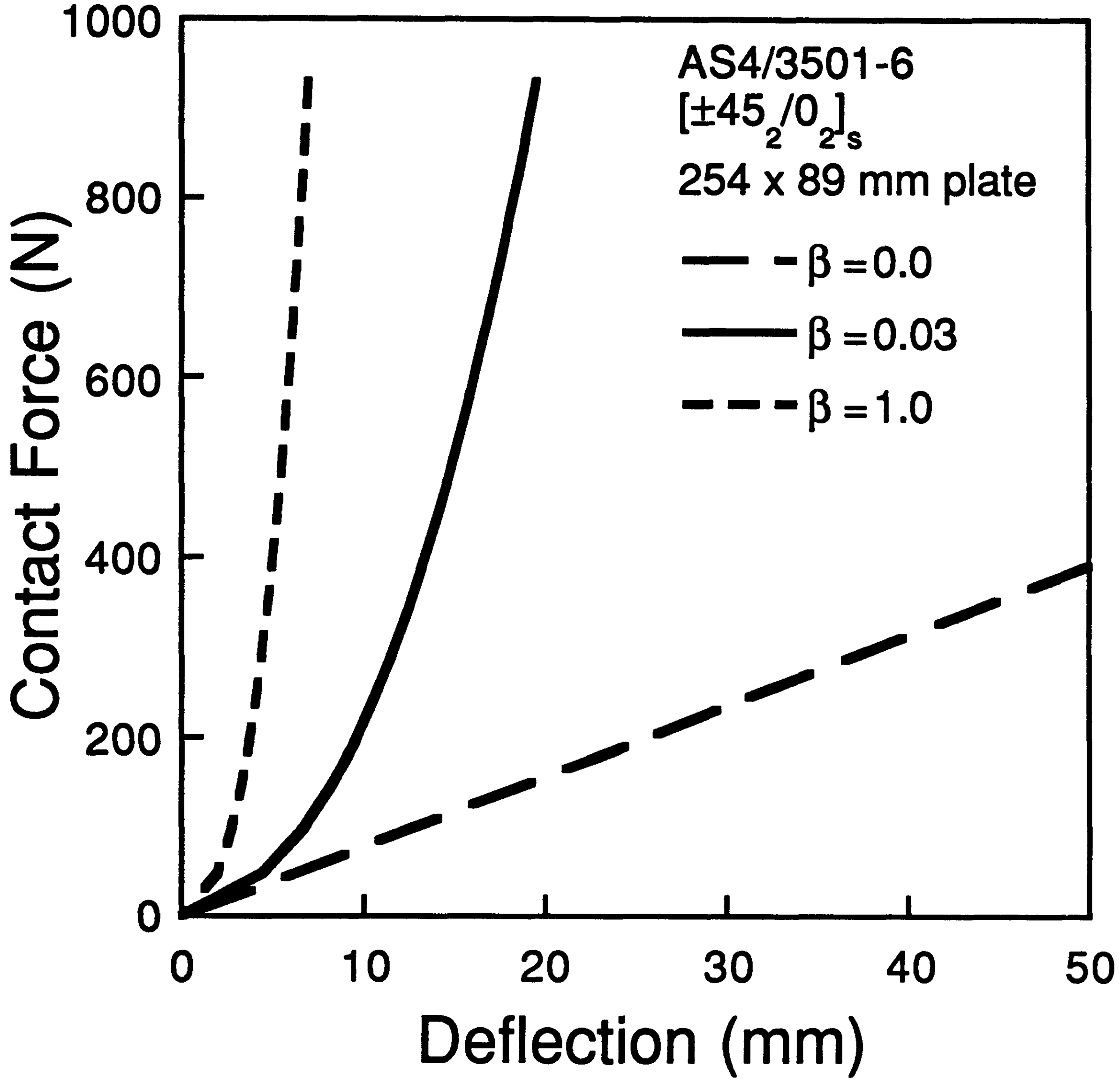

Figure 4.10 Analytical force-deflection results for various values of β for an AS4/3501-6 $[\pm45_2/0_2]_s$ 254 mm span specimen.

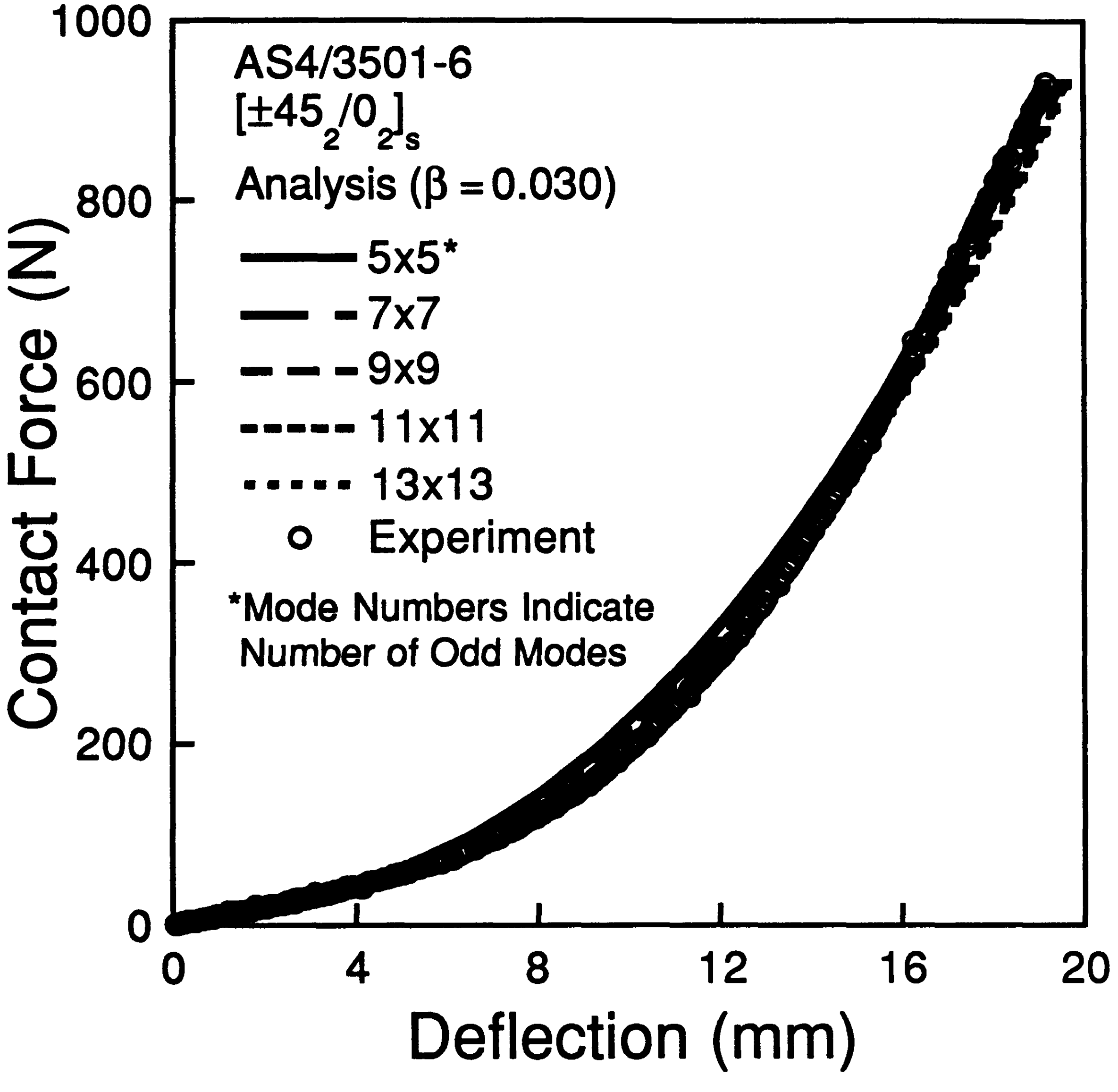

Figure 4.11 Convergence of force-deflection curves for an AS4/3501-6 [±$45_2/0_2$]$_s$ 254 mm span specimen indented to 930 N.

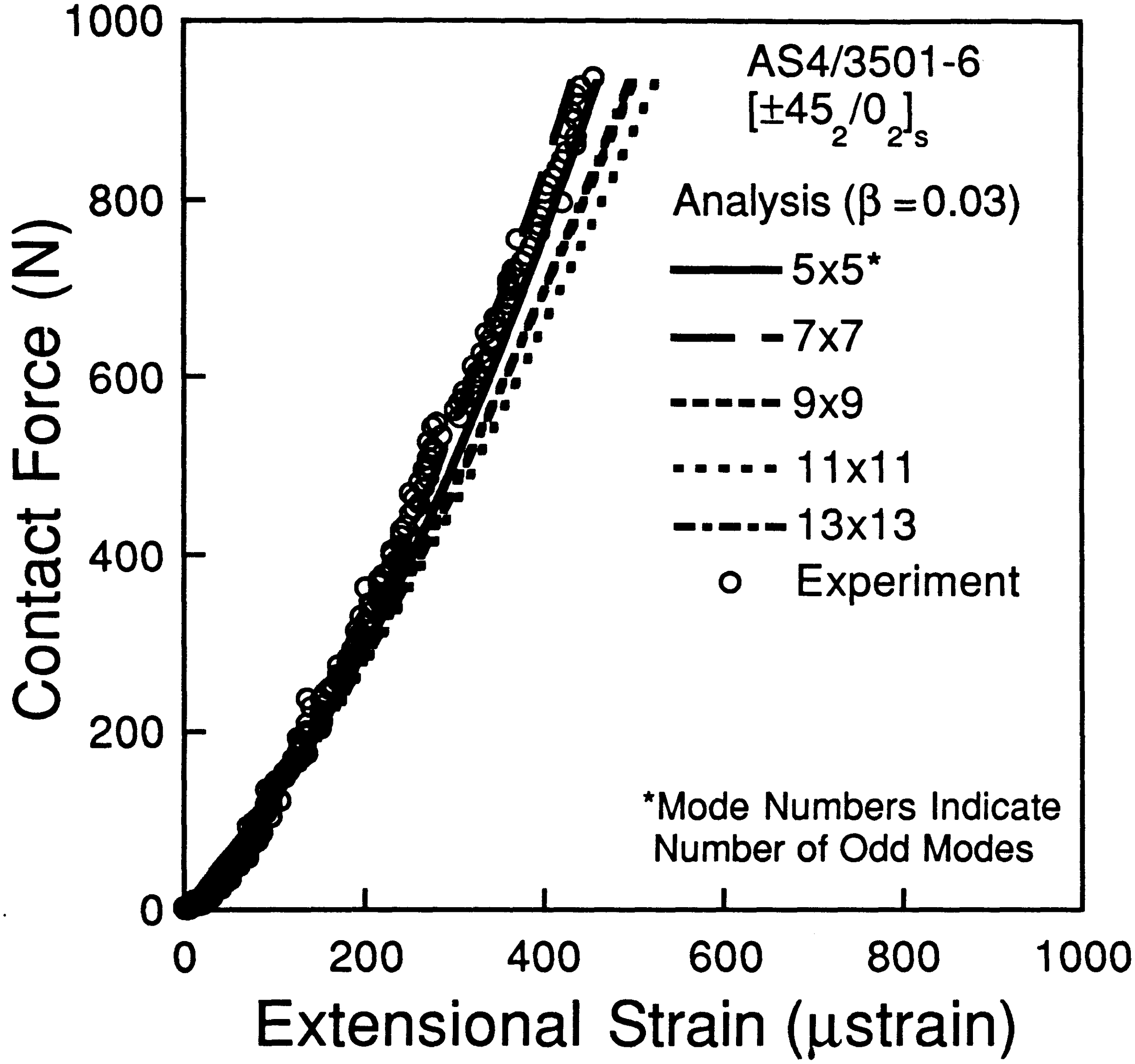

Figure 4.12 Convergence of force-extensional strain curves at position 3-4 (strain gage scheme A) for an AS4/3501-6 [±45$_2$/0$_2$]$_s$ 254 mm span specimen indented to 930 N.

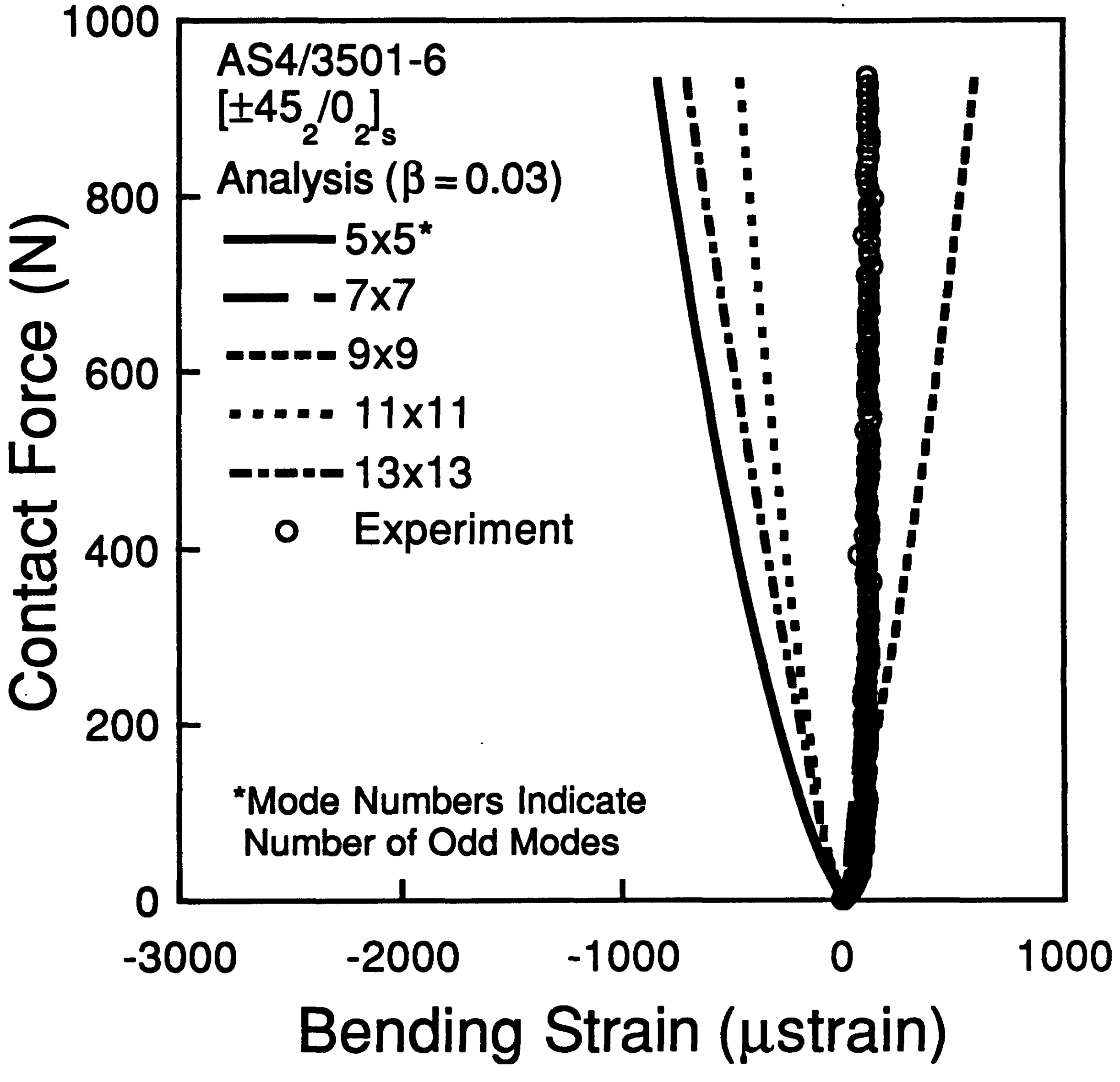

Figure 4.13 Convergence of force-bending strain curves for gage 4 (strain gage scheme A) for an AS4/3501-6 $[\pm45_2/0_2]_s$ 254 mm span specimen indented to 930 N.

Chapter 5

EXPERIMENTAL AND ANALYTICAL RESULTS

The experimental results include force-deflection, force-indentation, and force-strain data taken during indentation, and X-ray photographs and sectioning transcriptions made of the specimens after indentation to determine the damage state. The analytical results include force-deflection and force-strain data output from the program STATIC1.

5.1 Contact Behavior

The results which address the contact relation between the indentor and the specimen are contained in this section. These results are presented as force-indentation plots.

Representative force-indentation data taken during a test using the rigid backface support boundary condition are shown in Figures 5.1 and 5.2. These two force-indentation curves show the indentation response for the maximum contact forces of 549 N and 1479 N and include both the loading and unloading of the specimen. The maximum indentations seen for the maximum contact forces 549 N and 1479 N were approximately 0.10 mm and 0.18 mm, respectively. It should be noted that the maximum indentation seen, 0.18 mm, is approximately 11% of the average laminate thickness. The curves also show that as the maximum contact force was increased, the difference between the indentation for loading and unloading at a particular force level increased. No permanent indentation was indicated by the data or observed after the contact force was removed.

Force-indentation data from the tests using the clamped-clamped boundary condition for a 254 mm span are shown in Figures 5.3 and 5.4 for

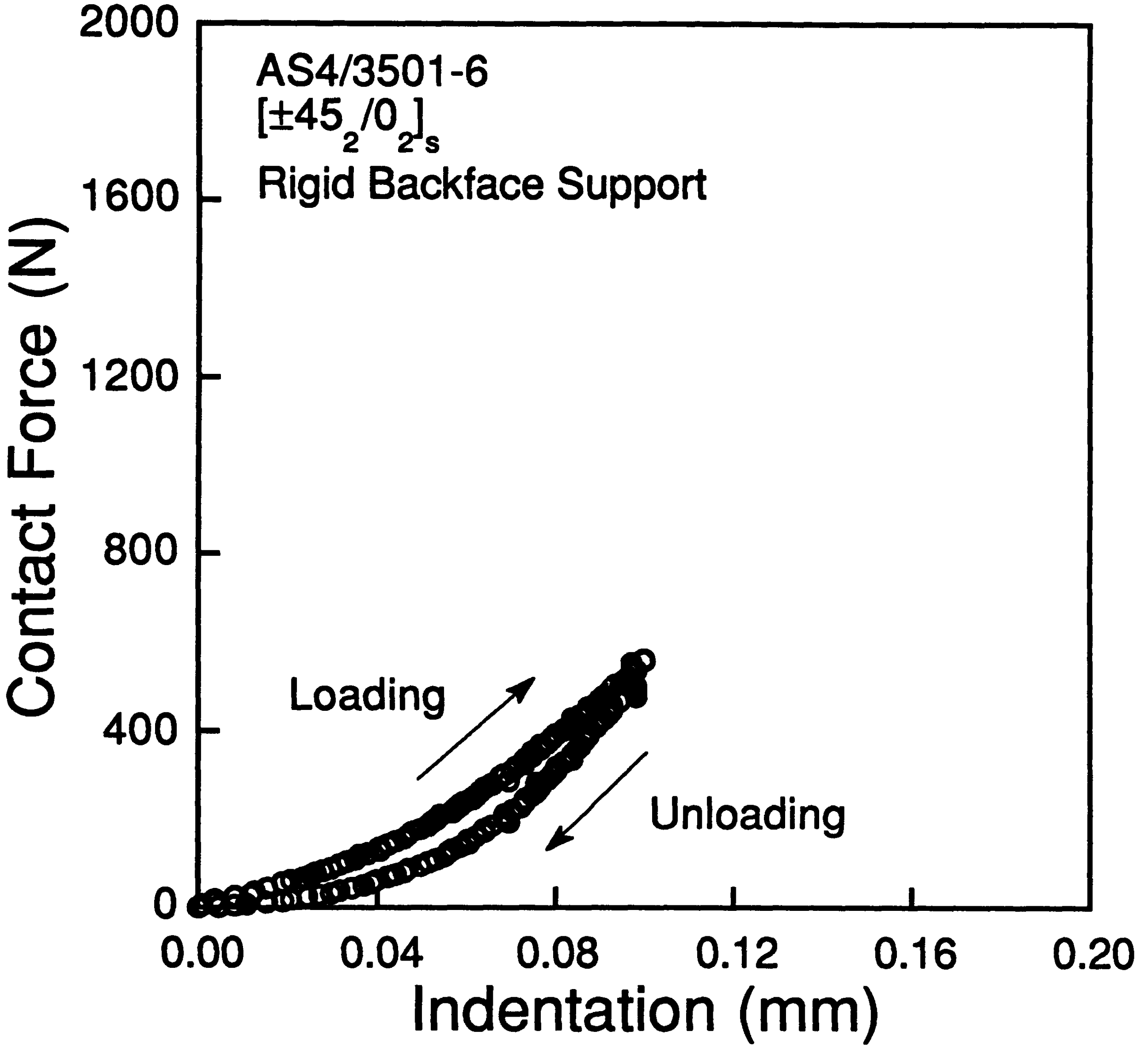

Figure 5.1 Force-indentation data for the specimen with a rigid backface support and loaded to a maximum contact force of 549 N.

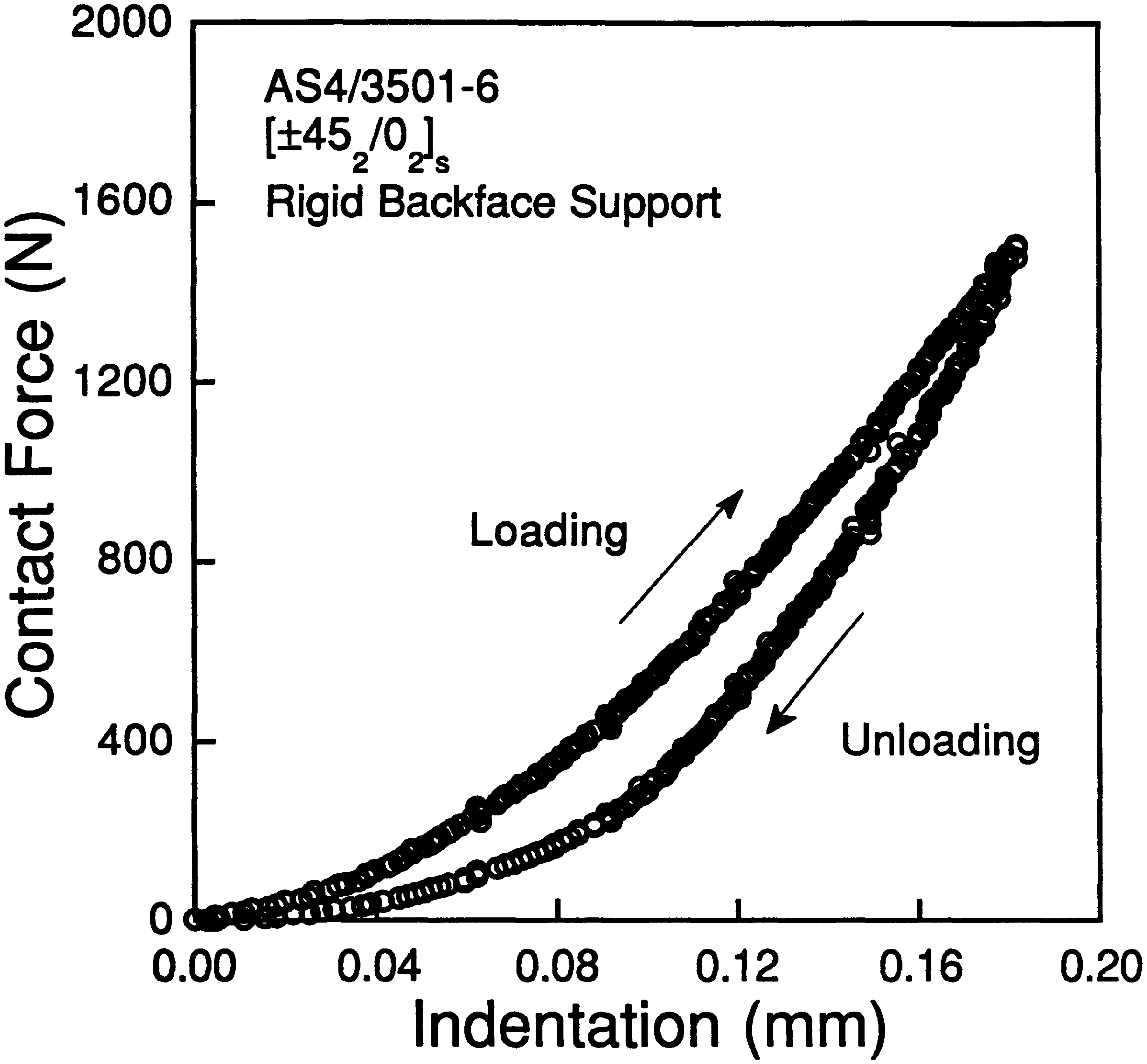

Figure 5.2 Force-indentation data for the specimen with a rigid backface support and loaded to a maximum contact force of 1479 N.

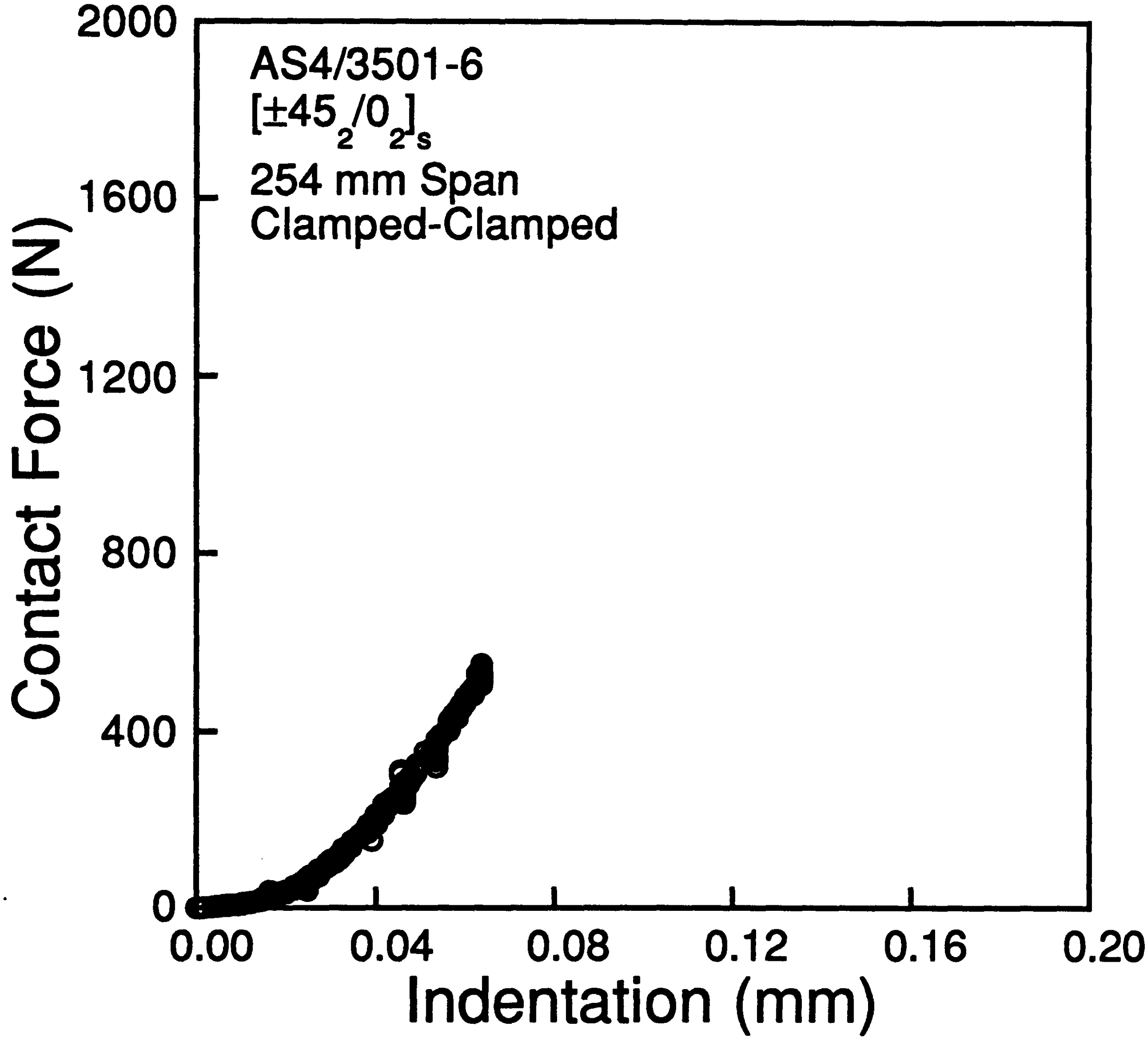

Figure 5.3 Force-indentation data for the specimen with a 254 mm span tested with a clamped-clamped support and loaded to a maximum contact force of 549 N.

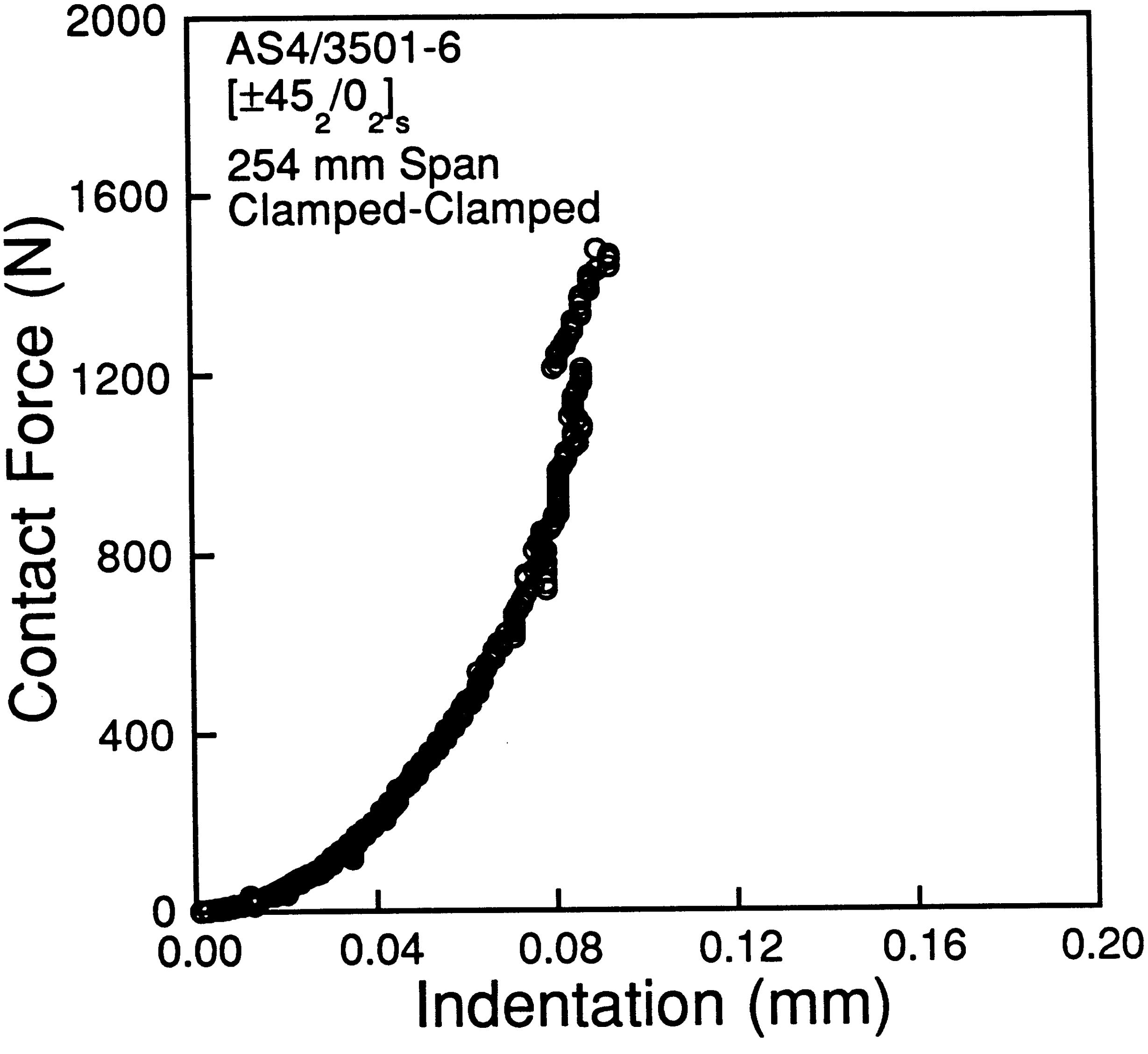

Figure 5.4 Force-indentation data for the specimen with a 254 mm span tested with a clamped-clamped support and loaded to a maximum contact force of 1479 N.

loading to maximum contact forces of 549 N and 1479 N. Similar force-indentation curves for the other maximum contact force levels tested are shown in Appendix B. The maximum indentations seen for the maximum contact forces 549 N and 1479 N are approximately 0.065 mm and 0.090 mm, respectively. The plot for the contact force 1479 N shows a discontinuity in the data at approximately 1200 N, possibly indicating that damage has occurred beneath the indentor. It should be noted that the indentation levels seen during these tests using the clamped-clamped boundary condition are consistently smaller by approximately half than the corresponding indentation during the rigid support tests.

The force-indentation data taken during a test to the maximum contact force of 930 N using the clamped-clamped boundary condition are shown in Figures 5.5 and 5.6. Two force-indentation curves are shown, one each for the spans of 31.75 mm and 508 mm. Variations in the force-indentation curves for the other spans tested are seen in the curves presented in Appendix B. This will be discussed in Chapter 6. The plots show indentation data for both loading and unloading of the specimen. The maximum indentations seen for the two spans shown were approximately 0.100 mm and 0.090 mm, respectively. Each of the plots shows a break in the data above 800 N, possibly indicating that damage has occurred beneath the indentor.

The force-indentation data was fit to the power relation:

$$F = k\alpha^{n} \tag{5.1}$$

to see how the data compared to Hertzian contact theory, where n equals 1.5 (as discussed in section 2.2), and to provide a basis for comparison for the data taken. Taking the logarithm of both sides of this equation gives:

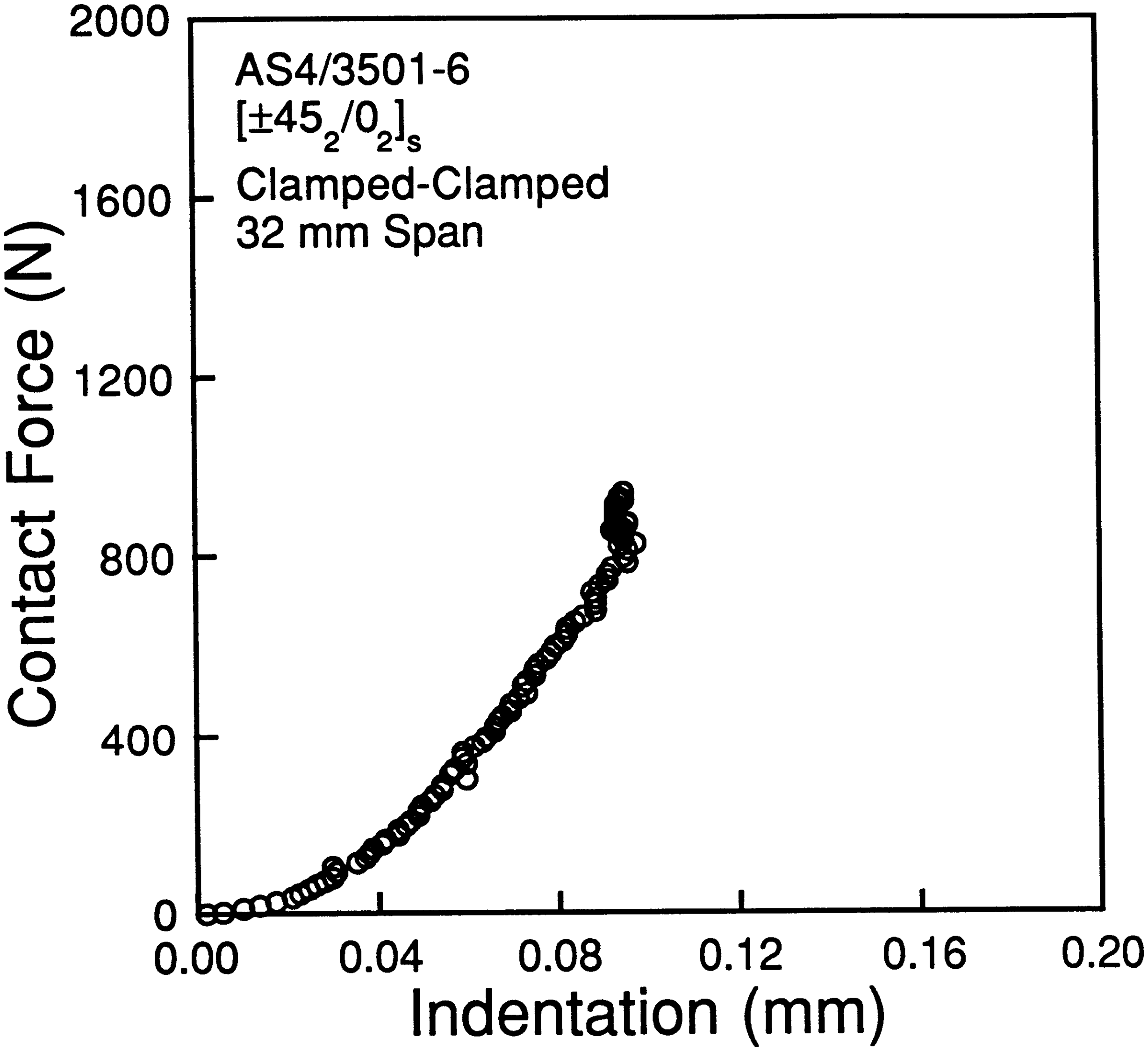

Figure 5.5 Force-indentation data for the specimen with a 32 mm span tested with a clamped-clamped support and loaded to a maximum contact force of 930 N.

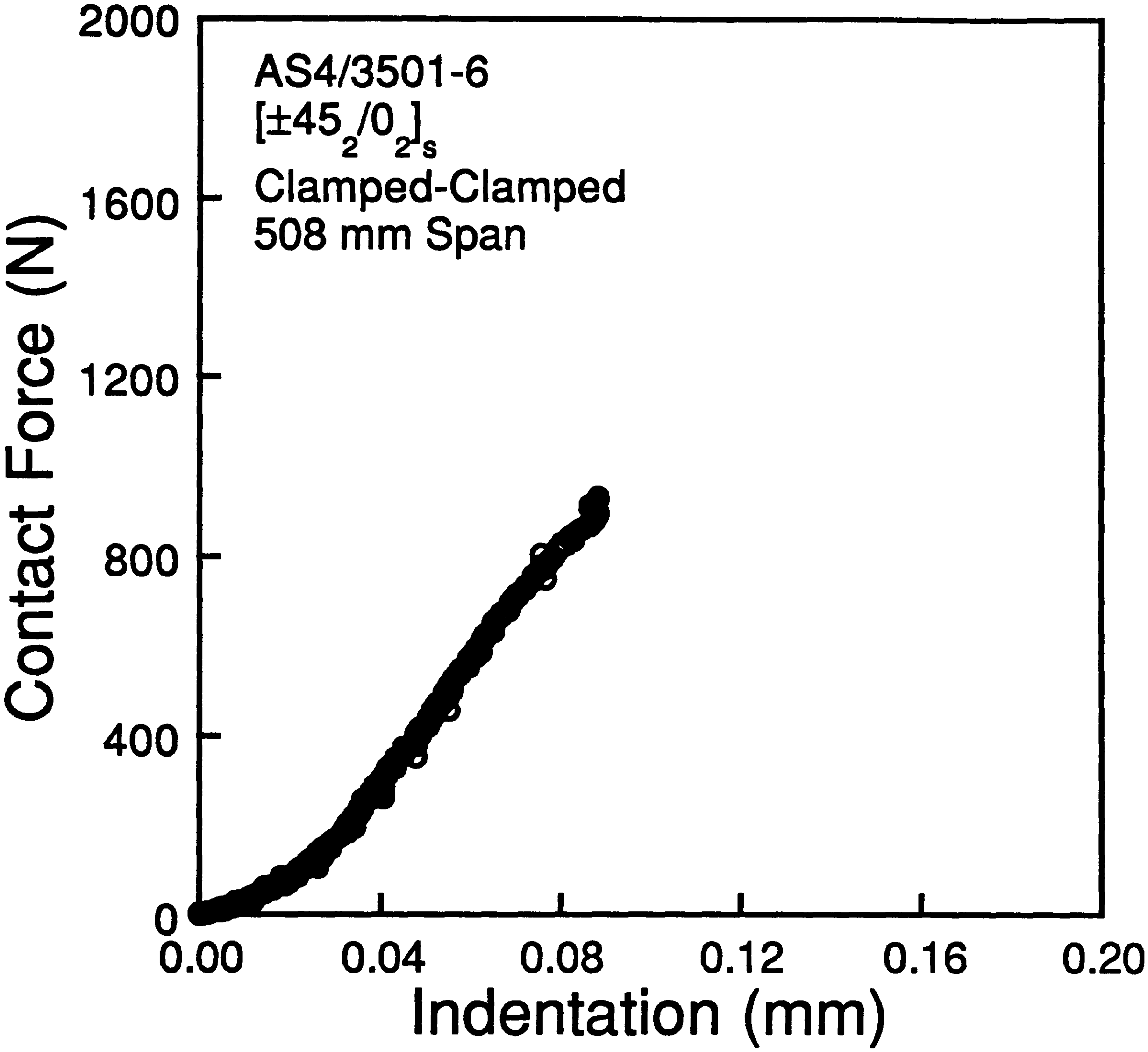

Figure 5.6 Force-indentation data for the specimen with a 508 mm span tested with a clamped-clamped support and loaded to a maximum contact force of 930 N.

$$log(\mathrm{F}) = log(\mathrm{k}) + \mathrm{n}\,log(\alpha) \qquad (5.2)$$

which is a straight line with a slope n and a $log(\mathrm{F})$ axis intercept of $log(\mathrm{k})$. By plotting the logarithm of the force data versus the logarithm of the indentation data, a linear regression can be done on the data. A line was fit through the data using the least squares method, yielding the slope and y-axis intercept of the line. The slope is the exponent n and the y-axis intercept of the line gives $log(\mathrm{k})$, from which the constant k is found. The correlation factor, R^2, was also determined for each log-log curve fit. This correlation factor indicates that the curve fit matches the data well when it has a value close to 1.0. An example of a log-log plot for the force-indentation data of Figure 5.1 is shown in Figure 5.7. The same log-log data was also fit to equation (5.2) while constraining n to the value of 1.5 used in Hertzian contact theory. Using this constrained curve fit, the values of k and the correlation factor, R^2, were determined from the data.

The value of the maximum indentation (α), n and R^2, and k, from the unconstrained curve fit for each maximum contact force and boundary condition and span are listed in Tables 5.1, 5.2, and 5.3, respectively. The maximum indentation obviously increases with the maximum contact force for both support conditions, but it should be again noted that the maximum indentation for the rigid backface support tests is consistently greater than the corresponding value for the clamped-clamped support condition. The maximum indentation values vary somewhat with span, but, if the high value for the 63.5 mm span is excluded, these values could be considered to be the same within the range of experimental error. The values of n for the rigid backface support boundary condition are

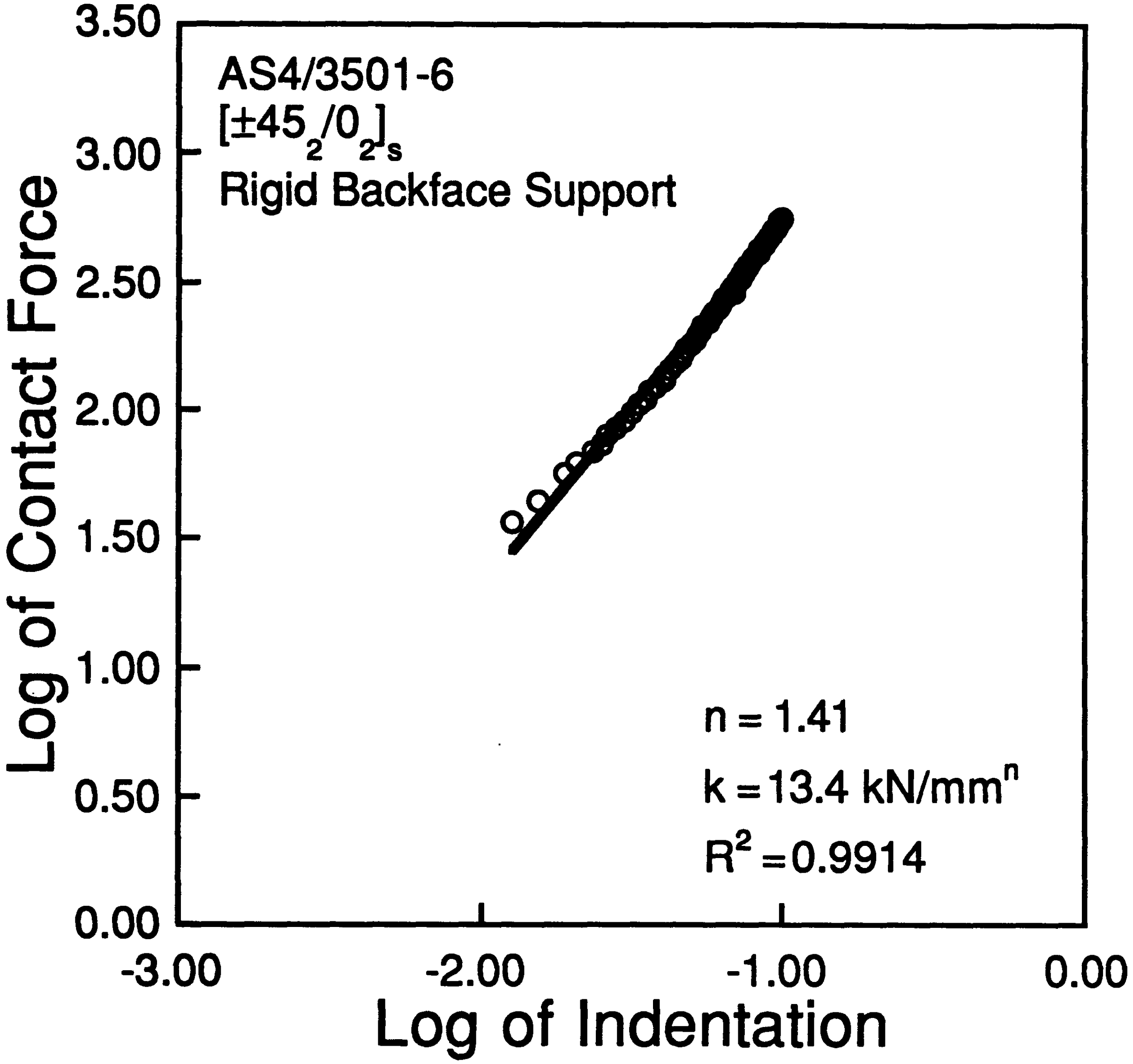

Figure 5.7 Log-log plot of force-indentation data from the test with a rigid backface support and loaded to a maximum contact force of 549 N.

Table 5.1 Table of values of the maximum indentation[a], α, for the unconstrained curve fit.

Maximum	Rigid	Span Length, mm					
Force, N	Support	32	63.5	127	254	381	508
444	0.100				0.052		
507					0.047		
549	0.100				0.064		
739					0.073		
930					0.085		
930	0.141	0.094	0.120	0.083	0.076	0.092	0.088
1183					0.083		
1479	0.181				0.092		

[a] All values in mm

Table 5.2 Table of values of the exponent, n, and the correlation factor[a], R^2, for the unconstrained curve fit.

Maximum Force, N	Rigid Support	Span Length, mm					
		32	63.5	127	254	381	508
444	1.92 (0.994)[a]				2.40 (0.939)		
507					1.88 (0.936)		
549	1.41 (0.991)				2.23 (0.993)		
739					1.55 (0.991)		
930					1.89 (0.997)		
930	1.71 (0.996)	1.97 (0.997)	1.96 (0.994)	1.74 (0.992)	1.72 (0.997)	1.87 (0.997)	1.67 (0.995)
1183					1.92 (0.988)		
1479	1.66 (0.997)				2.01 (0.986)		

[a] Values in parentheses are correlation factors.

Table 5.3 Table of values of the contact stiffness[a], k, for the unconstrained curve fit.

Maximum Force, N	Rigid Support	Span Length, mm					
		32	63.5	127	254	381	508
444	34.3				407		
507					152		
549	13.4				260		
739					43.8		
930					84.0		
930	27.1	87.8	60.0	70.3	74.4	72.0	61.0
1183					107		
1479	25.1				146		

[a] All values in kN/mm^n.

consistently smaller than the corresponding values for the clamped-clamped support condition. The values of n and k vary greatly in some cases for increasing maximum contact force or for increasing span length. However, it is felt that they remain constant within the range of experimental error. The correlation factors shown in Table 5.2 indicate that the least squares curve fits appear to correspond well with the log-log data. Note that the dimensions of k are [Force/Length^n], so that the value of n varies the dimensions of k. This fact makes comparing values of k for specimens which show different values of n of questionable benefit.

The values of k and R^2 from the constrained curve fit for each maximum contact force and boundary condition and span are listed in Table 5.4. The values of k are consistently smaller for the rigid support tests. However, the values of k do not follow any obvious relationship with the span or maximum contact force. The correlation factors indicate that the rigid support tests fit the Hertzian contact theory, where n is equal to 1.5, better than the clamped-clamped boundary condition tests. Obviously, since the unconstrained fit uses two parameters and the constrained fit uses one parameter, the tests show generally poorer correlation for the constrained curve fit than for the unconstrained curve fit. However, this does not necessarily mean that the value of n equal to 1.5 is invalid, especially for the rigid support case.

5.2 Bending Behavior

The results of the experimental and analytical investigation into the bending behavior of the specimens are contained in this section. The experimental results are presented as force-deflection plots made from data obtained from the testing machine stroke (as discussed in Chapter 3, this

Table 5.4 Table of values of the contact stiffness[a], k, and the correlation factor[b], R^2, for the constrained curve fit.

Maximum Force, N	Rigid Support	Span Length, mm					
		32	63.5	127	254	381	508
444	10.6 (0.947)[b]				34.4 (0.987)		
507					39.8 (0.898)		
549	17.5 (0.987)				24.1 (0.886)		
739					34.7 (0.977)		
930					23.1 (0.955)		
930	15.5 (0.980)	23.6 (0.941)	17.2 (0.939)	32.2 (0.972)	35.2 (0.980)	22.6 (0.959)	34.8 (0.985)
1183					25.2 (0.966)		
1479	17.1 (0.987)				30.4 (0.909)		

[a] All values in kN/mm^n.

[b] Values in parentheses are correlation factors.

data was only taken for the tests using specimens with a 254 mm span that were not strain gaged) and force-strain plots from data obtained from the strain gages (refer to the illustrations shown in Figures 3.2 and 3.3 for the positions of these gages). The analytical results using 9 by 9 odd modes and a β-factor of 0.030, as determined in Chapter 4 to best fit the experimental data, are presented with the force-deflection and force-strain plots to compare the results.

5.2.1 Force-Deflection

The force-deflection data taken during a test using the clamped-clamped boundary condition on a specimen with a 254 mm span loaded to the maximum contact force of 1479 N is shown in Figure 5.8. Force-deflection curves for the other maximum contact force levels tested are shown in Appendix B. When overplotted, the force-deflection data in Figure 5.8 and Appendix B shows this behavior to be consistent from specimen to specimen. The maximum deflections seen in these tests are compiled in Table 5.5.

It should be noted that the largest deflection observed, 23.0 mm, is approximately fourteen times the average laminate thickness Deflections of this magnitude, relative to the laminate thickness of 1.60 mm, constitute "large deflection" behavior [27]. A characteristic of this type of behavior is nonlinear force-deflection curves, as seen in Figure 5.8. The deflection starts off linear in a region below a contact force of approximately 100 N, but becomes nonlinear after that as the plate shows a stiffening behavior. This stiffening effect during large deflections is termed "membrane stiffening" because the geometry of the plate under large deflection bending causes

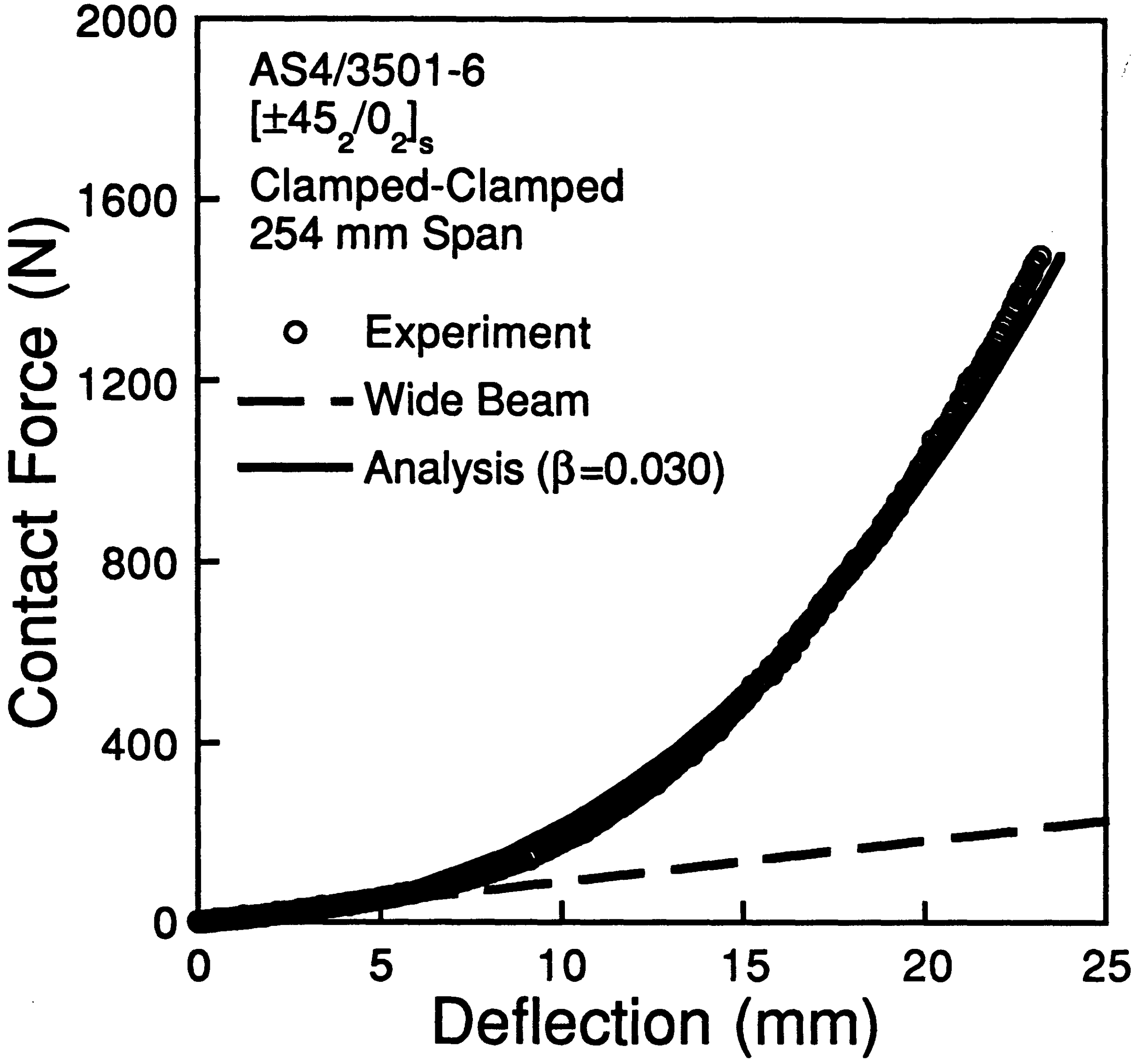

Figure 5.8 Experimental and analytical force-deflection results for a 254 mm specimen loaded to a maximum contact force of 1479 N using a clamped-clamped boundary condition.

Table 5.5 Table of the maximum deflections of a specimen with a 254 mm span for various maximum contact forces.

Maximum Force, N	Maximum Deflection, mm
444	13.7
507	14.2
549	15.4
739	17.2
930	19.2
1183	20.8
1479	23.2

forces acting in the plane of the plate, or membrane forces, to become non-negligible.

Force-deflection results from the wide beam and the nonlinear plate analyses for the case of a maximum contact force of 1479 N are also shown in Figure 5.8. Analytical force-deflection curves for the other maximum contact force levels tested are shown in Appendix B. The small deflection portion of the force-deflection data in Figure 5.8 is well predicted by the wide beam analysis. Since this is a linear analysis, it does not account for the membrane stiffening effect and it is not expected to predict large deflections. The important issue with this analysis is that it shows that the nonlinear analysis matches a simple, known analysis for small deflections.

The nonlinear analysis curve in Figure 5.8 matches the experimental force-deflection data well. The geometrical nonlinearity factor β, which is discussed in section 4.5, is used to model the unknown flexibility of the boundary conditions. A value of 0.030 was found to best match the experimental data. Nine by nine odd modes were used because the analysis was converged at that number of modes (see Chapter 4). The good agreement between this analysis and the experimental data points to the fact that including the geometrical nonlinearity accounting for the membrane stiffening effect is important to correctly model the large deflection bending effects during a static indentation event.

5.2.2 Force-Strain

The force-strain data taken during a test using the clamped-clamped boundary condition on a specimen with a 254 mm span loaded to a maximum contact force of 930 N are shown in Figures 5.9, 5.10, and 5.11. These plots show strain data for loading of the specimen only. The strain

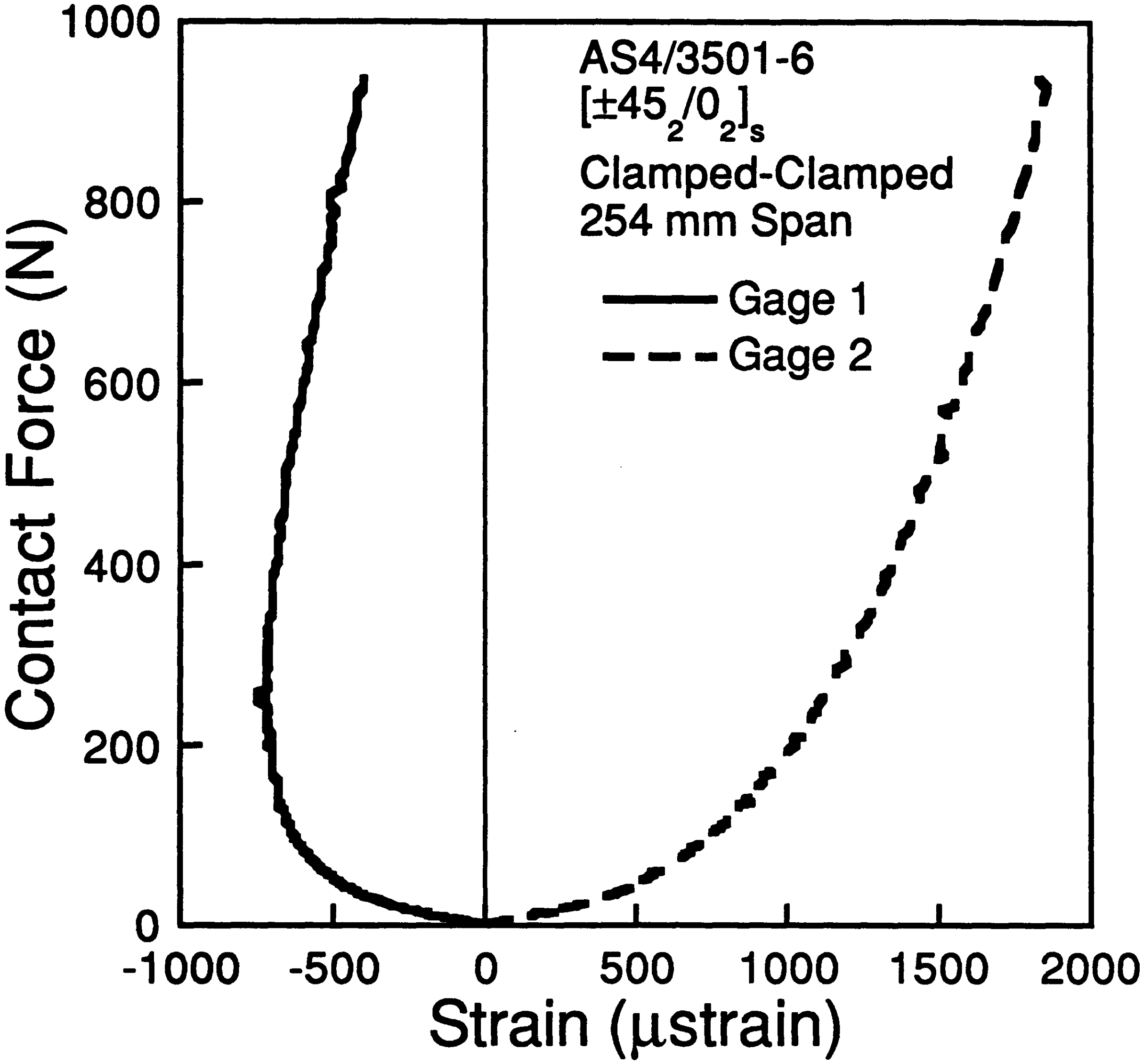

Figure 5.9 Force-strain data from gages 1 and 2 (see Figure 3.2) for the specimen with a 254 mm span in a clamped-clamped support and tested to a maximum contact force of 930 N.

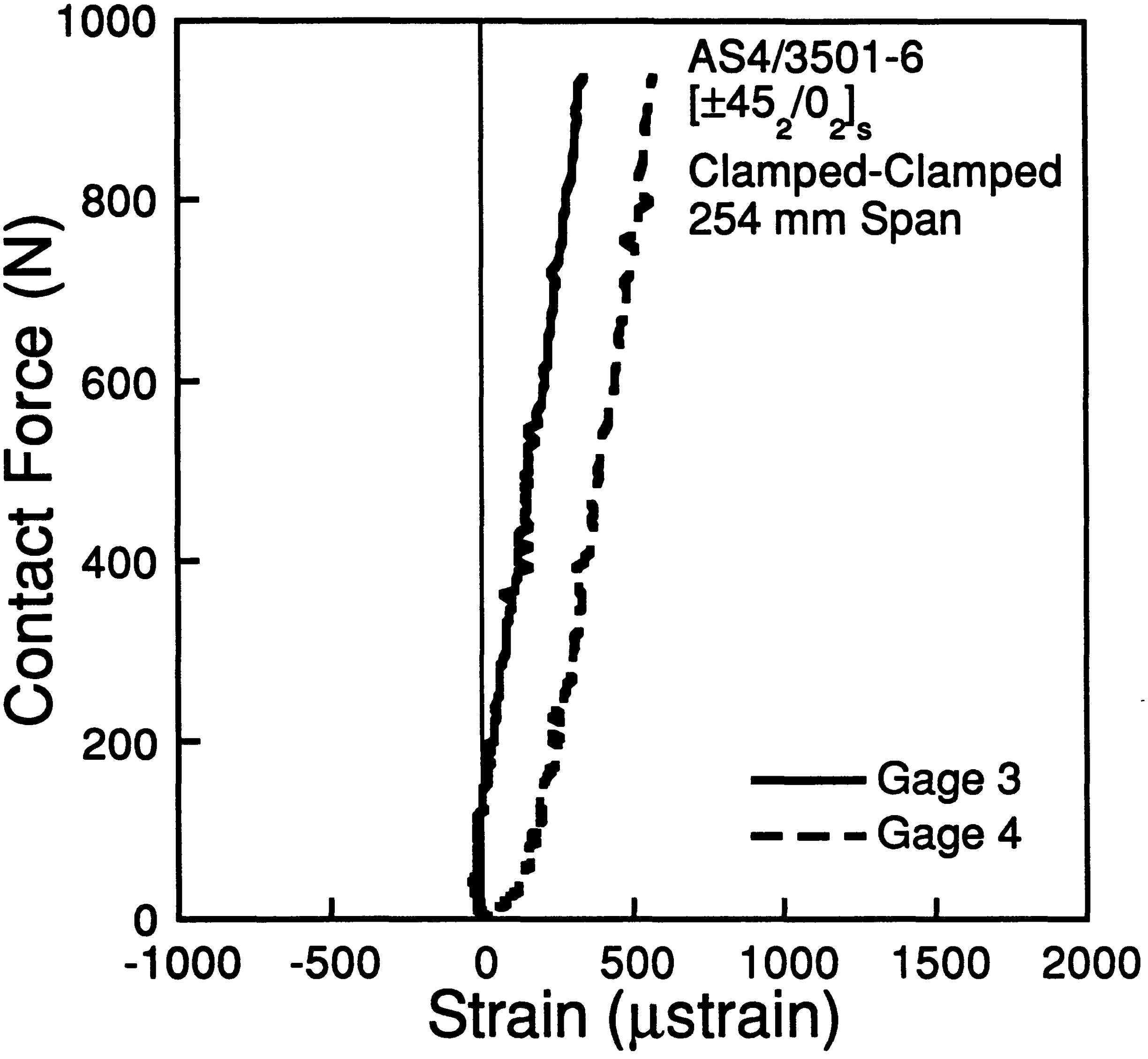

Figure 5.10 Force-strain data from gages 3 and 4 (see Figure 3.2) for the specimen with a 254 mm span in a clamped-clamped support and tested to a maximum contact force of 930 N.

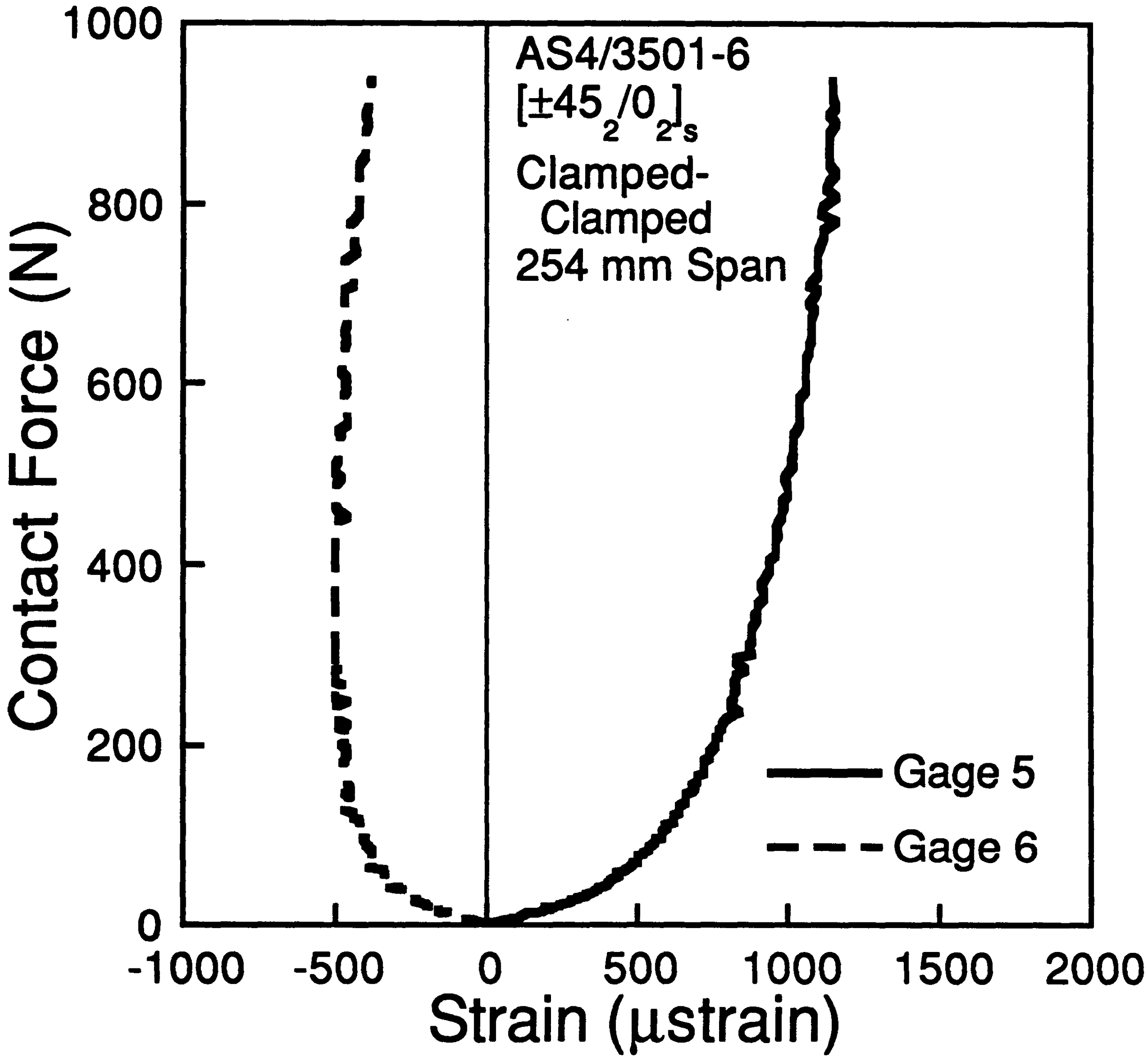

Figure 5.11 Force-strain data from gages 5 and 6 (see Figure 3.2) for the specimen with a 254 mm span in a clamped-clamped support and tested to a maximum contact force of 930 N.

data for this test was collected at the locations shown in Figure 3.2. These specimens were gaged to define the distribution of the strain along the span of the specimen. Figures 5.9 and 5.11 show strain data for the gages nearer the contact point and the clamped boundary, respectively. Note that the strains registered on the top and bottom faces reverse sign between these two points on the plate, indicating the change in curvature of the plate. Also note that the strain data shown in Figure 5.10 are of a much smaller magnitude than the data shown in the other two figures. This is because the gages recording this data were very near the inflection point on the plate where the curvature of the plate changes. At this point, the curvature of the plate would be zero. In these figures, it is clear that the strains on the top and bottom face of the laminate are not symmetric about zero, as one would expect for a case of pure bending. From this result, it is immediately obvious that there is a nonzero strain acting at the midplane of the laminate, making it necessary to look at the two components of the strain on the laminate - extension and bending, as is done later.

The force-strain data taken during a test using the clamped-clamped boundary condition for a 254 mm span loaded to a maximum contact force of 1479 N are shown in Figures 5.12, 5.13, 5.14, and 5.15. The strain data for this test was collected at the locations shown in Figure 3.3. These plots show strain data for loading of the specimen only. The major difference between these tests and those examined in the previous case was the location of the strain gages. These specimens were gaged to examine the possibility of wrapping around the indentor and the effect of the boundary condition on the strain at the end of the plate. The data for the gages near the clamped boundary, given in Figure 5.12, shows slight nonsymmetry about zero, indicating only small extensional strains acting at this point.

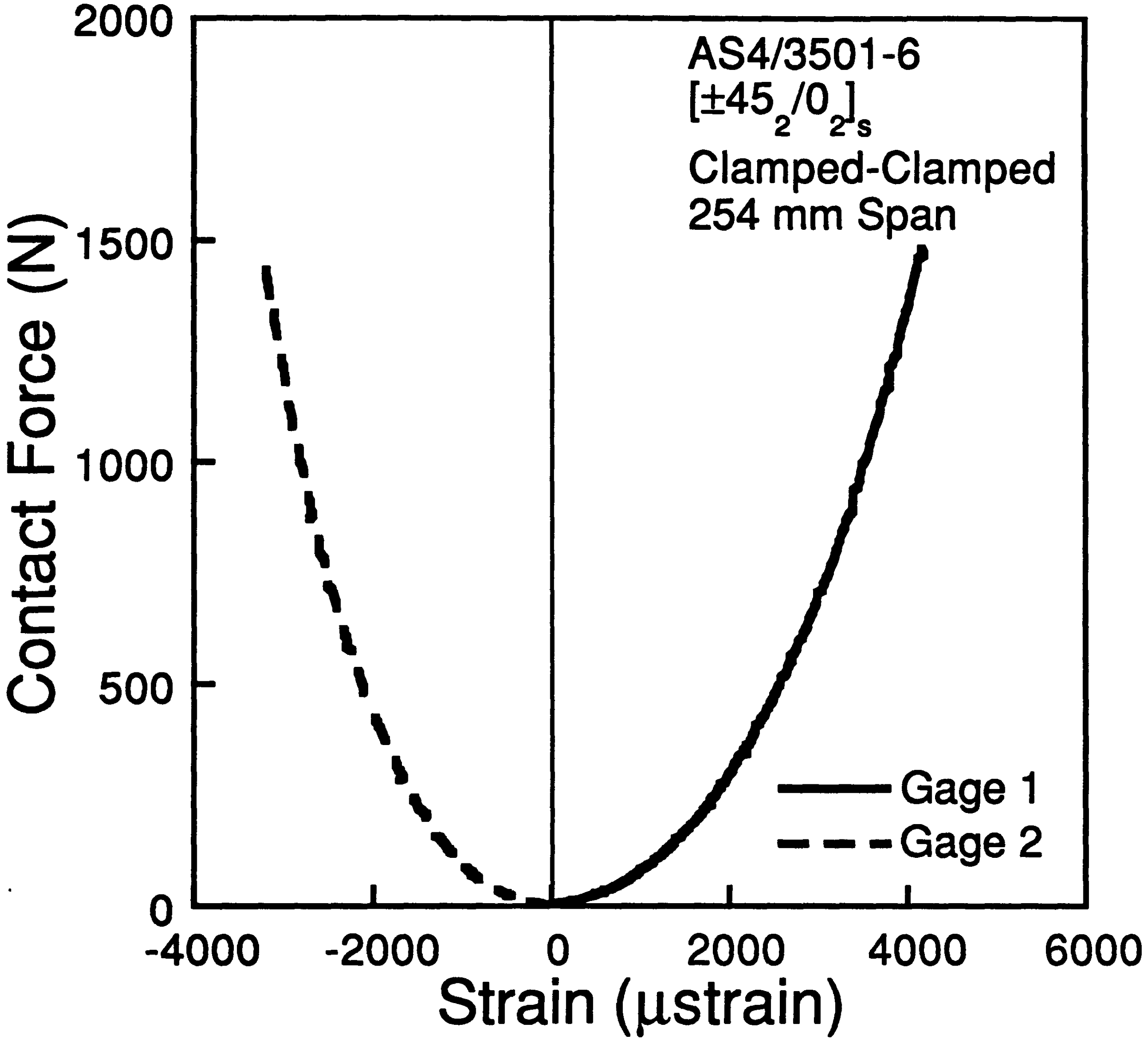

Figure 5.12 Force-strain data from gages 1 and 2 (see Figure 3.3) for the specimen with a 254 mm span in a clamped-clamped support and tested to a maximum contact force of 1479 N.

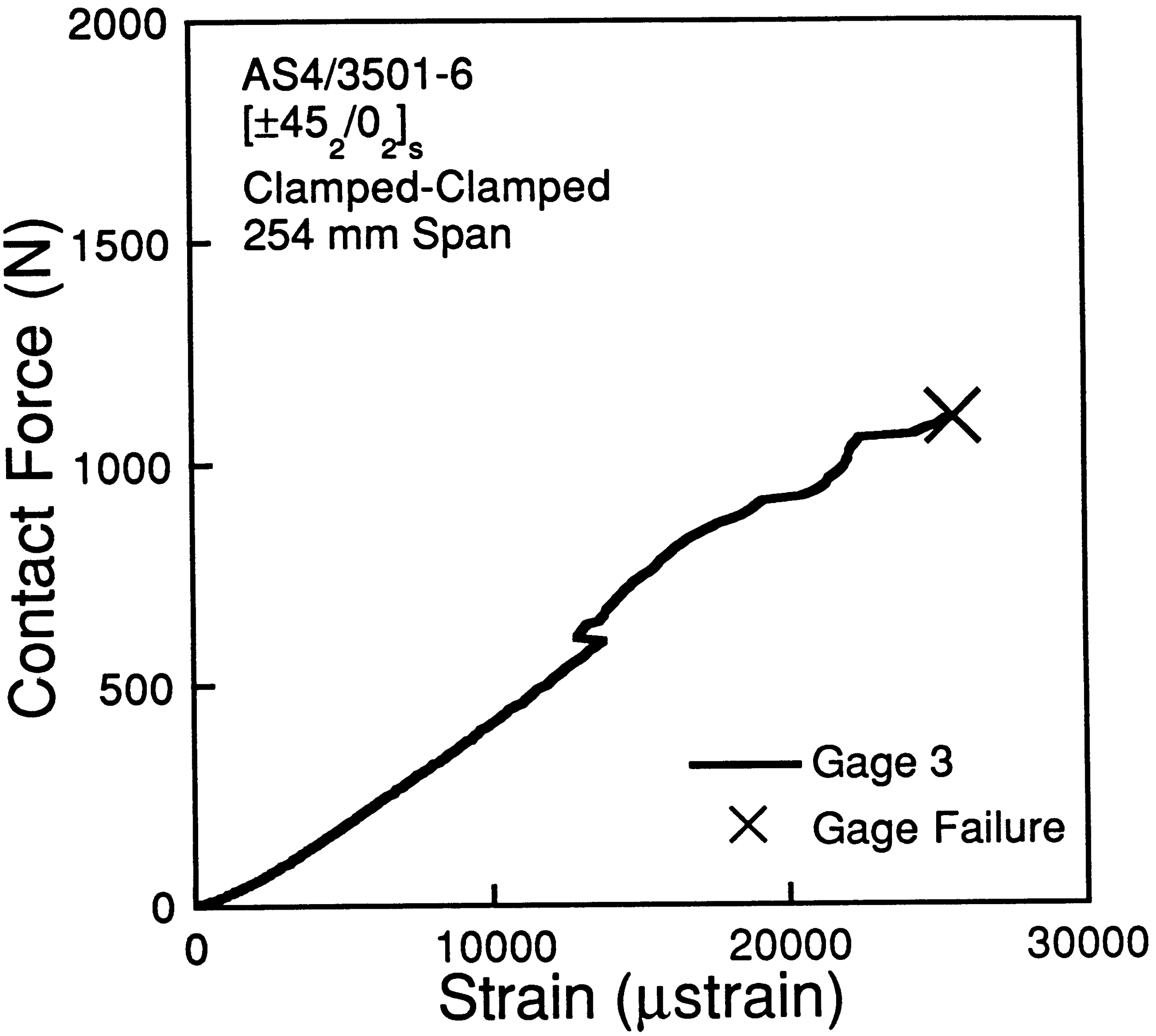

Figure 5.13 Force-strain data from gage 3 (see Figure 3.3) for the specimen with a 254 mm span in a clamped-clamped support and tested to a maximum contact force of 1479 N.

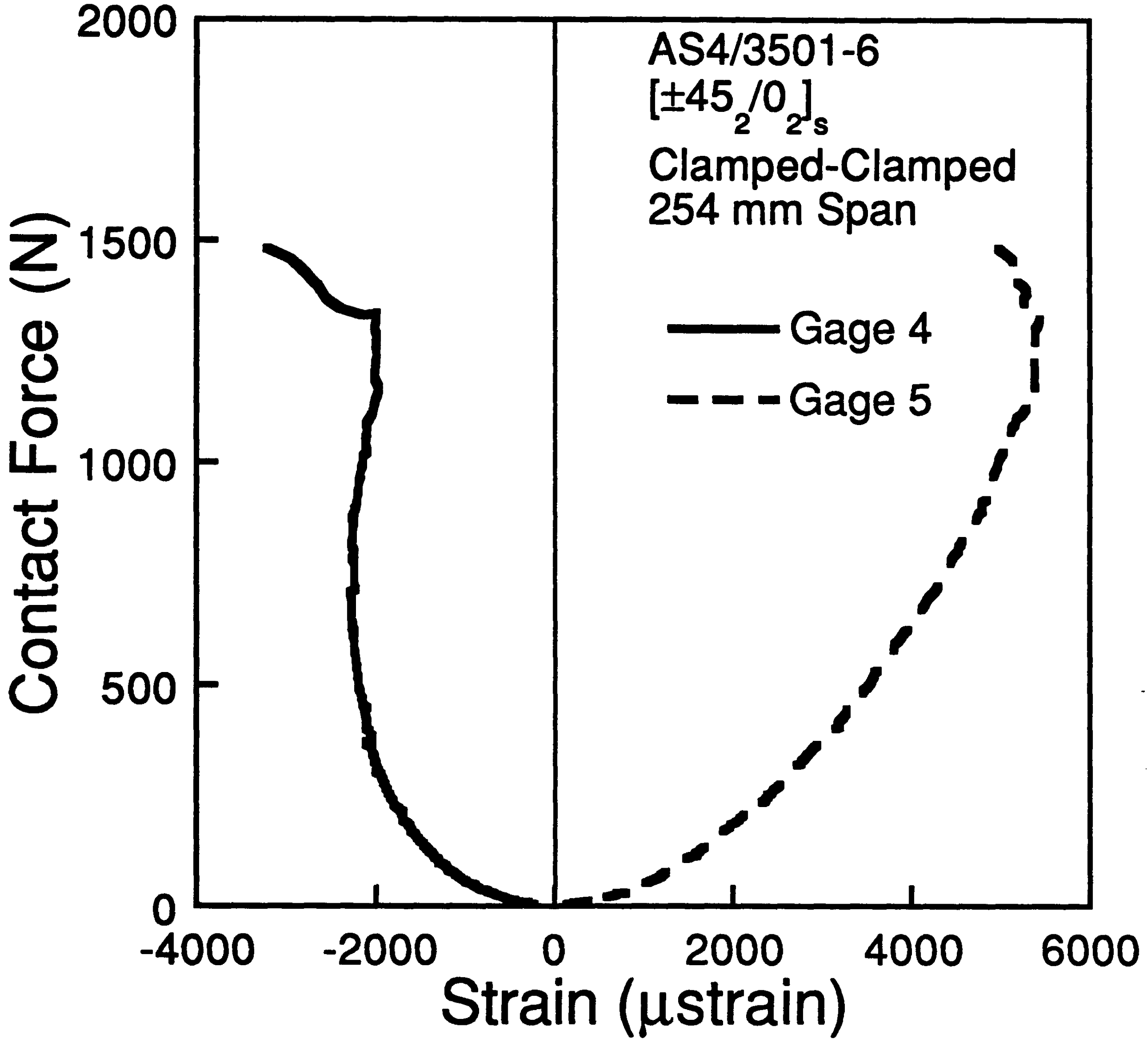

Figure 5.14 Force-strain data from gages 4 and 5 (see Figure 3.3) for the specimen with a 254 mm span in a clamped-clamped support and tested to a maximum contact force of 1479 N.

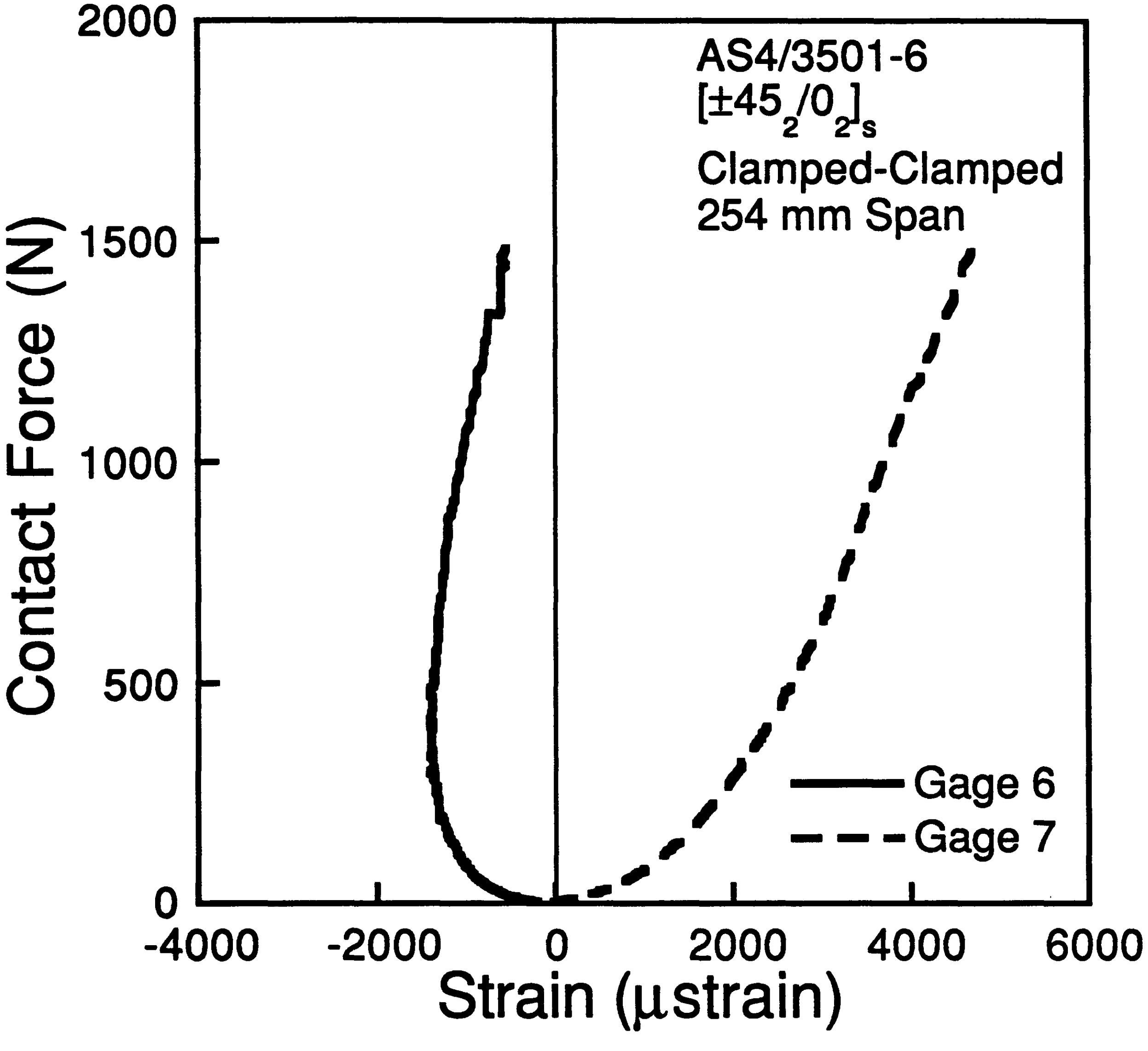

Figure 5.15 Force-strain data from gages 6 and 7 (see Figure 3.3) for the specimen with a 254 mm span in a clamped-clamped support and tested to a maximum contact force of 1479 N.

The data for the gage directly opposite the contact point, given in Figure 5.13, shows smooth behavior until approximately 600 N where there is a break in the data which may indicate that damage is occurring. It should be noted that the data at this location for the other spans tested showed breaks in the data at approximately the same force level: 450 to 600 N. It should also be noted that a "cracking noise" was audible during the tests for each of the specimens when the load reached approximately 450 to 500 N. The data for the gages near the contact point are shown in Figures 5.14 and 5.15. The gages nearer the contact point (gages 4 and 5) show larger strain magnitudes than the gages farther away. These gages nearer the contact point also show a sharp change in the strain behavior at approximately 1300 N which could indicate damage. In these figures it is again clear that the strains on the top and bottom face of the laminate are not symmetric about zero. This result shows that there is a nonzero strain acting at the midplane of the laminate, making it necessary to look at the two components of the strain on the laminate - extension and bending.

The force-strain data was reduced into its components, extensional and bending strain, by using the following equations. The midplane or extensional strain is given by,

$$\varepsilon^o = \frac{\varepsilon_u + \varepsilon_l}{2} \tag{5.3}$$

and the bending strain at a point on the lower surface of the specimen is given by:

$$z_l \kappa = \frac{\varepsilon_l - \varepsilon_u}{2} \tag{5.4}$$

where ε_u and ε_l are the strains on the upper and lower faces† (respectively) at a point along the longitudinal centerline of the laminate and z_l is the through-the-thickness coordinate of the lower face of the laminate. Similarly, the bending strain at a point on the upper surface of the specimen is given by:

$$z_u \kappa = \frac{\varepsilon_u - \varepsilon_l}{2} \tag{5.5}$$

where z_u is the through-the-thickness coordinate of the upper face of the laminate. The extensional strain at the three gage positions from gage scheme A (shown in Figure 3.2) are shown in Figures 5.16 through 5.21 for the various spans tested to a maximum contact load of 930 N. The bending strain on the bottom face at the same gage positions from scheme A are shown in Figures 5.22 through 5.27 for the same cases. Similarly, the extensional strain at the three positions from gage scheme B (shown in Figure 3.3) are shown in Figures 5.28 through 5.33 for the various spans tested to a maximum contact load of 1479 N, while the bending strain on the bottom face at the same gage positions from scheme B are shown in Figures 5.34 through 5.39 for the same cases.

Referring to the graphs for the specimens loaded to 930 N, there are some points which are immediately obvious. The extensional strain changes character as span increases, appearing nonlinear with force for the smaller spans (32 and 63.5 mm) and linear with force, except at very low contact force levels, for the other spans. The maximum extensional strain at each position is listed in Table 5.6. Note that, as discussed in Chapter 3, gages 1 and 2 were omitted from the specimens with a 32 mm

---

† The upper face is the side which the indentor contacts and the lower face is the side opposite the upper face.

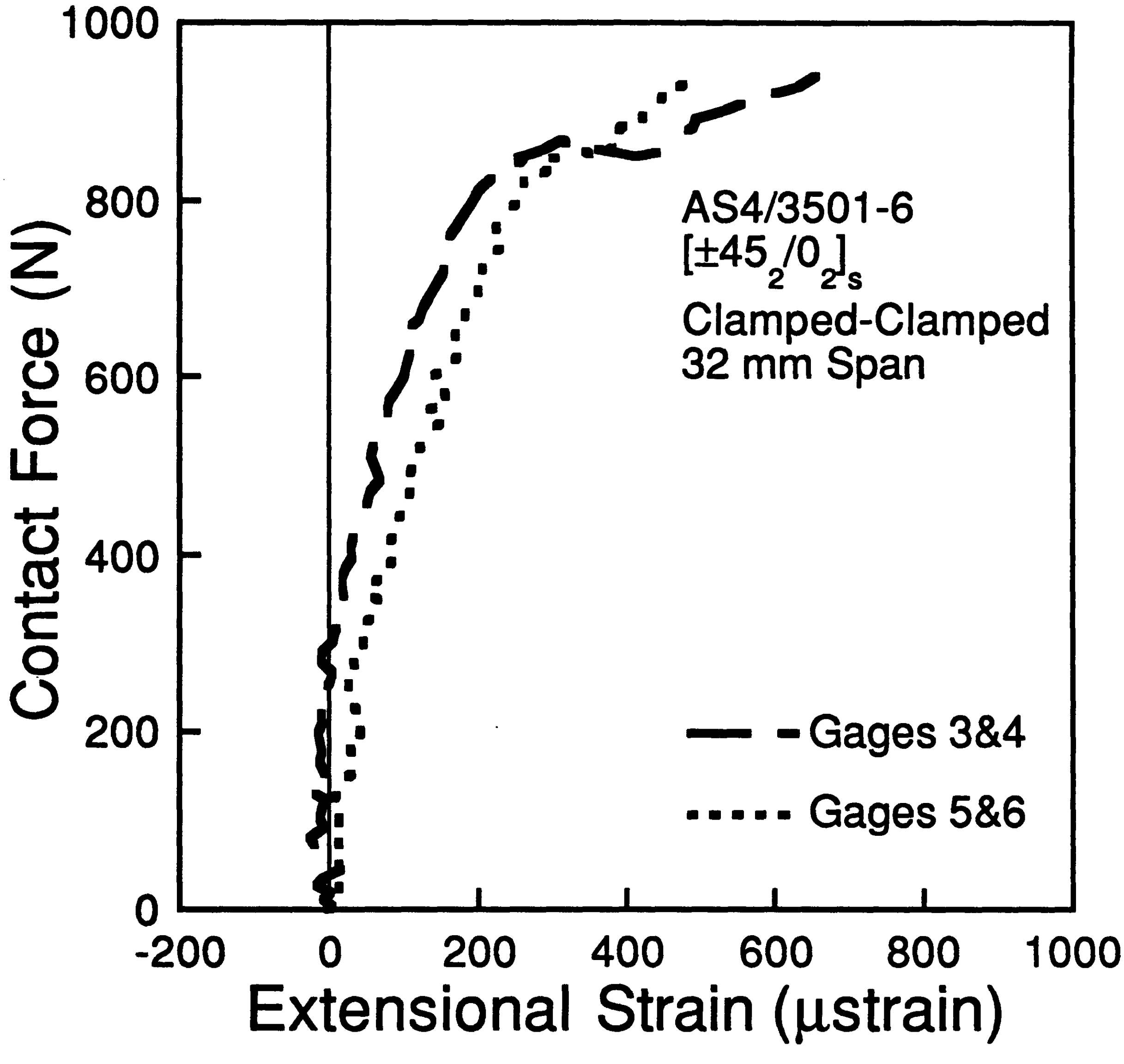

Figure 5.16 Force-extensional strain data for the specimen with a 32 mm span in a clamped-clamped support and tested to a maximum contact force of 930 N. (See Figure 3.2 for gage locations. Note that there is no gage 1 or 2 for the 32 mm configuration.)

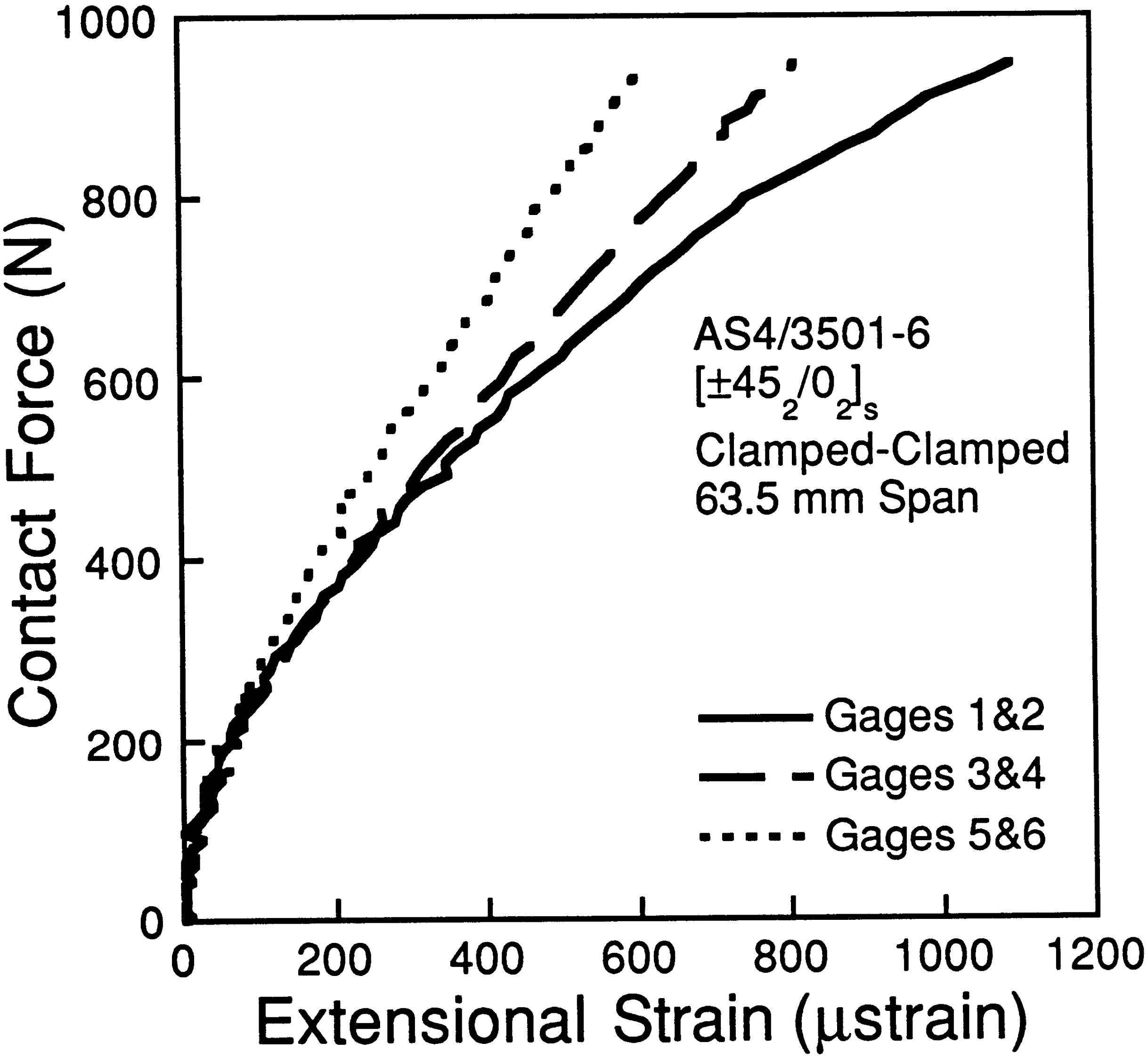

Figure 5.17 Force-extensional strain data for the specimen with a 63.5 mm span in a clamped-clamped support and tested to a maximum contact force of 930 N. (See Figure 3.2 for gage locations.)

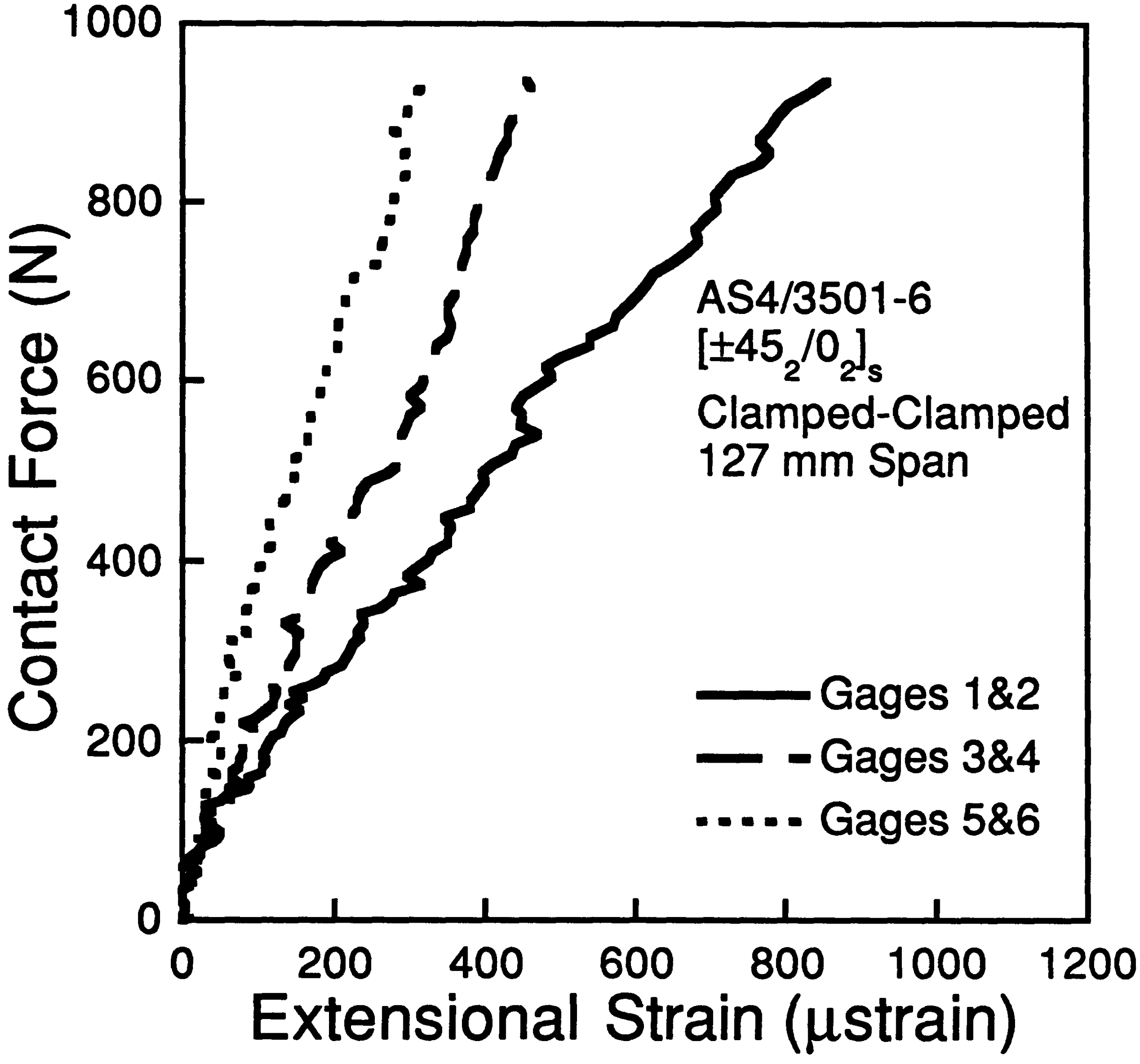

Figure 5.18 Force-extensional strain data for the specimen with a 127 mm span in a clamped-clamped support and tested to a maximum contact force of 930 N. (See Figure 3.2 for gage locations.)

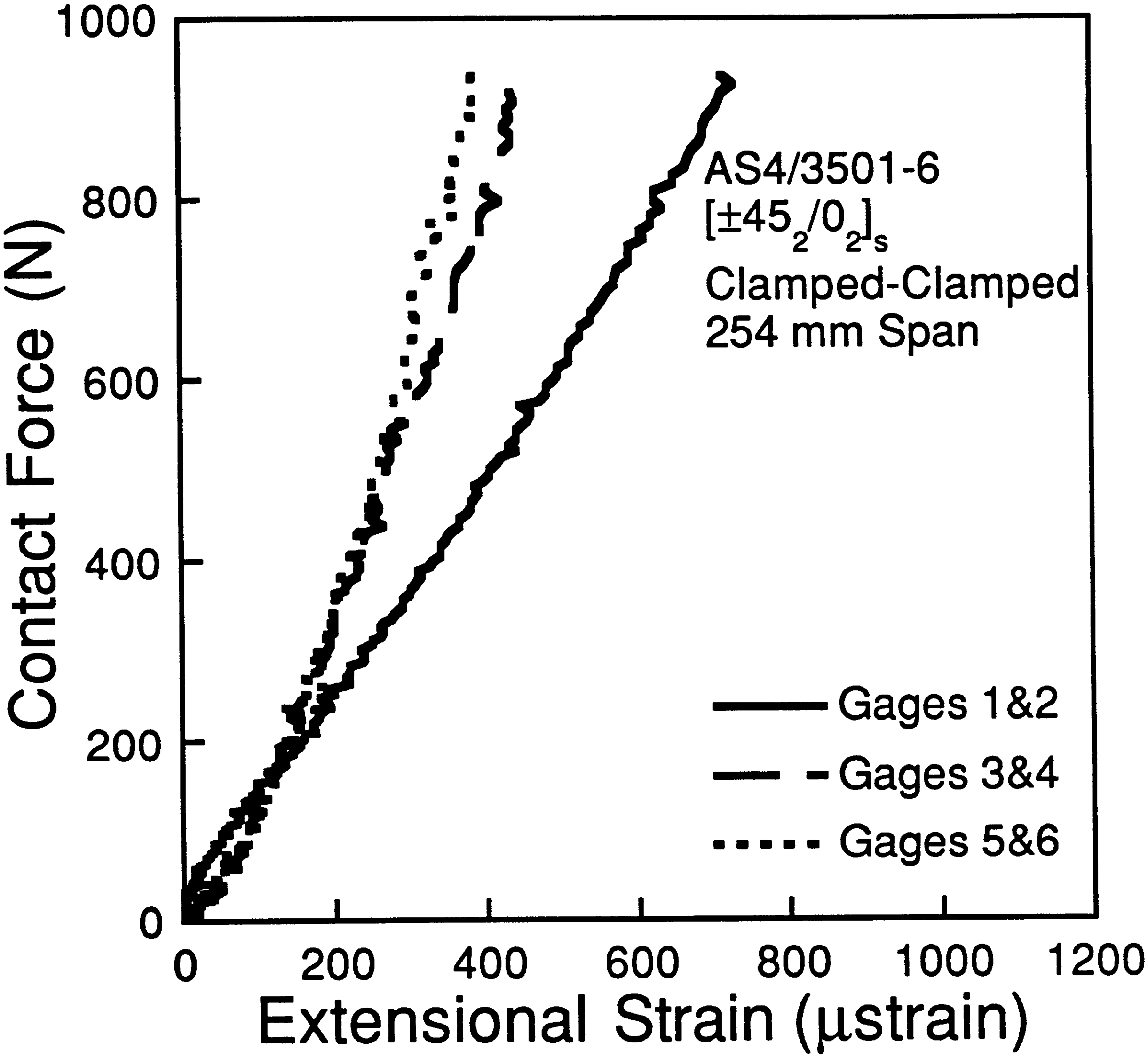

Figure 5.19 Force-extensional strain data for the specimen with a 254 mm span in a clamped-clamped support and tested to a maximum contact force of 930 N. (See Figure 3.2 for gage locations.)

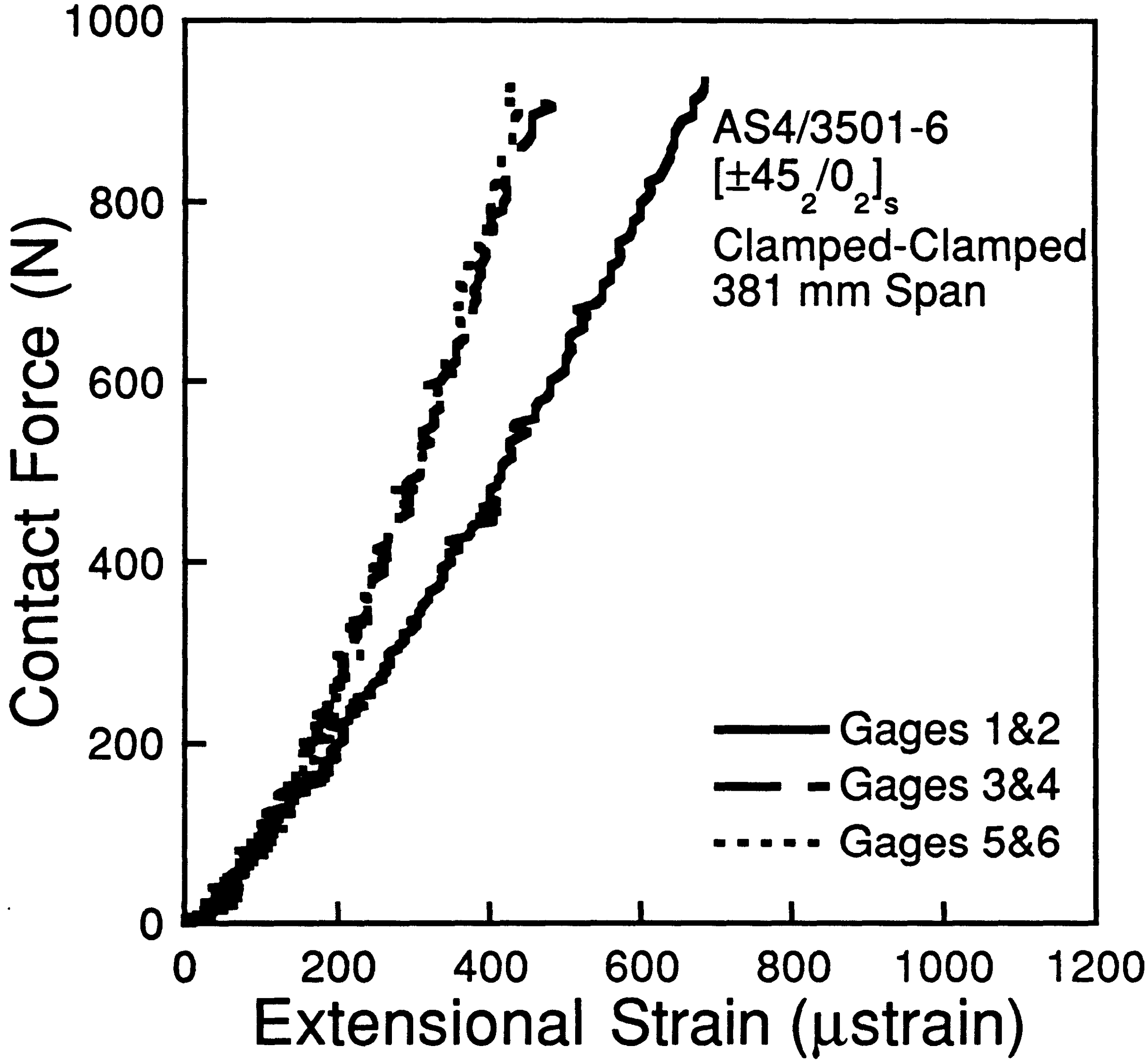

Figure 5.20 Force-extensional strain data for the specimen with a 381 mm span in a clamped-clamped support and tested to a maximum contact force of 930 N. (See Figure 3.2 for gage locations.)

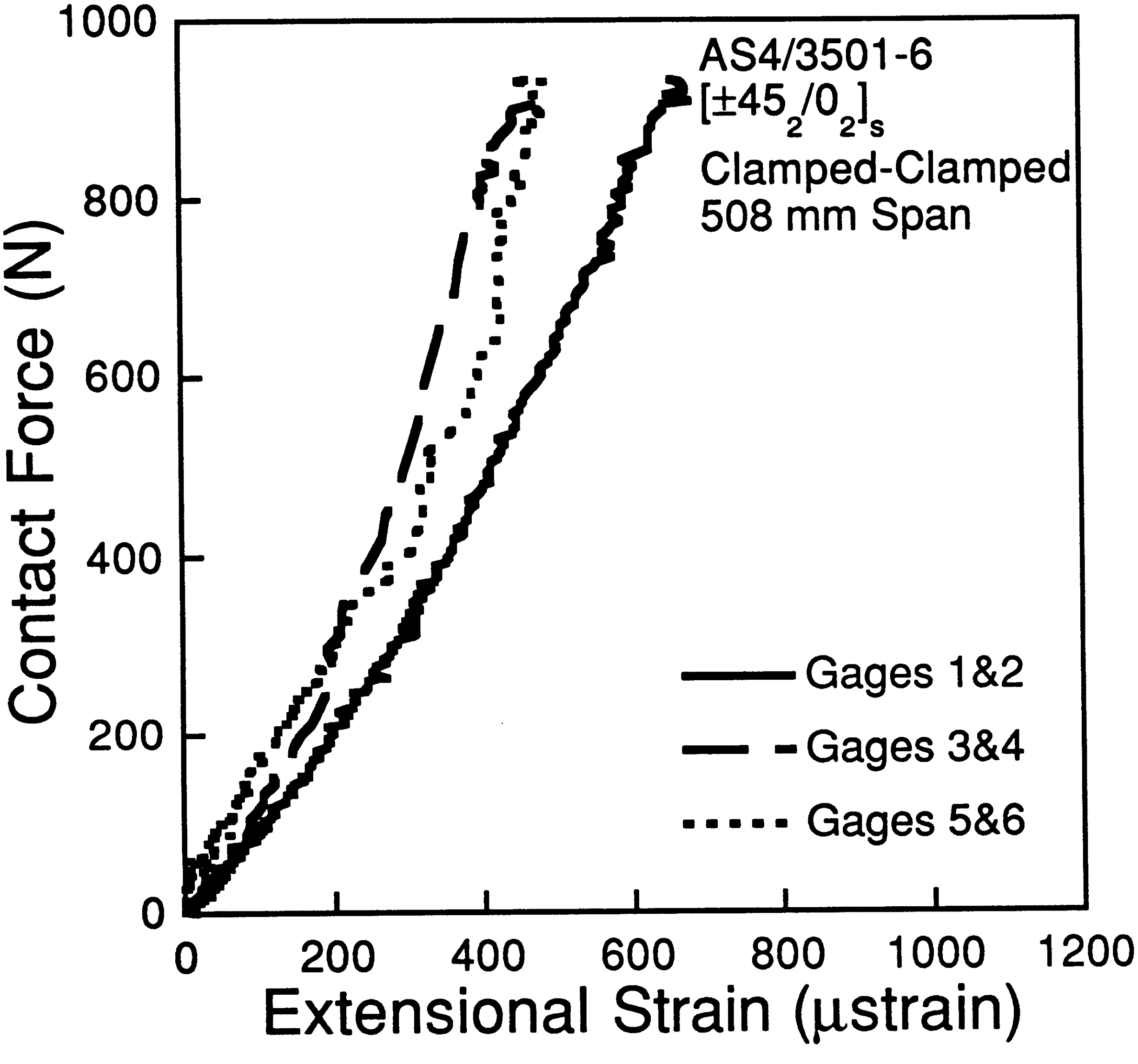

Figure 5.21 Force-extensional strain data for the specimen with a 508 mm span in a clamped-clamped support and tested to a maximum contact force of 930 N. (See Figure 3.2 for gage locations.)

Table 5.6 Table of maximum extensional strains[a] for specimens of different spans in a clamped-clamped support and tested to a maximum contact force of 930 N.

	Span Length, mm					
Position[b]	32	63.5	127	254	381	508
1/2	--[c]	1100	850	725	675	675
3/4	650	800	450	425	450	500
5/6	475	600	300	400	450	500

[a] All values in microstrain.

[b] Strain gage positions as given in Figure 3.2.

[c] There was no gage 1 or 2 for the 32 mm configuration as discussed in the text.

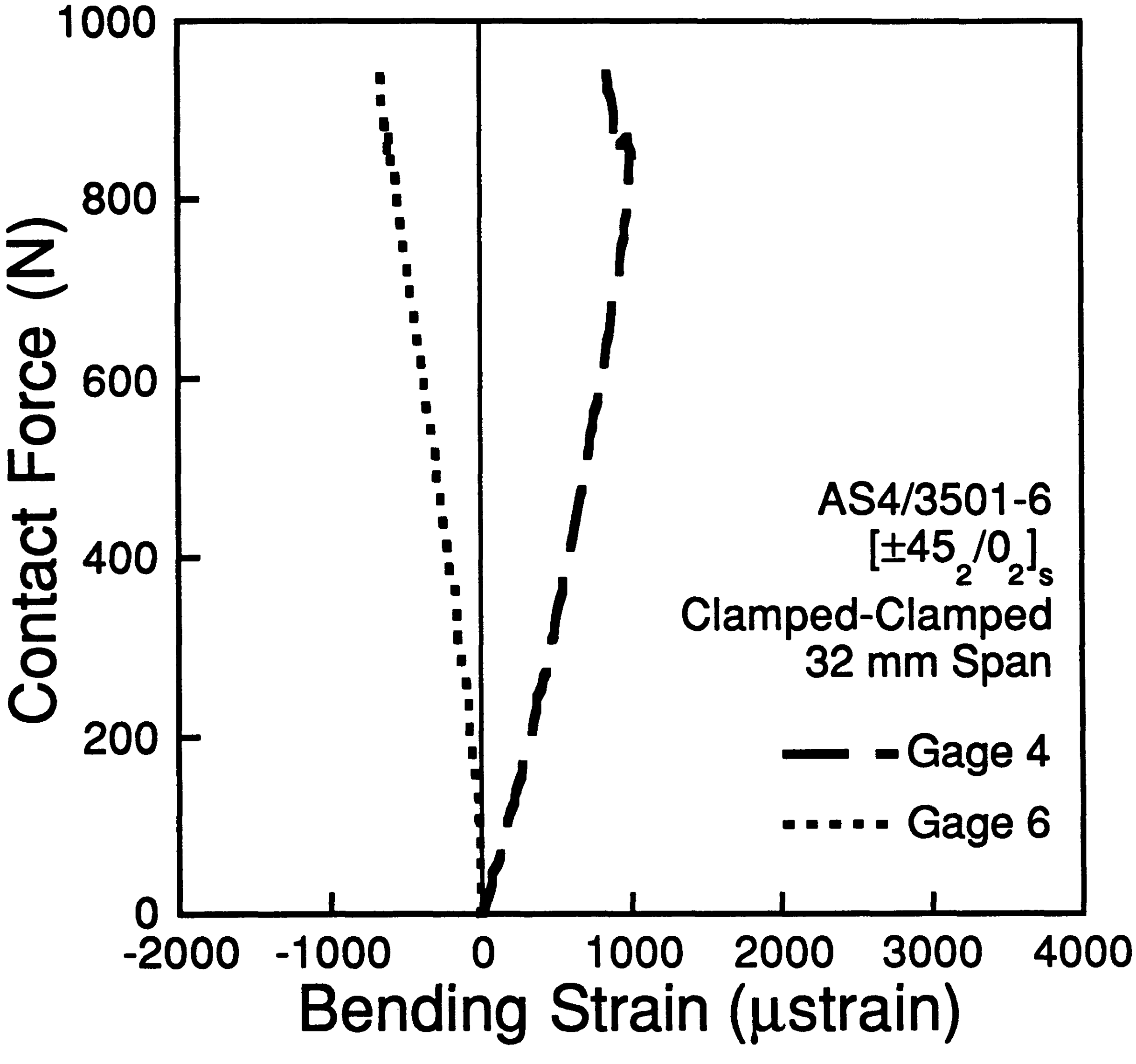

Figure 5.22 Force-bending strain data for the specimen with a 32 mm span in a clamped-clamped support and tested to a maximum contact force of 930 N. (See Figure 3.2 for gage locations. Note that there is no gage 1 or 2 for the 32 mm configuration.)

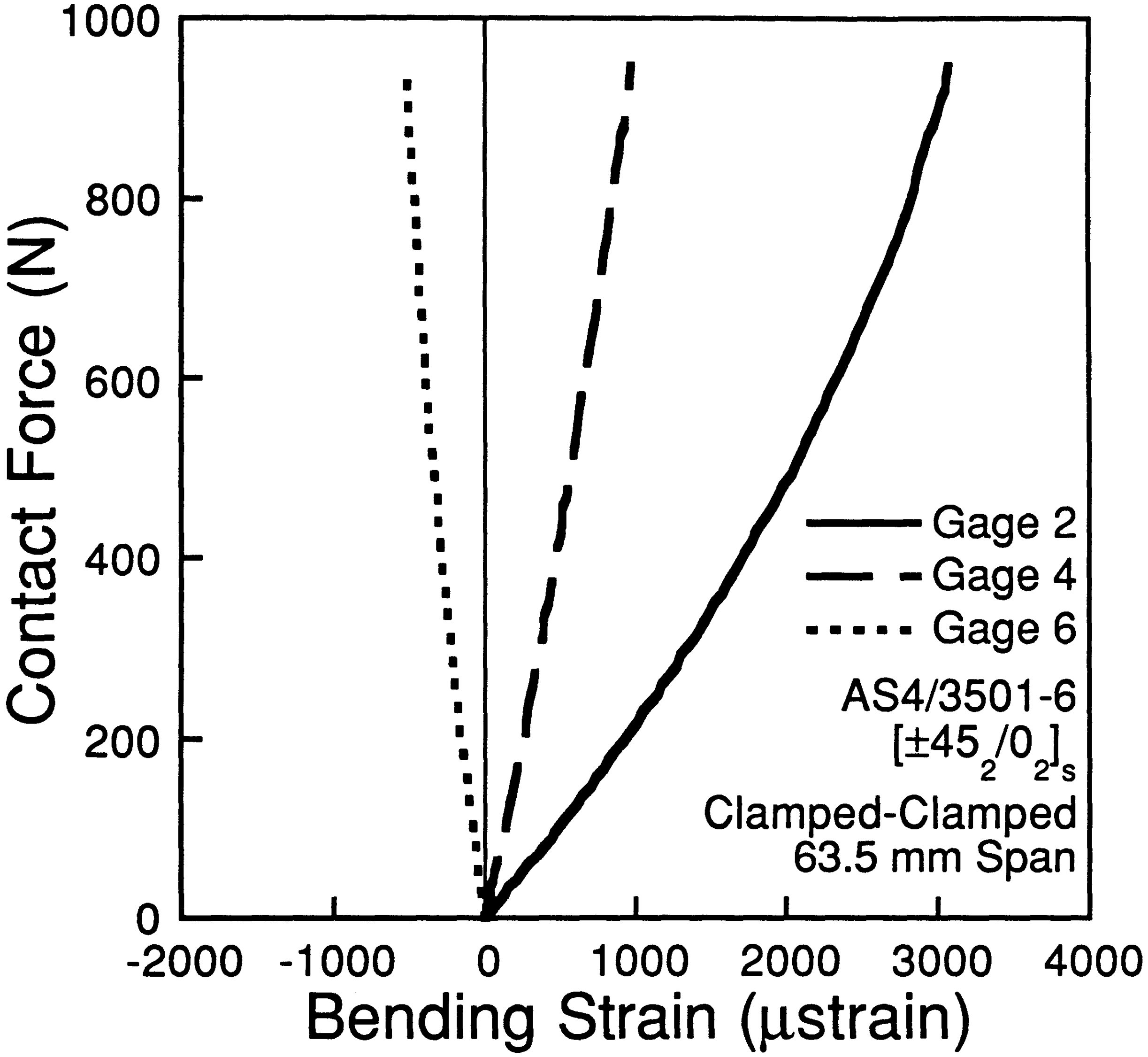

Figure 5.23 Force-bending strain data for the specimen with a 63.5 mm span in a clamped-clamped support and tested to a maximum contact force of 930 N. (See Figure 3.2 for gage locations.)

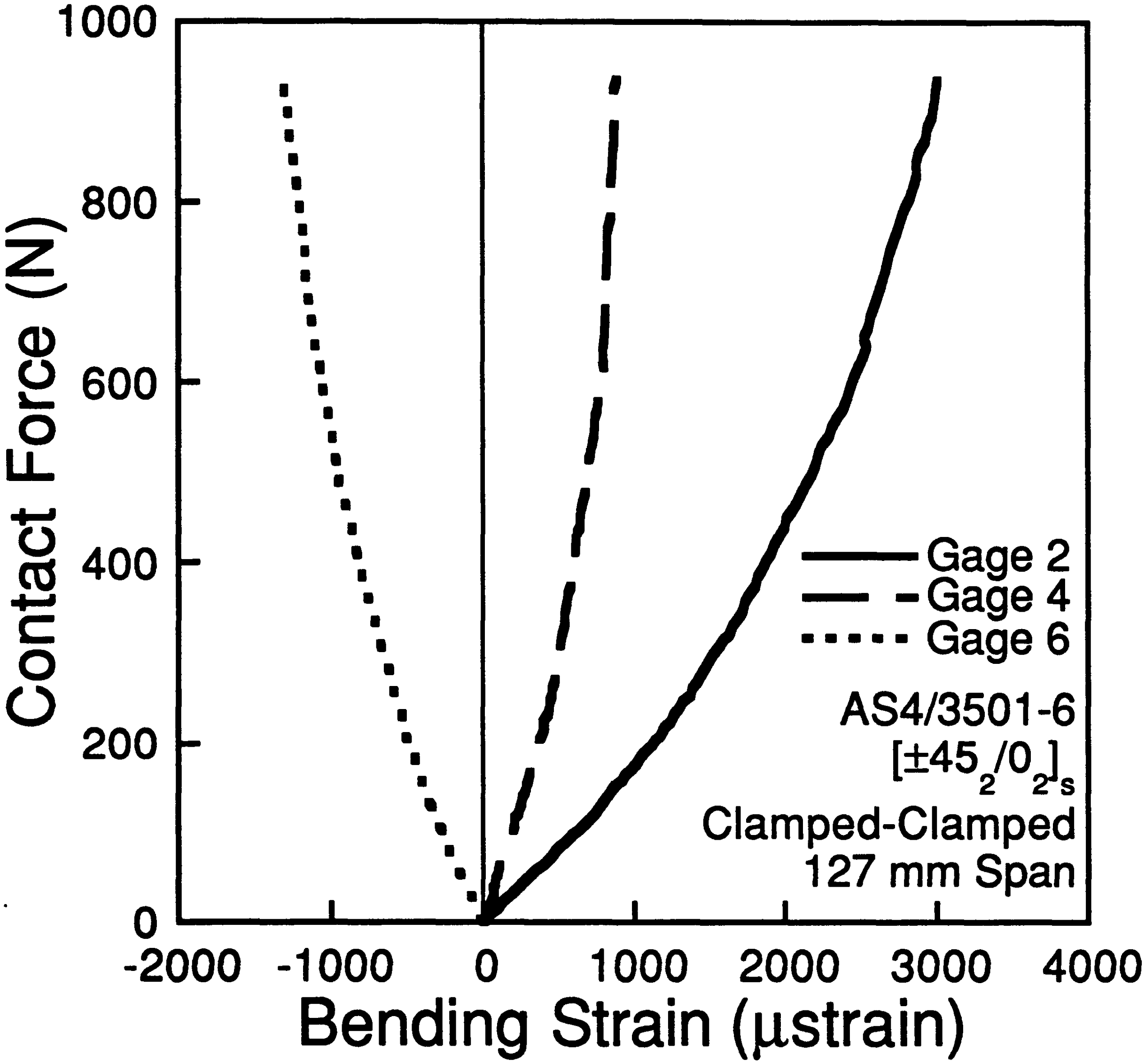

Figure 5.24 Force-bending strain data for the specimen with a 127 mm span in a clamped-clamped support and tested to a maximum contact force of 930 N. (See Figure 3.2 for gage locations.)

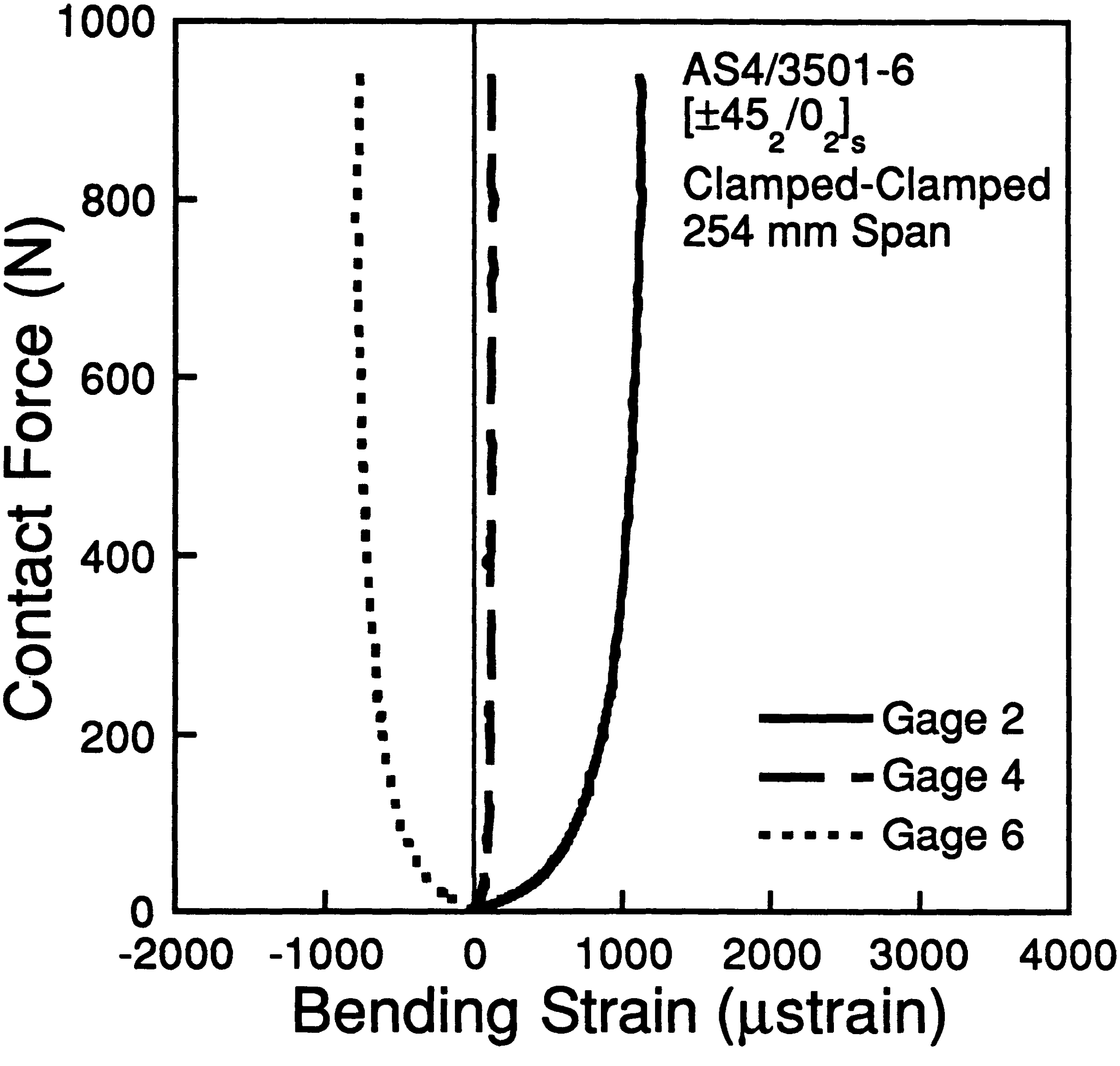

Figure 5.25 Force-bending strain data for the specimen with a 254 mm span in a clamped-clamped support and tested to a maximum contact force of 930 N. (See Figure 3.2 for gage locations.)

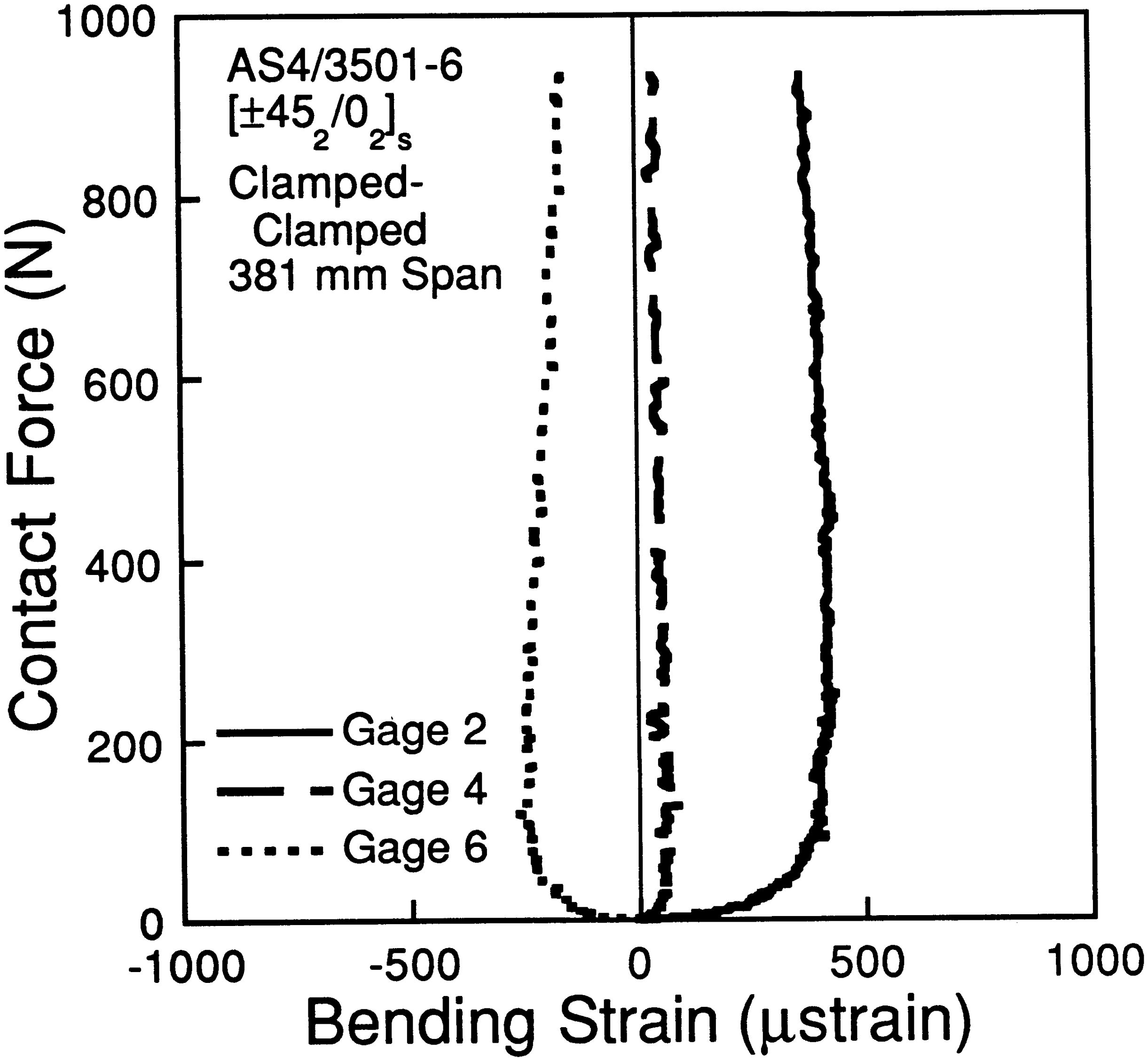

Figure 5.26 Force-bending strain data for the specimen with a 381 mm span in a clamped-clamped support and tested to a maximum contact force of 930 N. (See Figure 3.2 for gage locations.)

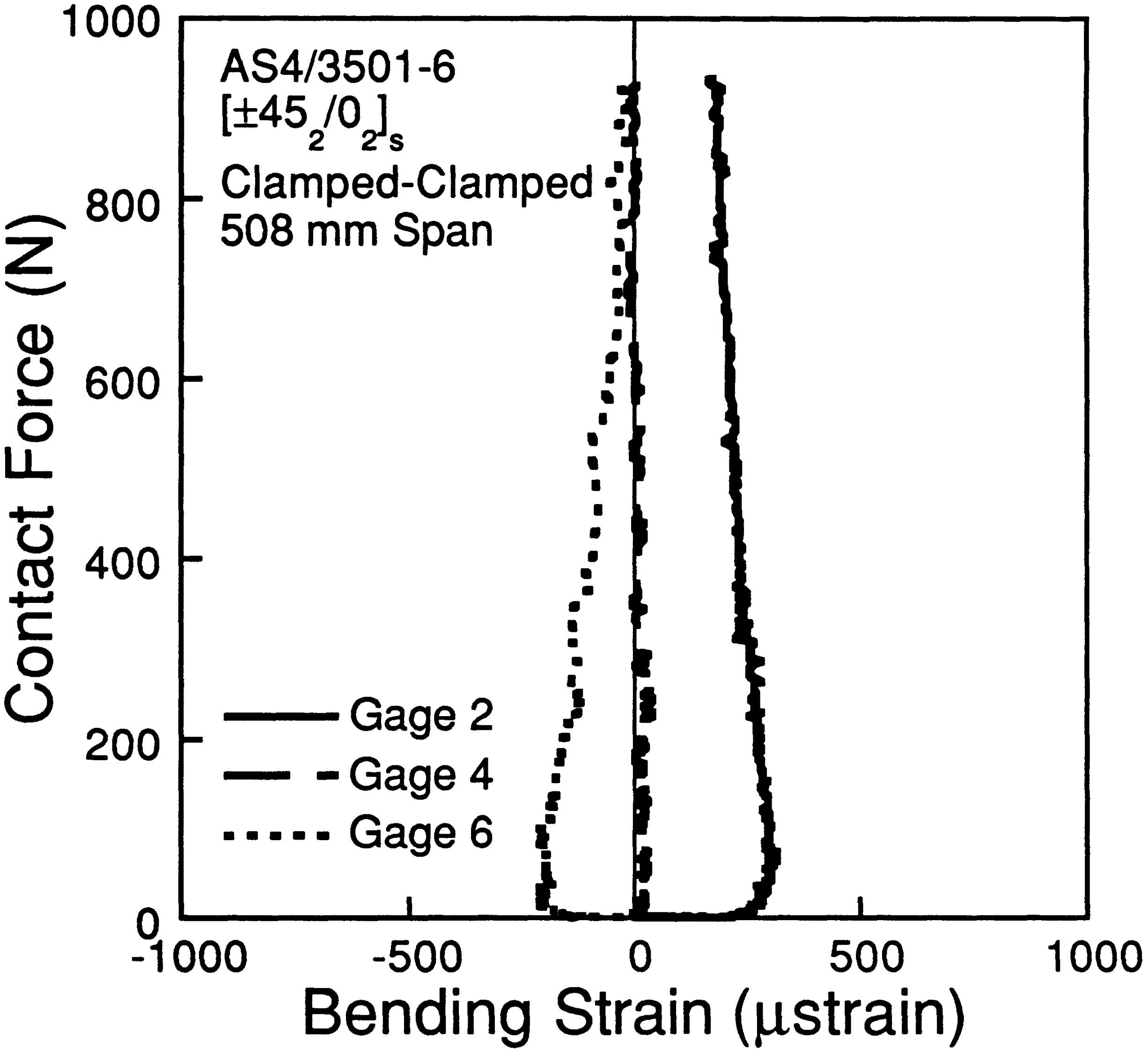

Figure 5.27 Force-bending strain data for the specimen with a 508 mm span in a clamped-clamped support and tested to a maximum contact force of 930 N. (See Figure 3.2 for gage locations.)

Table 5.7 Table of maximum bending strains[a] for specimens of different spans in a clamped-clamped support and tested to a maximum contact force of 930 N.

Gage[b]	Span Length, mm					
	32	63.5	127	254	381	508
2	--[c]	3080	3000	1140	430[d]	310[d]
4	1000	970	890	130	70[d]	30[d]
6	-660	-520	-1310	-780	-250[d]	-210[d]

[a] All values in microstrain.

[b] Strain gage positions as given in Figure 3.2.

[c] There was no gage 1 or 2 for the 32 mm configuration as discussed in the text.

[d] Maximum did not occur at maximum force level.

span because that span did not have space to fit the full compliment of strain gages. The general trend appears to be that the maximum extensional strain decreases with increasing span. It should be noted that, for the larger spans, the extensional strain at positions 3/4 and 5/6 appear to reach approximately the same strain level. The maximum bending strain at each position is listed in Table 5.7. The general trend appears to be that the maximum bending strain, at a position on a plate, decreases more rapidly with increasing span than the extensional strain, except for gage 6. For the spans greater than 127 mm, the bending strains reach a plateau where the strain no longer changes appreciably with increasing force. This plateau occurs after the "elbow" in the force-bending strain curve. This "elbow" in the curve is observed to occur at a decreasing contact force level as the specimen span length increases. The bending strains decrease after this point for the 381 mm and 508 mm spans.

There are observations which can be made regarding the graphs for the specimens loaded to 1479 N. For each span, the extensional strain curves for locations 4/5 and 6/7 are very similar, but the values for location 6/7 are consistently lower, except for the 381 mm case. The maximum extensional strain at these locations is approximately 2000 microstrain for spans less than 254 mm but grows in the larger spans. The maximum extensional strains are compiled in Table 5.8. The extensional strain for location 1/2 (represented by gages 6 and 7 for the 32 mm span, as discussed in Chapter 3) shows a maximum strain of approximately 2000 microstrain for spans less than 127 mm. However, the maximum strain drops to approximately 500 microstrain and remains constant at that level for larger spans. It should be noted that in many of the specimens, a drop or large change in the extensional strains occurs above approximately 1300 N at

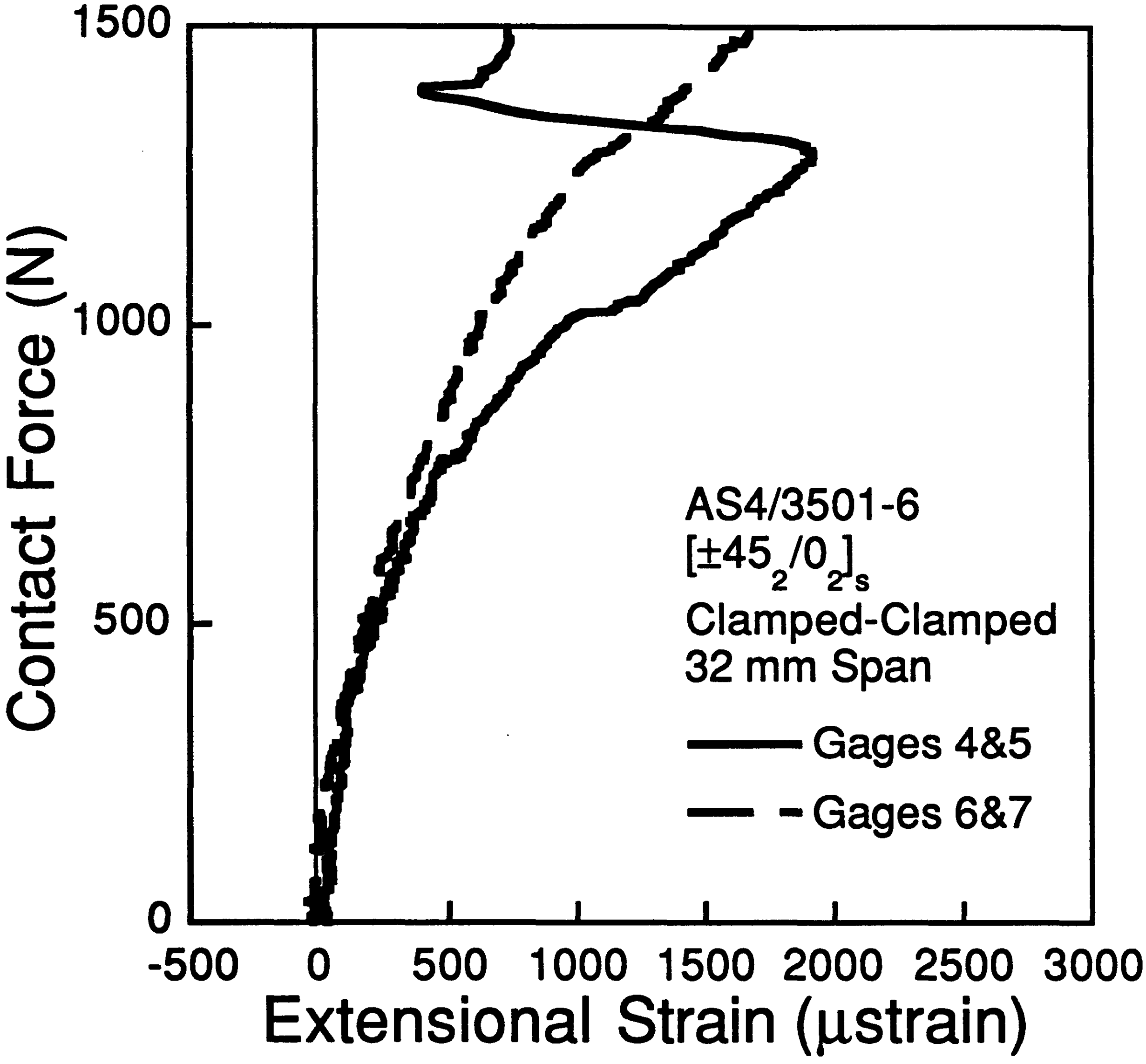

Figure 5.28 Force-extensional strain data for the specimen with a 32 mm span in a clamped-clamped support and tested to a maximum contact force of 1479 N. (See Figure 3.3 for gage locations. Note that there is no gage 1 or 2 for the 32 mm configuration.)

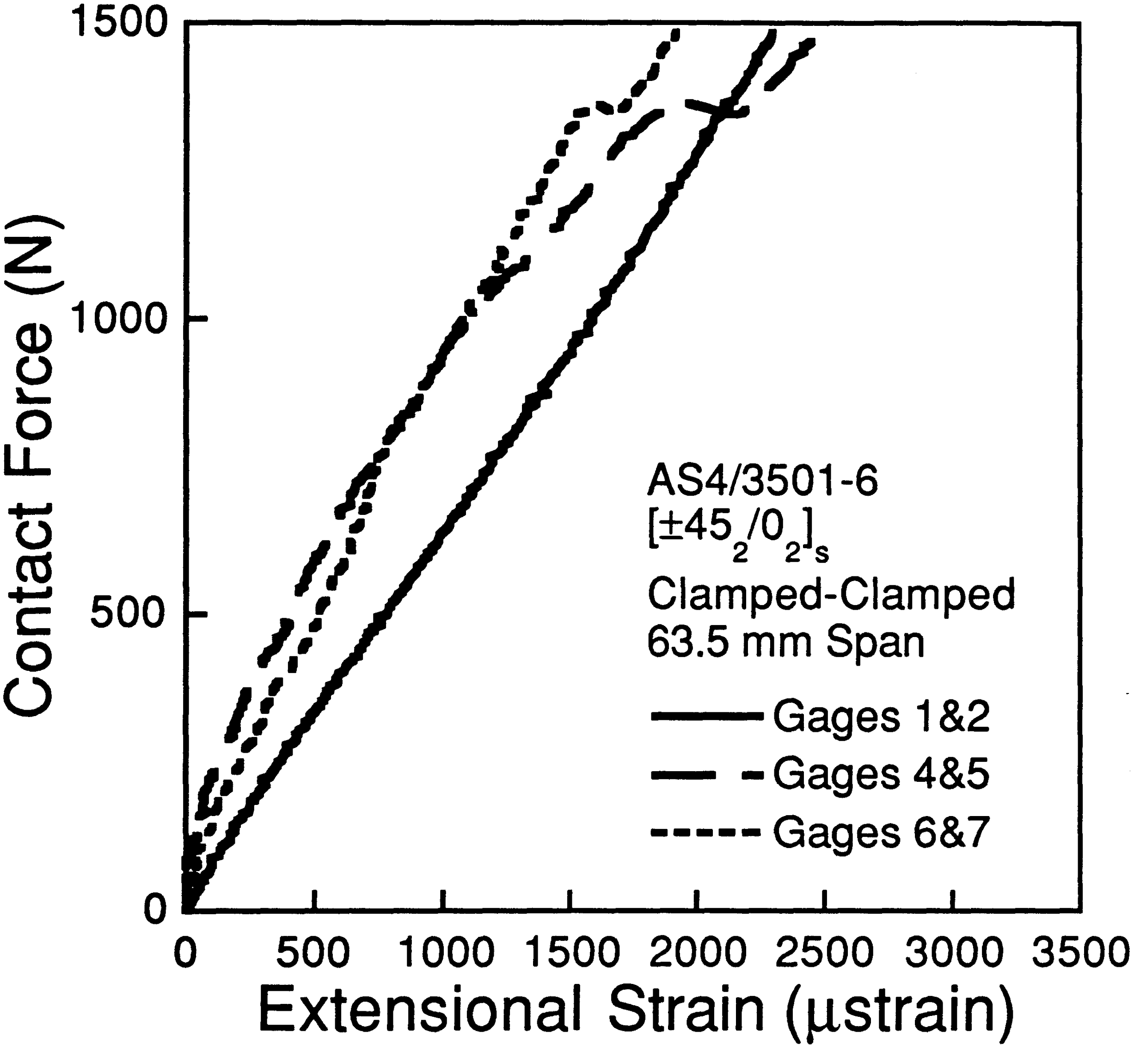

Figure 5.29 Force-extensional strain data for the specimen with a 63.5 mm span in a clamped-clamped support and tested to a maximum contact force of 1479 N. (See Figure 3.3 for gage locations.)

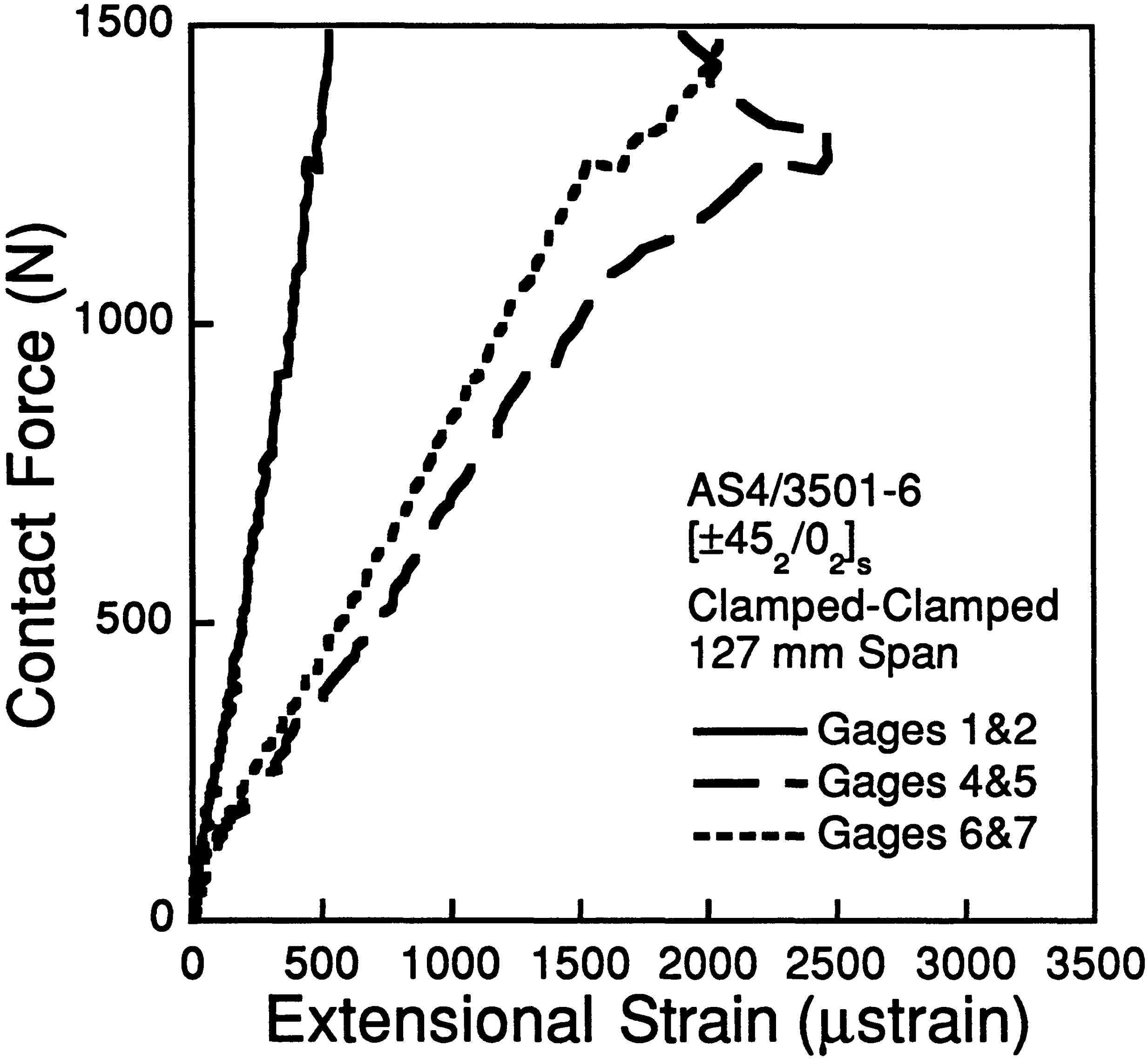

Figure 5.30 Force-extensional strain data for the specimen with a 127 mm span in a clamped-clamped support and tested to a maximum contact force of 1479 N. (See Figure 3.3 for gage locations.)

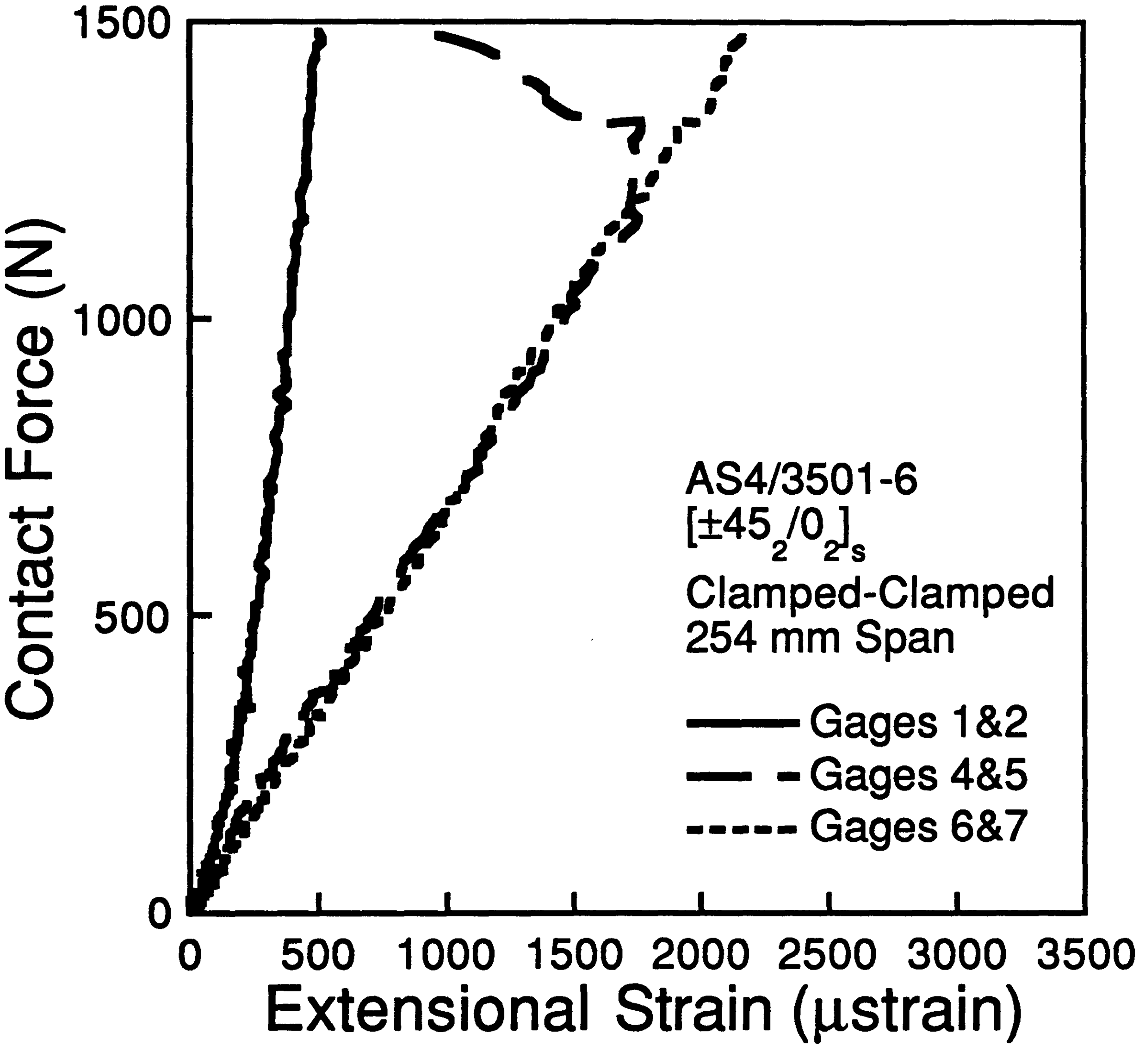

Figure 5.31 Force-extensional strain data for the specimen with a 254 mm span in a clamped-clamped support and tested to a maximum contact force of 1479 N. (See Figure 3.3 for gage locations.)

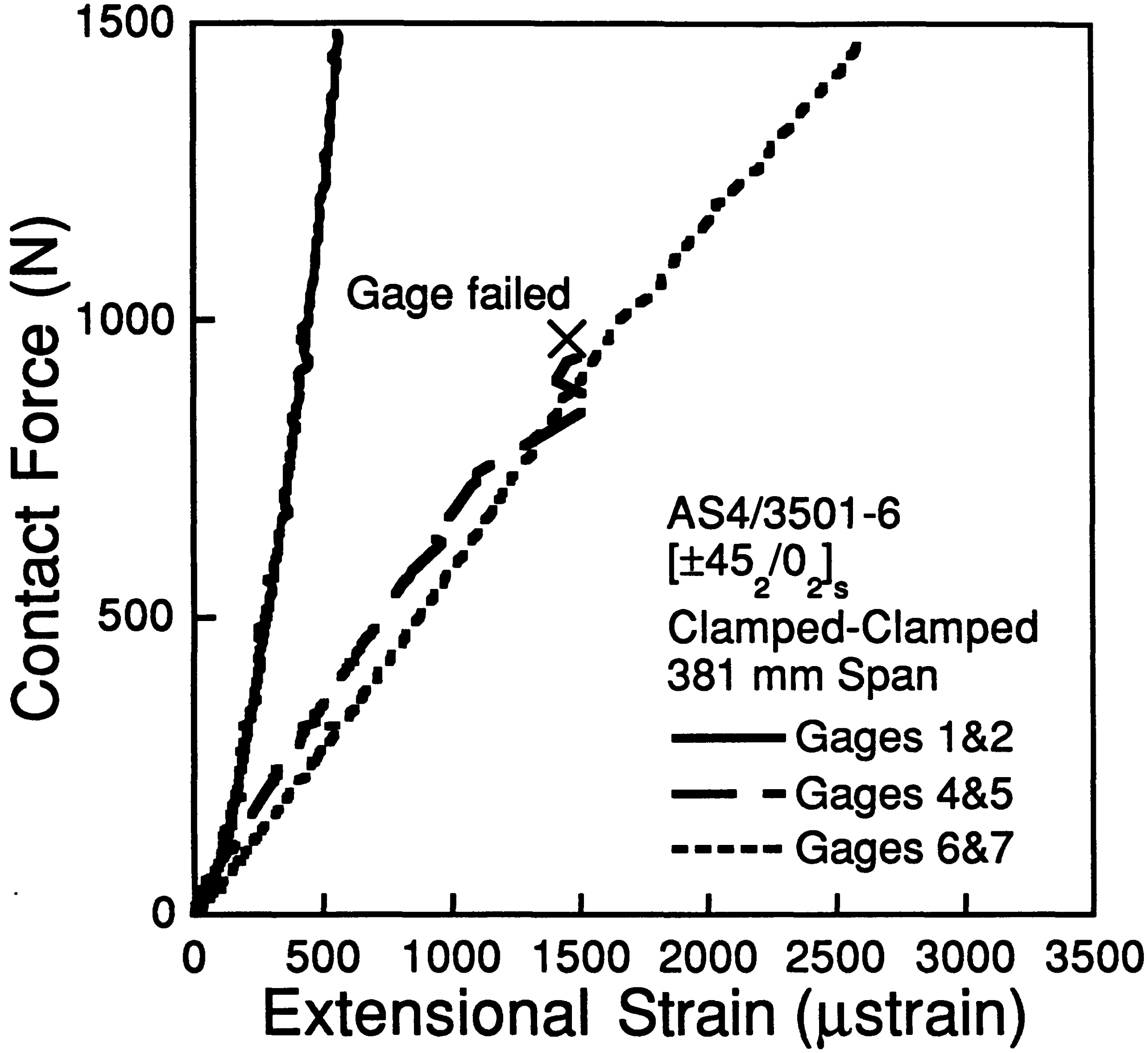

Figure 5.32 **Force-extensional strain data for the specimen with a 381 mm span in a clamped-clamped support and tested to a maximum contact force of 1479 N. (See Figure 3.3 for gage locations.)**

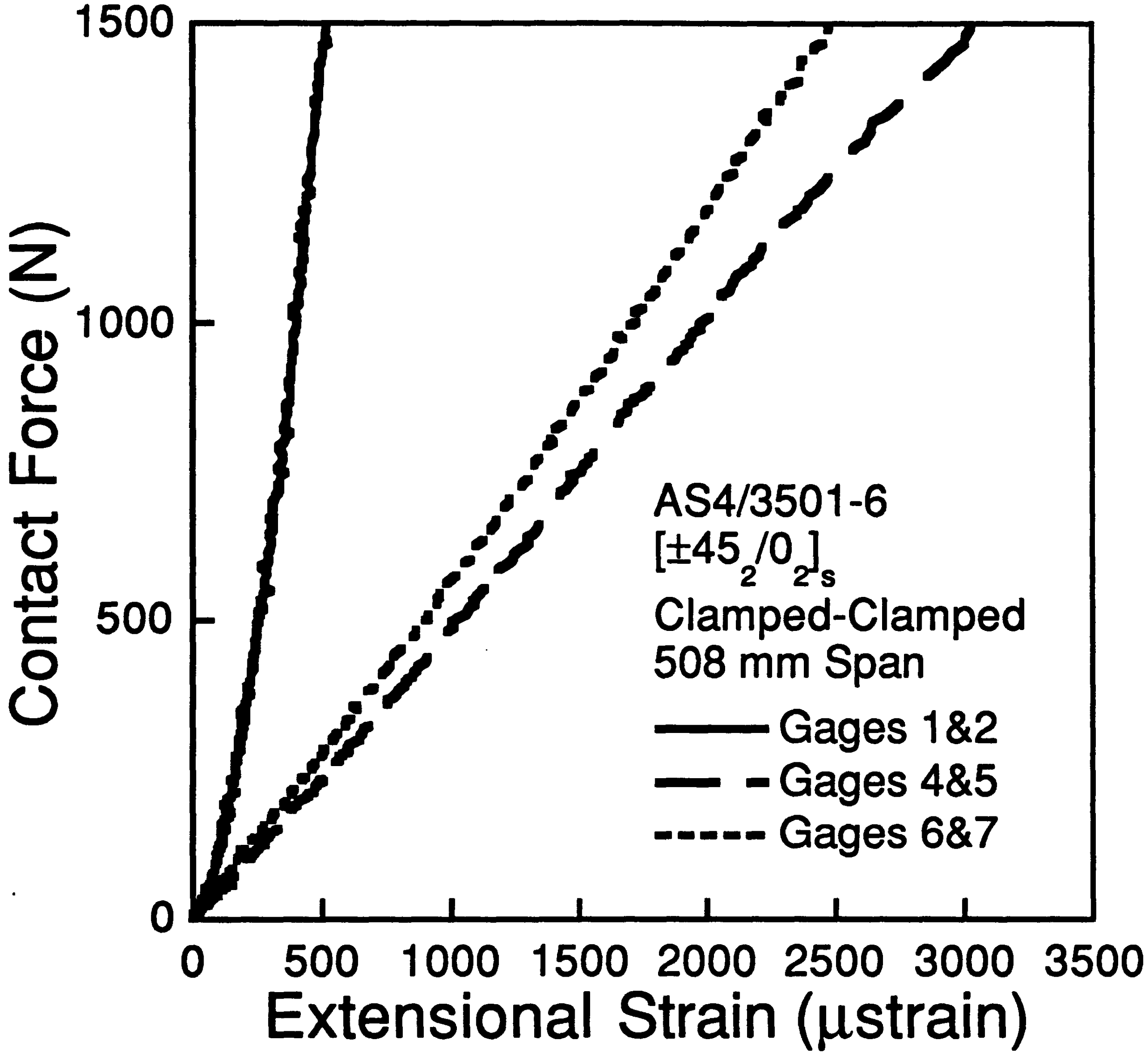

Figure 5.33 Force-extensional strain data for the specimen with a 508 mm span in a clamped-clamped support and tested to a maximum contact force of 1479 N. (See Figure 3.3 for gage locations.)

Table 5.8 Table of maximum extensional strains[a] for specimens of different spans in a clamped-clamped support and tested to a maximum contact force of 1479 N.

	Span Length, mm					
Position[b]	32	63.5	127	254	381	508
1/2	--[c]	2300	500	500	600	600
4/5	2000[d]	2500	2500[d]	1700[d]	--[e]	3000
6/7	1700	2000	2100	2200	2600	2500

[a] All values in microstrain.

[b] Strain gage positions as given in Figure 3.3.

[c] There was no gage 1 or 2 for the 32 mm configuration as discussed in the text.

[d] Maximum did not occur at maximum force level.

[e] This gage failed at a low force, therefore presenting a maximum would be misleading.

Table 5.9 Table of extensional strains[a] at 930 N for specimens of different spans in a clamped-clamped support and tested to a maximum contact force of 1479 N.

	Span Length, mm					
Position[b]	32	63.5	127	254	381	508
1/2	--[c]	1500	300	400	400	400
4/5	900	1000	1300	1300	1500	1900
6/7	600	1000	1100	1300	1500	1600

[a] All values in microstrain.

[b] Strain gage positions as given in Figure 3.3.

[c] There was no gage 1 or 2 for the 32 mm configuration as discussed in the text.

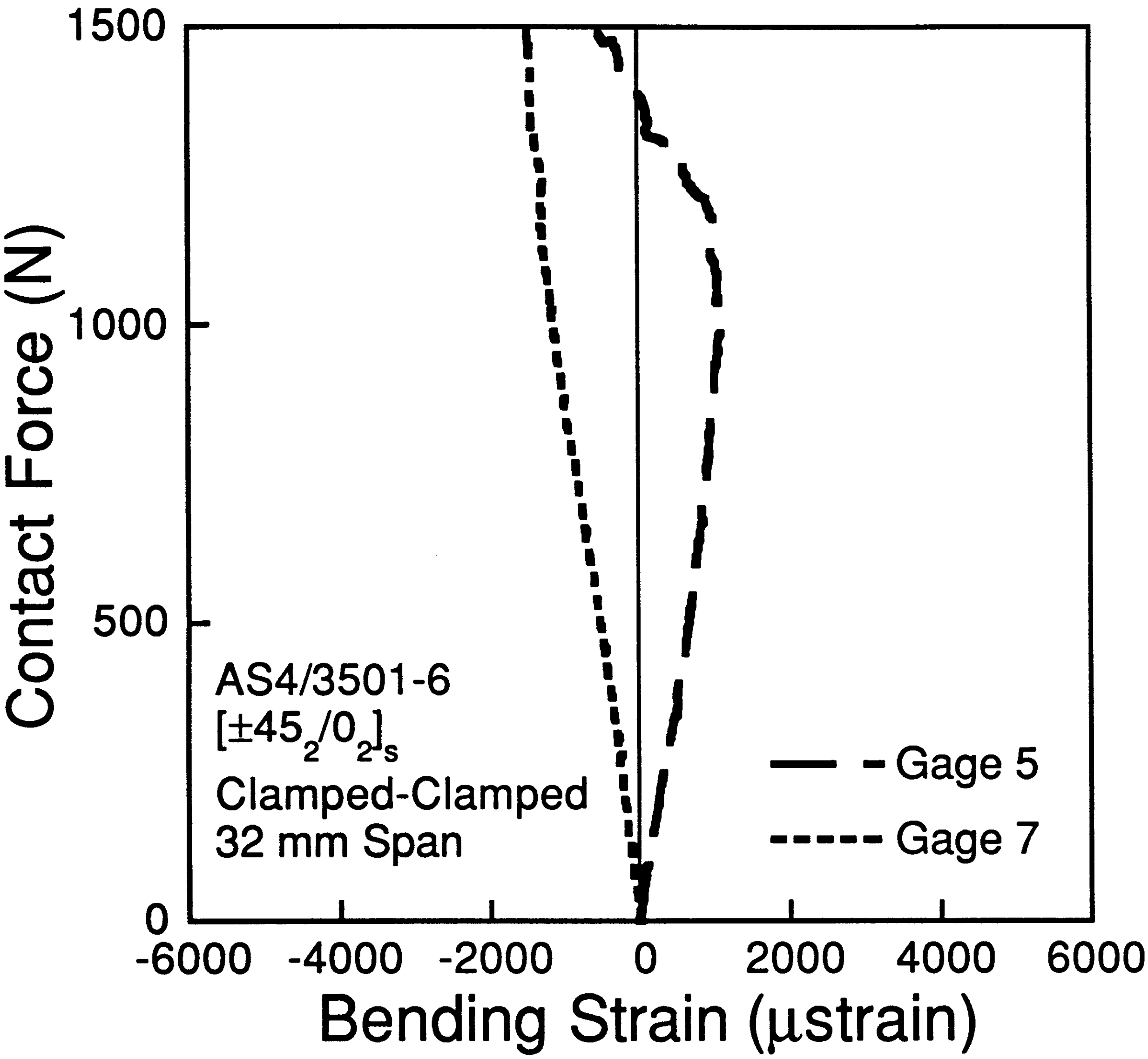

Figure 5.34 Force-bending strain data for the specimen with a 32 mm span in a clamped-clamped support and tested to a maximum contact force of 1479 N. (See Figure 3.3 for gage locations. Note that there is no gage 1 or 2 for the 32 mm configuration.)

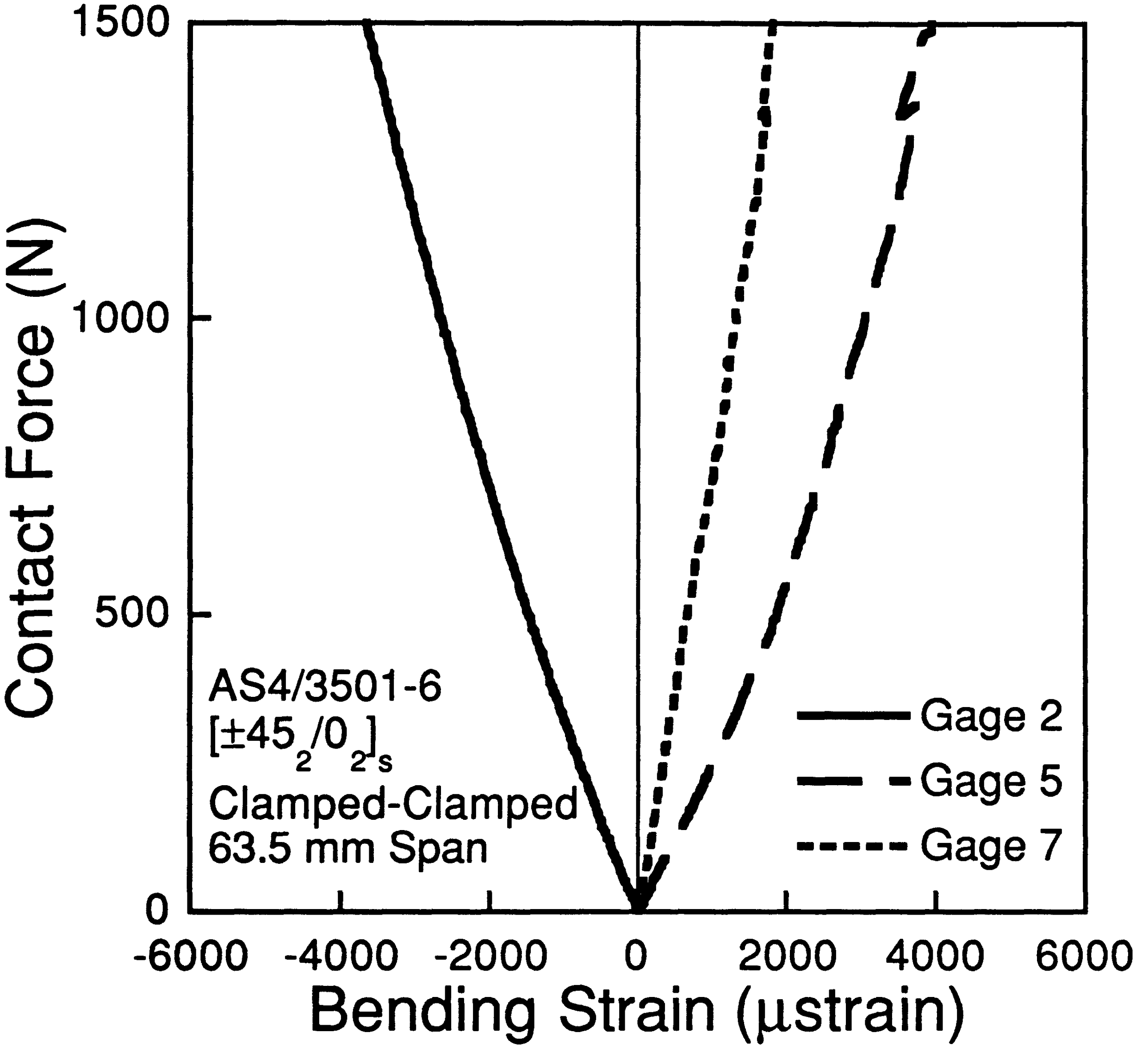

Figure 5.35 Force-bending strain data for the specimen with a 63.5 mm span in a clamped-clamped support and tested to a maximum contact force of 1479 N. (See Figure 3.3 for gage locations.)

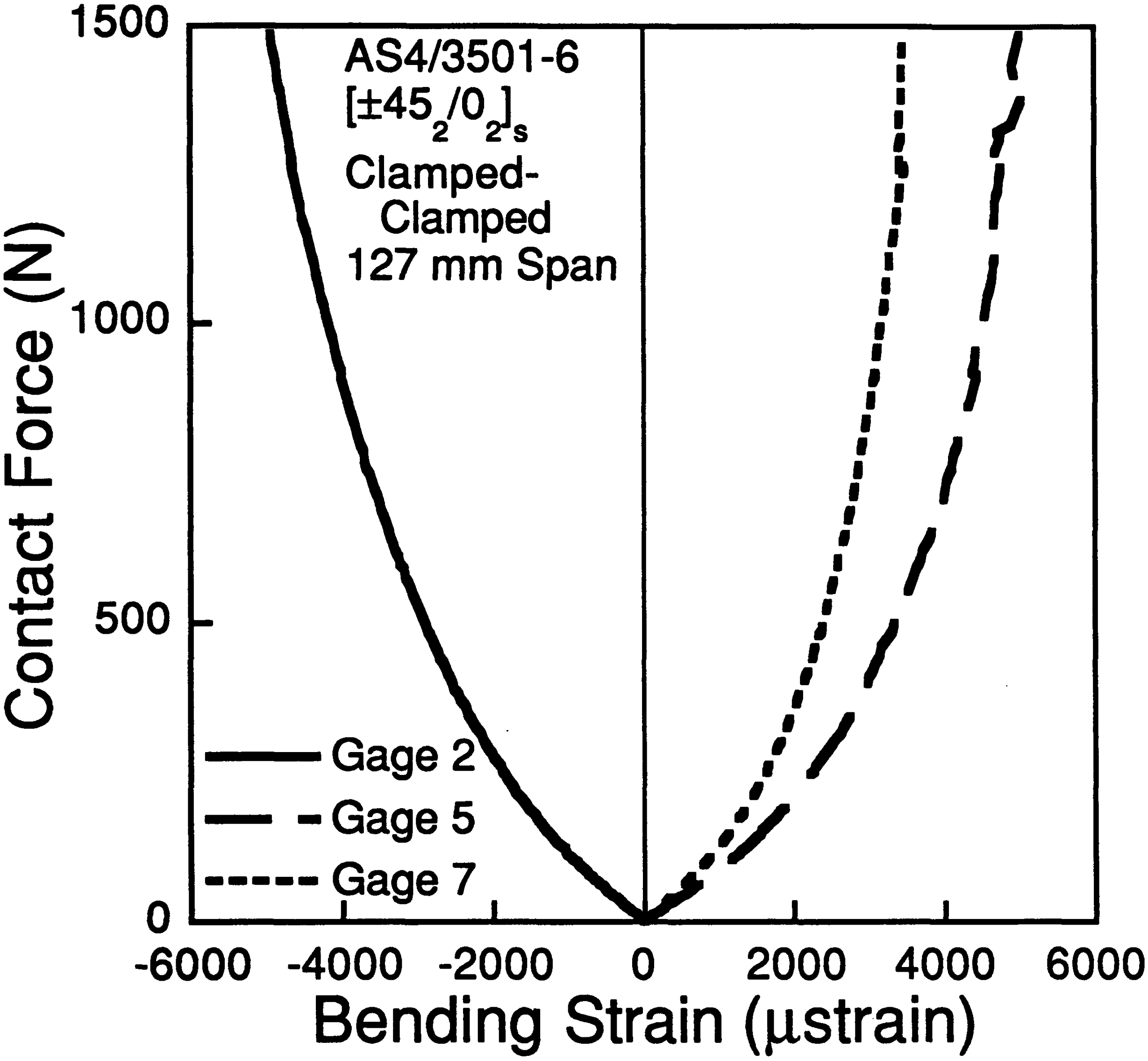

Figure 5.36 Force-bending strain data for the specimen with a 127 mm span in a clamped-clamped support and tested to a maximum contact force of 1479 N. (See Figure 3.3 for gage locations.)

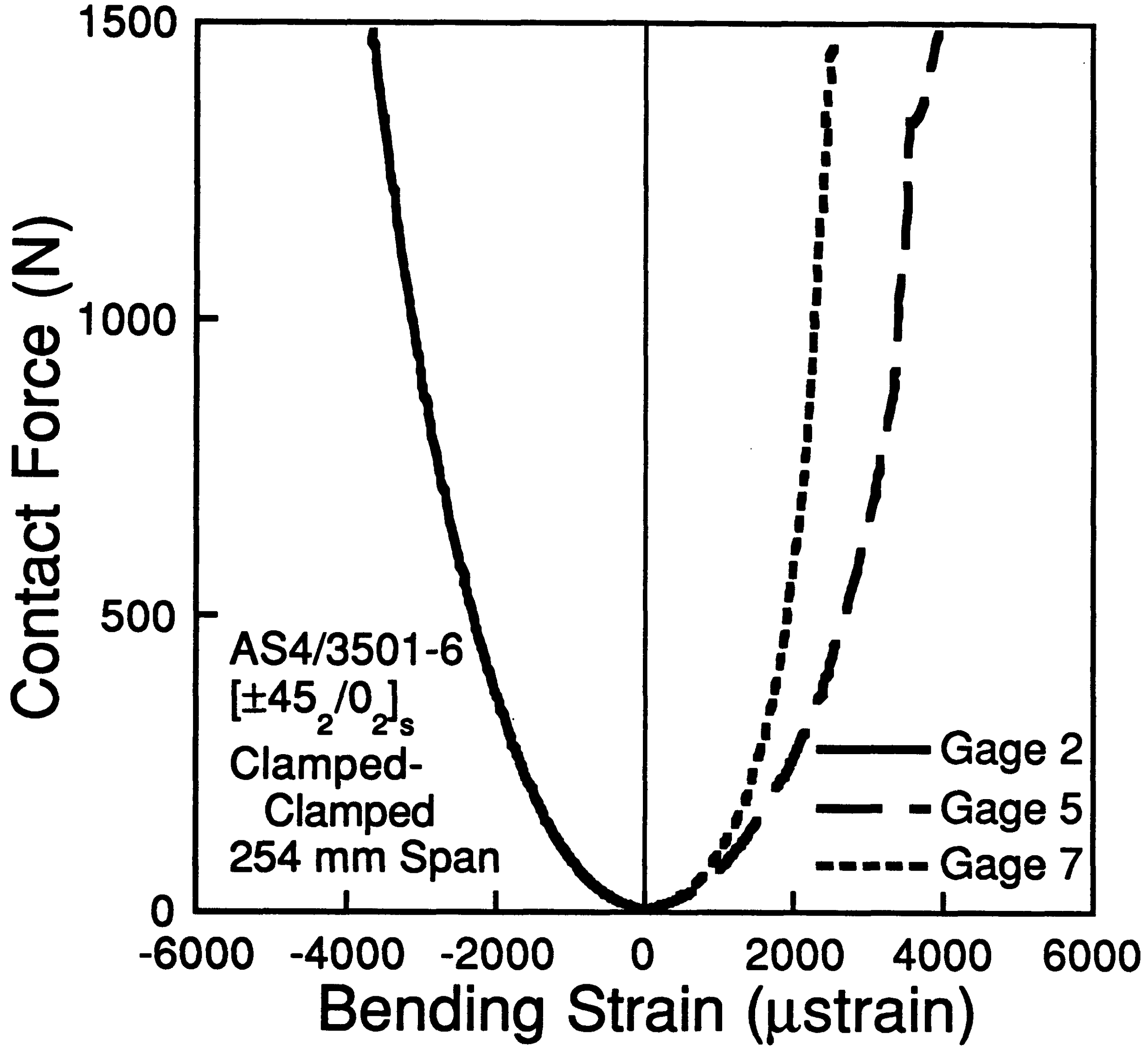

Figure 5.37 Force-bending strain data for the specimen with a 254 mm span in a clamped-clamped support and tested to a maximum contact force of 1479 N. (See Figure 3.3 for gage locations.)

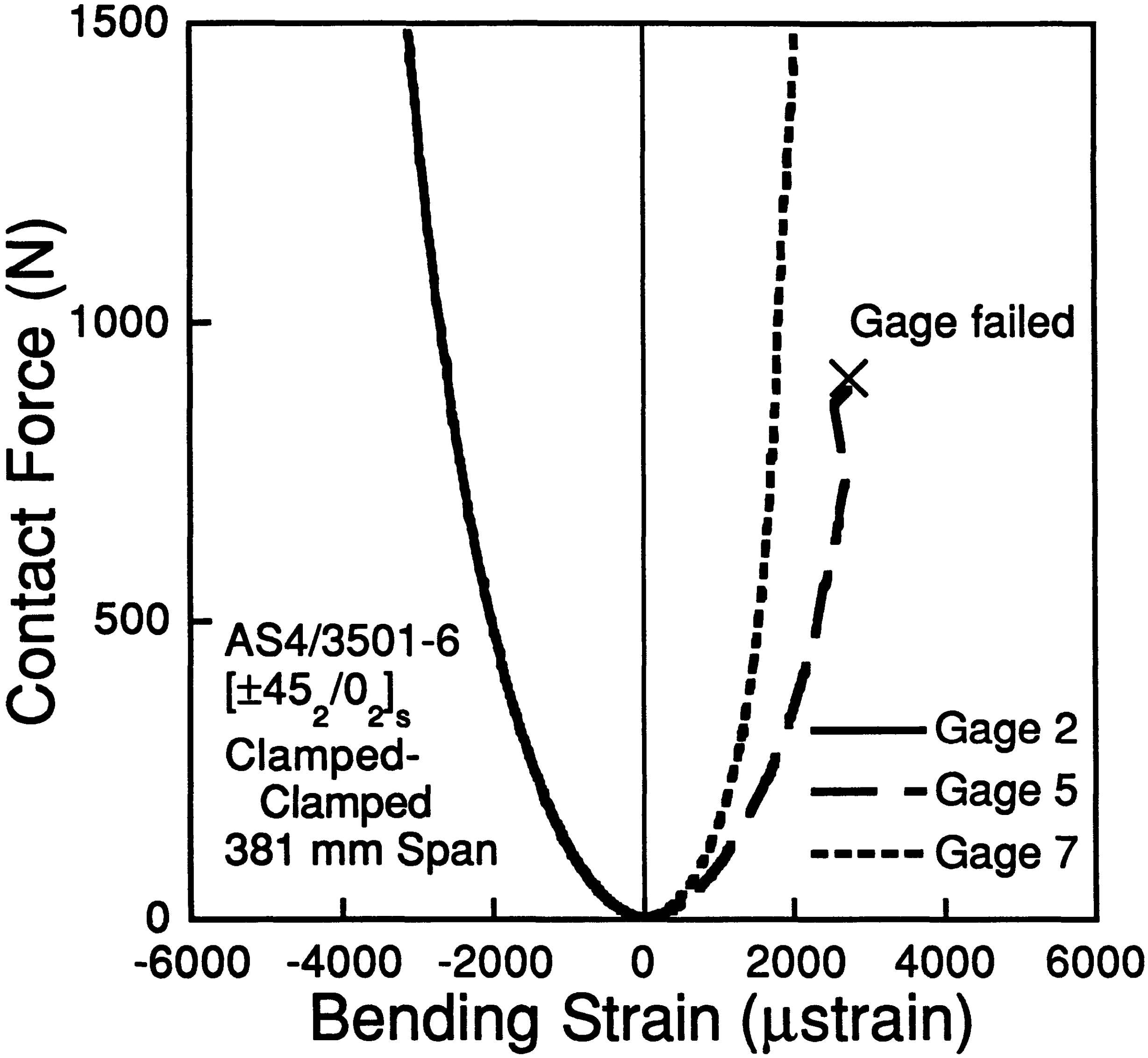

Figure 5.38 Force-bending strain data for the specimen with a 381 mm span in a clamped-clamped support and tested to a maximum contact force of 1479 N. (See Figure 3.3 for gage locations.)

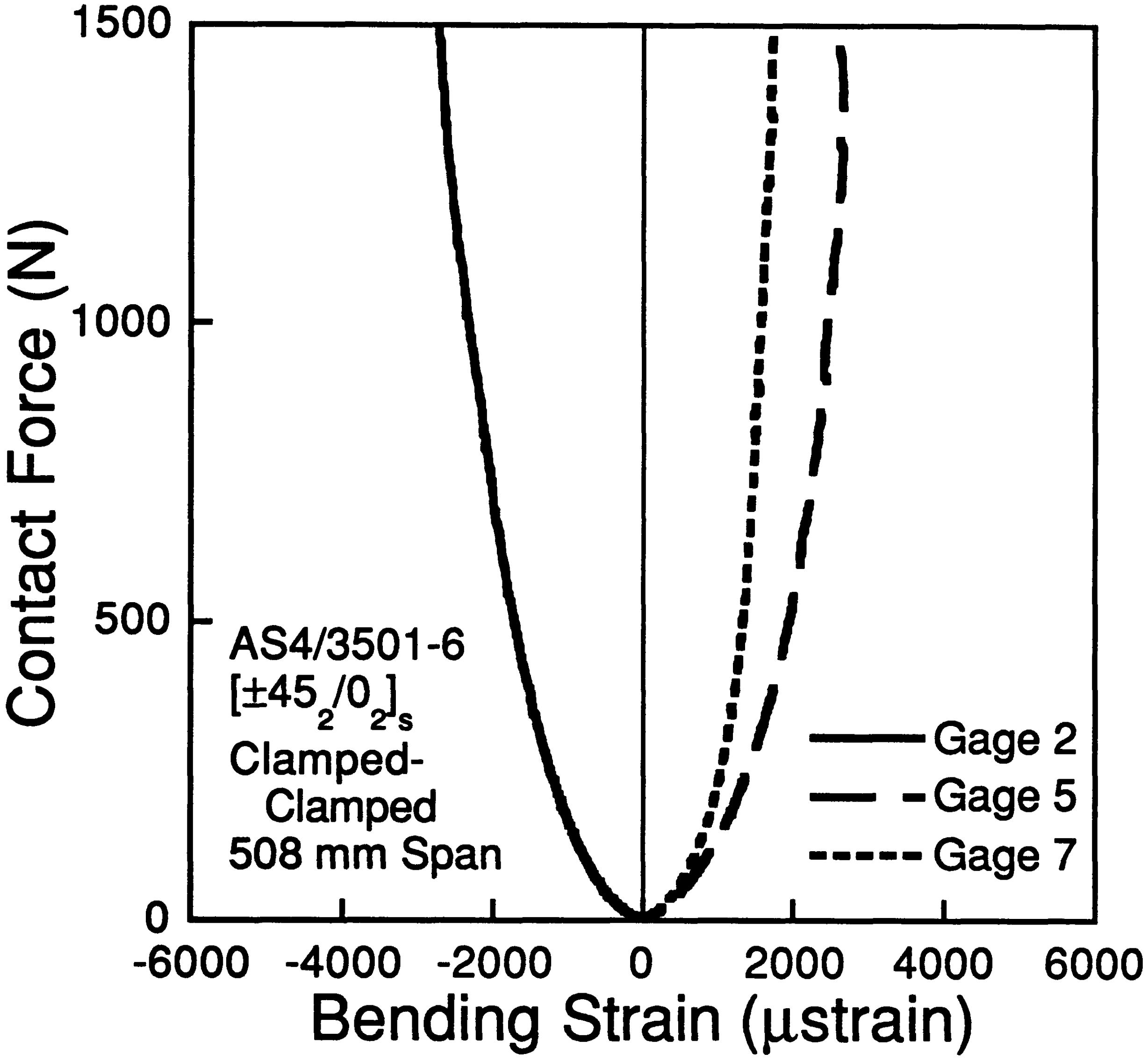

Figure 5.39 Force-bending strain data for the specimen with a 508 mm span in a clamped-clamped support and tested to a maximum contact force of 1479 N. (See Figure 3.3 for gage locations.)

Table 5.10 Table of maximum bending strains[a] for specimens of different spans in a clamped-clamped support and tested to a maximum contact force of 1479 N.

	Span Length, mm					
Gage[b]	32	63.5	127	254	381	508
2	--[c]	-3500	-5000	-3500	-3500	-2500
5	2500[d]	4000	5000	3500	--[e]	2500
7	3000	2000	3500	2500	2000	2000

[a] All values in microstrain.

[b] Strain gage positions as given in Figure 3.3.

[c] There was no gage 1 or 2 for the 32 mm configuration as discussed in the text.

[d] Maximum did not occur at maximum force level.

[e] This gage failed at a low force, therefore presenting a maximum would be misleading.

location 4/5 which may indicate that the damage has grown to that point on the plate. It can also be seen that for positions 4/5 and 6/7 in the tests to 1479 N, the extensional strains are much greater, at the same force, than those seen at any of the other strain gage locations from schemes A and B. This can be seen by comparing the values in Tables 5.9 and 5.6. This is especially evident for the specimens with a span of 127 mm or greater. Also, the bending strains for gages 2 and 5 have a similar magnitude but opposite sign for every span except the 32 mm span (as mentioned previously, there was insufficient space to fit the full compliment of strain gages on a specimen with this span). The maximum bending strains at each gage location on the plate are compiled in Table 5.10. The bending strains measured at gage 7 for each of the spans show consistently smaller strains than those seen for the other two gages. Otherwise, the bending strains show the same pattern in the specimens tested to 1479 N as those tested to 930 N of more linear behavior for smaller spans and nonlinear behavior with a less pronounced "elbow" for larger spans.

The force-extensional strain data from the nonlinear plate analysis, done for the case of a plate with a 254 mm span loaded to 930 N, and the similar experimental case are shown in Figures 5.40, 5.41, and 5.42. The force-bending strain data from the nonlinear plate analysis and the experiment are shown in Figures 5.43, 5.44, and 5.45. The geometrical nonlinearity factor, β, in the analysis was set to 0.030. This is the same value which was determined to correctly model the deflections in section 4.5. Nine by nine odd modes were used because the analysis was converged for deflection and extensional strain at that number of modes. The nonlinear analysis curves for extensional strain match the experimental force-extensional strain data well, with the exception of position 1/2 (Figure

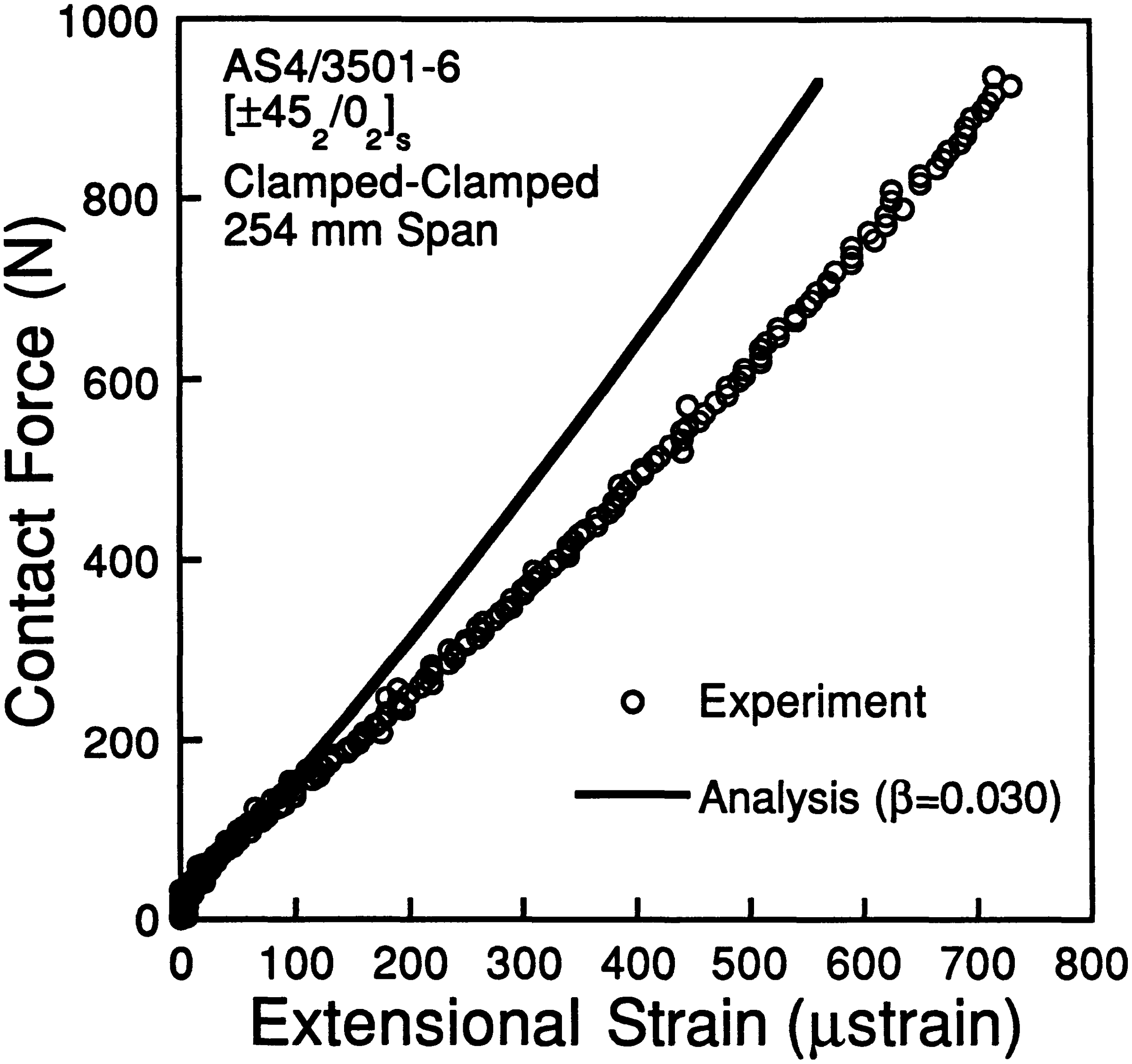

Figure 5.40 Experimental and analytical force-extensional strain data at the position for gages 1 and 2 (see Figure 3.2) for a specimen with a 254 mm span in a clamped-clamped support and tested to a maximum contact force of 930 N.

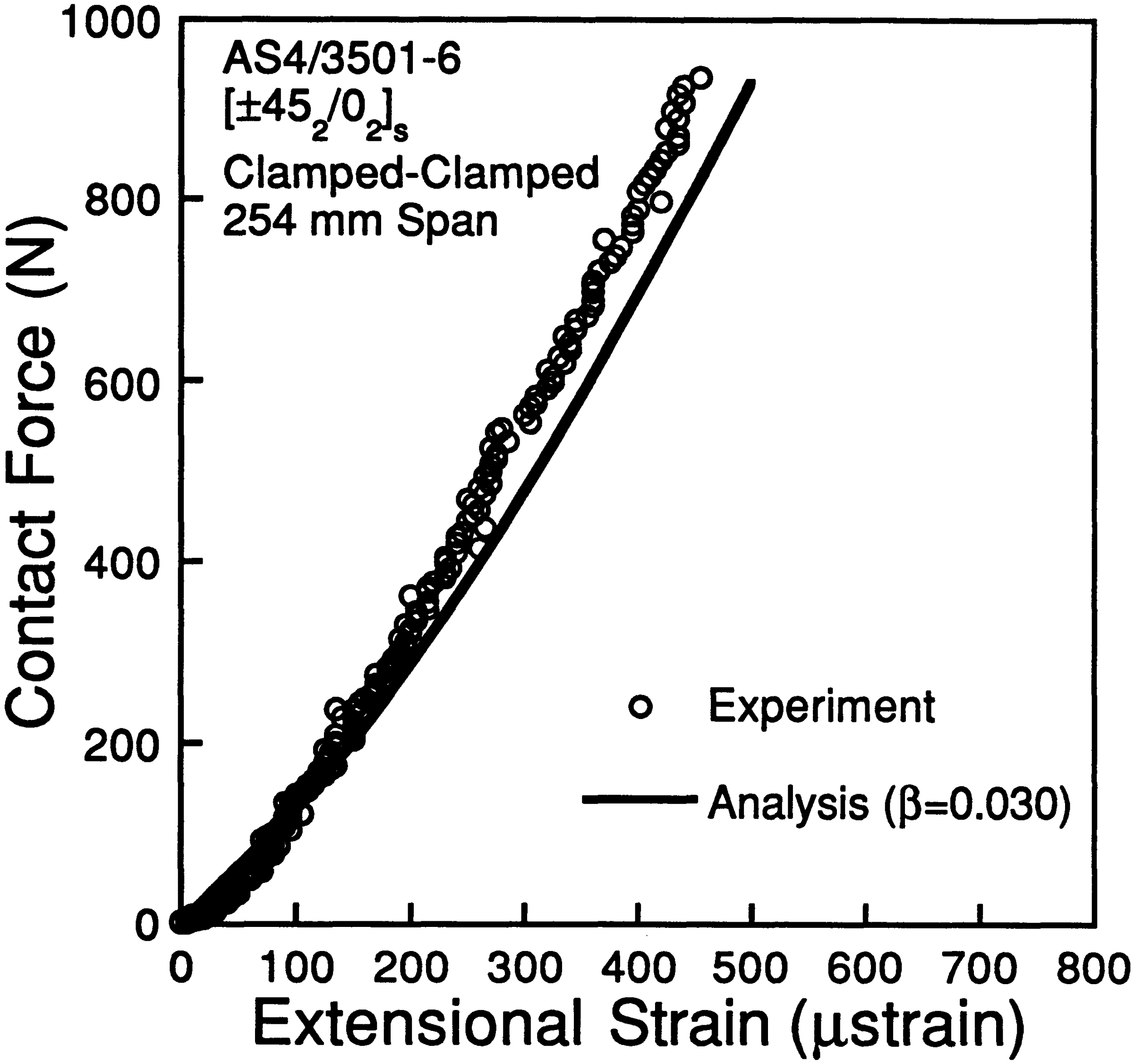

Figure 5.41 Experimental and analytical force-extensional strain data at the position for gages 3 and 4 (see Figure 3.2) for a specimen with a 254 mm span in a clamped-clamped support and tested to a maximum contact force of 930 N.

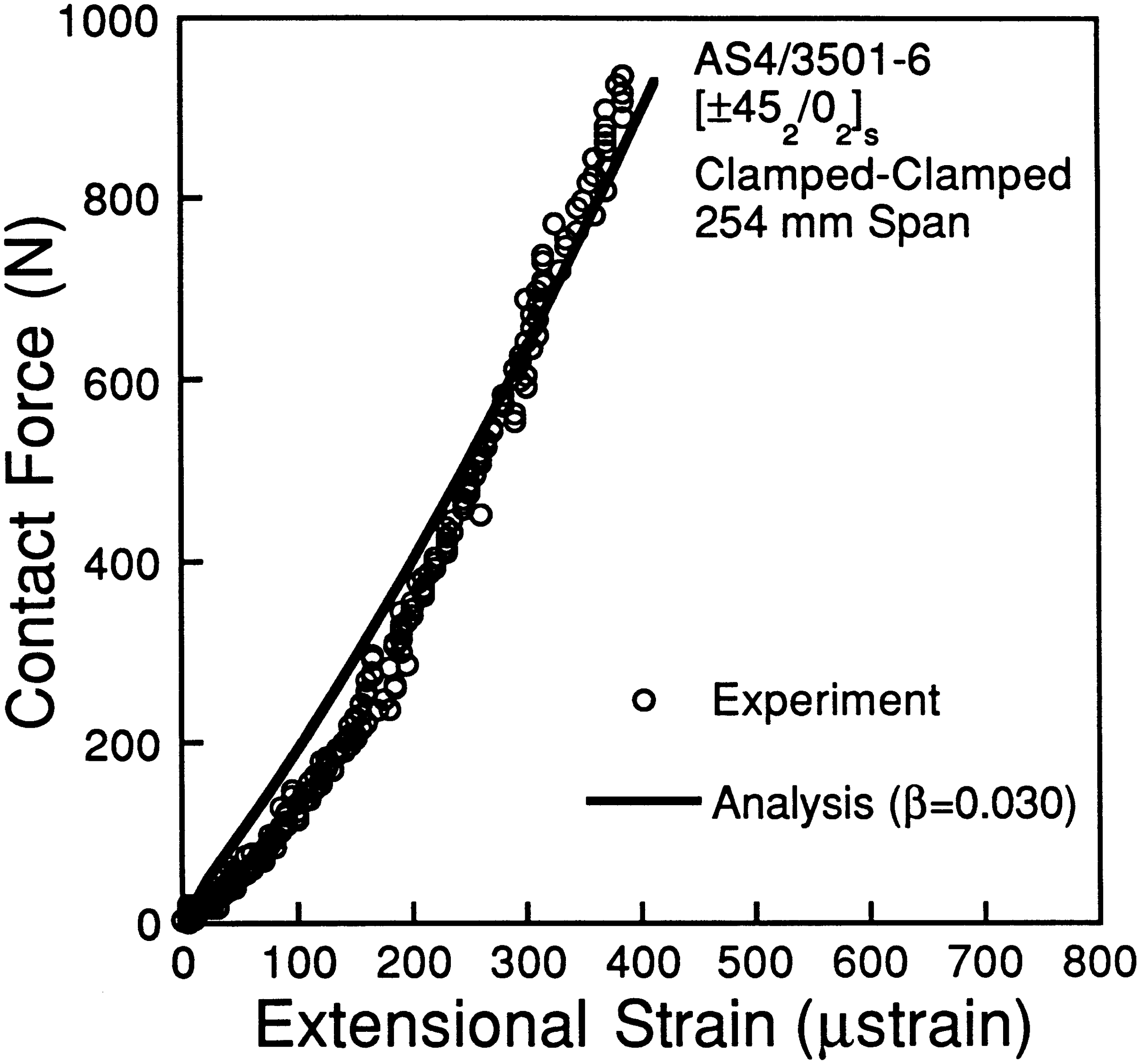

Figure 5.42 Experimental and analytical force-extensional strain data at the position for gages 5 and 6 (see Figure 3.2) for a specimen with a 254 mm span in a clamped-clamped support and tested to a maximum contact force of 930 N.

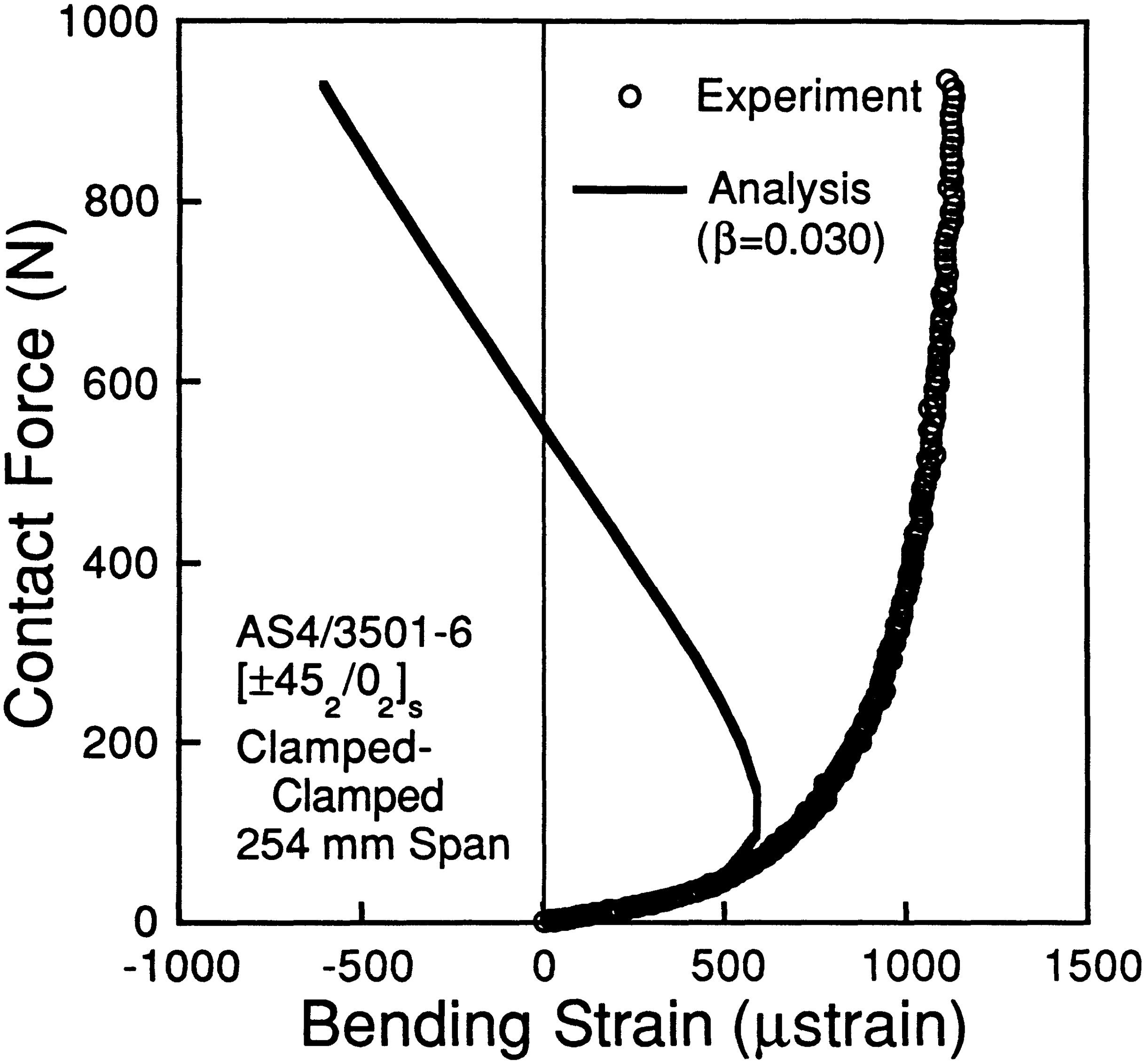

Figure 5.43 Experimental and analytical force-bending strain data at the position for gage 2 (see Figure 3.2) for a specimen with a 254 mm span in a clamped-clamped support and tested to a maximum contact force of 930 N.

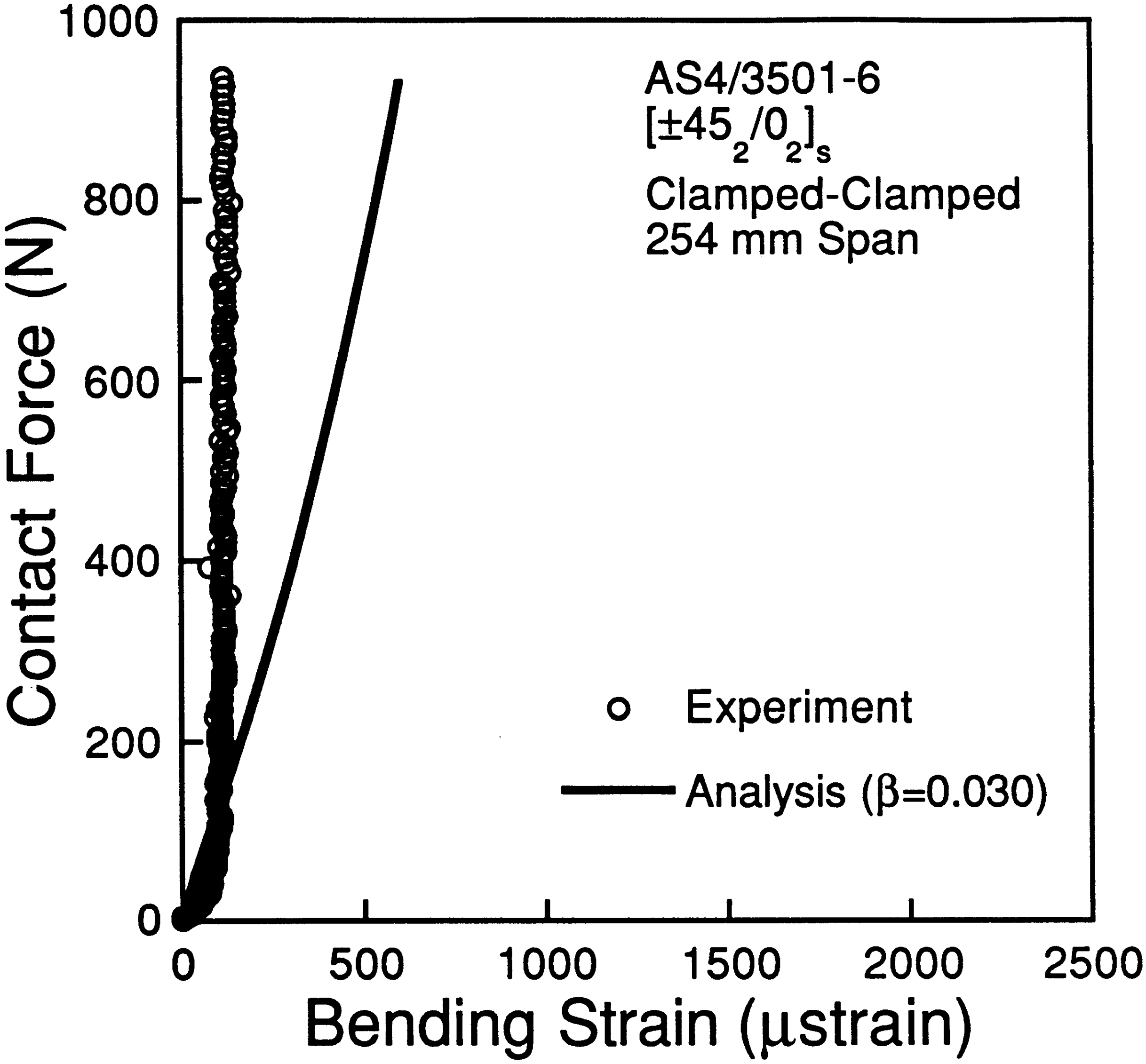

Figure 5.44 Experimental and analytical force-bending strain data at the position for gage 4 (see Figure 3.2) for a specimen with a 254 mm span in a clamped-clamped support and tested to a maximum contact force of 930 N.

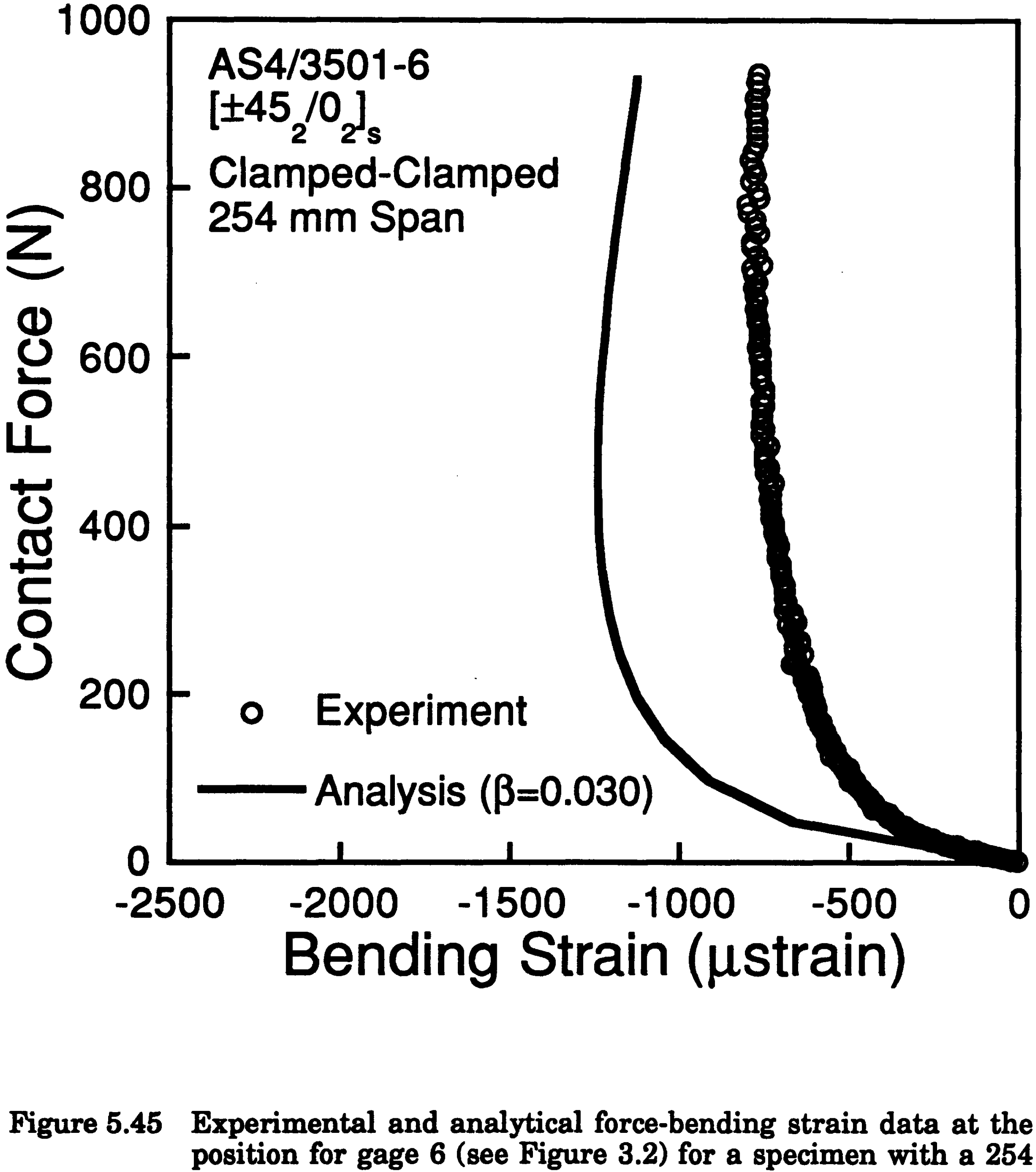

Figure 5.45 Experimental and analytical force-bending strain data at the position for gage 6 (see Figure 3.2) for a specimen with a 254 mm span in a clamped-clamped support and tested to a maximum contact force of 930 N.

5.40), which differ by approximately 22% at the maximum force level. The nonlinear analysis does not appear to predict the bending strains well. However, it does capture the general trends of the bending strains as the analysis captures both the nonlinear shape of the bending strain curve and the leveling off and reduction of the bending strains at high forces, as shown in Figures 5.43 and 5.45, except for gage 4, as shown in Figure 5.44. It should also be noted that the bending strains from the analysis predict the experimental strains well at low forces (below 100 N) where the plate is experiencing small deflections, and the behavior is linear.

5.3 Damage

The damage results are presented in this section via X-ray photographs taken of damage in the plane of the specimen and transcriptions of the damage observed in a cross-section through the thickness with a microscope, both as described in section 3.4. The transcriptions of the damage in a cross-section are useful in determining the through-the-thickness location of damage and its approximate shape. Note that the transcriptions are not to scale through-the-thickness. The X-ray photographs provide a more accurate description of the planar shape and extent of the damage in the laminate, but no through-the-thickness specifics.

Following the format of the discussion in section 5.1, damage for the tests using the rigid backface support boundary condition should be shown first. However, no damage was seen through either X-ray photography or microscopic examination for any of the maximum contact force levels (up to 1479 N) for which specimens were tested with this support condition.

The damage results outlining a make-up of the progression of damage during loading, using different specimens for each load level, are shown in Figures 5.46 through 5.50. These results represent the damage which occurred during tests on specimens with a 254 mm span using the clamped-clamped boundary condition. An X-ray and a transcription are shown for the maximum contact forces of 549 N, 739 N, 930 N, 1183 N and 1479 N. Damage was not observed at load levels below 549 N (444 N and 507 N). The first damage observed, as shown in Figure 5.46, occurred in a specimen loaded to a maximum contact force of 549 N and consists of a matrix crack extending approximately 8 mm, in the +45° plies nearer the backface, on each side of the hole used for injection of the DiB dye. The transcription of the microscopic examination was inconclusive as the crack could not be observed in the cross-section examined. However, a small delamination, which is not apparent in the X-ray photograph, was observed in the cross-section.

An increased extent of damage is seen at the higher force levels. The next step in the progression of damage that resulted from these tests consists of further matrix cracking and delaminations. This damage is seen to occur in the specimen loaded to a maximum contact force of 930 N as shown in Figure 5.48. The delaminations appear very small, indicating that they may have initiated from the matrix cracks at approximately this force level. The delamination is oriented along the +45° direction. The examination of the sectioned specimen under microscope showed that the delamination had occurred in the interface between the +45° and -45° plies nearer the back face of the laminate. Other delaminations were seen to occur in both interfaces between the -45° and 0° plies, with a matrix crack running between them at an angle through the 0° plies. The final step

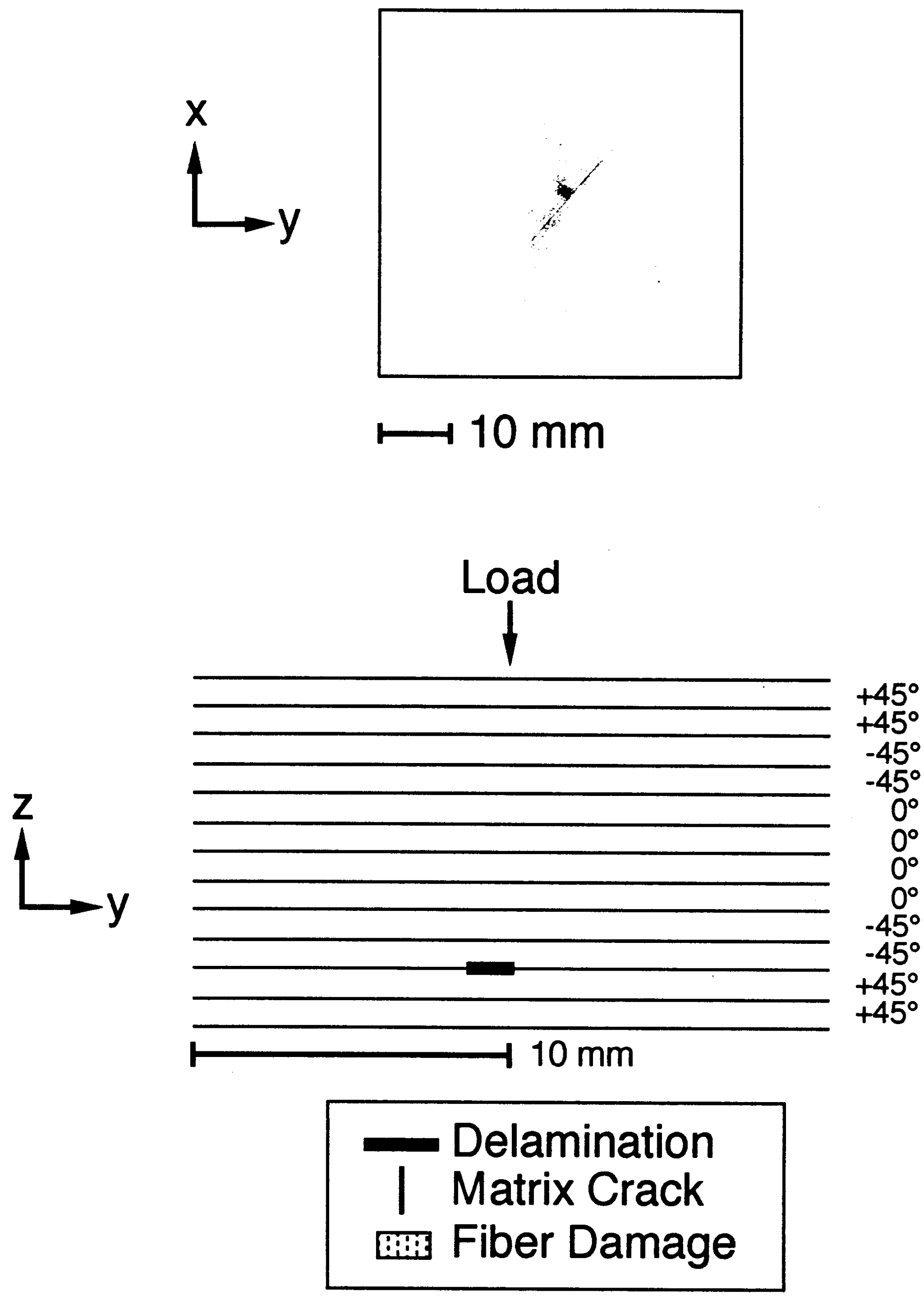

Figure 5.46 Damage in the specimen with a 254 mm span tested in a clamped-clamped support to a maximum contact force of 549 N via *(top)* X-ray photograph and *(bottom)* transcription of a cross-section.

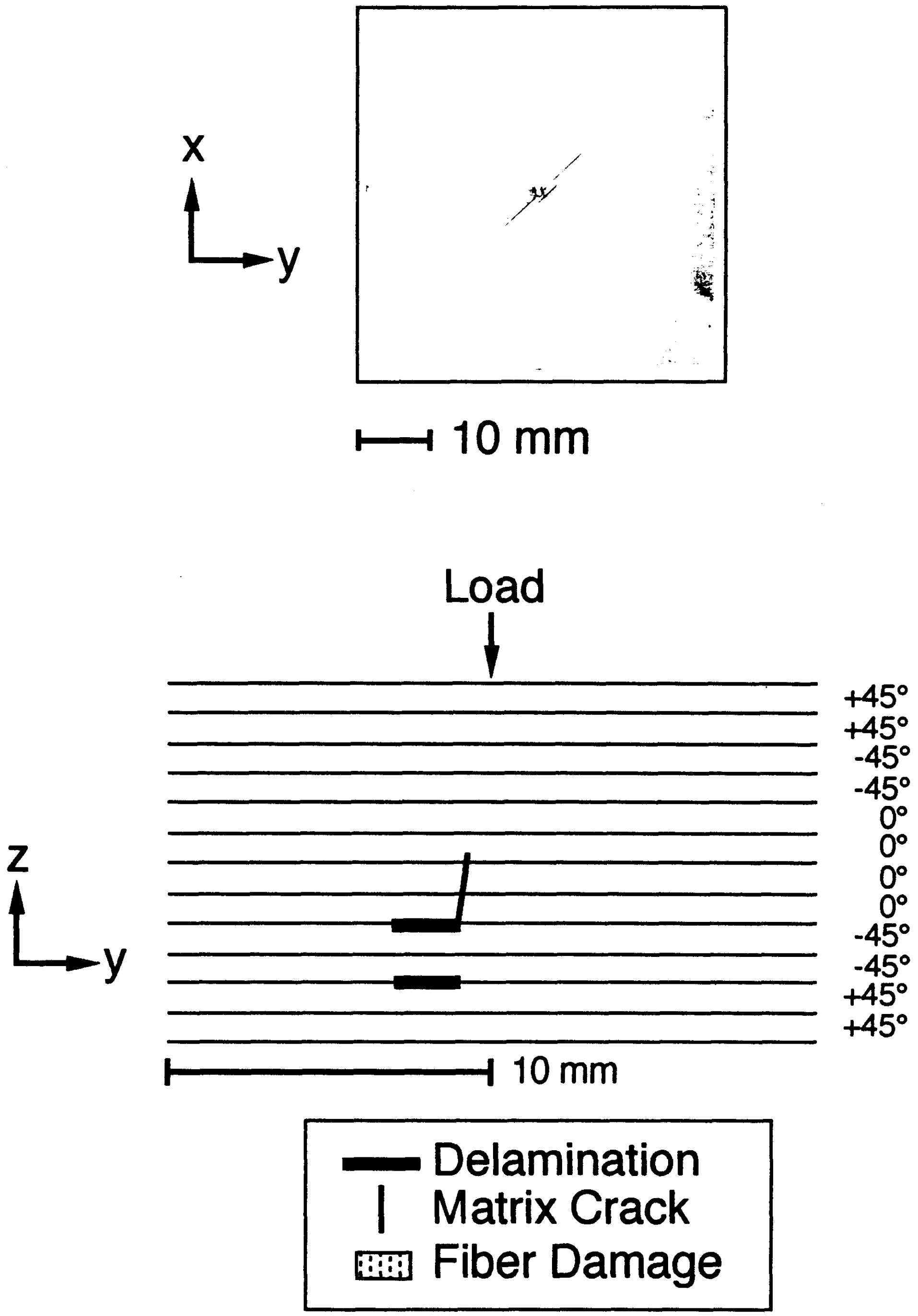

Figure 5.47 Damage in the specimen with a 254 mm span tested in a clamped-clamped support to a maximum contact force of 739 N via *(top)* X-ray photograph and *(bottom)* transcription of a cross-section.

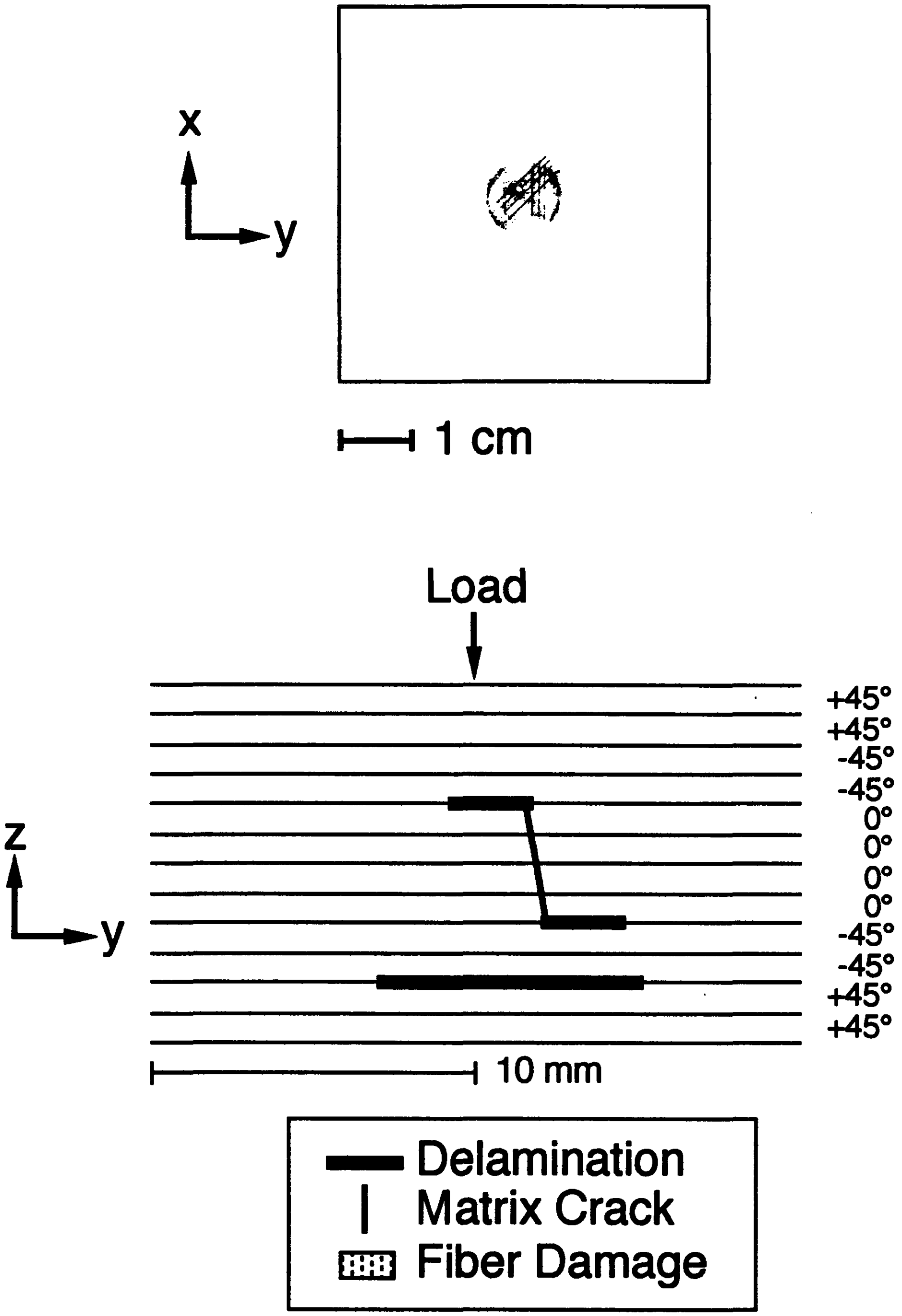

Figure 5.48 Damage in the specimen with a 254 mm span tested in a clamped-clamped support to a maximum contact force of 930 N via *(top)* X-ray photograph and *(bottom)* transcription of a cross-section.

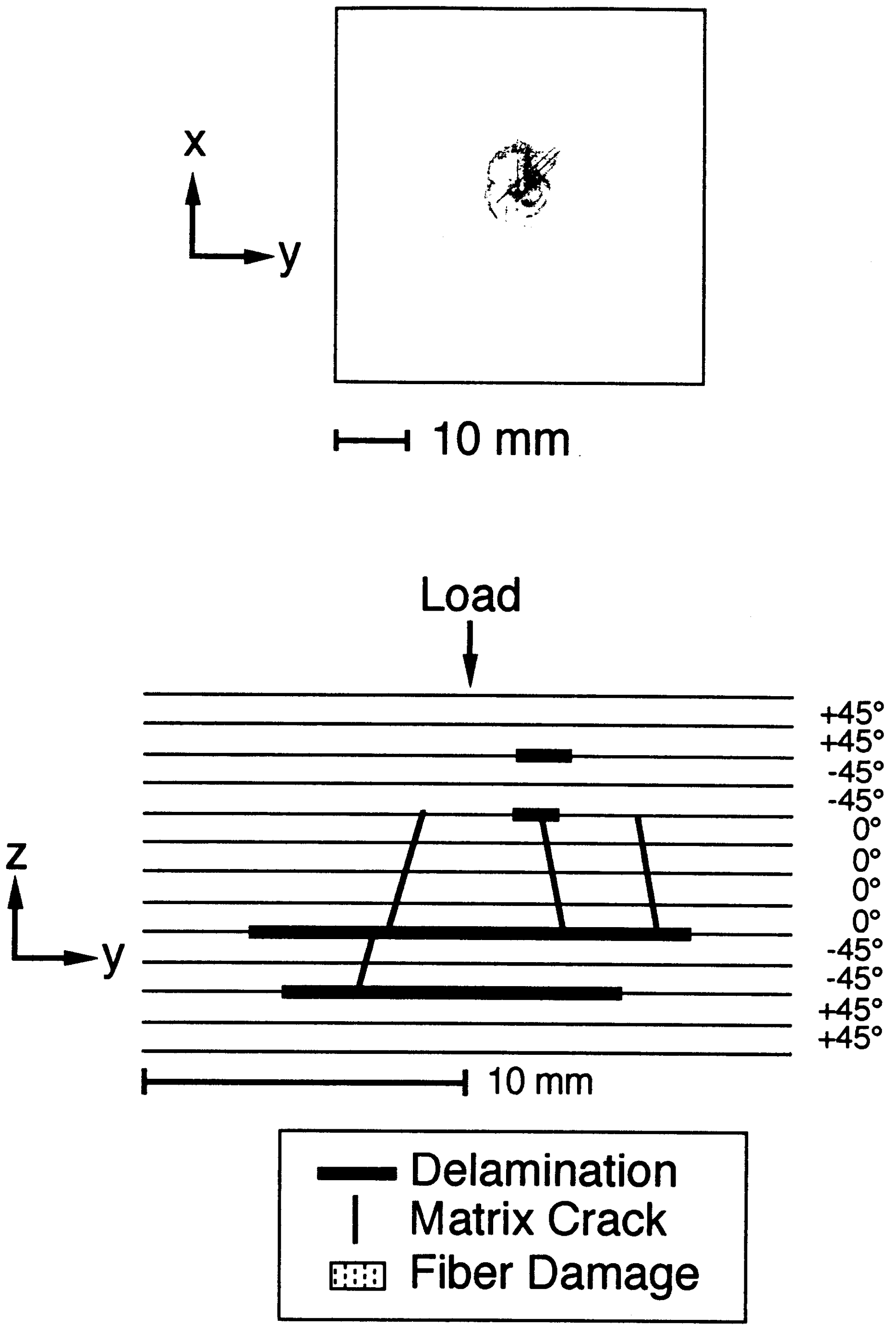

Figure 5.49 Damage in the specimen with a 254 mm span tested in a clamped-clamped support to a maximum contact force of 1183 N via *(top)* X-ray photograph and *(bottom)* transcription of a cross-section.

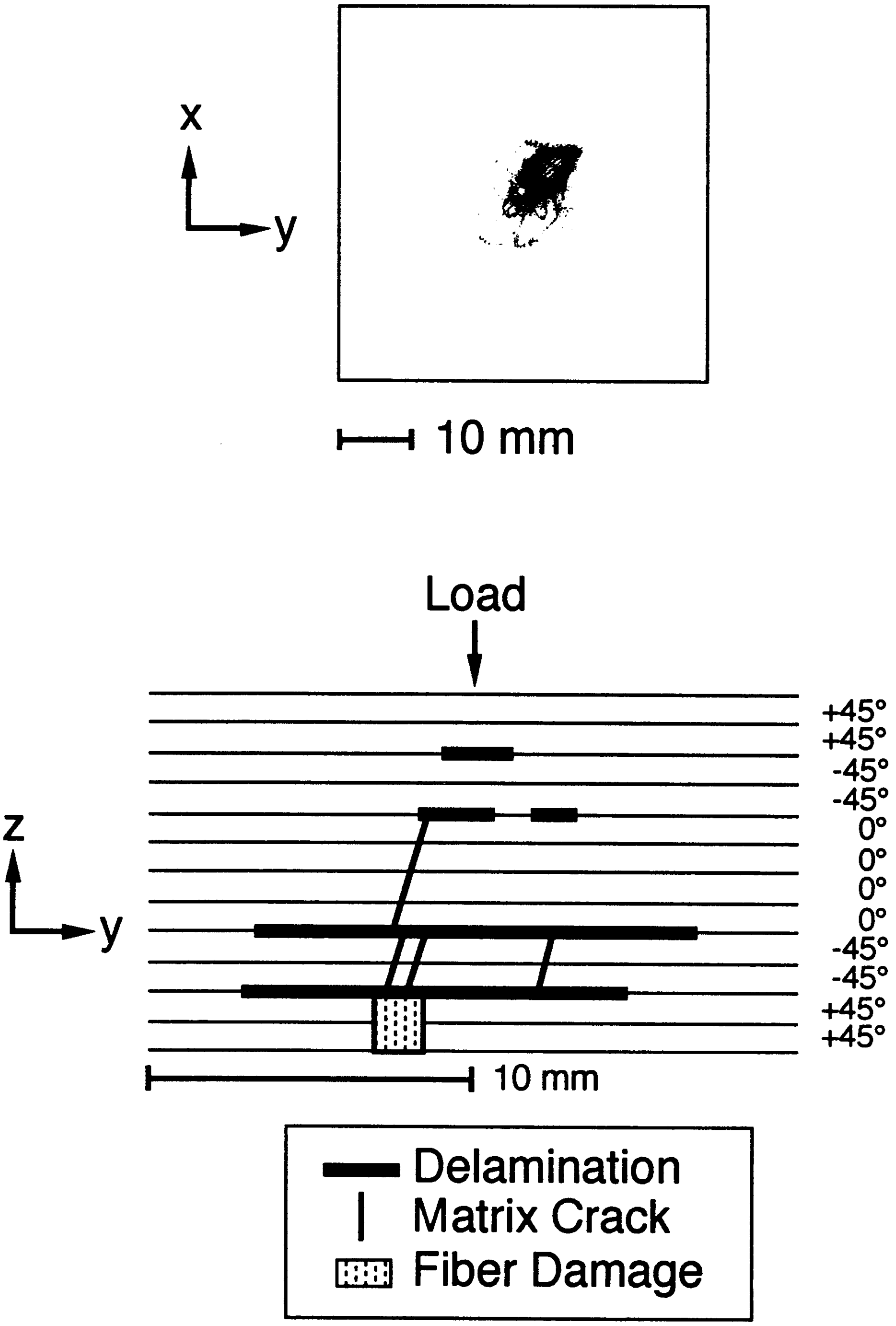

Figure 5.50 Damage in the specimen with a 254 mm span tested in a clamped-clamped support to a maximum contact force of 1479 N via *(top)* X-ray photograph and *(bottom)* transcription of a cross-section.

observed in the progression of damage consists of matrix cracking, further growth of delaminations, and fiber damage in the plies at the backface of the laminate. This damage resulted from loading the specimen to a maximum contact force of 1479 N and is shown in Figure 5.50. The largest delamination appears as an elongated ellipse extending in the +45° direction from the hole used to inject the DiB dye. The examination of the sectioned specimen under microscope showed that the largest area of delamination occurred in the interface between the +45° and -45° plies nearer the back face of the laminate, while delaminations could be seen in every interface. Matrix cracks were observed between delaminations in the -45°/0° and +45°/-45° interfaces nearer the backface of the specimen. An area of massive matrix and fiber damage was seen in the +45° plies at the backface of the specimen. This transcription shows that the extent of damage increases toward the back face of the laminate (away from the point of indentation).

The damage that occurs for specimens of different spans loaded to a maximum contact force of 930 N using the clamped-clamped boundary condition is observed to be similar in type, location, and extent. This is also observed for the specimens loaded to a maximum contact force of 1479 N. This can be seen through the X-ray photographs and transcriptions shown for the maximum contact force of 930 N in Figures 5.51 through 5.56 and the maximum contact force of 1479 N in Figures 5.57 through 5.62. The damage shown in Figures 5.51 through 5.56 is similar to the damage seen for the specimen with a 254 mm span loaded to a maximum contact force of 930 N, consisting of cracking and some small delaminations. The damage shown in Figures 5.57 through 5.62 is similar to the damage seen for the specimen with a 254 mm span loaded to a maximum contact force of

1479 N. This damage again consists of matrix cracking and delaminations for each span length. The most prominent delamination appears as an elongated ellipse extending in the +45° direction from the hole at the center. The examination of each sectioned span under microscope showed that the largest area of delamination occurred in the interface between the +45° and -45° plies nearer the back face of the laminate, while delaminations could be seen at every interface. Also, matrix cracks extend between the delaminations at the -45°/0° interfaces at an angle through the 0° plies. These transcription show that the extent of damage increases toward the back face of the laminate (away from the point of indentation). The important point to note is that for both maximum force levels, the damage appears to be of similar type, extent, and location regardless of the span length that was tested.

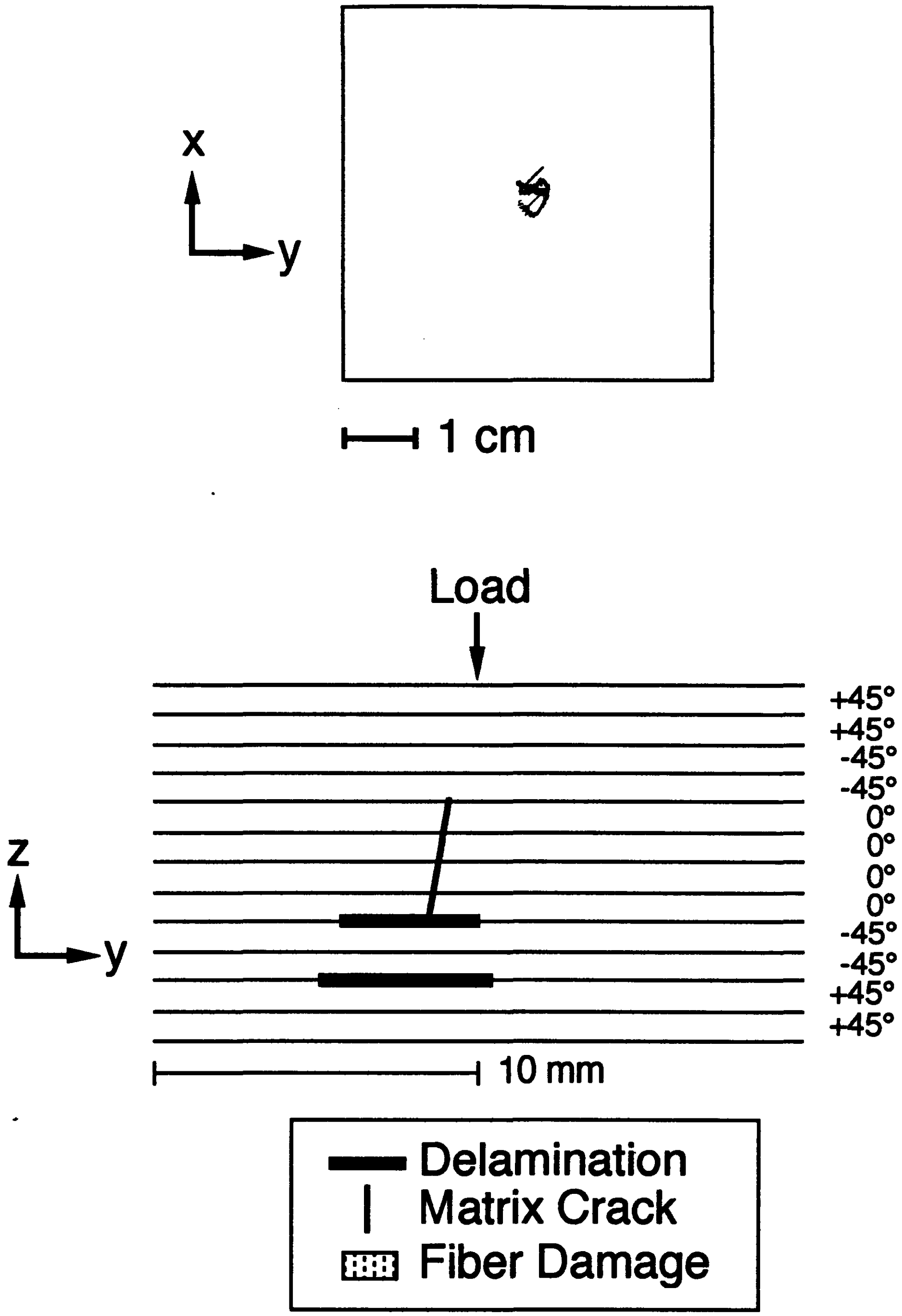

Figure 5.51 Damage in the specimen with a 32 mm span tested in a clamped-clamped support to a maximum contact force of 930 N via *(top)* X-ray photograph and *(bottom)* transcription of a cross-section.

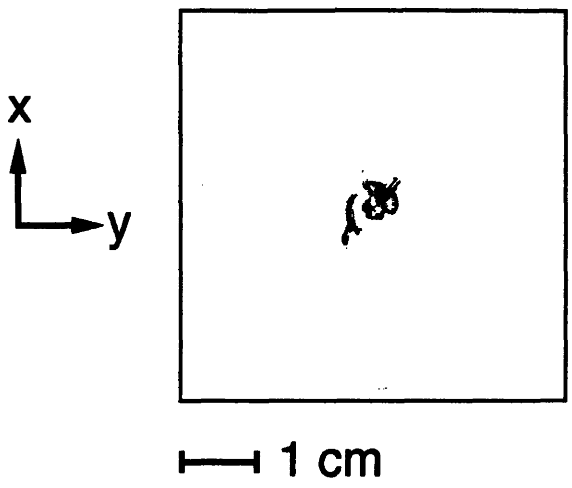

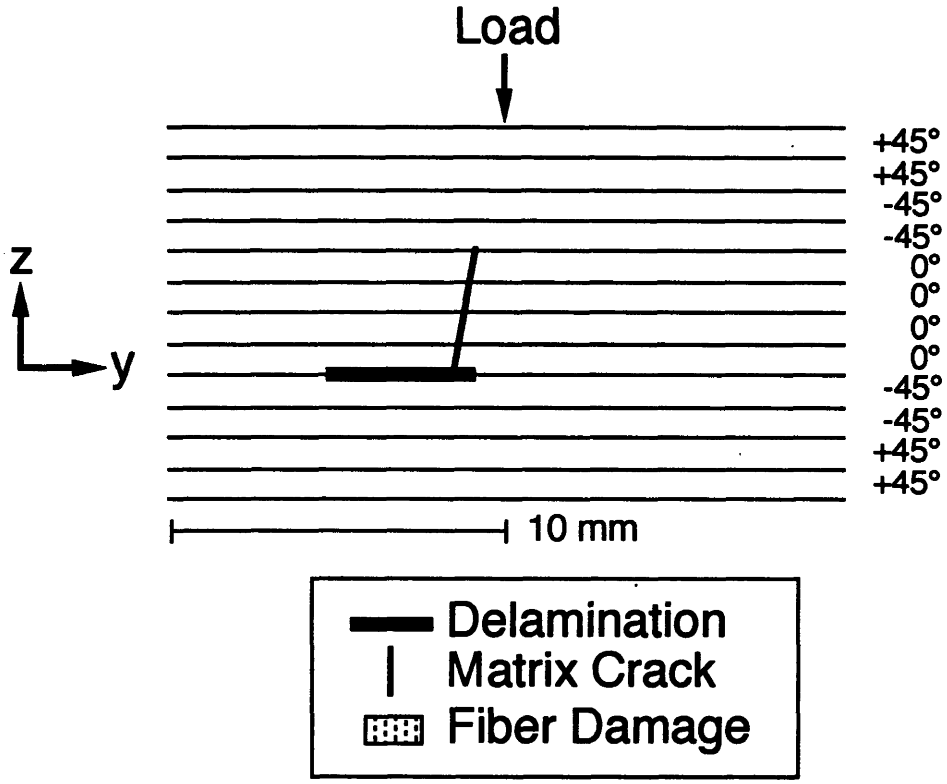

Figure 5.52 Damage in the specimen with a 63.5 mm span tested in a clamped-clamped support to a maximum contact force of 930 N via *(top)* X-ray photograph and *(bottom)* transcription of a cross-section.

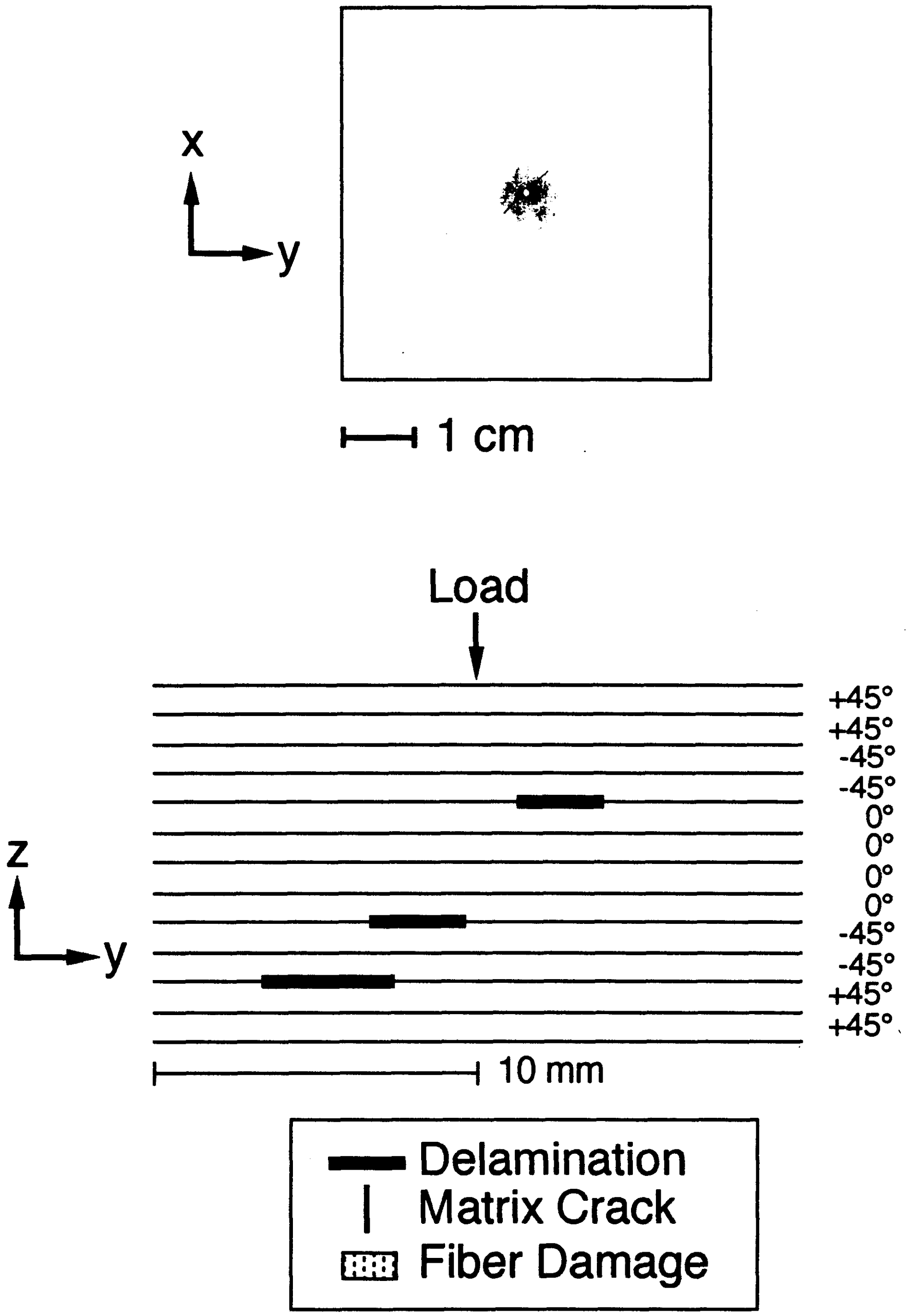

Figure 5.53 Damage in the specimen with a 127 mm span tested in a clamped-clamped support to a maximum contact force of 930 N via *(top)* X-ray photograph and *(bottom)* transcription of a cross-section.

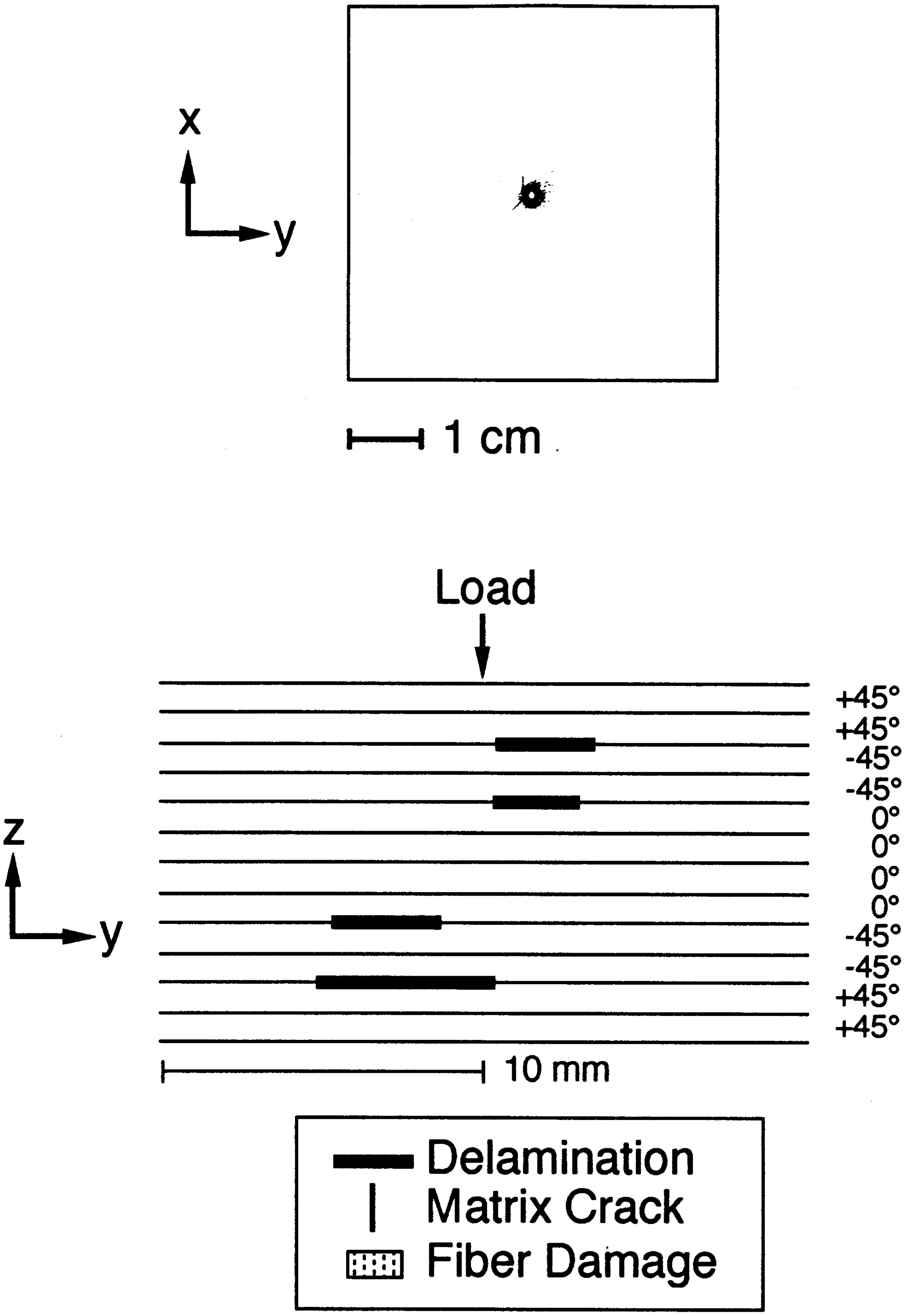

Figure 5.54 Damage in the specimen with a 254 mm span tested in a clamped-clamped support to a maximum contact force of 930 N via *(top)* X-ray photograph and *(bottom)* transcription of a cross-section.

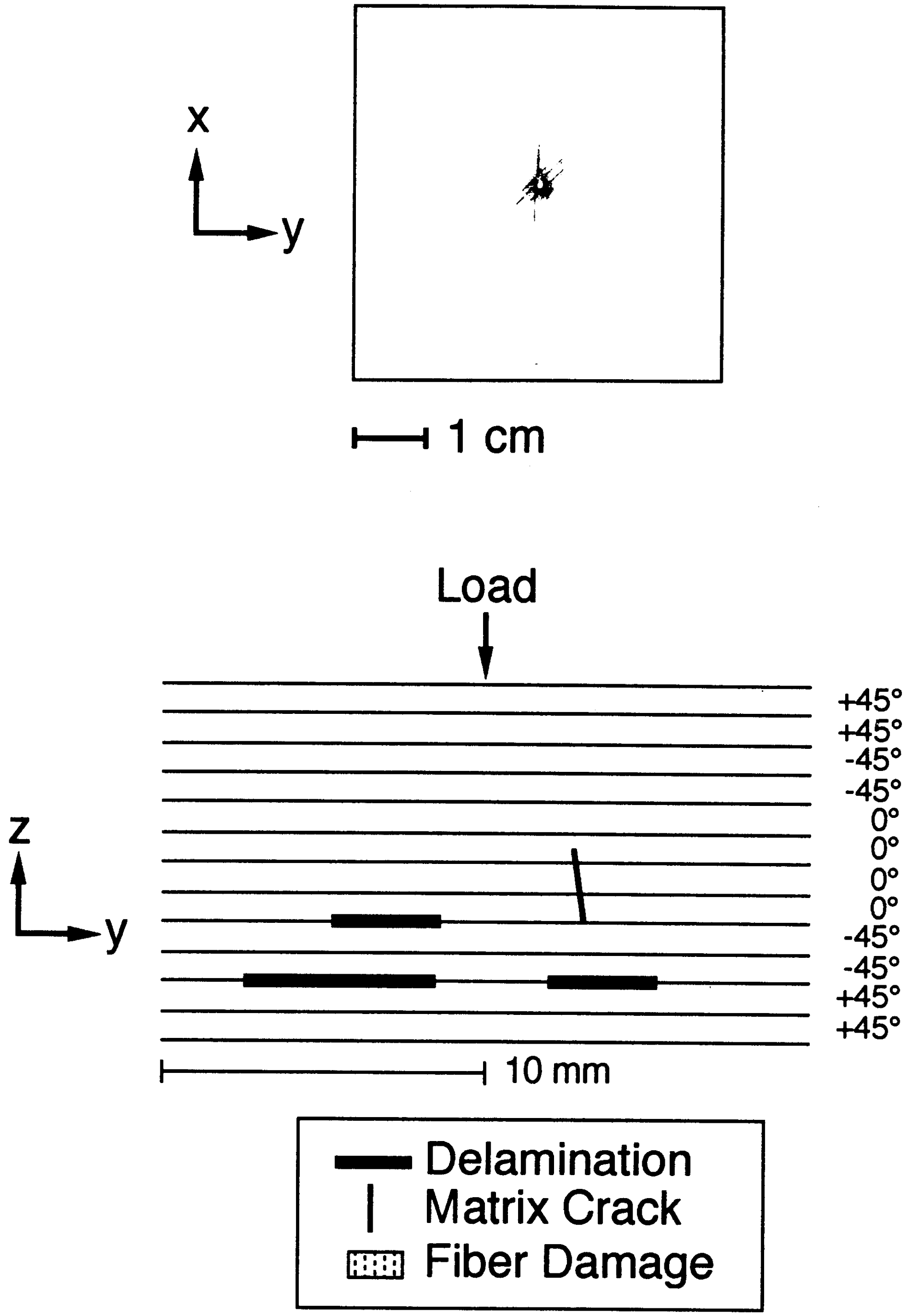

Figure 5.55 Damage in the specimen with a 381 mm span tested in a clamped-clamped support to a maximum contact force of 930 N via *(top)* X-ray photograph and *(bottom)* transcription of a cross-section.

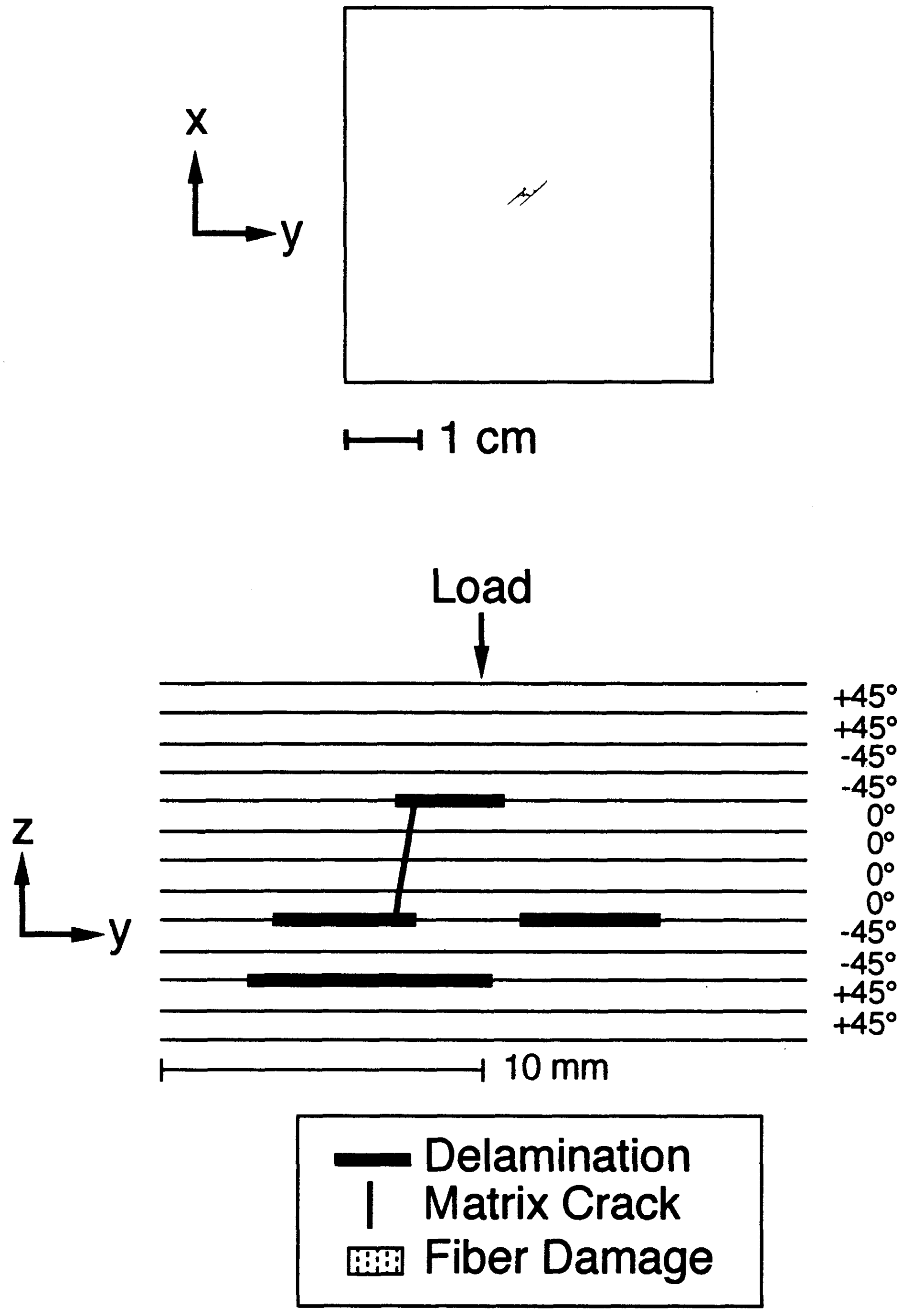

Figure 5.56 Damage in the specimen with a 508 mm span tested in a clamped-clamped support to a maximum contact force of 930 N via *(top)* X-ray photograph and *(bottom)* transcription of a cross-section.

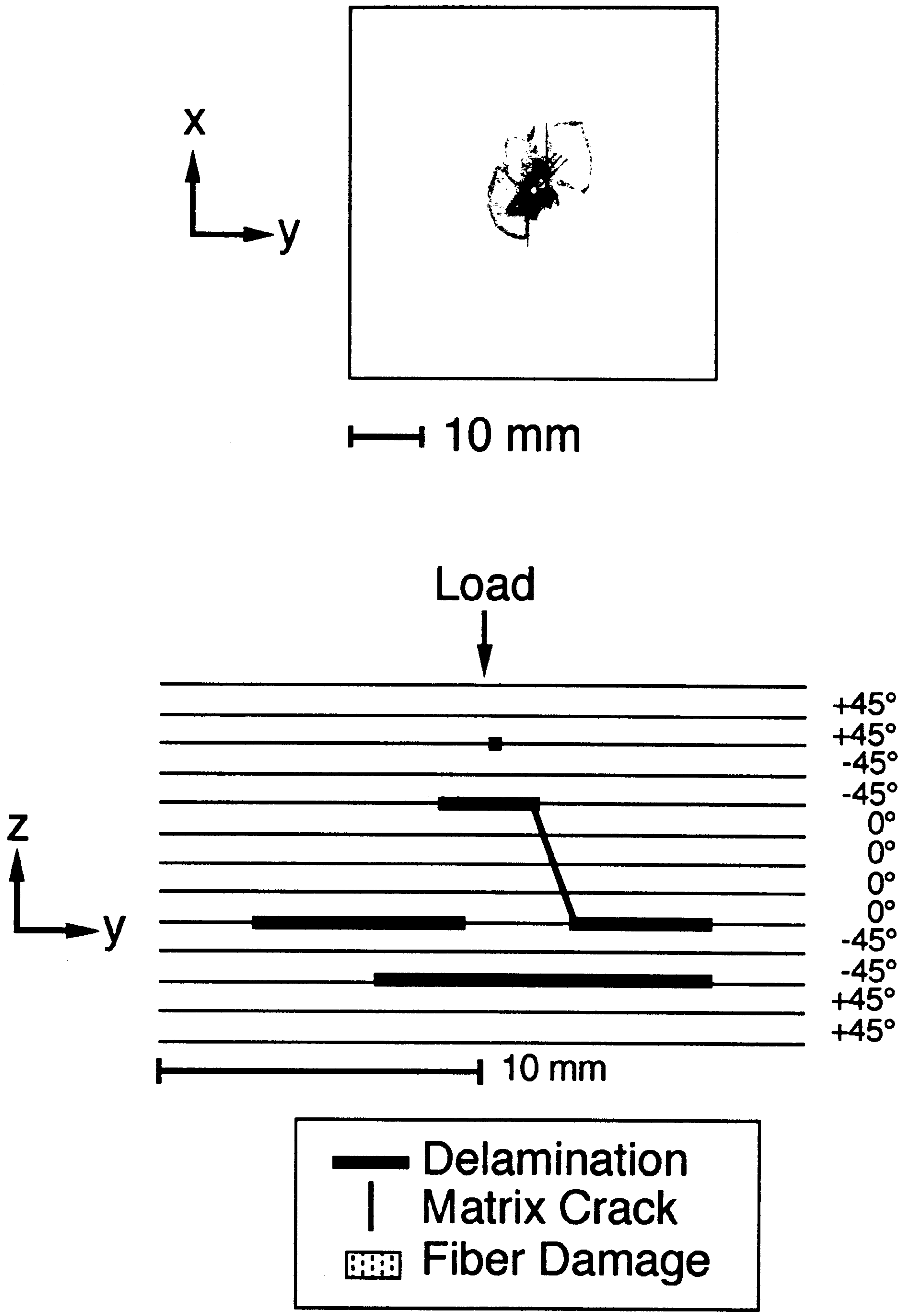

Figure 5.57 Damage in the specimen with a 32 mm span tested in a clamped-clamped support to a maximum contact force of 1479 N via *(top)* X-ray photograph and *(bottom)* transcription of a cross-section.

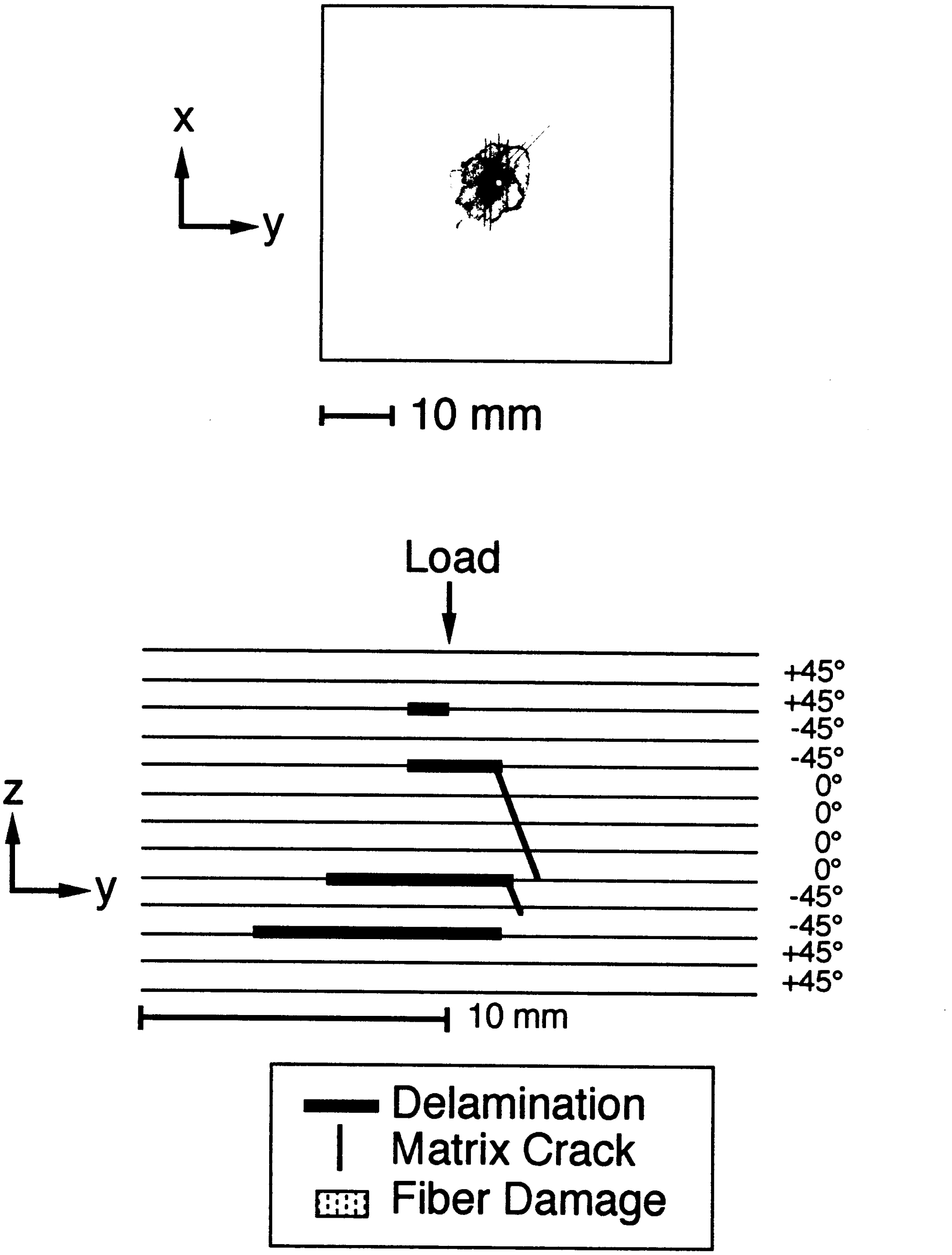

Figure 5.58 Damage in the specimen with a 63.5 mm span tested in a clamped-clamped support to a maximum contact force of 1479 N via *(top)* X-ray photograph and *(bottom)* transcription of a cross-section.

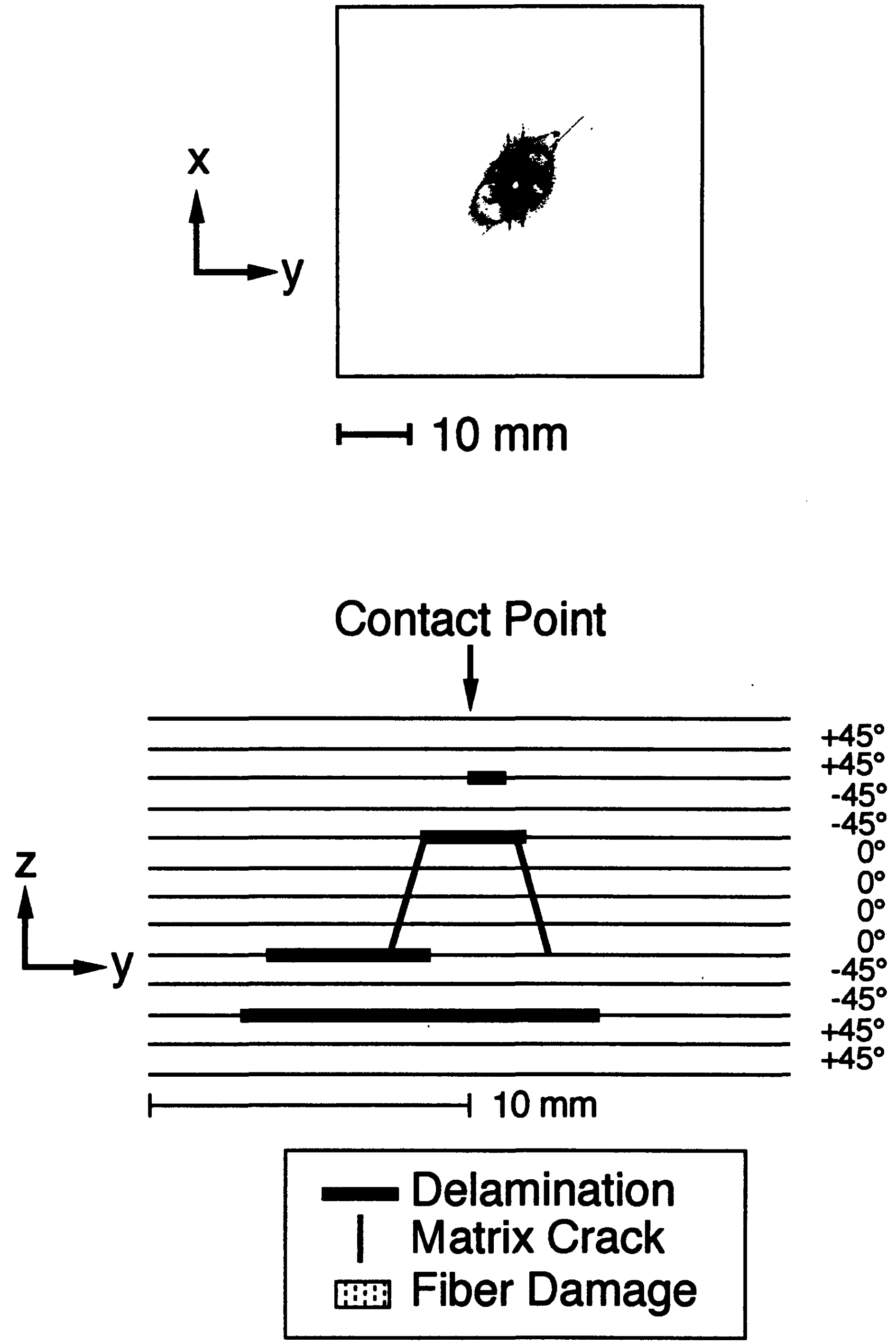

Figure 5.59 Damage in the specimen with a 127 mm span tested in a clamped-clamped support to a maximum contact force of 1479 N via *(top)* X-ray photograph and *(bottom)* transcription of a cross-section.

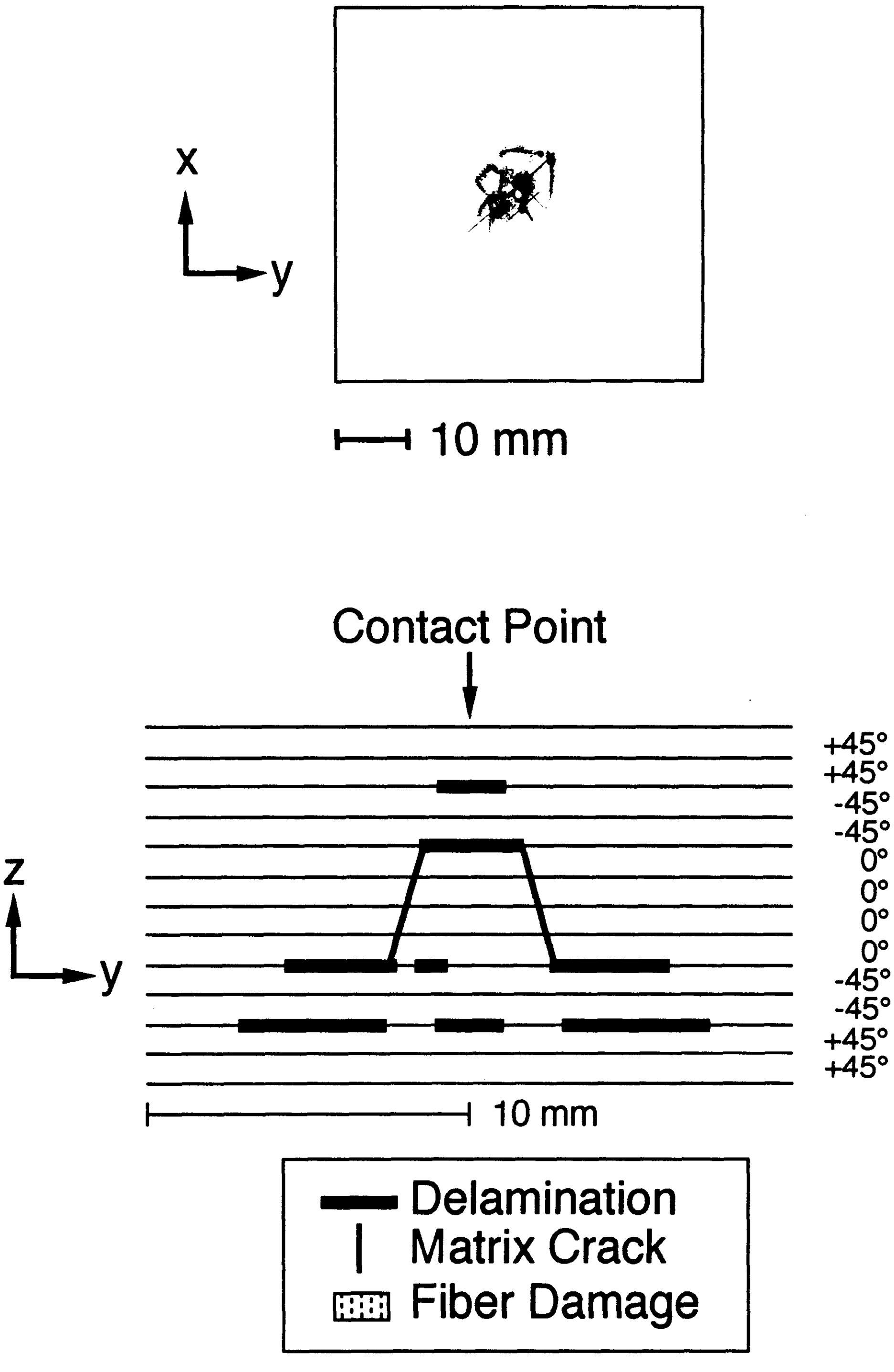

Figure 5.60 Damage in the specimen with a 254 mm span tested in a clamped-clamped support to a maximum contact force of 1479 N via *(top)* X-ray photograph and *(bottom)* transcription of a cross-section.

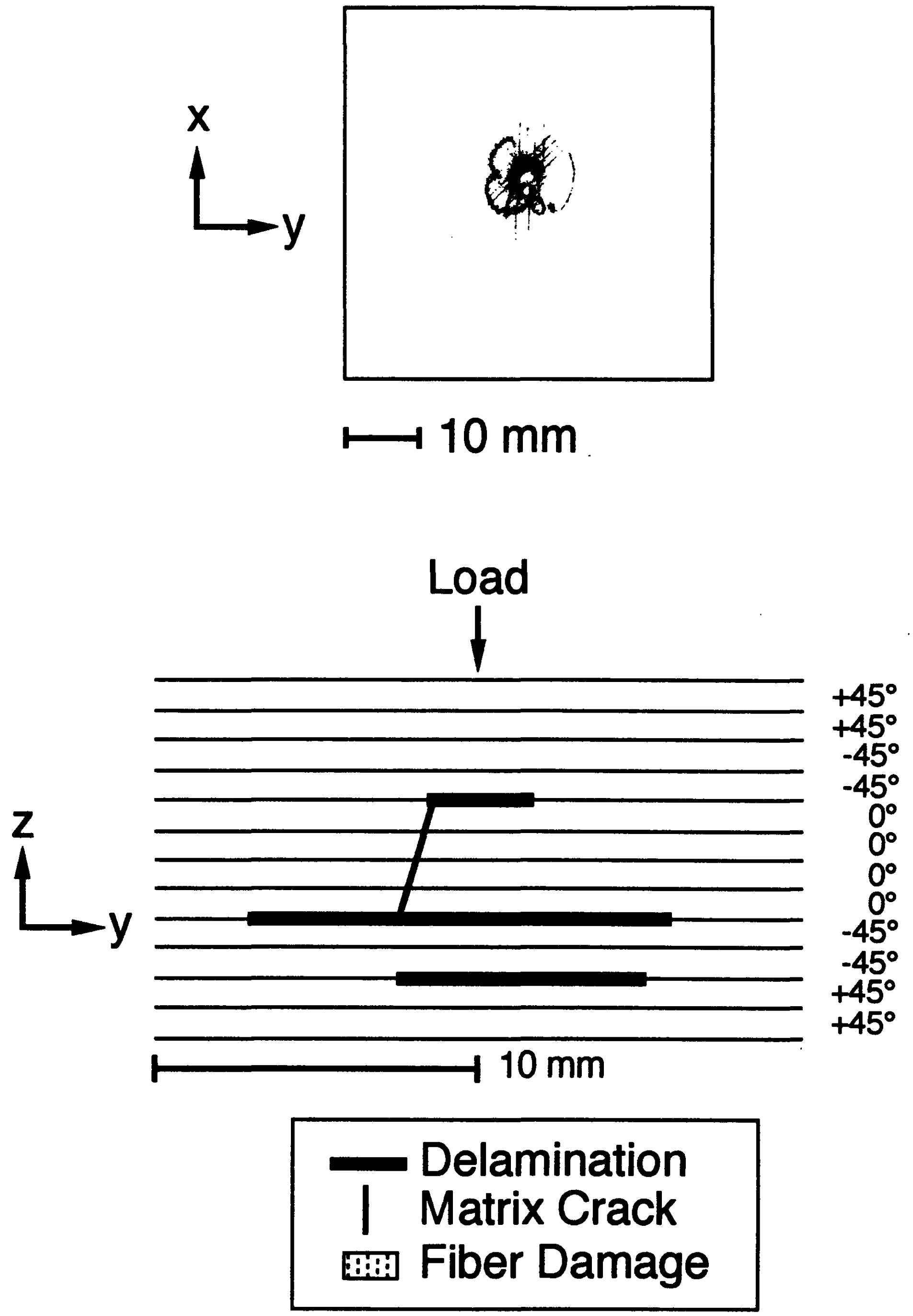

Figure 5.61 Damage in the specimen with a 381 mm span tested in a clamped-clamped support to a maximum contact force of 1479 N via *(top)* X-ray photograph and *(bottom)* transcription of a cross-section.

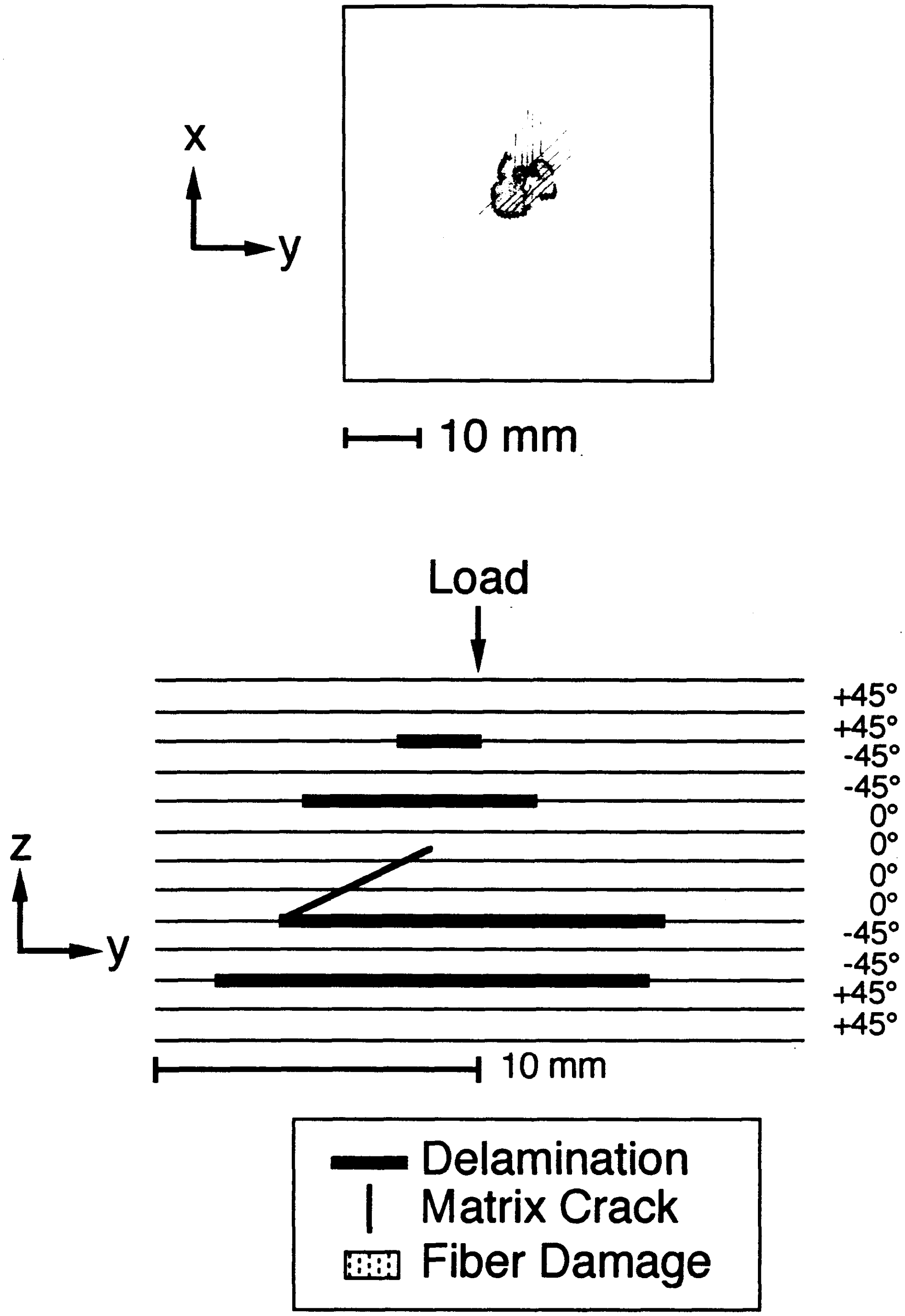

Figure 5.62 Damage in the specimen with a 508 mm span tested in a clamped-clamped support to a maximum contact force of 1479 N via *(top)* X-ray photograph and *(bottom)* transcription of a cross-section.

Chapter 6

DISCUSSION OF RESULTS

The goals of this investigation are to understand how the structural parameters of plate span and boundary condition influence the (impact) damage resistance, to evaluate the ability of the nonlinear analysis to predict the indentation event, and to understand how static indentation results compare with impact results. These issues will be addressed in this chapter through observations that can be made from the data obtained from the indentation experiments and analysis as reported in Chapter 5.

6.1 Effects of Boundary Condition

Two boundary conditions were used in this investigation, clamped-clamped and rigid backface support, as described in Chapter 3. These boundary conditions provide different supports for the specimen: the rigid backface support fixes the deflection of the backface of the specimen to zero and therefore has a nonzero through-the-thickness stress on the backface opposite the indentor; whereas the clamped-clamped support fixes only the ends of the specimen, allowing the specimen to bend, and has zero through-the-thickness stress on the backface opposite the indentor. These conditions cause different behavior to occur as observed in the test data. For example, the clamped specimens undergo deflections as high as 23 mm while the specimens supported on the backface have zero deflection.

In the tests with rigid backface support, consistently different indentation behavior occurred as compared to that from tests with the clamped-clamped condition. This is manifested in terms of higher indentations for the rigid backface support condition than those seen at the same force level for the clamped-clamped condition. The maximum indentations for the rigid backface support condition were approximately two times larger than the corresponding indentation for the clamped-clamped case as shown in Table 5.1. The indentations could be smaller for the clamped-clamped case because the global bending, which is allowed in this case, allows the indentor to contact the specimen over a greater area. This larger contact area results because the spherical indentor contacts the curved plate over a larger arc as the plate curves more (increased bending) with increased force. This situation hinges on the fact that the indentor is spherical and the specimens are undergoing approximately cylindrical bending, allowing "smooth" contact over a continuous surface on both the indentor and the plate. The contact force is therefore distributed over a larger area, producing lower peak contact stresses and therefore less indentation. The total contact force, which is the integral of the stress over the contact area, remains constant for the two cases, but, since the contact area changes, the maximum contact stress is larger for the rigid support case. This effect is illustrated in Figure 6.1. In addition to this effect, the through-thickness stress (σ_{zz}) on the backface opposite the indentor is nonzero for the rigid backface support. This causes the average through-thickness stress in a specimen which has a rigid backface support to be higher than the average through-thickness stress in a clamped specimen. Because the average through-thickness strain and therefore the indentation is proportional to the average through-thickness stress, this can also result in higher indentations for the cases with a rigid backface support.

The values of the local contact stiffness, k, for the rigid backface support condition were observed to be smaller than the corresponding

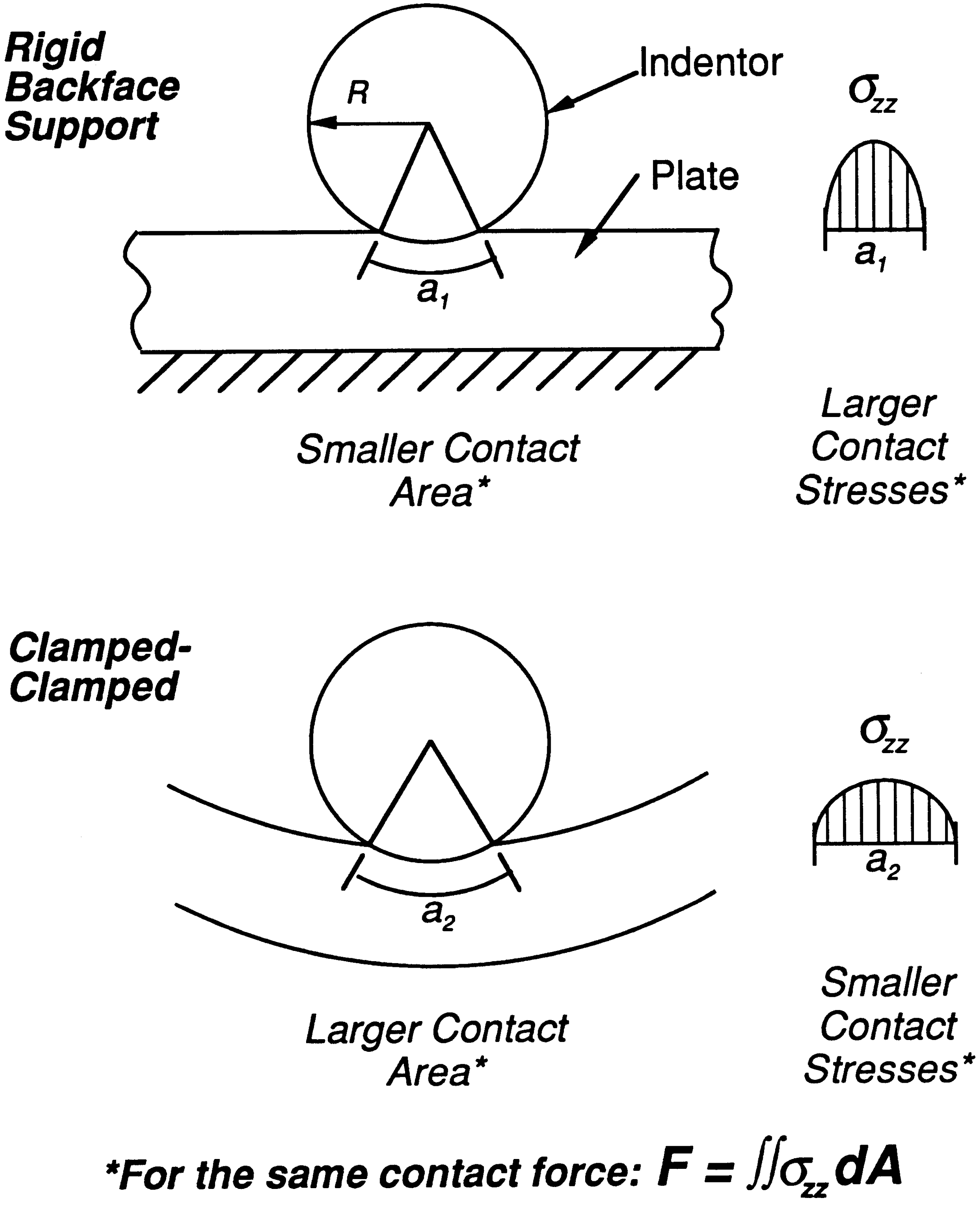

Figure 6.1 Illustration of the contact stress state for the rigid backface support and clamped-clamped boundary conditions.

values for the clamped-clamped case, as shown in Tables 5.3. From the constrained curve fit, the values of the contact stiffness for the rigid backface support condition were seen to be on the order of one-half of those seen for the clamped-clamped condition (see Table 5.4)†. The smaller values of k indicate that a specimen which is supported on the backface is more locally compliant through-the-thickness on a structural basis than a corresponding specimen which is clamped on two ends. In this latter case, the local compliance is affected by the structural conditions due to an apparent interaction with the bending. The values of the contact relation exponent, n, for the rigid backface support condition were observed to be smaller than the corresponding values for the clamped-clamped case, as shown in Tables 5.2. The constrained fit also showed that, on average, the data from the rigid backface support tests was fit better using an exponent of 1.5 than the clamped-clamped data. The values of n for the rigid backface support lie closer to the value of 1.5 expected from Hertzian contact theory. This result is expected because the rigid backface support condition more closely imitates the Hertzian assumption of contact with an elastic half-space [12]. The values of n for the clamped-clamped case, which are closer to two, do not match the Hertzian value. This discrepancy results because the half-space assumption of Hertzian contact theory is not a good approximation, in this case, due to the bending which occurs in the clamped-clamped plate and the fact that the through-thickness stress will be zero on the backface.

---

† The constrained curve fit yields values for the contact stiffness which are more easily compared than the unconstrained fit because they have consistent units (kN/mm^n, where n is equal to 1.5 for the constrained fit, but may be any value for the unconstrained fit).

Another important difference between cases with the two different boundary conditions is that the rigid support cases show no damage up to loads of 1479 N while the clamped-clamped cases show a progression of damage for the same forces tested, beginning at loads between 507 N and 549 N. Again, the explanation is that bending is allowed in the clamped case. This causes a difference in the stress state in the plates: the clamped-clamped plate transmits the contact stresses to the boundaries through global bending stresses along the whole span of the plate, whereas the plate supported on its backface transmits the contact stresses to the boundary on the backface through local through-the-thickness stresses. This situation results in large in-plane (bending) stresses in the clamped plate. The bending stresses are tensile in the back half of the laminate and increase in magnitude toward the backface. This causes matrix cracking and delaminations with the amount of such damage increasing toward the backface of the laminate as observed in the damage descriptions in Chapter 5. This pattern of backface damage has been seen previously in thinner laminates which are allowed to bend globally [33]. Damage incipience and progression was not investigated past a contact load of 1479 N for the rigid backface support condition so the type and location of damage which will develop in this case is not known. However, evidence exists [33] that thicker laminates show cracking and delamination, in the plies nearer the contact surface, which results from high local contact (through-the-thickness) stresses. This situation is similar to the rigid backface support condition which appears thick due to the support. As a result, it is expected that if higher force levels had been tested, damage in specimens with a rigid backface support would initiate in the plies near the upper face, where the local stresses are highest, and consist of matrix cracking and delamination. However, the creation of this type of damage, which is similar to that seen previously [33], would have to be verified.

6.2 Effects of Span

In this investigation, specimens in the clamped-clamped boundary condition with a range of spans between 32 mm and 508 mm were loaded to two different maximum contact forces, 930 N and 1479 N, as described in Chapter 3. The different bending effects, which this variety of plates experience, are most evident from the observation that, at the same force level, specimens with larger spans undergo larger deflections than specimens with smaller spans. This is because a longer specimen has a longer moment arm from the point of application of force to the boundary which creates a larger bending moment and therefore a larger deflection for larger spans.

The contact behavior may also be affected by the span. This may be seen if the force-indentation data for each of the different kinds of tests is overplotted. Overplots for the rigid backface support tests loaded to different maximum contact forces, the tests on the specimens with a 254 mm span in a clamped-clamped support loaded to different maximum contact forces, and the tests on specimens with different spans in a clamped-clamped support are shown in Figures 6.2, 6.3, and 6.4, respectively. The rigid support data is consistent (within experimental error) for each of the tests to a maximum contact force, as is the clamped-clamped data. However, the data for different spans shows a variation that does not have an obvious relationship with span, as seen in Figure 6.4. Because there is such a wide variation in the data for different spans when compared to the other tests, it is likely that span affects the relationship. Unfortunately, the small sample

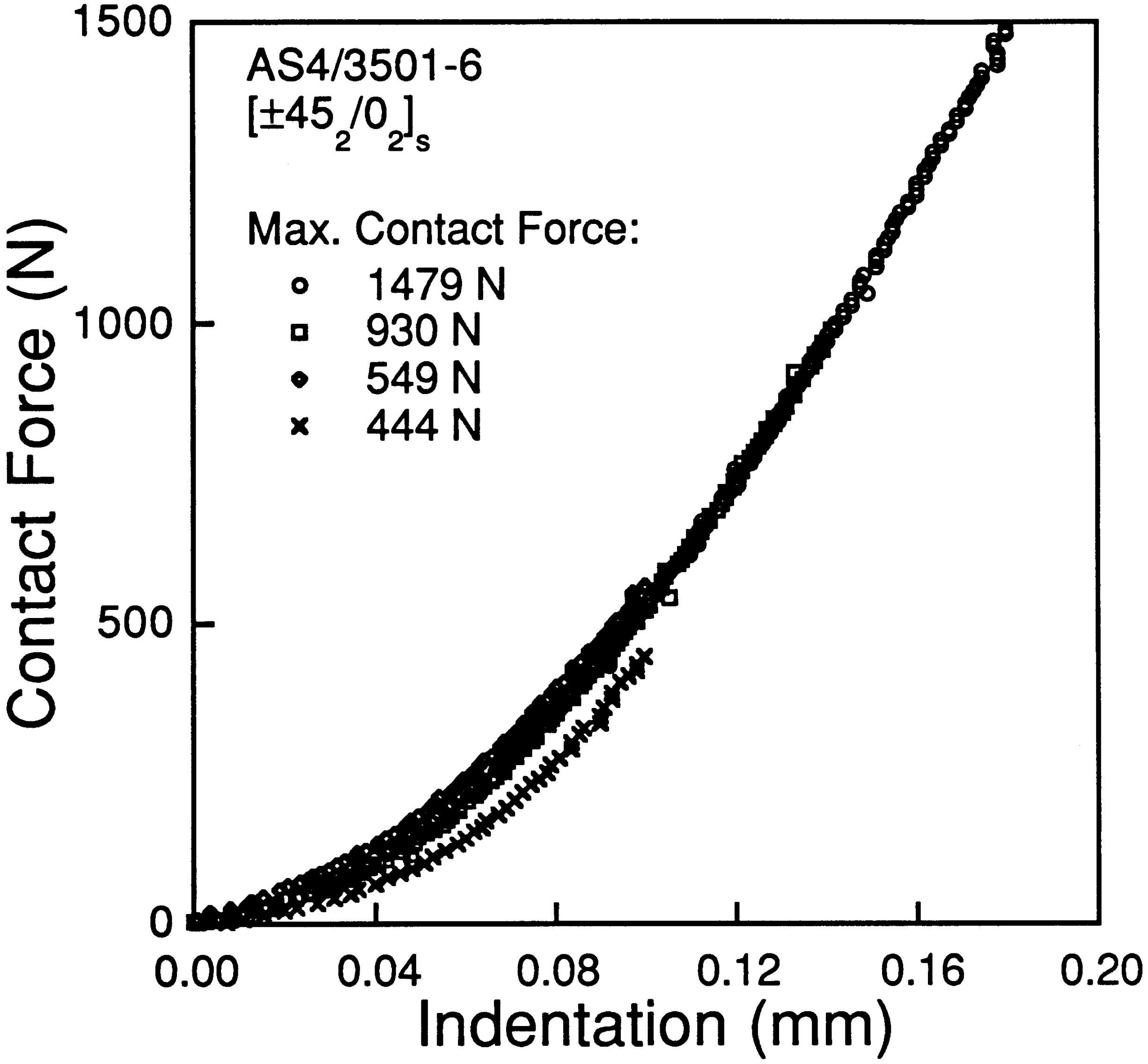

Figure 6.2 Overplotted force-indentation data for tests to different maximum contact forces with a rigid backface support boundary condition.

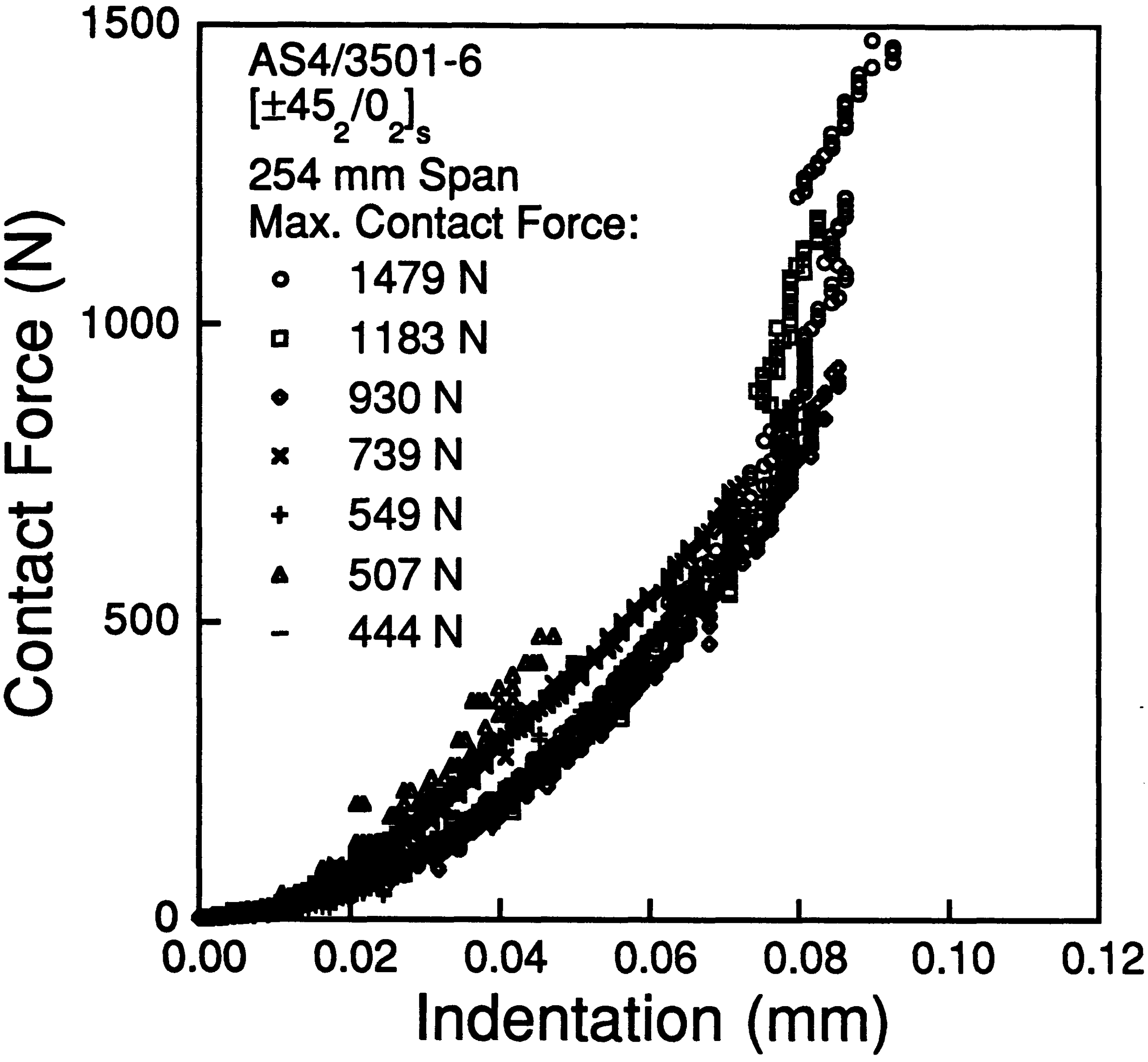

Figure 6.3 Overplotted force-indentation data for tests to different maximum contact forces using specimens with a 254 mm span and a clamped-clamped boundary condition.

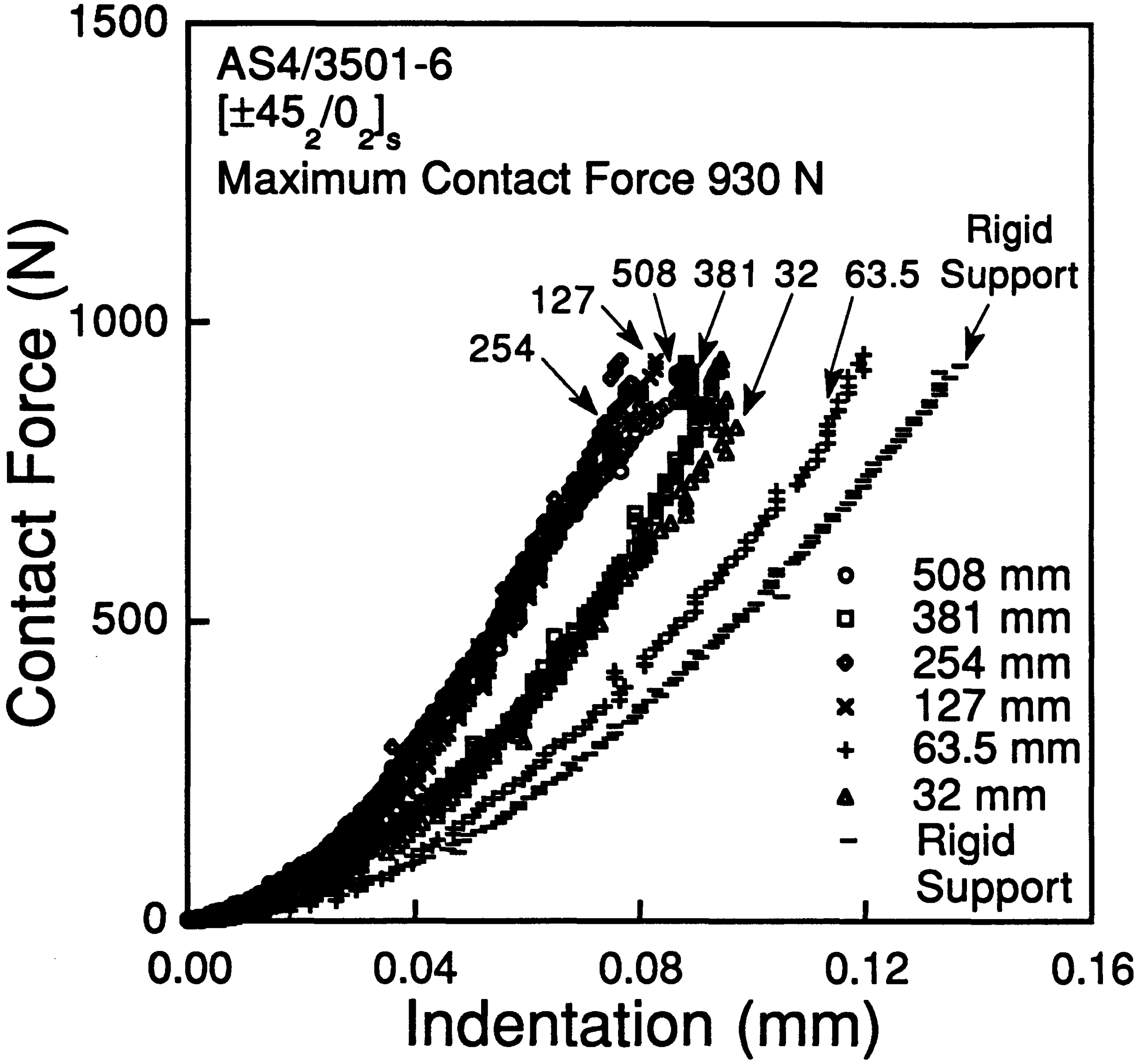

Figure 6.4 Overplotted force-indentation data for specimens with different spans loaded to a maximum contact force of 930 N using a clamped-clamped boundary condition.

of data for each span is not sufficient to definitively say what that relationship is. The general trend may be that the indentations decrease for a given force as span increases, but this would have to be determined conclusively through more tests.

If the range of indentations seen for contact forces of 200 N (indentation range approximately equal to ±0.01 mm) and 500 N (indentation range approximately equal to ±0.02 mm) in Figure 6.3 can be considered representative of the range of data for the force-indentation results, then, by accounting for this variability, it could be concluded that the indentation at a given force level decreases with increasing span. This can be seen if the indentation is plotted, accounting for the variability for each force, against specimen span as seen in Figures 6.5 and 6.6 for contact force levels of 200 N and 500 N, respectively. In these figures, a line, which decreases monotonically with span, can be drawn through the range of variability of the indentations, indicating that a monotonically decreasing relationship may exist between span and indentation. The data may also indicate that span does not affect indentation because a horizontal line (indicating the indentation is not affected by span) may also be drawn through the range of variability of the indentations. Additionally, because it allows no bending, the rigid backface case effectively acts as a zero span plate. In this way, the rigid backface support can be thought of as the upper limit on indentations for specimens of different spans (for this reason, the rigid support test to a force level of 930 N was included in Figure 6.4). This also indicates that indentation may decrease as span increases. If this behavior were occurring, it could be explained in the same way as the difference between indentations for the different boundary conditions. The global bending creates a larger contact area, distributing the contact force

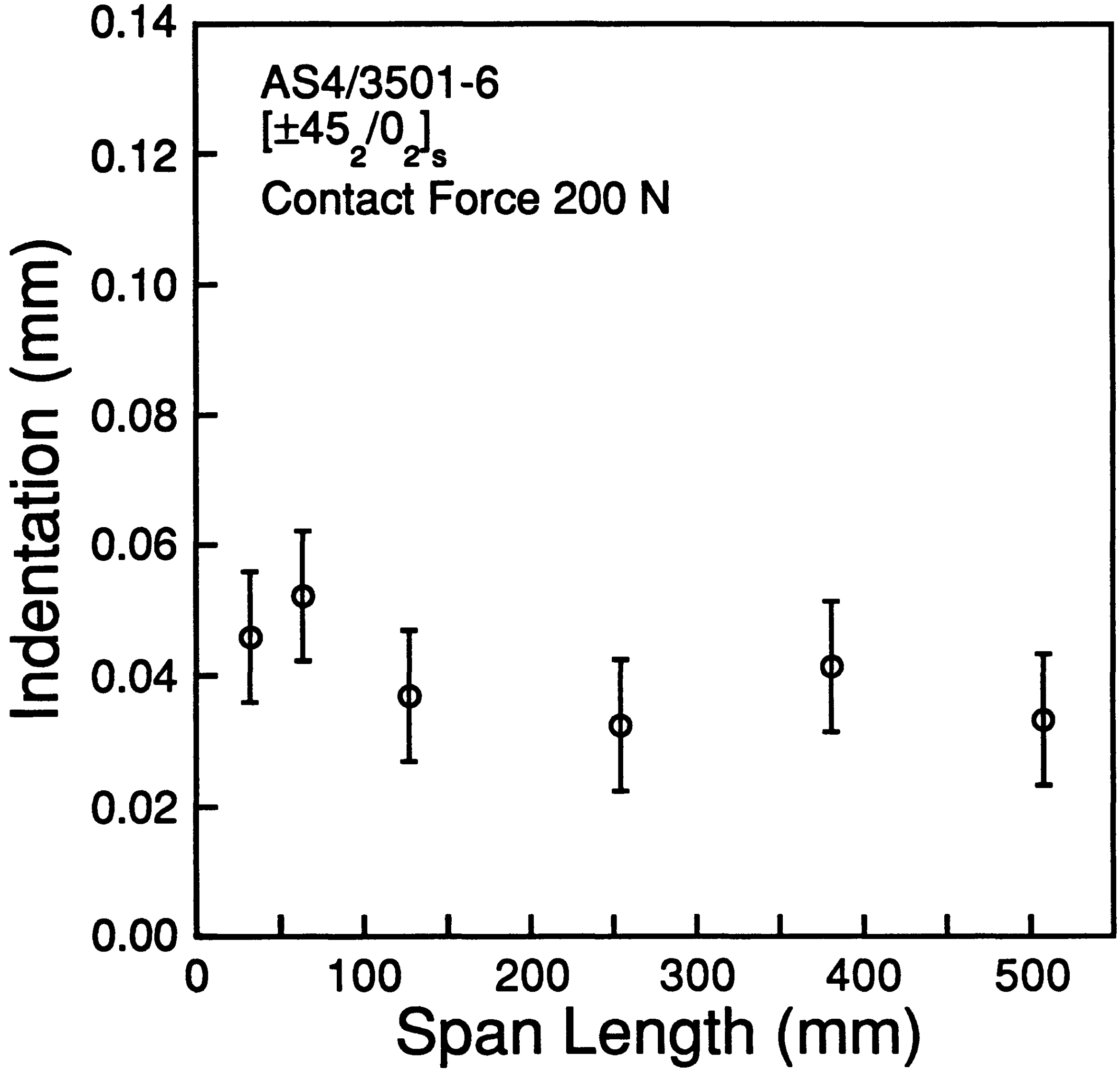

Figure 6.5 Force-indentation data, including the range of data variation, for specimens with different spans loaded to a maximum contact force of 200 N using a clamped-clamped boundary condition.

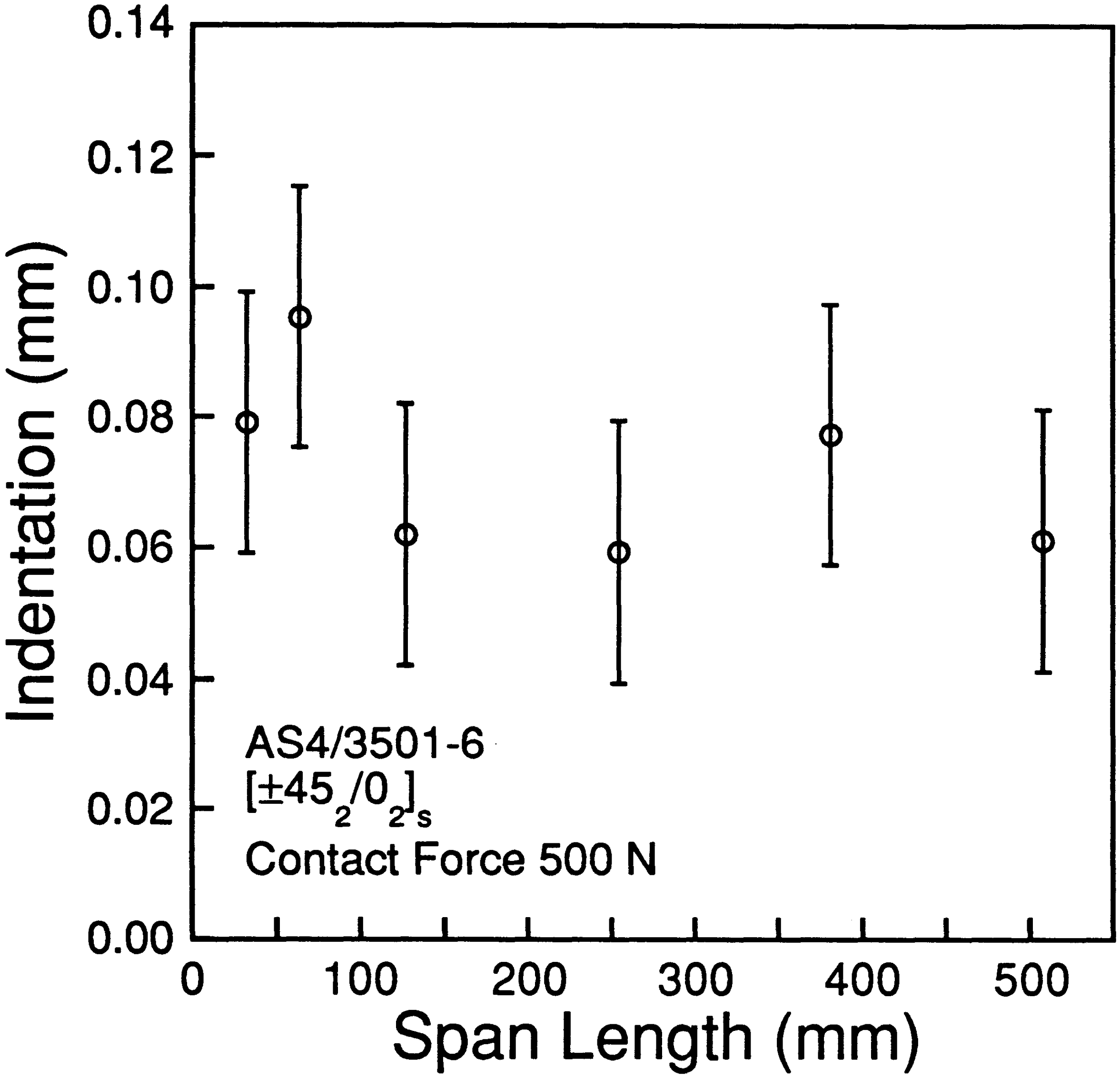

Figure 6.6 Force-indentation data, including the range of data variation, for specimens with different spans loaded to a maximum contact force of 500 N using a clamped-clamped boundary condition.

over a larger area, producing less contact stress and therefore less indentation. The global bending increases with increasing span, causing the contact area to increase as the span increases Again, this is caused because the spherical indentor contacts the curved plate over a larger arc as the plate curves more (increased bending) with increased bending. This will cause the contact stresses to be lower in the case of larger spans and cause smaller indentations. A similar situation has been described for increasing indentations in a previous investigation of contact behavior [15]. Such logic may differ depending upon the shape of the indentor.

It should be noted from the arguments above that changes in bending should influence the contact relationship regardless of the reason they occur. This is because the magnitude of the bending moment in the plate does not depend on whether it was created by an increase in the force, or an increase in the moment arm. Because of this, an increase in bending which occurs due to the application of force should change the contact behavior in the same way as an increase in bending which occurs due to an increase in span. This means that specimens loaded to different contact forces, which will obviously see increased amounts of bending as the load is increased, should have values of n and k which change with force. However, this effect needs further verification because it could not be determined in the specimens with a 254 mm span which were tested to different maximum contact forces.

While the rigid support case can be qualitatively thought of as an extreme case representing a "zero span" plate, this representation does not explain the large difference in contact behavior between even the specimen with the shortest span and the rigid backface support case. There are two effects at work in the different boundary conditions (as mentioned previously): the difference between allowing bending and not allowing bending, which leads to the statement that the rigid case effectively acts as a zero span plate; and the difference between the stress states on the backface of the specimen. The most likely explanation for the large difference in the contact behavior is that both effects are influencing the force-indentation response. However, the contribution of each of these effects needs to be individually determined.

The span of the plate is also observed to have an effect on the strain behavior of the plate. The maximum bending strains decrease more rapidly with increasing span than the extensional strain at a position on the plate, as seen in Figure 6.7. This is because the extensional strain becomes more dominant than the bending strain in the plate as the span of the specimen increases - the membrane effect is greater for longer specimens which experience larger deflections. This change in behavior of the specimens from bending-dominated behavior toward membrane-dominated behavior can be seen by considering the results for specimens with different spans shown in Figure 6.7. Extensional strain at a given contact force increases with span, indicating that membrane forces become more important as the plate size grows. For plates with spans longer than 254 mm, the extensional strain dominates the strain behavior. For smaller spans, bending strain dominates. This indicates that, at higher contact forces, the specimens with spans longer than 254 mm were behaving more like membranes than the smaller span specimens.

The development of membrane behavior in the larger span plates can also be seen as the magnitude of the deflection increases. The bending strains actually decrease for the cases of the specimens with 381 mm and 508 mm spans as the load increases beyond some value. This behavior can

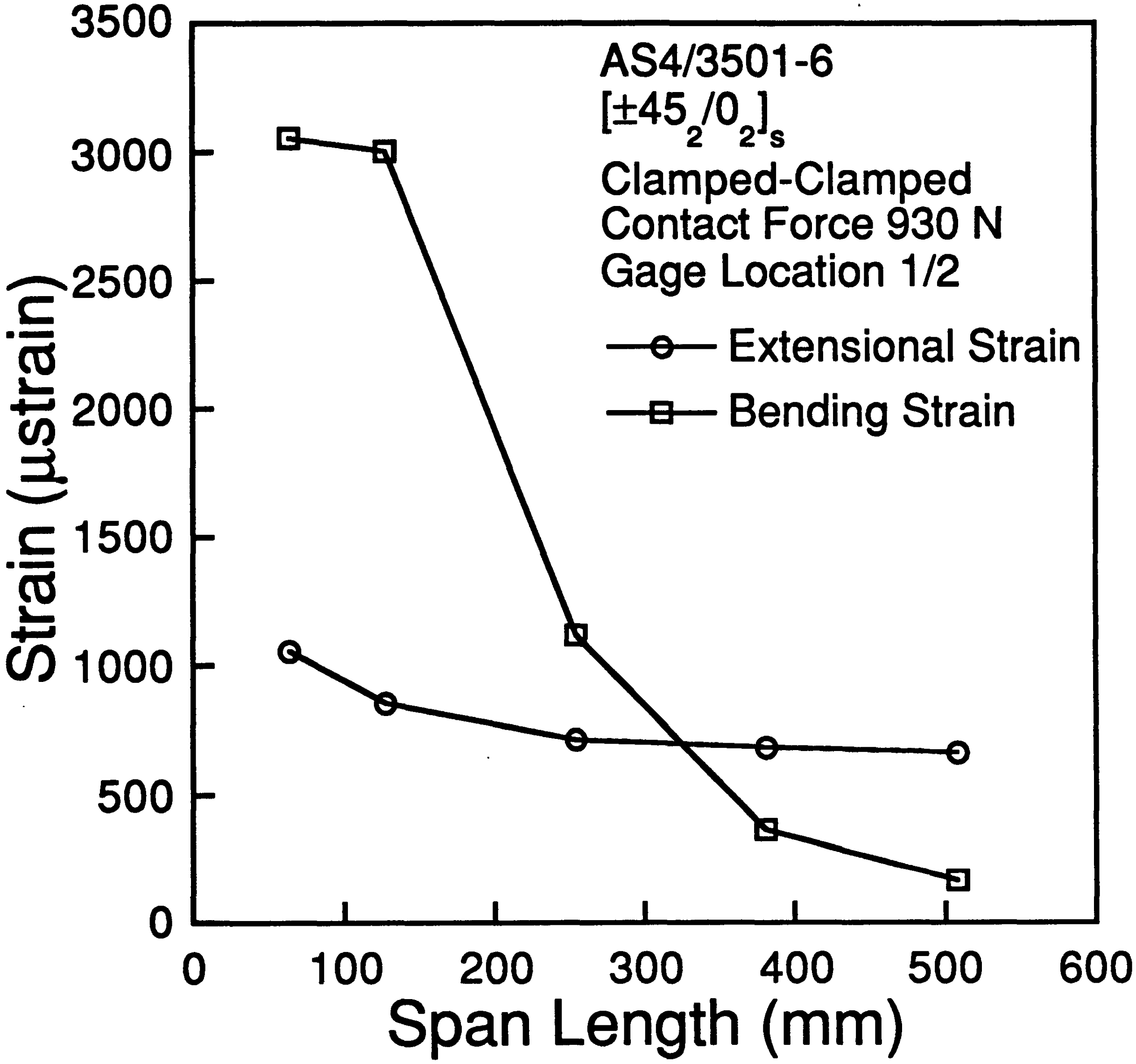

Figure 6.7 **Extensional and bending strain results shown at gage location 1/2 from gage scheme A (see Figure 3.2) for a contact force of 930 N and all plate spans.**

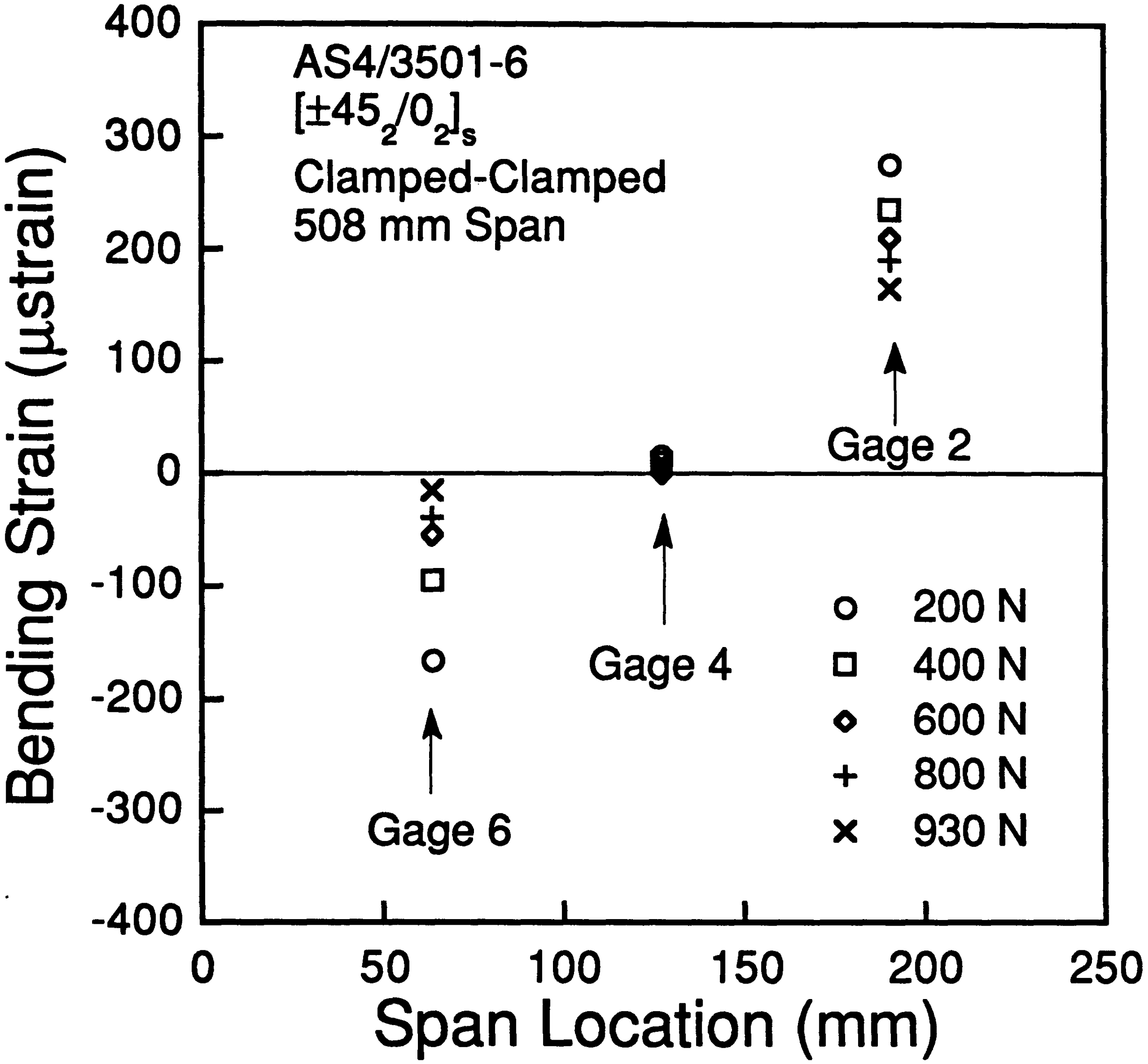

Figure 6.8 **Bending strain results shown at the span locations from gage scheme A (see Figure 3.2) for selected representative forces for a plate with a 508 mm span in a clamped-clamped boundary condition.**

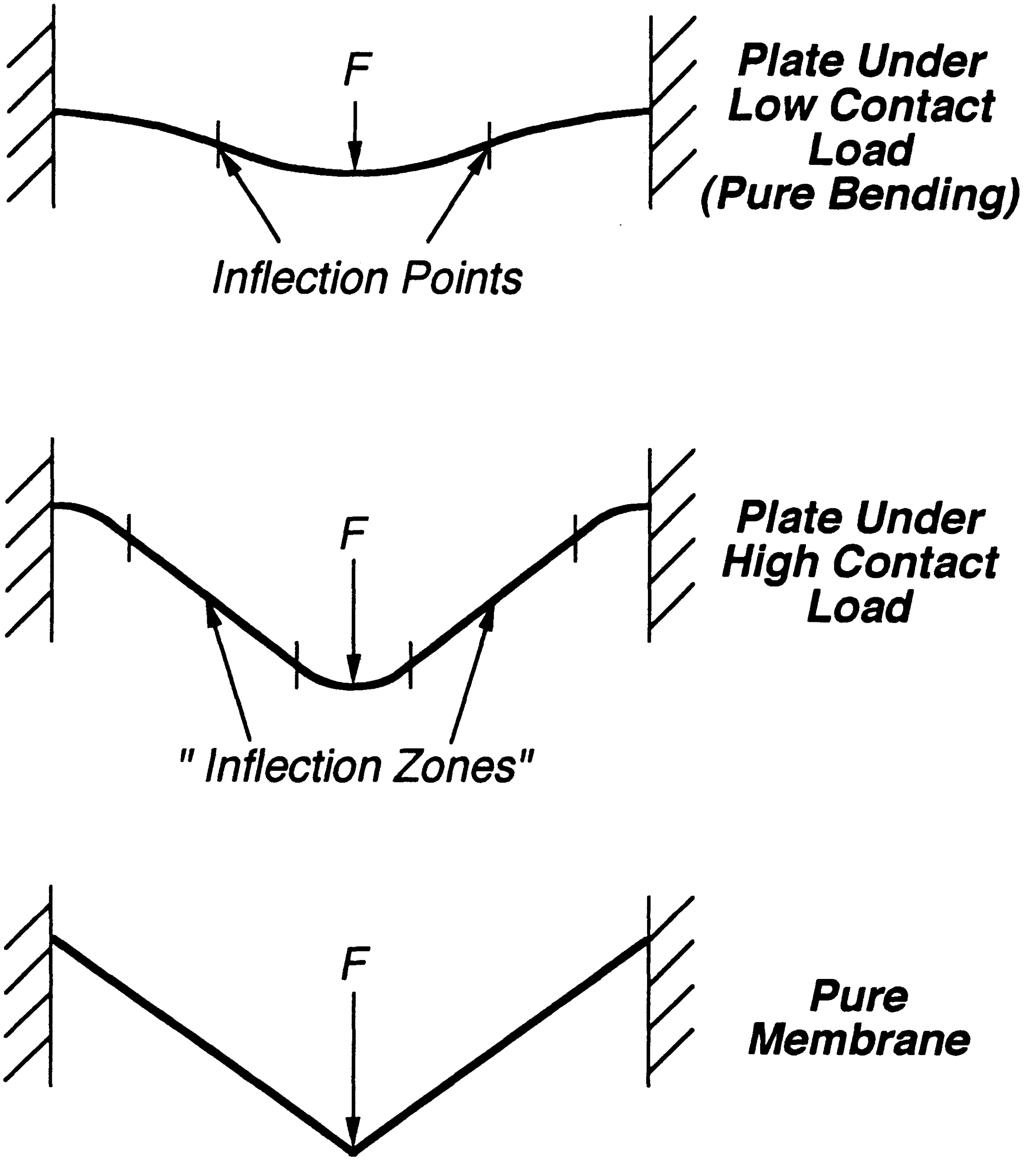

Figure 6.9 Illustration of the bending relaxation effect.

be seen clearly in Figure 6.8 which shows the bending strain at the scheme A gage locations (see Figure 3.2) for selected forces for a specimen with a 508 mm span. This relaxation in the bending, which occurs at very large deflections, can be explained due to the expansion of the point of inflection to a region of inflection. This is illustrated in Figure 6.9. There is an inflection point on a plate where the curvature of the plate, and therefore the bending strain, is zero. This is the point where the curvature of the plate changes from positive to negative. As the deflection of the plate becomes large, the inflection point becomes more like an inflection zone - a characteristic which shows that the plate is behaving more like a membrane. In the inflection zone, the plate flattens out again so that the bending strain approaches zero. In the limit, the plate behaves completely as a membrane.

The bending strain relaxation seen in Figures 5.26 and 5.27 can be thought of as the inflection zone extending as the contact force increases, reducing the bending strain of the plate in that region. The bending strains nearer the inflection point on the plate decrease as span increases because the larger plates begin to behave more like membranes. This can be seen as the relaxation effect develops and becomes more pronounced as the span of the plate increases, as shown in Figure 6.10. In this figure, it can be seen that the bending strains in the middle of the plate decrease toward zero as the span of the plate increases and that the length of the region over which this occurs grows as span increases.

The extensional strains can be seen to scale with the contact force. The extensional strains for each span, at each gage location along the span (from scheme A, Figure 3.2, and scheme B, Figure 3.3) are shown in Figures 6.11, 6.12, and 6.13 for the contact forces 200 N, 600 N, and 930 N.

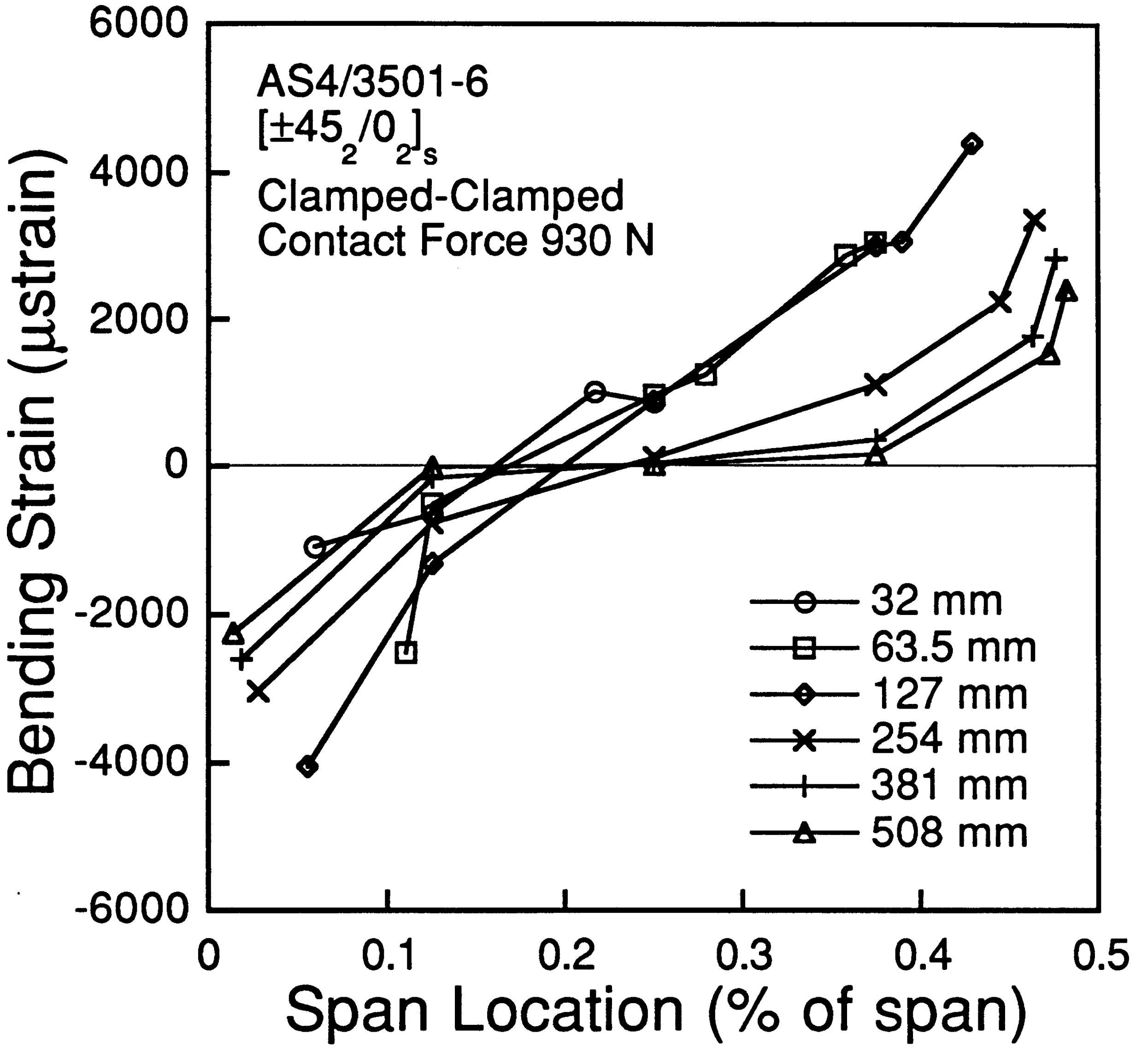

Figure 6.10 Bending strain results from the gages in schemes A and B (Figures 3.2 and 3.3) versus span locations, given as a percent of span, and at a contact force of 930 N for each plate span in a clamped-clamped boundary condition.

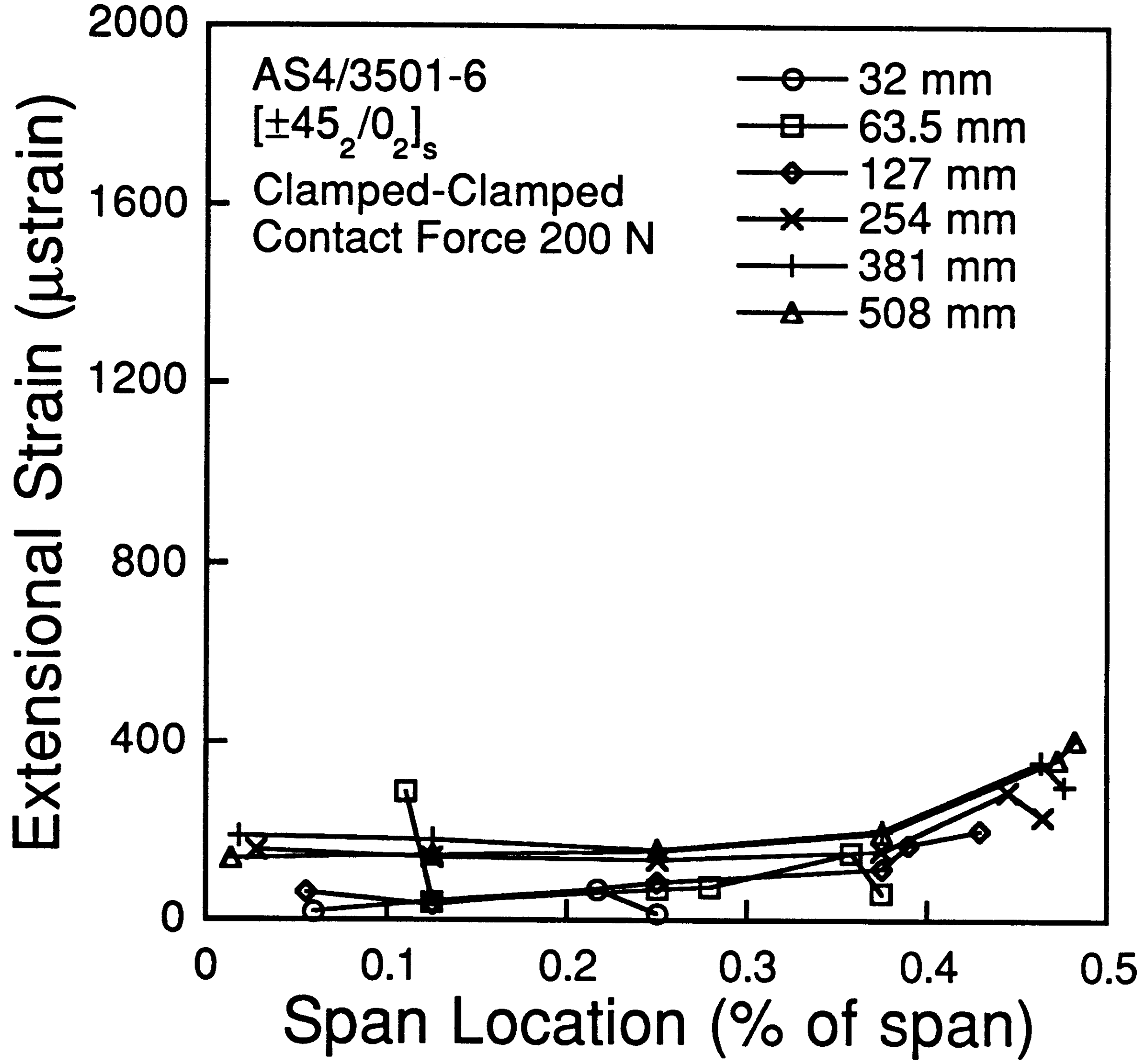

Figure 6.11 Extensional strain results from the gages in schemes A and B (Figures 3.2 and 3.3) versus span locations, given as a percent of span, and at a contact force of 200 N for each plate span in a clamped-clamped boundary condition.

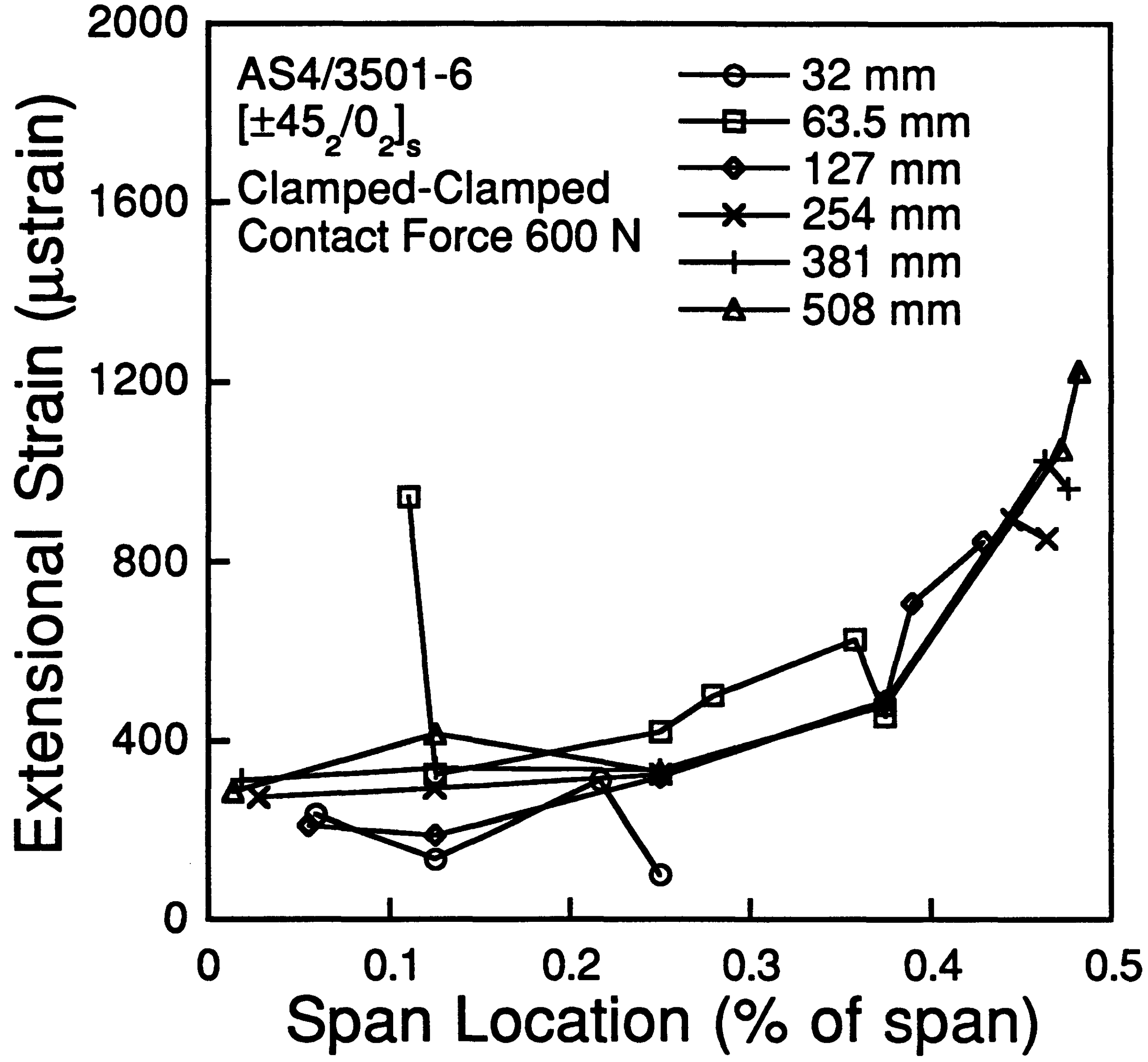

Figure 6.12 Extensional strain results from the gages in schemes A and B (Figures 3.2 and 3.3) versus span locations, given as a percent of span, and at a contact force of 600 N for each plate span in a clamped-clamped boundary condition.

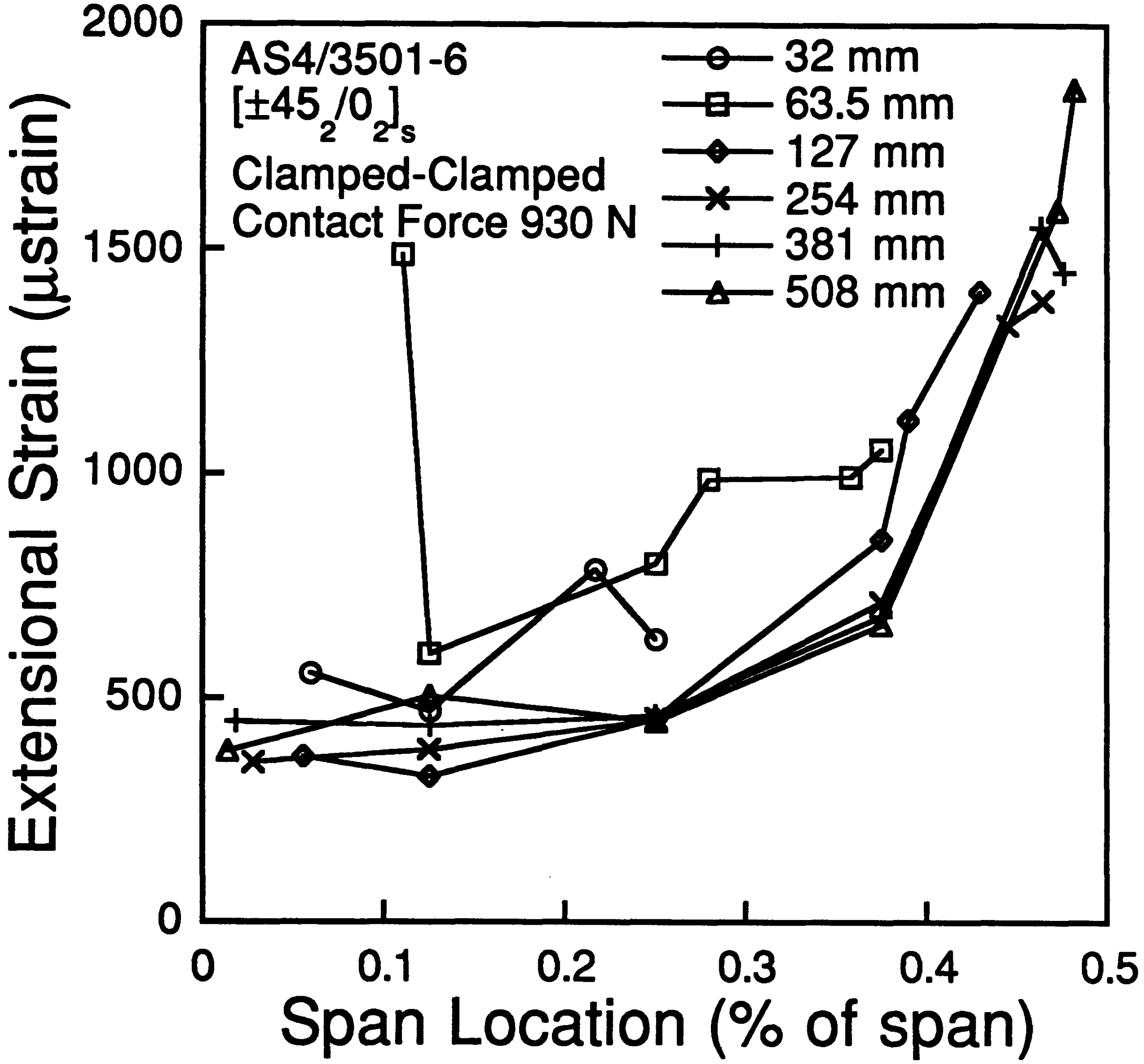

Figure 6.13 **Extensional strain results from the gages in schemes A and B (Figures 3.2 and 3.3) versus span locations, given as a percent of span, and at a contact force of 930 N for each plate span in a clamped-clamped boundary condition.**

In this series of figures, the extensional strains along the length of each plate span overplot for each contact force. However, the extensional strains for the smaller plate sizes deviate slightly from this pattern as the force increases. This is most likely due to the fact that these specimens have a low span to width aspect ratio resulting in behavior which is more "plate-like" (the bending is no longer cylindrical) than "beam-like" in the larger spans with a higher aspect ratio. The precise mechanism which causes the higher extensional strains is not known, but the low aspect ratio is the most likely cause. If this is so, the increase in extensional strain seen nearer the contact point for the larger spans as the contact force increases might also be explained as a result of the local non-cylindrical bending which occurs in this area. The extensional strain decreases away from the contact point as the plate takes on more cylindrical bending or "beam-like" characteristics.

The bending strains can be seen to scale with the bending moment at the boundary of the plate (the contact force multiplied by the moment arm: half the span). The bending strains for each span, at each gage location along the span (from scheme A, Figure 3.2, and scheme B, Figure 3.3) are shown in Figures 6.14 and 6.15 for bending moments of 5 Nm and 15 Nm, respectively. The same information for only the four largest spans are shown in Figure 6.16 for a bending moment of 60 Nm. The specimens of the two smaller spans were not loaded high enough to create this moment level. In this series of figures, the bending strains along the length of each plate span overplot only for the lowest bending moment level. At the higher bending moments, the difference between specimens of different spans increases as the bending relaxation effect starts to dominate the bending

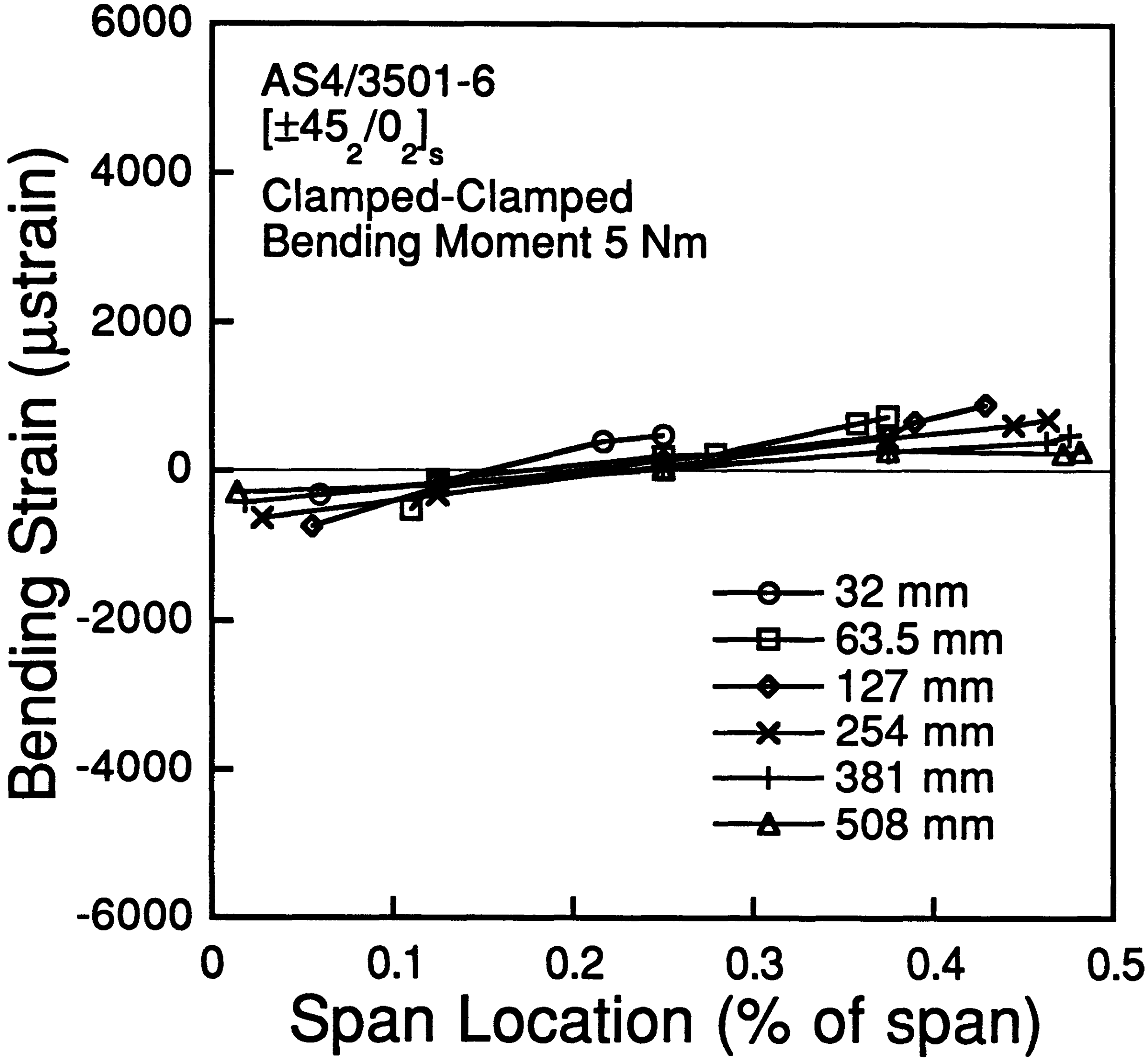

Figure 6.14 Bending strain results from the gages in schemes A and B (Figures 3.2 and 3.3) versus span locations, given as a percent of span, and at a bending moment of 5 Nm for each plate span in a clamped-clamped boundary condition.

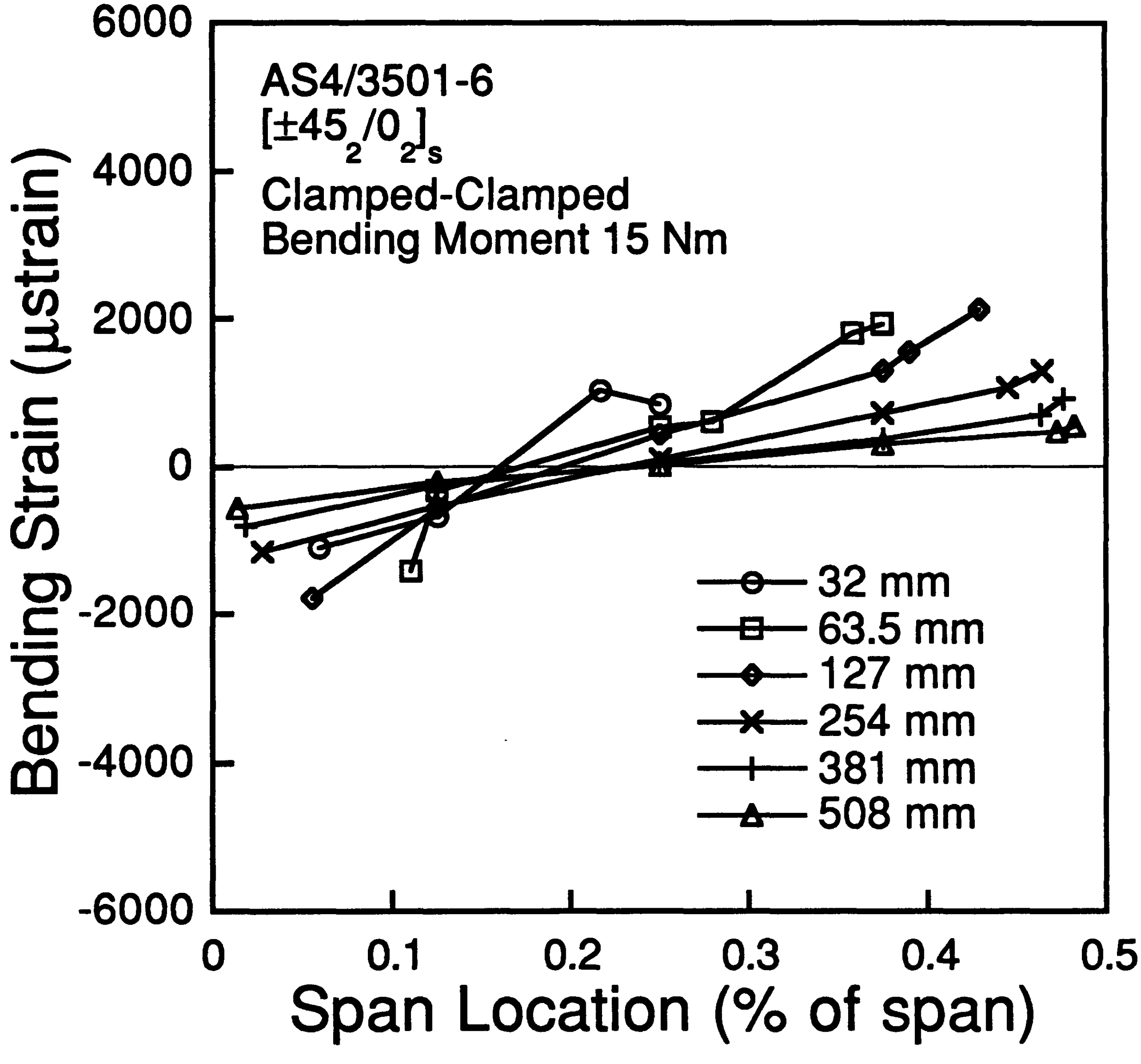

Figure 6.15 Bending strain results from the gages in schemes A and B (Figures 3.2 and 3.3) versus span locations, given as a percent of span, and at a bending moment of 15 Nm for each plate span in a clamped-clamped boundary condition.

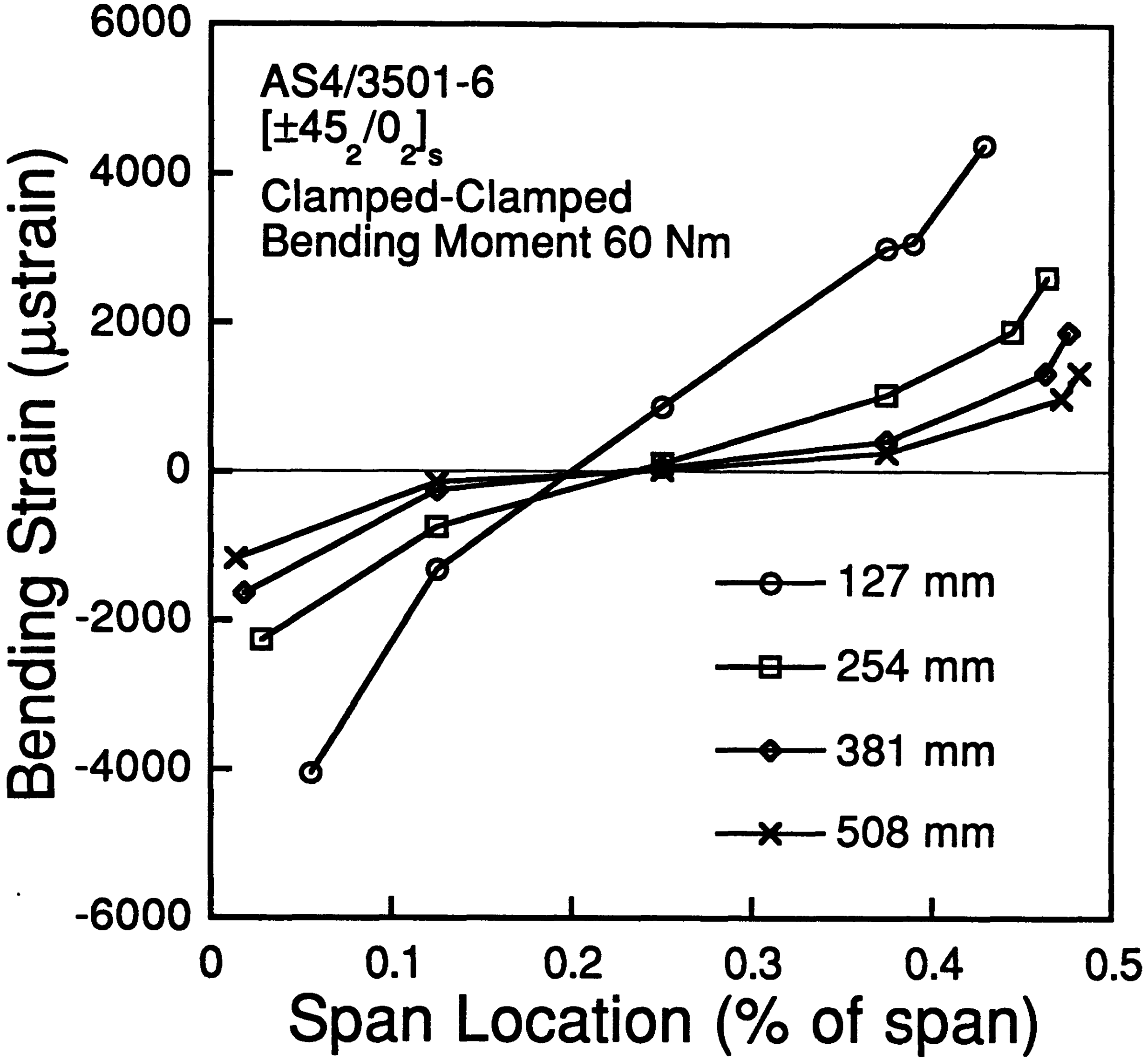

Figure 6.16 Bending strain results from the gages in schemes A and B (Figures 3.2 and 3.3) versus span locations, given as a percent of span, and at a bending moment of 60 Nm for each plate span in a clamped-clamped boundary condition.

response of the plate, causing the bending strain to deviate from the pure bending response as seen for the lower forces.

If the span of the plate can affect the indentation response, it is possible that it may influence other local effects. It was observed for specimens with a span of 127 mm or greater that the extensional strains at positions 4/5 and 6/7 (gage scheme B, see Figure 3.3) are much greater, at the same force, than those seen at any of the other strain gage locations from both schemes A and B. Furthermore, the extensional strains at locations 4/5 and 6/7 increase with span while the extensional strains for the other gages, from both schemes A and B, seem to be approaching a constant value along the length of the plate as span increases. These points were observed through a comparison of the values of extensional strain at each of the gage locations from both schemes for all the spans, as shown in Figure 6.17. In this figure, the extensional strain at the gages near the contact point (those with the highest span location) for each span is seen to increase, except for the specimens with the 63.5 mm span. This seems to indicate that span is having an effect on extensional strain behavior local to the contact point, which may be an indication of "wrapping". Wrapping has been defined as a local bending of the plate to conform to the indentor [16]. An observation which supports this is seen when comparing the extensional strain data from the analysis with the experimental data. The nonlinear analysis curves for extensional strain match the experimental force-extensional strain data well with the exception of position 1/2 (Figure 5.40) which is closest to the contact point. The discrepancy between experiment and analysis at that point could be explained as local effects (possibly wrapping) resulting from the contact between the indentor and the plate which are not accounted for in the analysis.

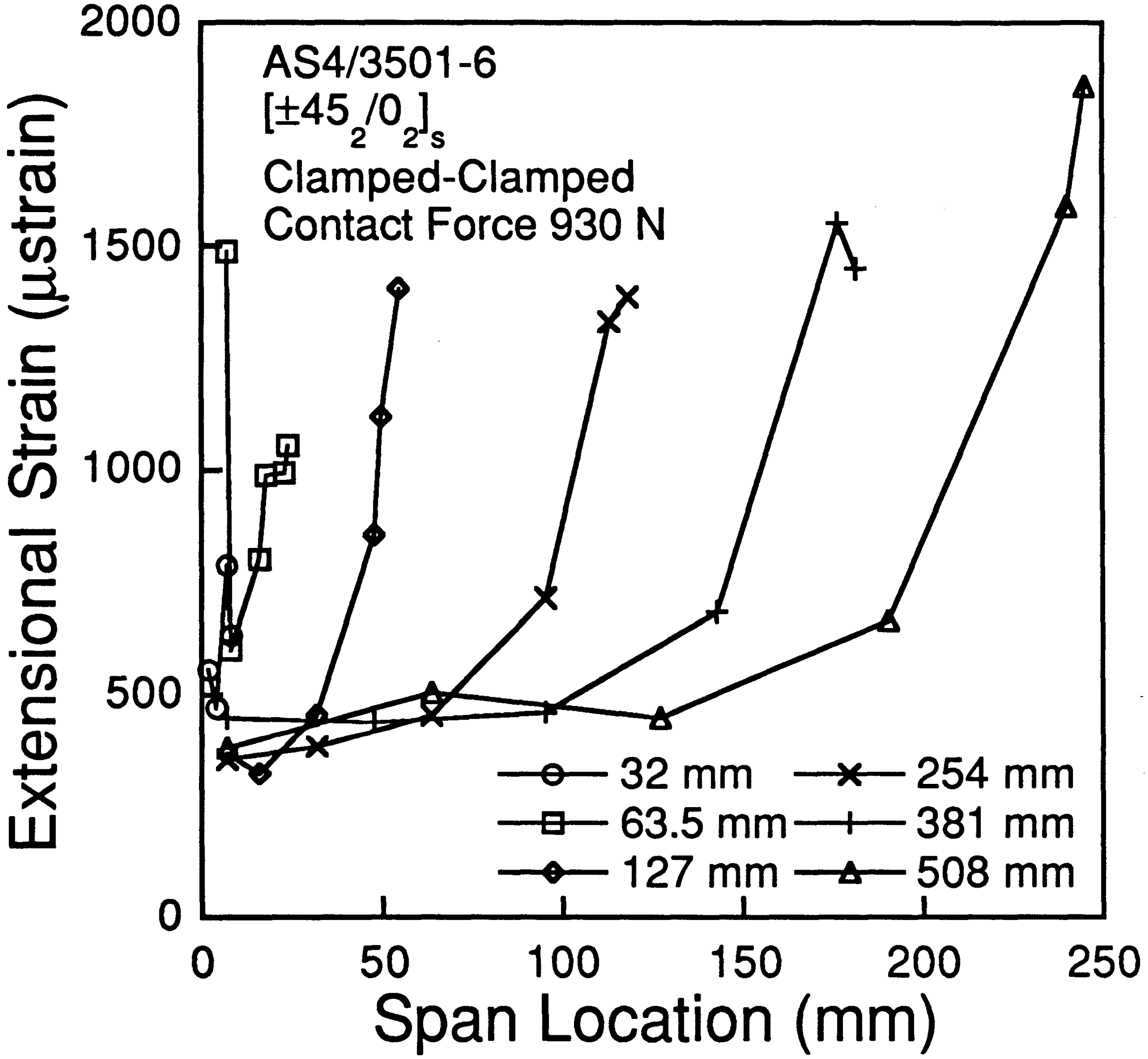

Figure 6.17 Extensional strain results shown at the span locations from gage schemes A and B (Figures 3.2 and 3.3) and at a contact force of 930 N for each plate span in a clamped-clamped boundary condition.

Not all the data seems to support the idea of wrapping, however. It was observed that the bending strains at gages 2 and 5 (gage scheme B) for the tests to 1479 N were of similar magnitude but opposite sign for all the spans tested (except the 32 mm span for which data was unavailable), as seen in Table 5.9. This can also be seen in Figure 6.10. The symmetry of the bending about the inflection point should cause bending strains at points equidistant from the boundary and the contact point to be equal in magnitude but opposite in sign, if local effects are neglected. This can be easily seen in the wide beam analysis developed in Chapter 4. From equation 4.5 (reiterated here as equation 6.1), it is obvious that the inflection point (where the curvature, κ_{11}, is equal to zero) will occur at the quarter span point:

$$\kappa_{11} = -\frac{\partial^2 w(x)}{\partial x^2} = -\frac{F}{2}\left(x - \frac{L}{4}\right)\left(\frac{D_{22}}{D_{22}D_{11} - D_{12}{}^2}\right) \tag{6.1}$$

While this is only rigorous for beams and not for plates, it is a good enough approximation to explain the behavior of these two gages. Since gage 2 is the same distance to the boundary as gage 5 is to the contact point, the similarity in the magnitude of the bending strains makes sense. However, this also seems to indicate that wrapping is not occurring at location 4/5 for any of the plates because a local bending effect should upset the symmetry in the bending strains and this is not observed.

The issue of wrapping needs further work. In the present work, the extensional strains obtained increase near the contact point. This may be a result of local shell effects. However, the bending strains do not seem to indicate any local effect at all. This indicates that wrapping behavior is not observed to affect the plate at the locations of gages 4 through 7 from gage scheme B. However, this does not indicate that wrapping is not occurring as wrapping may influence an area which is very local to, or directly beneath, the indentor and can, therefore, not be measured via the strain gages in this work. As a result, the issue of wrapping should receive attention in future works. This effect has been identified as possibly influencing the bending response [36].

With all of the differences in behavior resulting from changing span, it would be expected that the damage would also show differences. However, the damage extent, type, and location through-the-thickness does not vary with changes in span. The progression of damage through two different maximum contact forces also appears similar for every span. However, these observations do not necessarily indicate that span has no effect on damage behavior. These observations are all made for a specimen in which damage has already initiated. The damage in a laminate will affect the stress state in the laminate, usually in ways that are not well understood, diminishing the ability to positively determine what relationships are occurring. This means that the results obtained for span in this investigation only indicate that the progression of damage, once initial damage has occurred, is similar for the range of spans tested. Because the initiation of damage for different spans was not investigated, the question of what relationship damage has to the span should be determined in future works through an investigation of how the damage incipience changes with span.

6.3 Evaluation of Analysis

The nonlinear analysis, developed in Chapter 4, was used to determine the global effects of a static indentation event on a plate. This analysis was compared to the experimental force-deflection, force-extensional strain, and force-bending strain data to determine the validity of the analysis and to identify parameters which may be important in static indentation events.

The force-deflection curves fit the experimental data well for a geometrical nonlinearity factor, β, equal to 0.03, as seen in Figure 5.8. The predicted deflection of the plate is seen to change by only a small amount for large variations in the β-factor, possibly indicating that there is a logarithmic relationship between β and this predicted deflection of the plate. The deflections were also seen to converge very quickly, providing good results for small numbers of modes. This is because the mode shapes used were designed to accurately define the bending shape of the plate and because β was well defined at the center of the plate. The latter point was due to the fact that effects from the in-plane boundary flexibility were averaged across both the span and the width, making the center point, arguably, the most accurate.

The nonlinear analysis curves for extensional strain match the experimental force-extensional strain data well, with the exception of position 1/2 (gage scheme A), which is shown in Figure 5.33. The discrepancy between experiment and analysis at that point can be explained as a local bending effect (possibly wrapping and/or local shell effects) resulting from the contact between the indentor and the plate which are not accounted for in the analysis. The slight difference between the experimental and analytical curves for position 5/6 (gage scheme A), which is shown in Figure 5.35, can be explained as a result of effects from St. Venant's principle - the grips might not grip evenly across the width of the plate and cause the distribution of stresses near the end of the plate to diverge from what is assumed in the analysis. The extensional strains were seen to converge more slowly than the deflection. A reason for the slower convergence is that the extensional strain is a first derivative which is extracted from the displacement-based analysis, removing it by a step from the conditions of convergence which are based on the displacement. Another reason for the slower convergence is that the extensional strains are calculated at specific points along the plate. As stated previously, the use of the β-factor ignores the pointwise shell effect, but rather accounts for the geometrical nonlinearity only on a global basis. This means that by using the β-factor, the effect of the flexible boundary condition is averaged over both in-plane directions.

At first glance, the nonlinear analysis does not appear to predict the bending strains well. However, this does not mean that the method of analysis is in error. The poor agreement is because not enough modes have been used to allow the bending strain to converge (see section 4.6). This indicates that higher mode cases are needed to accurately predict the bending strains using this method. However, as discussed in Chapter 4, investigation of higher mode cases becomes difficult due to the size of the matrices involved in setting up and solving the nonlinear equations. As a result, the convergence of the bending strains could not be fully investigated due to limitations of the available computational facilities and time. It should be noted (on the positive side) that the analysis seems to account for the relaxation of the bending strain, as seen in Figure 5.38, even if it has not converged to the experimental data. A reason for the slow convergence is that the bending strain is a second derivative which is extracted from the displacement-based analysis. In other words, the deflection, for which the analysis was formulated, must be diluted twice to arrive at bending strain.

Another reason for inaccuracy of the analysis is that bending calculations must be done at a specific point through-the-thickness of the plate. By using the β-factor, which takes into account only the change in length along the through-the-thickness centerline, the effect of the flexible boundary condition is averaged across the thickness of the plate. This compounds the problem of using an average β-factor across the in-plane directions of the plate and could certainly cause slow convergence or inaccuracies in the method. More modes and possibly a better quantification of the local shell effects are needed to fully determine the ability of this method to accurately predict strains.

Finally, it should be mentioned that despite its limitations, the β-factor appears to work well in accounting for the global effects of the flexibility of the in-plane boundary conditions. This has allowed the deflection and extensional strain behavior to be matched closely with analysis, by accounting for this flexibility. The β-factor gives insight into the effect of a flexible in-plane boundary on the deflection, as shown in Figure 6.18, and the extensional strain of a plate, as shown in Figure 6.19. The extreme case of this flexible boundary, where β is equal to zero, is seen to increase the deflection and decrease the extensional strain in the plate. These points highlight the fact that the ideal boundary conditions modeled in this nonlinear analysis will not perfectly model boundary conditions even in a controlled experimental environment. Therefore, it is not expected that the ideal boundary conditions in this analysis could properly model the boundary conditions of a plate in a realistic structure. Such conditions are not ideal due to intentional design or variability in manufacturing. This indicates that the β-factor would be useful when modeling boundary conditions in realistic situations. The β-factor would, however, need to be

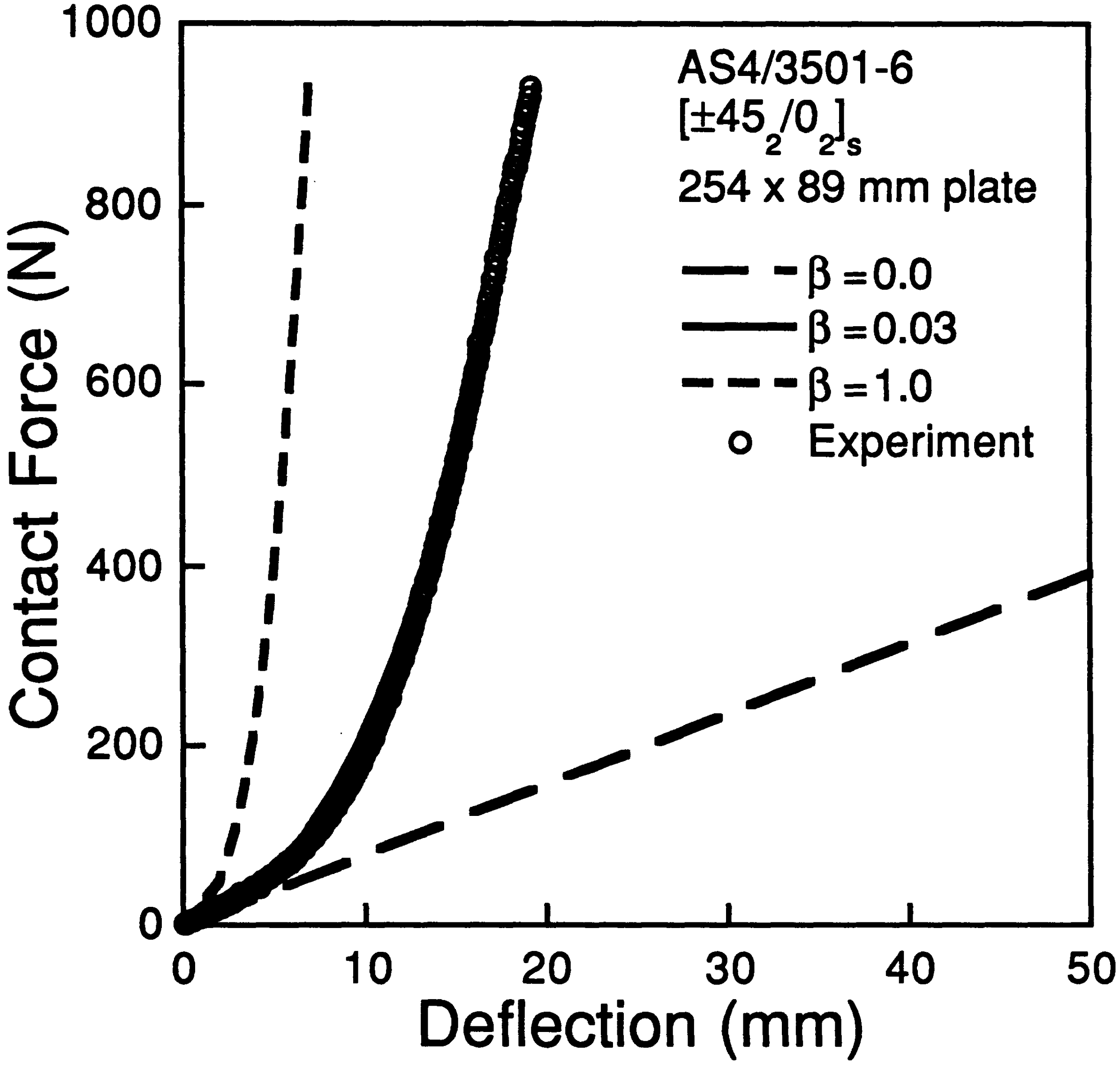

Figure 6.18 Experimental and analytical (for various values of β) force-deflection results for a specimen with a 254 mm span and loaded to 930 N.

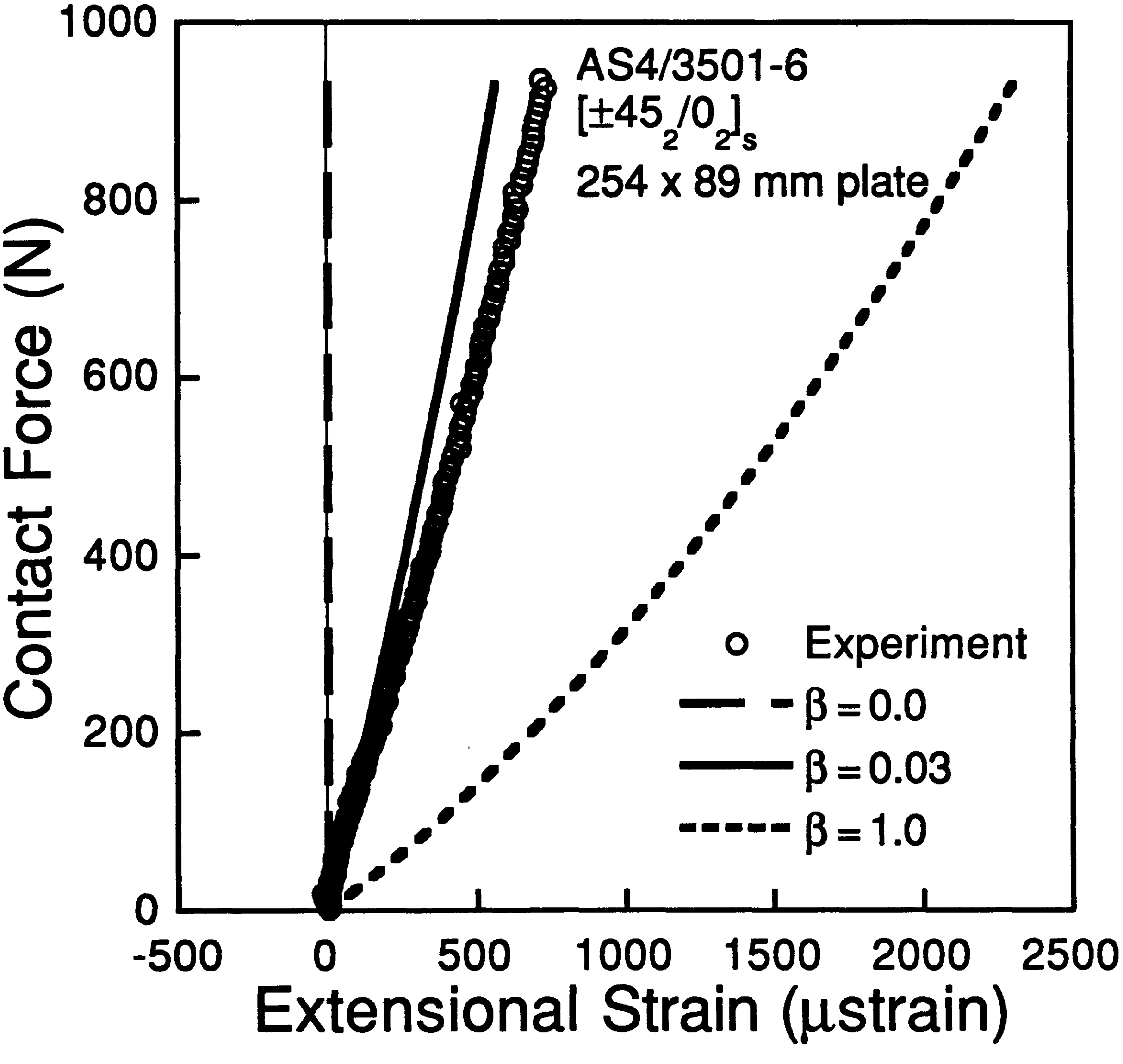

Figure 6.19 Experimental and analytical (for various values of *β*) force-extensional strain data at position 1/2 (strain gage scheme A) for a specimen with a 254 mm span and loaded to 930 N.

measured for each case. Furthermore, better accuracy in predicting the bending strains may not be possible without accounting for the local shell effect. Despite this, the β-factor has successfully taken the in-plane boundary flexibility into account for modeling static force-deflection and force-extensional strain data and previously to model impact force-time histories [32, 36].

6.4 Comparison with Impact Results

In this investigation, specimens with a 254 mm span with a clamped-clamped boundary condition were loaded to seven different maximum force levels. These force levels were determined from the maximum contact forces seen in previous impact experiments for the same material and laminate [10]. Each of the maximum contact forces corresponds to a particular impact velocity as seen in Table 6.1. The results from these static indentation tests are compared with the impact tests using force as the parameter for comparison. Force has been shown to be a useful parameter for evaluating impact phenomena [1] and in this case it is the only practical parameter to use as a basis of comparison between the two tests.

The force-deflection behavior can be seen to be different for the static and impact cases. The deflection during an impact is determined by twice integrating a force-time history (taken from reference [10]) to arrive at a force-deflection plot. This procedure is also discussed in detail in that work. A plot of the force-deflection behavior for a maximum contact force of 1479 N for both the impact and static tests is shown in Figure 6.20. It is observed from this data that the deflection seen in the static test is approximately twice the deflection seen in the impact test, at the same

Table 6.1 Table of the maximum contact forces and the corresponding impact velocities for a specimen with a 254 mm span in a clamped-clamped boundary condition [10].

Impact Velocity, m/s	Maximum Force, N
1.0	444
1.3	507
1.4	549
1.5	739
2.0	930
2.6	1183
3.0	1479

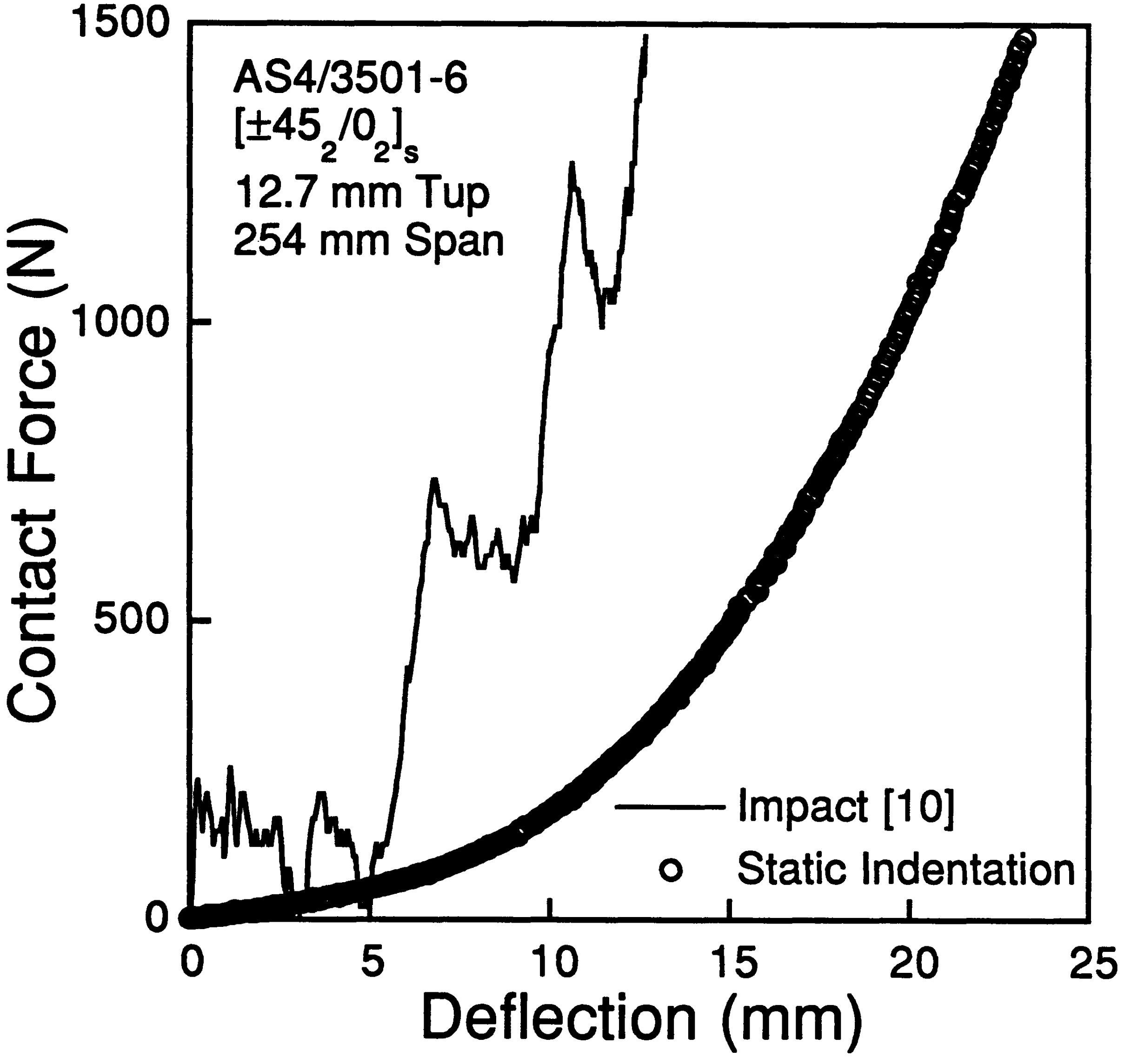

Figure 6.20 Force-deflection results for specimens with a 254 mm span in a clamped-clamped boundary condition statically loaded to a maximum contact force of 1479 N and impacted at a velocity of 3.0 m/s.

force. However, the curves both show similar overall nonlinear behavior (if the predominant first mode response of the impact data is considered), indicating that, although the magnitude is different, generally similar membrane effects are occurring in both specimens. It should also be noted that the rigid backface support condition can also be represented on this figure as the vertical line at zero deflection since no bending is allowed for this case. Observing this leads to the conclusion that the impact behavior for the clamped-clamped boundary condition is bounded by the static indentation behavior for the rigid backface support and clamped-clamped boundary conditions. This also implies that the static force-indentation behavior for the two boundary conditions may also bound the behavior in the impact case, although this would have to be verified.

The damage that results in a specimen for both the static and impact tests loaded to the same maximum contact force can be seen to be similar in certain aspects and different in others. For both cases, the first damage was seen for the test that was run to a maximum contact force of 549 N. The types of damage and through-the-thickness location are also the same. In both cases, cracks develop in the +45° plies nearer the backface of the laminate and are accompanied by delaminations at higher force levels. In both cases the damage extent is seen to increase toward the lower face of the laminate. As described earlier, the increase in the damage toward the backface of the laminate can be explained as a result of the higher bending stresses on the backface of the laminate. However, the overall extent of the delaminations appears somewhat smaller for the static indentation tests as can be seen in Figure 6.21. Damage incipience needs to be better defined to compare the damage which occurs in static and impact tests. The extent of the damage may not relate for the two cases due to dynamic effects. The

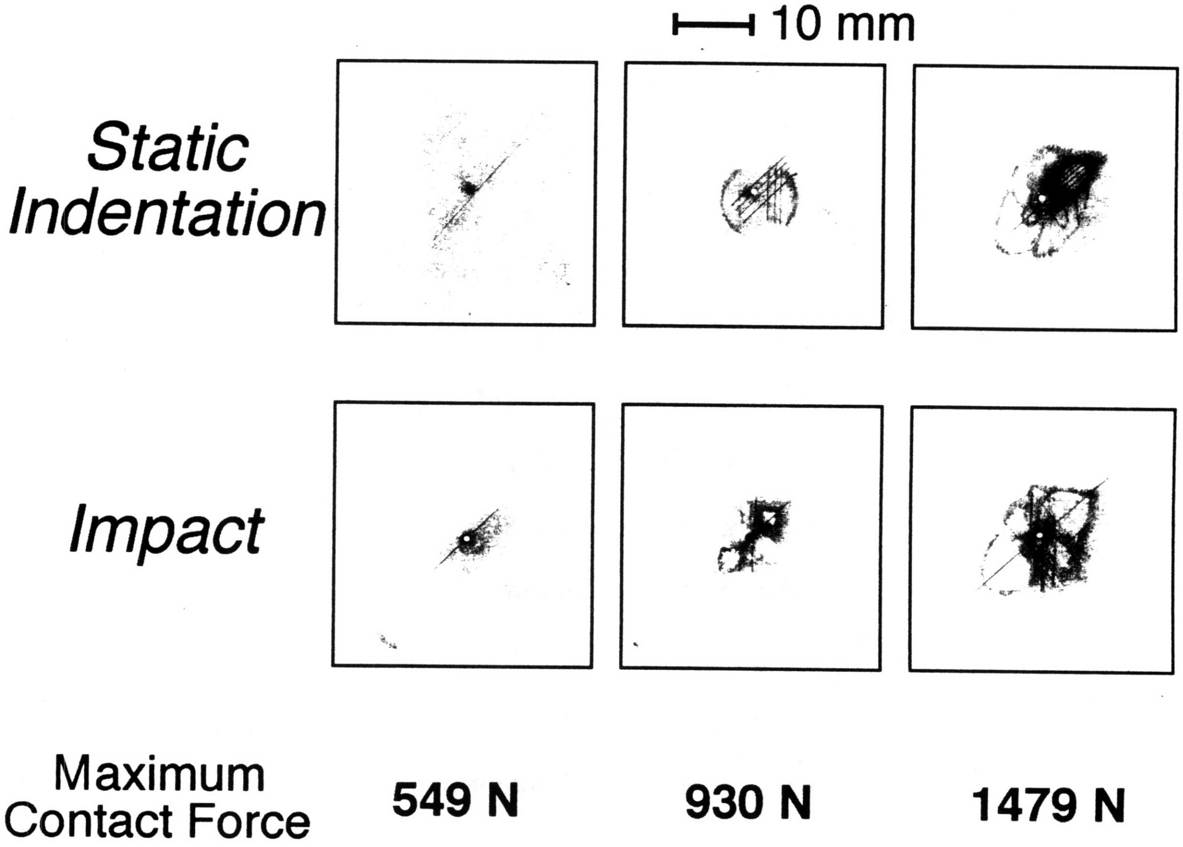

Figure 6.21 X-ray photographs showing the damage extent for *(top)* static indentation tests and *(bottom)* impact tests [10], which experienced the same maximum contact force.

extent of the damage also may not relate for the two cases because the internal stress state will change once damage occurs. There is no simple way to determine how this could interact with the overall bending stresses and local effects to alter the extent of damage.

Static tests are useful in investigating certain aspects of impact behavior. As seen here, the results of the static tests can be used to bound the global bending and indentation characteristics of an impact event and to understand general trends in behavior. However, caution must be used when directly applying results from static tests to quantify impact damage resistance, both in terms of damage incipience and damage extent. Clearly, plate geometry and boundary condition influence the indentation and bending response of a plate during impact and static events, but further work is needed to determine the relationship that exists between the damage incipience and damage extent in static and impact events for the plate geometries and boundary conditions examined here.

Chapter 7

CONCLUSIONS AND RECOMMENDATIONS

In this work, the effect of different structural parameters on the indentation and bending behavior of laminated plates was investigated through the use of static indentation. These different structural parameters include two boundary conditions, rigid backface support and clamped-clamped, and six different spans in the clamped-clamped boundary condition. The local indentation, bending, and damage response was studied for each case and, where possible, compared to previous impact test results. Additionally, a nonlinear analysis was developed to model the bending response of a plate under static loading and results from this analysis were compared to the experimental results.

The conclusions which can be drawn from this investigation are:

1. The maximum indentations for the rigid backface support condition are approximately two times larger than the corresponding indentation for the clamped-clamped case.

2. The force-indentation responses can be fit with the contact relationship $F = k\alpha^n$. The values of the exponent, n, for the rigid backface support lie closer to the value of 1.5 expected from Hertzian contact theory than the values for the clamped-clamped case, which are closer to two.

3. The force-indentation curves for the tests on specimens with different spans in a clamped-clamped support indicate that force-indentation

behavior may decrease monotonically or remain constant with increasing span. However, this relationship could not be determined conclusively.

4. The force-deflection behavior for both the impact tests and the static tests show similar overall nonlinear behavior, indicating that, although the magnitude is different, generally similar membrane effects are occurring in both specimens. The analysis also shows that membrane stiffening is important for the plates tested.

5. Membrane behavior was observed to become more dominant in plates with larger spans and at increased force levels.

6. Until nonlinear effects dominate, strain behavior does not change with span if location on the plate is normalized by span and the extensional strains are compared on the basis of contact force, while the bending strains are compared on the basis of bending moment at the boundary of the plate.

7. For specimens with a span of 127 mm or greater, the extensional strains may be influenced by local effects. However, the bending strains show no indication of being influenced by local effects.

8. The analytical force-deflection curves fit the experimental data well using a fitting factor, β, to account for flexibility of the in-plane boundary conditions. The deflections were also seen to converge very quickly, providing good results with a small numbers of modes.

9. The nonlinear analysis curves for extensional strain generally match the experimental force-extensional strain data well with the exception of the extensional strains at a location one-eighth of the span from the contact point. However, the extensional strains were seen to converge more slowly than the deflection.

10. The analysis accounts for the relaxation of the bending strain, but local shell effects need to be included to predict the values accurately.

11. The specimens tested with a rigid support show no damage up to loads of 1479 N (the maximum utilized) while the specimens tested with a clamped-clamped support show a progression of damage for the same forces tested, beginning at loads between 507 N and 549 N for both static and impact tests.

12. The damage in the specimens consists of cracks in the +45° plies nearer the backface of the laminate which are accompanied by delaminations at higher force levels. The damage extent is seen to increase toward the lower face of the laminate for both impacted and statically loaded specimens.

13. The damage extent, type, and location through-the-thickness for a contact force does not vary with changes in span. However, the influence of span on the contact force and type and location of damage at damage incipience was not determined.

14. Using force as the parameter for comparison, the types of damage and through-the-thickness location are the same for both impact and static tests. However, the overall extent of the damage appears smaller for specimens loaded to the same contact force level in the static indentation tests as that seen in impact tests.

15. The force-deflection behavior for the clamped-clamped boundary condition in the impact tests is bounded by the static force-deflection behavior for the rigid backface support and clamped-clamped boundary conditions.

16. In order to reliably use the static indentation test in assessing (impact) damage resistance, further work is needed to determine the relationship that exists between the damage incipience and damage extent in static and impact events for the plate geometries and boundary conditions examined here, as well as others.

Based on the results of this investigation, recommendations for further research are:

1. Investigate the effect of boundary conditions (including rigid backface support) and specimen span on the damage incipience for both impact and static tests.

2. Confirm whether or not the indentation decreases with increasing bending curvature through indentation tests which allow plates to

undergo different amounts of bending caused both by changing span and changing force.

3. Determine the individual contributions of the local through-thickness stress state and the overall bending characteristics to the difference in force-indentation response seen in specimens tested with the rigid backface support and the clamped-clamped support.

4. Further investigate the development of membrane behavior in plates with different geometries. Specifically, use the relationships between bending strain and bending moment and between extensional strain and contact force at a location on the plate normalized to span to examine at what contact force and specimen geometry (aspect ratio, length, thickness, etc.) membrane behavior becomes important.

5. Determine the change in behavior and important scaling parameters for the bending, indentation, and damage characteristics for specimens with different geometries to better understand how these parameters might influence the damage resistance for realistic geometries.

6. Investigate the possibility of wrapping occurring near the contact point. Specifically, identify the effects this behavior might have on the resulting damage in the plate and the range of contact forces or indentations under which this behavior will develop.

7. Include the local shell effect in the nonlinear analysis as developed in order to achieve better accuracy in predicting the bending strains which would enable prediction of the occurrence of damage in the plate.

8. Identify the physical meaning of the β-factor in terms of the flexibility of the in-plane boundary conditions through experiment and analysis.

9. Determine whether or not the indentation response of a specimen in a clamped-clamped boundary condition during an impact event is bounded by the indentation responses of specimens in a clamped-clamped boundary condition and a rigid backface support condition, as the deflection is.

10. Determine the relationship that exists between the damage incipience and damage extent in static and impact events for different plate geometries and boundary conditions.

REFERENCES

1. Lagace, P. A., Williamson, J. E., Tsang, P. H. W., Wolf, E., and Thomas, S. A., "A Preliminary Proposition for a Test Method to Measure (Impact) Damage Resistance", *Journal of Reinforced Plastics and Composites*, Vol. 12, No. 5, May, 1993, pp. 584-601.

2. Jackson, W. C. and Poe, C. C., "The Use of Impact Force as a Scale Parameter for the Impact Response of Composite Laminates", NASA-TM-104189, January, 1992.

3. Abrate, S., "Impact on Laminated Composite Materials", *Applied Mechanics Review*, Vol. 44, No. 4, April, 1991, pp. 155-190.

4. Cairns, D. S. and Lagace, P. A., "A Consistent Engineering Methodology for the Treatment of Impact in Composite Materials", *Journal of Reinforced Plastics and Composites*, Vol. 11, No. 4, 1992, pp. 395-412.

5. Lee, S.-M. and Zahuta, P., "Instrumented Impact and Static Indentation of Composites", *Journal of Composite Materials*, Vol. 25, No. 2, February, 1991, pp. 204-222.

6. Sjöblom, P. O., Hartness, J. T., and Cordell, T. M., "On Low-Velocity Impact Testing of Composite Materials", *Journal of Composite Materials*, Vol. 22, No. 1, January, 1988, pp. 30-52.

7. Elber, W., "Failure Mechanics in Low-Velocity Impacts on Thin Composite Plates", NASA-TP-2152, April, 1983.

8. Kwon, Y. S. and Sankar, B. V., "Indentation Damage in Graphite/Epoxy Laminates", *Proceedings of the American Society for Composites, Sixth Technical Conference*, Albany, New York, 1991, pp. 483-492.

9. Williamson, J. E., "Response Mechanisms in the Impact of Graphite/Epoxy Honeycomb Sandwich Panels", Department of Aeronautics and Astronautics, Massachusetts Institute of Technology, Cambridge, MA, S.M. Thesis, 1991.

10. Wolf, E., "Impact Damage Mechanisms in Several Laminated Material Systems", Department of Aeronautics and Astronautics, Massachusetts Institute of Technology, Cambridge, MA, S.M. Thesis, 1992.

11. Yang, S. H. and Sun, C. T., "Indentation Law for Composite Laminates", *Composite Materials: Testing and Design (sixth Conference)*, 1982, pp. 425-449.

12. Hertz, H., "Uber die Beruhrung fester Elastischer Korper", *Journal Reine Angle Math*, Vol. 92, 1881, pp. 155.

13. Goldsmith, W., *Impact*, Arnold, London, 1960,

14. Sun, C. T., Sankar, B. V., and Tan, T. M., "Dynamic Response of SMC to Impact of a Steel Ball", *The Winter Meeting of the American Society of Mechanical Engineers*, Washington, D.C., 1981,

15. Tan, T. M. and Sun, C. T., "Use of Statical Indentation Laws in the Impact Analysis of Laminated Composite Plates", *Journal of Applied Mechanics*, Vol. 52, March, 1985, pp. 6-12.

16. Keer, L. M. and Miller, G. R., "Contact Between an Elastically Supported Circular Plate and a Rigid Indenter", *International Journal of Engineering Sciences*, Vol. 21, No. 6, 1983, pp. 681-690.

17. Keer, L. M. and Ballarini, R., "Smooth Contact Between a Rigid Indenter and an Initially Stressed Orthotropic Beam", *AIAA Journal*, Vol. 21, No. 7, July, 1983, pp. 1035-1042.

18. Cairns, D. S. and Lagace, P. A., "Thick Composite Plates Subjected to Lateral Loading", *Journal of Applied Mechanics*, Vol. 54, September, 1987, pp. 611-616.

19. Sankar, B. V., "An Integral Equation for the Problem of Smooth Indentation of Orthotropic Beams", *International Journal of Solids and Structures*, Vol. 25, No. 3, 1989, pp. 327-337.

20. Lin, H. J. and Lee, Y. J., "Use of Statical Indentation Laws in the Impact Analysis of Composite Laminated Plates and Shells", *Journal of Applied Mechanics*, Vol. 57, September, 1990, pp. 787-789.

21. Cairns, D. S., "A Simple, Elasto-Plastic Contact Law for Composites", *Journal of Reinforced Plastics and Composites*, Vol. 10, July, 1991, pp. 423-433.

22. Oda, J. and Kubota, T., "Approximate Solution on the Elastic Contact Problems Between Two-Layered Bodies", *AIAA/ASME/ASCE/AHS/ASC Structures, Structural Dynamics and Materials Conference*, Dallas, TX, 1992,

23. Chen, C.-F. and Frederick, D., "Contact of Isotropic Square Plates with Rigid Spherical Indenters", *International Journals of Solids and Structures*, Vol. 30, No. 5, 1993, pp. 637-650.

24. vonKármán, T., *Encyklopaedie der Mathematischen Wissenschaften*, Vol. 4, 1910, pp. 394.

25. Timoshenko, S. and Woinowsky-Kreiger, S., *Theory of Plates and Shells*, McGraw-Hill, NY, 1959,

26. Levy, S., "Square Plate with Clamped Edges Under Normal Pressure Producing Large Deflections", TN 847, NACA, May, 1942.

27. Chia, C. Y., "Finite Deflections of Uniformly Loaded, Clamped, Rectangular, Anisotropic Plates", *AIAA Journal*, Vol. 10, No. 11, November, 1972, pp. 1399-1400.

28. Zaghloul, S. A. and Kennedy, J. B., "Nonlinear Behavior of Symmetrically Laminated Plates", *Journal of Applied Mechanics*, Vol. 42, March, 1975, pp. 234-236.

29. Reddy, J. N., "A Simple Higher-Order Theory for Laminated Composite Plates", *Journal of Applied Mechanics*, Vol. 51, December, 1984, pp. 745-752.

30. Savithri, S. and Varadan, T. K., "Large Deflection Analysis of Laminated Composite Plates", *International Journal of Non-Linear Mechanics*, Vol. 28, No. 1, 1993, pp. 1-12.

31. Kant, T. and Mallikarjuna, "Non-Linear Dynamics of Laminated Plates with Higher-Order Theory and C^0 Finite Elements", *International Journal of Non-Linear Mechanics*, Vol. 26, No. 3/4, 1991, pp. 335-343.

32. Matsuhashi, H., Graves, M. J., Dugundji, J., and Lagace, P. A., "Effect of Membrane Stiffening in Transient Impact Analysis of Composite Laminated Plates", *34th SDM Conference*, La Jolla, CA, 1993,

33. Cantwell, W. J. and Morton, J., "Geometrical Effects in the Low Velocity Impact Response of CFRP", *Composite Structures*, Vol. 12, 1989, pp. 39-59.

34. Meyer, P. I., "Low Velocity Hard-Object Impact of Filament-Wound Kevlar/Epoxy Composite", *Composites Science and Technology*, Vol. 33, No. 4, 1988, pp. 279-293.

35. Ryan, K. F., "Dynamic Response of Graphite/Epoxy Plates Subjected to Impact Loading", Department of Aeronautics and Astronautics, Massachusetts Institute of Technology, Cambridge, MA, S.M. Thesis, 1989.

36. Matsuhashi, H., "Nonlinear Analysis of Composite Laminated Plates Subjected to Impact", Department of Aeronautics and Astronautics, Massachusetts Institute of Technology, Cambridge, MA, S.M. Thesis, 1992.

37. Lagace, P. A., Beaumont, M., Brewer, J. C., and Varnerin, C. F., "TELAC Manufacturing Course Class Notes", TELAC Report No. 88-4b, Massachusetts Institute of Technology, September, 1991.

38. Beer, F. P. and Johnson, E. R., *Mechanics of Materials*, McGraw-Hill, Inc., New York, 1981,

39. Love, A. E. H., *A Treatise on the Mathematical Theory of Elasticity*, Dover Publications, New York, 1927,

40. Reissner, E., "The Effect of Transverse Shear Deformation on the Bending of Elastic Plates", *Journal of Applied Mechanics*, Vol. 18, June, 1945, pp. 67-69.

41. Whitney, J. M. and Pagano, N. J., "Shear Deformation in Heterogeneous Anisotropic Plates", *Journal of Applied Mechanics*, Vol. 37, No. 4, December, 1970, pp. 1031-1036.

42. Dugundji, J., "Simple Expression for Higher Vibration Modes of Uniform Euler Beams", *AIAA Journal*, Vol. 26, No. 8, August, 1988, pp. 1013-1014.

43. Strang, G., *Introduction to Applied Mathematics*, Wellesley-Cambridge Press, Wellesley, MA, 1986,

44. Press, W. H., Flannery, B. P., Teukolsky, S. A., and Vetterling, W. T., *Numerical Recipes (FORTRAN Version)*, Cambridge University Press, New York, 1989,

APPENDIX A: GENERALIZED BEAM FUNCTIONS

To implement the Rayleigh-Ritz method, it is necessary to define shape functions which approximate the deformed shape of the plate. Dugundji [42] derived approximate beam shape functions (generalized beam functions) for various bending modes and boundary conditions. Although these generalized beam functions are approximations to the traditional beam shape functions, the difference between the two becomes negligible when the mode number is greater than two.

The generalized beam functions are written in the form:

$$\phi_n(x) = \sqrt{2}\sin(\beta_n x + \theta) + A e^{-\beta_n x} + B e^{-\beta_n (1-x)} \tag{A.1}$$

where the constants or shape parameters β_n, θ, A, and B are given in Table A.1 for some common boundary conditions. All modes are normalized such that the mode shape $\phi_n(x)$ satisfies the condition:

$$\int_0^1 \phi_n{}^2(x)\,dx = 1 \tag{A.2}$$

These modes also apply for the case of n equal to one with less than a 1% error, except for the clamped-free case. The form of equation (A.1) has the advantage that generalized beam functions can be written in one single parametric form and easily evaluated numerically.

The shape functions are implemented in the analysis presented in this work by specifying the mode shape which best approximates the shape of a displacement or rotation. This is done by using the form of equation (A.1) for the clamped-clamped boundary condition in the x-direction and the free-free boundary condition in the y-direction, as determined by the values in Table A.1.

Table A.1 Euler Beam Elastic Mode Shape Parameters [42].

Boundary Condition[a]	β_n	θ	A	B
CL–CL	$(n+1/2)\pi$	$-\pi/4$	1	$(-1)^{n+1}$
FR–FR	$(n+1/2)\pi$	$+3\pi/4$	1	$(-1)^{n+1}$

[a] CL = clamped, and FR = free.

APPENDIX B

All of the force-indentation, force-deflection, and force-strain data obtained in this investigation is presented in this section. Analytical curves showing strain results, comparisons of β-factors, and convergence of strain results are also presented here. The contents of this section are summarized in Table B.1.

Table B.1 Appendix B Contents

Figure Descriptions	Figure Numbers
Comparisons of β-factors	B.1 - B.6
Analytical strain results	B.7 - B.12
Convergence of strain results	B.13 - B.18
Force-indentation data from tests of specimens with a rigid backface support	B.19 - B.22
Force-indentation data from tests of specimens with a 254 mm span in the clamped-clamped boundary condition	B.23 - B.29
Force-indentation data from tests to a maximum contact force of 930 N on specimens of various spans in the clamped-clamped boundary condition	B.30 - B.35
Force-deflection data from tests of specimens with a 254 mm span in the clamped-clamped boundary condition	B.36 - B.42
Force-strain data from tests to a maximum contact force of 930 N on specimens of various spans in the clamped-clamped boundary condition	B.43 - B.59
Force-strain data from tests to a maximum contact force of 1479 N on specimens of various spans in the clamped-clamped boundary condition	B.60 - B.82

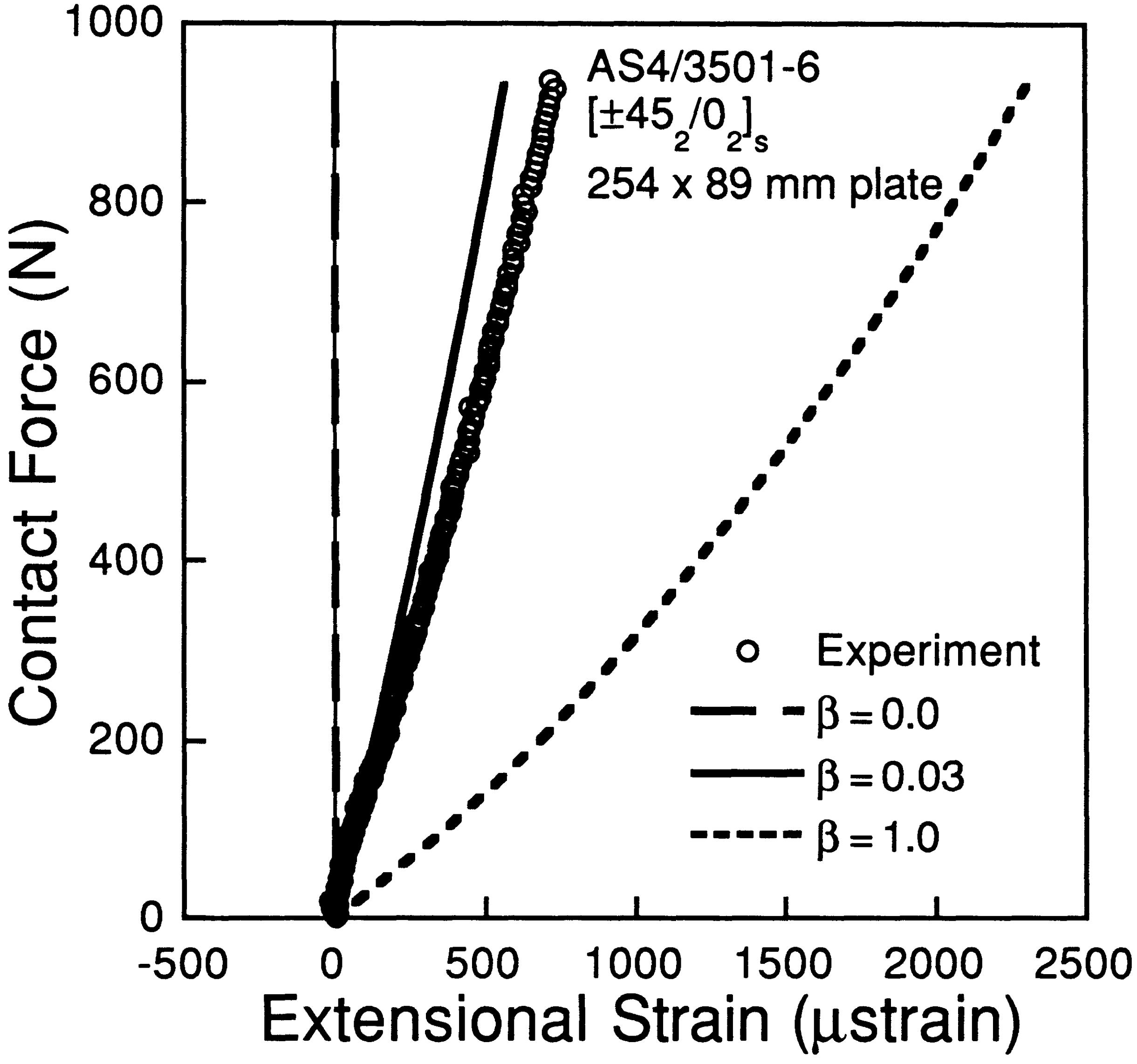

Figure B.1 Experimental force-extensional strain data and analytical force-extensional strain results for various values of β at position 1-2 (strain gage scheme A) for an AS4/3501-6 [±45$_2$/0$_2$]$_s$ 254 mm span specimen indented to 930 N.

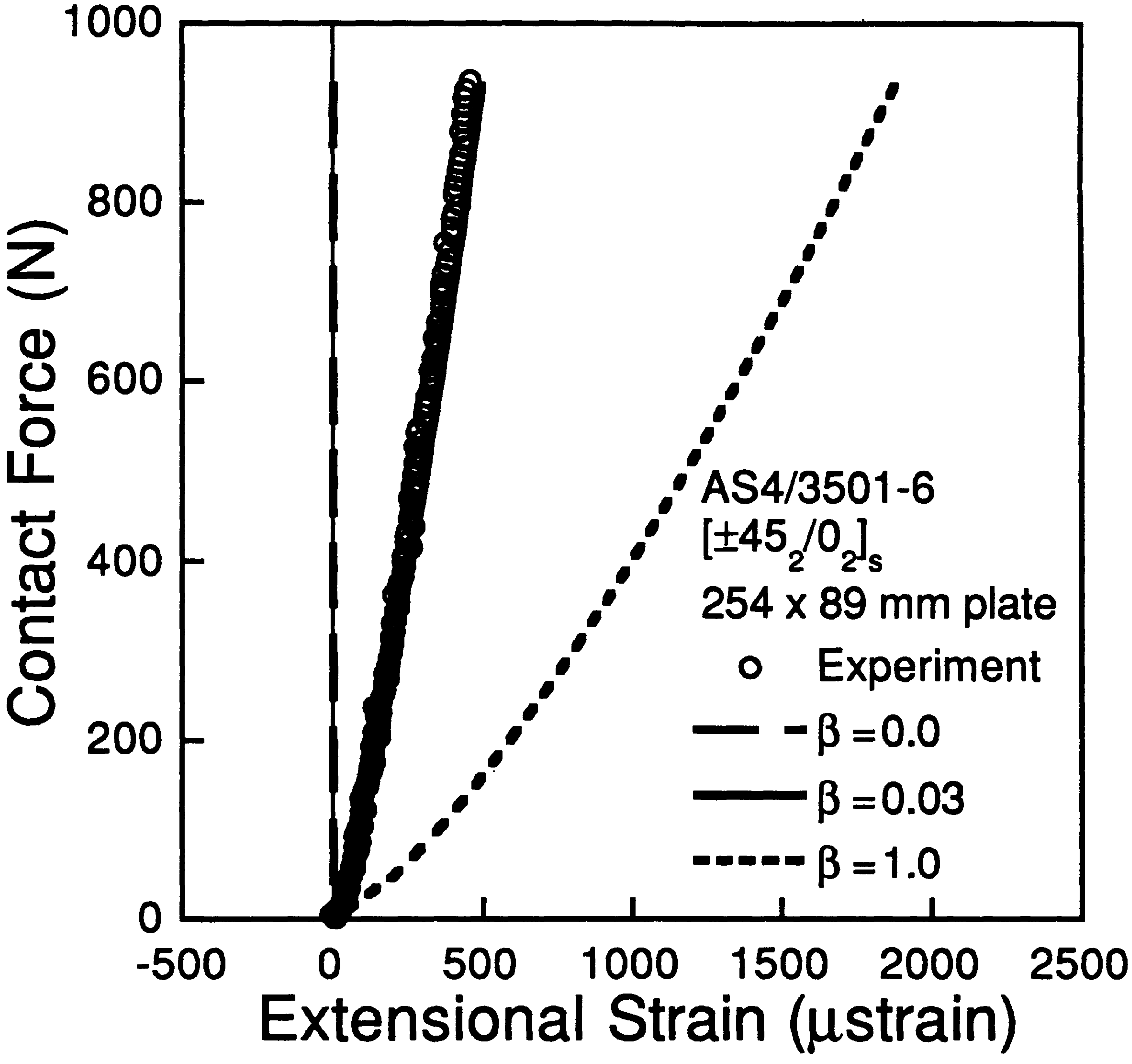

Figure B.2 Experimental force-extensional strain data and analytical force-extensional strain results for various values of β at position 3-4 (strain gage scheme A) for an AS4/3501-6 $[\pm45_2/0_2]_s$ 254 mm span specimen indented to 930 N.

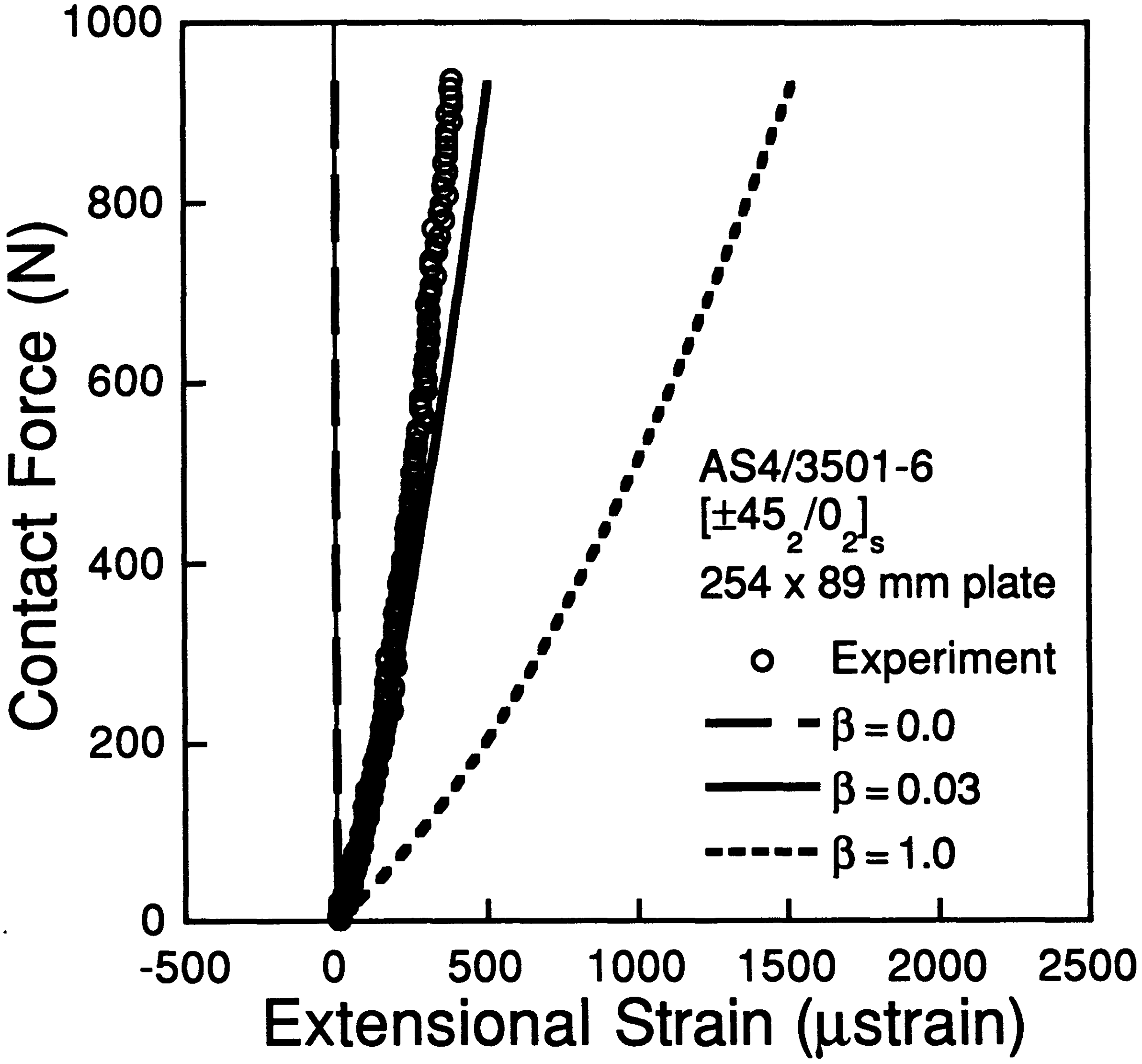

Figure B.3 Experimental force-extensional strain data and analytical force-extensional strain results for various values of *β* at position 5-6 (strain gage scheme A) for an AS4/3501-6 [$\pm 45_2/0_2]_s$ 254 mm span specimen indented to 930 N.

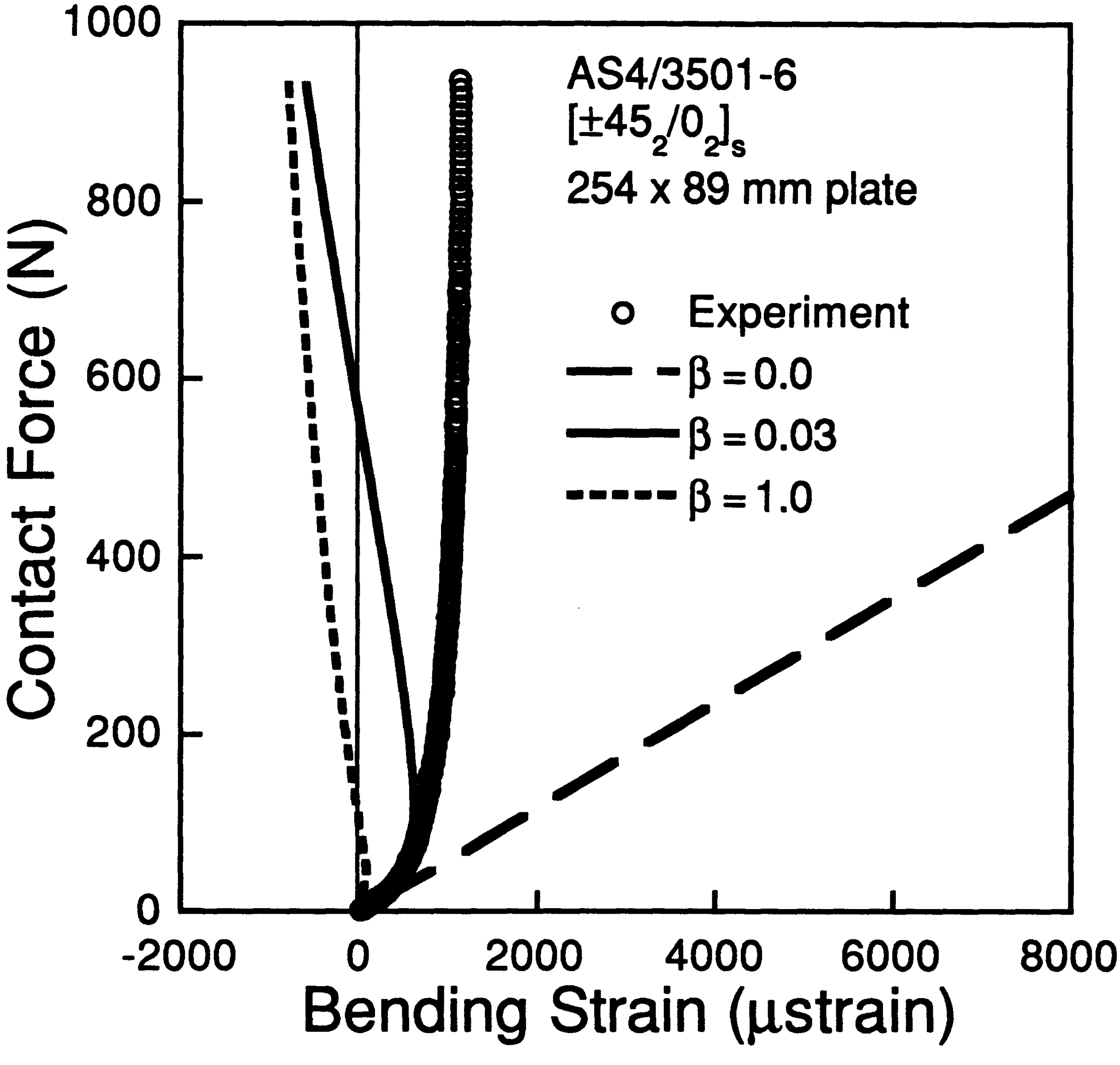

Figure B.4 Experimental force-bending strain data and analytical force-bending strain results for various values of *β* for gage 2 (strain gage scheme A) for an AS4/3501-6 $[\pm45_2/0_2]_s$ 254 mm span specimen indented to 930 N.

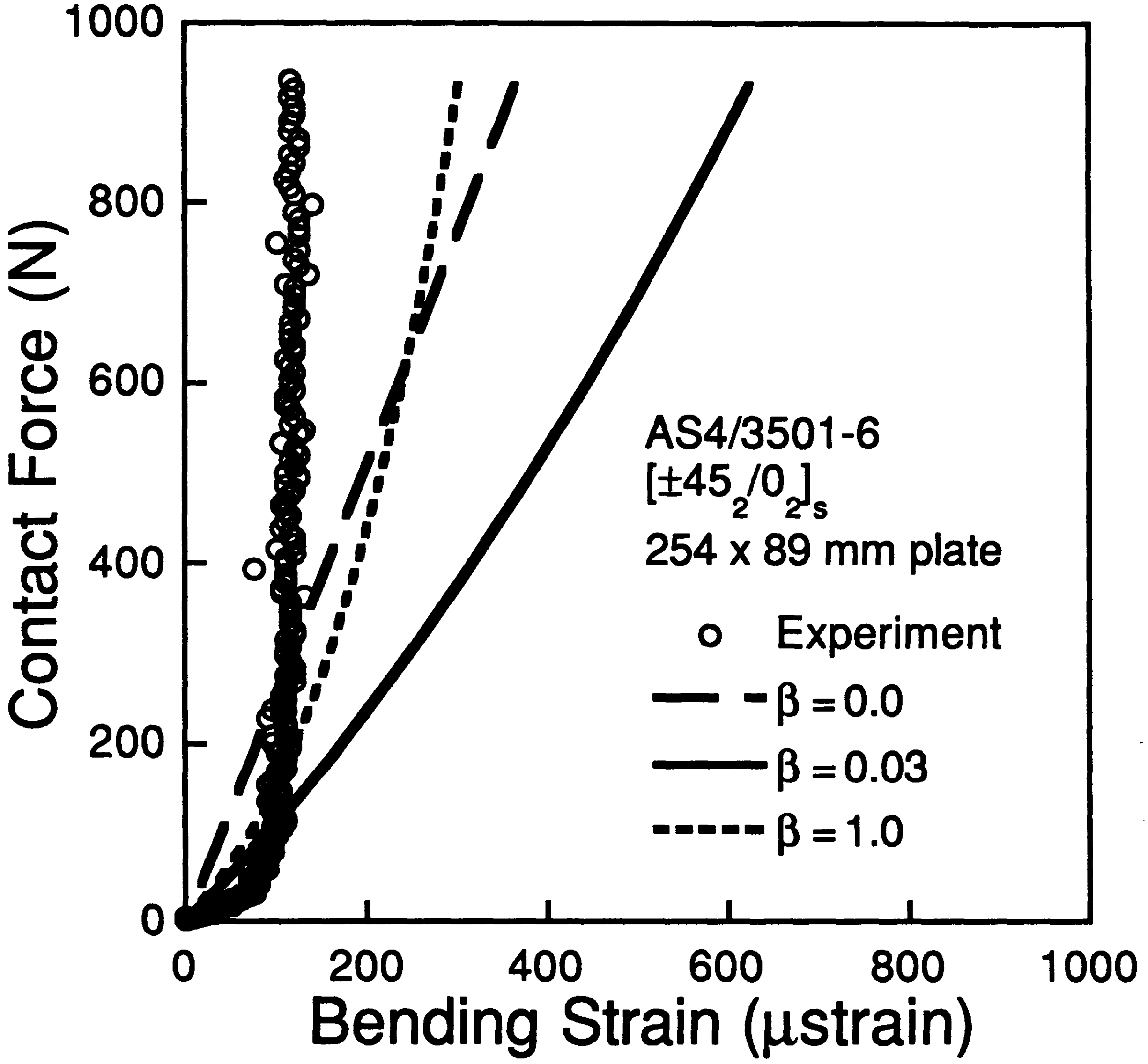

Figure B.5 **Experimental force-bending strain data and analytical force-bending strain results for various values of β for gage 4 (strain gage scheme A) for an AS4/3501-6 [±45$_2$/0$_2$]$_s$ 254 mm span specimen indented to 930 N.**

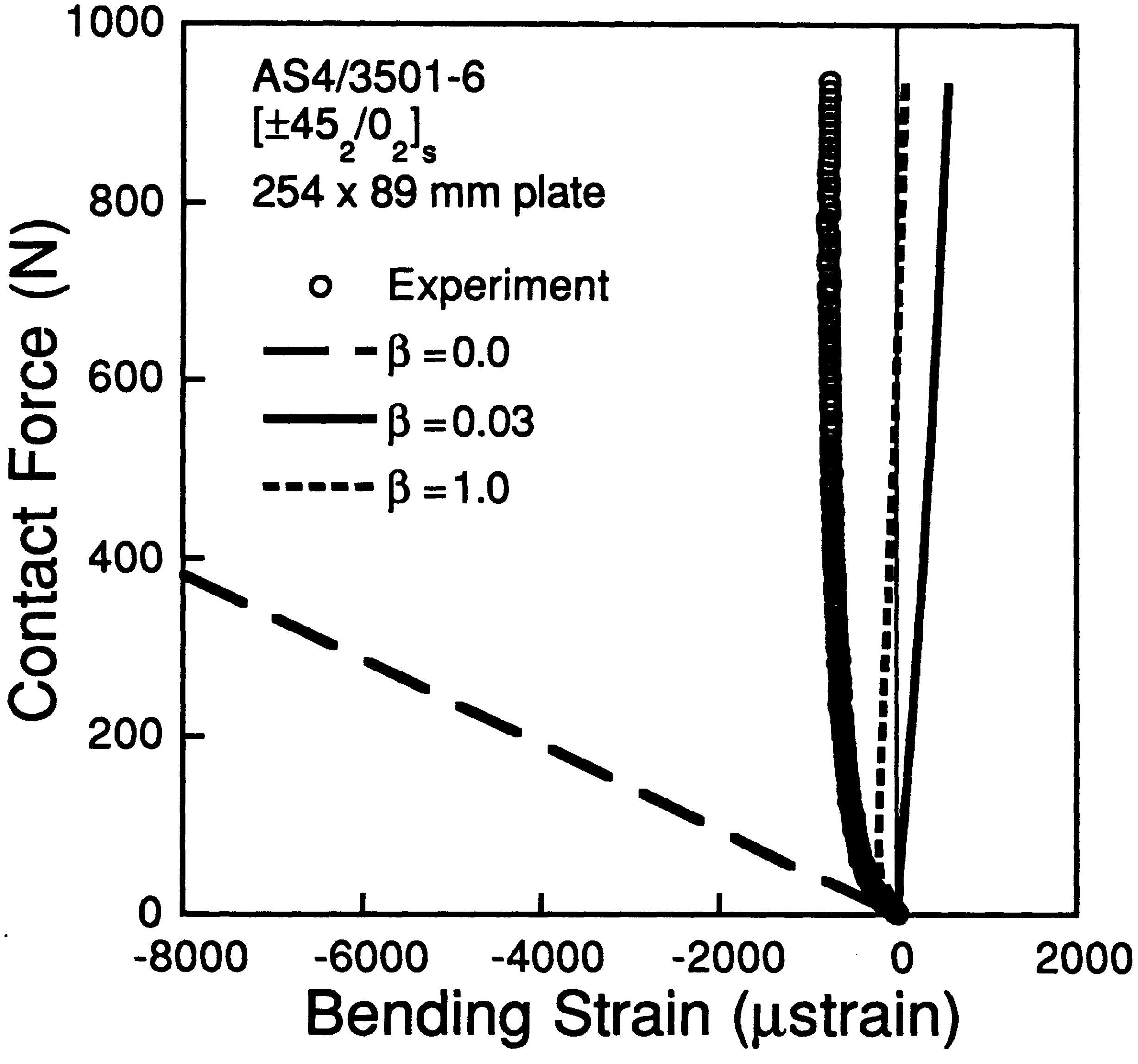

Figure B.6 Experimental force-bending strain data and analytical force-bending strain results for various values of β for gage 6 (strain gage scheme A) for an AS4/3501-6 $[\pm45_2/0_2]_s$ 254 mm span specimen indented to 930 N.

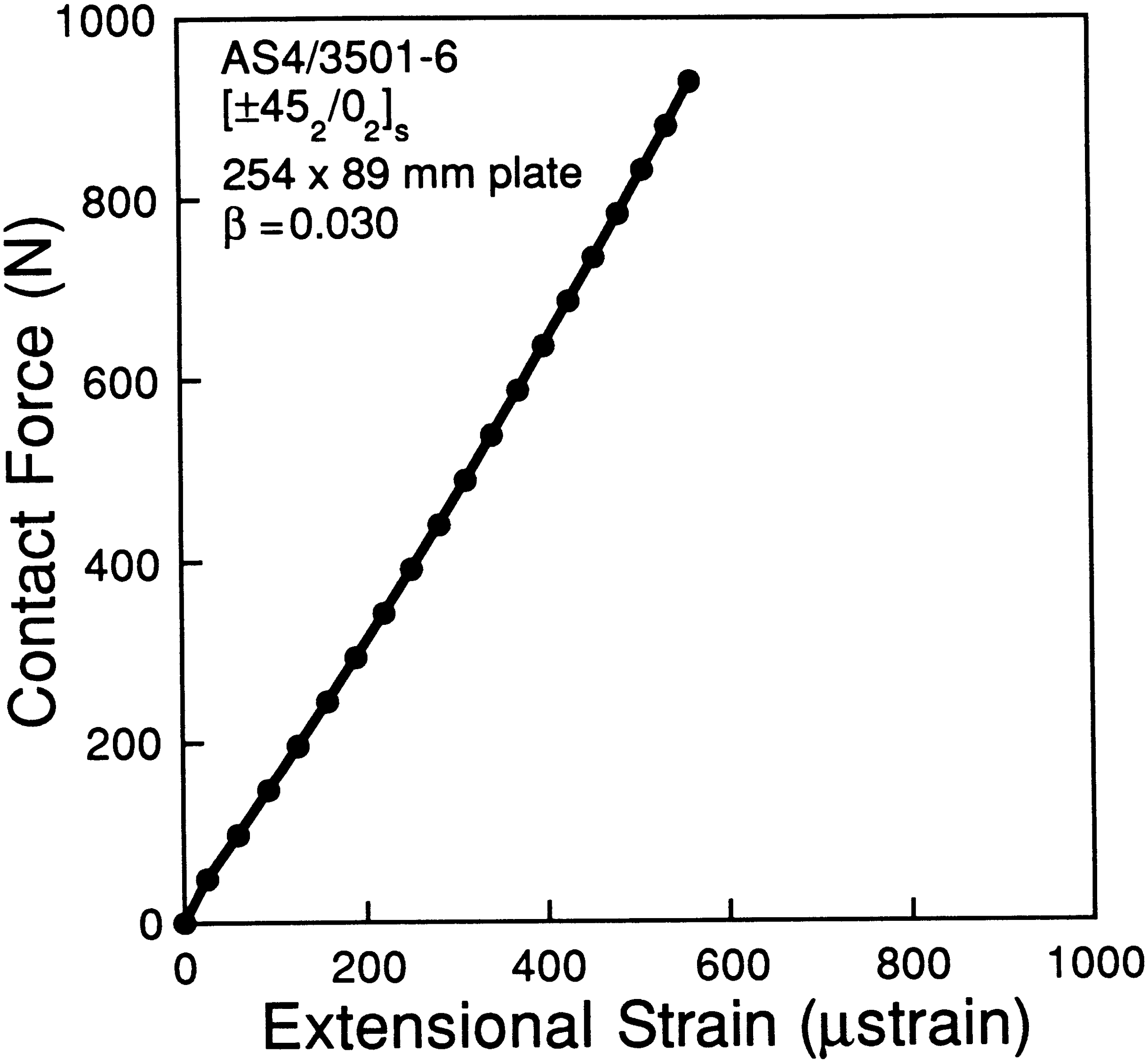

Figure B.7 Analytical force-extensional strain curve at position 1-2 (strain gage scheme A) for an AS4/3501-6 [$\pm45_2/0_2$]$_s$ 254 mm span specimen indented to 930 N.

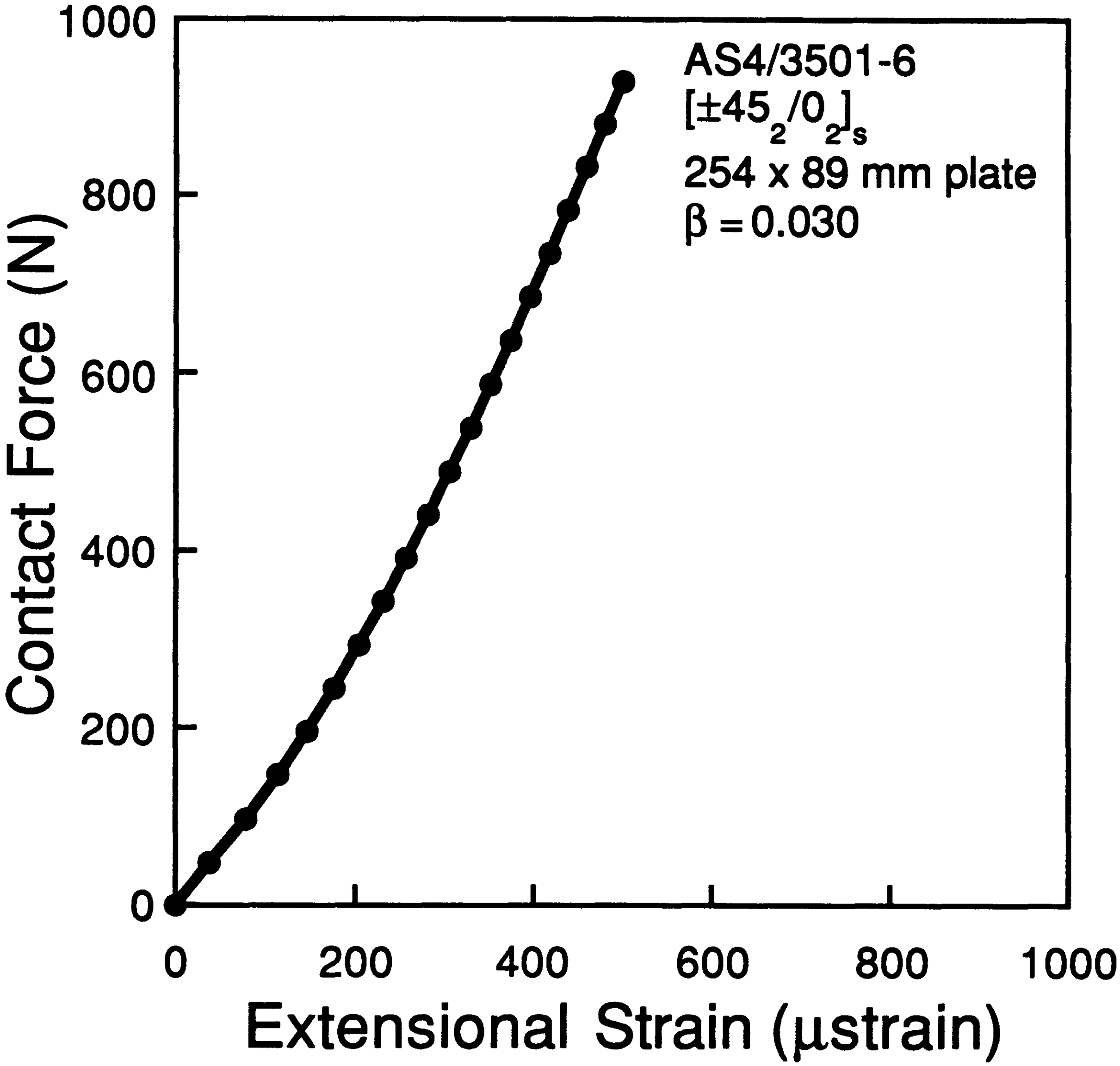

Figure B.8 **Analytical force-extensional strain curve at position 3-4 (strain gage scheme A) for an AS4/3501-6 $[\pm 45_2/0_2]_s$ 254 mm span specimen indented to 930 N.**

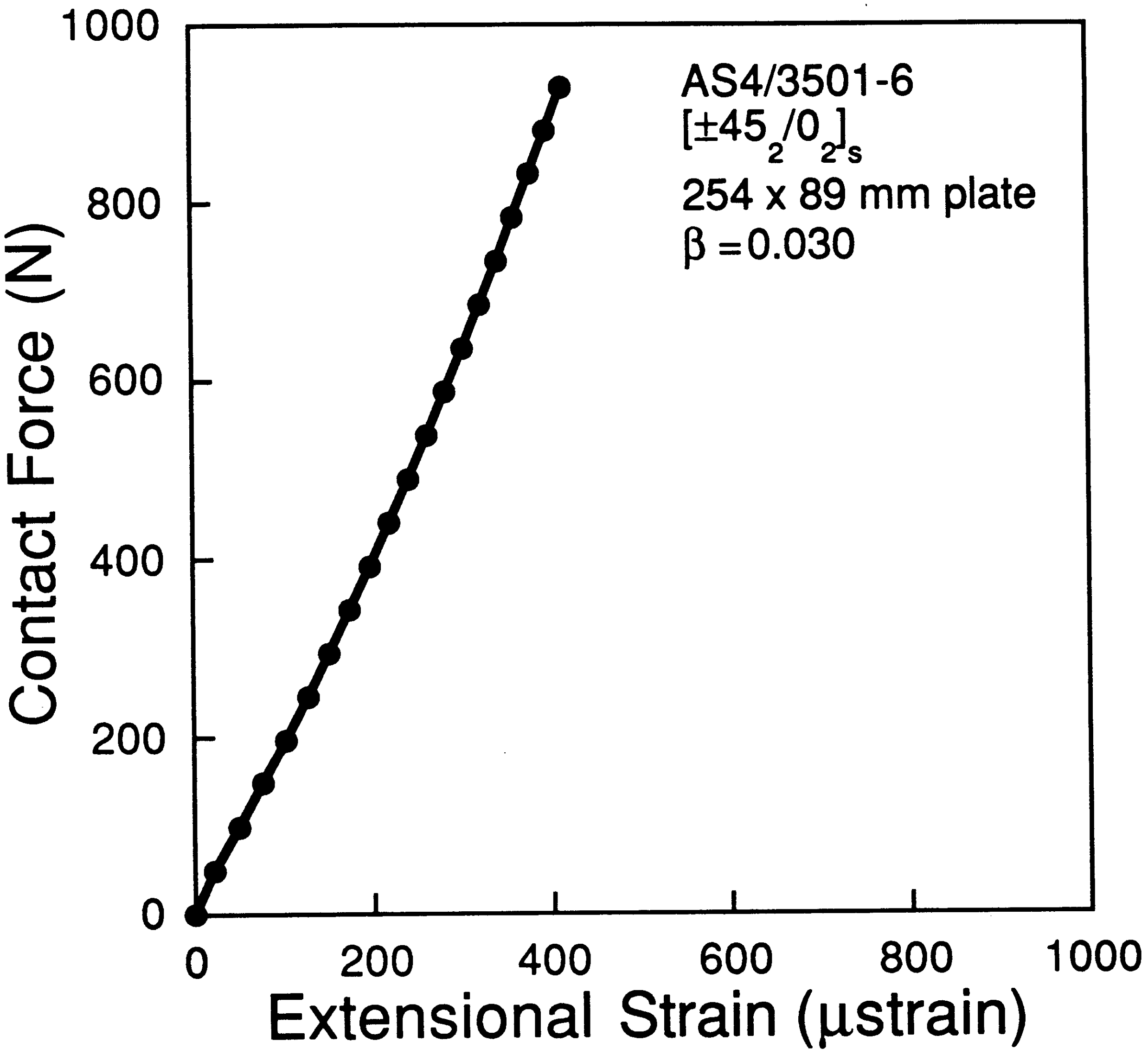

Figure B.9 Analytical force-extensional strain curve at position 5-6 (strain gage scheme A) for an AS4/3501-6 [±45$_2$/0$_2$]$_s$ 254 mm span specimen indented to 930 N.

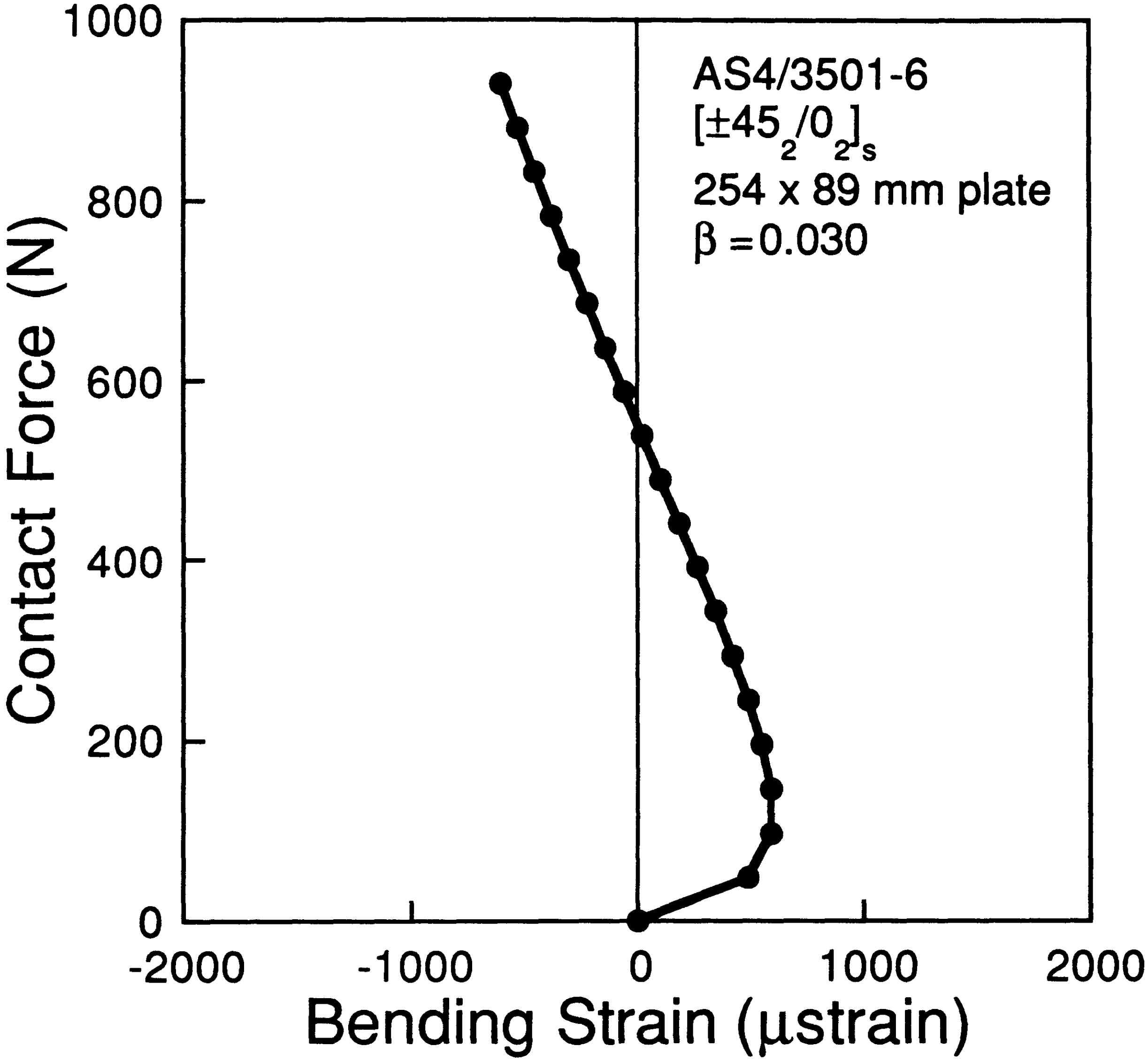

Figure B.10 Analytical force-bending strain curve for gage 2 (strain gage scheme A) for an AS4/3501-6 $[\pm45_2/0_2]_s$ 254 mm span specimen indented to 930 N.

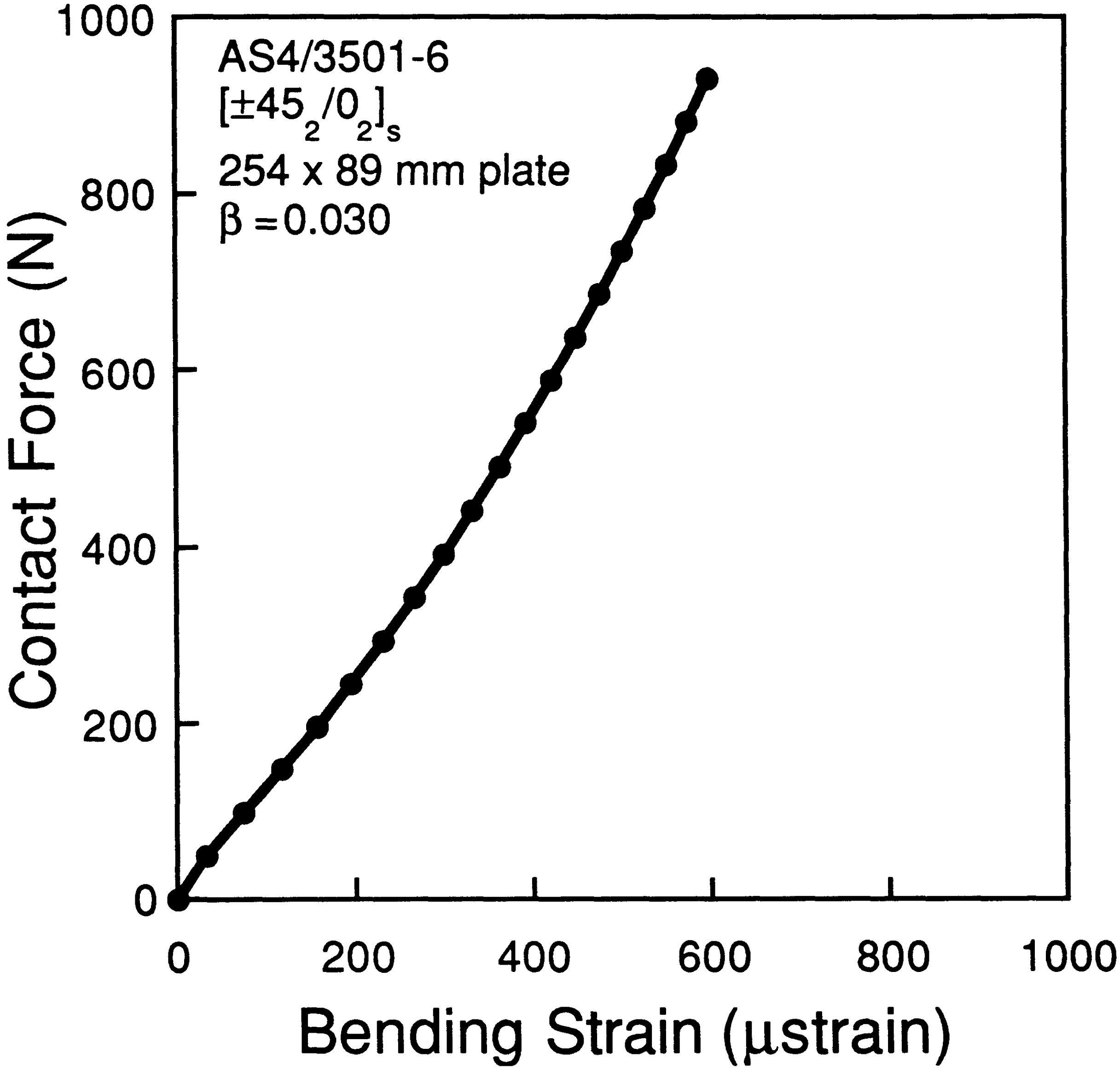

Figure B.11 Analytical force-bending strain curve for gage 4 (strain gage scheme A) for an AS4/3501-6 [±45$_2$/0$_2$]$_s$ 254 mm span specimen indented to 930 N.

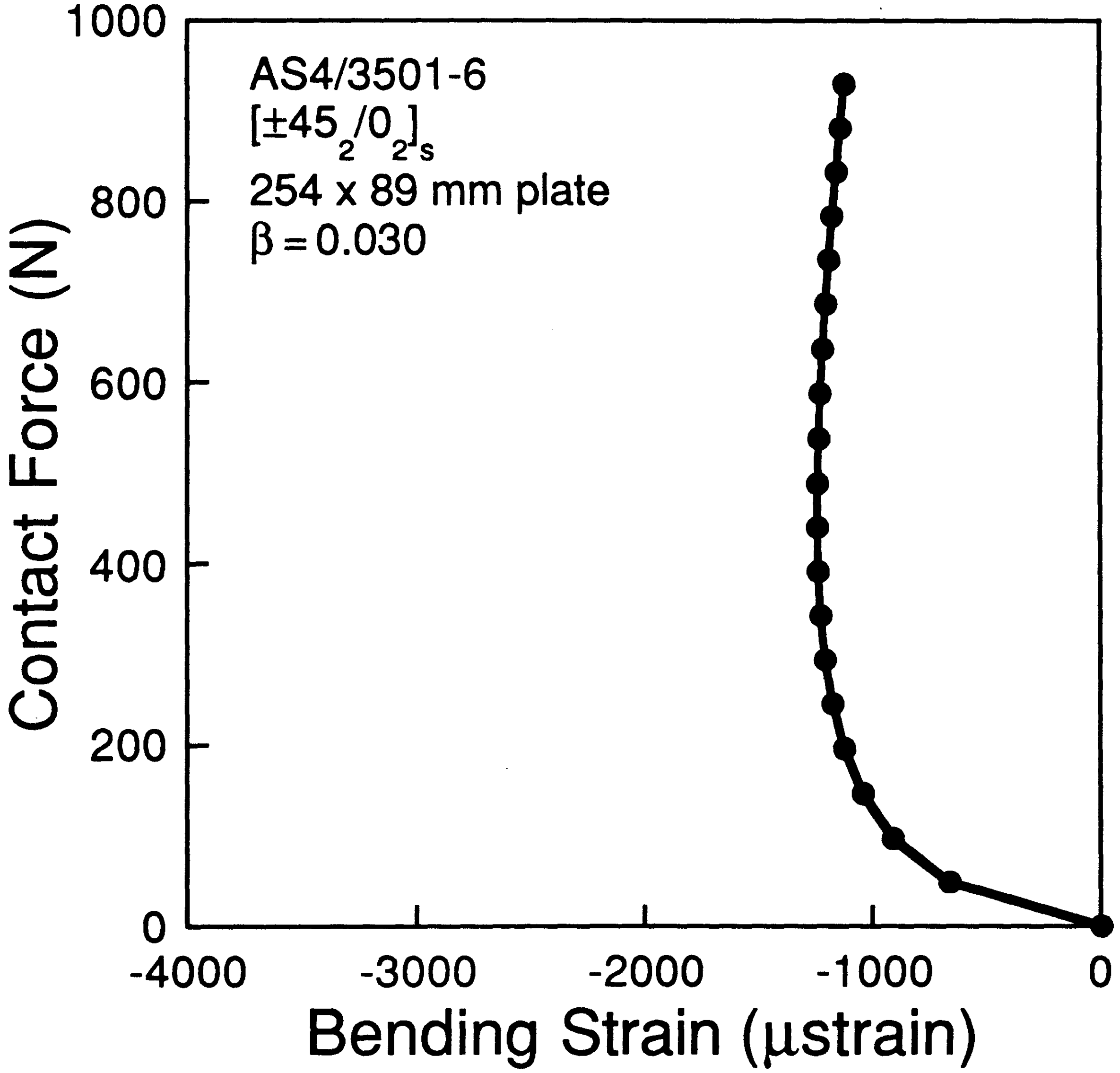

Figure B.12 Analytical force-bending strain curve for gage 6 (strain gage scheme A) for an AS4/3501-6 $[\pm 45_2/0_2]_s$ 254 mm span specimen indented to 930 N.

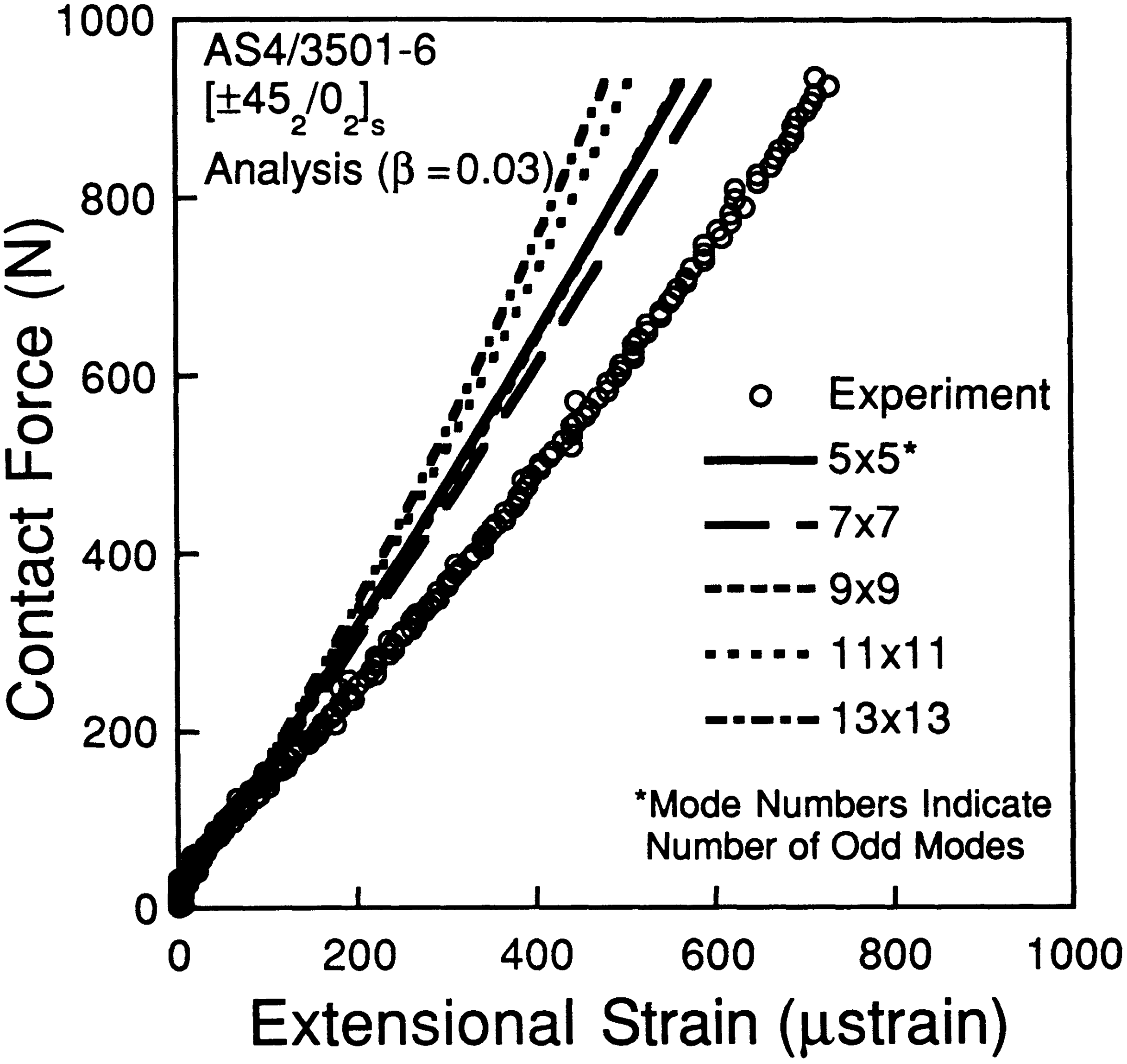

Figure B.13 Convergence of force-extensional strain curves at position 1-2 (strain gage scheme A) for an AS4/3501-6 [$\pm45_2/0_2]_s$ 254 mm span specimen indented to 930 N.

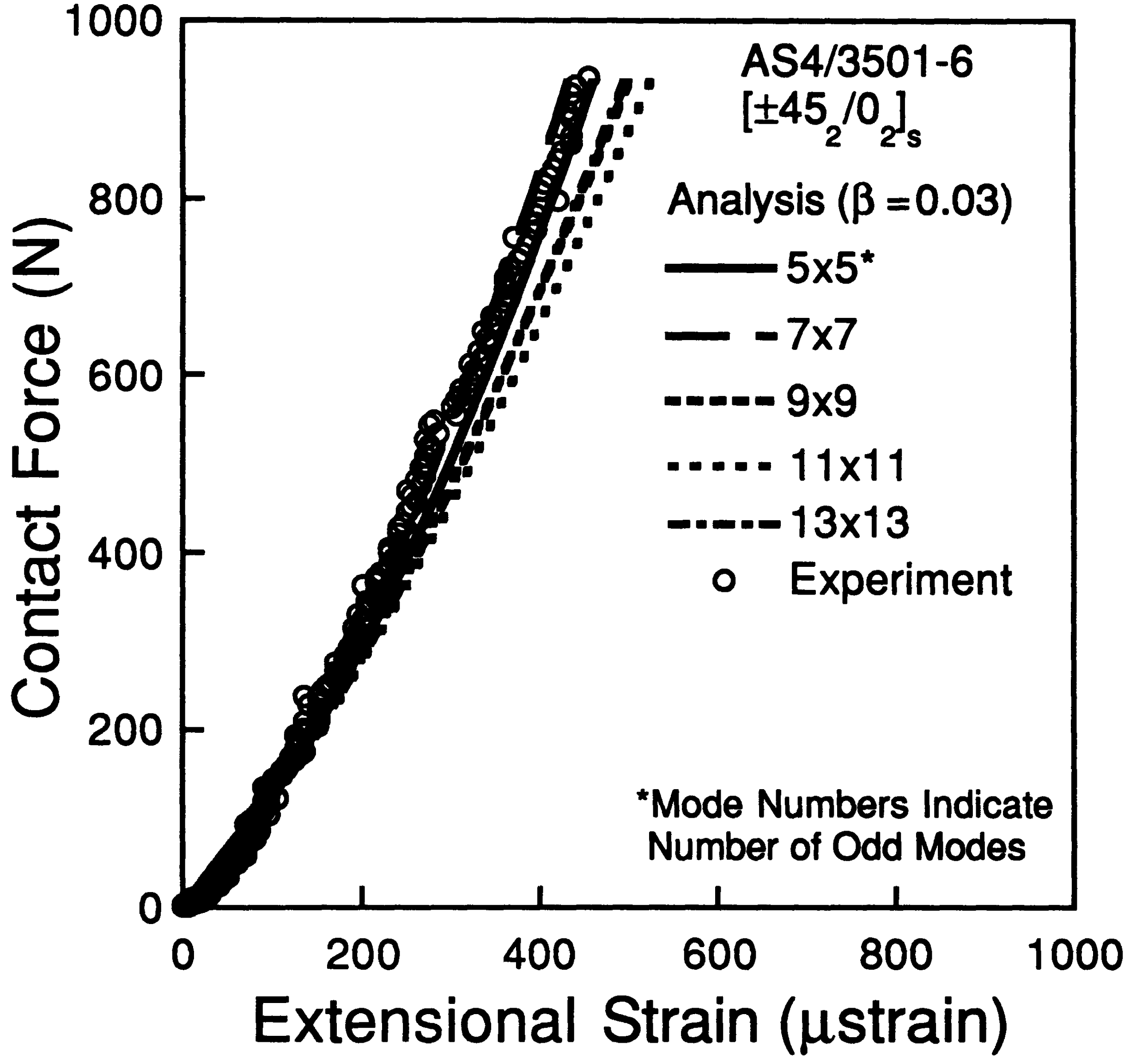

Figure B.14 Convergence of force-extensional strain curves at position 3-4 (strain gage scheme A) for an AS4/3501-6 [$\pm45_2/0_2$]$_s$ 254 mm span specimen indented to 930 N.

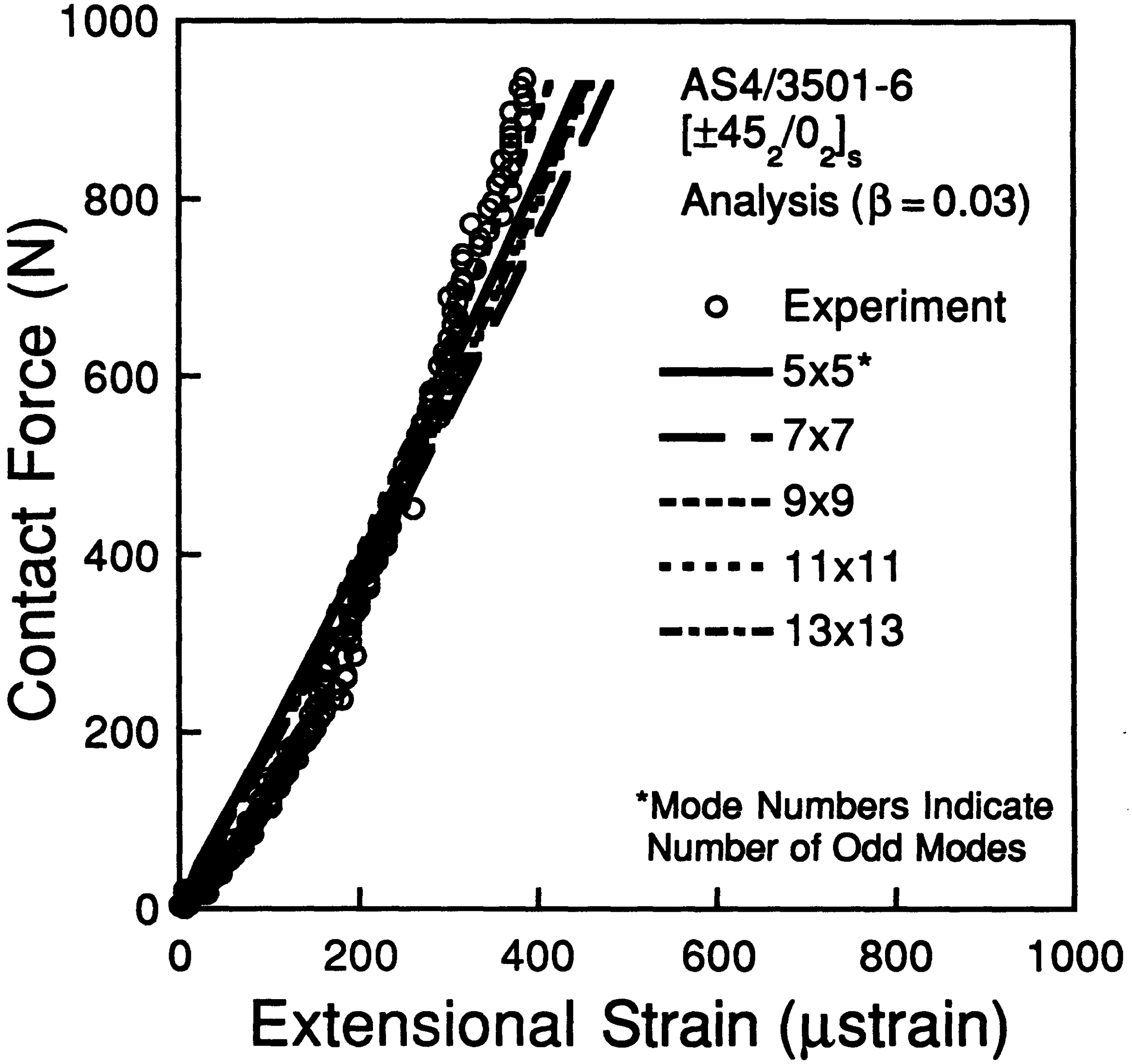

Figure B.15 Convergence of force-extensional strain curves at position 5-6 (strain gage scheme A) for an AS4/3501-6 [$\pm45_2/0_2]_s$ 254 mm span specimen indented to 930 N.

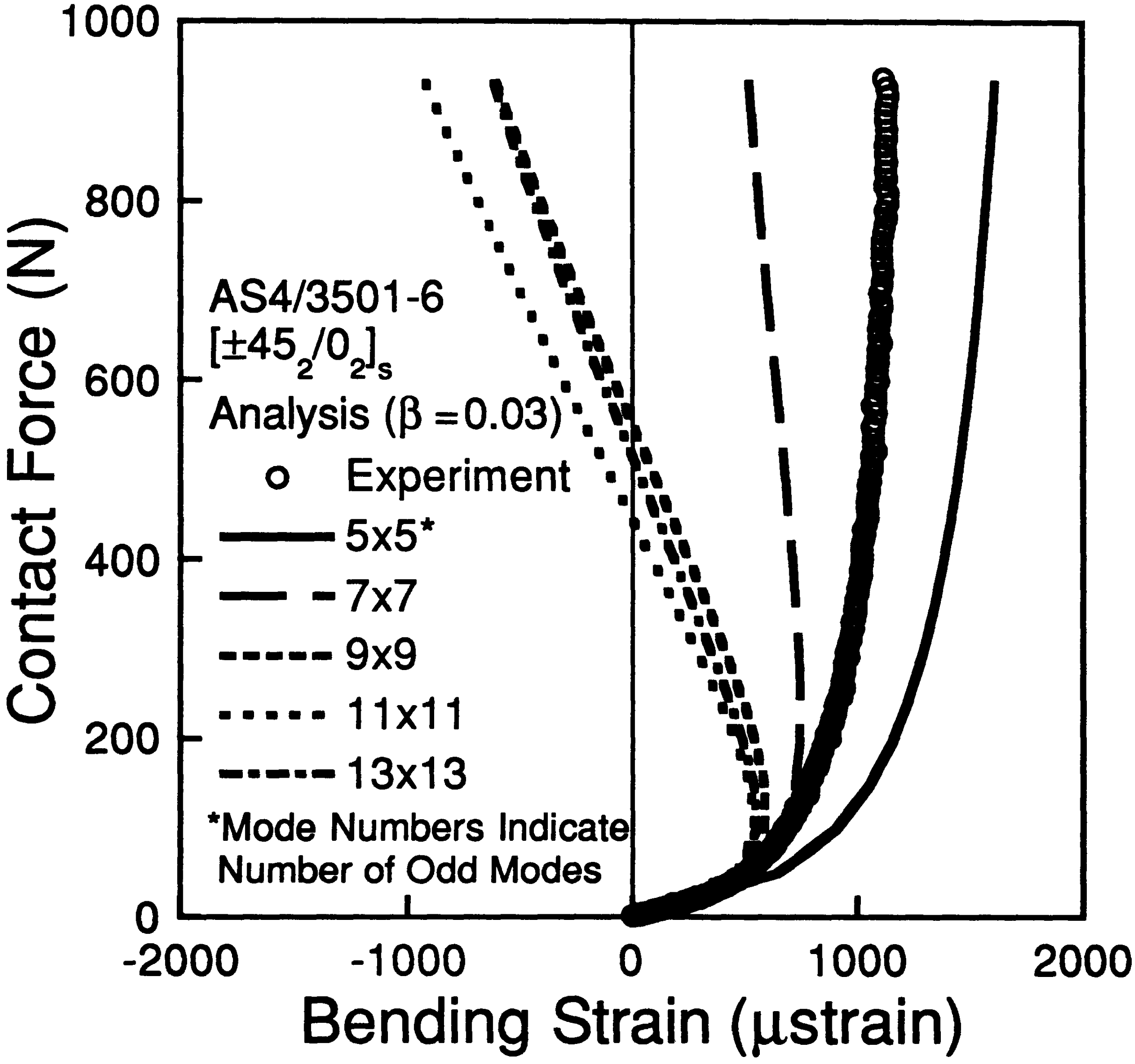

Figure B.16 Convergence of force-bending strain curves for gage 2 (strain gage scheme A) for an AS4/3501-6 [±$45_2/0_2$]$_s$ 254 mm span specimen indented to 930 N.

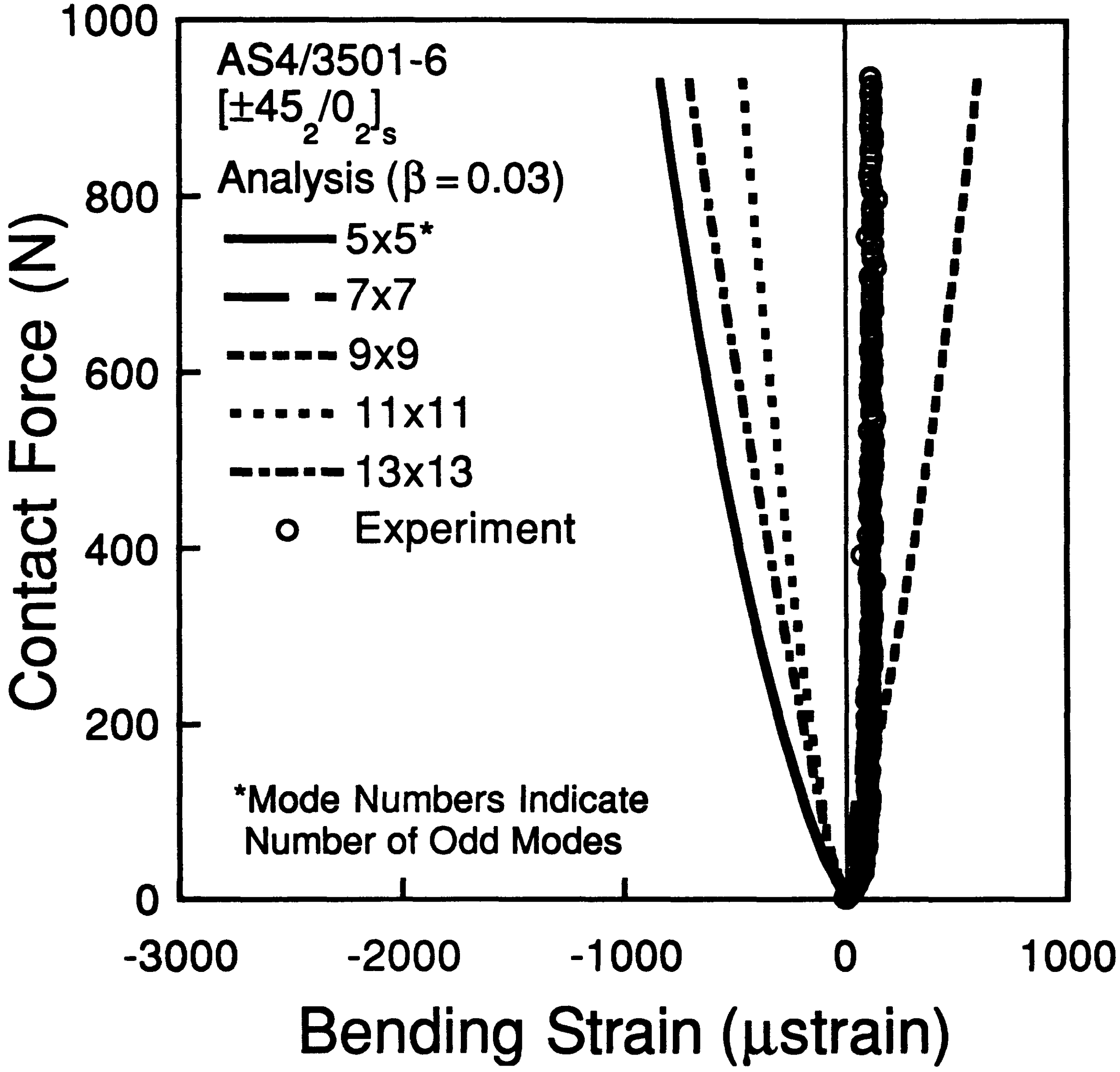

Figure B.17 Convergence of force-bending strain curves for gage 4 (strain gage scheme A) for an AS4/3501-6 [$\pm45_2/0_2$]$_s$ 254 mm span specimen indented to 930 N.

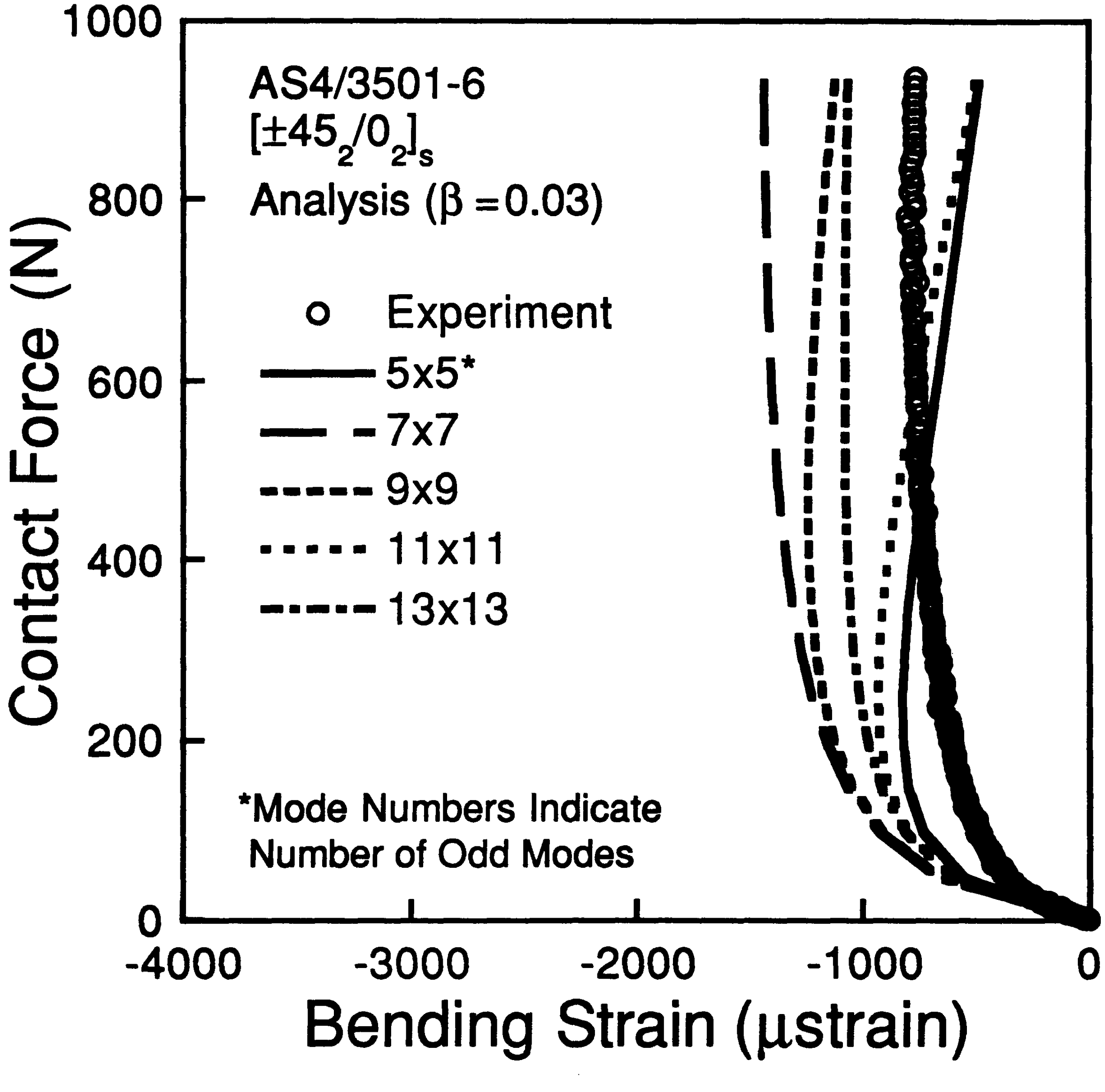

Figure B.18 Convergence of force-bending strain curves for gage 6 (strain gage scheme A) for an AS4/3501-6 [±45$_2$/0$_2$]$_s$ 254 mm span specimen indented to 930 N.

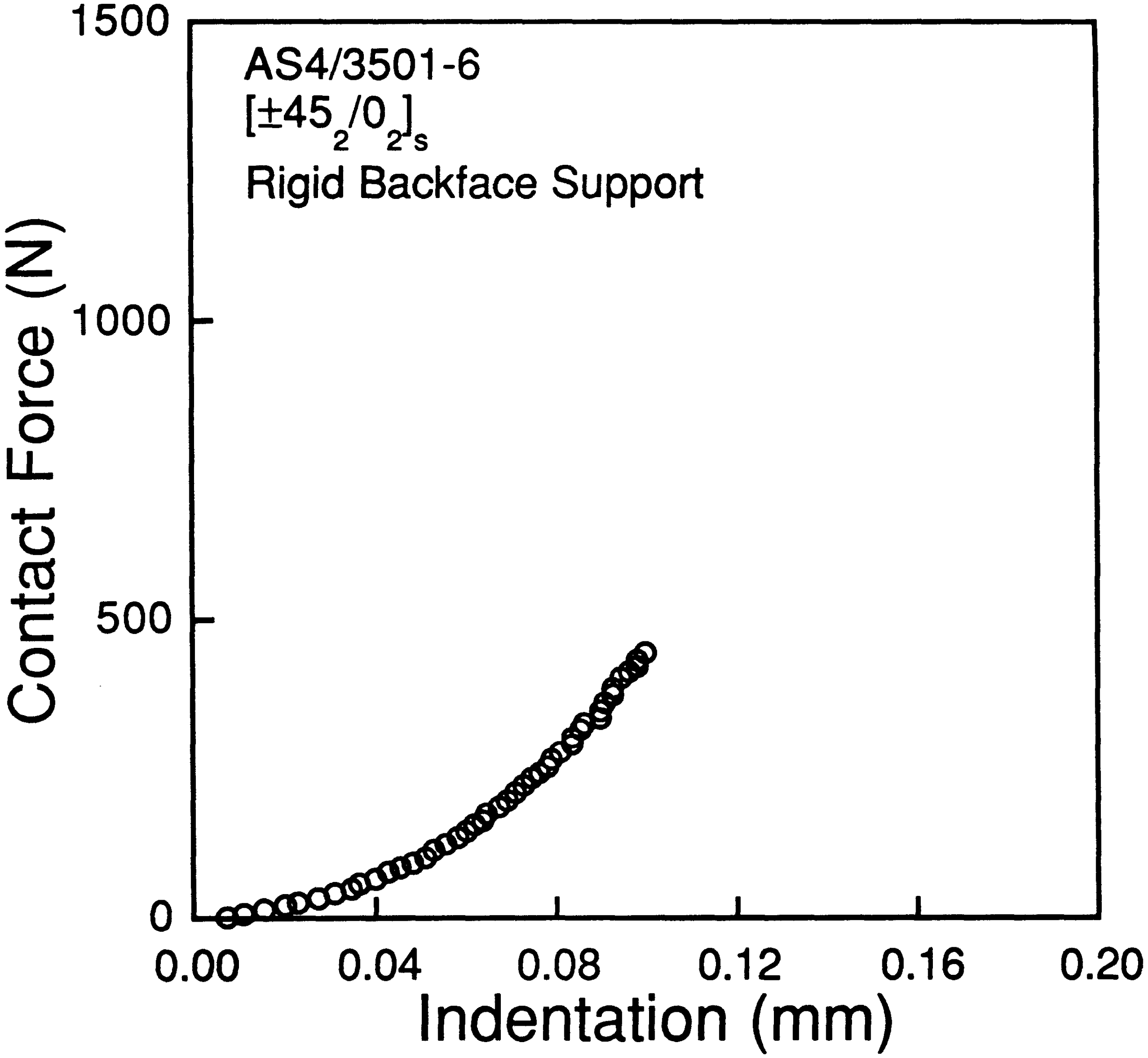

Figure B.19 Force-indentation data for the specimen with a rigid backface support and loaded to a maximum contact force of 444 N.

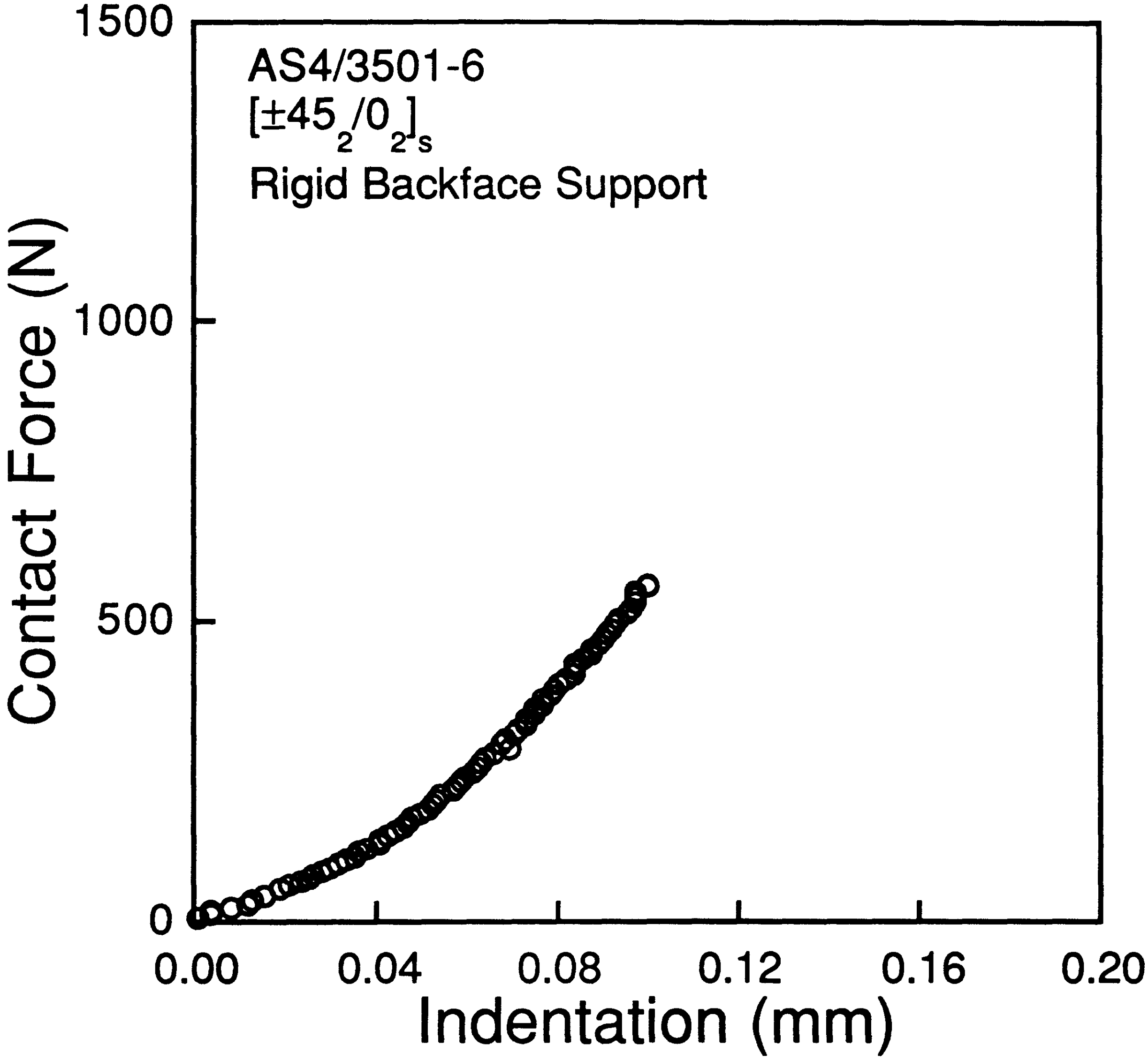

Figure B.20 Force-indentation data for the specimen with a rigid backface support and loaded to a maximum contact force of 549 N.

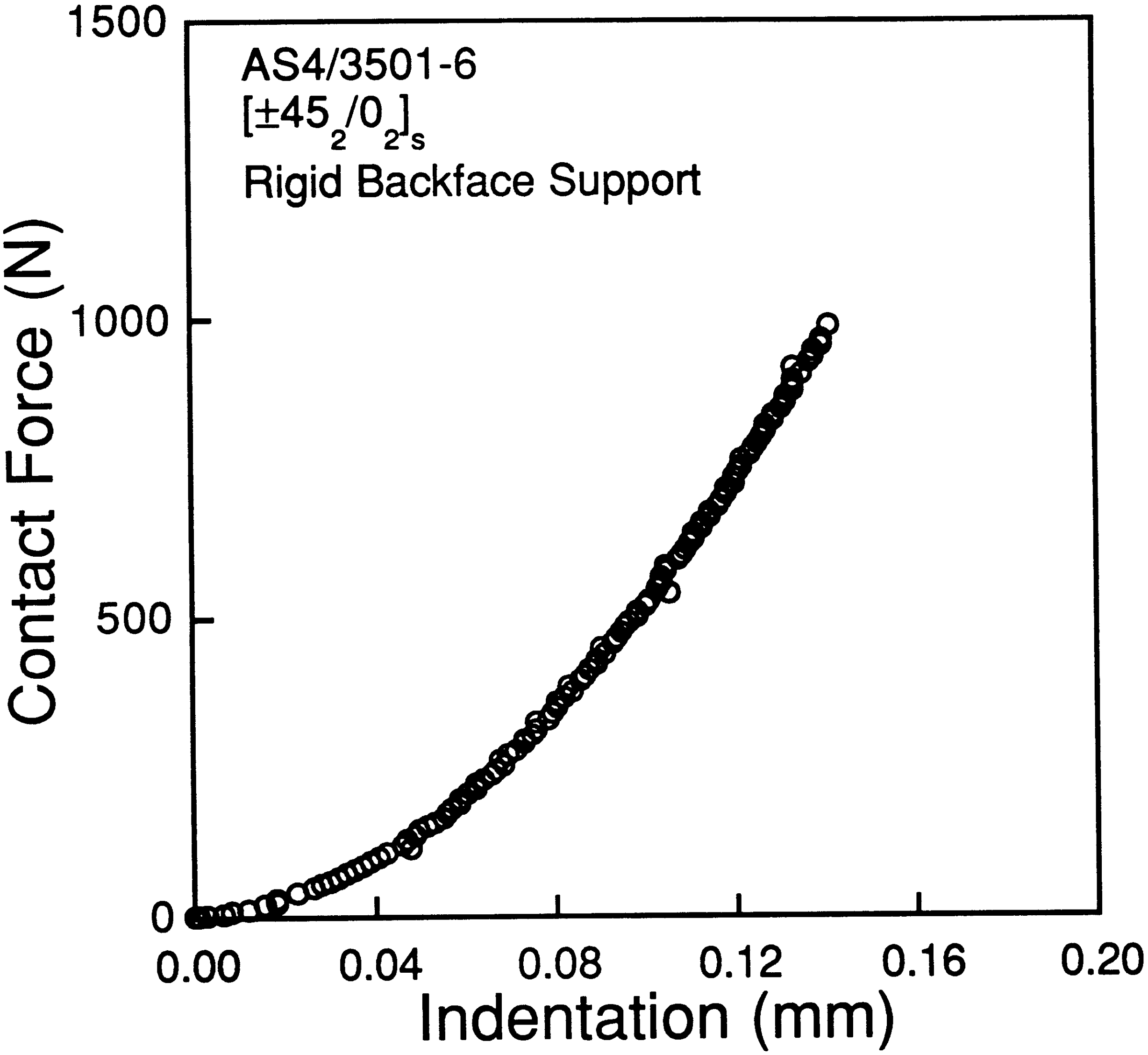

Figure B.21 Force-indentation data for the specimen with a rigid backface support and loaded to a maximum contact force of 930 N.

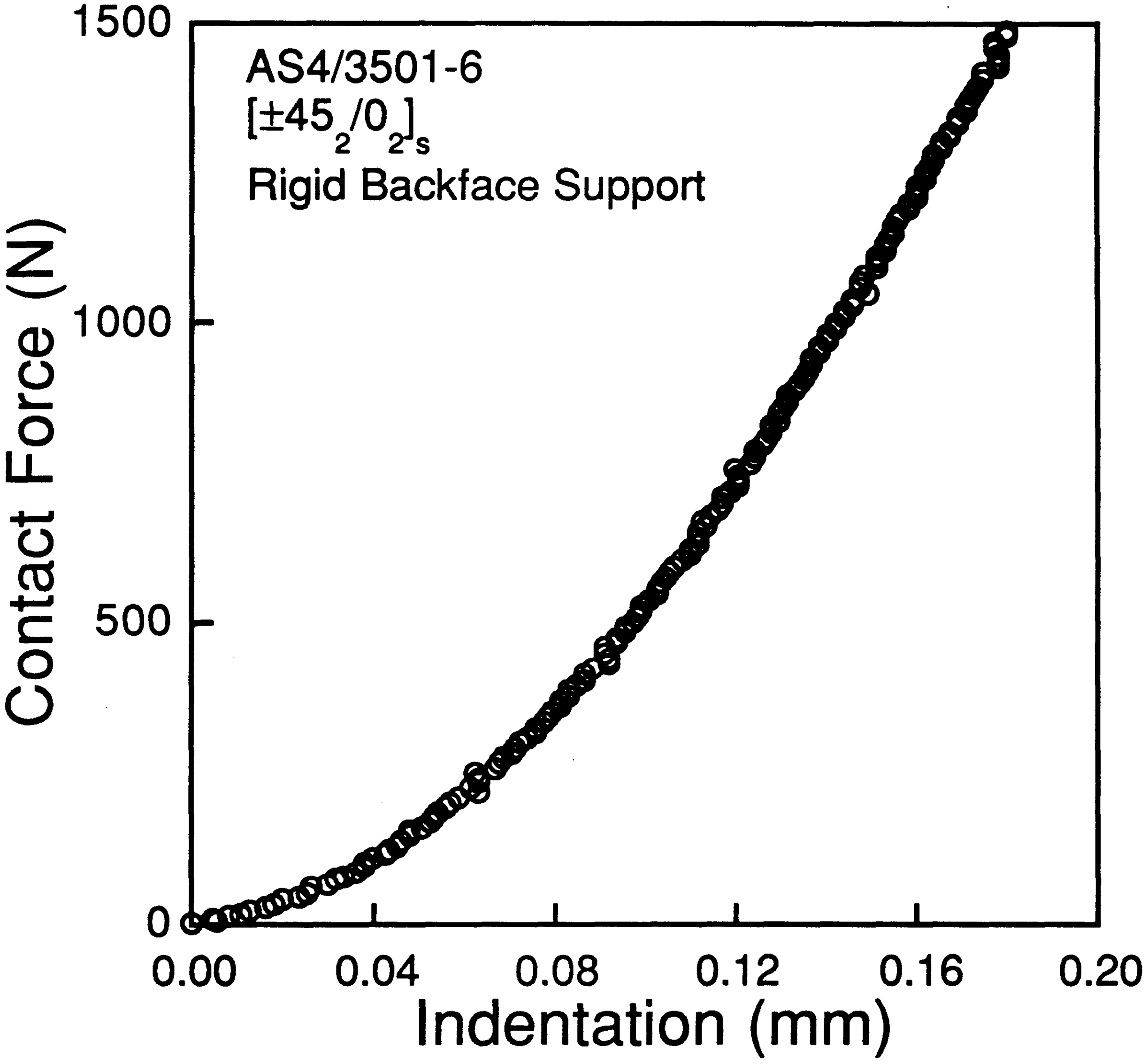

Figure B.22 Force-indentation data for the specimen with a rigid backface support and loaded to a maximum contact force of 1479 N.

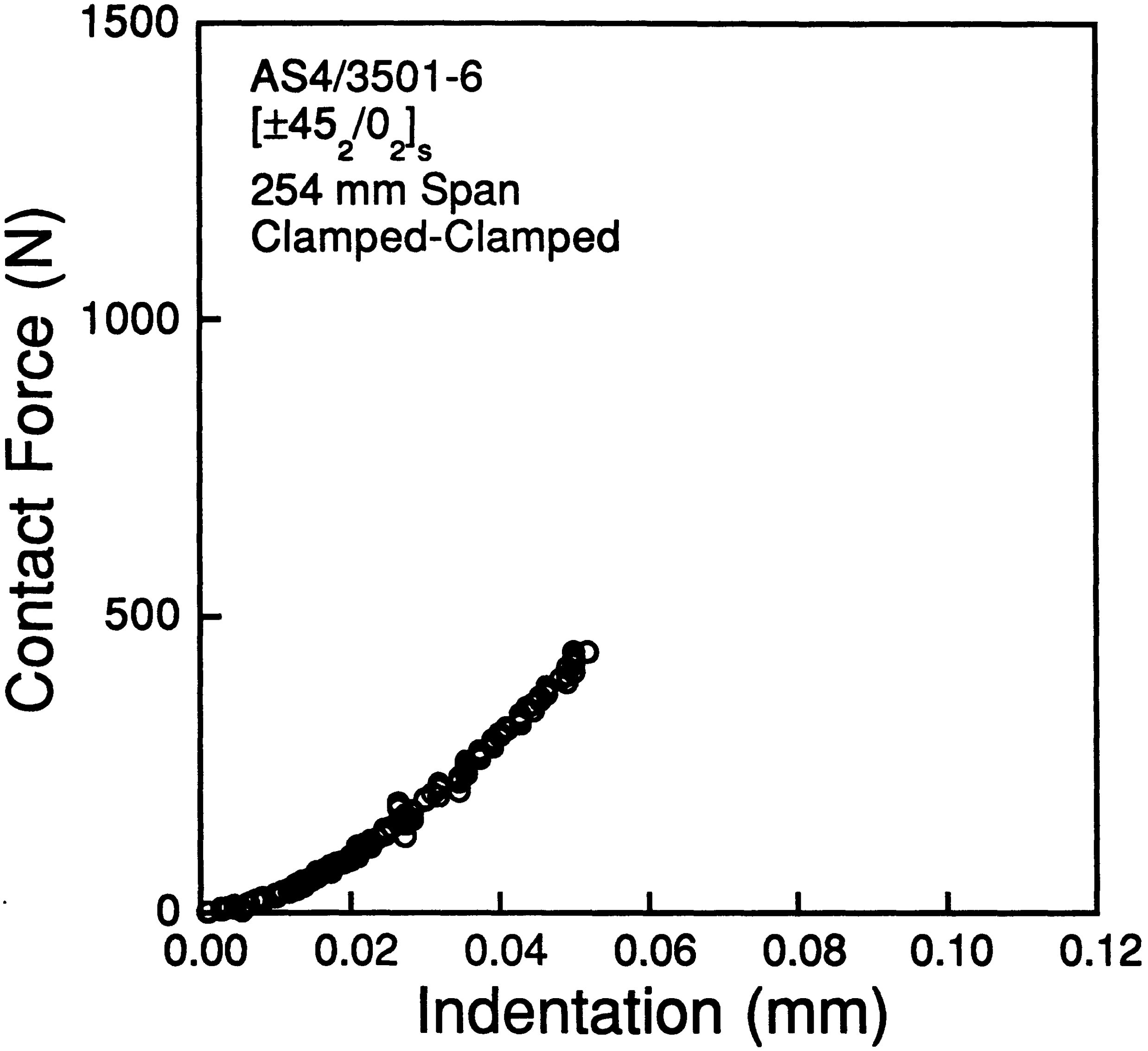

Figure B.23 Force-indentation data for the specimen with a 254 mm span tested with a clamped-clamped support and loaded to a maximum contact force of 444 N.

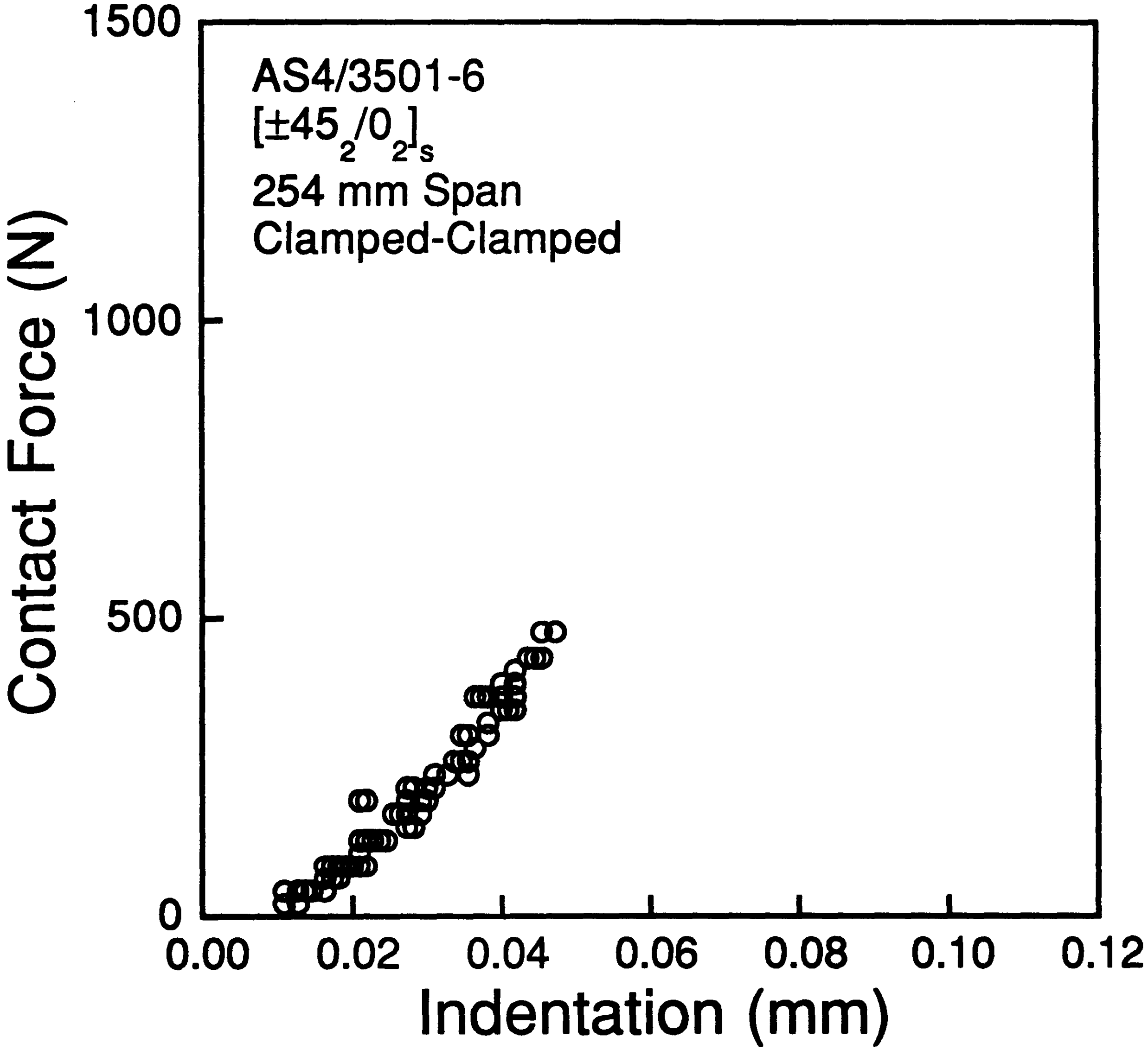

Figure B.24 Force-indentation data for the specimen with a 254 mm span tested with a clamped-clamped support and loaded to a maximum contact force of 507 N.

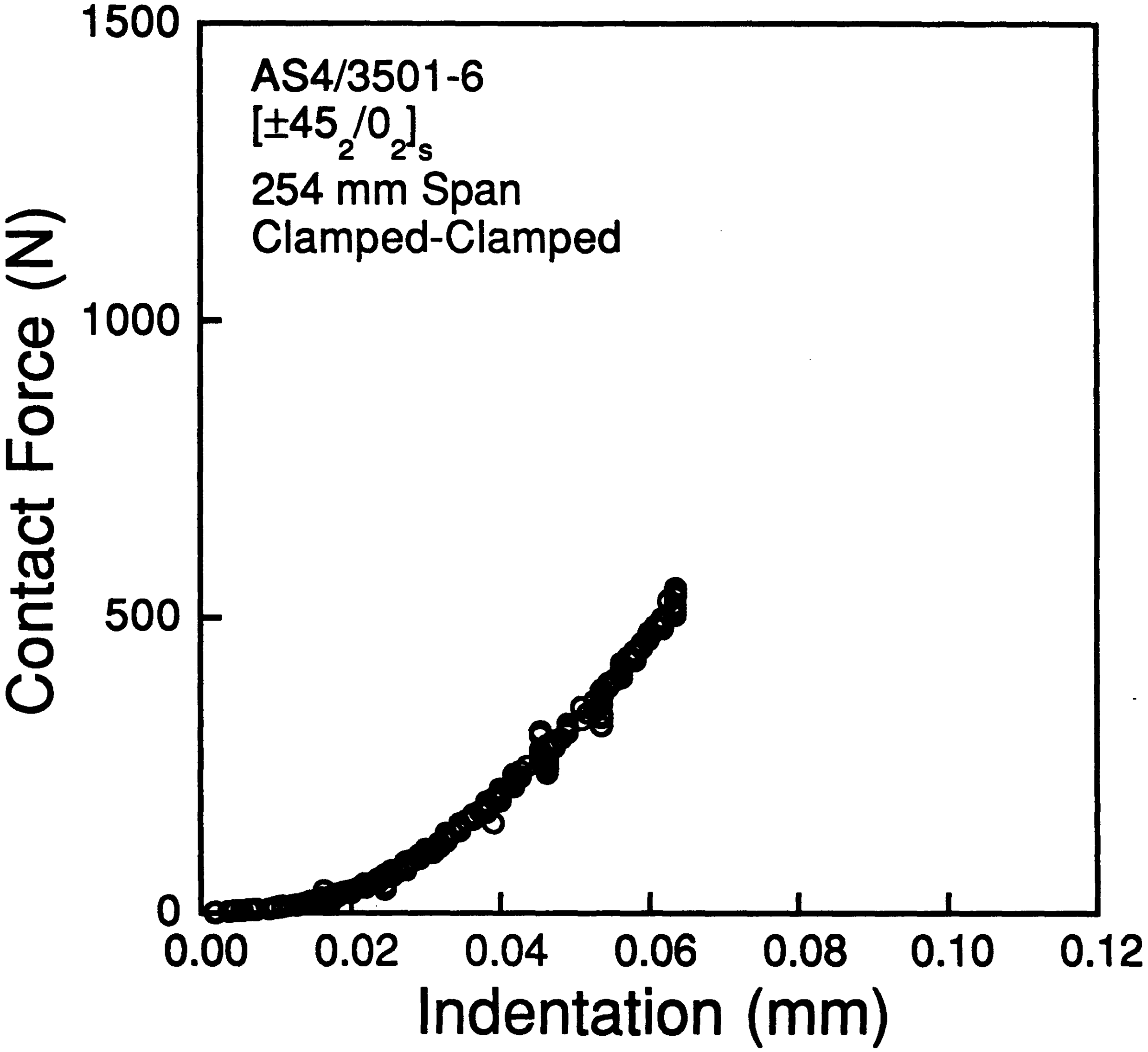

Figure B.25 Force-indentation data for the specimen with a 254 mm span tested with a clamped-clamped support and loaded to a maximum contact force of 549 N.

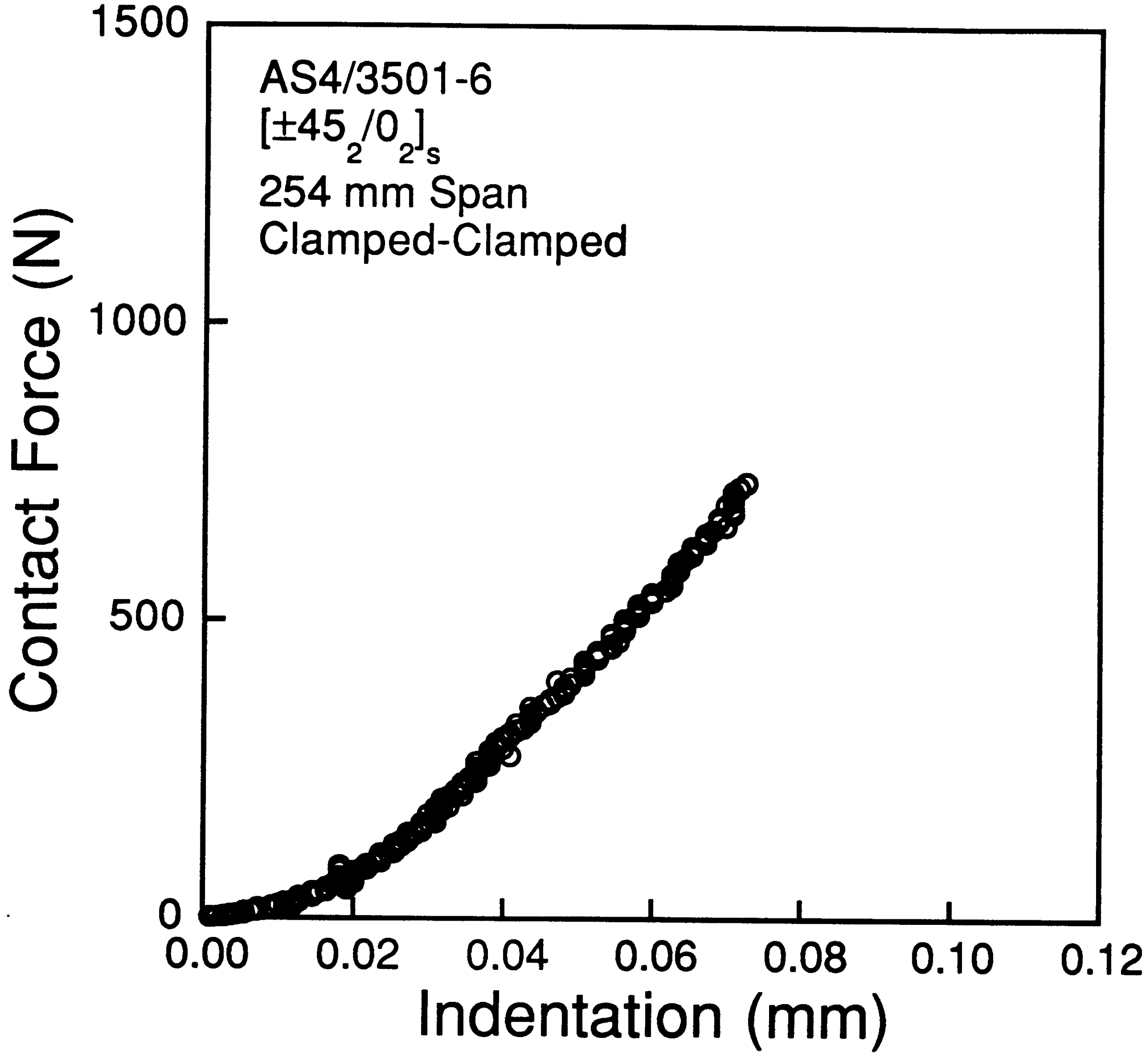

Figure B.26 Force-indentation data for the specimen with a 254 mm span tested with a clamped-clamped support and loaded to a maximum contact force of 739 N.

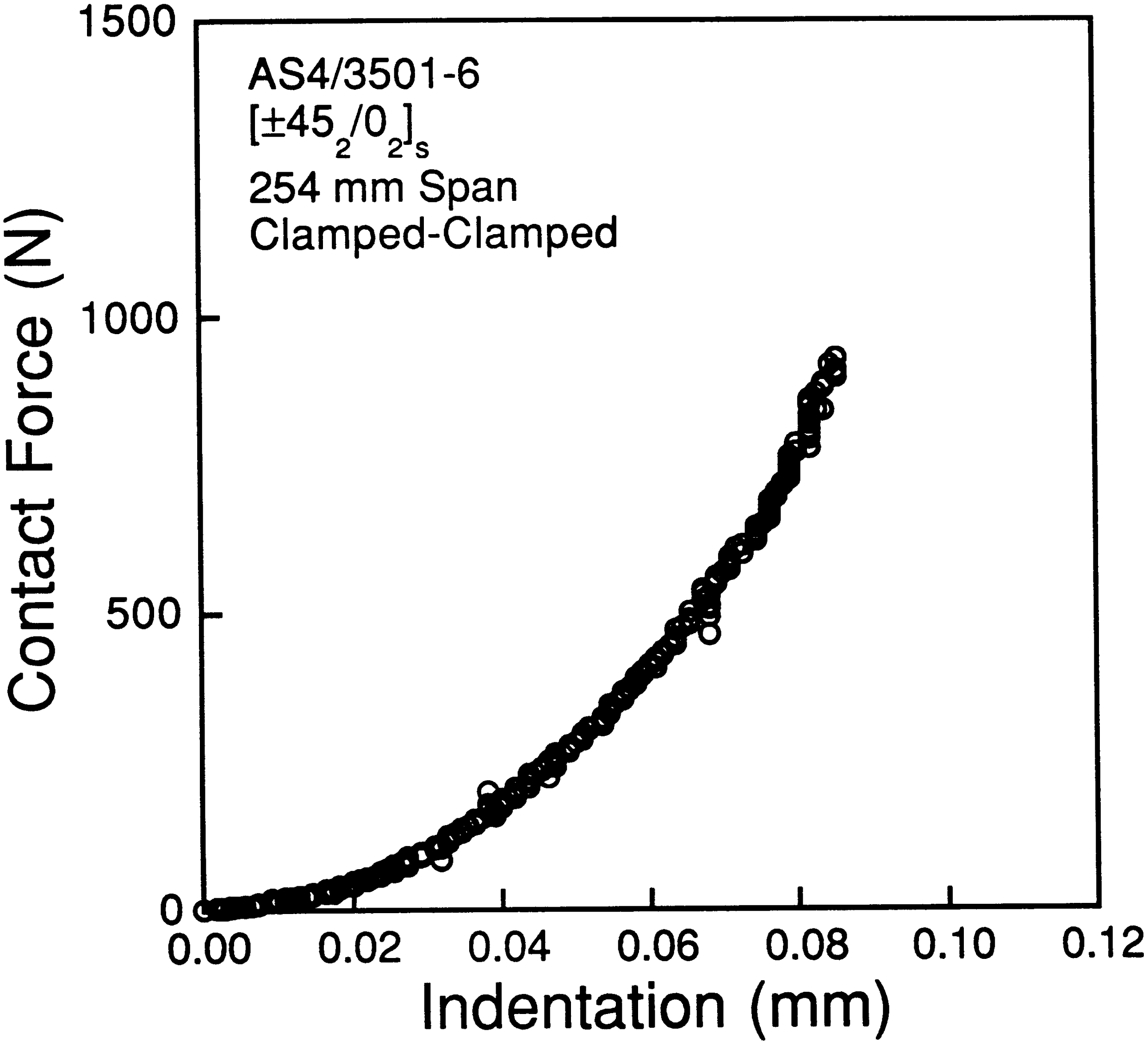

Figure B.27 Force-indentation data for the specimen with a 254 mm span tested with a clamped-clamped support and loaded to a maximum contact force of 930 N.

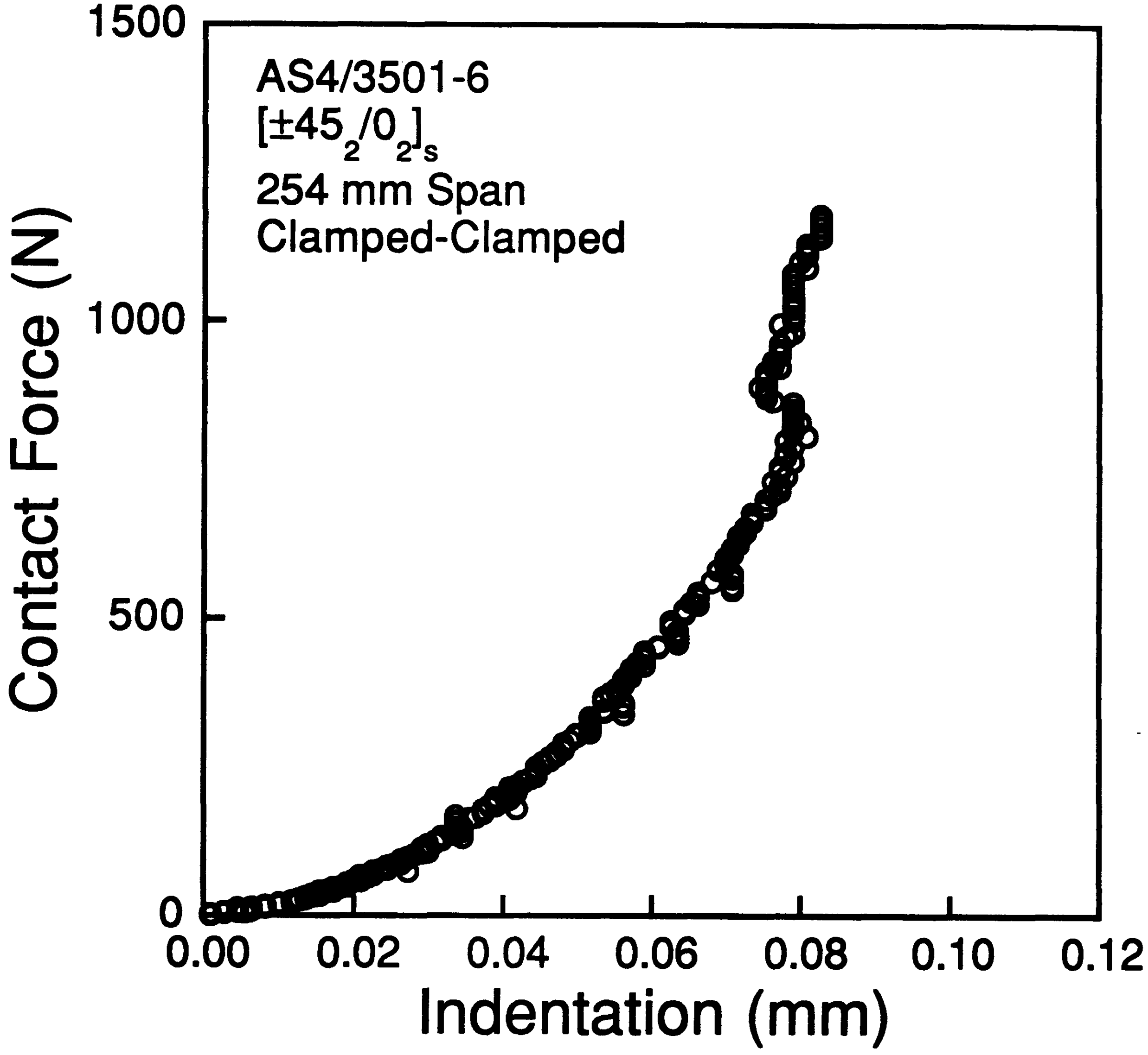

Figure B.28 Force-indentation data for the specimen with a 254 mm span tested with a clamped-clamped support and loaded to a maximum contact force of 1183 N.

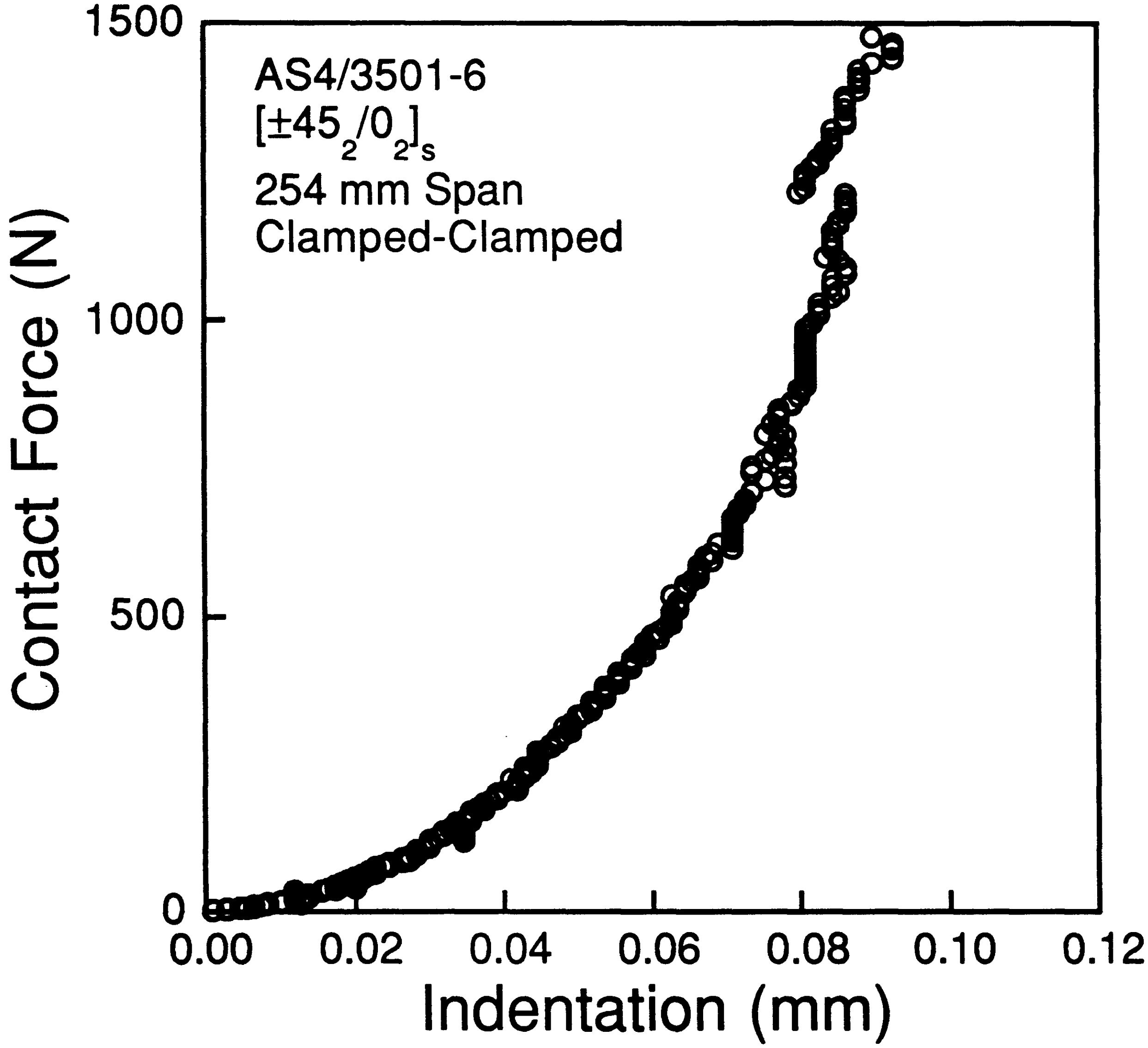

Figure B.29 Force-indentation data for the specimen with a 254 mm span tested with a clamped-clamped support and loaded to a maximum contact force of 1479 N.

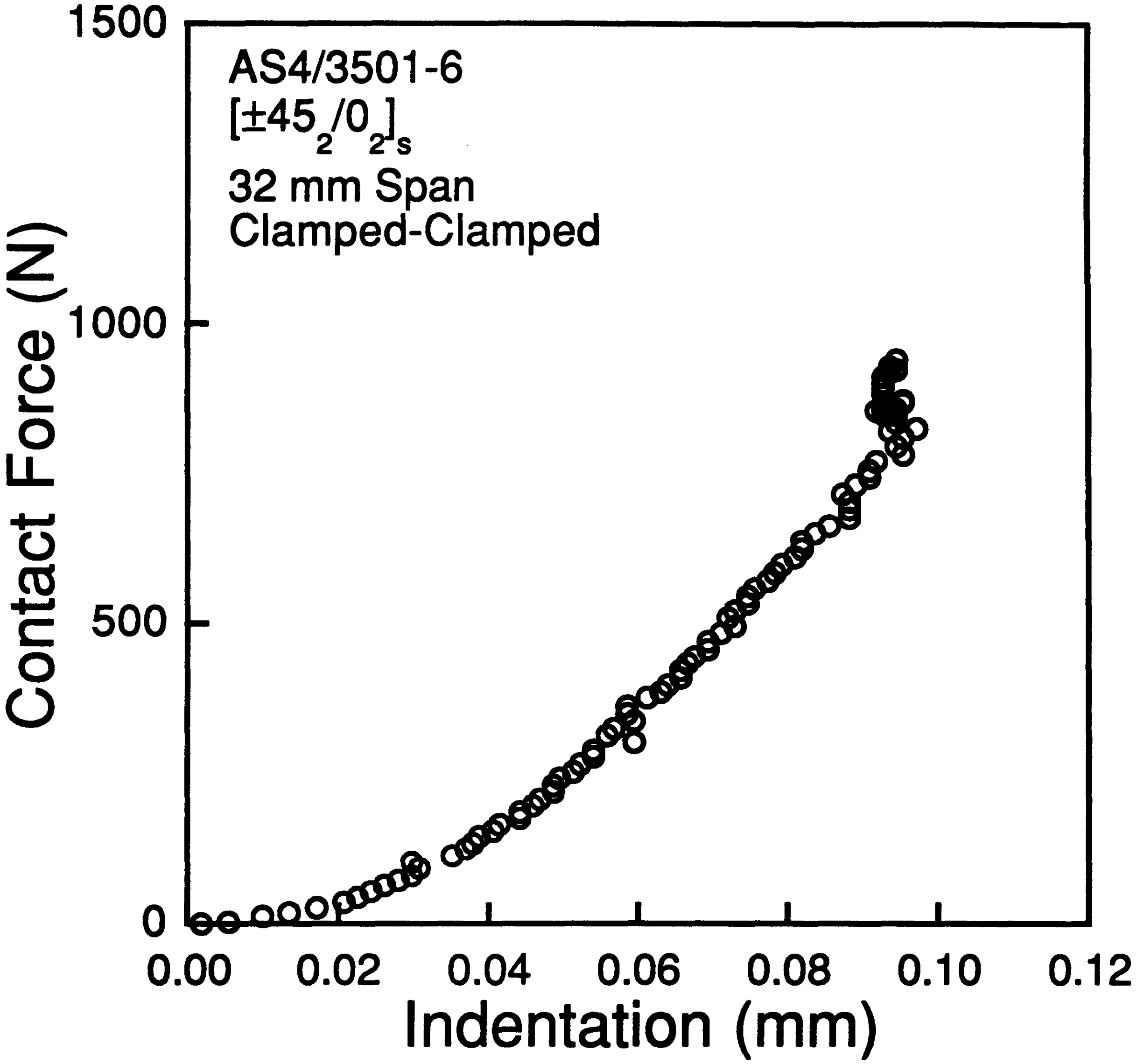

Figure B.30 Force-indentation data for the specimen with a 32 mm span tested with a clamped-clamped support and loaded to a maximum contact force of 930 N.

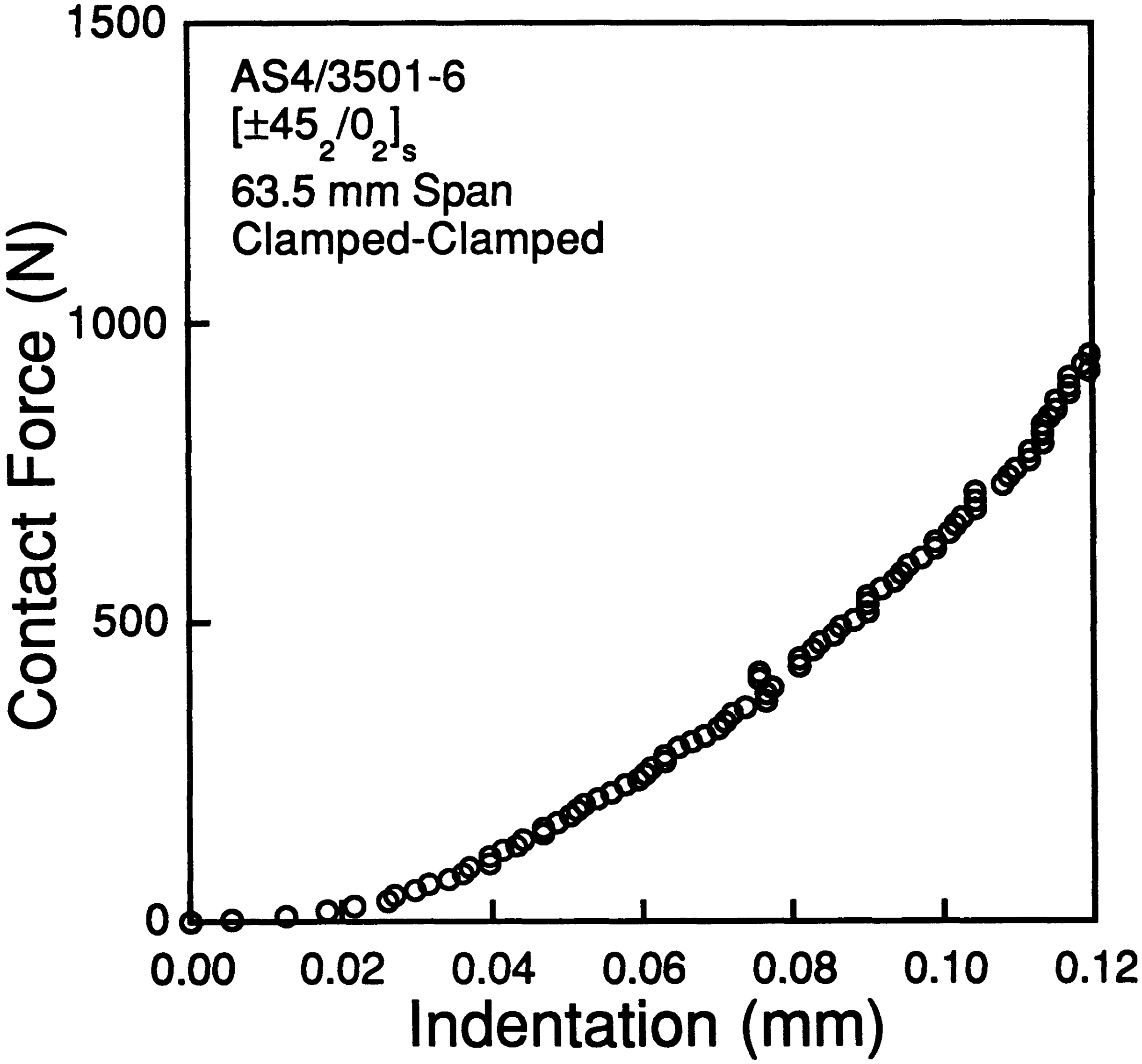

Figure B.31 Force-indentation data for the specimen with a 63.5 mm span tested with a clamped-clamped support and loaded to a maximum contact force of 930 N.

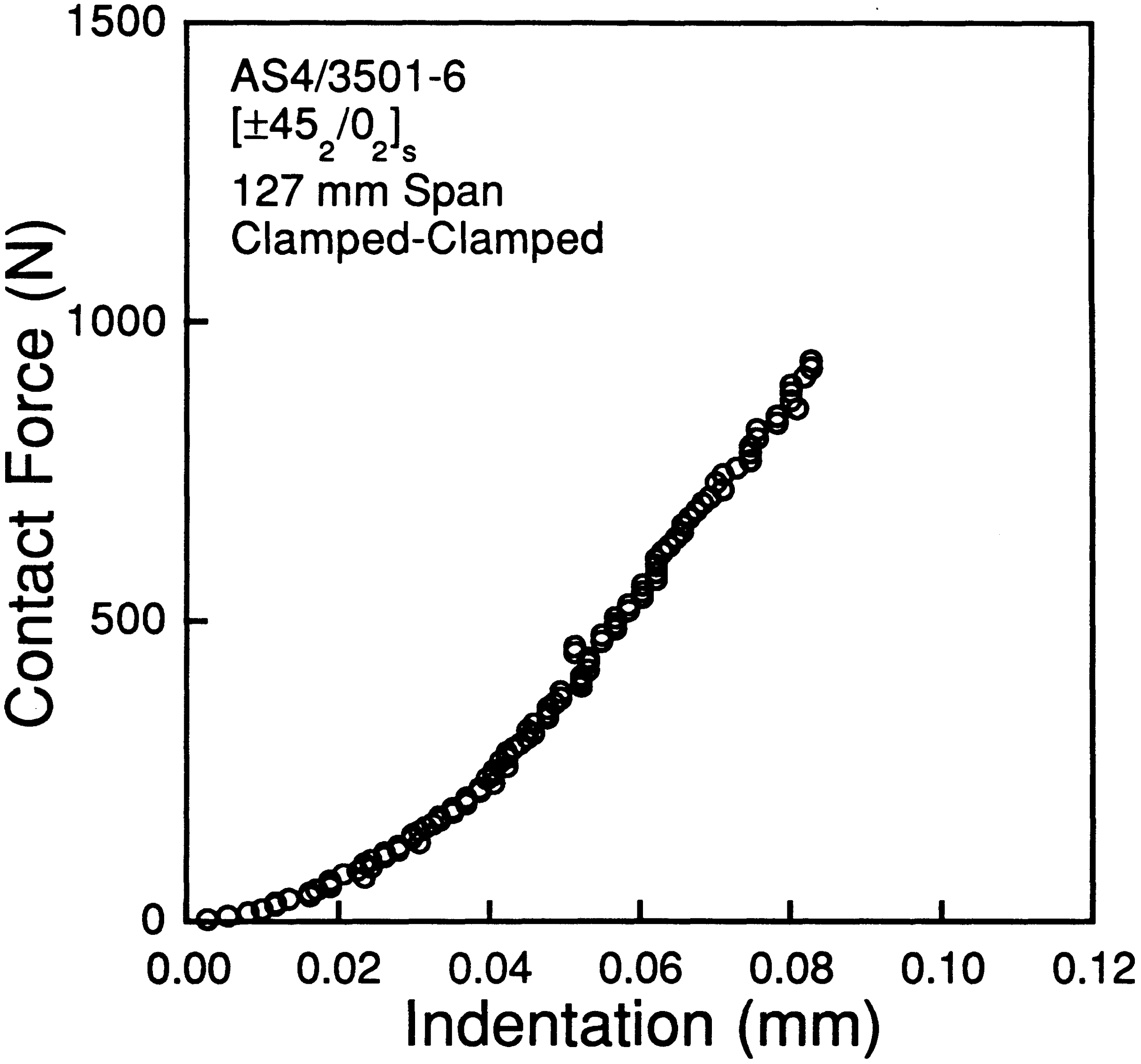

Figure B.32 Force-indentation data for the specimen with a 127 mm span tested with a clamped-clamped support and loaded to a maximum contact force of 930 N.

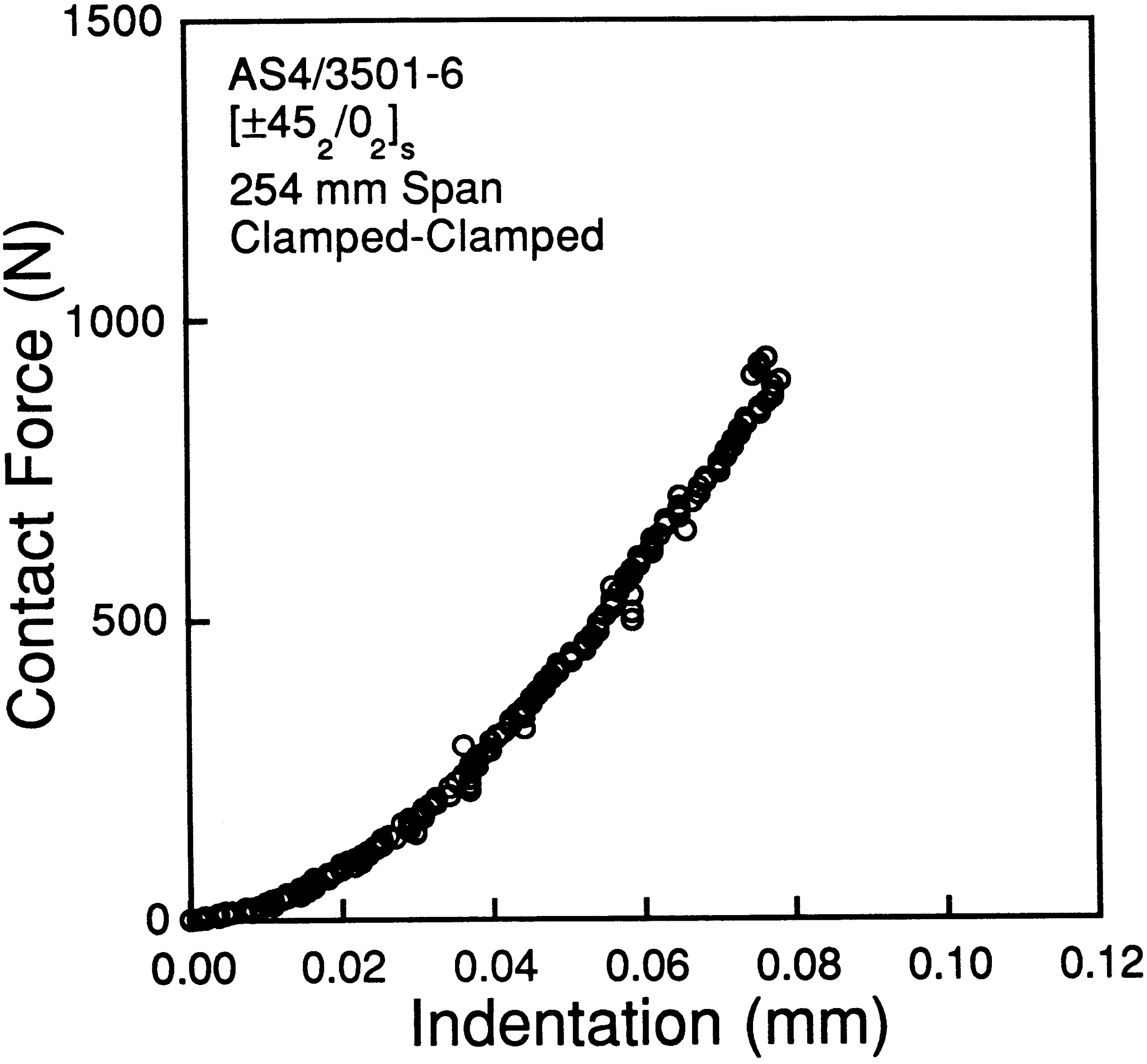

Figure B.33 Force-indentation data for the specimen with a 254 mm span tested with a clamped-clamped support and loaded to a maximum contact force of 930 N.

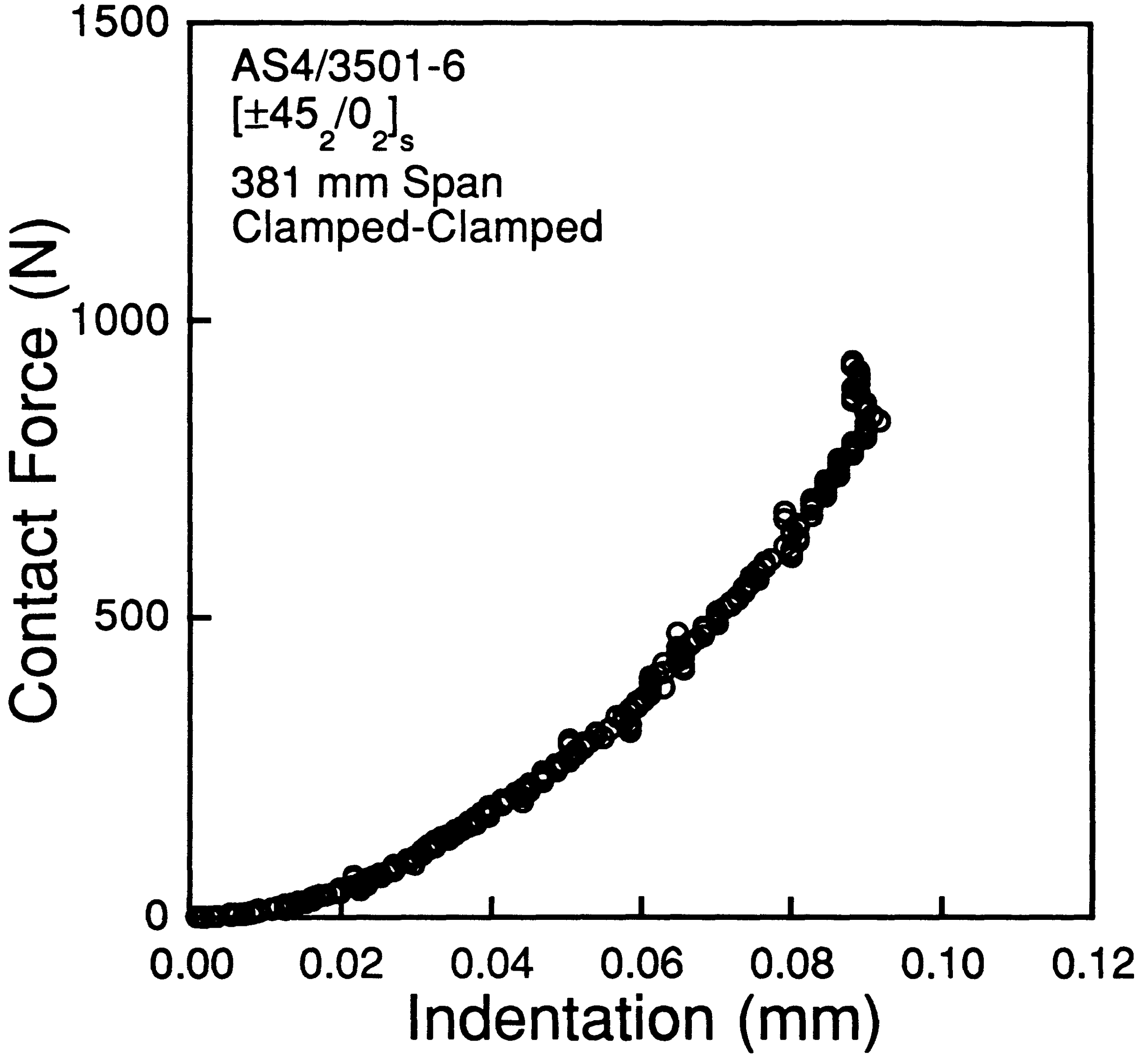

Figure B.34 Force-indentation data for the specimen with a 381 mm span tested with a clamped-clamped support and loaded to a maximum contact force of 930 N.

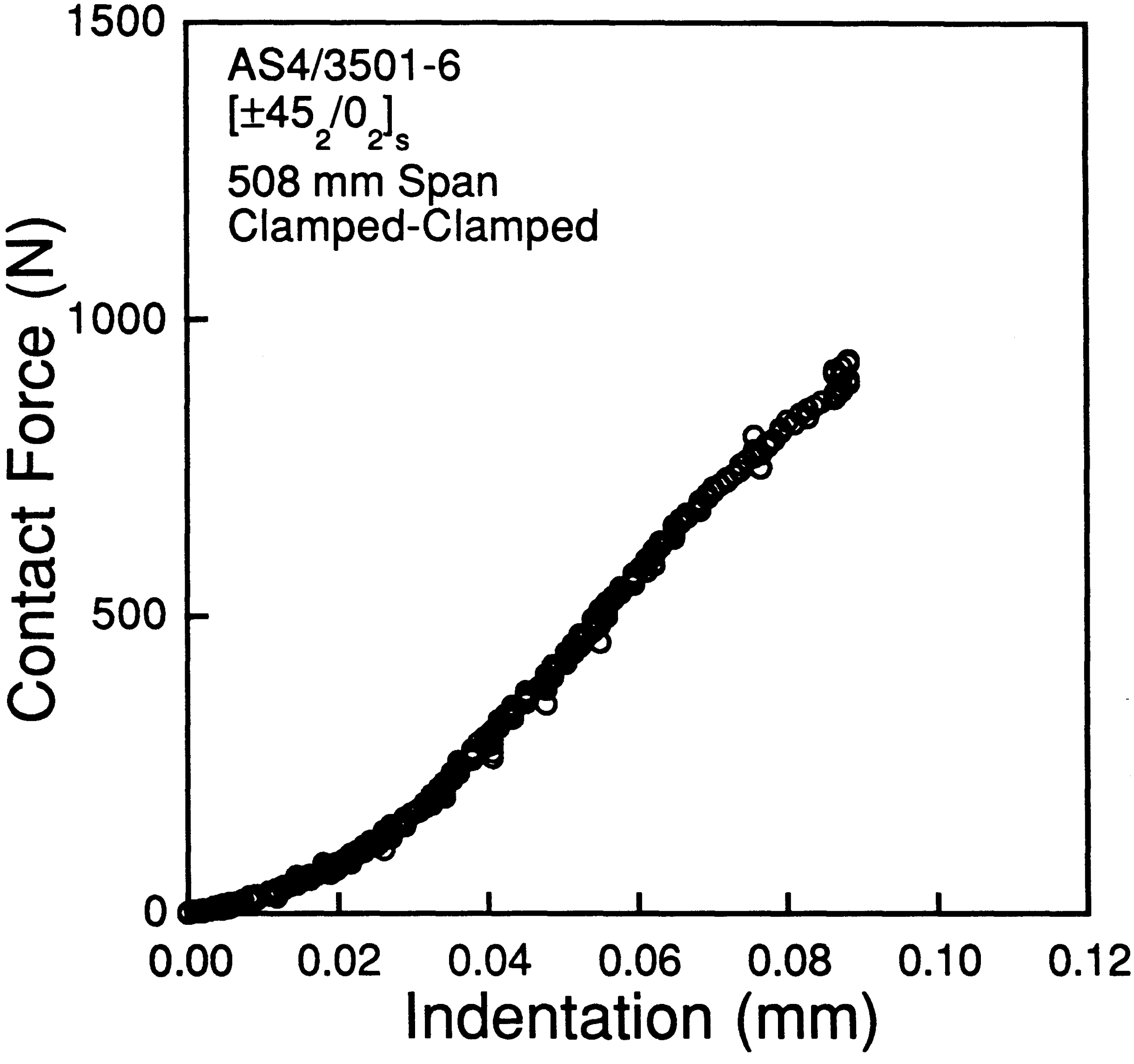

Figure B.35 Force-indentation data for the specimen with a 508 mm span tested with a clamped-clamped support and loaded to a maximum contact force of 930 N.

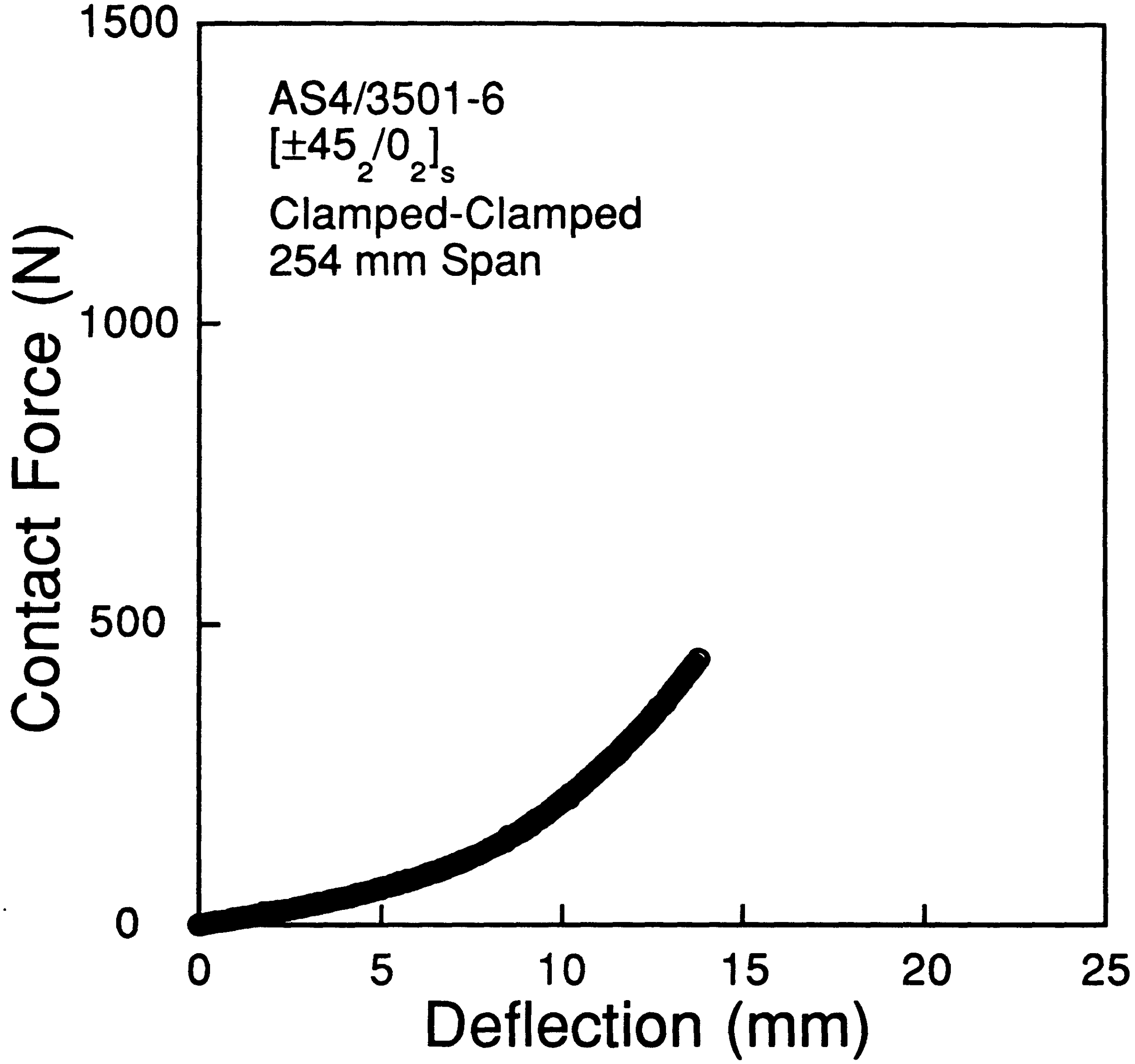

Figure B.36 Force-deflection data for a 254 mm specimen loaded to a maximum contact force of 444 N using a clamped-clamped boundary condition.

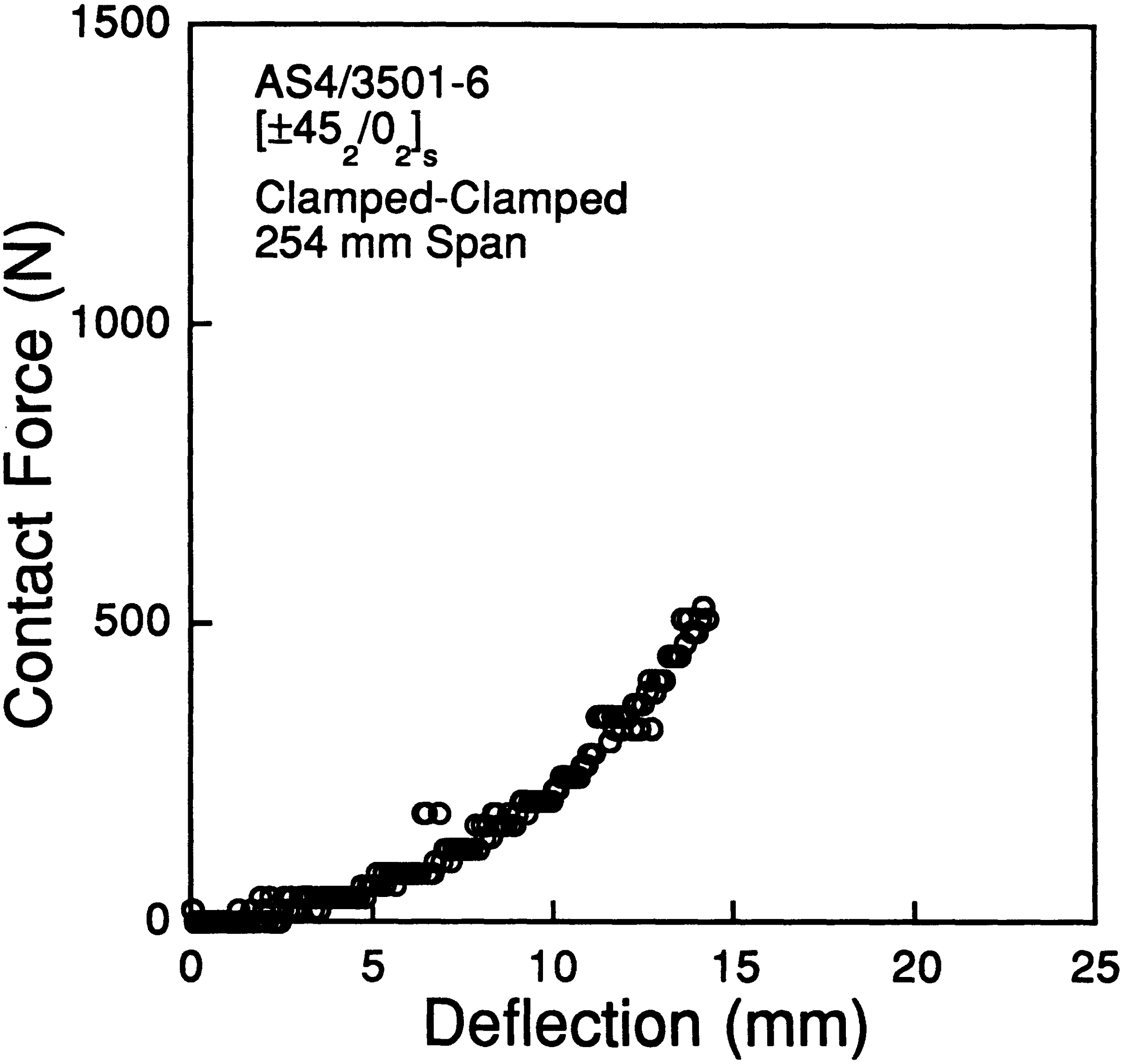

Figure B.37 Force-deflection data for a 254 mm specimen loaded to a maximum contact force of 507 N using a clamped-clamped boundary condition.

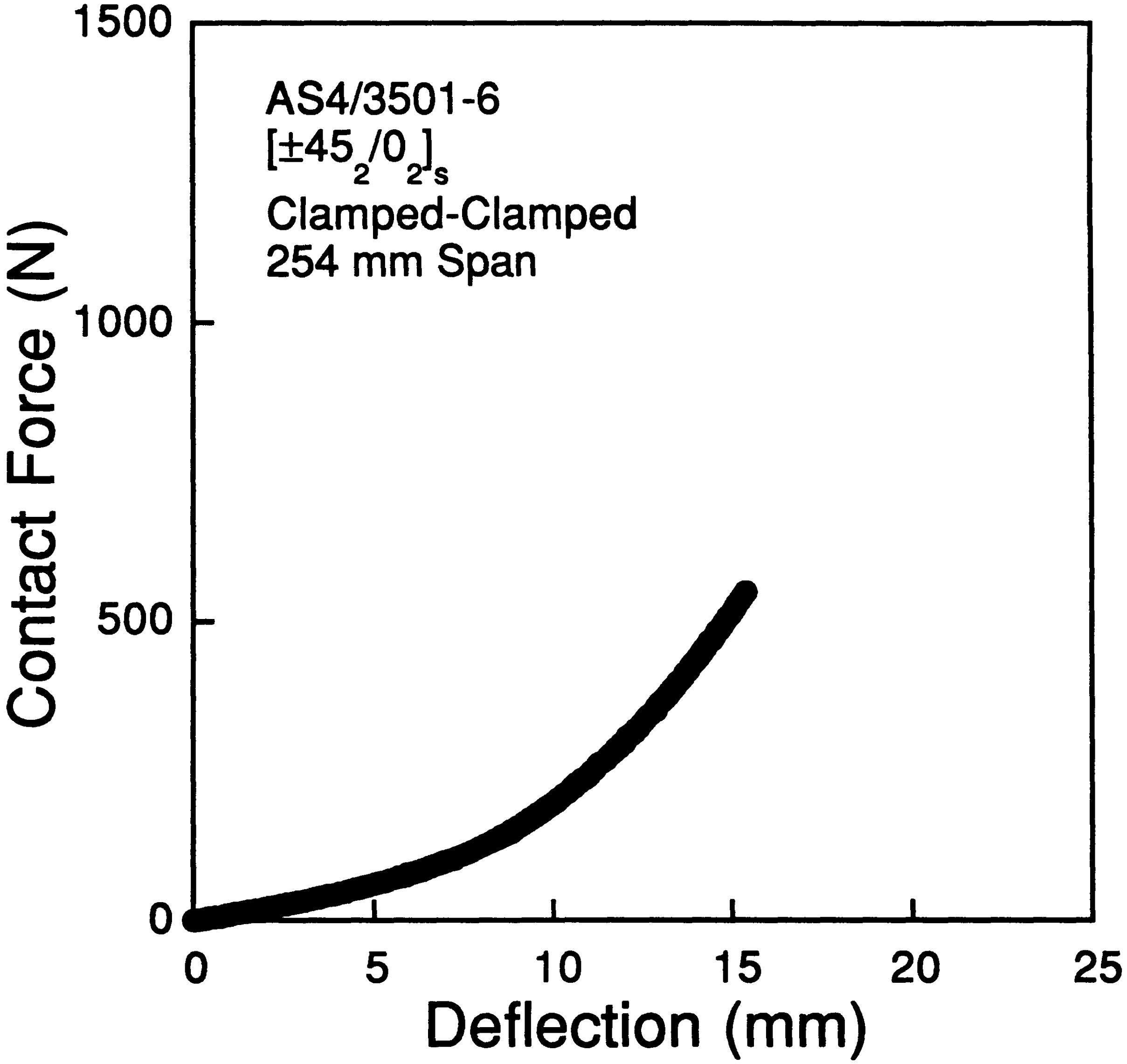

Figure B.38 Force-deflection data for a 254 mm specimen loaded to a maximum contact force of 549 N using a clamped-clamped boundary condition.

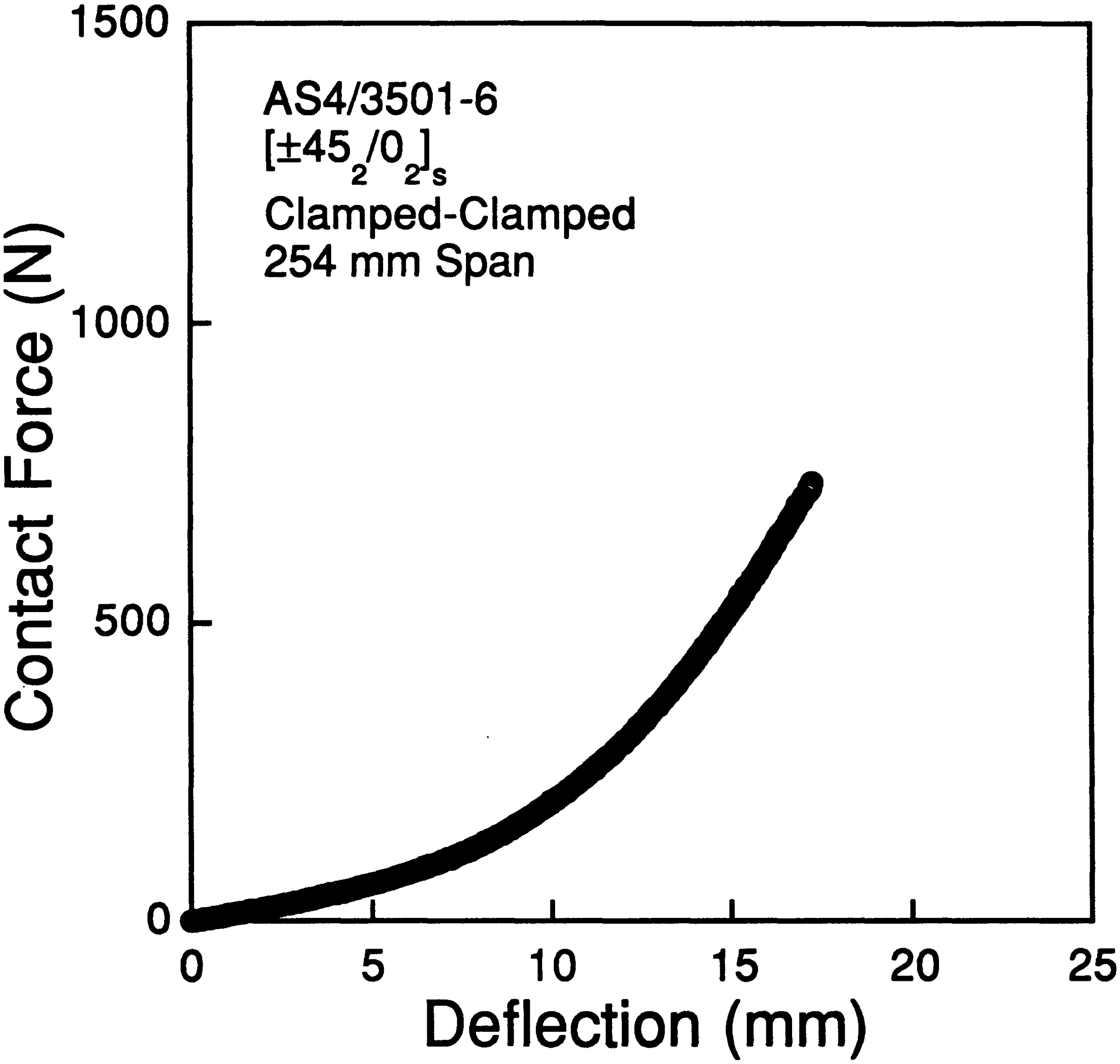

Figure B.39 Force-deflection data for a 254 mm specimen loaded to a maximum contact force of 739 N using a clamped-clamped boundary condition.

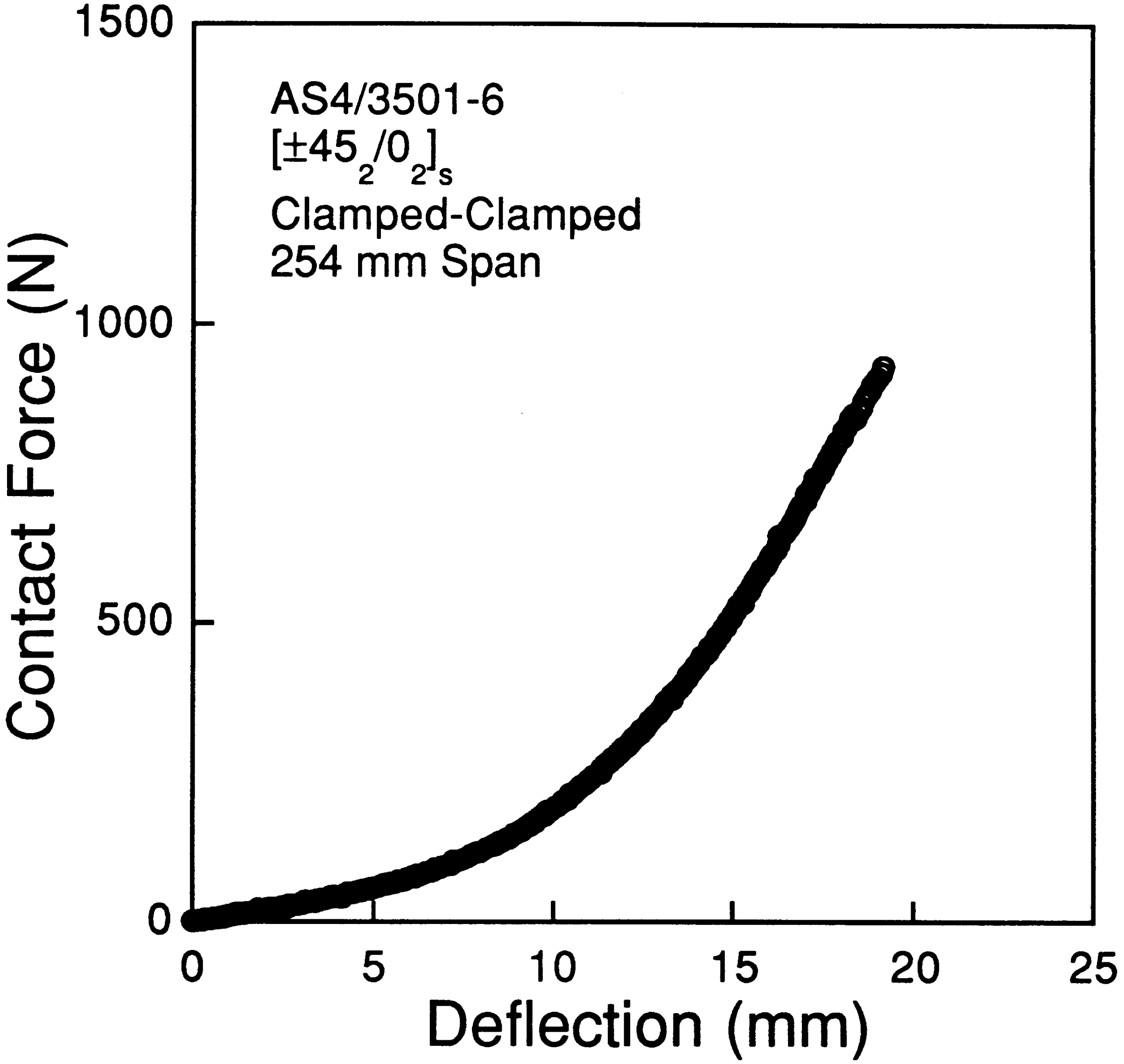

Figure B.40 Force-deflection data for a 254 mm specimen loaded to a maximum contact force of 930 N using a clamped-clamped boundary condition.

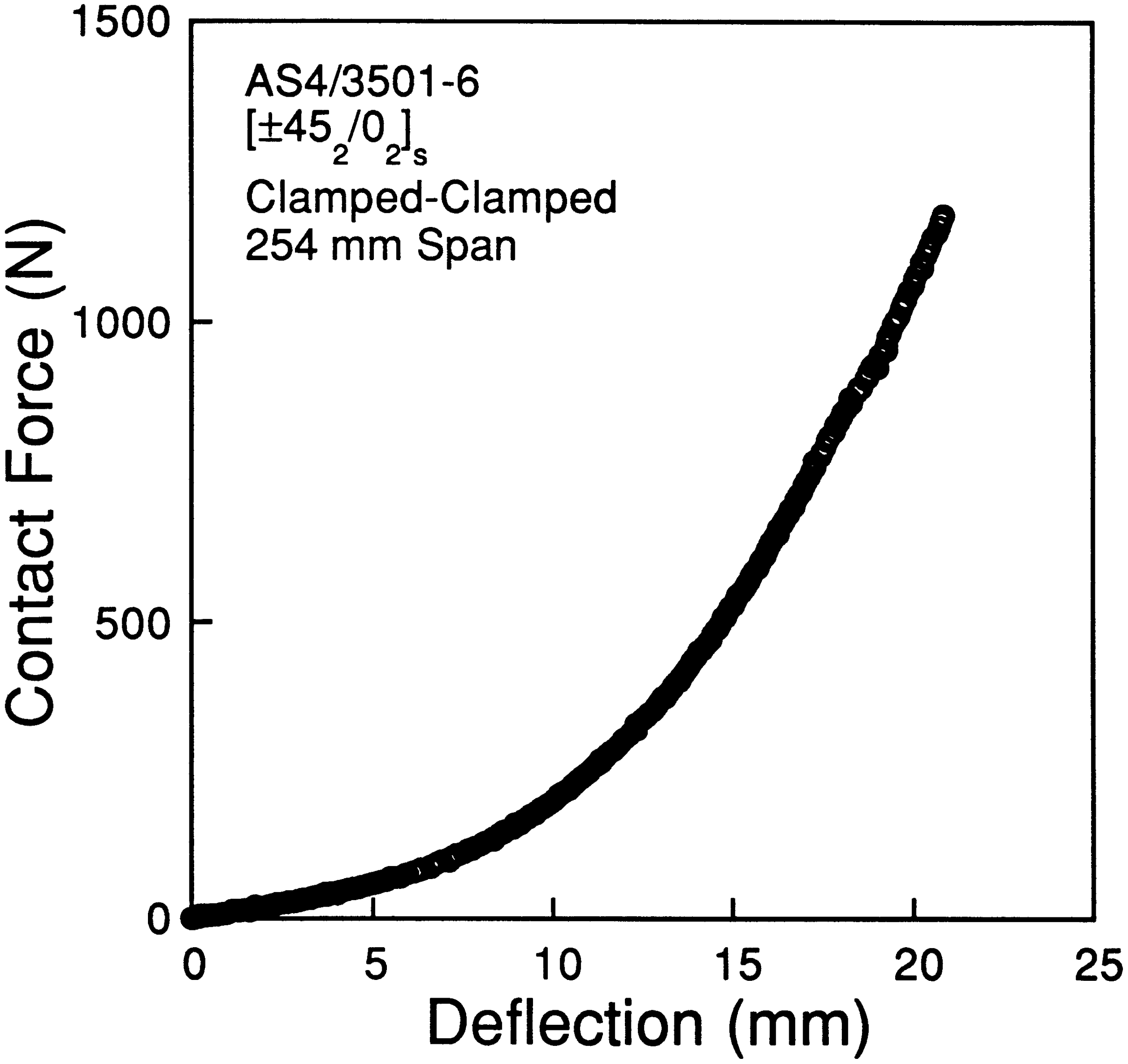

Figure B.41 Force-deflection data for a 254 mm specimen loaded to a maximum contact force of 1183 N using a clamped-clamped boundary condition.

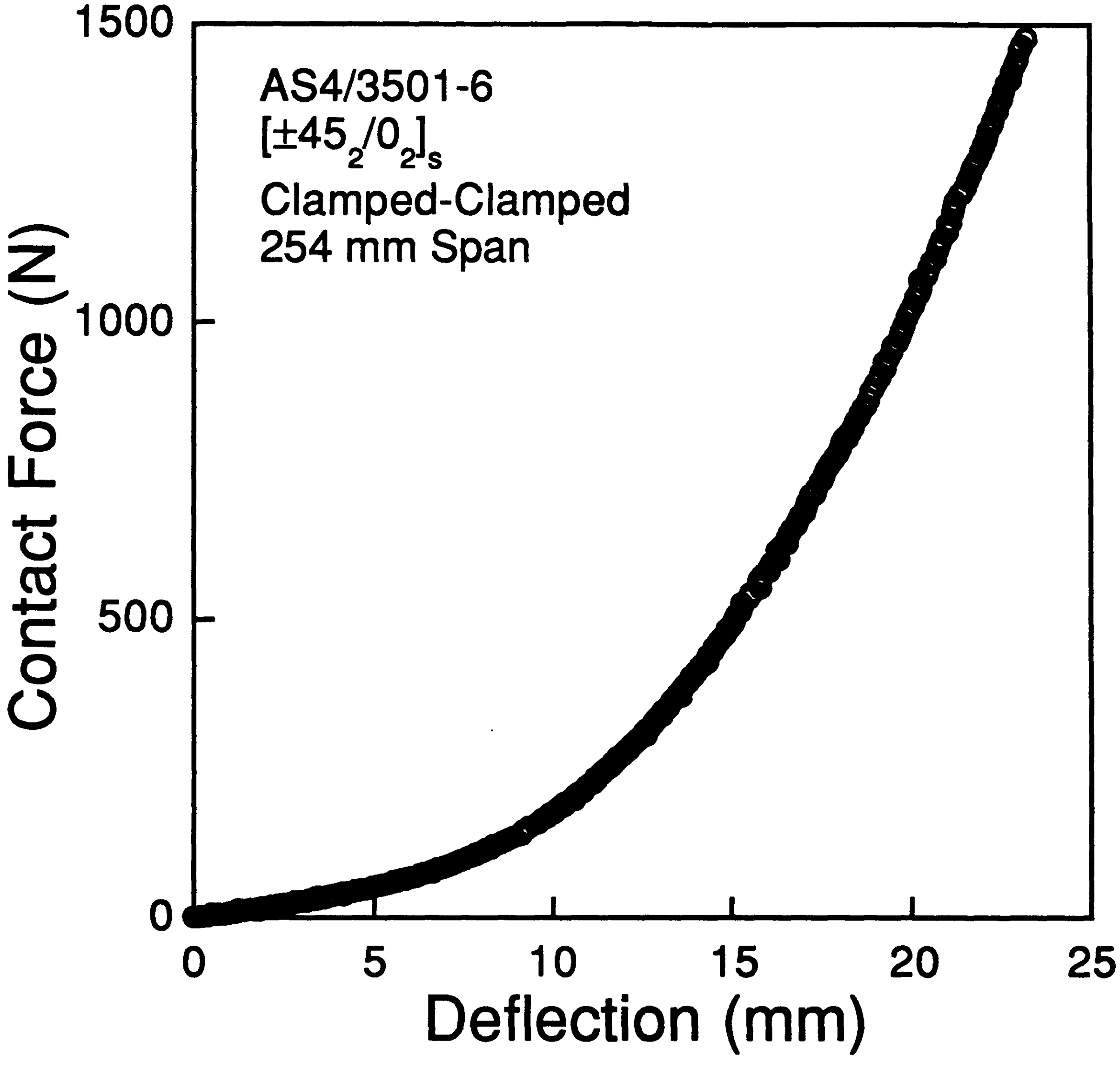

Figure B.42 Force-deflection data for a 254 mm specimen loaded to a maximum contact force of 1479 N using a clamped-clamped boundary condition.

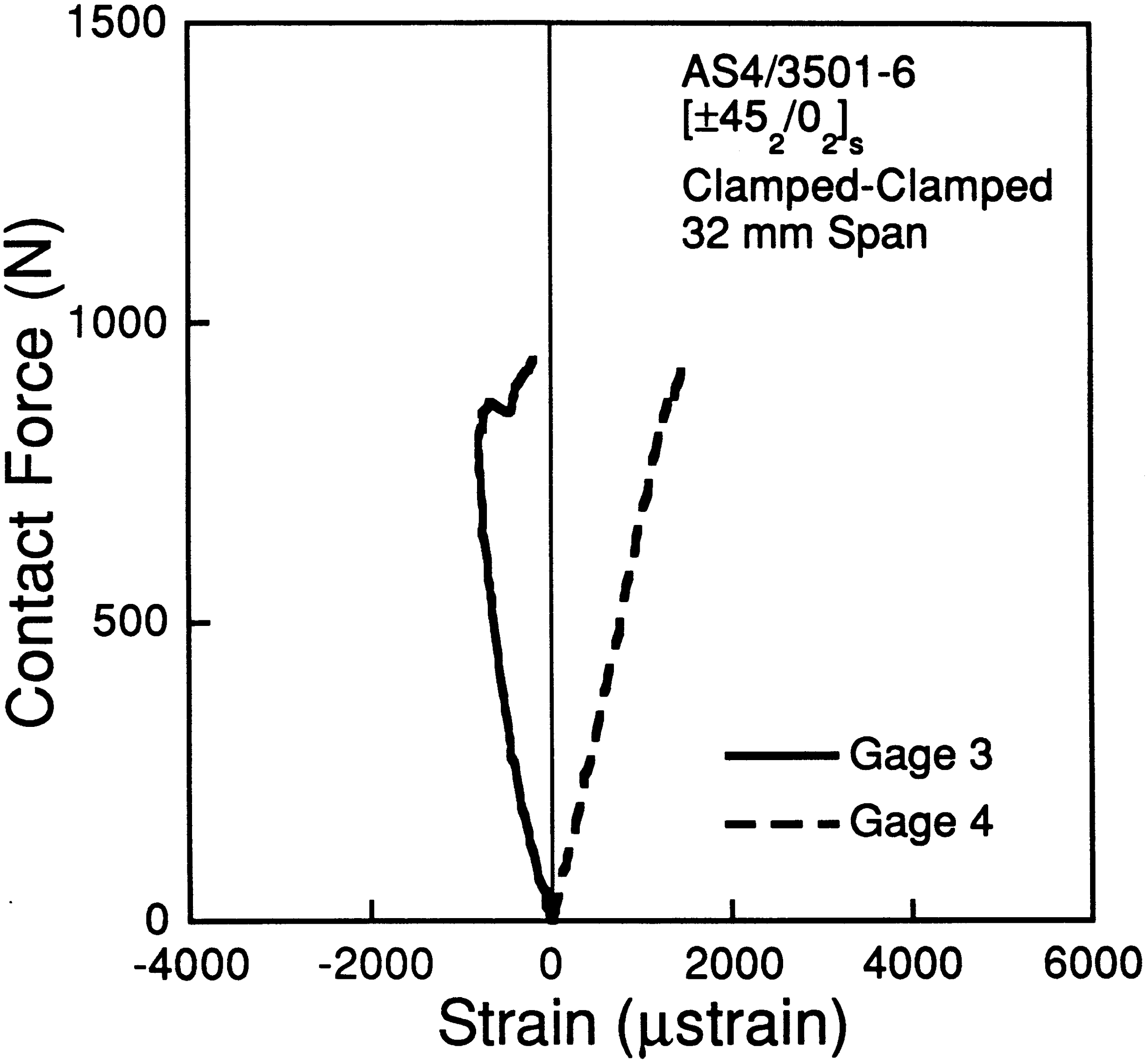

Figure B.43 Force-strain data from gages 3 and 4 (see Figure 3.2) for the specimen with a 32 mm span in a clamped-clamped support and tested to a maximum contact force of 930 N.

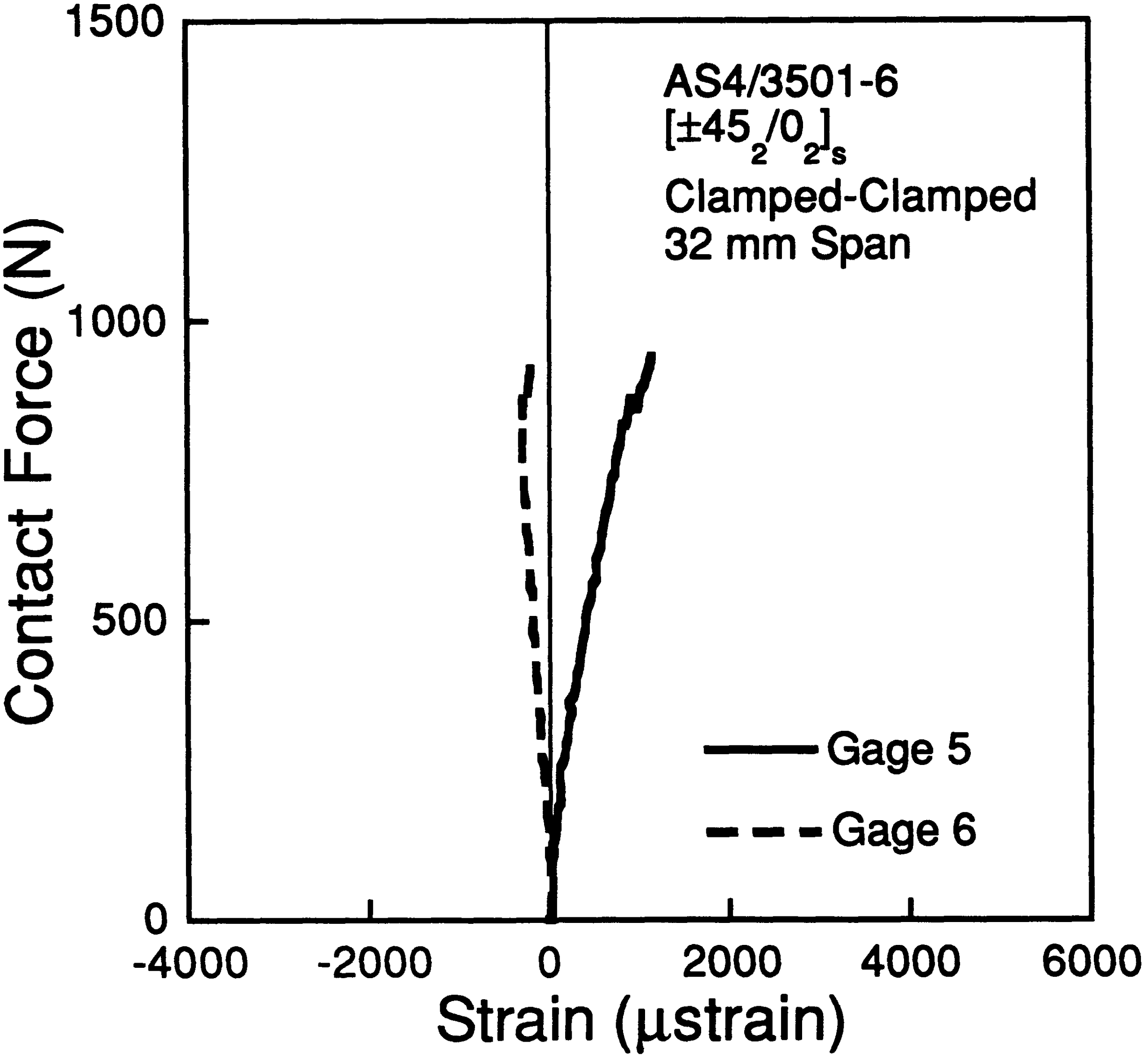

Figure B.44 Force-strain data from gages 5 and 6 (see Figure 3.2) for the specimen with a 32 mm span in a clamped-clamped support and tested to a maximum contact force of 930 N.

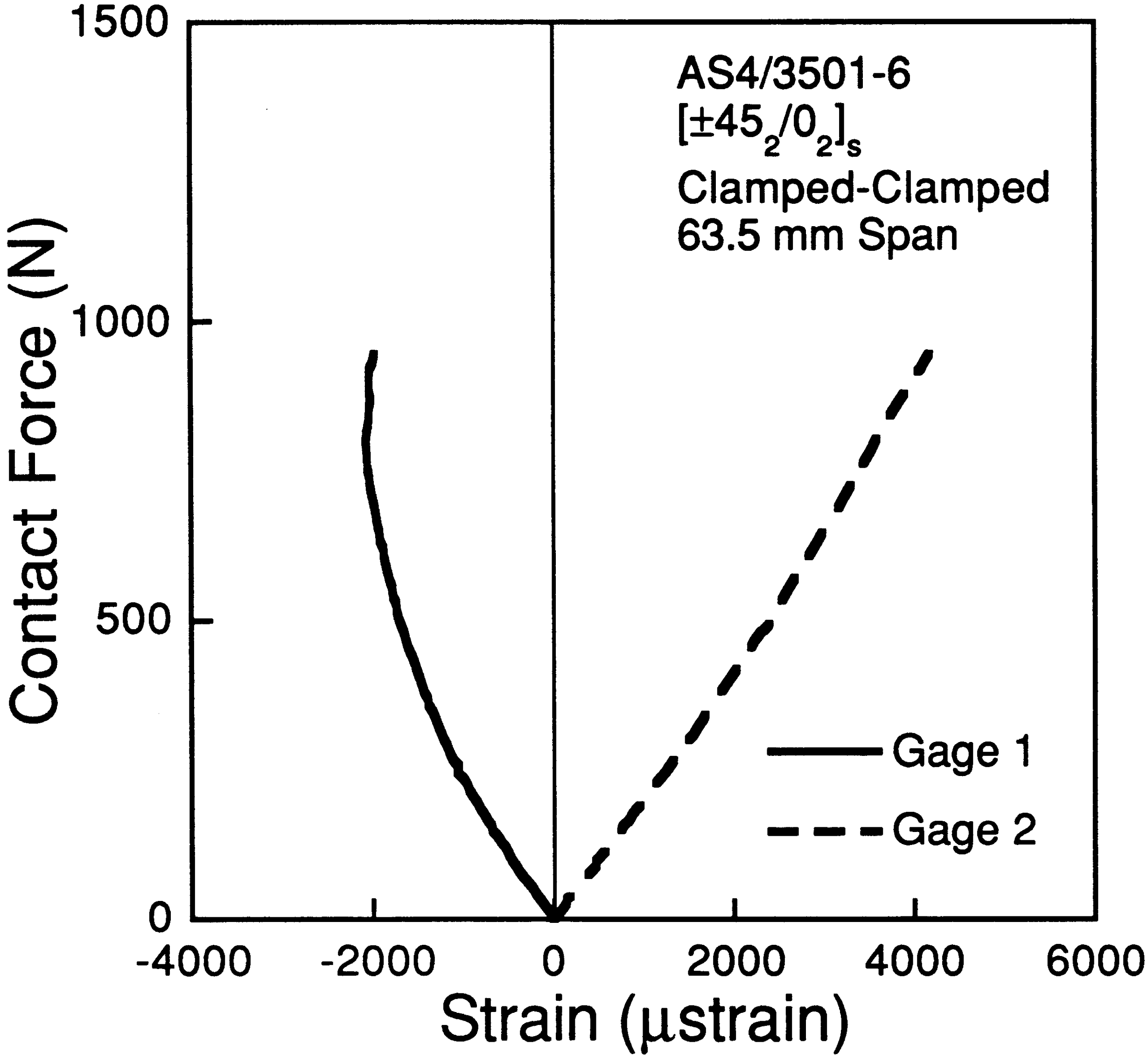

Figure B.45 Force-strain data from gages 1 and 2 (see Figure 3.2) for the specimen with a 63.5 mm span in a clamped-clamped support and tested to a maximum contact force of 930 N.

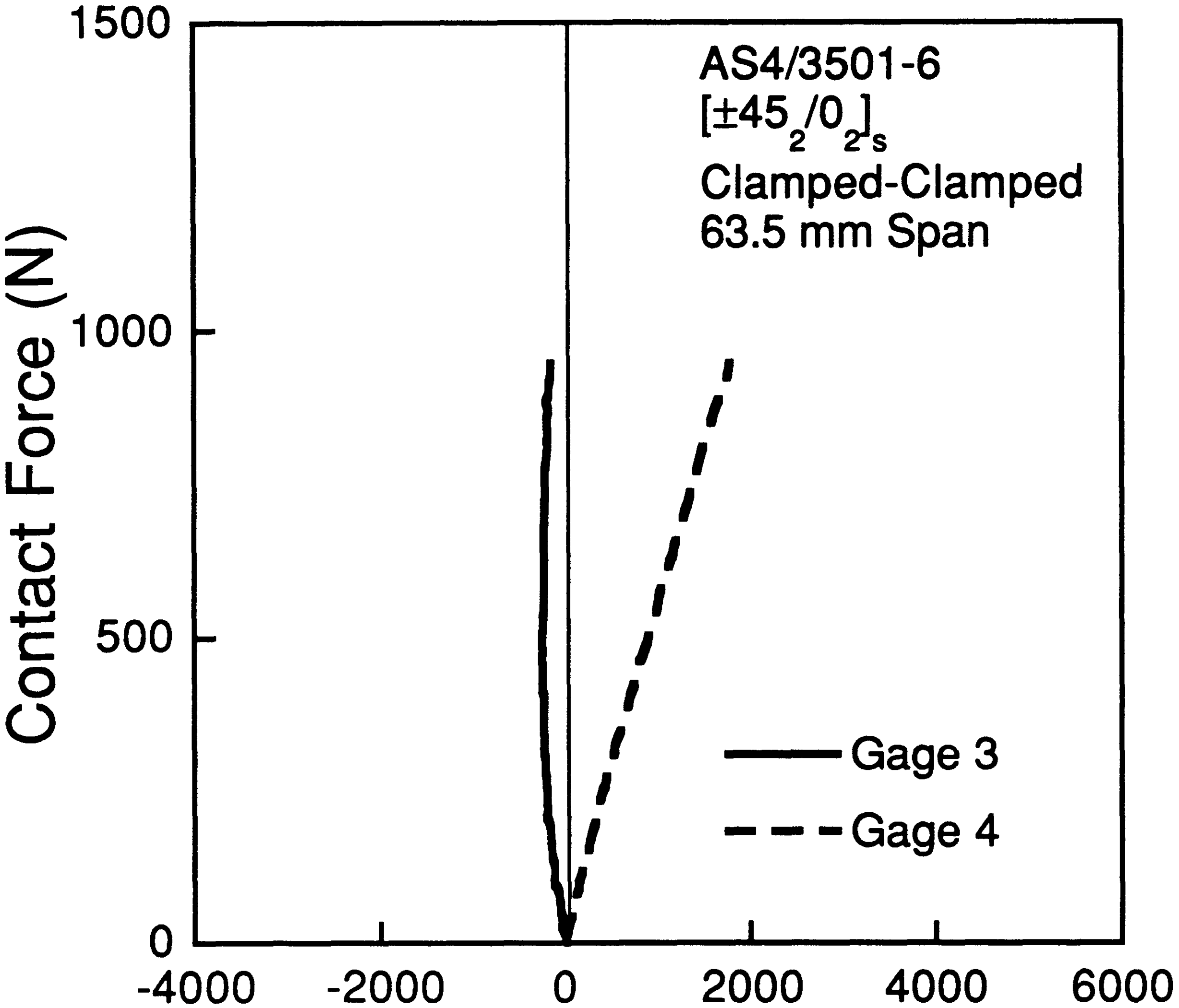

Figure B.46 Force-strain data from gages 3 and 4 (see Figure 3.2) for the specimen with a 63.5 mm span in a clamped-clamped support and tested to a maximum contact force of 930 N.

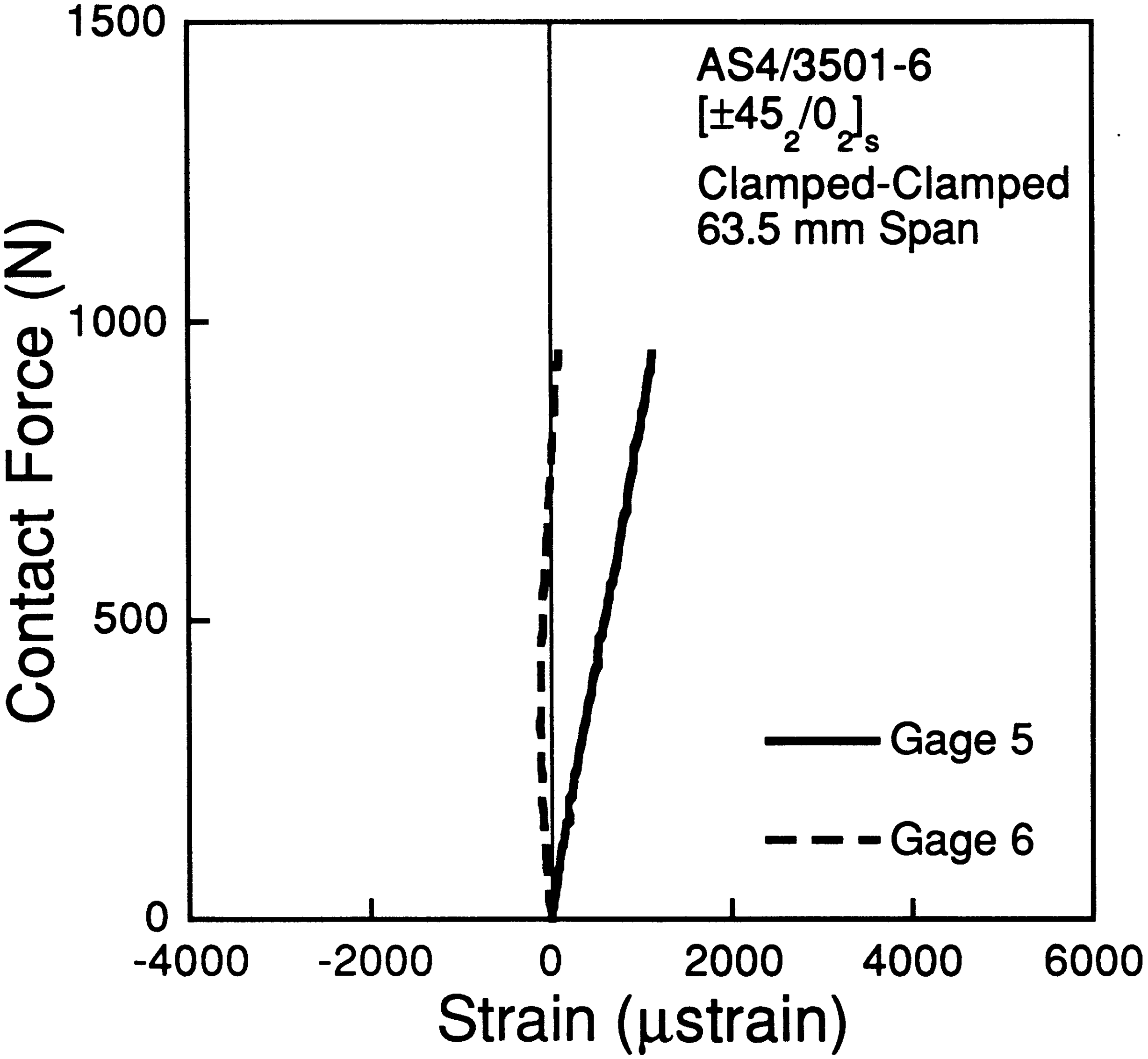

Figure B.47 Force-strain data from gages 5 and 6 (see Figure 3.2) for the specimen with a 63.5 mm span in a clamped-clamped support and tested to a maximum contact force of 930 N.

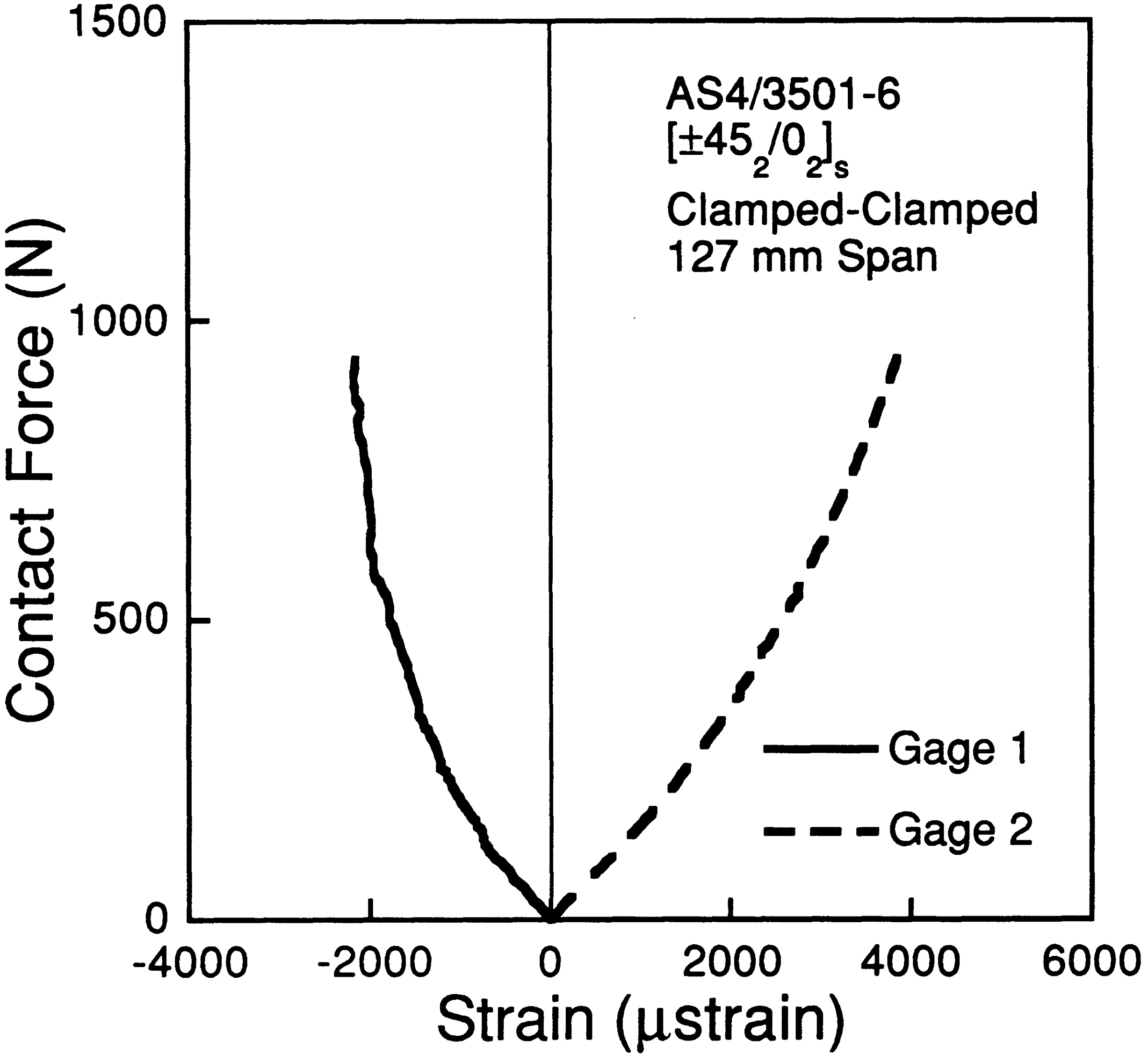

Figure B.48 Force-strain data from gages 1 and 2 (see Figure 3.2) for the specimen with a 127 mm span in a clamped-clamped support and tested to a maximum contact force of 930 N.

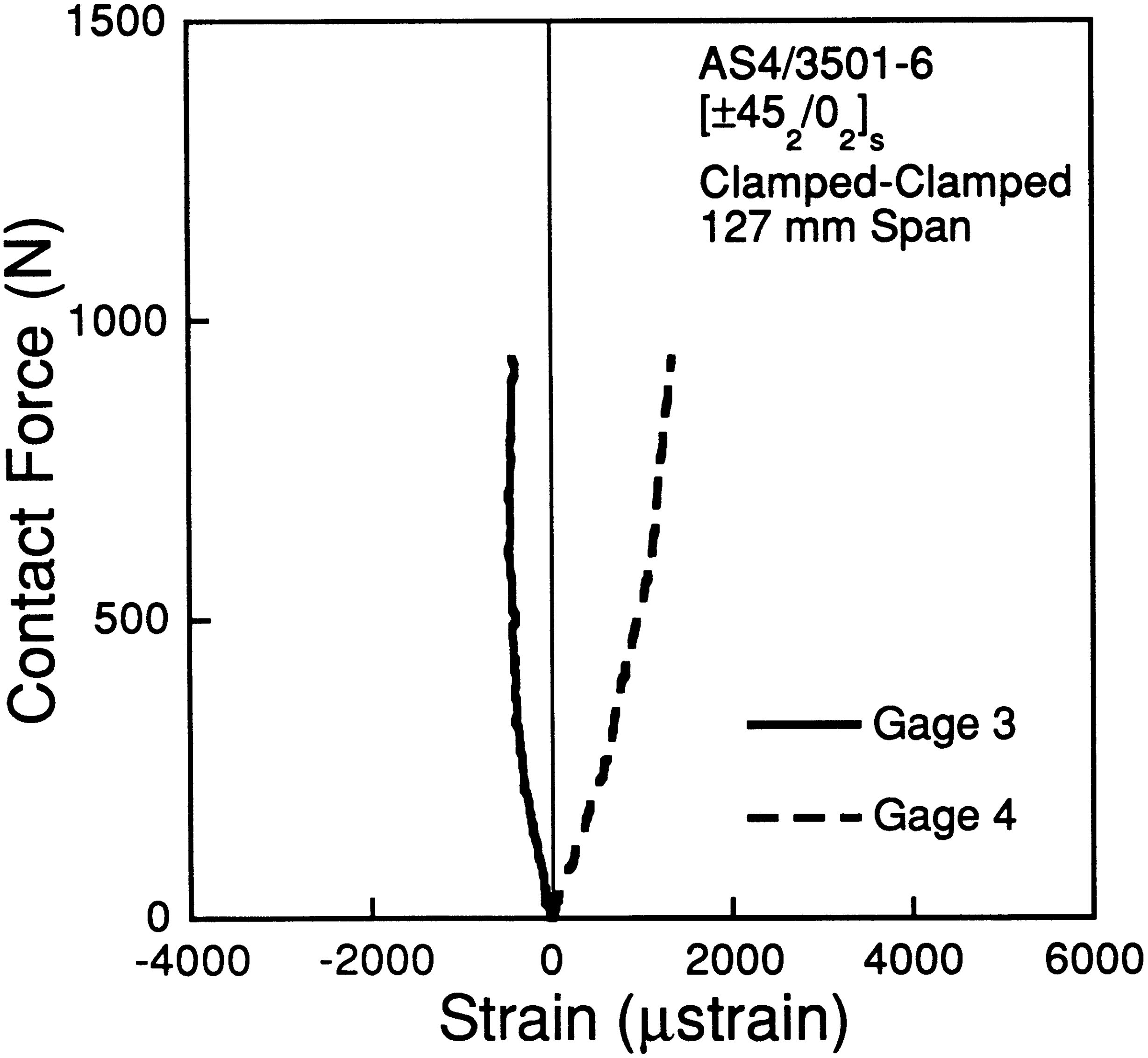

Figure B.49 Force-strain data from gages 3 and 4 (see Figure 3.2) for the specimen with a 127 mm span in a clamped-clamped support and tested to a maximum contact force of 930 N.

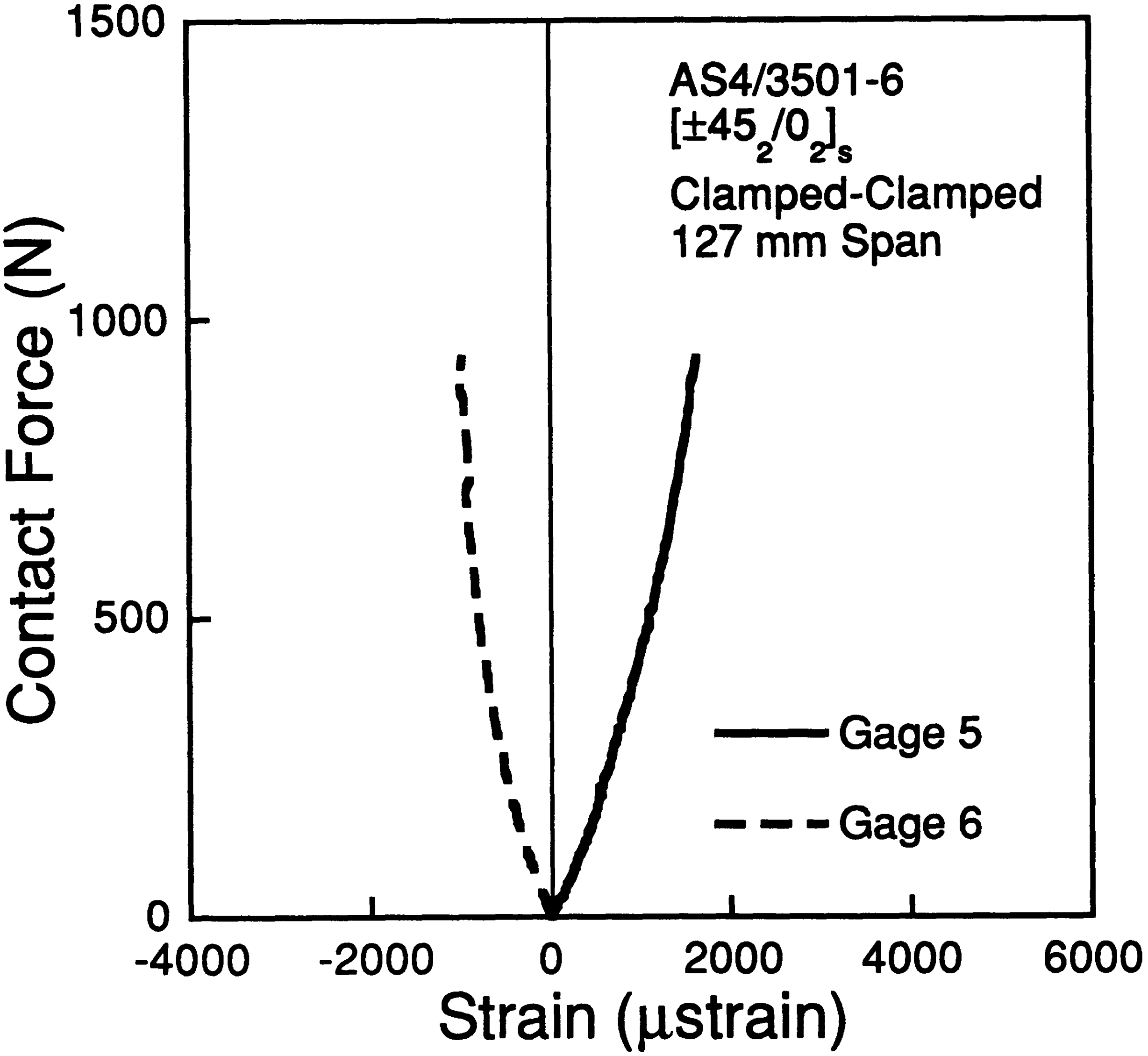

Figure B.50 Force-strain data from gages 5 and 6 (see Figure 3.2) for the specimen with a 127 mm span in a clamped-clamped support and tested to a maximum contact force of 930 N.

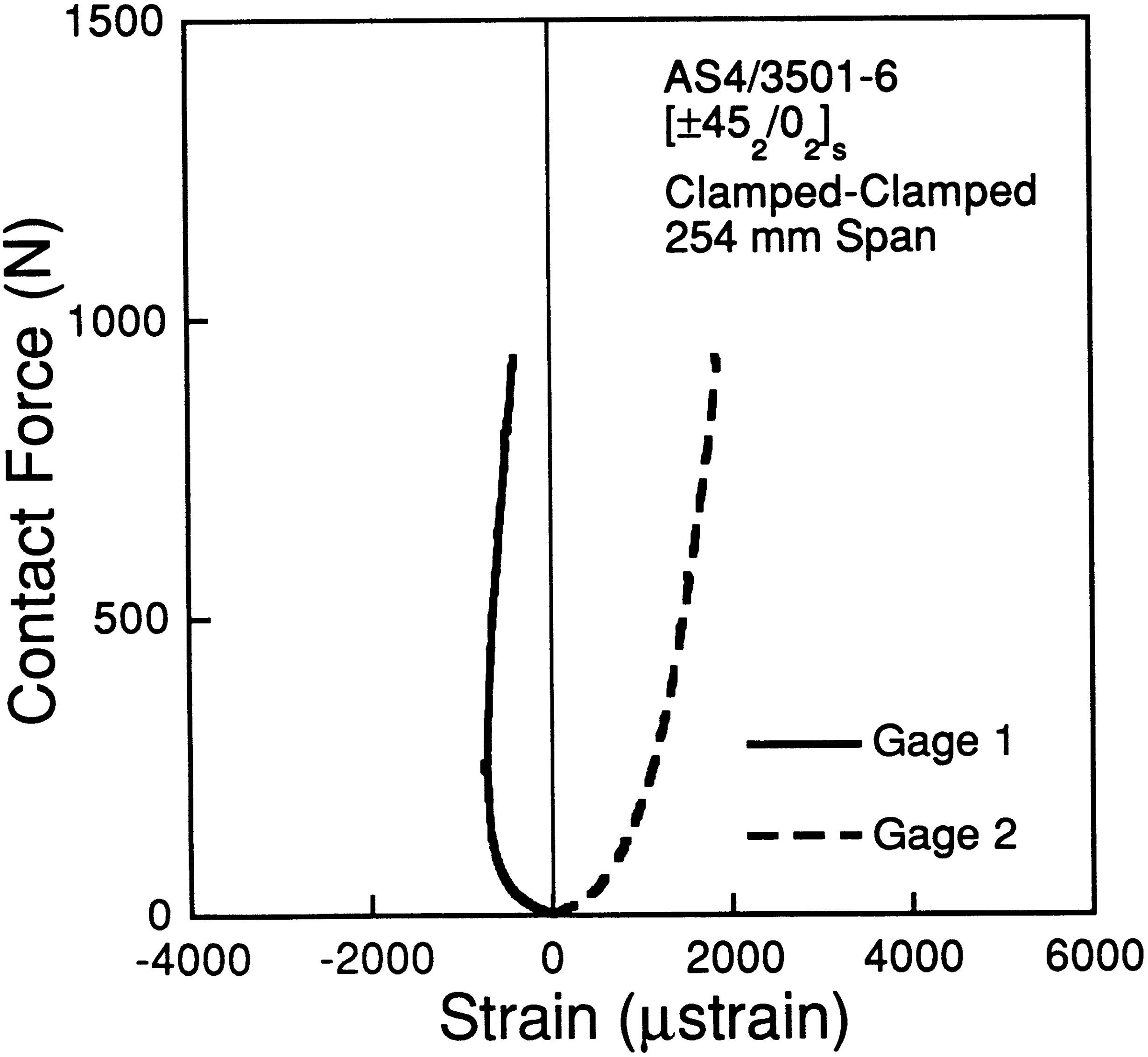

Figure B.51 Force-strain data from gages 1 and 2 (see Figure 3.2) for the specimen with a 254 mm span in a clamped-clamped support and tested to a maximum contact force of 930 N.

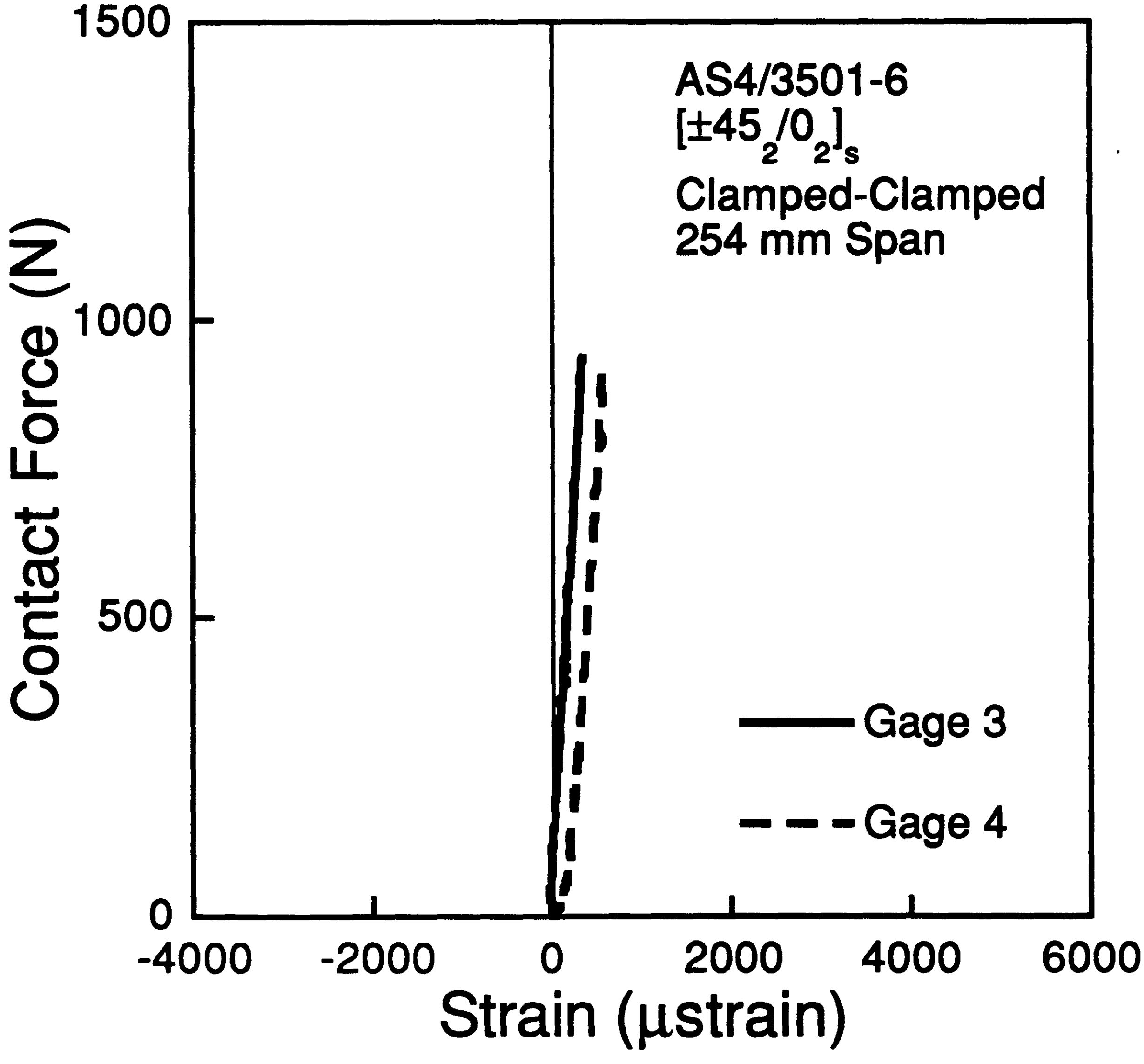

Figure B.52 Force-strain data from gages 3 and 4 (see Figure 3.2) for the specimen with a 254 mm span in a clamped-clamped support and tested to a maximum contact force of 930 N.

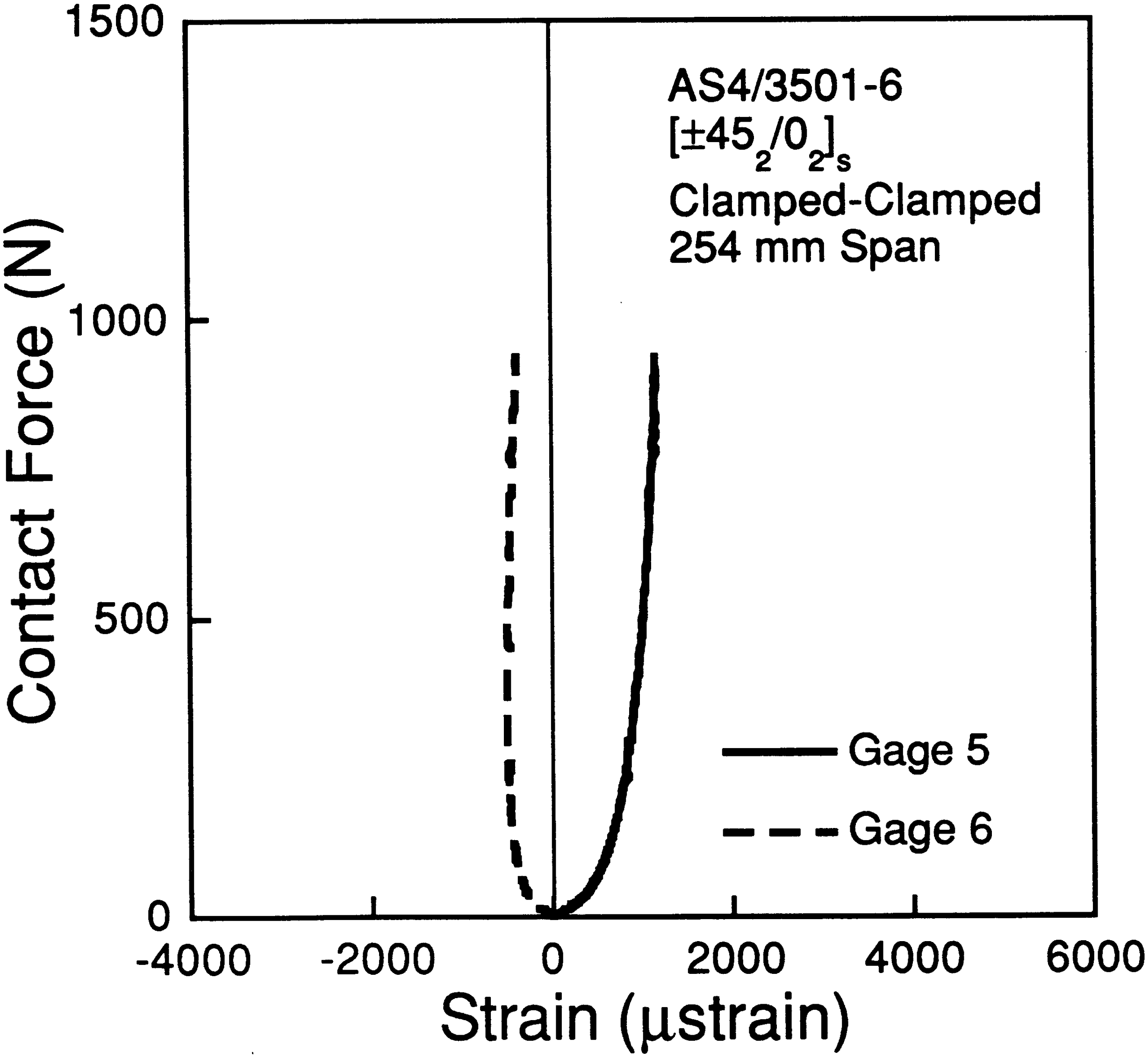

Figure B.53 Force-strain data from gages 5 and 6 (see Figure 3.2) for the specimen with a 254 mm span in a clamped-clamped support and tested to a maximum contact force of 930 N.

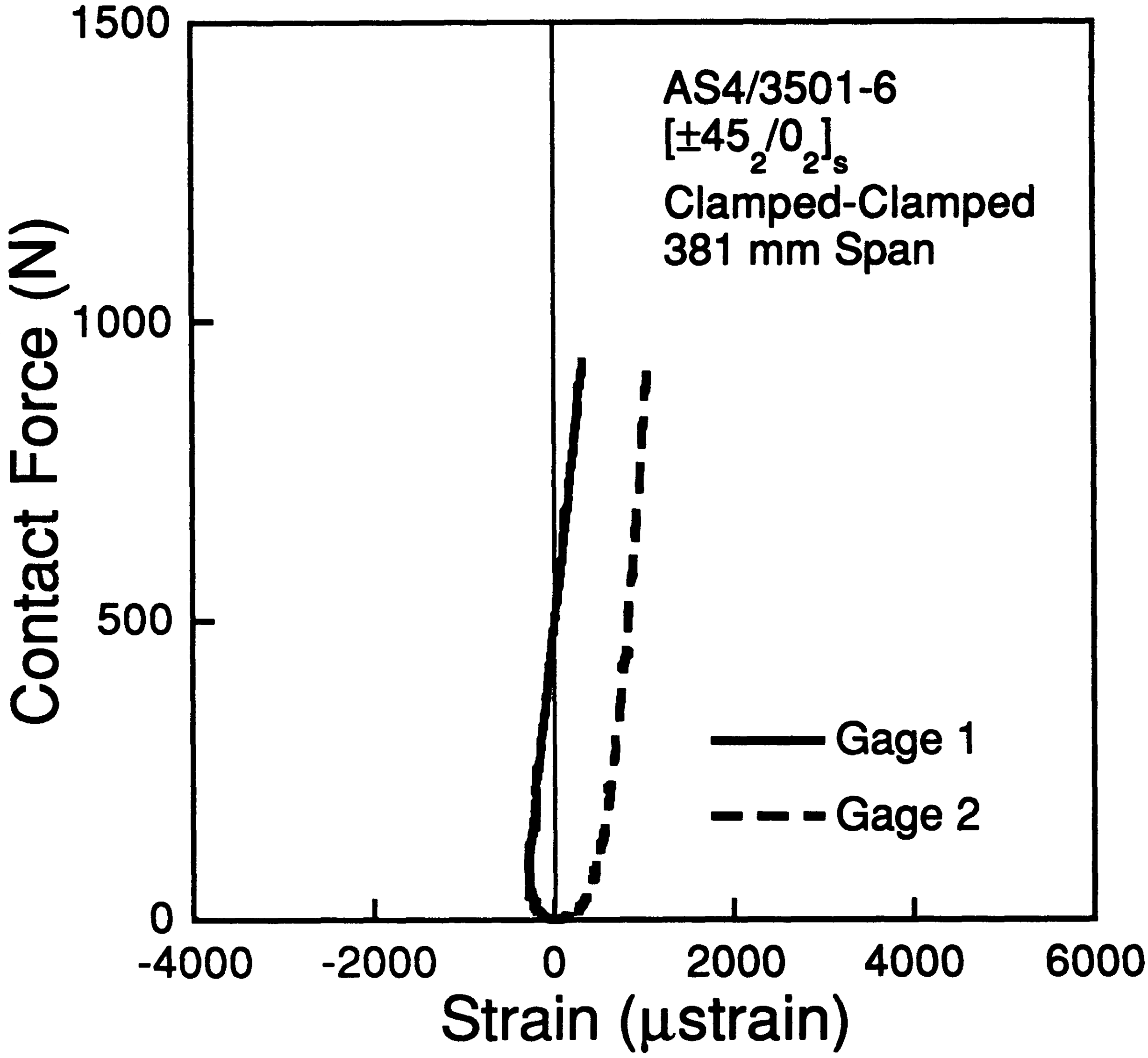

Figure B.54 Force-strain data from gages 1 and 2 (see Figure 3.2) for the specimen with a 381 mm span in a clamped-clamped support and tested to a maximum contact force of 930 N.

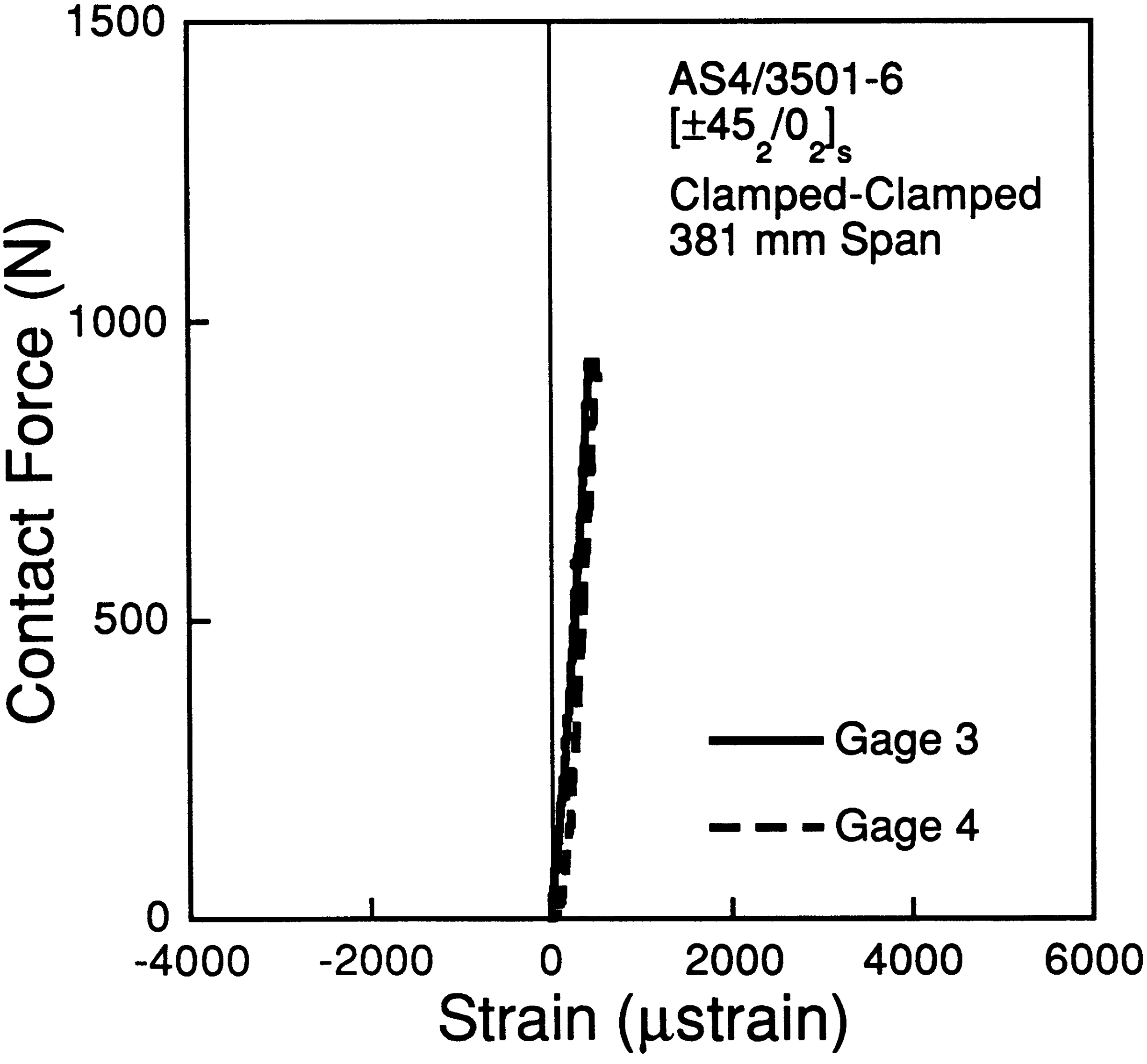

Figure B.55 Force-strain data from gages 3 and 4 (see Figure 3.2) for the specimen with a 381 mm span in a clamped-clamped support and tested to a maximum contact force of 930 N.

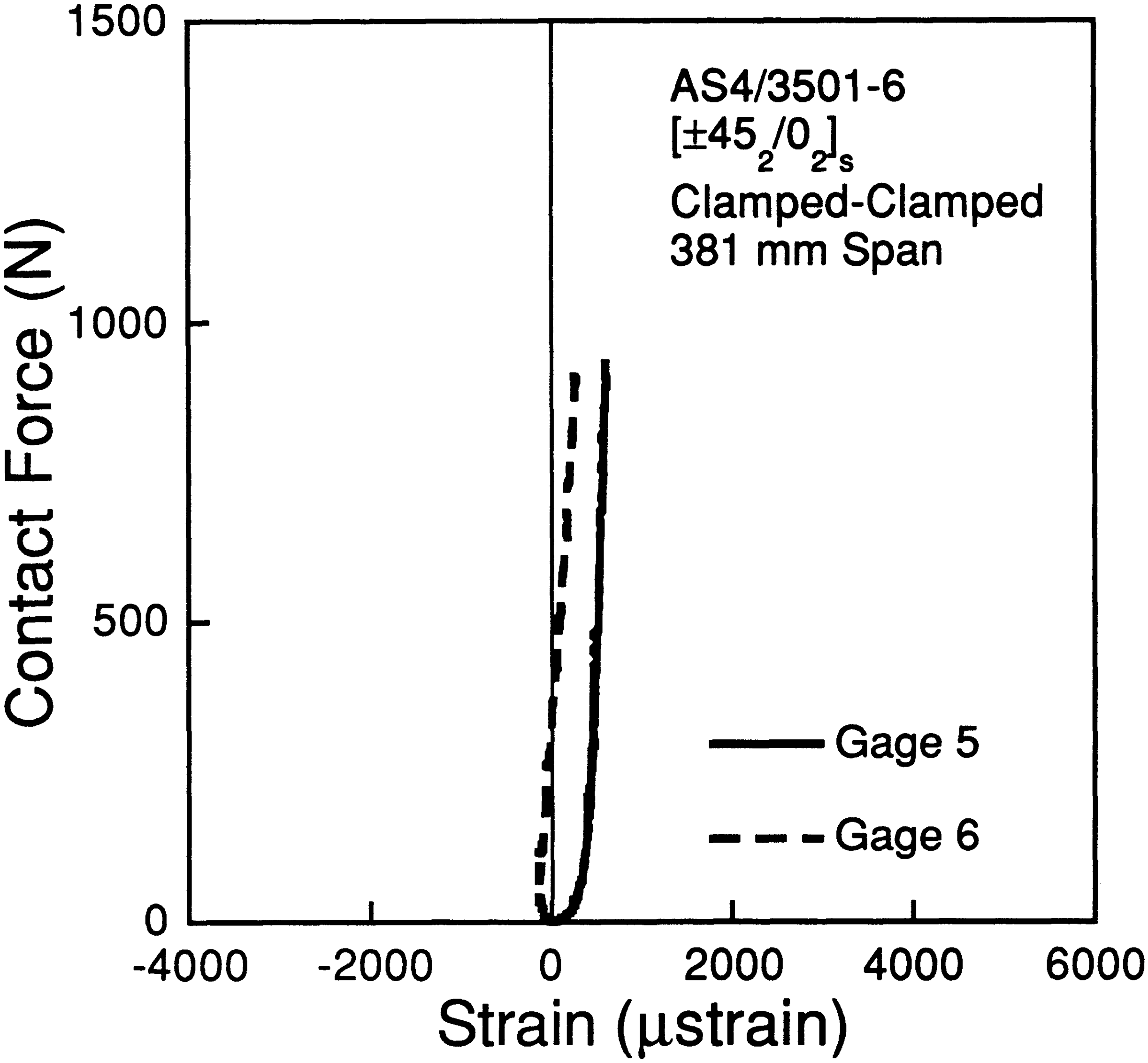

Figure B.56 Force-strain data from gages 5 and 6 (see Figure 3.2) for the specimen with a 381 mm span in a clamped-clamped support and tested to a maximum contact force of 930 N.

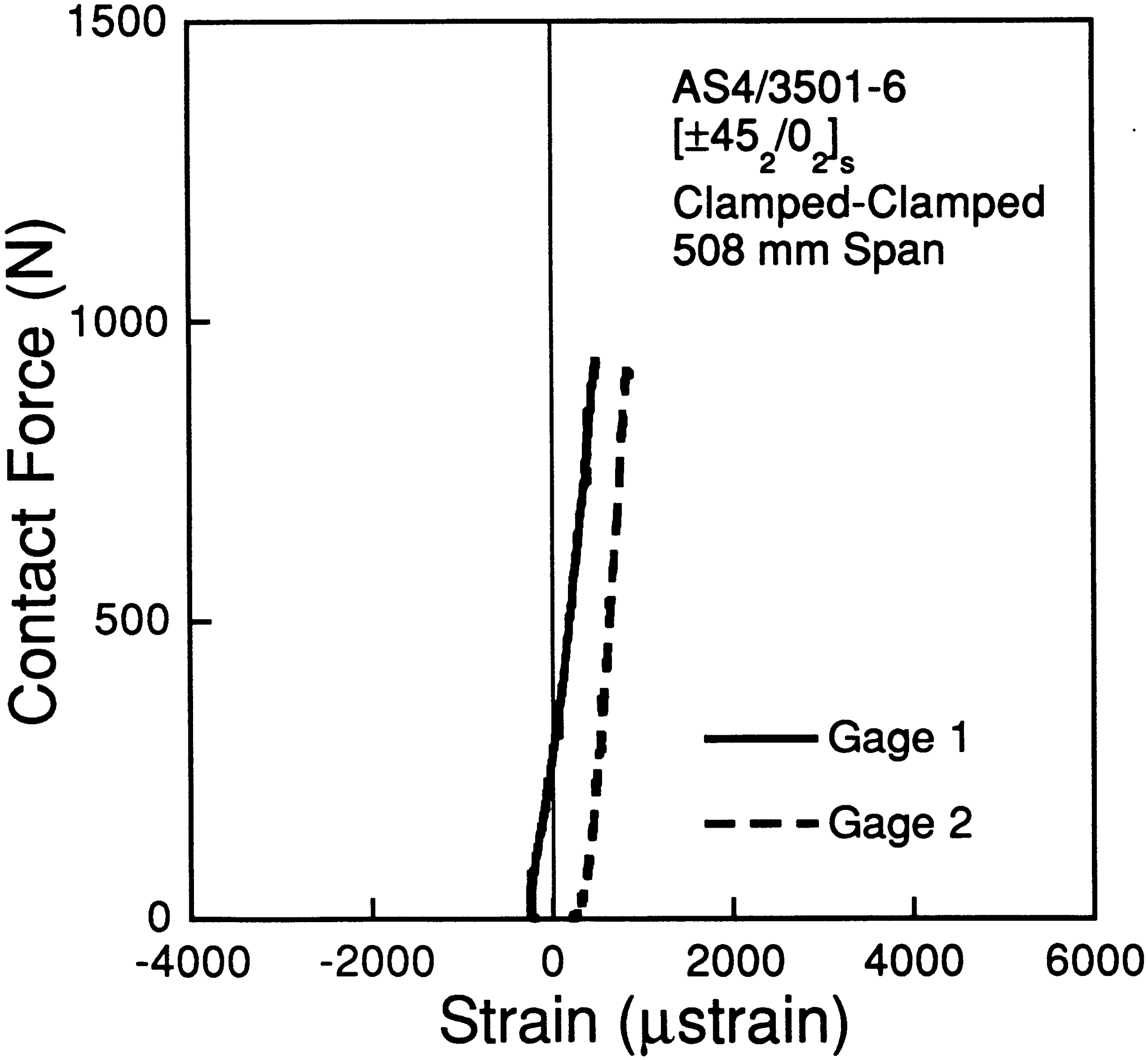

Figure B.57 Force-strain data from gages 1 and 2 (see Figure 3.2) for the specimen with a 508 mm span in a clamped-clamped support and tested to a maximum contact force of 930 N.

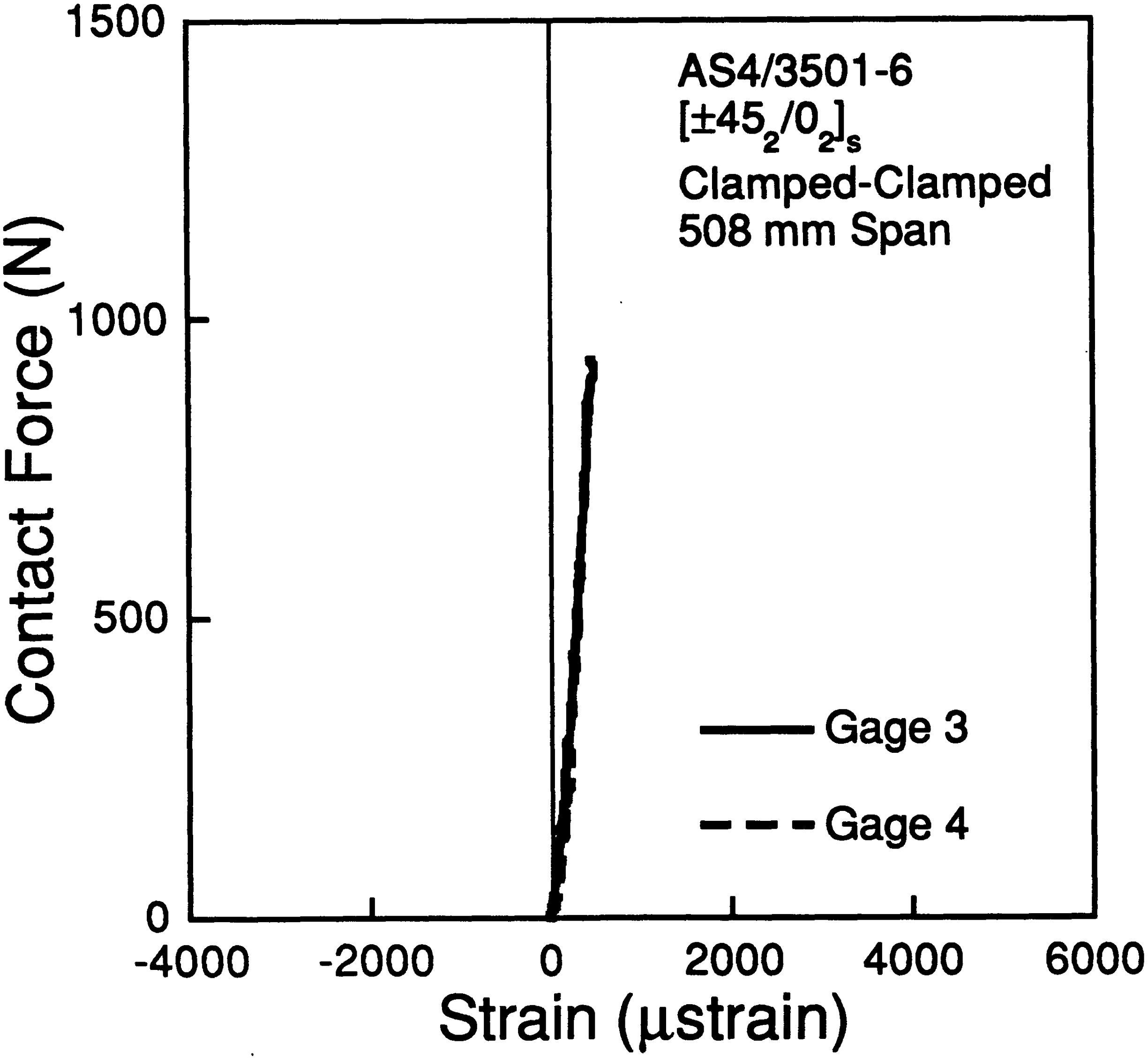

Figure B.58 Force-strain data from gages 3 and 4 (see Figure 3.2) for the specimen with a 508 mm span in a clamped-clamped support and tested to a maximum contact force of 930 N.

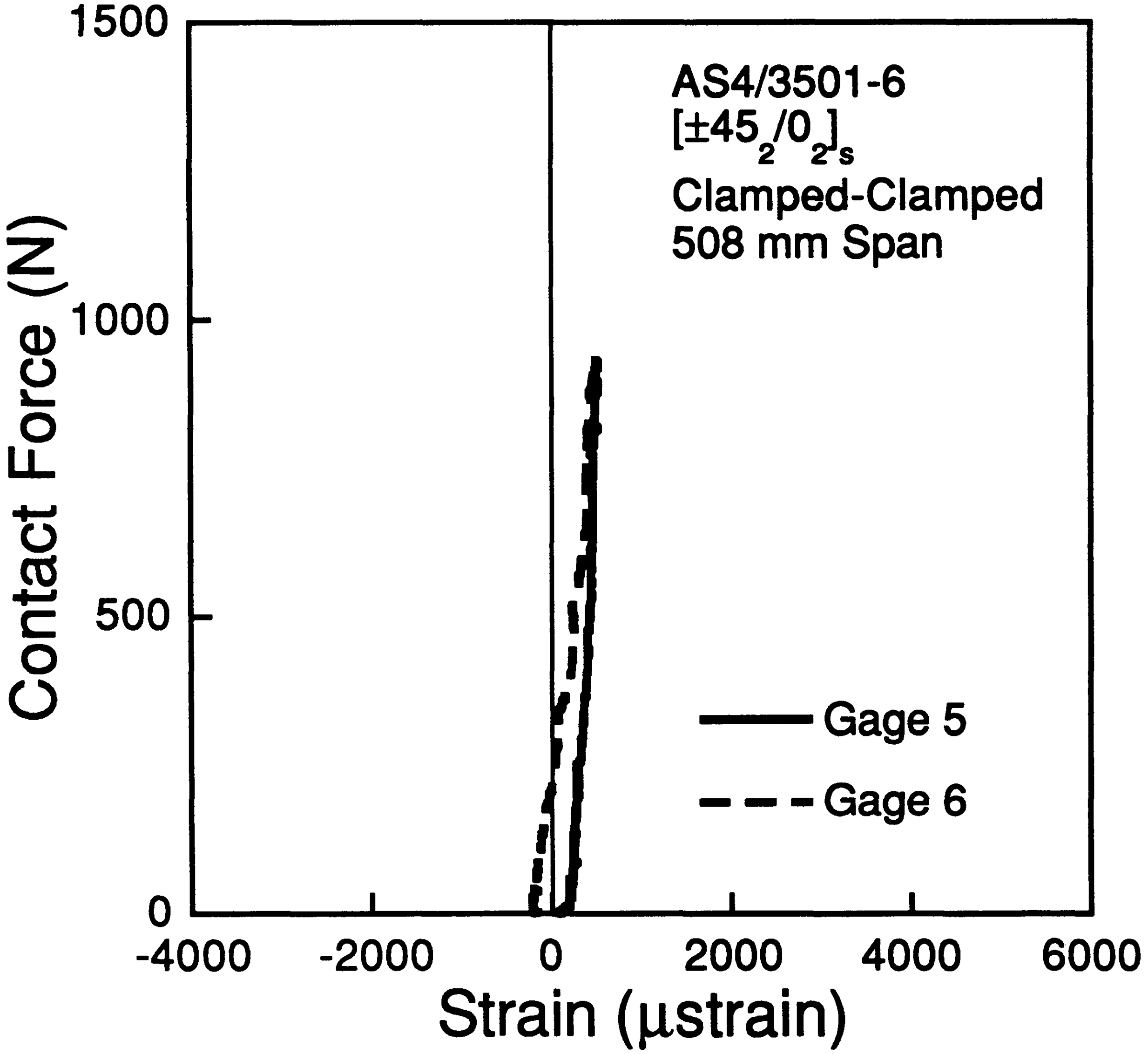

Figure B.59 Force-strain data from gages 5 and 6 (see Figure 3.2) for the specimen with a 508 mm span in a clamped-clamped support and tested to a maximum contact force of 930 N.

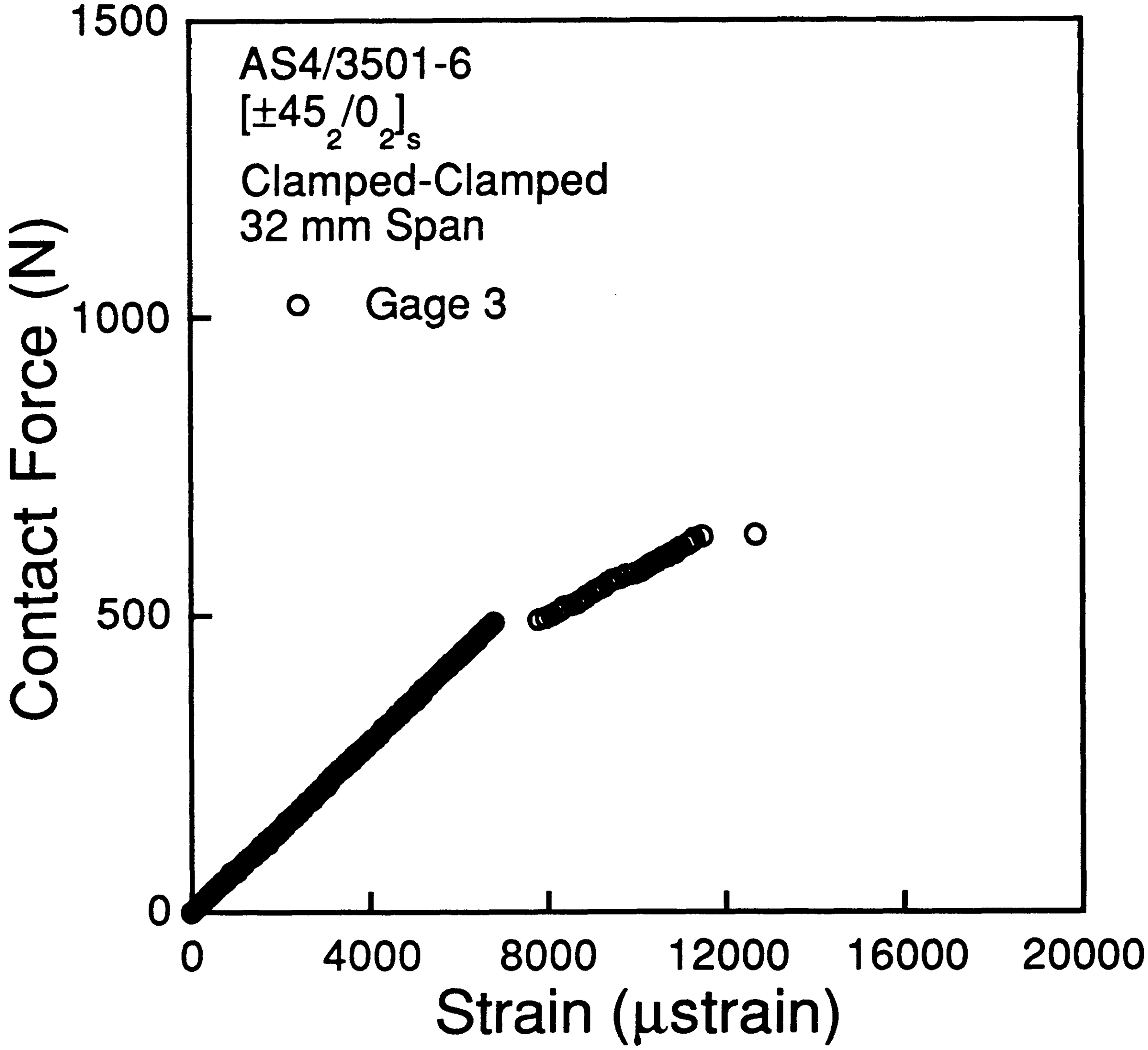

Figure B.60 Force-strain data from gage 3 (see Figure 3.3) for the specimen with a 32 mm span in a clamped-clamped support and tested to a maximum contact force of 1479 N.

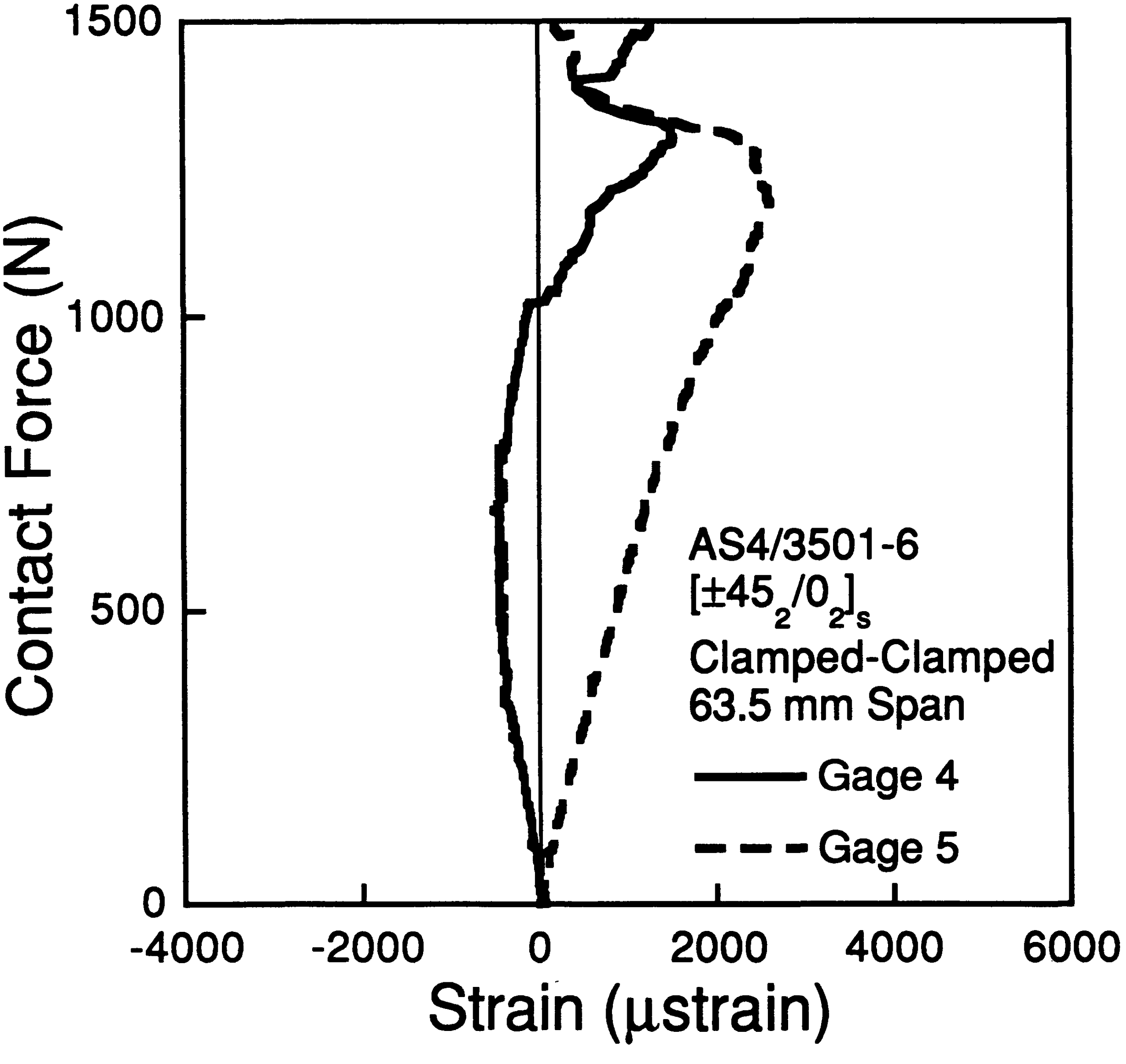

Figure B.61 Force-strain data from gages 4 and 5 (see Figure 3.3) for the specimen with a 32 mm span in a clamped-clamped support and tested to a maximum contact force of 1479 N.

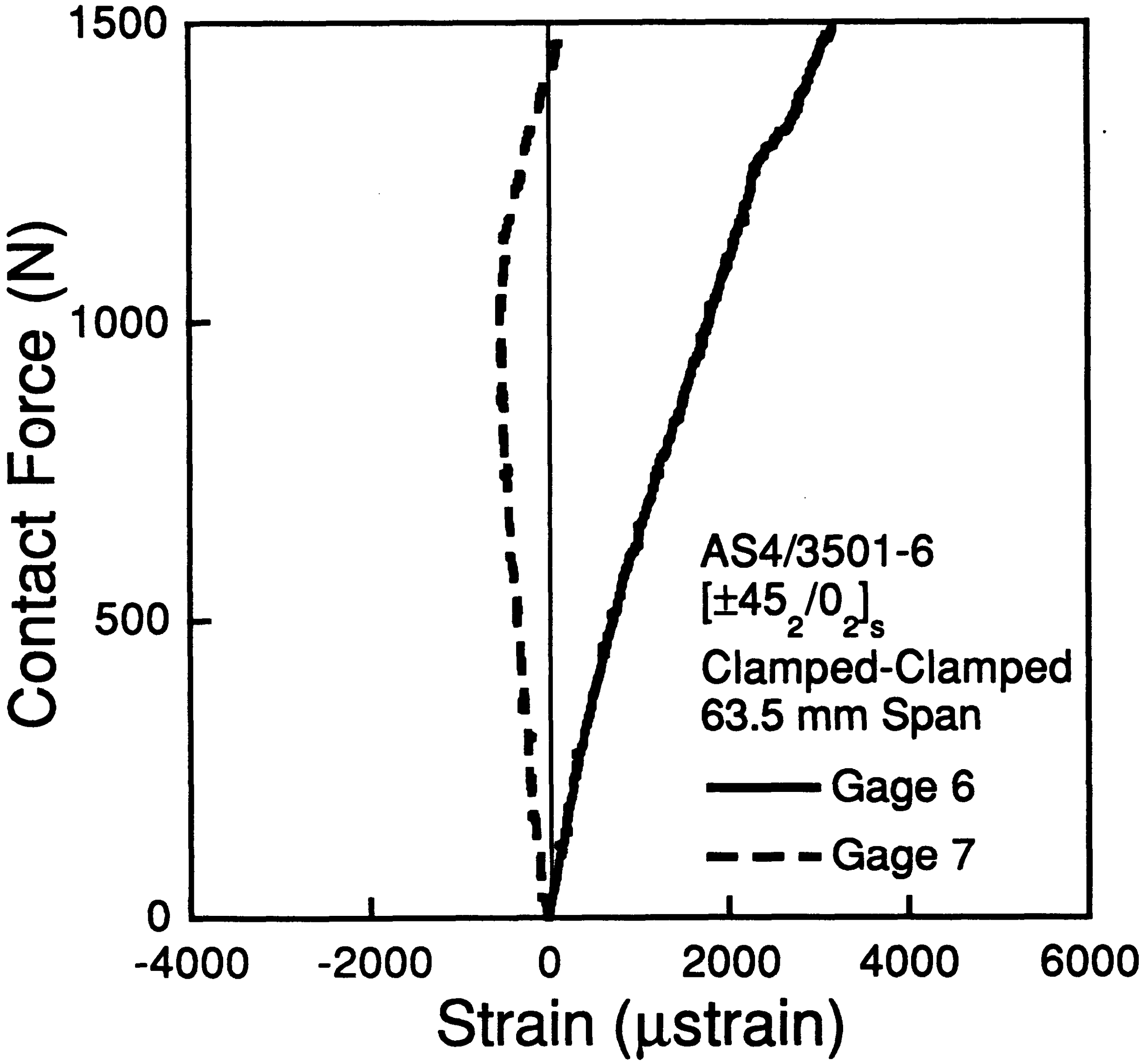

Figure B.62 Force-strain data from gages 6 and 7 (see Figure 3.3) for the specimen with a 32 mm span in a clamped-clamped support and tested to a maximum contact force of 1479 N.

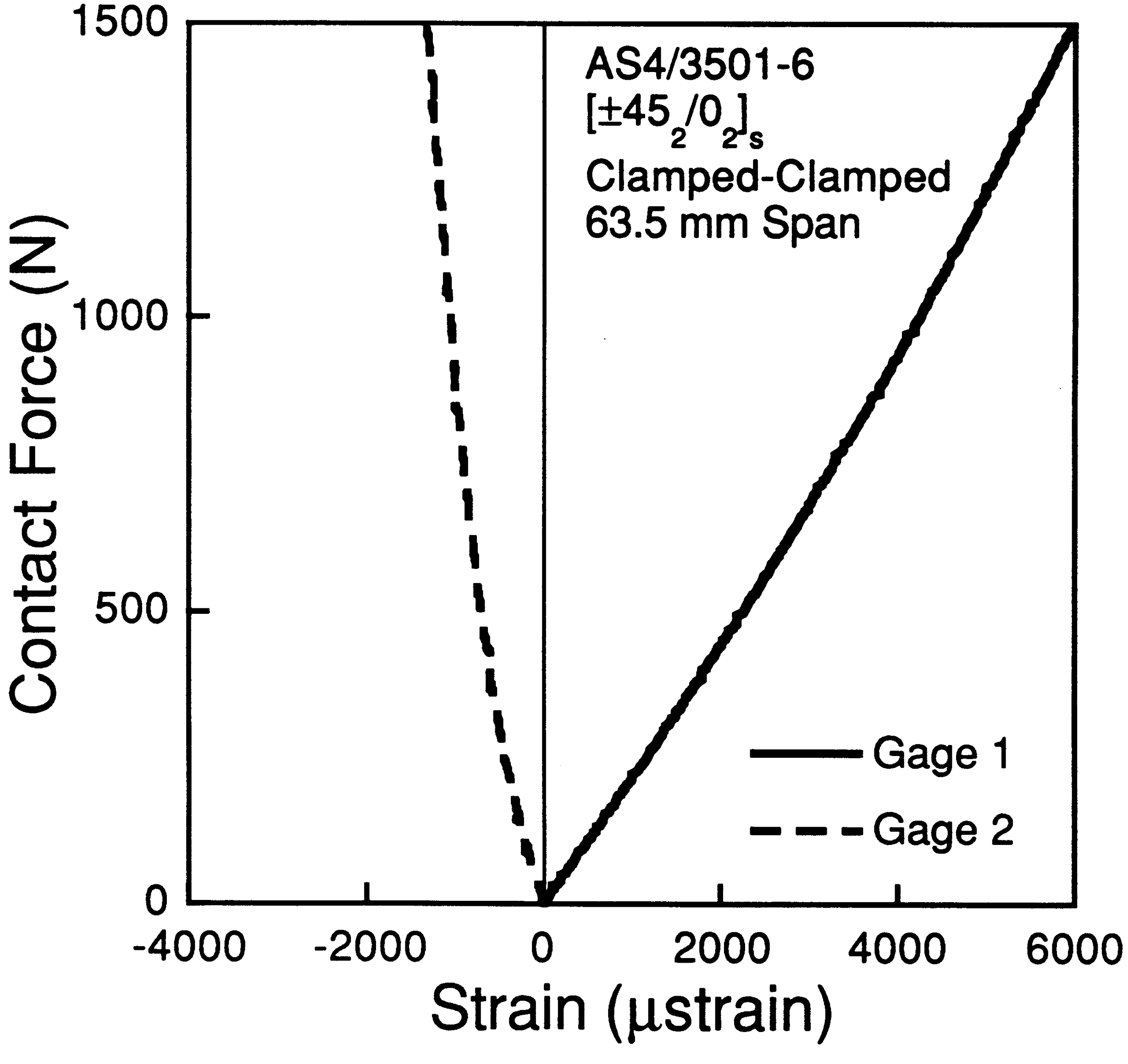

Figure B.63 Force-strain data from gages 1 and 2 (see Figure 3.3) for the specimen with a 63.5 mm span in a clamped-clamped support and tested to a maximum contact force of 1479 N.

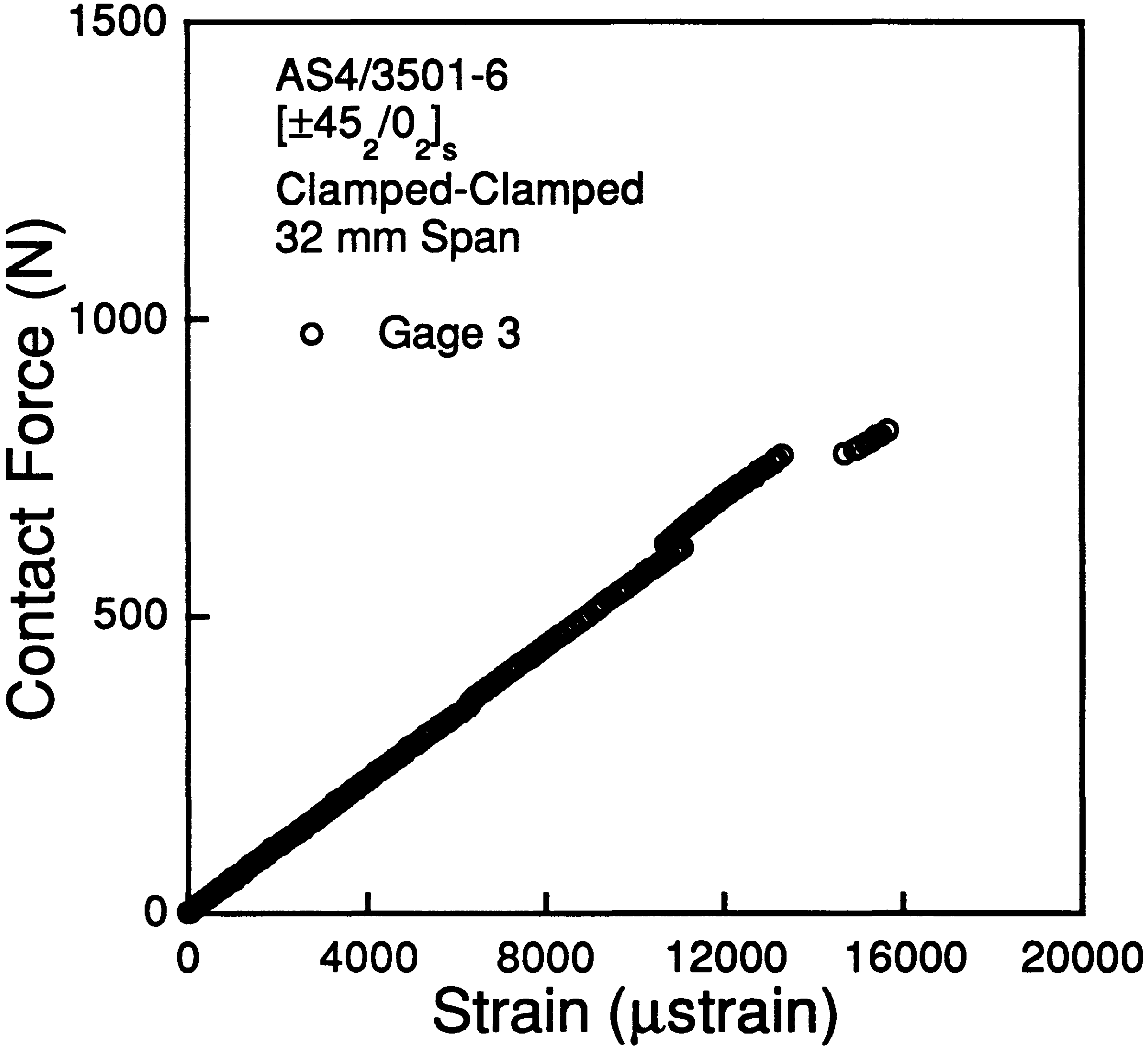

Figure B.64 Force-strain data from gage 3 (see Figure 3.3) for the specimen with a 63.5 mm span in a clamped-clamped support and tested to a maximum contact force of 1479 N.

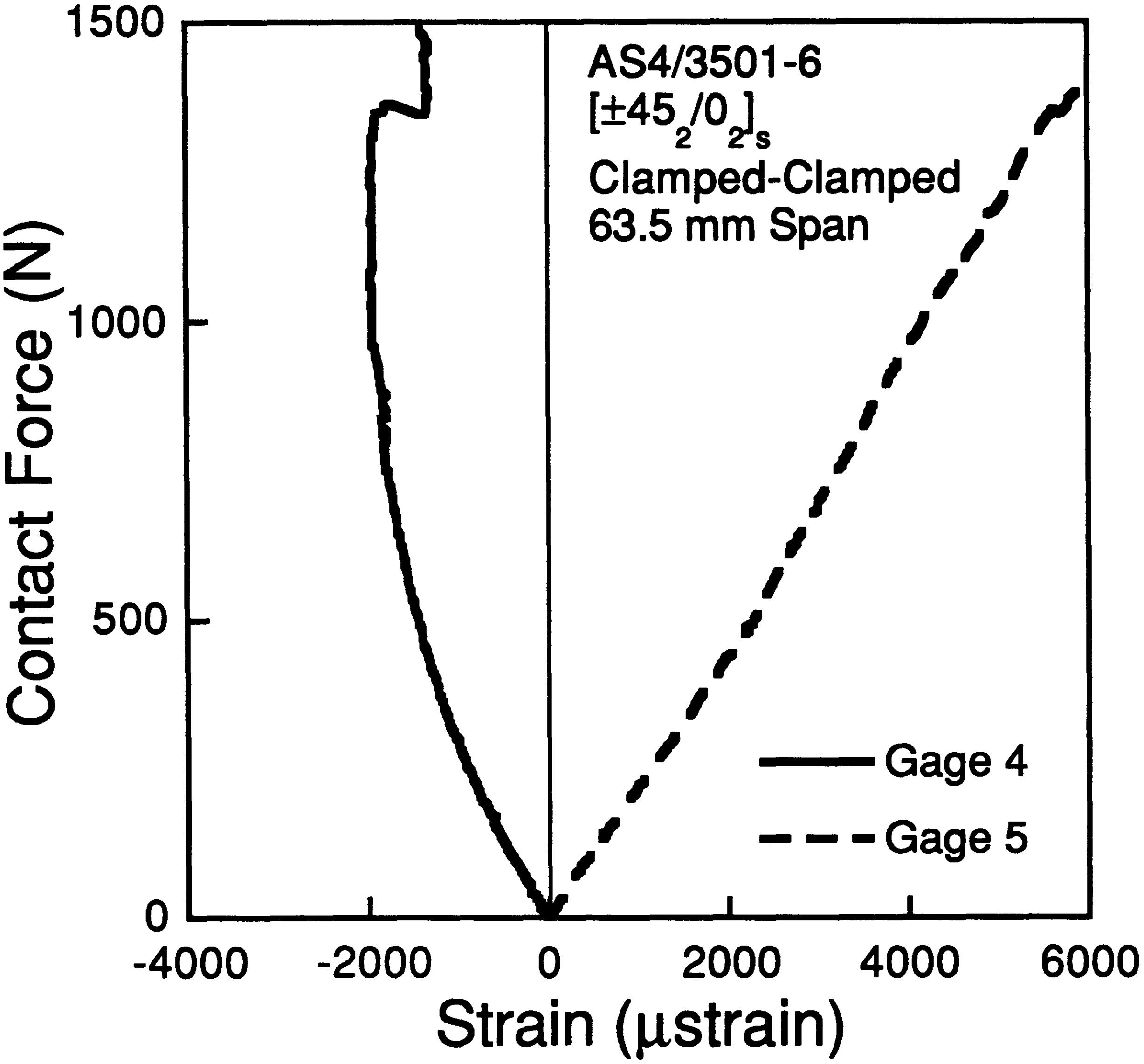

Figure B.65 Force-strain data from gages 4 and 5 (see Figure 3.3) for the specimen with a 63.5 mm span in a clamped-clamped support and tested to a maximum contact force of 1479 N.

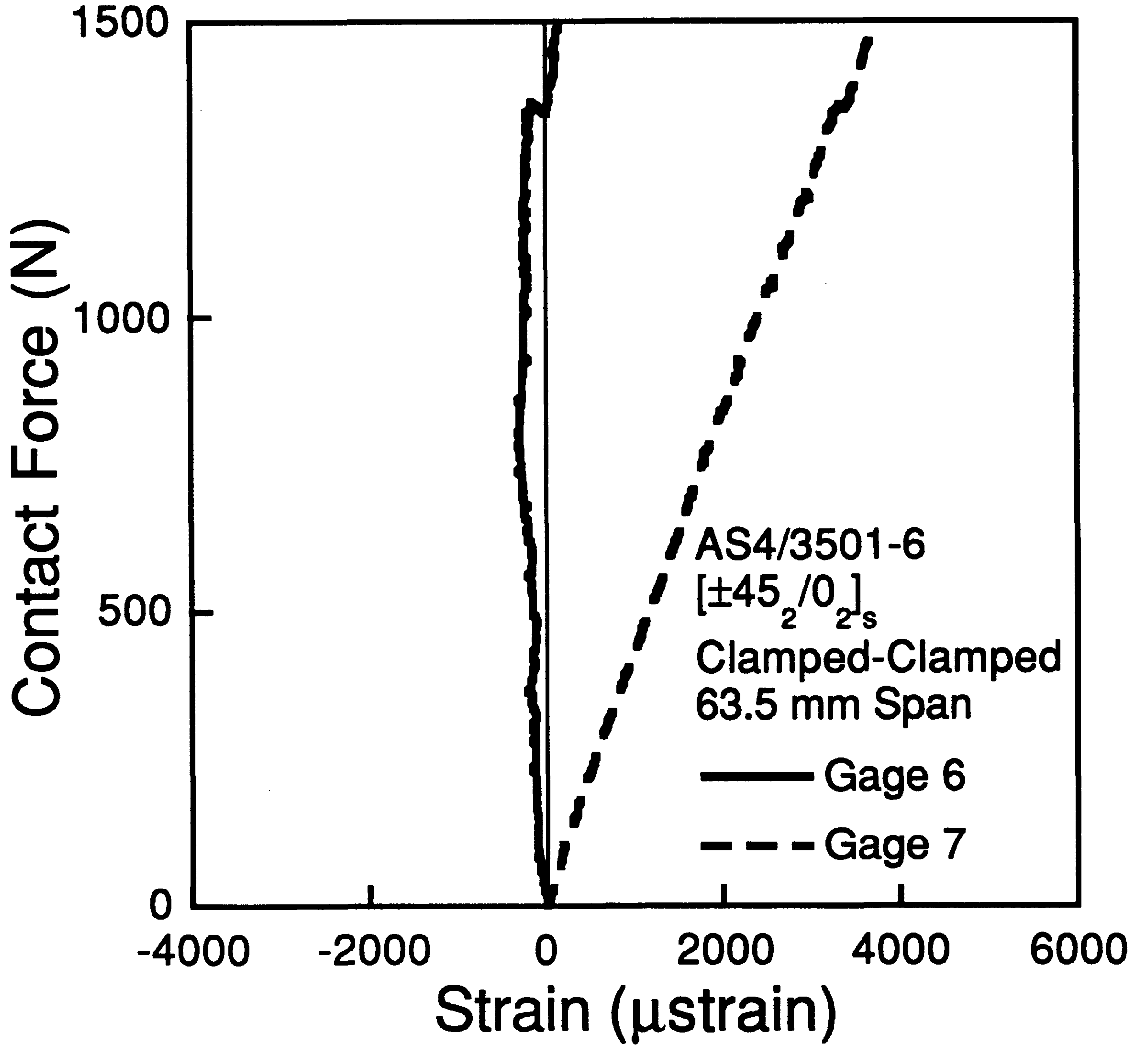

Figure B.66 Force-strain data from gages 6 and 7 (see Figure 3.3) for the specimen with a 63.5 mm span in a clamped-clamped support and tested to a maximum contact force of 1479 N.

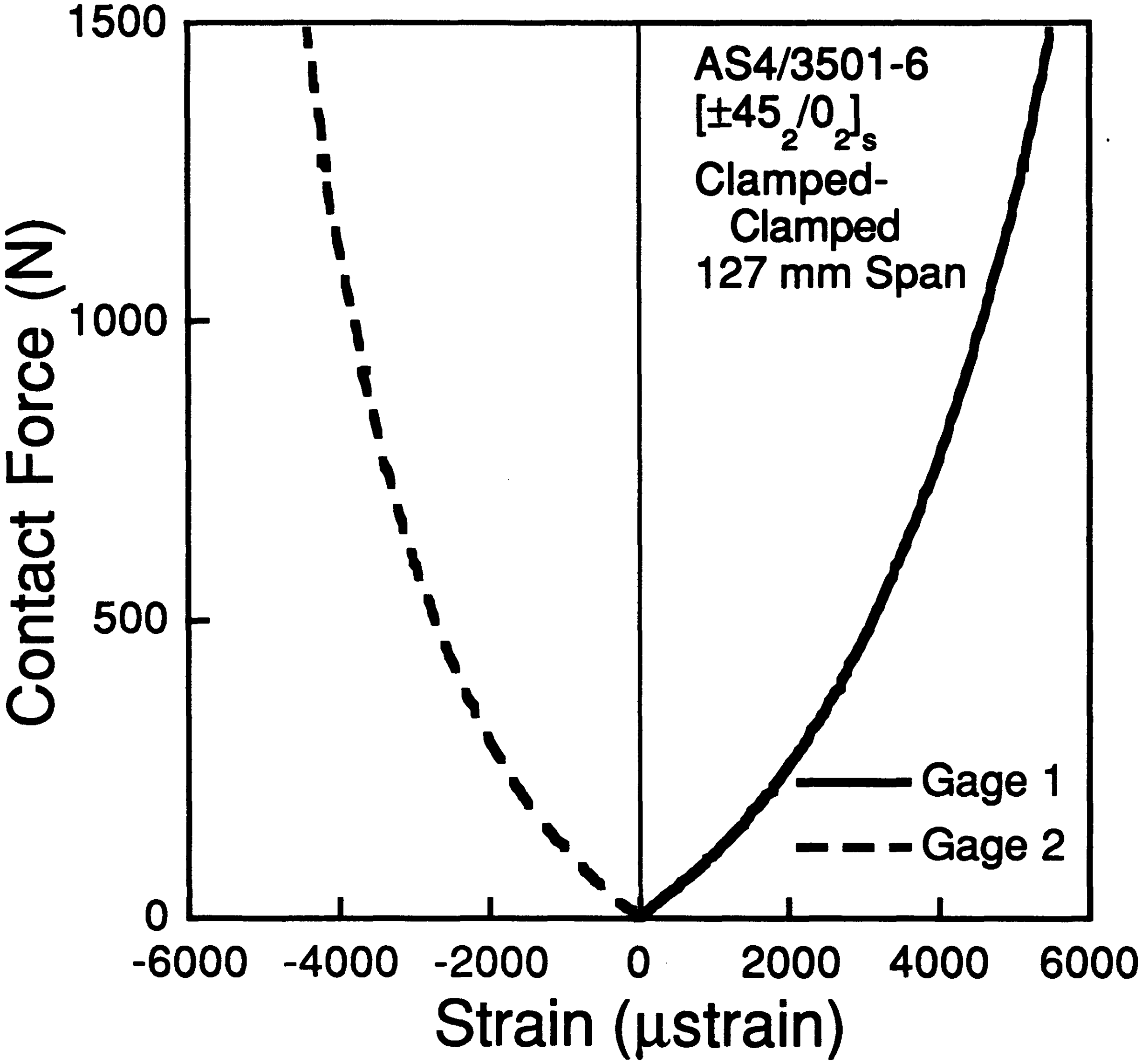

Figure B.67 Force-strain data from gages 1 and 2 (see Figure 3.3) for the specimen with a 127 mm span in a clamped-clamped support and tested to a maximum contact force of 1479 N.

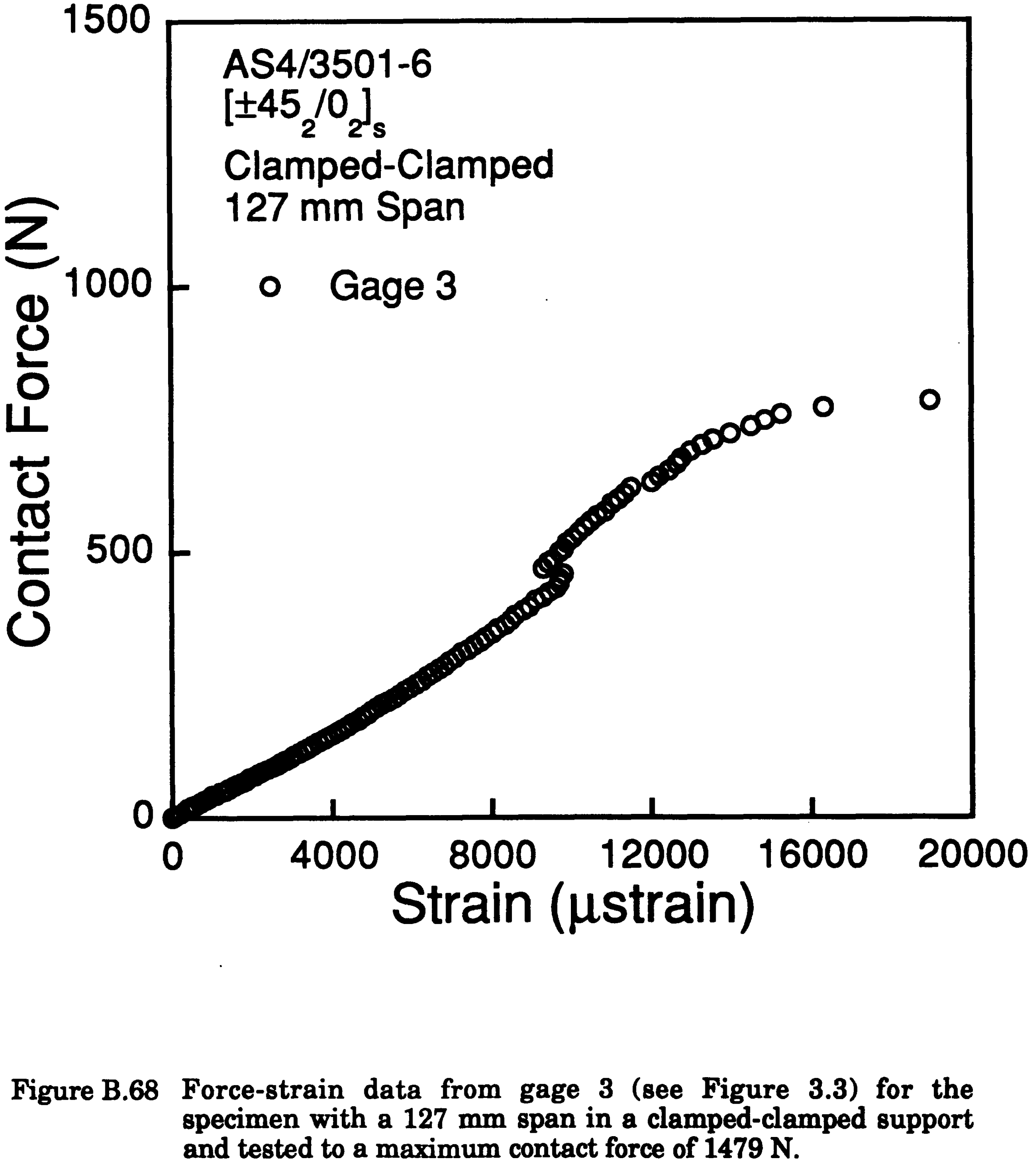

Figure B.68 Force-strain data from gage 3 (see Figure 3.3) for the specimen with a 127 mm span in a clamped-clamped support and tested to a maximum contact force of 1479 N.

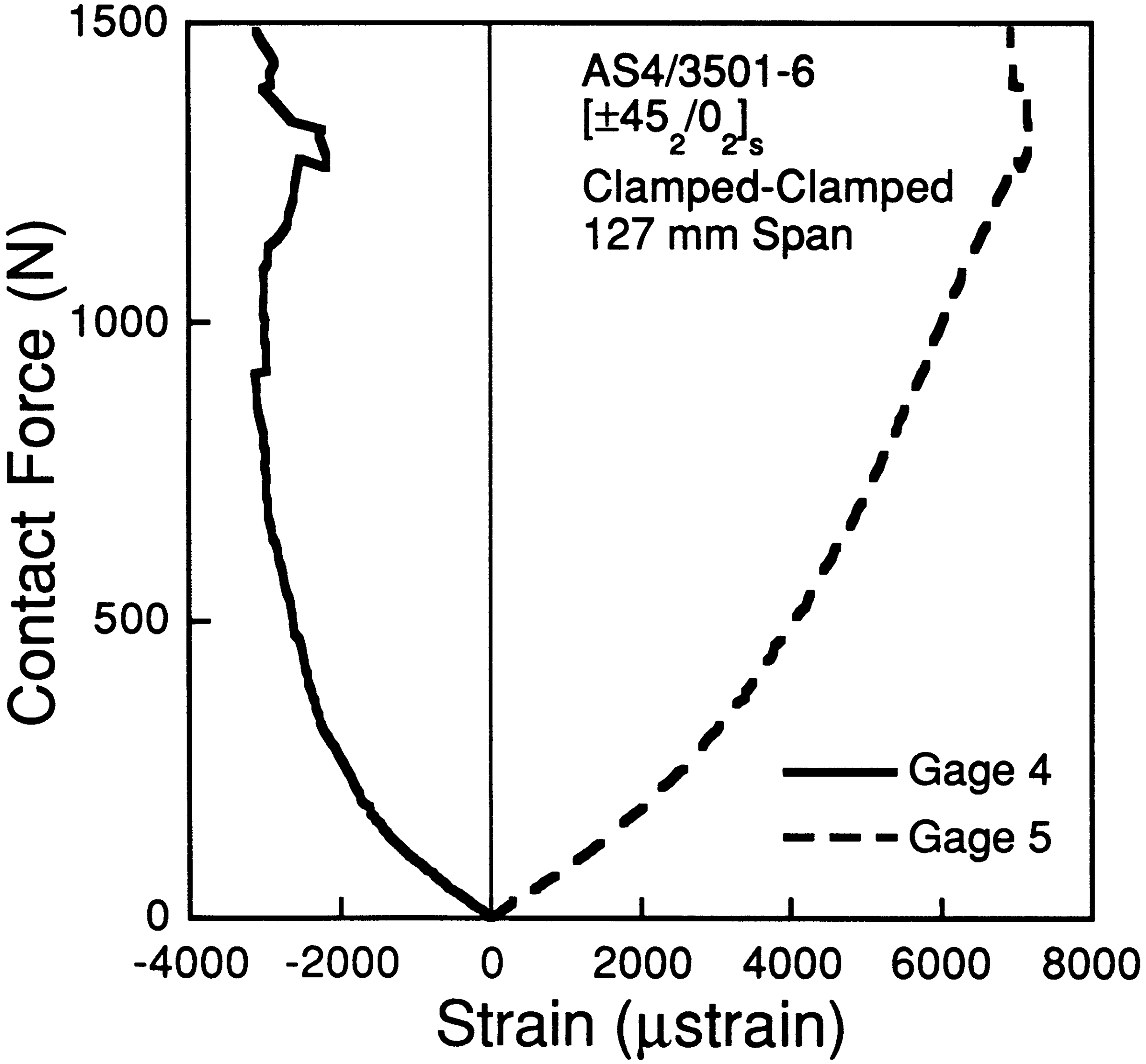

Figure B.69 Force-strain data from gages 4 and 5 (see Figure 3.3) for the specimen with a 127 mm span in a clamped-clamped support and tested to a maximum contact force of 1479 N.

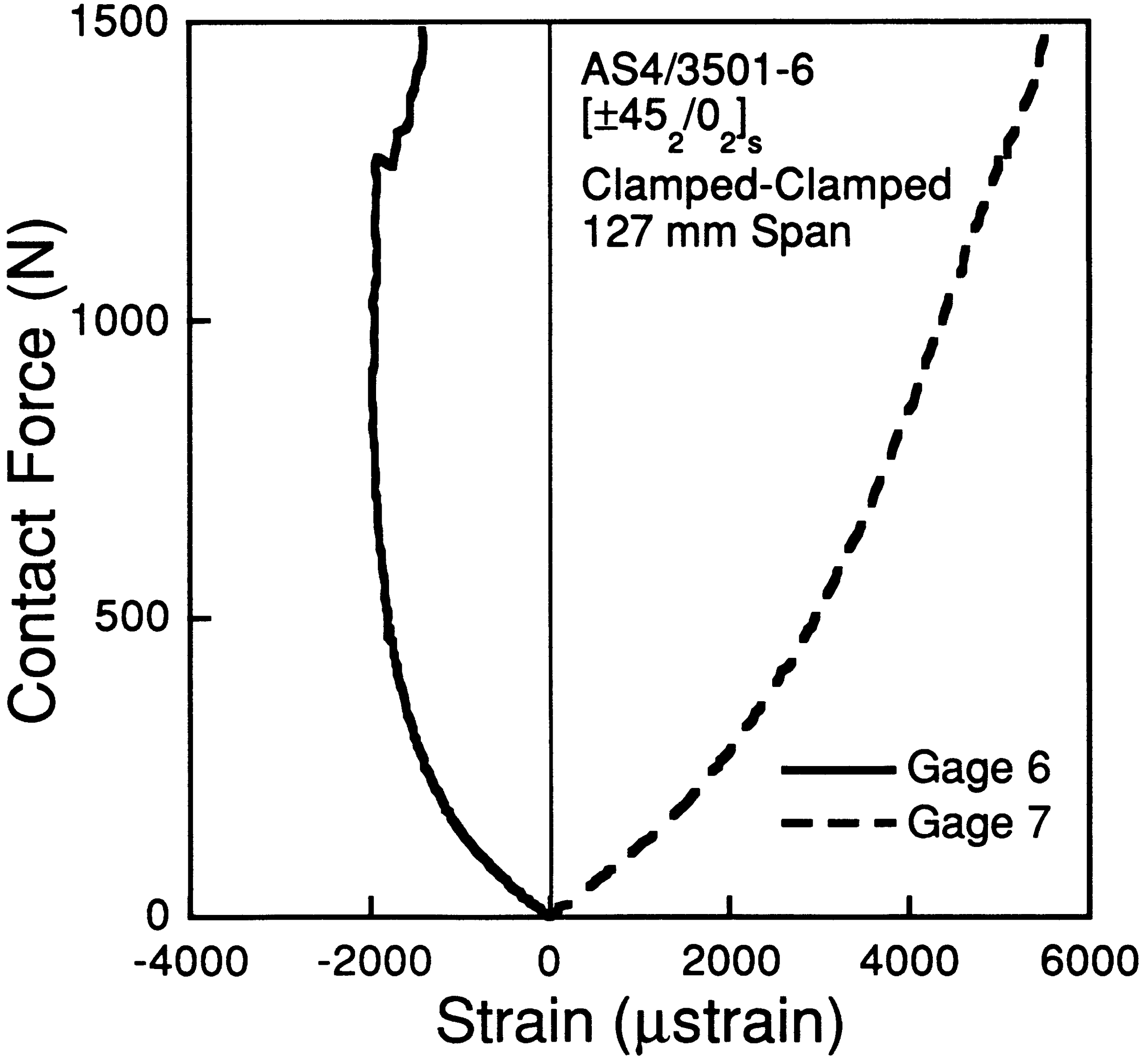

Figure B.70 Force-strain data from gages 6 and 7 (see Figure 3.3) for the specimen with a 127 mm span in a clamped-clamped support and tested to a maximum contact force of 1479 N.

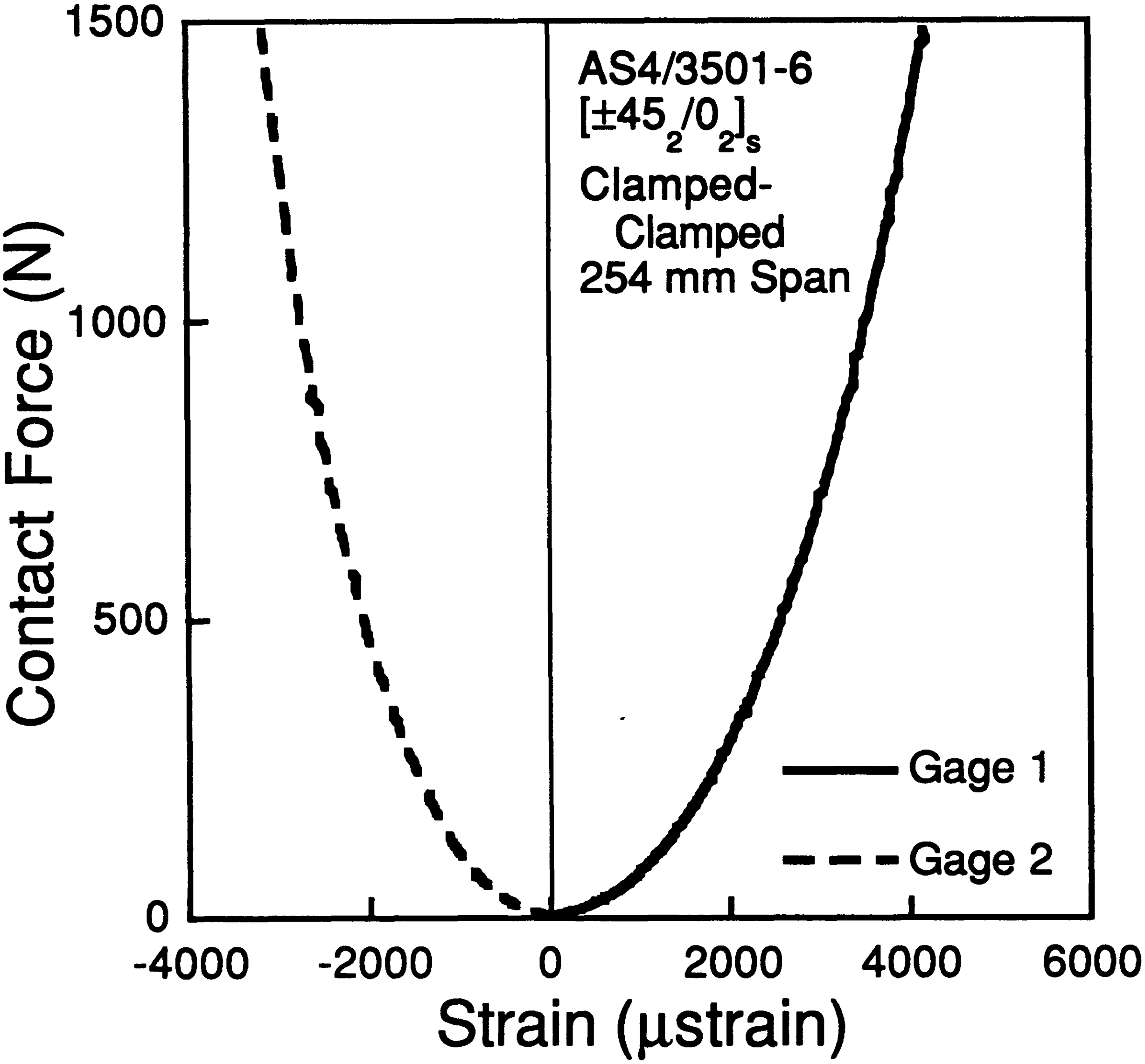

Figure B.71 Force-strain data from gages 1 and 2 (see Figure 3.3) for the specimen with a 254 mm span in a clamped-clamped support and tested to a maximum contact force of 1479 N.

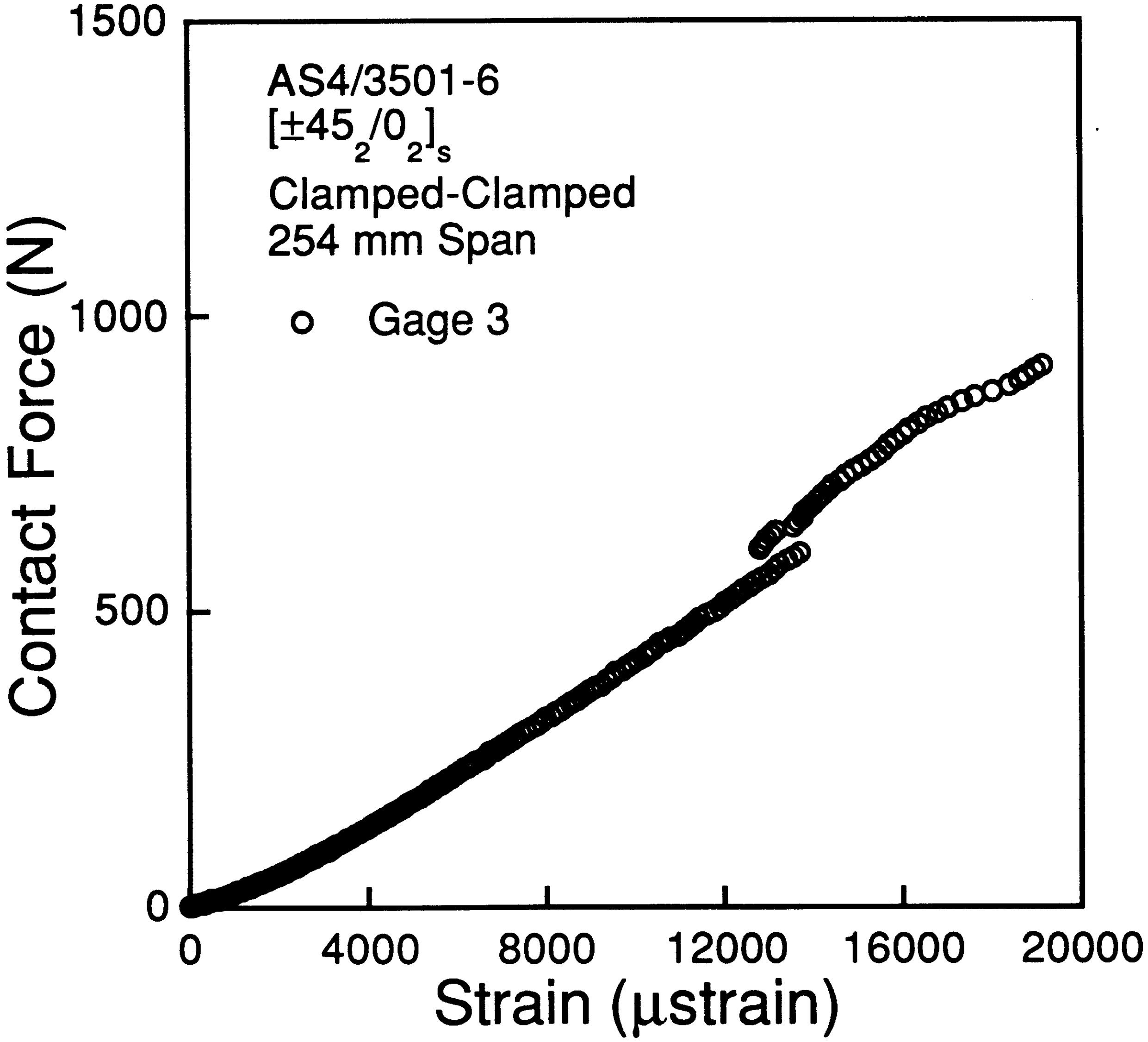

Figure B.72 Force-strain data from gage 3 (see Figure 3.3) for the specimen with a 254 mm span in a clamped-clamped support and tested to a maximum contact force of 1479 N.

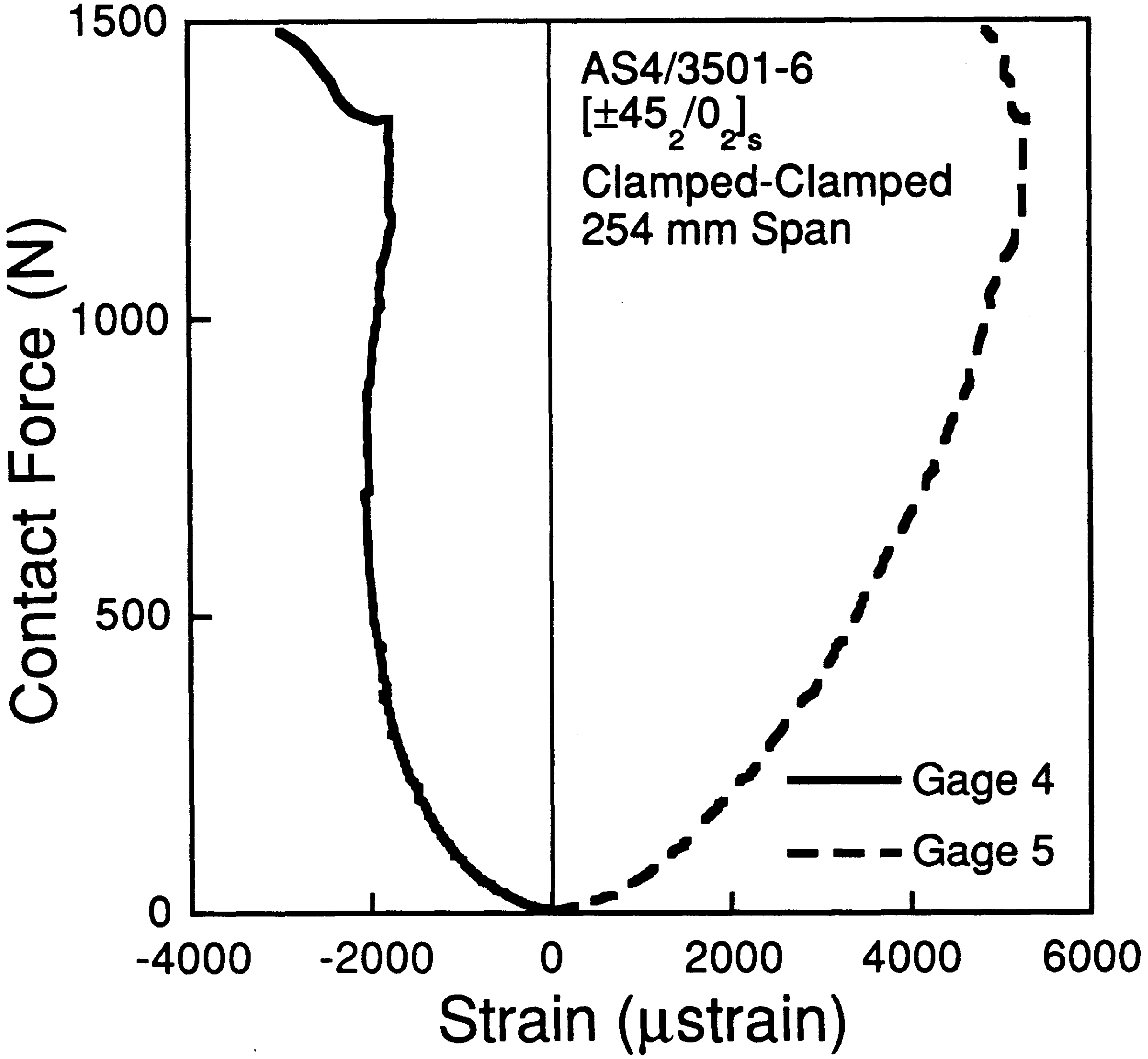

Figure B.73 Force-strain data from gages 4 and 5 (see Figure 3.3) for the specimen with a 254 mm span in a clamped-clamped support and tested to a maximum contact force of 1479 N.

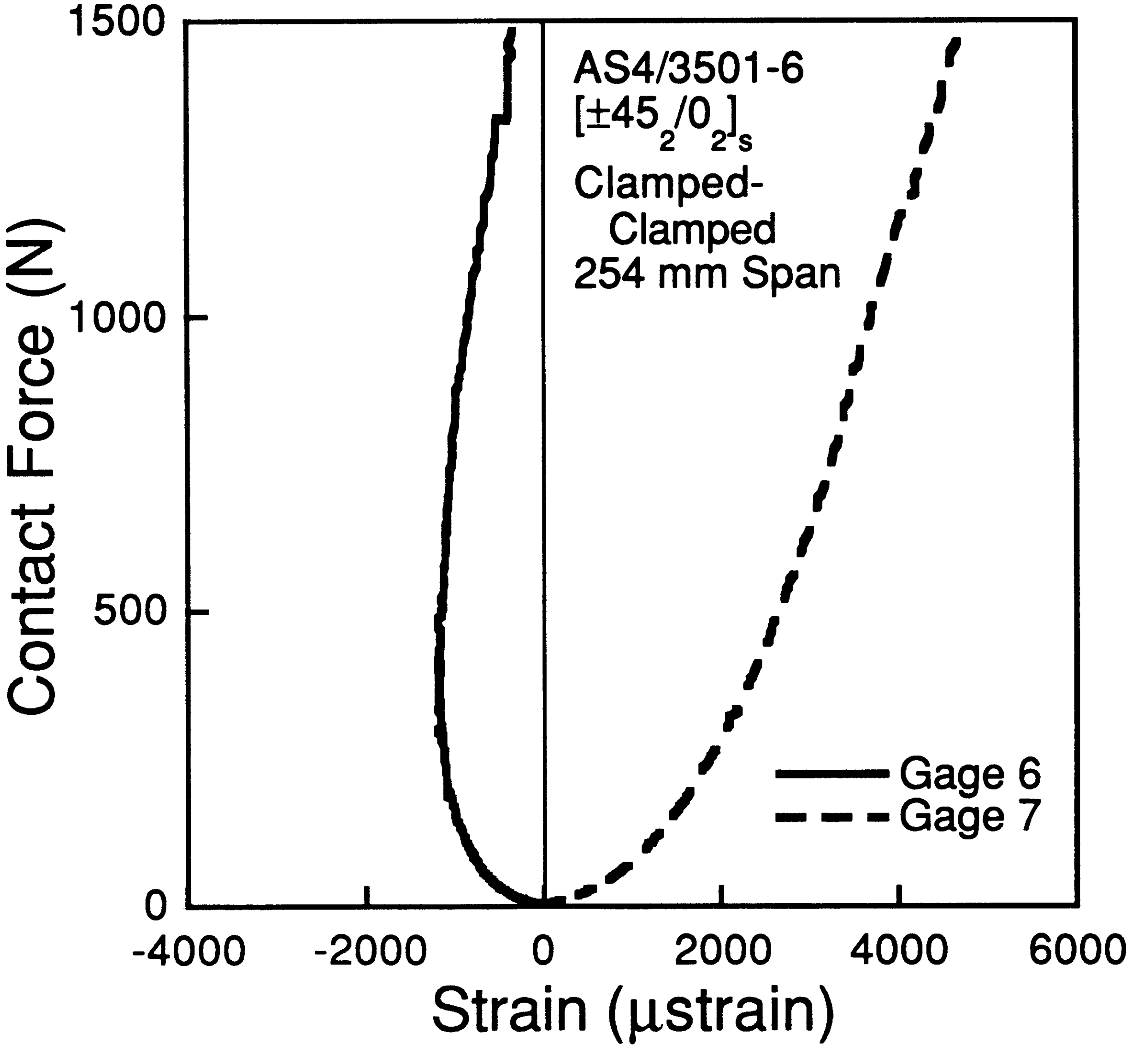

Figure B.74 Force-strain data from gages 6 and 7 (see Figure 3.3) for the specimen with a 254 mm span in a clamped-clamped support and tested to a maximum contact force of 1479 N.

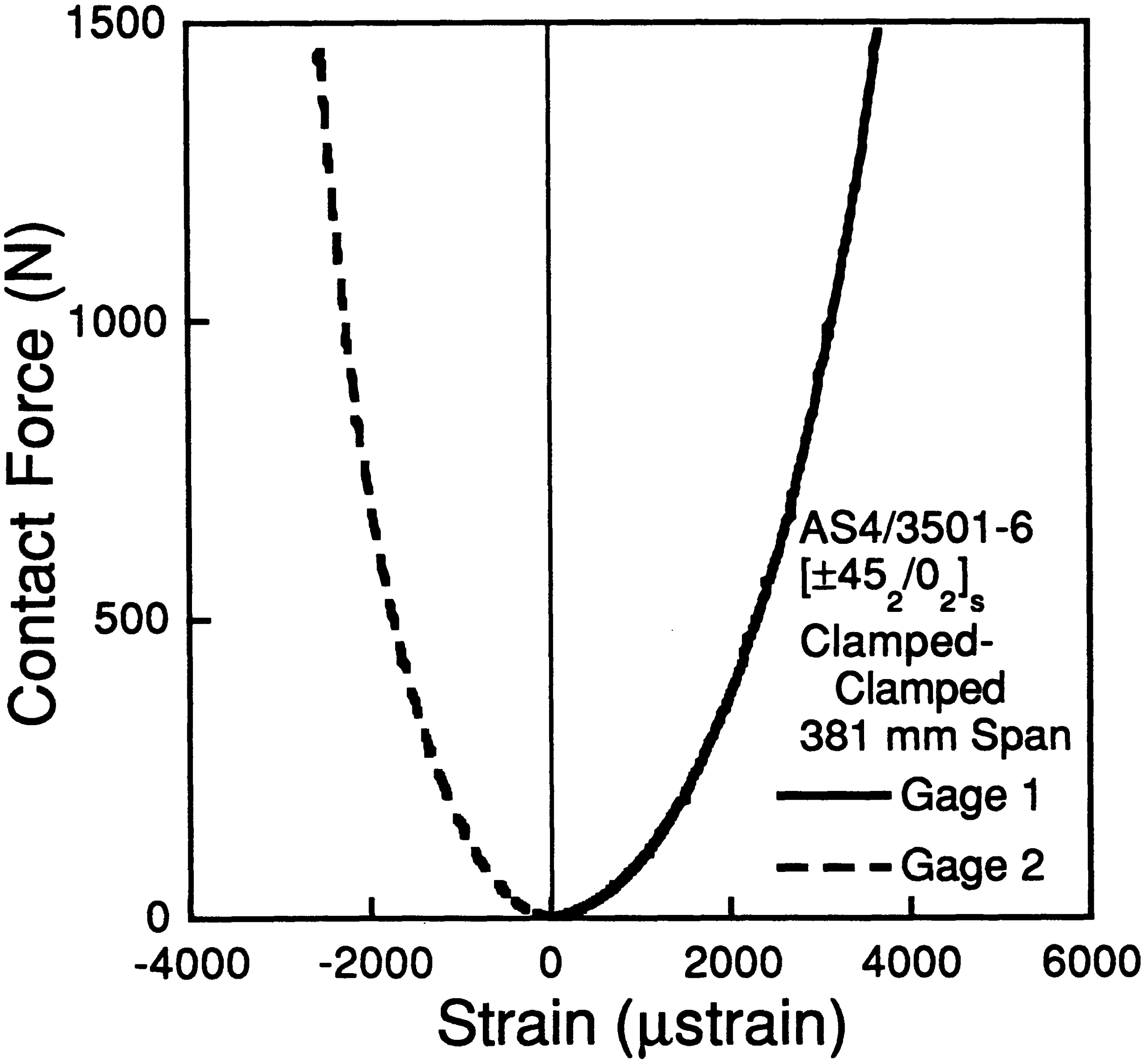

Figure B.75 Force-strain data from gages 1 and 2 (see Figure 3.3) for the specimen with a 381 mm span in a clamped-clamped support and tested to a maximum contact force of 1479 N.

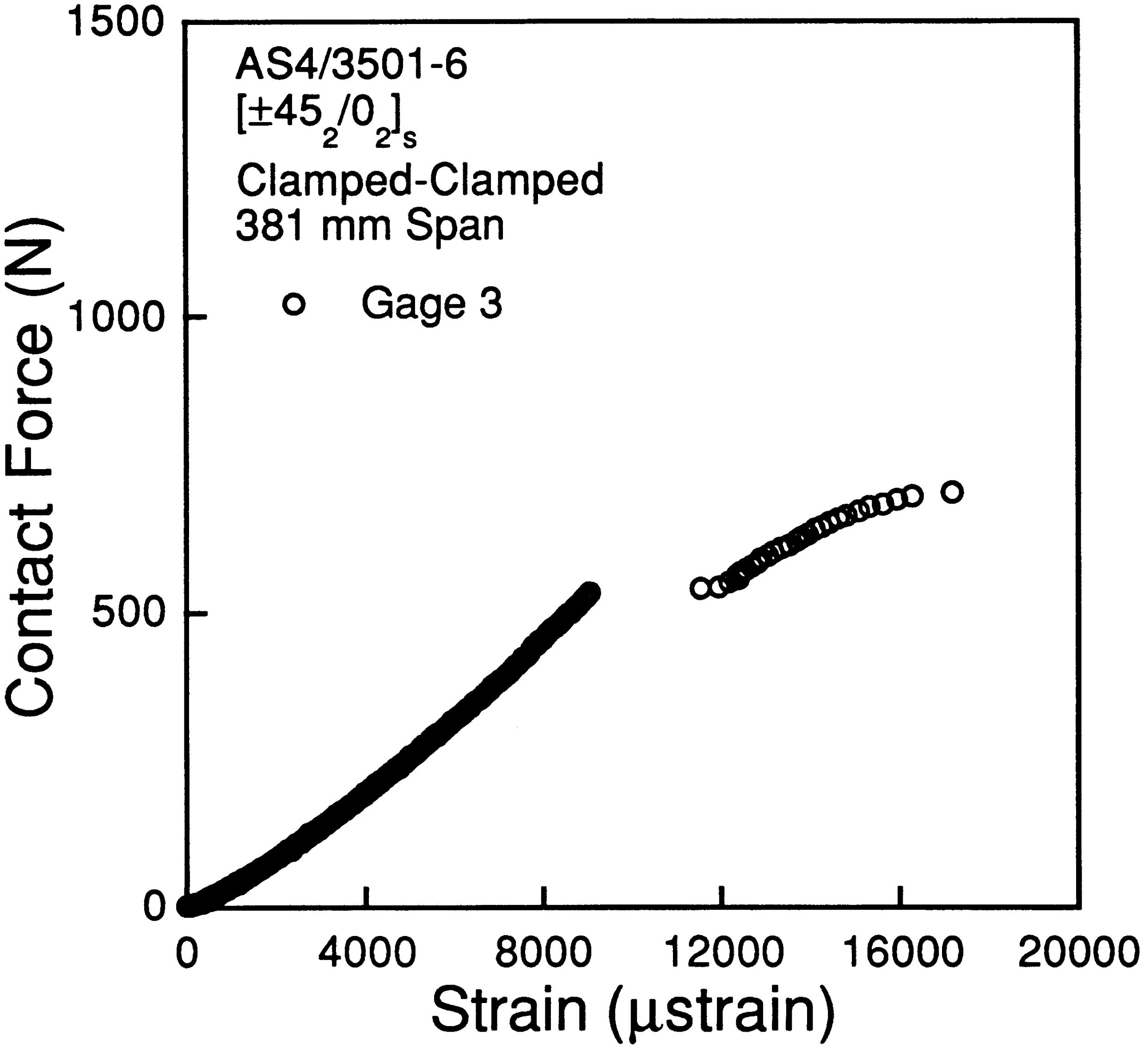

Figure B.76 Force-strain data from gage 3 (see Figure 3.3) for the specimen with a 381 mm span in a clamped-clamped support and tested to a maximum contact force of 1479 N.

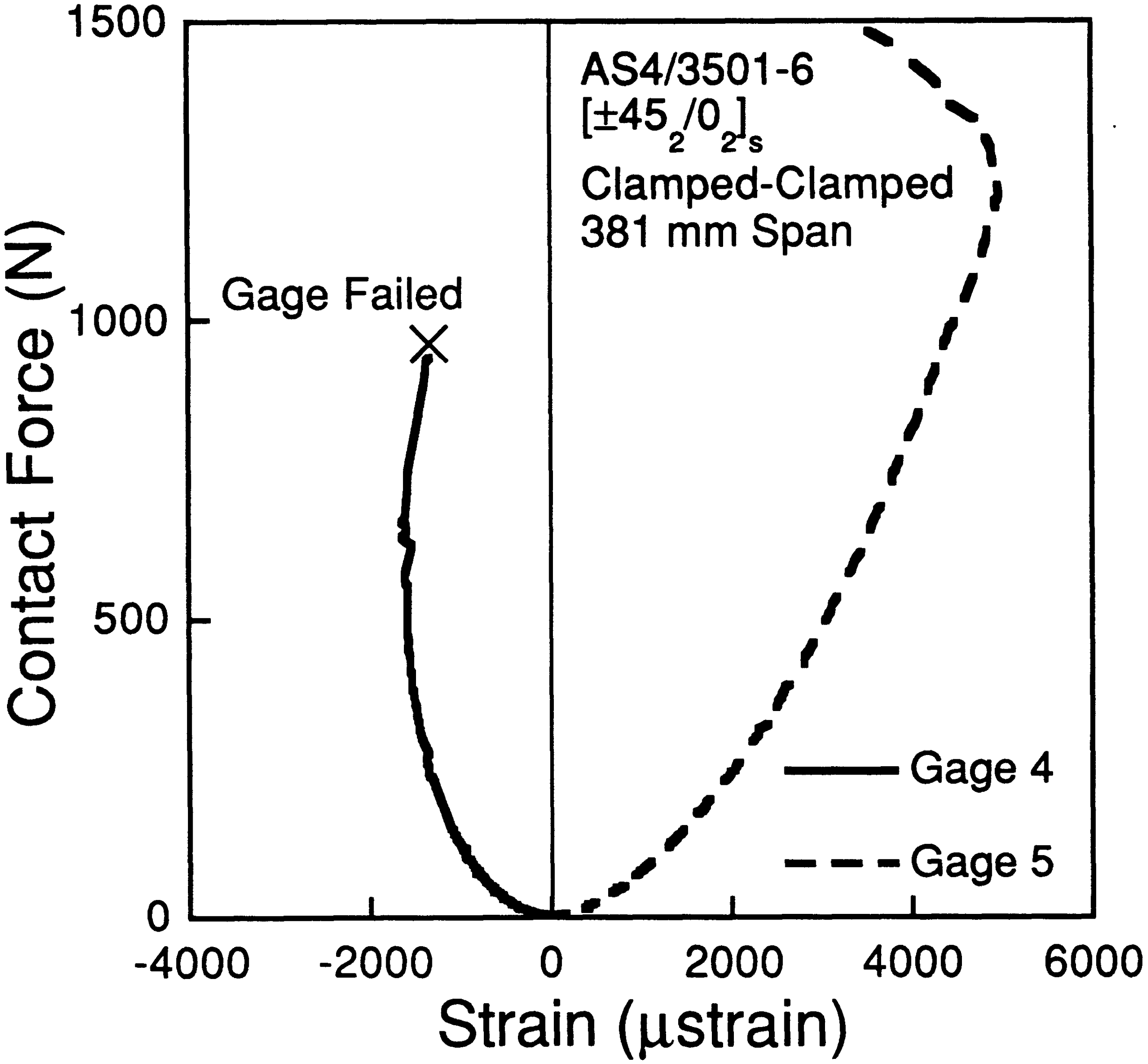

Figure B.77 Force-strain data from gages 4 and 5 (see Figure 3.3) for the specimen with a 381 mm span in a clamped-clamped support and tested to a maximum contact force of 1479 N.

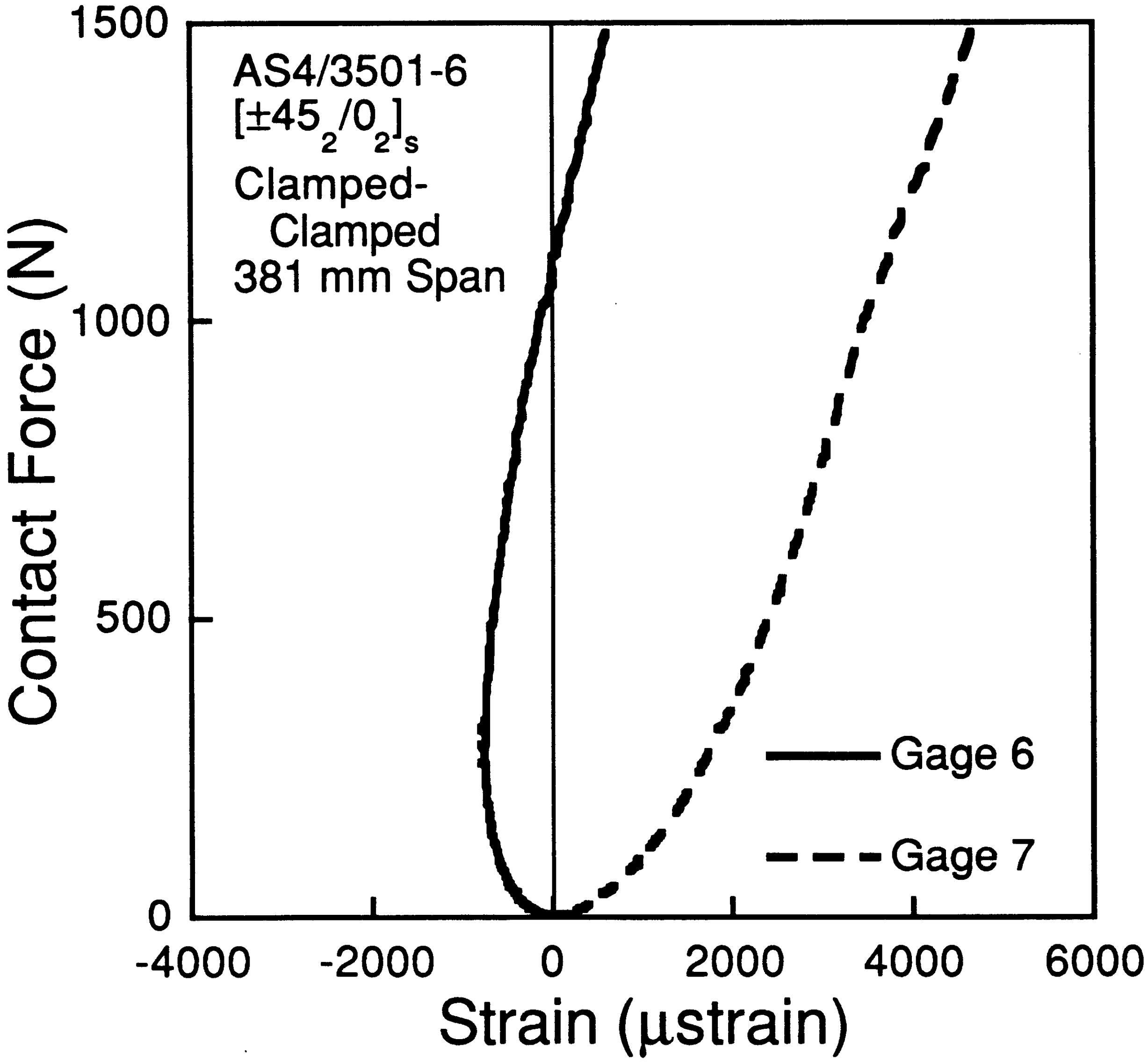

Figure B.78 Force-strain data from gages 6 and 7 (see Figure 3.3) for the specimen with a 381 mm span in a clamped-clamped support and tested to a maximum contact force of 1479 N.

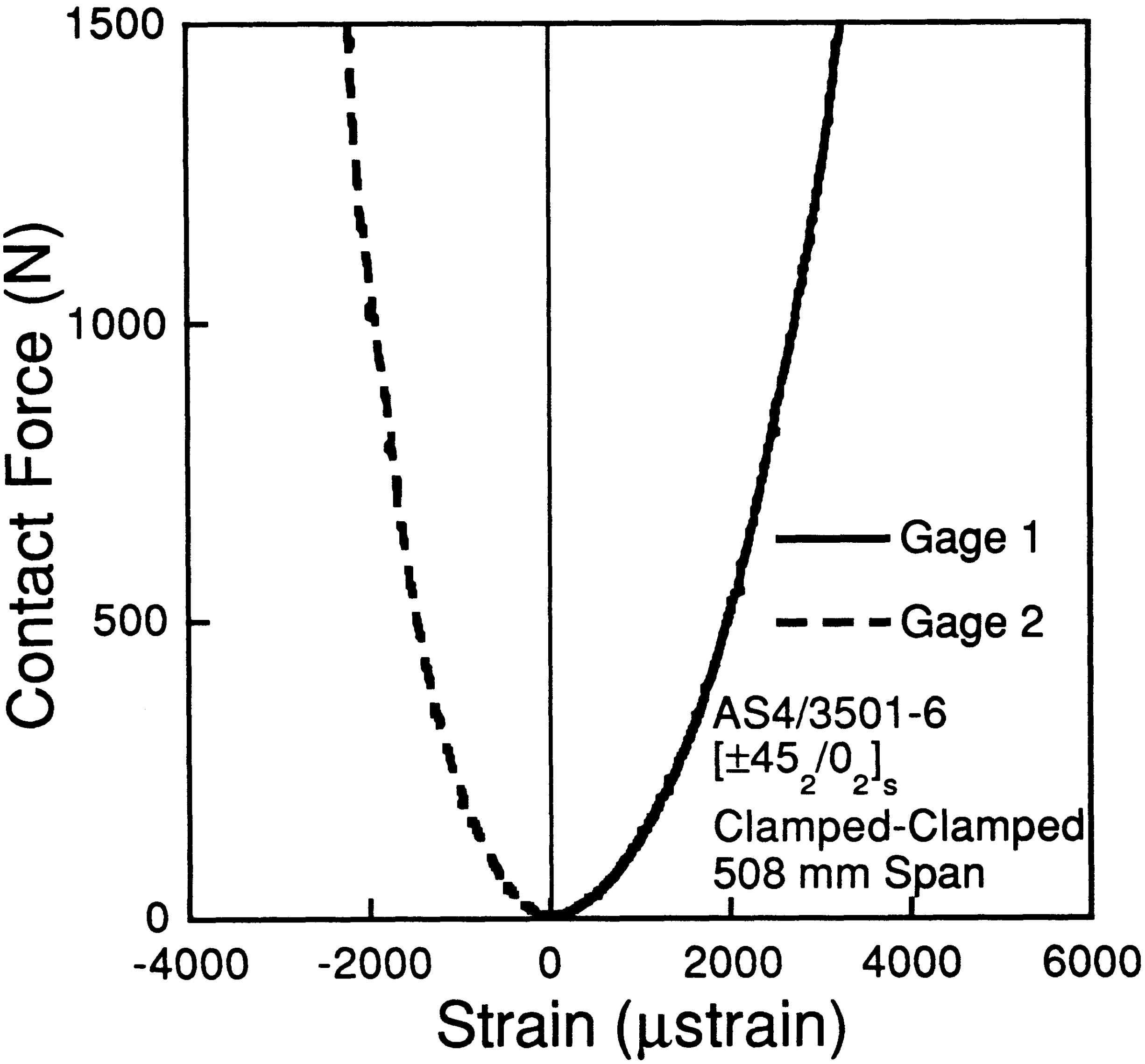

Figure B.79 Force-strain data from gages 1 and 2 (see Figure 3.3) for the specimen with a 508 mm span in a clamped-clamped support and tested to a maximum contact force of 1479 N.

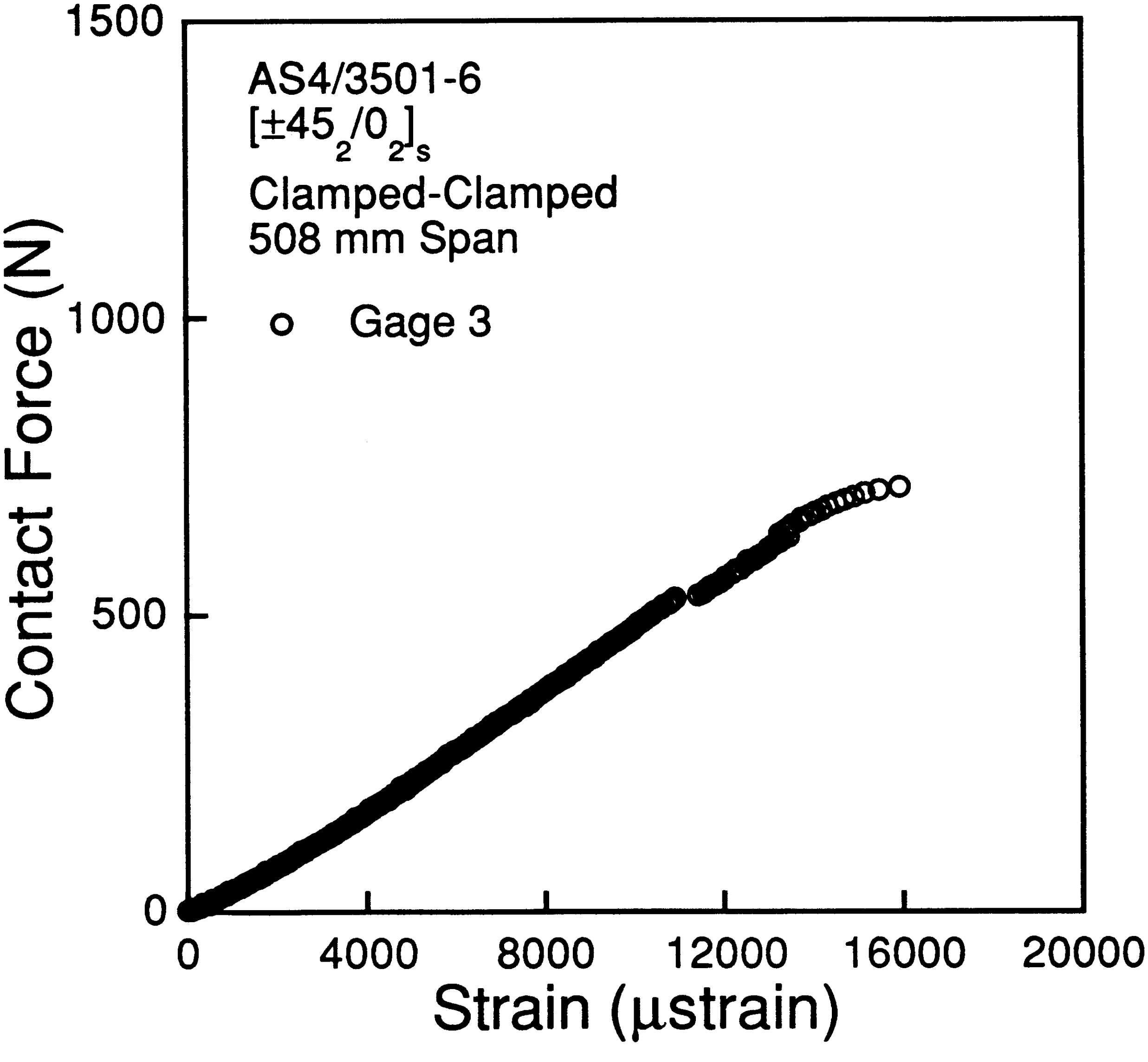

Figure B.80 Force-strain data from gage 3 (see Figure 3.3) for the specimen with a 508 mm span in a clamped-clamped support and tested to a maximum contact force of 1479 N.

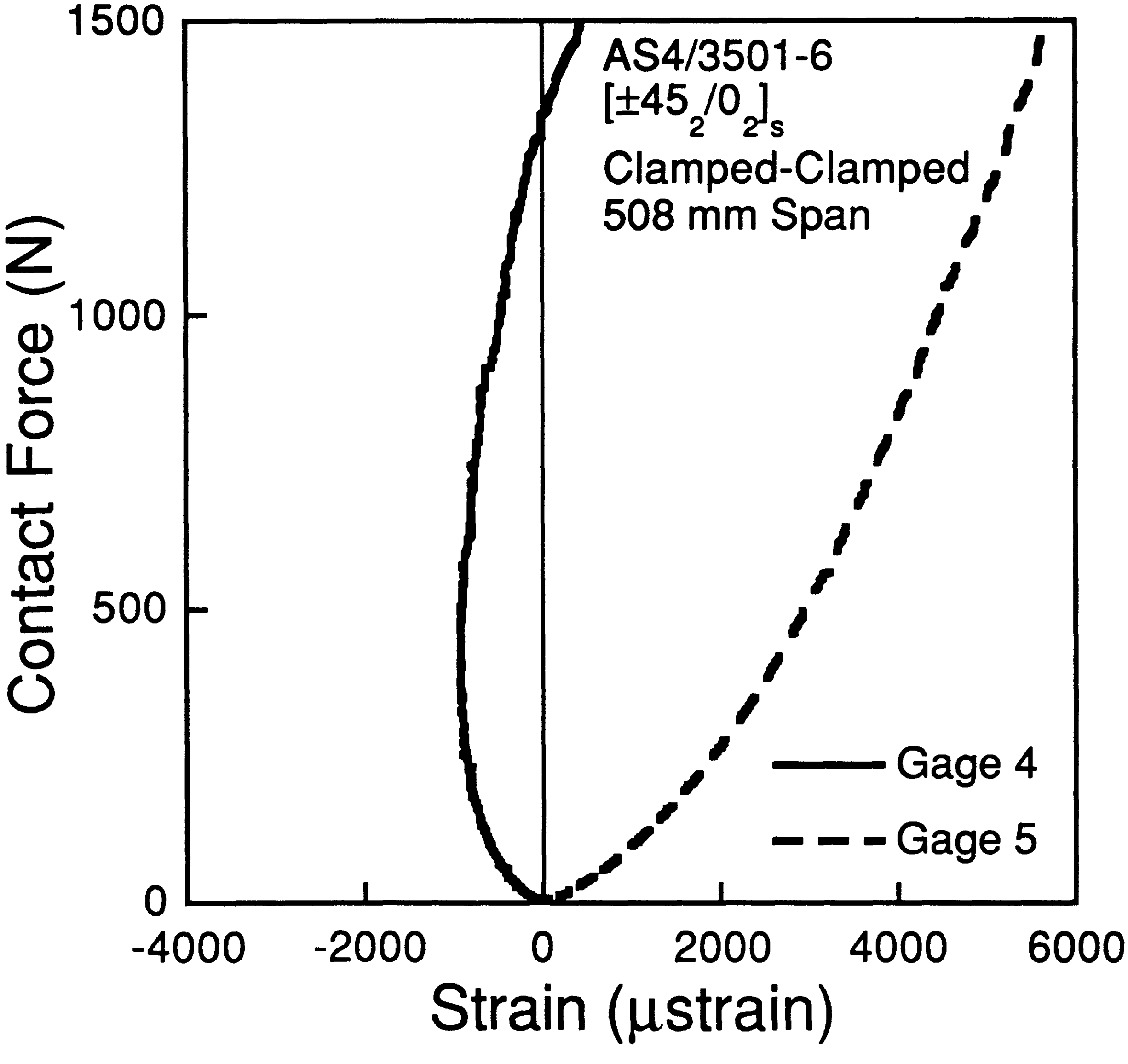

Figure B.81 Force-strain data from gages 4 and 5 (see Figure 3.3) for the specimen with a 508 mm span in a clamped-clamped support and tested to a maximum contact force of 1479 N.

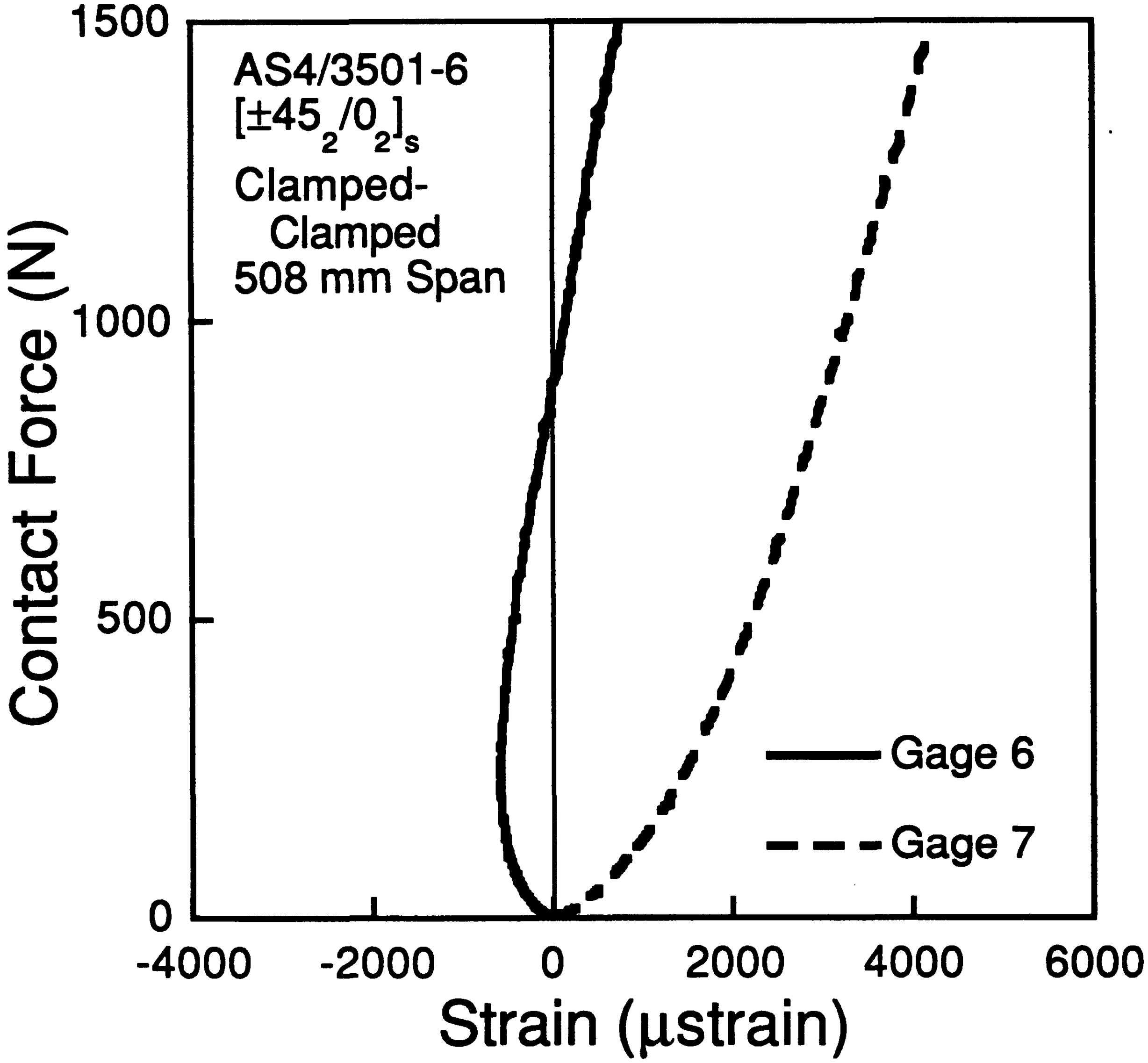

Figure B.82 Force-strain data from gages 6 and 7 (see Figure 3.3) for the specimen with a 508 mm span in a clamped-clamped support and tested to a maximum contact force of 1479 N.

APPENDIX C: PROGRAM STATIC1

An explanation of the input data file "Stiff.dat" for the program STATIC1 is presented first, followed by a sample output file, "Solve.out". The program listing for STATIC1, as described in Chapter 4, is provided at the end of this Appendix.

This program has several redundant parts and parts which are not used in normal operation. These parts were used in the development and debugging of the program. These parts facilitate splitting the program into parts which may be used as separate programs. This was done during development to speed the evaluation and debugging of the latter parts of the program. The stiffness matrix parts of the program may be used as one program, outputting the matrices to stiffness data files (the names of which are designated in the input file). The solution part may also be used as a stand-alone program, reading the output files from the stiffness matrix part and then solving the equations. Splitting the program this way has the advantage that the stiffness matrices do not have to be recalculated every time a solution of the equations is desired for a particular plate geometry. This saves significantly on the total time to run multiple cases and adds flexibility in terms of rerunning cases that may have had mistakes in the input file without having to rerun the whole program. The drawback is that appropriate storage space for the large nonlinear stiffness matrix must be available - the matrices for a 9 by 9 odd modes only case would require approximately 10 megabytes of storage space using this alternate scheme.

C.1 Sample Input

An example of the input data file "Stiff.dat" is provided here. The input parameters outlined in Table 4.1 are utilized in this example. The data listed is for an AS4/3501-6 $[\pm 45_2/0_2]_s$ laminate of dimensions 254 by 89 mm, using 9 by 9 odd modes only, a β-factor of 0.030, clamped-clamped boundary conditions in the x-direction, and free-free boundary conditions in the y-direction. This file requests the program to output data at twenty forces between 930 N and zero and for five locations on the x-direction (longitudinal) centerline of the plate, at one-eighth span intervals (0, 1/8, 1/4, 3/8, and 1/2 span). Following the listing for the data file is a line by line explanation of the required input data.

```
AS4/3501-6 [+-45 2/0 2]s 254 x 89 mm
Nonlinearity Factor beta = 0.030
9x9 Odd Modes only
Max. Contact Force 930N, Strain Gauge Scheme 1
Psx Psy  u   v   w
1 1 0.030
3 4 3 4 7 4 3 7 3 4
5 5 5 5 5 5
1
0.254 0.089 0.001608
125547200.0 54249900.0 37682300.0 0.0 0.0 42568300.0
17.0715 15.3645 11.2721 5.121 5.121 12.3249
6920000.0 8060000.0 0.0 0.833
0.0
20
0.0 0.0 0.0 0.0 0.0 0.0 0.0 0.0 0.0 0.0 0.0 0.0 0.0 0.0 0.0
0.0 0.0 0.0 0.0 0.0 0.0 0.0 0.0 0.0 0.0
930. 20
0.000001
5
0.127000 0.095250 0.063500 0.031750 0.000000
0.044500 0.044500 0.044500 0.044500 0.044500
'5xStiff1','5xStiff3'
'Solve.out'
```

The format of the input data file, "stiff.dat", is described as follows:

line 1-5: comment lines (program does not read)
line 6 : Ibx, Iby, beta
line 7 : IBCX(N), IBCY(N)
line 8 : NCX, NCY, NDX, NDY, NX, NY
line 9 : IEO
line 10 : XL, YL, THICK
line 11 : A11, A22, A12, A16, A26, A66
line 12 : D11, D22, D12, D16, D26, D66
line 13 : G44, G55, G45, sc
line 14 : cf
line 15 : LOOP
line 16 : E(I)
line 17 : F, NF
line 18 : ERR
line 19 : NKX
line 20 : X(1,I)
line 21 : X(2,I)
line 22 : OSTR1,OSTR3
line 23 : OSTR4

where,

Ibx, Iby : nonlinearity index numbers (integer) in the x and y direction
1 => include nonlinear effect
0 => do not include nonlinear effect (linear)

beta : degree of in-plane flexibility ranging from 0.0 to 1.0
0.0 => perfectly sliding case
1.0 => perfectly clamped case

IBCX, IBCY : index numbers for the boundary conditions in x and y directions for the u, v, and w displacements followed by the Ψ_x and Ψ_y rotation variables (input as x and y boundary conditions for the u displacement, then x and y boundary conditions for the v displacement, and so on)
1 => simply supported - simply supported
2 => clamped - free
3 => clamped - clamped
4 => free - free
5 => simply supported - clamped
6 => simply supported - free
7 => free - free even modes only (to be used when even modes are needed for the free-free boundary condition during odd modes only cases)

NCX, NCY : number of u modes in the x and y directions
NDX, NDY : number of v modes in the x and y directions
NX, NY : number of w modes in the x and y directions

Note that if odd modes are used, the number input will be (N+1)/2, or the number of odd modes, where N is the desired number of modes

IEO : switch for turning off even modes
0 => both odd and even modes
1 => odd modes only

XL, YL : dimensions of plate in the x and y directions (m)

THICK : thickness of the plate (m)

A's : tensor components of A matrix (N/m)
D's : tensor components of D matrix (N-m)
G's : shear stiffness components (N/m)

sc : shear correction factor

cf : for point loading, let cf = 0.0 (This program is capable of dealing with double-cosine type distributed patch loading, although this has not been verified. In the case where patch loading is used, this is the dimension, in (m), of the square shape of the patched loading.)

LOOP : max. number of Newton-Raphson iterations allowed

E(I) : first guess at w amplitudes in Newton-Raphson - there must be NX*NY guesses for the program to work

F : magnitude of contact force desired in (N)

NF : no. of force calculations (=1 just calculates for F) with interval F/NF

ERR : convergence condition on percentage change between current and previous guess in Newton-Raphson method

NKX : number of locations where data is to be calculated

X(1,I) : X coordinate of desired data location in (m)

X(2,I) : Y coordinate of desired data location in (m)

OSTR1&3 : Input filename for stiffness matrices, 18 chars. max, must be written within apostrophes like: 'xxxxxxx'

OSTR4 : Output filename for final solution, 18 characters max, must be written within apostrophes like: 'xxxxxxx'

C.2 Sample Output

A sample output data file, "Solve.out", as specified in the input file "Stiff.dat" listed in section C.1, is provided here. The first three lines give a heading summarizing some of the input information for future identification of the file. The first line indicates the number of modes input, in this case indicating the actual number of modes used. Since this is a 9 by 9 odd modes only case, the actual number of modes used will be five in each direction. The other lines are self-explanatory. After the heading data comes a listing of the raw modal amplitudes, $\underline{E}_i$ and $\underline{A}_i$, calculated by the program. These may be useful in debugging the program or identifying nonconvergence. After this comes the output data, which lists from left to right, the x and y locations (in meters) at which the data is calculated, the force (in Newtons) for which the data is calculated, the deflection (in meters), the extensional strain (in m/m), and the bending strain (in m/m) at the listed location and force. This is repeated for all the locations and forces desired, as prescribed in the input file. The format of the output file was designed for easy conversion to spreadsheet formats used on Apple Macintosh® computers for data reduction.

```
This is a  5 x  5 mode case
The beta factor is -> 0.03000
The initial guess vector is ->
 0.0000D+00  0.0000D+00  0.0000D+00  0.0000D+00  0.0000D+00
 0.0000D+00  0.0000D+00  0.0000D+00  0.0000D+00  0.0000D+00
 0.0000D+00  0.0000D+00  0.0000D+00  0.0000D+00  0.0000D+00
 0.0000D+00  0.0000D+00  0.0000D+00  0.0000D+00  0.0000D+00
 0.0000D+00  0.0000D+00  0.0000D+00  0.0000D+00  0.0000D+00
ØØØØØØØØØØØØØØØ
The E, A Vectors for force    930.0 are ->
 0.1059D-01 -0.4612D-03  0.7354D-04  0.1577D-06  0.5737D-05
-0.5126D-04  0.4931D-06 -0.5085D-05 -0.3567D-06 -0.1273D-05
 0.2300D-05 -0.9956D-06  0.5743D-06 -0.5755D-04  0.2548D-04
-0.9878D-06  0.4431D-04 -0.2312D-04  0.8012D-05 -0.5047D-05
 0.9611D-05 -0.8586D-05  0.1505D-05 -0.2236D-05  0.2673D-06

-0.1056D-01  0.4439D-03 -0.7326D-04 -0.5251D-05 -0.8001D-05
```

```
 0.4733D-04 -0.2721D-05  0.3281D-05 -0.1922D-05 -0.2758D-06
-0.2153D-05  0.2776D-06 -0.6818D-06  0.5922D-04 -0.2503D-04
 0.7873D-07 -0.3999D-04  0.2126D-04 -0.7416D-05  0.3722D-05
-0.9229D-05  0.7516D-05 -0.1588D-05  0.1403D-05 -0.5354D-06
===============
 X-Coord    Y-Coord       Force         w             Ep011         Kap11
0.127000   0.044500     930.0       0.1967e-01    0.5478e-19    0.1149e-01
0.095250   0.044500     930.0       0.1515e-01    0.4789e-03   -0.6172e-03
0.063500   0.044500     930.0       0.9348e-02    0.4946e-03   -0.7001e-03
0.031750   0.044500     930.0       0.3709e-02    0.4535e-03   -0.1064e-02
0.000000   0.044500     930.0       0.1013e-03    0.5294e-07   -0.8494e-02
0.127000   0.044500     881.1       0.1921e-01    0.5106e-19    0.1111e-01
0.095250   0.044500     881.1       0.1481e-01    0.4580e-03   -0.5510e-03
0.063500   0.044500     881.1       0.9134e-02    0.4754e-03   -0.6701e-03
0.031750   0.044500     881.1       0.3610e-02    0.4335e-03   -0.1067e-02
0.000000   0.044500     881.1       0.9896e-04    0.5055e-07   -0.8179e-02
0.127000   0.044500     832.1       0.1873e-01    0.4738e-19    0.1072e-01
0.095250   0.044500     832.1       0.1447e-01    0.4367e-03   -0.4831e-03
0.063500   0.044500     832.1       0.8912e-02    0.4558e-03   -0.6396e-03
0.031750   0.044500     832.1       0.3507e-02    0.4131e-03   -0.1069e-02
0.000000   0.044500     832.1       0.9656e-04    0.4814e-07   -0.7859e-02
0.127000   0.044500     783.2       0.1824e-01    0.4375e-19    0.1032e-01
0.095250   0.044500     783.2       0.1411e-01    0.4150e-03   -0.4135e-03
0.063500   0.044500     783.2       0.8682e-02    0.4359e-03   -0.6085e-03
0.031750   0.044500     783.2       0.3401e-02    0.3925e-03   -0.1072e-02
0.000000   0.044500     783.2       0.9408e-04    0.4569e-07   -0.7533e-02
0.127000   0.044500     734.2       0.1772e-01    0.4016e-19    0.9906e-02
0.095250   0.044500     734.2       0.1373e-01    0.3929e-03   -0.3422e-03
0.063500   0.044500     734.2       0.8442e-02    0.4156e-03   -0.5768e-03
0.031750   0.044500     734.2       0.3291e-02    0.3715e-03   -0.1074e-02
0.000000   0.044500     734.2       0.9150e-04    0.4322e-07   -0.7200e-02
0.127000   0.044500     685.3       0.1718e-01    0.3662e-19    0.9479e-02
0.095250   0.044500     685.3       0.1334e-01    0.3704e-03   -0.2692e-03
0.063500   0.044500     685.3       0.8193e-02    0.3948e-03   -0.5444e-03
0.031750   0.044500     685.3       0.3177e-02    0.3501e-03   -0.1076e-02
0.000000   0.044500     685.3       0.8880e-04    0.4071e-07   -0.6861e-02
0.127000   0.044500     636.3       0.1662e-01    0.3315e-19    0.9038e-02
0.095250   0.044500     636.3       0.1293e-01    0.3475e-03   -0.1945e-03
0.063500   0.044500     636.3       0.7931e-02    0.3736e-03   -0.5115e-03
0.031750   0.044500     636.3       0.3058e-02    0.3283e-03   -0.1078e-02
0.000000   0.044500     636.3       0.8598e-04    0.3816e-07   -0.6514e-02
0.127000   0.044500     587.4       0.1603e-01    0.2975e-19    0.8582e-02
0.095250   0.044500     587.4       0.1250e-01    0.3241e-03   -0.1182e-03
0.063500   0.044500     587.4       0.7657e-02    0.3519e-03   -0.4779e-03
0.031750   0.044500     587.4       0.2934e-02    0.3061e-03   -0.1078e-02
0.000000   0.044500     587.4       0.8302e-04    0.3558e-07   -0.6159e-02
0.127000   0.044500     538.4       0.1541e-01    0.2642e-19    0.8109e-02
0.095250   0.044500     538.4       0.1204e-01    0.3002e-03   -0.4038e-04
0.063500   0.044500     538.4       0.7368e-02    0.3296e-03   -0.4436e-03
0.031750   0.044500     538.4       0.2805e-02    0.2834e-03   -0.1078e-02
0.000000   0.044500     538.4       0.7991e-04    0.3296e-07   -0.5795e-02
0.127000   0.044500     489.5       0.1475e-01    0.2318e-19    0.7617e-02
0.095250   0.044500     489.5       0.1156e-01    0.2758e-03    0.3870e-04
0.063500   0.044500     489.5       0.7063e-02    0.3067e-03   -0.4088e-03
0.031750   0.044500     489.5       0.2669e-02    0.2603e-03   -0.1076e-02
0.000000   0.044500     489.5       0.7661e-04    0.3029e-07   -0.5422e-02
0.127000   0.044500     440.5       0.1405e-01    0.2004e-19    0.7106e-02
0.095250   0.044500     440.5       0.1105e-01    0.2509e-03    0.1187e-03
```

```
0.063500  0.044500    440.5      0.6738e-02   0.2830e-03   -0.3733e-03
0.031750  0.044500    440.5      0.2525e-02   0.2367e-03   -0.1072e-02
0.000000  0.044500    440.5      0.7309e-04   0.2758e-07   -0.5038e-02
0.127000  0.044500    391.6      0.1331e-01   0.1702e-19    0.6571e-02
0.095250  0.044500    391.6      0.1050e-01   0.2253e-03    0.1991e-03
0.063500  0.044500    391.6      0.6389e-02   0.2586e-03   -0.3372e-03
0.031750  0.044500    391.6      0.2373e-02   0.2125e-03   -0.1066e-02
0.000000  0.044500    391.6      0.6933e-04   0.2481e-07   -0.4641e-02
0.127000  0.044500    342.6      0.1250e-01   0.1412e-19    0.6010e-02
0.095250  0.044500    342.6      0.9899e-02   0.1991e-03    0.2791e-03
0.063500  0.044500    342.6      0.6013e-02   0.2331e-03   -0.3005e-03
0.031750  0.044500    342.6      0.2210e-02   0.1878e-03   -0.1055e-02
0.000000  0.044500    342.6      0.6526e-04   0.2199e-07   -0.4231e-02
0.127000  0.044500    293.7      0.1162e-01   0.1137e-19    0.5419e-02
0.095250  0.044500    293.7      0.9243e-02   0.1722e-03    0.3570e-03
0.063500  0.044500    293.7      0.5601e-02   0.2065e-03   -0.2633e-03
0.031750  0.044500    293.7      0.2034e-02   0.1624e-03   -0.1039e-02
0.000000  0.044500    293.7      0.6081e-04   0.1909e-07   -0.3803e-02
0.127000  0.044500    244.7      0.1065e-01   0.8784e-20    0.4791e-02
0.095250  0.044500    244.7      0.8513e-02   0.1446e-03    0.4305e-03
0.063500  0.044500    244.7      0.5144e-02   0.1784e-03   -0.2255e-03
0.031750  0.044500    244.7      0.1842e-02   0.1363e-03   -0.1014e-02
0.000000  0.044500    244.7      0.5587e-04   0.1611e-07   -0.3354e-02
0.127000  0.044500    195.8      0.9556e-02   0.6398e-20    0.4117e-02
0.095250  0.044500    195.8      0.7679e-02   0.1161e-03    0.4952e-03
0.063500  0.044500    195.8      0.4624e-02   0.1485e-03   -0.1873e-03
0.031750  0.044500    195.8      0.1629e-02   0.1093e-03   -0.9757e-03
0.000000  0.044500    195.8      0.5025e-04   0.1304e-07   -0.2878e-02
0.127000  0.044500    146.8      0.8273e-02   0.4241e-20    0.3381e-02
0.095250  0.044500    146.8      0.6693e-02   0.8663e-04    0.5426e-03
0.063500  0.044500    146.8      0.4014e-02   0.1160e-03   -0.1484e-03
0.031750  0.044500    146.8      0.1385e-02   0.8152e-04   -0.9147e-03
0.000000  0.044500    146.8      0.4365e-04   0.9835e-08   -0.2364e-02
0.127000  0.044500     97.9      0.6683e-02   0.2362e-20    0.2553e-02
0.095250  0.044500     97.9      0.5452e-02   0.5609e-04    0.5530e-03
0.063500  0.044500     97.9      0.3252e-02   0.7973e-04   -0.1084e-03
0.031750  0.044500     97.9      0.1093e-02   0.5267e-04   -0.8104e-03
0.000000  0.044500     97.9      0.3540e-04   0.6469e-08   -0.1788e-02
0.127000  0.044500     48.9      0.4447e-02   0.8411e-21    0.1550e-02
0.095250  0.044500     48.9      0.3667e-02   0.2449e-04    0.4679e-03
0.063500  0.044500     48.9      0.2171e-02   0.3788e-04   -0.6486e-04
0.031750  0.044500     48.9      0.7040e-03   0.2290e-04   -0.6024e-03
0.000000  0.044500     48.9      0.2368e-04   0.2893e-08   -0.1092e-02
0.127000  0.044500      0.0      0.4248e-14   0.2879e-45    0.9964e-15
0.095250  0.044500      0.0      0.3639e-14   0.2073e-28    0.8017e-15
0.063500  0.044500      0.0      0.2083e-14   0.4561e-28   -0.6573e-16
0.031750  0.044500      0.0      0.5781e-15   0.1840e-28   -0.7981e-15
0.000000  0.044500      0.0      0.2300e-16   0.2730e-32   -0.7280e-15
```

C.3 Program Listing

```
C ====================================================================
      PROGRAM STATIC1
C ====================================================================
C
C Program developed by Stephen A. Thomas,
C Adapted from the program GLOBAL1 developed by Hiroto Matsuhashi,
C Technology Laboratory for Advanced Composites,
C Department of Aeronautics and Astronautics, MIT, 1993.
C
C Copyright c1993 Massachusetts Institute of Technology
C
C Permission to use, copy, and modify this software and its
C documentation for internal purposes only and without fee is hereby
C granted provided that the above copyright notice and this permission
C appear on all copies of the code and supporting documentation.
C For any other use of this software, in original or modified form,
C including but not limited to, adaptation as the basis of a commercial
C software or hardware product, or distribution in whole or in part,
C specific prior permission and/or the appropriate licenses must be
C obtained from MIT.  This software is provided "as is" without any
C warranties whatsoever, either express or implied, including but
C not limited to the implied warranties of merchantability and fitness
C for a particular purpose.  This software is a research program, and
C MIT does not represent that it is free of errors or bugs or suitable
C for any particular task.
C
C ====================================================================
C
C  This program analyzes both linear and nonlinear global response
C  of a shear deformable composite laminated plate subjected to static
C  contact loading.  The deflection, extensional strain and bending
C  strain are output for any given point on the plate
C
C ====================================================================
C
C
C     [ Variables ]
C
      IMPLICIT DOUBLE PRECISION (A-H, O-Z)
      DOUBLE PRECISION M1,M2,M3,
     &                 K1aa,K1ab,K1ae,K1bb,K1be,K1ee,
     &                 Kigg,KI,KIII
C
      PARAMETER ( N1=7, N2=N1**2, N4=N2**3,
     &            N5=N2*2, Pi=3.14159265 )
C
      DIMENSION IBCX(5),IBCY(5)
      DIMENSION THETAX(5),THETAY(5),AX(5),AY(5)
      DIMENSION BETAX(5,N1),BETAY(5,N1),BX(5,N1),BY(5,N1)
      DIMENSION CX(5,N1),CY(5,N1),DX(5,N1),DY(5,N1),EX(5,N1),EY(5,N1)
      DIMENSION M1(N2),M2(N2),M3(N2)
      DIMENSION K1aa(N2,N2),K1ab(N2,N2),K1ae(N2,N2)
      DIMENSION K1bb(N2,N2),K1be(N2,N2),K1ee(N2,N2)
      DIMENSION Kigg(N5,N5)
      DIMENSION KI(N2,N2),Ri(N2)
      DIMENSION KIII(N2,N4)
      CHARACTER OSTR1*18,OSTR3*18
```

```
C
C
C
C      ===============
C      * Main Program
C      ===============
C
C
       CALL INPUT(IEO,Ibx,Iby,IBCX,IBCY,NX,NY,XL,YL,
     &            NCX,NCY,NDX,NDY,
     &            A11,A22,A12,A16,A26,A66,
     &            D11,D22,D12,D16,D26,D66,
     &            G44,G55,G45,cf,OSTR1,OSTR3)
C
       NXY = NX*NY
       NC = NCX*NCY
       ND = NDX*NDY
       NEN = NC+ND
C
C
       IF(IEO .EQ. 0) THEN
C
       WRITE(6,*)'ASSIGNING FULL X BEAM FUNCTIONS...'
          CALL BOUND(IBCX,NX,AX,THETAX,BETAX,BX,CX,DX,EX)
C
       WRITE(6,*)'ASSIGNING FULL Y BEAM FUNCTIONS...'
          CALL BOUND(IBCY,NY,AY,THETAY,BETAY,BY,CY,DY,EY)
C
       ENDIF
C
C
       IF(IEO .EQ. 1) THEN
C
       WRITE(6,*)'ASSIGNING ODD MODE X BEAM FUNCTIONS...'
          CALL BOUND1(IBCX,NX,AX,THETAX,BETAX,BX,CX,DX,EX)
C
       WRITE(6,*)'ASSIGNING ODD MODE Y BEAM FUNCTIONS...'
          CALL BOUND1(IBCY,NY,AY,THETAY,BETAY,BY,CY,DY,EY)
C
       ENDIF
C
C
       CALL INGRL1(NX,NY,NCX,NCY,NDX,NDY,IEO,
     &             AX,AY,THETAX,THETAY,
     &             BETAX,BETAY,BX,BY,
     &             CX,CY,DX,DY,EX,EY,
     &             A11,A22,A12,A16,A26,A66,
     &             D11,D22,D12,D16,D26,D66,
     &             G44,G55,G45,XL,YL,
     &             M1,M2,M3,Ri,cf,
     &             K1aa,K1ab,K1ae,K1bb,K1be,K1ee,Kigg)
C
C
       CALL ARRANG(NX,NY,iKaa,iKab,jKab,iKae,iKbb,iKbe,
     &              M1,M2,K1aa,K1ab,K1ae,K1bb,K1be)
C
C
       CALL CONDEN(NX,NY,iKaa,iKab,jKab,iKae,iKbb,iKbe,
```

```
     &              K1aa,K1ab,K1ae,K1bb,K1be,K1ee,KI)
C
C
      CALL INTGRL3(Ibx,Iby,NX,NY,AX,AY,THETAX,THETAY,IEO,
     &             BETAX,BETAY,BX,BY,
     &             CX,CY,DX,DY,EX,EY,
     &             A11,A22,A12,A16,A26,A66,
     &             XL,YL,KIII)
C
C
      WRITE(6,*)'Now lets solve this puppy...'
      CALL NRSOL(Ri,KI,KIII,AX,AY,THETAX,THETAY,
     &           BETAX,BETAY,BX,BY,CX,CY,DX,DY,EX,EY)
C
C
      WRITE(6,*)'DONE...'
C
      STOP
      END
C
C
C ==========================================================================
C
C
C     SUBROUTINE LIBRARIES
C
C
C ==========================================================================
C
C
C --------------------------------------------------------------------------
      SUBROUTINE  INPUT(IEO,Ibx,Iby,IBCX,IBCY,NX,NY,XL,YL,
     &                  NCX,NCY,NDX,NDY,
     &                  A11,A22,A12,A16,A26,A66,
     &                  D11,D22,D12,D16,D26,D66,
     &                  G44,G55,G45,cf,OSTR1,OSTR1)
C --------------------------------------------------------------------------
C
C  This subroutine reads data from the existing input data file called
C  "stiff.dat".  The format of the "stiff.dat" is described as follows;
C
C  line 1-5: comment line (program does not read)
C  line 6  : Ibx, Iby, beta
C  line 7  : IBCX(N), IBCY(N)
C  line 8  : NCX, NCY, NDX, NDY, NX, NY
C  line 9  : IEO
C  line 10 : XL, YL, THICK
C  line 11 : A11, A22, A12, A16, A26, A66
C  line 12 : D11, D22, D12, D16, D26, D66
C  line 13 : G44, G55, G45, sc
C  line 14 : cf
C  line 15 : Data not used here
C  line 16 : Data not used here
C  line 17 : Data not used here
C  line 18 : Data not used here
C  line 19 : Data not used here
C  line 20 : Data not used here
C  line 21 : Data not used here
```

```
C  line 22 : OSTR1,OSTR3
C  line 23 : Data not used here
C
C  where,
C
C     Ibx, Iby  : non linearity index numbers (integer) in the x and y
C                 direction
C                 1   =>  include nonlinear effect
C                 0   =>  do not include nonlinear effect (linear)
C
C     IBCX, IBCY: index numbers for the boundary conditions in x and y
C                 directions for each displacement or rotation variable
C                 1   =>  simply supported - simply supported
C                 2   =>  clamped - free
C                 3   =>  clamped - clamped
C                 4   =>  free - free
C                 5   =>  simply supported - clamped
C                 6   =>  simply supported - free
C
C     NCX, NCY  : number of u modes in the x and y directions
C     NDX, NDY  : number of v modes in the x and y directions
C     NX, NY    : number of w modes in the x and y directions
C
C     IEO       : switch for turning off even modes
C                 0   =>  both odd and even modes
C                 1   =>  odd modes only
C
C     XL, YL    : dimensions of plate in the x and y directions (m)
C
C     THICK     : thickness of the plate (m)
C
C     A's       : tensor components of A matrix (N/m)
C     D's       : tensor components of D matrix (N-m)
C     G's       : shear stiffness components (N/m)
C     sc        : shear correction factor
C
C     cf        : dimension of the square shape of the patched loading
C                 for point loading, let cf = 0.0
C                 (This program is capable of dealing with double-cosine
C                  type distributed patch loading, although this has not
C                  been verified yet.)
C
C     OSTR1&3   : Output filenames for stiffness matrices, 18 chars max,
C                 must be written within apostrophes like:  'xxxxxxx'
C
C ----------------------------------------------------------------------
C
C
C     [ Variables ]
C
      IMPLICIT DOUBLE PRECISION (A-H, O-Z)
      DIMENSION IBCX(5),IBCY(5)
      CHARACTER OSTR1*18,OSTR3*18
C
C
      OPEN( UNIT=10, FILE='stiff.dat', STATUS='OLD' )
C
C
```

```
      READ(10,*)
      READ(10,*)
      READ(10,*)
      READ(10,*)
      READ(10,*)
      READ(10,*) Ibx,Iby,beta
      READ(10,*) IBCX(1),IBCY(1),IBCX(2),IBCY(2),IBCX(3),IBCY(3),
     &           IBCX(4),IBCY(4),IBCX(5),IBCY(5)
      READ(10,*) NCX,NCY,NDX,NDY,NX,NY
      READ(10,*) IEO
      READ(10,*) XL,YL,THICK
      READ(10,*) A11,A22,A12,A16,A26,A66
      READ(10,*) D11,D22,D12,D16,D26,D66
      READ(10,*) G44,G55,G45,sc
      READ(10,*) cf
      READ(10,*)
      READ(10,*)
      READ(10,*)
      READ(10,*)
      READ(10,*)
      READ(10,*)
      READ(10,*)
      READ(10,*) OSTR1,OSTR3
      READ(10,*)
C
C
      G44 = sc*sc*G44
      G55 = sc*sc*G55
      G45 = sc*sc*G45
C
C
      CLOSE( UNIT=10 )
C
C
      RETURN
      END
C
C
C ---------------------------------------------------------------------
      SUBROUTINE BOUND(IBC,N,A,THETA,BETA,B,C,D,E)
C ---------------------------------------------------------------------
C
C  This subroutine determines the euler beam elastic mode shape
C  parameters depending on the boundary condition of each x and y
C  direction based on the Generalized Beam Functions described in
C  Appendix A.
C
C ---------------------------------------------------------------------
C
C
C     [ Variables ]
C
      IMPLICIT DOUBLE PRECISION (A-H, O-Z)
      INTEGER IBC,N
C
      PARAMETER ( N1=7, PI = 3.14159265 )
C
      DIMENSION IBC(5)
```

```
      DIMENSION THETA(5),A(5)
      DIMENSION BETA(5,N1),B(5,N1),C(5,N1),D(5,N1),E(5,N1)
C
C
      DO 10 ki=1,5
      J=0
      IF(IBC(ki) .EQ. 1) THEN
         A(ki) = 0.
         THETA(ki) = 0.
         DO 201 I=1,N
            BETA(ki,I) = (1.*I)*PI
            B(ki,I) = 0.
            C(ki,I) = 1.
            D(ki,I) = 0.
            E(ki,I) = 0.
 201     CONTINUE
      ENDIF
C
C
      IF(IBC(ki) .EQ. 2) THEN
         A(ki) = 1.
         THETA(ki) = -PI/4.
         DO 202 I=1,N
            BETA(ki,I) = (1.*I-0.5)*PI
            B(ki,I) = (-1.)**(I+1)
            C(ki,I) = 1.
            D(ki,I) = 0.
            E(ki,I) = 0.
 202     CONTINUE
      ENDIF
C
C
      IF(IBC(ki) .EQ. 3) THEN
         A(ki) = 1.
         THETA(ki) = -PI/4.
         DO 203 I=1,N
            BETA(ki,I) = (1.*I+0.5)*PI
            B(ki,I) = (-1.)**(I+1)
            C(ki,I) = 1.
            D(ki,I) = 0.
            E(ki,I) = 0.
 203     CONTINUE
      ENDIF
C
C
      IF(IBC(ki) .EQ. 4) THEN
         A(ki) = 1.
         THETA(ki) = 3.*PI/4.
         BETA(ki,1) = 1.
         BETA(ki,2) = 1.
         B(ki,1) = 0.
         B(ki,2) = 0.
         C(ki,1) = 0.
         C(ki,2) = 0.
         D(ki,1) = 0.
         D(ki,2) = 1.
         E(ki,1) = 1.
         E(ki,2) = 1.
```

```
            DO 204 I=1,N-2
               J=I+2
               BETA(ki,J) = (1.*I+0.5)*PI
               B(ki,J) = (-1.)**(I+1)
               C(ki,J) = 1.
               D(ki,J) = 0.
               E(ki,J) = 0.
 204        CONTINUE
         ENDIF
C
C
         IF(IBC(ki) .EQ. 5) THEN
            A(ki) = 0.
            THETA(ki) = 0.
            DO 205 I=1,N
               BETA(ki,I) = (1.*I+0.25)*PI
               B(ki,I) = (-1.)**(I+1)
               C(ki,I) = 1.
               D(ki,I) = 0.
               E(ki,I) = 0.
 205        CONTINUE
         ENDIF
C
C
         IF(IBC(ki) .EQ. 6) THEN
            A(ki) = 0.
            THETA(ki) = 0.
            DO 206 I=1,N
               BETA(ki,I) = (1.*I+0.25)*PI
               B(ki,I) = (-1.)**(I)
               C(ki,I) = 1.
               D(ki,I) = 0.
               E(ki,I) = 0.
 206        CONTINUE
         ENDIF
C
C
         IF(IBC(ki) .EQ. 7) THEN
            A(ki) = 0.
            THETA(ki) = PI/2.
            BETA(ki,1) = 1.
            BETA(ki,2) = 1.
            B(ki,1) = 0.
            B(ki,2) = 0.
            C(ki,1) = 0.
            C(ki,2) = 0.
            D(ki,1) = 1.
            D(ki,2) = 0.
            E(ki,1) = 1.
            E(ki,2) = 1.
            DO 207 I=1,N-2
               J=I+2
               BETA(ki,J) = (1.*I)*PI
               B(ki,J) = 0.
               C(ki,J) = 1./(1.*I)**2.
               D(ki,J) = 0.
               E(ki,J) = 0.
 207        CONTINUE
```

```
      ENDIF
 10   CONTINUE
C
C
      RETURN
      END
C
C
C ------------------------------------------------------------------
      SUBROUTINE BOUND1(IBC,N,A,THETA,BETA,B,C,D,E)
C ------------------------------------------------------------------
C
C  This subroutine determines the euler beam elastic mode shape
C  parameters for the odd modes only case depending on the boundary
C  condition of each x and y direction based on the Generalized Beam
C  Functions described in Appendix A.
C
C ------------------------------------------------------------------
C
C
C     [ Variables ]
C
      IMPLICIT DOUBLE PRECISION (A-H, O-Z)
      INTEGER IBC,N
C
      PARAMETER ( N1=7, PI = 3.14159265 )
C
      DIMENSION IBC(5)
      DIMENSION THETA(5),A(5)
      DIMENSION BETA(5,N1),B(5,N1),C(5,N1),D(5,N1),E(5,N1)
C
C
C
      DO 10 ki=1,5
      J=0
      IF(IBC(ki) .EQ. 1) THEN
         A(ki) = 0.
         THETA(ki) = 0.
         DO 201 I=1,N
            BETA(ki,I) = ((I*2.)-1.)*PI
            B(ki,I) = 0.
            C(ki,I) = 1.
            D(ki,I) = 0.
            E(ki,I) = 0.
 201     CONTINUE
      ENDIF
C
C
      IF(IBC(ki) .EQ. 2) THEN
         A(ki) = 1.
         THETA(ki) = -PI/4.
         DO 202 I=1,N
            BETA(ki,I) = (1.*((I*2.)-1.)-0.5)*PI
            B(ki,I) = (-1.)**(((I*2)-1)+1)
            C(ki,I) = 1.
            D(ki,I) = 0.
            E(ki,I) = 0.
 202     CONTINUE
```

```
      ENDIF
C
C
      IF(IBC(ki) .EQ. 3) THEN
         A(ki) = 1.
         THETA(ki) = -PI/4.
         DO 203 I=1,N
            BETA(ki,I) = ((I*2.-1.)+0.5)*PI
            B(ki,I) = (-1.)**((I*2-1)+1)
            C(ki,I) = 1.
            D(ki,I) = 0.
            E(ki,I) = 0.
 203     CONTINUE
      ENDIF
C
C
      IF(IBC(ki) .EQ. 4) THEN
         A(ki) = 1.
         THETA(ki) = 3.*PI/4.
         BETA(ki,1) = 1.
         B(ki,1) = 0.
         C(ki,1) = 0.
         D(ki,1) = 0.
         E(ki,1) = 1.
         DO 204 I=1,N-1
            J=I+1
            BETA(ki,J) = (((I*2.-1.))+0.5)*PI
            B(ki,J) = (-1.)**(((I*2-1))+1)
            C(ki,J) = 1.
            D(ki,J) = 0.
            E(ki,J) = 0.
 204     CONTINUE
      ENDIF
C
C
      IF(IBC(ki) .EQ. 5) THEN
         A(ki) = 0.
         THETA(ki) = 0.
         DO 205 I=1,N
            BETA(ki,I) = ((I*2.-1.)+0.25)*PI
            B(ki,I) = (-1.)**((I*2-1)+1)
            C(ki,I) = 1.
            D(ki,I) = 0.
            E(ki,I) = 0.
 205     CONTINUE
      ENDIF
C
C
      IF(IBC(ki) .EQ. 6) THEN
         A(ki) = 0.
         THETA(ki) = 0.
         DO 206 I=1,N
            BETA(ki,I) = (1.*I+0.25)*PI
            B(ki,I) = (-1.)**(I)
            C(ki,I) = 1.
            D(ki,I) = 0.
            E(ki,I) = 0.
 206     CONTINUE
```

```
      ENDIF
C
C
      IF(IBC(ki) .EQ. 7) THEN
         A(ki) = 0.
         THETA(ki) = PI/2.
         BETA(ki,1) = 1.
         B(ki,1) = 0.
         C(ki,1) = 0.
         D(ki,1) = 1.
         E(ki,1) = 1.
         DO 207 I=1,N-1
            J=I+1
            BETA(ki,J) = ((2.*I)-1.)*PI
            B(ki,J) = 0.
            C(ki,J) = 1./((2.*I)-1.)**2.
            D(ki,J) = 0.
            E(ki,J) = 0.
 207     CONTINUE
      ENDIF
 10   CONTINUE
C
C
      RETURN
      END
C
C
C ----------------------------------------------------------------------
      SUBROUTINE INGRL1(NX,NY,NCX,NCY,NDX,NDY,IEO,
     &                  AX,AY,THETAX,THETAY,
     &                  BETAX,BETAY,BX,BY,
     &                  CX,CY,DX,DY,EX,EY,
     &                  A11,A22,A12,A16,A26,A66,
     &                  D11,D22,D12,D16,D26,D66,
     &                  G44,G55,G45,XL,YL,
     &                  M1,M2,M3,Ri,cf,
     &                  K1aa,K1ab,K1ae,K1bb,K1be,K1ee,Kigg)
C ----------------------------------------------------------------------
C
C  This subroutine computes each matrix component for the stiffness
C  matrix [K] (the linear term).
C
C ----------------------------------------------------------------------
C
C
C      [ Variables ]
C
      IMPLICIT DOUBLE PRECISION (A-H, O-Z)
      DOUBLE PRECISION l,m,n,M1,M2,M3,
     &                 Kaa,Kab,Kae,Kbb,Kbe,Kee,
     &                 K1aa,K1ab,K1ae,K1bb,K1be,K1ee,
     &                 Kigg
C
      PARAMETER ( N1=7, N2=N1**2, N4=N2**3,
     &            N5=N2*2, Pi=3.14159265 )
C
      DIMENSION THETAX(5),THETAY(5),AX(5),AY(5)
      DIMENSION BETAX(5,N1),BETAY(5,N1),BX(5,N1),BY(5,N1)
```

```
      DIMENSION CX(5,N1),CY(5,N1),DX(5,N1),DY(5,N1),EX(5,N1),EY(5,N1)
      DIMENSION M1(N2),M2(N2),M3(N2)
      DIMENSION K1aa(N2,N2),K1ab(N2,N2),K1ae(N2,N2)
      DIMENSION K1bb(N2,N2),K1be(N2,N2),K1ee(N2,N2)
      DIMENSION Kigg(N5,N5)
      DIMENSION Ri(N2)
      DIMENSION DUMMY(N2)
C
C
C     ---------------------------------------------------------------
C     * Defining Beam Functions & Derivatives of Beam Functions
C     ---------------------------------------------------------------
C
C
C
      f(i,x)   = ((BETAX(1,i)*SQRT(2.)*COS(BETAX(1,i)*x+THETAX(1))
     &           -BETAX(1,i)*AX(1)*EXP(-BETAX(1,i)*x)
     &           +BETAX(1,i)*BX(1,i)*EXP(-BETAX(1,i)*(1.-x)))*CX(1,i)
     &           +DX(1,i)*(-2.))/XL
C
C
      df(i,x)  =((-(BETAX(1,i)**2)*SQRT(2.)*SIN(BETAX(1,i)
     &                                          *x+THETAX(1))
     &           +(BETAX(1,i)**2)*AX(1)*EXP(-BETAX(1,i)*x)
     &           +(BETAX(1,i)**2)*BX(1,i)*EXP(-BETAX(1,i)
     &                                       *(1.-x)))
     &           *CX(1,i))/(XL*XL)
C
C
      g(i,y)   = (SQRT(2.)*SIN(BETAY(1,i)*y+THETAY(1))
     &           +AY(1)*EXP(-BETAY(1,i)*y)
     &           +BY(1,i)*EXP(-BETAY(1,i)*(1.-y)))*CY(1,i)
     &           +2.*EY(1,i)*(DY(1,i)*(-y)+0.5)
C
C
      dg(i,y)  =((BETAY(1,i)*SQRT(2.)*COS(BETAY(1,i)*y+THETAY(1))
     &           -BETAY(1,i)*AY(1)*EXP(-BETAY(1,i)*y)
     &           +BETAY(1,i)*BY(1,i)*EXP(-BETAY(1,i)*(1.-y)))
     &           *CY(1,i)+DY(1,i)*(-2.))/YL
C
C
      h(i,x)   = (SQRT(2.)*SIN(BETAX(2,i)*x+THETAX(2))
     &           +AX(2)*EXP(-BETAX(2,i)*x)
     &           +BX(2,i)*EXP(-BETAX(2,i)*(1.-x)))*CX(2,i)
     &           +2.*EX(2,i)*(DX(2,i)*(-x)+0.5)
C
C
      dh(i,x)  =((BETAX(2,i)*SQRT(2.)*COS(BETAX(2,i)*x+THETAX(2))
     &           -BETAX(2,i)*AX(2)*EXP(-BETAX(2,i)*x)
     &           +BETAX(2,i)*BX(2,i)*EXP(-BETAX(2,i)*(1.-x)))
     &           *CX(2,i)+DX(2,i)*(-2.))/XL
C
C
      l(i,y)   = ((BETAY(2,i)*SQRT(2.)*COS(BETAY(2,i)*y+THETAY(2))
     &           -BETAY(2,i)*AY(2)*EXP(-BETAY(2,i)*y)
     &           +BETAY(2,i)*BY(2,i)*EXP(-BETAY(2,i)*(1.-y)))
     &           *CY(2,i)+DY(2,i)*(-2.))/YL
C
C
```

```
      dl(i,y) =((-(BETAY(2,i)**2)*SQRT(2.)*SIN(BETAY(2,i)
     &                                         *y+THETAY(2))
     &          +(BETAY(2,i)**2)*AY(2)*EXP(-BETAY(2,i)*y)
     &          +(BETAY(2,i)**2)*BY(2,i)*EXP(-BETAY(2,i)
     &                                      *(1.-y)))
     &          *CY(2,i))/(YL*YL)
C
C
      m(i,x)  = (SQRT(2.)*SIN(BETAX(3,i)*x+THETAX(3))
     &          +AX(3)*EXP(-BETAX(3,i)*x)
     &          +BX(3,i)*EXP(-BETAX(3,i)*(1.-x)))*CX(3,i)
     &          +2.*EX(3,i)*(DX(3,i)*(-x)+0.5)
C
C
      dm(i,x) =((BETAX(3,i)*SQRT(2.)*COS(BETAX(3,i)*x+THETAX(3))
     &          -BETAX(3,i)*AX(3)*EXP(-BETAX(3,i)*x)
     &          +BETAX(3,i)*BX(3,i)*EXP(-BETAX(3,i)*(1.-x)))
     &          *CX(3,i)+DX(3,i)*(-2.))/XL
C
C
      n(i,y)  = (SQRT(2.)*SIN(BETAY(3,i)*y+THETAY(3))
     &          +AY(3)*EXP(-BETAY(3,i)*y)
     &          +BY(3,i)*EXP(-BETAY(3,i)*(1.-y)))*CY(3,i)
     &          +2.*EY(3,i)*(DY(3,i)*(-y)+0.5)
C
C
      dn(i,y) =((BETAY(3,i)*SQRT(2.)*COS(BETAY(3,i)*y+THETAY(3))
     &          -BETAY(3,i)*AY(3)*EXP(-BETAY(3,i)*y)
     &          +BETAY(3,i)*BY(3,i)*EXP(-BETAY(3,i)*(1.-y)))
     &          *CY(3,i)+DY(3,i)*(-2.))/YL
C
C
      o(i,x)  = (SQRT(2.)*SIN(BETAX(4,i)*x+THETAX(4))
     &          +AX(4)*EXP(-BETAX(4,i)*x)
     &          +BX(4,i)*EXP(-BETAX(4,i)*(1.-x)))*CX(4,i)
     &          +2.*EX(4,i)*(DX(4,i)*(-x)+0.5)
C
C
      do(i,x) =((BETAX(4,i)*SQRT(2.)*COS(BETAX(4,i)*x+THETAX(4))
     &          -BETAX(4,i)*AX(4)*EXP(-BETAX(4,i)*x)
     &          +BETAX(4,i)*BX(4,i)*EXP(-BETAX(4,i)*(1.-x)))
     &          *CX(4,i)+DX(4,i)*(-2.))/XL
C
C
      p(i,y)  = (SQRT(2.)*SIN(BETAY(4,i)*y+THETAY(4))
     &          +AY(4)*EXP(-BETAY(4,i)*y)
     &          +BY(4,i)*EXP(-BETAY(4,i)*(1.-y)))*CY(4,i)
     &          +2.*EY(4,i)*(DY(4,i)*(-y)+0.5)
C
C
      dp(i,y) =((BETAY(4,i)*SQRT(2.)*COS(BETAY(4,i)*y+THETAY(4))
     &          -BETAY(4,i)*AY(4)*EXP(-BETAY(4,i)*y)
     &          +BETAY(4,i)*BY(4,i)*EXP(-BETAY(4,i)*(1.-y)))
     &          *CY(4,i)+DY(4,i)*(-2.))/YL
C
C
      q(i,x)  = (SQRT(2.)*SIN(BETAX(5,i)*x+THETAX(5))
     &          +AX(5)*EXP(-BETAX(5,i)*x)
```

```
     &           +BX(5,i)*EXP(-BETAX(5,i)*(1.-x)))*CX(5,i)
     &           +2.*EX(5,i)*(DX(5,i)*(-x)+0.5)
C
C
      dq(i,x) =((BETAX(5,i)*SQRT(2.)*COS(BETAX(5,i)*x+THETAX(5))
     &           -BETAX(5,i)*AX(5)*EXP(-BETAX(5,i)*x)
     &           +BETAX(5,i)*BX(5,i)*EXP(-BETAX(5,i)*(1.-x)))
     &           *CX(5,i)+DX(5,i)*(-2.))/XL
C
C
      r(i,y)  =  (SQRT(2.)*SIN(BETAY(5,i)*y+THETAY(5))
     &           +AY(5)*EXP(-BETAY(5,i)*y)
     &           +BY(5,i)*EXP(-BETAY(5,i)*(1.-y)))*CY(5,i)
     &           +2.*EY(5,i)*(DY(5,i)*(-y)+0.5)
C
C
      dr(i,y) =((BETAY(5,i)*SQRT(2.)*COS(BETAY(5,i)*y+THETAY(5))
     &           -BETAY(5,i)*AY(5)*EXP(-BETAY(5,i)*y)
     &           +BETAY(5,i)*BY(5,i)*EXP(-BETAY(5,i)*(1.-y)))
     &           *CY(5,i)+DY(5,i)*(-2.))/YL
C
C
      xunit = XL/20.
      yunit = YL/20.
      NXY = NX*NY
      NC = NCX*NCY
      ND = NDX*NDY
C
C
C     ----------------------------------------------------
C     * Calculations help determine if zeros will occur on
C       the diagonals in the stiffness matrices.
C     ----------------------------------------------------
C
      i = 0
      DO 310 ix = 1, NX
         DO 311 iy = 1, NY
            i = i+1
C
            j = 0
            DO 312 jx = 1, NX
               DO 313 jy = 1, NY
                  j = j+1
C
                  xM1 = 0.
                  xM2 = 0.
                  xM3 = 0.
C
                  yM1 = 0.
                  yM2 = 0.
                  yM3 = 0.
C
                  x = -0.05
                  y = -0.05
C
                  IF(IEO .EQ. 1) NNN = 11
                  IF(IEO .EQ. 0) NNN = 21
C
```

```
                  DO 314 II = 1, NNN
C
                     x = x+0.05
                     y = y+0.05
C
                     rc    = 1.
                     IF((II .EQ. 1) .OR. (II .EQ. 21)) rc = 2.
                     IF(IEO .EQ. 1) THEN
                        IF((II .EQ. 1) .OR. (II .EQ. 11)) rc=2.
                     ENDIF
C
                     xM1 = xM1+f(ix,x)*f(jx,x)*xunit/rc
                     xM2 = xM2+h(ix,x)*h(jx,x)*xunit/rc
                     xM3 = xM3+q(ix,x)*q(jx,x)*xunit/rc
C
                     yM1 = yM1+g(iy,y)*g(jy,y)*yunit/rc
                     yM2 = yM2+l(iy,y)*l(jy,y)*yunit/rc
                     yM3 = yM3+r(iy,y)*r(jy,y)*yunit/rc
C
 314              CONTINUE
C
                  IF(i .EQ. j) THEN
                     M1(i) = xM1 * yM1
                     M2(i) = xM2 * yM2
                     M3(i) = xM3 * yM3
                  ENDIF
C
                  IF(IEO .EQ. 1) THEN
                     IF(i .EQ. j) THEN
                        M1(i) = xM1 * yM1 * 4.
                        M2(i) = xM2 * yM2 * 4.
                        M3(i) = xM3 * yM3 * 4.
                     ENDIF
                  ENDIF
C
 313           CONTINUE
 312        CONTINUE
C
 311     CONTINUE
 310  CONTINUE
C
C
C     -----------------------------------------------------
C     * Calculating stiffness matrix components by numerical
C       integration using "Extended Trapezoidal Rule"
C     -----------------------------------------------------
C
      WRITE(6,*)'CYPHERIN UP THAT THERE STIFFNESS THINGY...'
C
      i = 0
      DO 300 ix = 1, NX
         DO 301 iy = 1, NY
            i = i+1
C
            j = 0
            DO 302 jx = 1, NX
               DO 303 jy = 1, NY
                  j = j+1
```

```
C
                  xKaa1 = 0.
                  xKaa2 = 0.
                  xKaa3 = 0.
                  xKaa4 = 0.
                  xKab1 = 0.
                  xKab2 = 0.
                  xKab3 = 0.
                  xKab4 = 0.
                  xKae1 = 0.
                  xKae2 = 0.
                  xKbb1 = 0.
                  xKbb2 = 0.
                  xKbb3 = 0.
                  xKbb4 = 0.
                  xKbe1 = 0.
                  xKbe2 = 0.
                  xKcc1 = 0.
                  xKcc2 = 0.
                  xKcc3 = 0.
                  xKcc4 = 0.
                  xKcd1 = 0.
                  xKcd2 = 0.
                  xKcd3 = 0.
                  xKcd4 = 0.
                  xKdd1 = 0.
                  xKdd2 = 0.
                  xKdd3 = 0.
                  xKdd4 = 0.
                  xKee1 = 0.
                  xKee2 = 0.
                  xKee3 = 0.
                  xKee4 = 0.
C
                  yKaa1 = 0.
                  yKaa2 = 0.
                  yKaa3 = 0.
                  yKaa4 = 0.
                  yKab1 = 0.
                  yKab2 = 0.
                  yKab3 = 0.
                  yKab4 = 0.
                  yKae1 = 0.
                  yKae2 = 0.
                  yKbb1 = 0.
                  yKbb2 = 0.
                  yKbb3 = 0.
                  yKbb4 = 0.
                  yKbe1 = 0.
                  yKbe2 = 0.
                  yKcc1 = 0.
                  yKcc2 = 0.
                  yKcc3 = 0.
                  yKcc4 = 0.
                  yKcd1 = 0.
                  yKcd2 = 0.
                  yKcd3 = 0.
                  yKcd4 = 0.
```

```
                  yKdd1 = 0.
                  yKdd2 = 0.
                  yKdd3 = 0.
                  yKdd4 = 0.
                  yKee1 = 0.
                  yKee2 = 0.
                  yKee3 = 0.
                  yKee4 = 0.
C
                  x = -0.05
                  y = -0.05
C
                  NNN = 21
                  IF(IEO .EQ. 1) NNN = 11
C
                  DO 304 II = 1, NNN
                     x = x+0.05
                     y = y+0.05
C
                     rc = 1.
                     IF((II .EQ. 1) .OR. (II .EQ. 21)) rc = 2.
C
                     IF(IEO .EQ. 1) THEN
                        IF((II .EQ. 1) .OR. (II .EQ. 11)) rc=2.
                     ENDIF
C
                     xKaa1 = xKaa1+df(ix,x)*df(jx,x)*xunit/rc
                     xKaa2 = xKaa2+df(ix,x)*f(jx,x)*xunit/rc
                     xKaa3 = xKaa3+f(ix,x)*df(jx,x)*xunit/rc
                     xKaa4 = xKaa4+f(ix,x)*f(jx,x)*xunit/rc
C
                     xKab1 = xKab1+df(ix,x)*h(jx,x)*xunit/rc
                     xKab2 = xKab2+df(ix,x)*dh(jx,x)*xunit/rc
                     xKab3 = xKab3+f(ix,x)*h(jx,x)*xunit/rc
                     xKab4 = xKab4+f(ix,x)*dh(jx,x)*xunit/rc
C
                     xKae1 = xKae1+f(ix,x)*dq(jx,x)*xunit/rc
                     xKae2 = xKae2+f(ix,x)*q(jx,x)*xunit/rc
C
                     xKbb1 = xKbb1+h(ix,x)*h(jx,x)*xunit/rc
                     xKbb2 = xKbb2+dh(ix,x)*h(jx,x)*xunit/rc
                     xKbb3 = xKbb3+h(ix,x)*dh(jx,x)*xunit/rc
                     xKbb4 = xKbb4+dh(ix,x)*dh(jx,x)*xunit/rc
C
                     xKbe1 = xKbe1+h(ix,x)*dq(jx,x)*xunit/rc
                     xKbe2 = xKbe2+h(ix,x)*q(jx,x)*xunit/rc
C
                     IF(ix.GT.NCX.OR.jx.GT.NCX) GOTO 100
                     xKcc1 = xKcc1+dm(ix,x)*dm(jx,x)*xunit/rc
                     xKcc2 = xKcc2+m(ix,x)*dm(jx,x)*xunit/rc
                     xKcc3 = xKcc3+dm(ix,x)*m(jx,x)*xunit/rc
                     xKcc4 = xKcc4+m(ix,x)*m(jx,x)*xunit/rc
 100                 CONTINUE
C
                     IF(ix.GT.NCX.OR.jx.GT.NDX) GOTO 110
                     xKcd1 = xKcd1+dm(ix,x)*o(jx,x)*xunit/rc
                     xKcd2 = xKcd2+dm(ix,x)*do(jx,x)*xunit/rc
                     xKcd3 = xKcd3+m(ix,x)*o(jx,x)*xunit/rc
```

```
                      xKcd4 = xKcd4+m(ix,x)*do(jx,x)*xunit/rc
 110                  CONTINUE
C
                      IF(ix.GT.NDX.OR.jx.GT.NDX) GOTO 120
                      xKdd1 = xKdd1+o(ix,x)*o(jx,x)*xunit/rc
                      xKdd2 = xKdd2+do(ix,x)*o(jx,x)*xunit/rc
                      xKdd3 = xKdd3+o(ix,x)*do(jx,x)*xunit/rc
                      xKdd4 = xKdd4+do(ix,x)*do(jx,x)*xunit/rc
 120                  CONTINUE
C
                      xKee1 = xKee1+dq(ix,x)*dq(jx,x)*xunit/rc
                      xKee2 = xKee2+dq(ix,x)*q(jx,x)*xunit/rc
                      xKee3 = xKee3+q(ix,x)*dq(jx,x)*xunit/rc
                      xKee4 = xKee4+q(ix,x)*q(jx,x)*xunit/rc
C
C
                      yKaa1 = yKaa1+g(iy,y)*g(jy,y)*yunit/rc
                      yKaa2 = yKaa2+g(iy,y)*dg(jy,y)*yunit/rc
                      yKaa3 = yKaa3+dg(iy,y)*g(jy,y)*yunit/rc
                      yKaa4 = yKaa4+dg(iy,y)*dg(jy,y)*yunit/rc
C
                      yKab1 = yKab1+g(iy,y)*dl(jy,y)*yunit/rc
                      yKab2 = yKab2+g(iy,y)*l(jy,y)*yunit/rc
                      yKab3 = yKab3+dg(iy,y)*dl(jy,y)*yunit/rc
                      yKab4 = yKab4+dg(iy,y)*l(jy,y)*yunit/rc
C
                      yKae1 = yKae1+g(iy,y)*r(jy,y)*yunit/rc
                      yKae2 = yKae2+g(iy,y)*dr(jy,y)*yunit/rc
C
                      yKbb1 = yKbb1+dl(iy,y)*dl(jy,y)*yunit/rc
                      yKbb2 = yKbb2+l(iy,y)*dl(jy,y)*yunit/rc
                      yKbb3 = yKbb3+dl(iy,y)*l(jy,y)*yunit/rc
                      yKbb4 = yKbb4+l(iy,y)*l(jy,y)*yunit/rc
C
                      yKbe1 = yKbe1+l(iy,y)*r(jy,y)*yunit/rc
                      yKbe2 = yKbe2+l(iy,y)*dr(jy,y)*yunit/rc
C
                      IF(iy.GT.NCY.OR.jy.GT.NCY) GOTO 130
                      yKcc1 = yKcc1+n(iy,y)*n(jy,y)*yunit/rc
                      yKcc2 = yKcc2+dn(iy,y)*n(jy,y)*yunit/rc
                      yKcc3 = yKcc3+n(iy,y)*dn(jy,y)*yunit/rc
                      yKcc4 = yKcc4+dn(iy,y)*dn(jy,y)*yunit/rc
 130                  CONTINUE
C
                      IF(iy.GT.NCY.OR.jy.GT.NDY) GOTO 140
                      yKcd1 = yKcd1+n(iy,y)*dp(jy,y)*yunit/rc
                      yKcd2 = yKcd2+n(iy,y)*p(jy,y)*yunit/rc
                      yKcd3 = yKcd3+dn(iy,y)*dp(jy,y)*yunit/rc
                      yKcd4 = yKcd4+dn(iy,y)*p(jy,y)*yunit/rc
 140                  CONTINUE
C
                      IF(iy.GT.NDY.OR.jy.GT.NDY) GOTO 150
                      yKdd1 = yKdd1+dp(iy,y)*dp(jy,y)*yunit/rc
                      yKdd2 = yKdd2+p(iy,y)*dp(jy,y)*yunit/rc
                      yKdd3 = yKdd3+dp(iy,y)*p(jy,y)*yunit/rc
                      yKdd4 = yKdd4+p(iy,y)*p(jy,y)*yunit/rc
 150                  CONTINUE
C
```

```
                     yKee1 = yKee1+r(iy,y)*r(jy,y)*yunit/rc
                     yKee2 = yKee2+r(iy,y)*dr(jy,y)*yunit/rc
                     yKee3 = yKee3+dr(iy,y)*r(jy,y)*yunit/rc
                     yKee4 = yKee4+dr(iy,y)*dr(jy,y)*yunit/rc
C
 304              CONTINUE
C
C
                  asm=1.
                  IF(IEO .EQ. 1) asm=4.
C
C
                  K1aa(i,j) =(D11 * xKaa1 * yKaa1
     &                       +D16 * xKaa2 * yKaa2
     &                       +D16 * xKaa3 * yKaa3
     &                       +D66 * xKaa4 * yKaa4
     &                       +G55 * xKaa4 * yKaa1)*asm
C
C
                  K1ab(i,j) =(D12 * xKab1 * yKab1
     &                       +D16 * xKab2 * yKab2
     &                       +D26 * xKab3 * yKab3
     &                       +D66 * xKab4 * yKab4
     &                       +G45 * xKab3 * yKab2)*asm
C
C
                  K1ae(i,j) =(G55 * xKae1 * yKae1
     &                       +G45 * xKae2 * yKae2)*asm
C
C
                  K1bb(i,j) =(D22 * xKbb1 * yKbb1
     &                       +D26 * xKbb2 * yKbb2
     &                       +D26 * xKbb3 * yKbb3
     &                       +D66 * xKbb4 * yKbb4
     &                       +G44 * xKbb1 * yKbb4)*asm
C
C
                  K1be(i,j) =(G45 * xKbe1 * yKbe1
     &                       +G44 * xKbe2 * yKbe2)*asm
C
C
                  IF(i.GT.NC.OR.j.GT.NC) GOTO 160
                  Kigg(i,j) =(A11 * xKcc1 * yKcc1
     &                       +A16 * xKcc2 * yKcc2
     &                       +A16 * xKcc3 * yKcc3
     &                       +A66 * xKcc4 * yKcc4)*asm
 160              CONTINUE
C
C
                  IF(i.GT.NC.OR.j.GT.ND) GOTO 170
                  Kigg(i,j+NC) =(A12 * xKcd1 * yKcd1
     &                          +A16 * xKcd2 * yKcd2
     &                          +A26 * xKcd3 * yKcd3
     &                          +A66 * xKcd4 * yKcd4)*asm
C
C
                  Kigg(j+NC,i) = Kigg(i,j+NC)
 170              CONTINUE
```

```
C
C
                  IF(i.GT.ND.OR.j.GT.ND) GOTO 180
                  Kigg(i+NC,j+NC) =(A22 * xKdd1 * yKdd1
     &                             +A26 * xKdd2 * yKdd2
     &                             +A26 * xKdd3 * yKdd3
     &                             +A66 * xKdd4 * yKdd4)*asm
 180              CONTINUE
C
C
                  Klee(i,j) =(G55 * xKee1 * yKee1
     &                       +G45 * xKee2 * yKee2
     &                       +G45 * xKee3 * yKee3
     &                       +G44 * xKee4 * yKee4)*asm
C
C
 303           CONTINUE
 302        CONTINUE
C
 301     CONTINUE
 300  CONTINUE
C
C
      NEN = NC + ND
      CALL INVERS(Kigg,NEN)
C
C
C     ------------------------------------------------------
C     * Compute force vector terms for concentrated loading
C     ------------------------------------------------------
C
      WRITE(6,*)'CYPHERIN UP THAT THERE FORCE THINGY...'
C
      x = 0.5
      y = 0.5
C
      i = 0
C
      DO 330 ix = 1, NX
         DO 331 iy = 1, NY
            i = i+1
            Ri(i) = q(ix,x)*r(iy,y)
C
C
 331     CONTINUE
 330  CONTINUE
C
      IF(cf .EQ. 0.) GOTO 345
C
C
C     ----------------------------------------------------------------
C     * Compute force vector terms for cosine distributed patch loading
C     ----------------------------------------------------------------
C
C
      af = cf/XL
      bf = cf/YL
C
```

```
      aunit = cf*cf/100.
C
      p0 = (Pi**2)/(4.*cf*cf)
C
      ij = 0
C
C
      DO 335 ix = 1, NX
         DO 336 iy = 1, NY
C
            x = 0.5-af/2.
            SUM = 0.
C
            DO 340 I = 1, 10
               y = 0.5-bf/2.
               x = x+af/10.
C
               DO 341 J = 1, 10
                  y = y+bf/10.
C
                  PR = COS(Pi/af*(x-0.5))*COS(Pi/bf*(y-0.5))
     &                 *q(ix,x)*r(iy,y)*aunit
C
                  SUM = SUM+PR
C
 341           CONTINUE
 340        CONTINUE
C
            ij = ij+1
            Ri(ij) = p0*SUM
C
 336     CONTINUE
 335  CONTINUE
C
C
 345  CONTINUE
C
C
      RETURN
      END
C
C
C -----------------------------------------------------------------------
      SUBROUTINE ARRANG(NX,NY,iKaa,iKab,jKab,iKae,iKbb,iKbe,
     &                  M1,M2,K1aa,K1ab,K1ae,K1bb,K1be)
C -----------------------------------------------------------------------
C
C  This subroutine rearranges the stiffness matrix [K], if there is any
C  singularity due to using the free-free beam boundary condition.
C
C -----------------------------------------------------------------------
C
C     [ Variables ]
C
      IMPLICIT DOUBLE PRECISION (A-H, O-Z)
      DOUBLE PRECISION M1,M2,
     &                 K1aa,K1ab,K1ae,K1bb,K1be
      INTEGER NX,NY,NXY
```

```
C
      PARAMETER ( N1=7, N2=N1**2 )
C
      DIMENSION M1(N2),M2(N2)
      DIMENSION NM1(N2),NM2(N2)
      DIMENSION K1aa(N2,N2),K1ab(N2,N2),K1ae(N2,N2)
      DIMENSION K1bb(N2,N2),K1be(N2,N2)
C
C
      NXY = NX*NY
C
      WRITE(6,*)'DOIN THE ARRANGE THING...'
C
      DO 250 i = 1, NXY
C
         NM1(i) = 0
         IF(M1(i) .EQ. 0.) NM1(i) = 1
C
         NM2(i) = 0
         IF(M2(i) .EQ. 0.) NM2(i) = 1
C
 250  CONTINUE
C
C
      iKaa = NXY
      iKab = NXY
      jKab = NXY
      iKae = NXY
      iKbb = NXY
      iKbe = NXY
C
C
      ii = 0
      DO 251 i = 1, NXY
         iKaa = iKaa-1
         iKab = iKab-1
         iKae = iKae-1
         IF(NM1(i) .EQ. 1) GOTO 251
         ii = ii+1
         iKaa = iKaa+1
         iKab = iKab+1
         iKae = iKae+1
         DO 252 j = 1, NXY
            K1aa(ii,j) = K1aa(i,j)
            K1ab(ii,j) = K1ab(i,j)
            K1ae(ii,j) = K1ae(i,j)
 252     CONTINUE
 251  CONTINUE
C
C
      IF(iKaa .EQ. NXY) GOTO 253
C
      jj = 0
      DO 254 j = 1, NXY
         IF(NM1(i) .EQ. 1) GOTO 254
         jj = jj+1
         DO 255 i = 1, iKaa
            K1aa(i,jj) = K1aa(i,j)
```

```
 255      CONTINUE
 254   CONTINUE
C
C
 253   CONTINUE
C
C
       ii = 0
       DO 256 i = 1, NXY
          iKbb = iKbb-1
          iKbe = iKbe-1
          IF(NM2(i) .EQ. 1) GOTO 256
          ii = ii+1
          iKbb = iKbb+1
          iKbe = iKbe+1
          DO 257 j = 1, NXY
             K1bb(ii,j) = K1bb(i,j)
             K1be(ii,j) = K1be(i,j)
 257      CONTINUE
 256   CONTINUE
C
C
       IF(iKbb .EQ. NXY) GOTO 260
C
       jj = 0
       DO 258 j = 1, NXY
          jKab = jKab-1
          IF(NM2(j) .EQ. 1) GOTO 258
          jKab = jKab+1
          jj = jj+1
          DO 259 i = 1, iKbb
             K1bb(i,jj) = K1bb(i,j)
 259      CONTINUE
          DO 261 i = 1, iKab
             K1ab(i,jj) = K1ab(i,j)
 261      CONTINUE
 258   CONTINUE
C
C
 260   CONTINUE
C
C
       RETURN
       END
C
C
C ----------------------------------------------------------------------
       SUBROUTINE CONDEN(NX,NY,iKaa,iKab,jKab,iKae,iKbb,iKbe,
      &                  K1aa,K1ab,K1ae,K1bb,K1be,K1ee,KI)
C ----------------------------------------------------------------------
C
C  This subroutine performs static condensation in order to reduce the
C  system of equations.
C
C ----------------------------------------------------------------------
C
C     [ Variables ]
C
```

```
      IMPLICIT DOUBLE PRECISION (A-H, O-Z)
      DOUBLE PRECISION K1aa,K1ab,K1ae,K1ba,K1bb,K1be,
     &                 K1ea,K1eb,K1ee,
     &                 KK,KI
      INTEGER NX,NY,NXY
C
      PARAMETER ( N1=7, N2=N1**2, N4=N2**3, N5=N2*2 )
C
      DIMENSION K1aa(N2,N2),K1ab(N2,N2),K1ae(N2,N2)
      DIMENSION K1ba(N2,N2),K1bb(N2,N2),K1be(N2,N2)
      DIMENSION K1ea(N2,N2),K1eb(N2,N2),K1ee(N2,N2),KK(N2,N5)
      DIMENSION KI(N2,N2),A(N5,N5)
      DIMENSION DUM(N2)
C
C
      NXY = NX*NY
C
      WRITE(6,*)'NOW ON TO STATIC CONDENSATION...'
C
C
C     -----------------------------
C     * Obtain transpose of matrix
C     -----------------------------
C
C
      DO 404 I = 1, iKab
         DO 405 J = 1, jKab
            K1ba(J,I) = K1ab(I,J)
 405     CONTINUE
 404  CONTINUE
C
C
      DO 406 I = 1, iKae
         DO 407 J = 1, NXY
            K1ea(J,I) = K1ae(I,J)
 407     CONTINUE
 406  CONTINUE
C
C
      DO 408 I = 1, iKbe
         DO 409 J = 1, NXY
            K1eb(J,I) = K1be(I,J)
 409     CONTINUE
 408  CONTINUE
C
C
C     ----------------------------------
C     * Compute inverse of [ K ] matrix
C     ----------------------------------
C
      WRITE(6,*)'INVERSE STIFFNESS...'
C
      DO 424 I = 1, iKaa
         DO 425 J = 1, iKaa
            A(I,J) = K1aa(I,J)
 425     CONTINUE
         DO 426 J = 1, jKab
            A(I,iKaa+J) = K1ab(I,J)
```

```
 426        CONTINUE
 424     CONTINUE
C
         DO 427 I = 1, iKbb
            DO 428 J = 1, iKab
               A(iKaa+I,J) = K1ba(I,J)
 428        CONTINUE
            DO 429 J = 1, iKbb
               A(iKaa+I,iKab+J) = K1bb(I,J)
 429        CONTINUE
 427     CONTINUE
C
         NN = iKaa+iKbb
C
C
         CALL INVERS(A,NN)
C
C        ----------------------------------------
C        * Recovering A&B from static condensation
C        ----------------------------------------
         CALL REMAT(A,NN,K1ae,iKae,K1be,iKbe,NXY)
C
C        ----------------------------------------
C        * Static condensation for [ K* ] matrix
C        ----------------------------------------
C
         WRITE(6,*)'STATIC CONDENSATION - JUST DO IT...'
C
         DO 440 I = 1, NXY
            DO 441 J = 1, NN
               SUM = 0.
               DO 442 JJ = 1, iKaa
                  PR = K1ea(I,JJ)*A(JJ,J)
                  SUM = SUM+PR
 442           CONTINUE
               DO 443 JJ = 1, iKbb
                  PR = K1eb(I,JJ)*A(JJ+iKaa,J)
                  SUM = SUM+PR
 443           CONTINUE
               KK(I,J) = SUM
 441        CONTINUE
 440     CONTINUE
C
C
         DO 444 I = 1, NXY
            DO 445 J = 1, NXY
               SUM = 0.
               DO 446 JJ = 1, iKaa
                  PR = KK(I,JJ)*K1ae(JJ,J)
                  SUM = SUM+PR
 446           CONTINUE
               DO 447 JJ = 1, iKbb
                  PR = KK(I,JJ+iKaa)*K1be(JJ,J)
                  SUM = SUM+PR
 447           CONTINUE
               A(I,J) = SUM
 445        CONTINUE
 444     CONTINUE
```

```
C
C
      DO 448 I = 1, NXY
         DO 449 J = 1, NXY
            KI(I,J) = Klee(I,J) - A(I,J)
 449     CONTINUE
 448  CONTINUE
C
C
      RETURN
      END
C
C
C -----------------------------------------------------------------------
      SUBROUTINE INVERS(A,N)
C -----------------------------------------------------------------------
C
C  This subroutine calculates the inverse of a given NxN matrix [A].
C  Taken from "Numerical Recipes for FORTRAN77"
C
C -----------------------------------------------------------------------
C
C     [ Variables ]
C
      IMPLICIT DOUBLE PRECISION (A-H, O-Z)
C
      PARAMETER ( N1=7, N2=N1**2, N5=N2*2 )
C
      DIMENSION A(N5,N5),Y(N5,N5),INDX(N5),B1(N5)
C
C
      DO 340 I = 1, N
         DO 341 J = 1, N
            Y(I,J) = 0.
 341     CONTINUE
         Y(I,I) = 1.
 340  CONTINUE
C
C
      CALL LUDCMP(A,N,INDX)
C
C
      DO 342 J = 1, N
         DO 345 I = 1, N
            B1(I) = Y(I,J)
 345     CONTINUE
C
C
         CALL LUBKSB(A,N,INDX,B1)
C
         DO 346 I = 1, N
            Y(I,J) = B1(I)
 346     CONTINUE
C
 342  CONTINUE
C
C
      DO 343 I = 1, N
```

```
         DO 344 J = 1, N
            A(I,J) = Y(I,J)
 344     CONTINUE
 343  CONTINUE
C
C
      RETURN
      END
C
C
C -----------------------------------------------------------------------
      SUBROUTINE LUDCMP(A,N,INDX)
C -----------------------------------------------------------------------
C
C  This subroutine performs LU decomposition.
C  Taken from "Numerical Recipes for FORTRAN77"
C
C -----------------------------------------------------------------------
C
C     [ Variables ]
C
      IMPLICIT DOUBLE PRECISION (A-H, O-Z)
C
      PARAMETER ( N1=7, N2=N1**2, N5=N2*2 )
      PARAMETER ( TINY=1.0E-16 )
C
      DIMENSION A(N5,N5),INDX(N5),VV(N5)
C
C
      D = 1.
C
C
      DO 350 I = 1, N
         AAMAX = 0.
         DO 351 J = 1, N
            IF(ABS(A(I,J)) .GT. AAMAX) AAMAX=ABS(A(I,J))
 351     CONTINUE
         IF(AAMAX .EQ. 0.) AAMAX=TINY
         VV(I) = 1./AAMAX
 350  CONTINUE
C
C
      DO 352 J = 1, N
C
         DO 353 I = 1, J-1
            SUM = A(I,J)
            DO 354 K = 1, I-1
               SUM = SUM - A(I,K)*A(K,J)
 354        CONTINUE
            A(I,J) = SUM
 353     CONTINUE
         AAMAX = 0.
C
         DO 355 I = J, N
            SUM = A(I,J)
            DO 356 K = 1, J-1
               SUM = SUM - A(I,K)*A(K,J)
 356        CONTINUE
```

```
            A(I,J) = SUM
            DUM = VV(I)*ABS(SUM)
            IF(DUM .GE. AAMAX) THEN
               IMAX = I
               AAMAX = DUM
            ENDIF
 355     CONTINUE
C
         IF(J .NE. IMAX) THEN
            DO 357 K = 1, N
               DUM = A(IMAX,K)
               A(IMAX,K) = A(J,K)
               A(J,K) = DUM
 357        CONTINUE
            D = -D
            VV(IMAX) = VV(J)
         ENDIF
C
         INDX(J) = IMAX
C
         IF(A(J,J) .EQ. 0.) A(J,J)=TINY
C
         IF(J .NE. N) THEN
            DUM = 1./A(J,J)
            DO 358 I = J+1, N
               A(I,J) = A(I,J)*DUM
 358        CONTINUE
         ENDIF
C
 352  CONTINUE
C
C
      RETURN
      END
C
C
C -------------------------------------------------------------------
      SUBROUTINE LUBKSB(A,N,INDX,B1)
C -------------------------------------------------------------------
C
C  This subroutine performs LU back-substitution.
C  Taken from "Numerical Recipes for FORTRAN77"
C
C -------------------------------------------------------------------
C
C     [ Variables ]
C
      IMPLICIT DOUBLE PRECISION (A-H, O-Z)
C
      PARAMETER ( N1=7, N2=N1**2, N5=N2*2 )
C
      DIMENSION A(N5,N5),INDX(N5),B1(N5)
C
C
      II = 0
C
C
      DO 360 I = 1, N
```

```
          LL = INDX(I)
          SUM = B1(LL)
          B1(LL) = B1(I)
C
          IF(II .NE. 0) THEN
             DO 361 J = II, I-1
                SUM = SUM - A(I,J)*B1(J)
 361         CONTINUE
          ELSE IF (SUM .NE. 0.) THEN
             II = I
          ENDIF
C
          B1(I) = SUM
 360   CONTINUE
C
C
       DO 362 I = N, 1, -1
          SUM = B1(I)
          DO 363 J = I+1, N
             SUM = SUM - A(I,J)*B1(J)
 363      CONTINUE
          B1(I) = SUM/A(I,I)
 362   CONTINUE
C
C
       RETURN
       END
C ----------------------------------------------------------------------
       SUBROUTINE REMAT(A,NN,K1ae,iKae,K1be,iKbe,NXY)
C ----------------------------------------------------------------------
C  This subroutine calculates the matrix for backing the A & B
C  amplitudes out of E and writes it to the output file.  The
C  subroutine name stands for "REcovery MATrix."  The matrix KUN,
C  which is written row by row, will be used in the solution program
C  to complete the operation of recovering A & B, which ultimately
C  allow the calculation of Yx and Yy.
C ----------------------------------------------------------------------
       DOUBLE PRECISION A,K1ae,K1be,SUM,PR,KUNrow
C
       PARAMETER ( N1=7, N2=N1**2, N5=N2*2 )
C
       DIMENSION A(N5,N5),K1ae(N2,N2),K1be(N2,N2),KUNrow(N2)
C
       OPEN( UNIT=9, FILE='KUNMAT', STATUS='NEW' )
C
       WRITE(6,*)'WRITING Psi x & Psi y Recovery Matrix...'
C
       WRITE(9,*)NN,iKae,iKbe
       DO 10 I = 1, NN
          DO 20 J = 1, NXY
             SUM = 0.
             DO 30 K = 1, iKae
                PR = -A(I,K)*K1ae(K,J)
                SUM = SUM+PR
 30          CONTINUE
             DO 40 K = 1, iKbe
                PR = -A(I,iKae+K)*K1be(K,J)
                SUM = SUM+PR
```

```
 40         CONTINUE
            KUNrow(J)=SUM
 20      CONTINUE
        WRITE(9,*) (KUNrow(L),L=1,NXY)
 10   CONTINUE
        WRITE(9,*)
C
      CLOSE( UNIT=9 )
C
      RETURN
      END
C
C
C ----------------------------------------------------------------------
      SUBROUTINE INTGRL3(Ibx,Iby,NX,NY,AX,AY,THETAX,THETAY,IEO,
     &                   BETAX,BETAY,BX,BY,
     &                   CX,CY,DX,DY,EX,EY,
     &                   A11,A22,A12,A16,A26,A66,
     &                   XL,YL,KIII)
C ----------------------------------------------------------------------
C
C  This subroutine computes the stiffness matrix for the nonlinear cubic
C  term.  Note that this matrix is a non-square matrix.
C
C ----------------------------------------------------------------------
C
C
C     [ Variables ]
C
      IMPLICIT DOUBLE PRECISION (A-H, O-Z)
      DOUBLE PRECISION KIII
      INTEGER NX,NY,NXY,i,j
C
      PARAMETER ( N1=7, N2=N1**2, N4=N2**3 )
C
      DIMENSION THETAX(5),THETAY(5),AX(5),AY(5)
      DIMENSION BETAX(5,N1),BETAY(5,N1),BX(5,N1),BY(5,N1)
      DIMENSION CX(5,N1),CY(5,N1),DX(5,N1),DY(5,N1),EX(5,N1),EY(5,N1)
      DIMENSION KIII(N2,N4)
C
C
C     ------------------------------------------------------------
C     * Defining Beam Functions & Derivatives of Beam Functions
C     ------------------------------------------------------------
C
C
      q(i,x)  = (SQRT(2.)*SIN(BETAX(5,i)*x+THETAX(5))
     &          +AX(5)*EXP(-BETAX(5,i)*x)
     &          +BX(5,i)*EXP(-BETAX(5,i)*(1.-x)))*CX(5,i)
     &          +2.*EX(5,i)*(DX(5,i)*(-x)+0.5)
C
C
      dq(i,x) =((BETAX(5,i)*SQRT(2.)*COS(BETAX(5,i)*x+THETAX(5))
     &          -BETAX(5,i)*AX(5)*EXP(-BETAX(5,i)*x)
     &          +BETAX(5,i)*BX(5,i)*EXP(-BETAX(5,i)*(1.-x)))
     &          *CX(5,i)+DX(5,i)*(-2.))/XL
C
C
```

```
       r(i,y)   = (SQRT(2.)*SIN(BETAY(5,i)*y+THETAY(5))
     &            +AY(5)*EXP(-BETAY(5,i)*y)
     &            +BY(5,i)*EXP(-BETAY(5,i)*(1.-y)))*CY(5,i)
     &            +2.*EY(5,i)*(DY(5,i)*(-y)+0.5)
C
C
       dr(i,y) =((BETAY(5,i)*SQRT(2.)*COS(BETAY(5,i)*y+THETAY(5))
     &            -BETAY(5,i)*AY(5)*EXP(-BETAY(5,i)*y)
     &            +BETAY(5,i)*BY(5,i)*EXP(-BETAY(5,i)*(1.-y)))
     &            *CY(5,i)+DY(5,i)*(-2.))/YL
C
C
C      ---------------------------------------------------------
C      * Calculating non-square stiffness matrix components for
C        nonlinear (cubic) term by numerical integration using
C        "Extended Trapezoidal Rule"
C      ---------------------------------------------------------
C
       WRITE(6,*)'CYPHERIN UP THAT NON-LINEAR STIFFNESS THINGY...'
C
       xunit = XL/20.
       yunit = YL/20.
C
C
       IF(Ibx .EQ. 0) THEN
          A11 = 0.
       ENDIF
C
       IF(Iby .EQ. 0) THEN
          A22 = 0.
       ENDIF
C
C
       i = 0
       DO 320 ix = 1, NX
          DO 321 iy = 1, NY
       WRITE(6,*)'Ho Hum...'
             i = i+1
             j = 0
             DO 322 kx = 1, NX
                DO 323 ky = 1, NY
                   DO 324 lx = 1, NX
                      DO 325 ly = 1, NY
                         DO 326 mx = 1, NX
                            DO 327 my = 1, NY
                               j = j+1
C
                               xKee1 = 0.
                               xKee4 = 0.
C
                               yKee1 = 0.
                               yKee4 = 0.
C
                               x = -0.05
                               y = -0.05
C
                               IF(IEO .EQ. 1) NNN = 11
                               IF(IEO .EQ. 0) NNN = 21
```

```
C
                              DO 328 KK = 1, NNN
C
                                 x = x+0.05
                                 y = y+0.05
C
C
                                 rc = 1.
                                 IF((KK .EQ. 1) .OR.
     &                              (KK .EQ. 21)) rc = 2.
                                 IF(IEO .EQ. 0) THEN
                                   IF((KK .EQ. 1) .OR.
     &                                (KK .EQ. 11)) rc=2.
                                 ENDIF
C
C
                                 xKee1 = dq(ix,x)*dq(kx,x)
     &                                  *dq(lx,x)*dq(mx,x)
     &                                  *xunit/rc + xKee1
C
C
                                 xKee4 = q(ix,x)*q(kx,x)
     &                                  *q(lx,x)*q(mx,x)
     &                                  *xunit/rc + xKee4
C
C
C
                                 yKee1 = r(iy,y)*r(ky,y)
     &                                  *r(ly,y)*r(my,y)
     &                                  *yunit/rc + yKee1
C
C
                                 yKee4 = dr(iy,y)*dr(ky,y)
     &                                  *dr(ly,y)*dr(my,y)
     &                                  *yunit/rc + yKee4
C
C
 328                          CONTINUE
C
                              asm=1.
                              IF(IEO .EQ. 1) asm=4.
C
                              KIII(i,j) = (0.5 * A11 * xKee1
     &                                               * yKee1
     &                                    +0.5 * A22 * xKee4
     &                                               * yKee4)* asm
C
C
 327                       CONTINUE
 326                    CONTINUE
 325                 CONTINUE
 324              CONTINUE
 323           CONTINUE
 322        CONTINUE
 321     CONTINUE
 320  CONTINUE
      WRITE(6,*)'Finally...'
C
```

```
C
      RETURN
      END
C
C
C ======================================================================
      SUBROUTINE NRSOL(Rhold,KI,KIII,AX,AY,THETAX,THETAY,
     &                  BETAX,BETAY,BX,BY,CX,CY,DX,DY,EX,EY)
C ======================================================================
      IMPLICIT DOUBLE PRECISION (A-H, O-Z)
      DOUBLE PRECISION KE,KdE,KI,Kigg,KiiS
      DOUBLE PRECISION Kiige,Kiieg,KIII,KUN
      PARAMETER ( N1=7, N2=N1**2, N3=N2**2, N4=N2**3,
     &            N5=N2*2, N6=N2*2, N7=N3*2 )
      DIMENSION A(N2),B(N2),C(N2),D(N2),E(N2),X(2,20)
      DIMENSION KUN(N5,N2),KE(N2),KdE(N2,N2)
      DIMENSION KI(N2,N2)
      DIMENSION KIII(N2,N4),R(N2),Rhold(N2)
      DIMENSION THETAX(5),THETAY(5),AX(5),AY(5)
      DIMENSION BETAX(5,N1),BETAY(5,N1),BX(5,N1),BY(5,N1)
      DIMENSION CX(5,N1),CY(5,N1),DX(5,N1),DY(5,N1),EX(5,N1),EY(5,N1)
      CHARACTER OSTR1*18,OSTR3*18,OSTR4*18,OSTR5*18
C
      CALL INPUT2(beta,NCX,NCY,NDX,NDY,NX,NY,XL,YL,
     &            THICK,NKX,X,LOOP,E,F,NF,ERR,
     &            OSTR1,OSTR3,OSTR4)
      NXY = NX*NY
      NC = NCX*NCY
      ND = NDX*NDY
      NEN = NC+ND
C
C  Psi x & Psi y Recovery Matrix
C
        WRITE(6,*)'Reading stiffnesses...'
            OPEN( UNIT=9, FILE='KUNMAT', STATUS='OLD' )
      READ(9,*)NN,iKae,iKbe
      DO 15 I = 1, NN
        READ(9,*)(KUN(I,L),L=1,NXY)
 15   CONTINUE
      READ(9,*)
            CLOSE( UNIT=9 )
C
C  Write header for output data
C
        WRITE(6,*)'Open Write File ...'
            OPEN( UNIT=12, FILE=OSTR4, STATUS='NEW' )
C
        WRITE(6,*)'The initial guess vector is ->'
        WRITE(6,210)(E(I),I=1,NXY)
        WRITE(6,*)
        WRITE(12,221)NX,NY
        WRITE(12,222)beta
        WRITE(12,*)'The initial guess vector is ->'
        WRITE(12,210)(E(I),I=1,NXY)
 221  FORMAT(1X,'This is a ',I2,' x ',I2,' mode case')
 222  FORMAT(1X,'The beta factor is ->',F8.5)
C
C Loop for calculating deflection at a succession of forces
```

```
C
      Q = F
      DO 150 K = 1,NF
C
        WRITE(6,102)K
        WRITE(6,*)
 102  FORMAT(' ','Force Number',I6)
C
        DO 160 I=1,NXY
          R(I) = 2*Rhold(I)*F
 160    CONTINUE
C
C  Goto Newton-Raphson subroutine to get E
C
      CALL NEWRAF(E,KI,KIII,R,NXY,NEN,LOOP,K,ERR,beta)
C         There is a good reason for this K^
C
C  Goto Recover subroutine to get A & B
C
      CALL RECOVR(KUN,NN,NXY,E,A,B,iKae,iKbe)
C
C  Write more header for output data
C
      IF(K.EQ.1)THEN
        WRITE(12,*)'000000000000000'
        WRITE(12,200)F
        WRITE(12,210)(E(I),I=1,NXY)
        WRITE(12,210)(A(I),I=1,NXY)
        WRITE(12,210)(C(I),I=1,NC)
        WRITE(12,210)(D(I),I=1,ND)
        WRITE(12,*)'==============='
        WRITE(12,*)' X-Coord    Y-Coord     Force       w           Ep011
     &        Kap11       Kap11w'
      ENDIF
 200  FORMAT(1X,'The E, A, C,& D Vectors for force ',F8.1,' are ->')
 210  FORMAT(9D12.4)
C
C  Goto Mode Shape subroutine to get final answer & output
C
      CALL MODSHP(F,E,A,C,NX,NY,NXY,NC,ND,NEN,XL,YL,
     &            beta,NKX,X,THICK,
     &            AX,AY,THETAX,THETAY,
     &            BETAX,BETAY,BX,BY,
     &            CX,CY,DX,DY,EX,EY)
C
C  Increment Force
C
      IF(NF.EQ.1)GOTO 150
      F = F - Q/(NF - 1)
 150  CONTINUE
C
            CLOSE( UNIT=12 )
      STOP
      END
C
C
C ======================================================================
C
```

```
C
C     SUBROUTINE LIBRARIES
C
C
C =====================================================================
C
C
C ---------------------------------------------------------------------
      SUBROUTINE INPUT2(beta,NCX,NCY,NDX,NDY,NX,NY,XL,YL,
     &                 THICK,NKX,X,LOOP,E,F,NF,ERR,
     &                 OSTR1,OSTR3,OSTR4)
C ---------------------------------------------------------------------
C
C  This subroutine reads data from the existing input data file called
C  "stiff.dat".  The format of "stiff.dat" is described as follows:
C
C  line 1-5: comment lines (program does not read)
C  line 6  : Ibx,Iby,beta
C  line 7  : Data not used here
C  line 8  : NCX, NCY, NDX, NDY, NX, NY
C  line 9  : Data not used here
C  line 10 : XL, YL, THICK
C  line 11 : Data not used here
C  line 12 : Data not used here
C  line 13 : Data not used here
C  line 14 : Data not used here
C  line 15 : LOOP
C  line 16 : E(I)
C  line 17 : F, NF
C  line 18 : ERR
C  line 19 : NKX
C  line 20 : X(1,I)
C  line 21 : X(2,I)
C  line 22 : OSTR1,OSTR3
C  line 23 : OSTR4
C
C  where,
C
C     beta      : degree of non linearity ranging from 0.0 to 1.0
C                 0.0 =>  linear case
C                 1.0 =>  perfectly nonlinear case
C
C     NCX, NCY  : number of u modes in the x and y directions
C     NDX, NDY  : number of v modes in the x and y directions
C     NX, NY    : number of w modes in the x and y directions
C
C     XL, YL    : dimensions of plate in the x and y directions (m)
C
C     LOOP      : max. number of Newton-Raphson iterations allowed
C
C     E(I)      : first guess at w amplitudes in Newton-Raphson
C
C     F         : magnitude of contact force desired
C
C     NF        : no. of force calculations (=1 just calculates for F)
C
C     ERR       : error between current and previous guess in
C                 Newton-Raphson
```

```
C
C     NKX       : number of locations where data is to be calculated
C
C     X(1,I)    : X coordinate of desired data location
C
C     X(2,I)    : Y coordinate of desired data location
C
C     OSTR1&3   : Input filename for stiffness matrices, 18 chars. max,
C                 must be written within apostrophes like:  'xxxxxxx'
C
C     OSTR4     : Output filename for final solution, 18 characters max,
C                 must be written within apostrophes like:  'xxxxxxx'
C
C ---------------------------------------------------------------------
C
C
C     [ Variables ]
C
      IMPLICIT DOUBLE PRECISION (A-H, O-Z)
      PARAMETER ( N1=7, N2=N1**2 )
      DIMENSION E(N2),X(2,20)
      CHARACTER OSTR1*18,OSTR3*18,OSTR4*18
C
        WRITE(6,*)'Reading input file...'
      OPEN( UNIT=14, FILE='stiff.dat', STATUS='OLD' )
C
      READ(14,*)
      READ(14,*)
      READ(14,*)
      READ(14,*)
      READ(14,*)
      READ(14,*) Ibx,Iby,beta
      READ(14,*)
      READ(14,*) NCX,NCY,NDX,NDY,NX,NY
      READ(14,*)
      READ(14,*) XL,YL,THICK
      READ(14,*)
      READ(14,*)
      READ(14,*)
      READ(14,*)
      READ(14,*)LOOP
      NXY=NX*NY
      READ(14,*)(E(I),I=1,NXY)
      READ(14,*)F,NF
      READ(14,*)ERR
      READ(14,*)NKX
      READ(14,*)(X(1,I),I=1,NKX)
      READ(14,*)(X(2,I),I=1,NKX)
      READ(14,*) OSTR1,OSTR3
      READ(14,*) OSTR4
C
      CLOSE( UNIT=14 )
C
      RETURN
      END
C ---------------------------------------------------------------------
      SUBROUTINE NEWRAF(E,KI,KIII,R,NXY,NEN,LOOP,K,ERR,beta)
C ---------------------------------------------------------------------
```

```
C  Subroutine uses the Newton-Raphson method to solve the non-linear
C  system of equations for the modal amplitudes, E.
C  We're using the Newton-Raphson method:
C                          [J]{E' - E} = -{G}
C  Which is of the form Ax = b
C              We have A:  [J] = KdE     We have b:  -{G} = -KE
C                           And we want x:  {E' - E}
C  We use LU decomposition to solve for x which is assigned to KE.
C  Since KE = {E' - E} we solve for the next guess:  E' = KE + E.
C  Actually the program just reassigns it to E for the next loop.
C  Convergence is checked by comparing the absolute value of the
C  difference between the current guess and the updated guess
C  (Abs(KE)) against a pre-determined error value, ERR.  The number
C  of Newton-Raphson iterations is limited to LOOP as a safety valve
C  against divergence.
C ---------------------------------------------------------------------
      IMPLICIT DOUBLE PRECISION (A-H, O-Z)
      DOUBLE PRECISION KE,KdE,KI,KIII,R
      PARAMETER ( N1=7, N2=N1**2, N3=N2**2, N4=N2**3,
     &                    N6=N2*2, N7=N3*2 )
      DIMENSION INDX(N6),E(N2),KE(N2),KdE(N2,N2)
      DIMENSION KI(N2,N2),KIII(N2,N4),R(N2)
C
        WRITE(6,*)
        WRITE(6,*)'Newton-Raphsoning...'
        WRITE(6,*)
C
      DO 1 I=1,NXY
        KE(I)=0.0
      DO 2 J=1,NXY
        KdE(I,J)=0.0
 2    CONTINUE
 1    CONTINUE
C
C  Newton-Raphson Loop
C
      DO 100 L = 1,LOOP
        WRITE(6,101)L
 101  FORMAT('+','Newton-Raphson Step Number ',I6)
C
C  Get the equations from this subroutine
C
      CALL EEQS(E,KE,KdE,KI,KIII,R,NXY,NEN,beta)
C
C  Do LU decomposition and solve for x (KE)
C
      CALL LUDCM2(KdE,NXY,N2,INDX)
      CALL LUBKS2(KdE,NXY,N2,INDX,KE)
C
      HOLD = 0.0
C
C  Calculate next guess from current guess
C
      DO 10 I = 1,NXY
        E(I) = KE(I) + E(I)
 10   CONTINUE
C
C  Check to see if the guesses have converged to within ERR
```

```
C
      DO 20 I = 1,NXY
        KE(I) = ABS(KE(I))
        IF(KE(I).GT.HOLD) HOLD = KE(I)
 20   CONTINUE
      IF(HOLD.LT.ERR) GOTO 25
 100  CONTINUE
 25   CONTINUE
C
C  End of Newton-Raphson Loop
C
      RETURN
      END
C ---------------------------------------------------------------------
      SUBROUTINE EEQS(E,KE,KdE,KI,KIII,R,NXY,NEN,beta)
C ---------------------------------------------------------------------
C  This subroutine determines the non-linear equations (g) and the
C  components of the Jacobian matrix (J) for use in the Newton-Raphson
C  root finding method as shown:
C
C                     J  [x    - x] = -g
C                      k   k+1   k      k
C ---------------------------------------------------------------------
      IMPLICIT DOUBLE PRECISION (A-H, O-Z)
      DOUBLE PRECISION KE,KdE,KI,KIII,R
      DOUBLE PRECISION E,dE1dE,dE2dE,dE3dE
      PARAMETER ( N1=7, N2=N1**2, N3=N2**2, N4=N2**3,
     &            N5=N2*3, N6=N2*2, N7=N3*2 )
      DIMENSION E(N2),KE(N2),KdE(N2,N2)
      DIMENSION KI(N2,N2),KIII(N2,N4),R(N2)
C
C Initialize Variables
C
      DO 1 I=1,NXY
      DO 2 J=1,NXY
        KE(I)=0.0
        KdE(I,J)=0.0
 2    CONTINUE
 1    CONTINUE
C
      DO 10 l = 1,NXY
      n = 0
      ms = 0
      KE(l) = R(l)
        DO 20 i = 1,NXY
C
C -> Linear Terms <-
C
C  Calculate a linear term in the equation (-g).
C
        KE(l) = (-1.)*KI(l,i)*E(i) + KE(l)
C
C  Determine the derivative of a linear term.
C
        IF (l.EQ.i)THEN
            dE1dE = 1.0
          ELSE
            dE1dE = 0.0
```

```
          ENDIF
C
C  Calculate a linear term in the Jacobian (J).
C
          DO 25 il = 1,NXY
          KdE(il,l) = KI(il,i)*dE1dE + KdE(il,l)
 25       CONTINUE
C
C -> Non-Linear Terms <-
C
          DO 30 j = 1,NXY
            DO 40 k = 1,NXY
            n = n + 1
C
C  Calculate a non-linear term in the equation (-g).
C
            KE(l) = (-1.)*beta*KIII(l,n)*E(i)*E(j)*E(k) + KE(l)
C
C  Determine the derivative of a non-linear term.
C
            IF(l.EQ.i.AND.l.EQ.j.AND.l.EQ.k)THEN
              dE3dE = 3.*E(i)**2.
              GOTO 50
              ENDIF
            IF(l.EQ.i.AND.l.EQ.j)THEN
              dE3dE = 2.*E(i)*E(k)
              GOTO 50
              ENDIF
            IF(l.EQ.j.AND.l.EQ.k)THEN
              dE3dE = 2.*E(j)*E(i)
              GOTO 50
              ENDIF
            IF(l.EQ.i.AND.l.EQ.k)THEN
              dE3dE = 2.*E(i)*E(j)
              GOTO 50
              ENDIF
            IF(l.EQ.i)THEN
              dE3dE = E(j)*E(k)
              GOTO 50
              ENDIF
            IF(l.EQ.j)THEN
              dE3dE = E(i)*E(k)
              GOTO 50
              ENDIF
            IF(l.EQ.k)THEN
              dE3dE = E(i)*E(j)
              GOTO 50
              ENDIF
            dE3dE = 0.0
 50         CONTINUE
C
C  Calculate a non-linear term in the Jacobian (J).
C
            DO 45 in = 1,NXY
            KdE(in,l) = beta*KIII(in,n)*dE3dE + KdE(in,l)
 45         CONTINUE
C
 40         CONTINUE
```

```
 30         CONTINUE
 20       CONTINUE
 10     CONTINUE
C
        RETURN
        END
C ---------------------------------------------------------------------
        SUBROUTINE LUDCM2(A,N,NP,INDX)
C ---------------------------------------------------------------------
C
C  This subroutine performs LU decomposition.
C  Taken from "Numerical Recipes for FORTRAN77"
C
C ---------------------------------------------------------------------
C       [ Variables ]
C
        IMPLICIT DOUBLE PRECISION (A-H, O-Z)
        PARAMETER ( N1=7, N2=N1**2, N6=N2*2 )
        PARAMETER ( TINY=1.0E-16 )
        DIMENSION A(NP,NP),INDX(NP),VV(N6)
C
        D = 1.
C
        DO 350 I = 1, N
           AAMAX = 0.
           DO 351 J = 1, N
              IF(ABS(A(I,J)) .GT. AAMAX) AAMAX=ABS(A(I,J))
 351       CONTINUE
           IF(AAMAX .EQ. 0.) AAMAX=TINY
           VV(I) = 1./AAMAX
 350    CONTINUE
C
        DO 352 J = 1, N
C
           DO 353 I = 1, J-1
              SUM = A(I,J)
              DO 354 K = 1, I-1
                 SUM = SUM - A(I,K)*A(K,J)
 354          CONTINUE
              A(I,J) = SUM
 353       CONTINUE
           AAMAX = 0.
C
           DO 355 I = J, N
              SUM = A(I,J)
              DO 356 K = 1, J-1
                 SUM = SUM - A(I,K)*A(K,J)
 356          CONTINUE
              A(I,J) = SUM
              DUM = VV(I)*ABS(SUM)
              IF(DUM .GE. AAMAX) THEN
                 IMAX = I
                 AAMAX = DUM
              ENDIF
 355       CONTINUE
C
           IF(J .NE. IMAX) THEN
              DO 357 K = 1, N
```

```
                DUM = A(IMAX,K)
                A(IMAX,K) = A(J,K)
                A(J,K) = DUM
 357         CONTINUE
             D = -D
             VV(IMAX) = VV(J)
          ENDIF
C
          INDX(J) = IMAX
C
          IF(A(J,J) .EQ. 0.) A(J,J)=TINY
C
          IF(J .NE. N) THEN
             DUM = 1./A(J,J)
             DO 358 I = J+1, N
                A(I,J) = A(I,J)*DUM
 358         CONTINUE
          ENDIF
C
 352   CONTINUE
C
       RETURN
       END
C ----------------------------------------------------------------------
       SUBROUTINE LUBKS2(A,N,NP,INDX,B1)
C ----------------------------------------------------------------------
C
C  This subroutine performs LU back-substitution.
C  Taken from "Numerical Recipes for FORTRAN77"
C ----------------------------------------------------------------------
C      [ Variables ]
C
       IMPLICIT DOUBLE PRECISION (A-H, O-Z)
       PARAMETER ( N1=7, N2=N1**2, N6=N2*2 )
       DIMENSION A(NP,NP),INDX(NP),B1(N6)
C
       II = 0
C
       DO 360 I = 1, N
          LL = INDX(I)
          SUM = B1(LL)
          B1(LL) = B1(I)
C
          IF(II .NE. 0) THEN
             DO 361 J = II, I-1
                SUM = SUM - A(I,J)*B1(J)
 361         CONTINUE
          ELSE IF (SUM .NE. 0.) THEN
             II = I
          ENDIF
C
          B1(I) = SUM
 360   CONTINUE
C
       DO 362 I = N, 1, -1
          SUM = B1(I)
          DO 363 J = I+1, N
             SUM = SUM - A(I,J)*B1(J)
```

```
 363      CONTINUE
          B1(I) = SUM/A(I,I)
 362  CONTINUE
C
      RETURN
      END
C -----------------------------------------------------------------------
      SUBROUTINE RECOVR(KUN,NN,NXY,E,A,B,iKae,iKbe)
C -----------------------------------------------------------------------
C  This subroutine recovers A & B from E using the matrix KUN,
C  calculated as a step of static condensation in the stiffness program.
C  A & B allow the calculation of Yx and Yy.
C -----------------------------------------------------------------------
      IMPLICIT DOUBLE PRECISION (A-H, O-Z)
      DOUBLE PRECISION KUN,E,A,B,SUM,PR
C
      PARAMETER ( N1=7, N2=N1**2, N5=N2*2 )
C
      DIMENSION KUN(N5,N2),E(N2),A(N2),B(N2)
C
      DO 10 I = 1, NN
            SUM = 0.
         DO 20 J = 1, NXY
               PR = KUN(I,J)*E(J)
               SUM = SUM+PR
 20      CONTINUE
            IF(I.LE.iKae)THEN
             A(I)=SUM
            ELSE
             B(I-iKae)=SUM
            ENDIF
 10   CONTINUE
      RETURN
      END
C
C -----------------------------------------------------------------------
      SUBROUTINE MODSHP(F,E,A,C,NX,NY,NXY,NC,ND,NEN,XL,YL,
     &                  beta,NKX,XY,THICK,
     &                  AX,AY,THETAX,THETAY,
     &                  BETAX,BETAY,BX,BY,
     &                  CX,CY,DX,DY,EX,EY)
C -----------------------------------------------------------------------
C  This subroutine calculates the deflection and strain at a series of
C  points on the plate.  It uses the assumed mode shapes and the modal
C  amplitudes solved for in the Newton-Raphson subroutine.
C -----------------------------------------------------------------------
      IMPLICIT DOUBLE PRECISION (A-H, O-Z)
      DOUBLE PRECISION Kap11,n,m,Kap110
      PARAMETER ( N1=7, N2=N1**2, N5=N2*2, N6=N2*2 )
      DIMENSION E(N2),C(N2),A(N2),XY(2,20)
      DIMENSION THETAX(5),THETAY(5),AX(5),AY(5)
      DIMENSION BETAX(5,N1),BETAY(5,N1),BX(5,N1),BY(5,N1)
      DIMENSION CX(5,N1),CY(5,N1),DX(5,N1),DY(5,N1),EX(5,N1),EY(5,N1)
C
C
      q(i,x)  = (SQRT(2.)*SIN(BETAX(5,i)*x+THETAX(5))
     &          +AX(5)*EXP(-BETAX(5,i)*x)
     &          +BX(5,i)*EXP(-BETAX(5,i)*(1.-x)))*CX(5,i)
```

```
     &           +2.*EX(5,i)*(DX(5,i)*(-x)+0.5)
C
C
      r(i,y)   = (SQRT(2.)*SIN(BETAY(5,i)*y+THETAY(5))
     &           +AY(5)*EXP(-BETAY(5,i)*y)
     &           +BY(5,i)*EXP(-BETAY(5,i)*(1.-y)))*CY(5,i)
     &           +2.*EY(5,i)*(DY(5,i)*(-y)+0.5)
C
C
      dq(i,x)  =((BETAX(5,i)*SQRT(2.)*COS(BETAX(5,i)*x+THETAX(5))
     &           -BETAX(5,i)*AX(5)*EXP(-BETAX(5,i)*x)
     &           +BETAX(5,i)*BX(5,i)*EXP(-BETAX(5,i)*(1.-x)))
     &           *CX(5,i)+DX(5,i)*(-2.))/XL
C
C
      n(i,y)   = (SQRT(2.)*SIN(BETAY(3,i)*y+THETAY(3))
     &           +AY(3)*EXP(-BETAY(3,i)*y)
     &           +BY(3,i)*EXP(-BETAY(3,i)*(1.-y)))*CY(3,i)
     &           +2.*EY(3,i)*(DY(3,i)*(-y)+0.5)
C
C
      m(i,x)   = (SQRT(2.)*SIN(BETAX(3,i)*x+THETAX(3))
     &           +AX(3)*EXP(-BETAX(3,i)*x)
     &           +BX(3,i)*EXP(-BETAX(3,i)*(1.-x)))*CX(3,i)
     &           +2.*EX(3,i)*(DX(3,i)*(-x)+0.5)
C
C
      dm(i,x)  =((BETAX(3,i)*SQRT(2.)*COS(BETAX(3,i)*x+THETAX(3))
     &           -BETAX(3,i)*AX(3)*EXP(-BETAX(3,i)*x)
     &           +BETAX(3,i)*BX(3,i)*EXP(-BETAX(3,i)*(1.-x)))
     &           *CX(3,i)+DX(3,i)*(-2.))/XL
C
C
      ddq(i,x) = CX(5,i)*((AX(5)*BETAX(5,i)**2.)/EXP(x*BETAX(5,i))
     &         + (BETAX(5,i)**2.*BX(5,i))/EXP((1. - x)*BETAX(5,i))
     &         - SQRT(2.)*BETAX(5,i)**2.
     &              *SIN(THETAX(5) + x*BETAX(5,i)))/(XL*XL)
C
C
      df(i,x)  =((-(BETAX(1,i)**2)*SQRT(2.)*SIN(BETAX(1,i)
     &                                 *x+THETAX(1))
     &           +(BETAX(1,i)**2)*AX(1)*EXP(-BETAX(1,i)*x)
     &           +(BETAX(1,i)**2)*BX(1,i)*EXP(-BETAX(1,i)
     &                       *(1.-x)))*CX(1,i))/(XL*XL)
C
C
      g(i,y)   = (SQRT(2.)*SIN(BETAY(1,i)*y+THETAY(1))
     &           +AY(1)*EXP(-BETAY(1,i)*y)
     &           +BY(1,i)*EXP(-BETAY(1,i)*(1.-y)))*CY(1,i)
     &           +2.*EY(1,i)*(DY(1,i)*(-y)+0.5)
C
C
C Cycle through x and y locations
C
      DO 10 KX = 1,NKX
        u = 0.0
        w = 0.0
        dw = 0.0
```

```
        du = 0.0
        dpsi = 0.0
        ddw = 0.0
        NW = 0
        x = XY(1,KX)/XL
        y = XY(2,KX)/YL
          DO 30 I = 1,NX
            DO 40 J = 1,NY
            NW = NW + 1
C
C  Calculate deflection
C
            w = w + E(NW)*q(I,x)*r(J,y)
C
C  Calculate derivatives of deflection in x direction (for strain)
C
            dw = dw + E(NW)*dq(I,x)*r(J,y)
            dpsi = dpsi + A(NW)*df(I,x)*g(J,y)
            ddw = ddw + E(NW)*ddq(I,x)*r(J,y)
C
            IF(NW.GT.NC) GOTO 200
            du = du + C(NW)*dm(I,x)*n(J,y)
            u = u + C(NW)*m(I,x)*n(J,y)
 200        CONTINUE
C
 40         CONTINUE
 30       CONTINUE
C
C  Calculate extensionsal strain, bending strain on top of plate,
C  and total strain on top and bottom of plate
C
            Ep011 = beta*(1./2.)*(dw*dw)
            Kap11 = (THICK/2.)*dpsi
            Kap110 = (THICK/2.)*ddw
C
      WRITE(12,100)XY(1,KX),XY(2,KX),F,w,Ep011,Kap11,Kap110
C
 10   CONTINUE
 100  FORMAT(1X,2(F8.6,','),F7.1,4(',',D12.4))
      RETURN
      END
```